

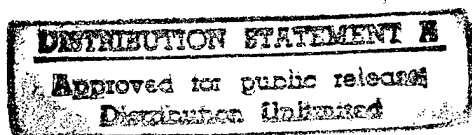
JPRS-JST-90-032

27 JUNE 1990



**FOREIGN
BROADCAST
INFORMATION
SERVICE**

JPRS Report



19980130 198

Science & Technology

Japan

MECHANISM OF SUPERCONDUCTIVITY

DTIC QUALITY INSPECTED 3

22161

SPRINGFIELD, VA
5285 PORT ROYAL RD
ATTN: PROCESS 103
NTIS

22161
45

REPRODUCED BY
U.S. DEPARTMENT OF COMMERCE
NATIONAL TECHNICAL INFORMATION SERVICE
SPRINGFIELD, VA. 22161

JPRS-JST-90-032
27 JUNE 1990

SCIENCE & TECHNOLOGY
JAPAN

MECHANISM OF SUPERCONDUCTIVITY

43070732 Tokyo RESEARCH REPORT ON MECHANISM OF SUPERCONDUCTIVITY
in English Mar 90 pp 1-439

[Second year report on "Mechanism of Superconductivity" supported
by the Grant-in-Aid of Science Research on Priority Areas
(No.031) from the Ministry of Education, Science and Culture]

CONTENTS

Table of Contents.....	1
Cu-O Network Dependent Properties of Single CuO ₂ -Sheet Compounds - Charge-Transfer Gap and Charge-Doping Effect - [Y. Tokura, T. Arima, et al.].....	6
New High-T _c Copper Oxide Superconductors: (Nd,Ce,Sr) ₂ CuO _{4-z} and (Ln,Ce,Ba) ₄ Cu ₃ O _{9-z} (Ln:Nd,Sm,Eu and Gd) [Jun Akimitsu, Hiroshi Sawa].....	11
Oxygen Contents and Superconductivity in Several High-T _c Oxides: Ba _{1-x} K _x BiO _{3-δ} , Tl ₂ Ba ₂ CuO _{6-δ} , PbBaSrYCu ₃ O _{7+δ} and Nd _{1.85-x} M _x Ce _{0.15} O _{4-δ} (M=La, Sm) [Y. Syono, M. Kikuchi, et al.].....	19
Preparation and Superconducting Properties of Pb ₂ Sr ₂ Y _{0.5} Ca _{0.5} Cu ₃ O _{8+δ} With Zero Resistance at 75 K [Y. Saito, Y. Koike, et al.].....	27

Thallium-Substitution Effects in Ferroelectric Bismuth Layer-Oxides [Masaaki Takashige, Fuminao Shimizu, et al.].....	32
Preparation and Characterization of Certain Cu-Oxides Stabilized in Layered Structures by the Use of High Pressures and High Oxygen Pressures [M. Takano, Y. Takeda].....	36
Absence of Superconductivity in the $(\text{La}_{1-x}\text{Sr}_x)_2\text{NiO}_4$ System [M. Takahashi, H. Twawaki, et al.].....	41
Carrier Density Dependence of the Transport Properties of $\text{La}_{2-x}\text{Sr}_{1+x}\text{Cu}_2\text{O}_{6+y}$ [Tsuyoshi Tamegai, Chiho Okada, et al.].....	44
Anisotropic Properties of $\text{La}_{8-x}\text{Sr}_x\text{Cu}_8\text{O}_{20-\delta}$ Epitaxial Thin Films [T. Murakami, Y. Enomoto, et al.].....	48
Ba-Y-Cu-O Films Prepared by Various RF Sputtering Techniques and Their Structure and Superconducting Properties [H. Morita, H. Fjuimori, et al.].....	53
Preparation of $(\text{Bi}_{1-x}\text{Pb}_x)_2\text{Sr}_2\text{Ca}_3\text{Cu}_4\text{O}_y$ Superconducting Film by a Single Composite Target Sputtering Method [Yoichiro Kawai, Toshifumi Terui ⁺ , et al.].....	56
Preparation of Oxide Superconductors by Oxidation of Amorphous Ln-Ce-Cu (Ln= Pr, Nd or Sm) Alloy Tapes [Kunio Matsuzaki, Koichi Shimizu*, et al.].....	61
Ultrahigh-Pressure Study of High T_c Oxides [H. Aoki, M. Kumazawa*, et al.].....	65
Growth of Superconducting Oxide Single Crystals by TSFZ Method [H. Kojima, I. Tanaka].....	67
Crystal Growth and Characterization of Oxide Superconductors and Related Compounds [H. Takei, H. Takeya, et al.].....	71
Single Crystal Growth of Superconducting Oxides and Related Compounds by the Flux, Floating Zone and Other Methods [T. Fukuda, T. Shishido, et al.].....	81
Cross Sectional Observation of Bi-O and Cu-O Layers by STM/STS in $\text{Bi}_2\text{Sr}_2\text{CaCu}_2\text{O}_y$ [K. Kitazawa, T. Hasegawa, et al.].....	88
Neutron and X-Ray Diffraction Studies on Crystal Structures of Oxide Superconductors [H. Asano].....	92

Oxygen Deficiency in 1-2-3-Type Oxide Superconductors [E. Takayama-Muromachi].....	97
Anomalous Properties of 2-1-4 Compounds [Y. Maeno, M. Kato, et al.].....	103
Ultrasonic Properties in $\text{La}_{2-x}\text{M}_x\text{CuO}_{4-\delta}$ (M=Ba and Sr) and Correlation Between T_c and Hole Concentration in the Cation-Substituted $\text{Bi}_2\text{Sr}_2\text{CaCu}_2\text{O}_{8+\delta}$ System [T. Fukase, Ye. Koike*, et al.].....	113
Comparison of High Pressure Effects on Transition Temperature in the Electron- and Hole-Doped Oxide Superconductors [S. Yomo*, C. Murayama*, et al.].....	119
Characteristics of Electronic Properties of High- T_c Oxides [Masatoshi Sato, Masafumi Sera, et al.].....	124
Specific Heat Study of $\text{Ba}_2\text{YCu}_3\text{O}_{6+y}$ ($6 \leq y \leq 7$) and Ni/Zn Substituted Samples [Y. Nakazawa, J. Takeya, et al.].....	134
Thermal Conductivity, Electrical Resistivity and Specific Heat of $\text{La}_{1.85}\text{Sr}_{0.15}\text{CuO}_4$ Superconductor [K. Mori, K. Noto*, et al.].....	139
Study of High-Temperature Superconductors in La-Sr-Cu-O and Pb-Doped Bi-Sr-Ca-Cu-O Systems [R. Yoshizaki].....	142
Hole Concentration Dependences of T_c in Cuprate Oxide Superconductors [K. Takita, H. Akinaga, et al.].....	147
Resistivity, Hall Coefficient and Transition Temperatures in Ag Doped Bi-Sr-Ca-Cu-O and Sb Doped (Bi,Pb)-Sr-Ca-Cu-O Superconductors [K. Oto, K. Murase, et al.].....	151
Magnetic Study in High- T_c Superconducting Oxides by AC-Complex Susceptibility [Kiichi Okuda, Satoru Noguchi, et al.].....	155
Anomalous Behaviors of Resistive Transition in High T_c -Phase Bi-Pb-Sr-Ca-Cu-O Thin Films in Magnetic Field [S. Mase, T. Fukami, et al.].....	159
Superconductivity and Magnetism of $\text{R}\text{Ba}_2\text{Cu}_3-x\text{M}_x\text{O}_y$ (R=La, Nd and Er; M=Ni and Zn) [Kazuko Sekizawa, Yoshiki Takano].....	167
Dependence of Meissner Effect on the Shape of the Specimens and Magnetic Field [K. Kitazawa, T. Matsushita*, et al.].....	171

Experimental and Theoretical High- T_c Research at Ibaraki University [Takekazu Ishida, Shokichi Kanno, et al.].....	180
Thermally Activated Behavior in Resistive Transition and Magnetic Relaxation of $YBa_2Cu_3O_z$ Films [N. Kobayashi, H. Kawabe*, et al.].....	188
Neutron, Xray Scattering and Neutron Depolarization Studies on Magnetism and Superconductivity in Cuprous Oxides Materials [Yasuo Endoh].....	193
Nuclear Spin-Lattice Relaxation in Highly Correlated Metallic and Superconducting Copper Oxides [H. Yasuoka, T. Shimizu, et al.].....	199
NQR and NMR Studies of Hole- and Electron-Doped $Ln_{2-x}M_xCuO_4$ [K. Kumagai, Y. Nakamura, et al.].....	205
Study of High- T_c Oxide Superconductor by NMR and Other Measurements (II)	
1. NMR [Y. Kitaoka, K. Ishida, et al.].....	210
2. Susceptibility and Resistivity [Y. Oda, M. Yamada].....	210
Proton NMR Studies of Hydrogen-Doped Superconductor $YBa_2Cu_3O_{6.94}H_x$ [H. Niki+, T. Higa*, et al.].....	220
Hydrogen Absorption in Some High- T_c Copper Oxides [H. Fujii, T. Takabatake, et al.].....	226
Study of High T_c Oxide by in-Beam Perturbed Angular Correlation [Fumio Komori, Nobuo Ikeda*, et al.].....	231
Magnetism Studies of Oxide-Superconductors by μ^+ SR [Nobuhiko Nishida].....	234
^{119}Sn and ^{57}Fe Mossbauer Study of $La_{2-x}Sr_xCuO_4$ [T. Shinjo, S. Nasu*, et al.].....	238
New Method for Accurate Analysis of Mossbauer Spectra of $YBa_2(Cu_{1-x}Fe_x)_3O_{7-\delta}$ [T. Tamaki, M. Nishizawa, et al.].....	243
Ion-Channeling Studies in Single-Crystal $YBa_2Cu_3O_{7-y}$ and $Bi_{2.2}Sr_{1.8}CaCu_2O_y$ [K. Yamaya, T. Haga, et al.].....	247
Electronic Structure of High- T_c Superconductor Studied by Photoemission and X-Ray Absorption [T. Takahashi, H. Matsuyama, et al.].....	253

Photoemission Study of Electron- and Hole-Doped Cu-Oxide Superconductors [A. Fujimori].....	259
Raman Studies of Spins and Carriers in Oxide Superconductors [S. Sugai].....	263
Correlation of the Infrared Anomaly and Superconductivity in $\text{YBa}_2(\text{Cu}_{1-x}\text{Co}_x)_3\text{O}_{7-\delta}$ [Kohji Ohbayashi, Hideaki Tukamoto, et al.].....	270
Hopping, Free Carrier and Super-conduction in FIR Optical Conductivity of Bi-Sr-Ca-Cu-O Thin Films [K. Nagasaka, M. Sato, et al.].....	275
Oxygen K-Edge Fine Structure of Tl-Ba-Ca-Cu-O Studied by Electron Energy Loss Spectroscopy [D. Shindo, K. Hiraga, et al.].....	285
Low-Energy Electron Energy Loss Spectroscopy on $\text{Bi}_2\text{Sr}_2\text{Ca}_{n-1}\text{Cu}_n\text{O}_{2n+4+x}$ ($n=1,2$) and Preparation of Thin Film Specimens by Molecular Beam Epitaxy [Atsushi Ando, Liu Kuang-Yu, et al.].....	290
Self-Interaction Correction to Local Spin Density Approximation in Solids [Y. Ishii, K. Terakura].....	294
Nature of Doped Electrons in $\text{Nd}_{2-x}\text{Ce}_x\text{CuO}_4$: Electronic Band Structures of Nd_2CuO_4 Type M_2CuO_4 ($\text{M}=\text{La, Ce and Th}$) [Katsuhiko Takegahara, Tadao Kasuya].....	298
Calculation of the Electronic State of Cu and Ni Compounds by Use of Extended Clusters [J. Kanamori, T. Nishino, et al.].....	303
Theory of Soft-X-Ray Spectroscopy in High- T_c Superconductors [A. Kotani].....	307
Self-Doping in Oxide Superconductors [J. Kondo].....	313
Hole Distribution in Cu-Oxide Superconductors [S. Maekawa, Y. Ohta, et al.].....	317
Theoretical Study of Tunneling Spectra in $\text{Ba}_{x-1}\text{K}_1\text{BiO}_3$ [Masafumi Shirai, Naoshi Suzuki, et al.].....	323
Electronic State and Superconductivity in Layered Copper Oxides [M. Tachiki, H. Matsumoto].....	328
Electronic States of the d-p Model [T. Matsuura, H. Jichi+, et al.].....	338

To Understand Electronic Properties of High Temperature Superconductors on the Basis of Fermi Liquid Theory. II [Hiroshi Kohno, Kosaku Yamada].....	342
Fermi Liquid Theory on the Basis of the Periodic Anderson Model With Spin-Orbit Coupling and Crystalline Field [K. Hanzawa, K. Yosida, et al.].....	347
A Modified Spin-Wave Theory of the Square-Lattice Antiferromagnet [K. Ohara, K. Yosida].....	347
T-Square Term of Electrical Resistivity [K. Yamada, M. Nakano, et al.].....	348
Functional Integral Approach to the Low Dimensional Antiferromagnets [K. Hatada, K. Yosida].....	348
Theory of Normal and Superconducting States of High Temperature Superconductors [Y. Nagaoka, Y. Ōno, et al.].....	349
Fluctuations in High Temperature Superconductors in Strong Magnetic Field [Toshihiko Tsuneto, Tyusuke Ikeda, et al.].....	357
Magnetic Properties of Time-Reversal Breaking Superconductors [M. Sigrist*, T. M. Rice**, et al.].....	360
Theoretical Study of Two-Dimensional CuO ₂ Systems [Masatoshi Imada].....	365
Hole Propagation in a 2D Quantum Spin-1/2 Antiferromagnet [Y. Takahashi, H. Tsunetsugu].....	368
The Holon-Doublon Operator Formalism [Sadao Nakajima].....	373
Slave-Fermion Theory of the t-t'-J Model [Daijiro Yoshioka].....	375
On the Stability of Flux State and Chiral Spin State [Hiroyuki Shiba, Masao Ogata*].....	382
Effective Hamiltonian for CuO ₂ Layers and Fractional Statistics [Hidetoshi Fukuyama].....	388
Organic Conductors Based on Unsymmetrical Donors DMPT and EDT-TTF [I. Ikemoto, K. Kikuchi, et al.].....	393
Design of Molecular Metals With Various Types of Band Structures -- One- Dimensional and Two-Dimensional p π Bands and p π -d Mixing Bands [Hayao Kobayashi, Reizo Kato, et al.].....	397

A Novel Type of Halogen-Bridged One-Dimensional Metal Complexes: Syntheses, Structures and Solid State Properties of $-\text{Ni(III)}-\text{X}-\text{Ni(III)}-$ Compounds (X=Cl and Br) [M. Yamashita, K. Hirao, et al.].....	403
Metal-to-Semiconductor Transition of an Organic Conductor, (EDT-TTF) $_2\text{AuBr}_2$ [T. Mori, H. Inokuchi].....	406
"2K-Superconducting State" in the Organic Superconductor β -(BEDT-TTF) $_2\text{I}_3$ " [S. Kagoshima, M. Hasumi, et al.].....	409
Unconventional Superconductivity in the Organic Superconductor, κ -(BEDT-TTF) $_2\text{Cu(NCS)}_2$ [Toshihiro Takahashi, Kazushi Kanoda].....	415
Anomalous Magnetotransport Phenomena in Organic Conductors [K. Kajita, Y. Nishio, et al.].....	421
(BEDT-TTF)-Based Organic Superconductors Studied at IMR, in 1989 [N. Toyota].....	425
Superconducting and Normal State Properties of Organic Metals (BEDT-TTF) $_2\text{X}$ [Madoka Tokumoto, Nobumori Kinoshita, et al.].....	430
Uniaxial Tensile Stress Effects on Organic Superconductors [T. Ishiguro, Y. Nogami].....	440

Preface	Y. Muto	i
Members of Science Research on Priority Area "Mechanism of Superconductivity"		iii

Part I. Oxide Superconductors ; Experiments

I-1 Sample Synthesis and Characterization

1. Cu-O Network Dependent Properties of Single CuO ₂ -Sheet Compounds - Charge-Transfer Gap and Charge-Doping Effect -	Y. Tokura, T. Arima, S. Koshihara, T. Ido, S. Ishibashi, H. Takagi and S. Uchida	1
2. New High-T _c Copper Oxide Superconductors : (Nd, Ce, Sr) ₂ CuO _{4-z} and (Ln, Ce, Ba) ₄ Cu ₃ O _{9-z} (Ln: Nd, Sm, Eu and Gd)	J. Akimitsu and H. Sawa	6
3. Oxygen Contents and Superconductivity in Several High-T _c Oxides : Ba _{1-x} K _x BiO _{3-δ} , Tl ₂ Ba ₂ CuO _{6-δ} , PbBaSrYCu ₃ O _{7+δ} and Nd _{1.85-x} M _x Ce _{0.15} O _{4-δ} (M = La, Sm)	Y. Syono, M. Kikuchi, K. Ueki, A. Tokiwa, K. Oh-ishi, S. Nakajima, T. Suzuki, M. Nagoshi, N. Kobayashi and Y. Muto	14
4. Preparation and Superconducting Properties of Pb ₂ Sr ₂ Y _{0.5} Ca _{0.5} Cu ₃ O _{8+δ} with Zero Resistance at 75 K	Y. Saito, Y. Koike, T. Noji, M. Masuzawa, H. Sunagawa, H. Kawabe and N. Kobayashi	22
5. Thallium-Substitution Effects in Ferroelectric Bismuth Layer-Oxides	M. Takashige, F. Shimizu, H. Suzuki and S. Sawada	27
6. Preparation and Characterization of Certain Cu-Oxides Stabilized in Layered Structures by the Use of High Pressures and High Oxygen Pressures	M. Takano and Y. Takeda	31
7. Absence of Superconductivity in the (La _{1-x} Sr _x) ₂ NiO ₄ System	M. Takahashi, H. Iwasaki, N. Kobayashi, S. Hosoya, T. Fukuda and Y. Muto	36
8. Carrier Density Dependence of the Transport Properties of La _{2-x} Sr _{1+x} Cu ₂ O _{6+y}	T. Tamegai, C. Okada and Y. Iye	39
9. Anisotropic Properties of La _{8-x} Sr _x Cu ₈ O _{20-δ} Epitaxial Thin Films	T. Murakami, Y. Enomoto and K. Moriwaki	43
10. Ba-Y-Cu-O Films Prepared by Various RF Sputtering Techniques and Their Structure and Superconducting Properties	H. Morita, H. Fujimori, Y. Koyanagi, K. Watanabe, K. Noto and Y. Muto	48
11. Preparation of (Bi _{1-x} Pb _x) ₂ Sr ₂ Ca ₃ Cu ₄ O _y Superconducting Film by a Single Composite Target Sputtering Method	Y. Kawai, T. Terui and Y. Maruyama	51
12. Preparation of Oxide Superconductors by Oxidation of Amorphous Ln-Ce-Cu (Ln = Pr, Nd or Sm) Alloy Tapes	K. Matsuzaki, K. Shimizu, A. Inoue and T. Masumoto	56
13. Ultrahigh-Pressure Study of High T _c Oxides	H. Aoki, M. Kumazawa, K. Kurita, S. Kobayashi, S. Ikehata, A. Nakamura, S. Katsumoto, F. Komori, T. Fujii, T. Ishii, K. Kinoshita and T. Yamada	60

14.	Growth of Superconducting Oxide Single Crystals by TSFZ Method	H. Kojima and I. Tanaka	62
15.	Crystal Growth and Characterization of Oxide Superconductors and Related Compounds	H. Takei, H. Takeya, F. Sakai, M. Koike and J. Akimoto	66
16.	Single Crystal Growth of Superconducting Oxides and Related Compounds by the Flux, Floating Zone and Other Methods	T. Fukuda, T. Shishido, S. Hosoya, N. Toyota, K. Ukei, T. Kajitani, D. Shindo, H. Iwasaki, M. Takahashi, M. Kikuchi, S. Nakajima, K. Ohishi, T. Sasaki and Y. Saito	76
17.	Cross Sectional Observation of Bi-O and Cu-O Layers by STM/STS in $\text{Bi}_2\text{Sr}_2\text{CaCu}_2\text{O}_y$	K. Kitazawa, T. Hasegawa, K. Kishio, M. Nanto and H. Suzuki	83
18.	Neutron and X-Ray Diffraction Studies on Crystal Structures of Oxide Superconductors	H. Asano	87
19.	Oxygen Deficiency in 1-2-3-Type Oxide Superconductors	E. Takayama-Muromachi	92
20.	Anomalous Properties of 2-1-4 Compounds	Y. Maeno, M. Kato, T. Suzuki, M. Kurisu and T. Fujita	98
21.	Ultrasonic Properties in $\text{La}_{2-x}\text{M}_x\text{CuO}_{4-\delta}$ ($\text{M} = \text{Ba}$ and Sr) and Correlation between T_c and Hole Concentration in the Cation-Substituted $\text{Bi}_2\text{Sr}_2\text{CaCu}_2\text{O}_{8+\delta}$ System	T. Fukase, Y. Koike, T. Goto, T. Nomoto, Y. Iwabuchi and T. Hanaguri	108
22.	Comparison of High Pressure Effects on Transition Temperature in the Electron- and Hole-Doped Oxide Superconductors	S. Yomo, C. Murayama, N. Môri, H. Takagi, S. Uchida and Y. Tokura	114

I-2 Transport, Thermal and Magnetic Properties

1.	Characteristics of Electronic Properties of High- T_c Oxides	M. Sato, M. Sera, S. Shamoto, M. Onoda, S. Yamagata and H. Fujishita	119
2.	Specific Heat Study of $\text{Ba}_2\text{YCu}_3\text{O}_y$ ($6 \leq y < 7$) and Ni/Zn Substituted Samples	Y. Nakazawa, J. Takeya and M. Ishikawa	129
3.	Thermal Conductivity, Electrical Resistivity and Specific Heat of $\text{La}_{1.85}\text{Sr}_{0.15}\text{CuO}_4$ Superconductor	K. Mori, K. Noto, Y. Ogiso, T. Igarashi, Y. Ishikawa and K. Sato	134
4.	Study of High-Temperature Superconductors in La-Sr-Cu-O and Pb-doped Bi-Sr-Ca-Cu-O Systems	R. Yoshizaki	137
5.	Hole Concentration Dependences of T_c in Cuprate Oxide Superconductors	K. Takita, H. Akinaga, T. Ohshima, Y. Orimoto, Y. Takeda and M. Takano	142
6.	Resistivity, Hall Coefficient and Transition Temperatures in Ag Doped Bi-Sr-Ca-Cu-O and Sb Doped (Bi, Pb)-Sr-Ca-Cu-O Superconductors	K. Oto, K. Murase and S. Takaoka	146
7.	Magnetic Study in High- T_c Superconducting Oxides by AC-Complex Susceptibility	K. Okuda, S. Noguchi and M. Yoshikawa	150
8.	Anomalous Behaviors of Resistive Transition in High T_c -Phase Bi-Pb-Sr-Ca-Cu-O Thin Films in Magnetic Field	S. Mase, T. Fukami, Y. Horie and A. A. A. Youssef	154
9.	Superconductivity and Magnetism of $\text{RBa}_2\text{Cu}_3-x\text{M}_x\text{O}_y$ ($\text{R} = \text{La}$, Nd and Er ; $\text{M} = \text{Ni}$ and Zn)	K. Sekizawa and Y. Takano	162

10.	Dependence of Meissner Effect on the Shape of the Specimens and Magnetic Field	K. Kitazawa, T. Matsushita, O. Nakamura, Y. Tomioka, N. Motohira, T. Tamura, T. Hasegawa, K. Kishio, I. Tanaka and H. Kojima	166
11.	Experimental and Theoretical High- T_c Research at Ibaraki University	T. Ishida, S. Kanno and T. Sasaki	175
12.	Thermally Activated Behavior in Resistive Transition and Magnetic Relaxation of $YBa_2Cu_3O_z$ Films	N. Kobayashi, H. Kawabe, K. Miyoshi, K. Watanabe, H. Yamane, H. Kurosawa, T. Hirai and Y. Muto	183

I-3 Electronic Structure

1.	Neutron, Xray Scattering and Neutron Depolarization Studies on Magnetism and Superconductivity in Cuprous Oxides Materials	Y. Endoh	189
2.	Nuclear Spin-Lattice Relaxation in Highly Correlated Metallic and Superconducting Copper Oxides	H. Yasuoka, T. Shimizu, T. Imai and Y. Yosinari	195
3.	NQR and NMR Studies of Hole- and Electron-Doped $Ln_{2-x}M_xCuO_4$	K. Kumagai, Y. Nakamura, I. Watanabe, M. Abe and H. Nakajima	201
4.	Study of High- T_c Oxide Superconductor by NMR and Other Measurements (II) 1. NMR	Y. Kitaoka, K. Ishida, K. Fujiwara, G-q. Zheng, T. Kondo and K. Asayama	206
	2. Susceptibility and Resistivity	Y. Oda and M. Yamada	
5.	Proton NMR Studies of Hydrogen-Doped Superconductor $YBa_2Cu_3O_{6.94}H_x$	H. Niki, T. Higa, S. Tomiyoshi, M. Omori, T. Kajitani, T. Sato, T. Shinohara, T. Suzuki, K. Yagasaki and R. Igei	216
6.	Hydrogen Absorption in Some High- T_c Copper Oxides	H. Fujii, T. Takabatake, K. Morimoto, W. Ye, S. Orimo, T. Ekino and T. Hihara	222
7.	Study of High T_c Oxide by in-Beam Perturbed Angular Correlation	F. Komori, N. Ikeda, O. Hashimoto, T. Fukuda, S. Katsumoto, T. Nomura, S. Kobayashi, S. Ikehata and T. Yamazaki	227
8.	Magnetism Studies of Oxide-Superconductors By μ^+SR	N. Nishida	230
9.	^{119}Sn and ^{57}Fe Mössbauer Study of $La_{2-x}Sr_xCuO_4$	T. Shinjo, S. Nasu, T. Mizutani, K. Shintaku, N. Hosoi, K. Matsukuma and T. Takabatake	234
10.	New Method for Accurate Analysis of Mössbauer Spectra of $YBa_2(Cu_{1-x}Fe_x)_3O_{7-\delta}$	T. Tamaki, M. Nishizawa, A. Ito and T. Fujita	239
11.	Ion-Channeling Studies in Single-Crystal $YBa_2Cu_3O_{7-y}$ and $Bi_{2.2}Sr_{1.8}CaCu_2O_y$	K. Yamaya, T. Haga and Y. Okajima	243
12.	Electronic Structure of High- T_c Superconductor Studied by Photoemission and X-Ray Absorption	T. Takahashi, H. Matsuyama, H. Katayama-Yoshida, T. Watanabe, T. Ejima, T. Kashiwakura, S. Suzuki, S. Sato, N. Kosugi, A. Yagishita, K. Tanaka, H. Maezawa, H. Fujimoto, K. Seki, K. Kamiya, S. Shamoto, M. Sato and H. Inokuchi	249
13.	Photoemission Study of Electron- and Hole-Doped Cu-Oxide Superconductors	A. Fujimori	255

14.	Raman Studies of Spins and Carriers in Oxide Superconductors	S. Sugai	259
15.	Correlation of the Infrared Anomaly and Superconductivity in $\text{YBa}_2(\text{Cu}_{1-x}\text{Co}_x)_3\text{O}_{7-\delta}$	K. Ohbayashi, H. Tukamoto, N. Ogita, M. Udagawa, Y. Aoki and T. Fujita	265
16.	Hopping, Free Carrier and Super-Conduction in FIR Optical Conductivity of Bi-Sr-Ca-Cu-O Thin Films	K. Nagasaka, M. Sato and N. Tonosaki	270
17.	Oxygen K-edge Fine Structure of Tl-Ba-Ca-Cu-O Studied by Electron Energy Loss Spectroscopy	D. Shindo, K. Hiraga, S. Nakajima, M. Kikuchi and Y. Syono	280
18.	Low-energy Electron Energy Loss Spectroscopy on $\text{Bi}_2\text{Sr}_2\text{Ca}_{n-1}\text{Cu}_n\text{O}_{2n+4+x}$ ($n=1,2$) and Preparation of Thin Film Specimens by Molecular Beam Epitaxy	A. Ando, L. Kuang-Yu, K. Saiki and A. Koma	285

Part II. Mechanisms of Superconductivity ; Theory

1.	Self-Interaction Correction to Local Spin Density Approximation in Solids	Y. Ishii and K. Terakura	289
2.	Nature of Doped Electrons in $\text{Nd}_{2-x}\text{Ce}_x\text{CuO}_4$: Electronic Band Structures of Nd_2CuO_4 Type M_2CuO_4 ($\text{M} = \text{La}, \text{Ce}$ and Th)	K. Takegahara and T. Kasuya	293
3.	Calculation of the Electronic State of Cu and Ni Compounds by Use of Extended Clusters	J. Konamori, T. Nishino and M. Takahashi	298
4.	Theory of Soft-X-Ray Spectroscopy in High- T_c Superconductors	A. Kotani	302
5.	Self-Doping in Oxide Superconductors	J. Kondo	308
6.	Hole Distribution in Cu-Oxide Superconductors	S. Maekawa, Y. Ohta and T. Tohyama	312
7.	Theoretical Study of Tunneling Spectra in $\text{Ba}_x\text{K}_{1-x}\text{BiO}_3$	M. Shirai, N. Suzuki and K. Motizuki	318
8.	Electronic State and Superconductivity in Layered Copper Oxides	M. Tachiki and H. Matsumoto	323
9.	Electronic States of the d-p Model	T. Matsuura, H. Jichu, Y. Ôno and Y. Kuroda	333
10.	To Understand Electronic Properties of High Temperature Superconductors on the Basis of Fermi Liquid Theory. II	H. Kohno and K. Yamada	337
11.	Fermi Liquid Theory on the Basis of the Periodic Anderson Model with Spin-Orbit Coupling and Crystalline Field (Abstract only)	K. Hanzawa, K. Yosida and K. Yamada	342
12.	A. Modified Spin-Wave Theory of the Square-Lattice Antiferromagnet (Abstract only)	K. Ohara and K. Yosida	342
13.	T-Square Term of Electrical Resistivity (Abstract only)	K. Yamada, M. Nakano, K. Yosida, K. Hanzawa and A. Sakurai	343
14.	Functional Integral Approach to the Low Dimensional Antiferromagnets (Abstract only)	K. Hatada and K. Yosida	343

15.	Theory of Normal and Superconducting States of High Temperature Superconductors Y. Nagaoka, Y. Ôno, T. Matsuura, Y. Kuroda, H. Jichu, K. Takano, K. Sano, I. Doi and D. S. Hirashima	344
16.	Fluctuations in High Temperature Superconductors in Strong Magnetic Physic T. Tsuneto, R. Ikeda and T. Ohmi	352
17.	Magnetic Properties of Time-Reversal Breaking Superconductors M. Sigrist, T. M. Rice and K. Ueda	355
18.	Theoretical Study of Two-Dimensional CuO ₂ Systems M. Imada	360
19.	Hole Propagation in a 2D Quantum Spin-1/2 Antiferromagnet Y. Takahashi and H. Tsunetsugu	363
20.	The Holon-Doublon Operator Formalism S. Nakajima	368
21.	Slave-Fermion Theory of the t-t'-J Model D. Yoshioka	370
22.	On the Stability of Flux State and Chiral Spin State H. Shiba and M. Ogata	377
23.	Effective Hamiltonian for CuO ₂ Layers and Fractional Statistics H. Fukuyama	383

Part III. Organic Superconductors

1.	Organic Conductors Based on Unsymmetrical Donors DMPT and EDT-TTF I. Ikemoto, K. Kikuchi and K. Saito	389
2.	Design of Molecular Metals with Various Types of Band Structures --- One-Dimensional and Two-Demensional pn Band and pn-d Mixing Bands H. Kobayashi R. Kato and A. Kobayashi	393
3.	A Novel Type of Halogen-Bridged One-Dimensional Metal Complexes : Syntheses, Structures and Solid State Properties of -Ni(III)-X-Ni(III)-Compounds (X = Cl and Br) M. Yamashita, K. Hirao, K. Toriumi, H. Okamoto, T. Mitani and Y. Wada	399
4.	Metal-to-Semiconductor Transition of an Organic Conductor, (EDT-TTF) ₂ AuBr ₂ T. Mori and H. Inokuchi	402
5.	"2K-Superconducting State" in the Organic Superconductor β-(BEDT-TTF) ₂ I ₃ S. Kagoshima, M. Hasumi, Y. Nogami, N. Kinoshita, M. Tokumoto, T. Sasaki, N. Toyota H. Anzai and G. Saito	405
6.	Unconventional Superconductivity in the Organic Superconductor, κ -(BEDT-TTF) ₂ Cu(NCS) ₂ T. Takahashi and K. Kanoda	411
7.	Anomalous Magnetotransport Phenomena in Organic Conductors K. Kajita, Y. Nishio, T. Takahashi, W. Sasaki, R. Kato, H. Kobayashi, A. Kobayashi and Y. Iye	417
8.	(BEDT-TTF)-based Organic Superconductors Studied at IMR, in 1989 N. Toyota	421
9.	Superconducting and Normal State Properties of Organic Metals (BEDT-TTF) ₂ X M. Tokumoto, N. Kinoshita, K. Murata, H. Bando, K. Yamaji and H. Anzai	426
10.	Uniaxial Tensile Stress Effects on Organic Superconductors T. Ishiguro and Y. Nogami	436

Cu-O Network Dependent Properties of Single CuO_2 -Sheet Compounds - Charge-Transfer Gap and Charge-Doping Effect -

Y.Tokura, T.Arima and S.Koshihara

Department of Physics, University of Tokyo, Tokyo 113, Japan

T.Ido, S.Ishibashi, H.Takagi and S.Uchida

Engineering Research Institute, University of Tokyo, Tokyo 113, Japan

Single crystals of parent families of oxide superconductors with single CuO_2 -sheets have been synthesized and their optical spectra for charge-transfer and two-magnon excitations have been measured to unravel the puzzling electronic structure. The effect of electron-doping on the charge-transfer gap has been also investigated for $\text{Nd}_{2-x}\text{Ce}_x\text{CuO}_4$ compounds.

INTRODUCTION

Superconducting copper oxide compounds with high transition temperature (T_c) possess two-dimensional (2D) sheets of corner-linked CuO_4 squares ($^{\circ}\text{CuO}_2$ -sheets) as a common structural unit. There are three modifications of the CuO_2 -sheets, as shown in Fig.1, depending on the presence or absence of apical oxygen(s) positioned above and/or below the Cu atoms, i.e. the 2D sheets of (a) Cu-O squares, (b) pyramids and (c) octahedra. The first-discovered high- T_c compound [1], alkaline earth-substituted La_2CuO_4 (see Fig.2(a)), show the 2D sheets of octahedra, while in most of other copper oxide compounds with higher T_c , such as $\text{YBa}_2\text{Cu}_3\text{O}_7$ and $\text{Bi}_2\text{Sr}_2\text{CaCu}_2\text{O}_8$, show adjacent multi-layers of pyramidal CuO_2 sheets. Recent discovery of electron-doping-induced high T_c [2] shows that the CuO_2 -sheets alone without apical oxygens (i.e. 2D array of Cu-O squares) also sustain superconducting carriers, as observed in Ce-substituted Nd_2CuO_4 (see Fig.2(d)). The quantitative understanding of electronic structures of various types of CuO_2 -sheets and their change upon the carrier-doping are undoubtedly one of the central issues to unravel the mechanism of high T_c . In this report, we investigate the optical properties in single crystals of semiconducting parent compounds of High T_c superconductors with a single CuO_2 -sheet per repeated unit. The change in the optical conductivity spectra with doping is also investigated for $\text{Nd}_{2-x}\text{Ce}_x\text{CuO}_4$ with electron-type charge-carriers.

P-TYPE AND N-TYPE BEHAVIOR IN CuO_2 SHEETS

In Fig.2 we show the crystal structures of copper oxide compounds investigated here, which respectively represent typical patterns of 2D Cu-O networks. All the structures show a well-defined network of a single Cu-O sheet within a repeated unit and hence in those compounds there is no complication due to the combination of two or more types of Cu-O planes as observed, for example, in the Y-Ba-Cu-O systems accompanying the both of pyramidal sheets and chains. This feature is important to obtain clear-cut observation about the Cu-O network dependence of the electronic structures. Single crystals of all these compounds were grown from the melt by using excess CuO or $\text{CuO}/\text{Bi}_2\text{O}_3$ mixture as flux, detailed procedures of which will be described elsewhere.

Of particular interest are the compounds which can sustain the excess charge in their CuO_2 sheets; (a) $\text{La}_{2-x}\text{Sr}_x\text{CuO}_4$, (c) $(\text{La},\text{Sm})_{2-x}\text{Sr}_x\text{CuO}_4$ [3] and (d) $\text{Nd}_{2-x}\text{Ce}_x\text{CuO}_4$. These compounds also represent three typical patterns of CuO network shown in Fig.1. Empirically, it has been established that the octahedral and pyramidal CuO_2 sheets can sustain hole-type carriers (i.e. P-type) and the CuO_2 sheets alone without apical oxygens electron-type carriers (N-type). In other words, the electron type carriers cannot be doped into the

octahedral nor pyramidal sheets like Fig.1(b,c), and hole type carriers not into square-type sheets (Fig.1(a)) with no apex. According to preliminary measurements of thermopower, the above empirical rule appears to be valid also for the infinite-layer compound (Ca,Sr)CuO₂ shown in Fig.2(e): it shows the N-type behavior though the doping level attained by substitution of Ca with rare-earth elements is quite low. Such a P- or N-type behaviour depending on the pattern of Cu-O networks implies the importance of electrostatic interaction between the doped carrier and surrounding ionic lattice [4,5].

ELECTRONIC STATES IN INSULATING CuO₂ SHEETS

In Fig.3 are plotted the optical conductivity spectra [6] for six members of Cu-O layered compounds listed in Fig.1 (a)-(f). The conductivity spectra were obtained by the Kramers-Kronig transformations of reflectivity data measured on the (001) faces of those single crystals at 290K with the polarization parallel to the Cu-O basal planes. Concerning the reflectivities at photon energies above 6eV, the reflectance data [7] taken with use of the synchrotron radiation source were utilized. In all the compounds investigated here, we have observed the strong optical transitions at energy of 1.5-2.0eV, below which the compounds show no optical active bands except for the optical phonon modes. These optical excitations are strongly polarized along the basal plane of CuO₂ (or parallel to the chain direction in Ca₂CuO₃) and the spectra for the light polarization normal to the sheets show no prominent structure in the photon energy region below 3eV [6]. On these bases, we have assigned these strong absorption bands to the charge-transfer gap excitation mainly from the O-2p to Cu-3d (upper Hubbard) state. The fairly sharp profile of the absorption peaks as observed indicates the excitonic character of the transition rather than the van Hove singularity.

Looking at Fig.3, one may notice the systematic change in the peak position with the number of apical oxygens coordinated around Cu; 2.0eV in octahedral CuO₂ sheets of La₂CuO₄, 1.8eV in pyramidal CuO₂-sheets of LaGdCuO₄, and 1.5eV in CuO₂-sheets with no apical oxygen in Nd₂CuO₄ and (Ca,Sr)CuO₂. This fact indicates that the relative position of the uppermost filled band (dominantly of O-2p σ character) and lowest unoccupied band (dominantly of Cu d_{x²-y²} character) is quite sensitive to the presence or absence of apical oxygen(s). On the other hand, the oscillator strength of the CT exciton-like absorption increases in going from octahedral to square CuO₂ sheets. The peak energies and oscillator strengths of the CT excitons are summarized in Table 1 for the representative 3 members of single-CuO₂-sheet compounds, La₂CuO₄ (octahedra), LaGdCuO₄ (pyramids) and Nd₂CuO₄ (squares). The oscillator strengths were approximately estimated by fitting the optical conductivity spectra of CT excitons with Lorentzian profiles.

In the Raman spectra of these compounds [6], fairly strong bands with the symmetry of A_{1g} and B_{1g} are observed around 3000cm⁻¹ (ca.0.4eV). The corresponding Raman bands in related copper oxide compounds have been assigned to the two-magnon excitation [8]. It was argued [8] that the peak position of the two-magnon Raman band is approximately equal to 2.7J, J, being the exchange energy between the localized spins on neighboring Cu sites. The observed Raman shifts for the 2-magnon excitations and estimated J-values are also listed in Table 1. In contrast to the systematic change of CT gap energies, the 2-magnon Raman shift appears not to be sensitive to the shape of CuO network.

Based on the observed values for CT and 2-magnon excitation, important features in electronic structures of CuO₂-sheets with various shapes can be discussed. The values of the oscillator strength (f) of CT excitations are quite large (f=0.2-0.5), indicating the strong hybridization between Cu-3d and O-2p orbitals and the strong exciton effect due to the coulombic final state interaction between the excited electron and hole. According to the simplified model for a single CuO₄ cluster, the oscillator strength of the optical CT excitation is approximately proportional to the degree of hybridization (t_{pd}/Δ)². Here, t_{pd} and Δ stand for the transfer energy and energy difference between the Cu 3d and O 2p orbitals. The transfer energy t_{pd} is known to be proportional to d⁻⁴, d being the distance between the neighboring Cu and O within CuO₂-sheet. In Table 1, the change in t_{pd} is shown using the value ($t_{pd}=t_0$) of La₂CuO₄. If we take the observed CT gap

energy as an approximation of Δ , we can estimate the relative strength of CT transitions. The calculated results for $(t_{pd}/\Delta)^2$ are also shown in Table 1 in arbitrarily normalized unit. The tendency is in good agreement with the observed results: The degree of hybridization between Cu-d and O-p orbitals is increased as the oxygen coordination around Cu is decreased. This is apparently due to the change in CT gap energy, which is superior to the change in t_{pd} .

In Table 1 are also listed the calculated values of J_s , in which the simple 2-band model is used with the appropriate values of correlation energies for Cu d-electron ($U_d=8\text{eV}$) and O p-electron ($U_p=4\text{eV}$). We used again the observed CT gap as an approximation of Δ and assumed $t_0=0.96\text{eV}$. The agreement with the experimentally derived values is fairly good. Rather small variation in J_s from material to material can be interpreted as a result of cancellation of respective change in t_{pd} and Δ .

EFFECT OF CARRIER-DOPING INTO CuO_2 -SHEETS

Up to now, controllable carrier-doping in CuO_2 sheets of single crystals have been capable only in $\text{La}_{2-x}\text{Sr}_x\text{CuO}_4$ and $\text{YBa}_2\text{Cu}_3\text{O}_{6+y}$, by changing the Sr concentration x and oxygen content y , respectively. The latter compound comprises two pyramidal sheets and a CuO_y chain per repeated unit and variation of oxygen content (y) modifies the chain structure, which may cause some complication in the interpretation of optical spectra. In single crystalline films of $\text{La}_{2-x}\text{Sr}_x\text{CuO}_4$, on the other hand, measurements of optical transmittance spectra have been performed by Suzuki [9], who has found doping-induced optical absorption bands in the infrared region and their systematic change with the Sr-concentration (x). (See also the paper by Tajima et al. in the Proceedings.) Here, we present the result for change in optical conductivity spectra observed in single crystals of the electron-doped counterpart $\text{Nd}_{2-x}\text{Ce}_x\text{CuO}_4$.

The E c reflectance spectra have been measured on single crystals of $\text{Nd}_{2-x}\text{Ce}_x\text{CuO}_4$ at 290K. The Ce-composition of each CuO-flux grown single crystal has been determined by the measurement of c -axis length as well as by the ICP method. The transformed optical conductivity spectra, which were obtained by Kramers-Kronig analyses of reflectivity data, are shown in Fig.4. For undoped samples ($x=0.0$) we also show the spectrum for the intentionally reduced sample which were annealed under the Ar/O_2 gas mixture with the partial O_2 -pressure of $\text{ca.}10^{-4}$ atm at 900 C. Referring to the cases of polycrystalline samples, the estimated oxygen vacancies is about 1% of the total stoichiometric oxygen content. It shows a blurred feature and the additional broad absorption below the CT gap. This indicates that the reducing procedure in Nd_2CuO_4 introduces the excess electrons which are responsible for the infrared absorption. Upon substitution of Nd with Ce, the introduced electrons in CuO_2 sheets cause the strong infrared absorption below 1.1eV. Remarkably, the isosbetic point is observed at $\text{ca.}1.1\text{eV}$ with increase of x , indicating that the electron-doping transfers the transition intensity from the CT excitation to the infrared excitations. Effective number of electrons relevant to the transition is given by integration of optical conductivity in the photon energy range of the absorption band. Therefore, the existence of isosbetic point with doping indicates that the electronic states giving rise to the CT excitation and infrared absorption are closely correlated with each other. In other words, the electronic states responsible for the CT gap excitation are modified by doped electrons to the ones relevant to the infrared absorption. This feature is contradictory to the simple picture that the doped carriers are accommodated in the upper-lying rigid band and causes the plasmon-like optical response. According to a preliminary estimation, the rate of intensity transfer from CT excitation to infrared band with increasing x (< 0.15) is approximately twice larger in $\text{Nd}_{2-x}\text{Ce}_x\text{CuO}_4$ than that for hole-doping case in $\text{La}_{2-x}\text{Sr}_x\text{CuO}_4$. This may be reflecting the stronger p-d hybridization in Nd_2CuO_4 .

REFERENCES

1. J.G.Bednorz and K.A.Muller, *Z. Phys. B* **64**, 189 (1986).
2. Y.Tokura, H.Takagi and S.Uchida, *Nature* **337**, 345 (1989).
3. Y.Tokura et al., *Phys.Rev. B* **40** 2568 (1989).
4. J.Kondo, *J.Phys.Soc.Jpn.* **58**, 2884 (1989).
5. J.B.Torrance and R.Metzger, *Phys.Rev.Lett.* **63**, 1515 (1989).
6. Y.Tokura et al., preprint (submitted for publication).
7. S.Tajima et al., *J.Opt.Soc. Am. B6*, 475 (1989).
8. K.B.Lyons, P.A.Fleury, J.P.Remeika and T.J.Negran, *Phys.Rev. B* **37**, 2353 (1988).
9. M.Suzuki, *Phys.Rev. B* **39**, 2312 (1989).

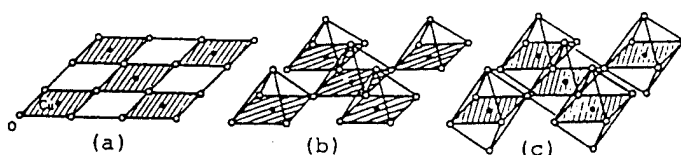


Fig.1. Three types of 2-dimensional Cu-O networks; (a) squares, (b) pyramids and (c) octahedra.

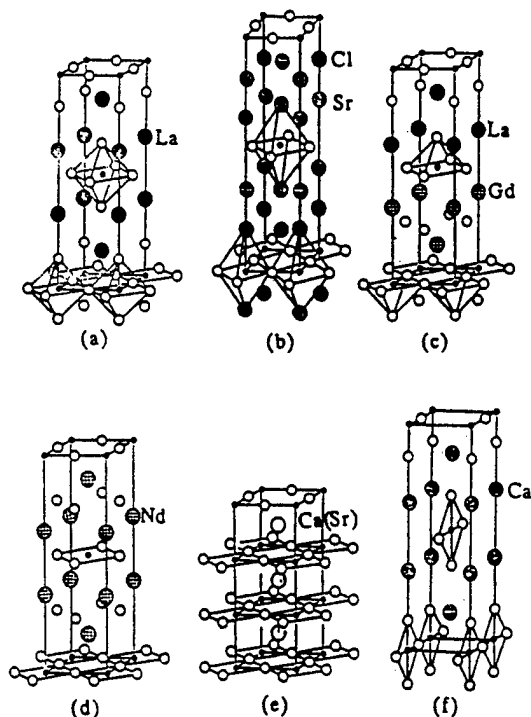


Fig.2. Crystal structures of Cu-O layered compounds; (a) La_2CuO_4 , (b) $\text{Sr}_2\text{CuO}_2\text{Cl}_2$, (c) $(\text{La,Gd})_2\text{CuO}_4$, (d) Nd_2CuO_4 , (e) $(\text{Ca,Sr})\text{CuO}_2$, and (f) Ca_2CuO_3 .

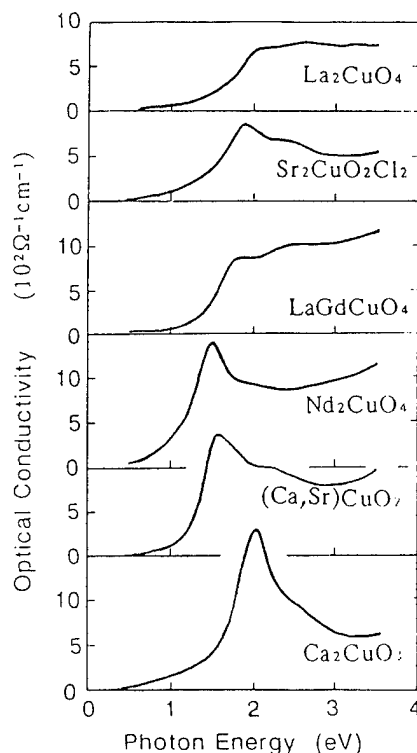


Fig.3. Optical conductivity spectra of single crystals of Cu-O layered compounds listed in Fig.2. In all the spectra the light E-vector is parallel to the basal plane.

Table 1 Physical parameters in CuO_2 -sheets.

compounds	La_2CuO_4	$(\text{La}, \text{Gd})_2\text{CuO}_4$	Nd_2CuO_4
Cu-O network (oxygen coordination)	octahedron (8)	pyramid (5)	square (4)
$d_{\text{Cu-O}}$ (CuO_2 -sheet)	1.905 Å	1.936 Å	1.973 Å
t_{pd}	t_0	$0.937t_0$	$0.869t_0$
Δ_{CT} (optical gap)	2.0 eV	1.8 eV	1.5 eV
f_{CT}	0.2 ₈	0.3 ₃	0.4 ₃
$(t_{\text{pd}}/\Delta)^2$ (arbitrarily normalized)	0.28	0.31	0.38
Raman shift ω_s (2-magnon band)	3200 cm^{-1}	2800 cm^{-1}	2900 cm^{-1}
J_s exp.*	0.14 eV	0.12 eV	0.13 eV
cal.*	0.142 eV	0.128 eV	0.133 eV

* assumed $U_d=8.0$ eV, $U_p=4.0$ eV, and $t_0=0.96$ eV.

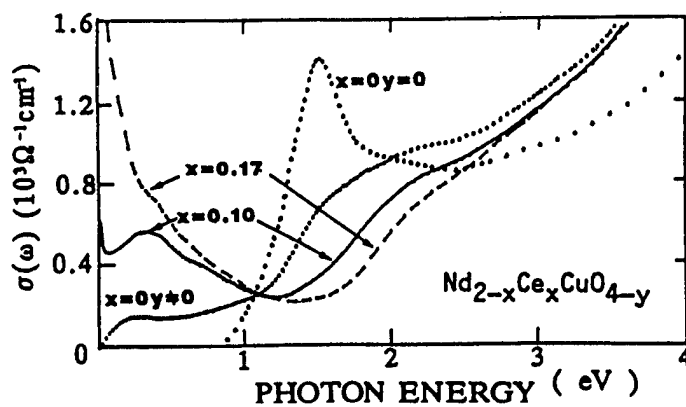


Fig.4. Optical conductivity spectra in single crystals of $\text{Nd}_{2-x}\text{Ce}_x\text{CuO}_{4-y}$.

New high- T_C copper oxide superconductors :
(Nd,Ce,Sr)₂CuO_{4-x} and (Ln,Ce,Ba)₄Cu₃O_{9-x} (Ln: Nd, Sm, Eu and Gd)

Jun Akimitsu and Hiroshi Sawa

Department of Physics, Aoyama-Gakuin University
6-16-1, Chitosedai, Setagaya-ku, Tokyo 157.

Two new high- T_C superconducting systems have been found by the resistivity and magnetization measurements. The crystal structures are proposed on the basis of Rietveld analysis of powder X-ray and TOF neutron diffraction data.

First is the Nd-Sr-Ce-Cu-O system with the highest onset transition temperature of about 28K. The structure comprises of alternating slabs of the K_2NiF_4 and Nd_2CuO_4 structures, and that all copper atoms are crystallographically equivalent with oxygen in fivefold (square-pyramidal) coordination.

Second is a family of superconducting system Ln-Ce-Ba-Cu-O (Ln : Nd, Sm, Eu and Gd) with the highest transition temperature of about 48K. The structure consists of alternating slabs of the $YBa_2Cu_3O_{7-y}$ and Nd_2CuO_4 structures, and that the copper-oxide framework is similar to $YBa_2Cu_3O_{7-y}$.

1. Introduction

Despite tremendous efforts for understandings of high- T_C superconductivity, the mechanism lying behind remains unsolved. The progress in this field has always been coupled with the discovery of new materials. It is, therefore, important to find the new materials even if the transition temperature is low.

In this paper, we add two new materials to the high- T_C superconducting oxides that have widely aroused interest.

One of them is the Nd-Ce-Sr-Cu-O system with an onset transition temperature of 28K[1]. The structure comprises of alternating slabs K_2NiF_4 - and Nd_2CuO_4 -type structures, and that there is only one Cu site in pyramidal coordination of oxygen[2]. This compound is the first case of the copper-based superconductor in which Cu ions take an only pyramidal five fold coordination.

Another is a family of superconducting system Ln-Ce-Ba-Cu-O (Ln : Nd, Sm, Eu and Gd) with a highest transition temperature of about 48K[3]. The structure consists of alternating blocks of the $YBa_2Cu_3O_{7-y}$ and Nd_2CuO_4 structures, and that the copper-oxide framework is similar to that of $YBa_2Cu_3O_{7-y}$.

2. Nd-Ce-Sr-Cu-O system

A sample with the composition of $(Nd_{1-x-y}Sr_xCe_y)_2CuO_{4-x}$ was prepared, of which details were already published elsewhere[1].

The standard four probe technique was used for resistivity measurements. Figure 1 shows the resistivity measurement for the specimens with the nominal composition of $Nd_2Sr_{0.5}Ce_{0.5}Cu_{1.2}O_x$. The onset and endpoint transition temperatures are 28K and 18K, respectively. The semiconducting behavior observed at low temperature is due to oxygen deficiency included in the sample. The maximum transition temperature is about 28K, although we observed different transition temperatures for different compositions.

Magnetization measurements were also performed with the SQUID magnetometer. Figure 2 shows a typical example of the diamagnetic susceptibility taken at 5Oe. Assuming that the density of the material is about 7.3, the superconducting volume fraction is about 24% at 4.2K. This indicates that the superconductivity is bulk in nature.

Powder X-ray diffraction was performed on a conventional X-ray spectrometer with the graphite monochromator. Figure 3 shows the typical X-ray diffraction pattern of $Nd_2Sr_{0.5}Ce_{0.5}Cu_{1.2}O_x$ taken at room temperature. The predominant lines can be ascribed to the tetragonal structure with $a = 3.855\text{\AA}$ and $c = 12.49\text{\AA}$. As far as the arrangement of the metal ions is concerned, the crystal structure is the same as that of La_2CuO_4 and/or Nd_2CuO_4 . Therefore, the present X-ray data suggest that the compound has the chemical formula of $(Nd_{1-x-y}Sr_xCe_y)_2CuO_{4-x}$. The oxygen positions, however, remain undetermined by the X-ray diffraction. The evidence that the $(Nd_{1-x-y}Sr_xCe_y)_2CuO_{4-x}$ is responsible for the superconductivity is the strong relationship between the superconductivity and the presence of this phase.

Takayama-Muromachi et al.[4] identified the superconducting phase by the combined use of X-ray diffraction and electron microscopy. Metal positions in this phase were confirmed to be identical with those in the K_2NiF_4 or Nd_2CuO_4 structure except the cationic order of Nd(Ce) and Sr. In addition, the possible space group was suggested to be $P4/nmm$, because $hk0$ reflections with $h+k=2n+1$ were absent in electron diffraction patterns. Subsequently, a convergent-beam electron diffraction study revealed that $(Nd_{1-x-y}Sr_xCe_y)_2CuO_{4-x}$ belongs to $P4/nmm$ [5].

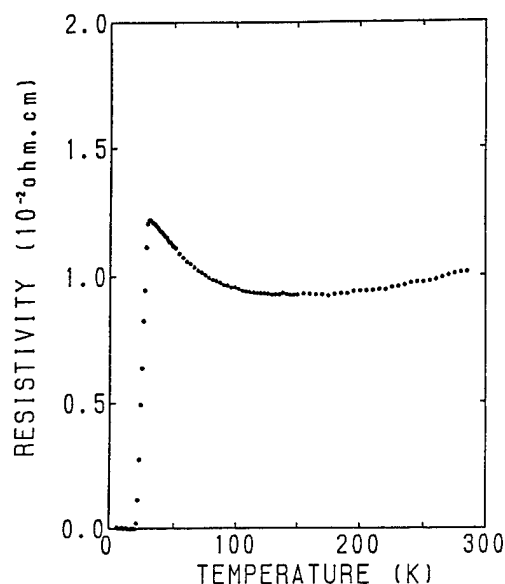


Figure 1. Temperature dependence of the resistivity nominally described as $Nd_2Sr_{0.5}Ce_{0.5}Cu_{1.2}O_z$.

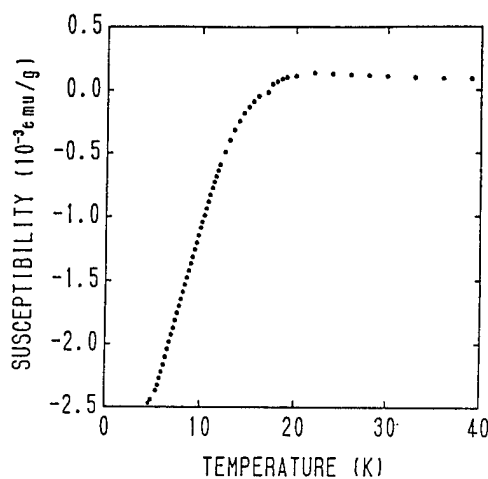


Figure 2. Meissner diamagnetism observed for the specimen with nominal composition of $Nd_2Sr_{0.5}Ce_{0.5}Cu_{1.2}O_z$.

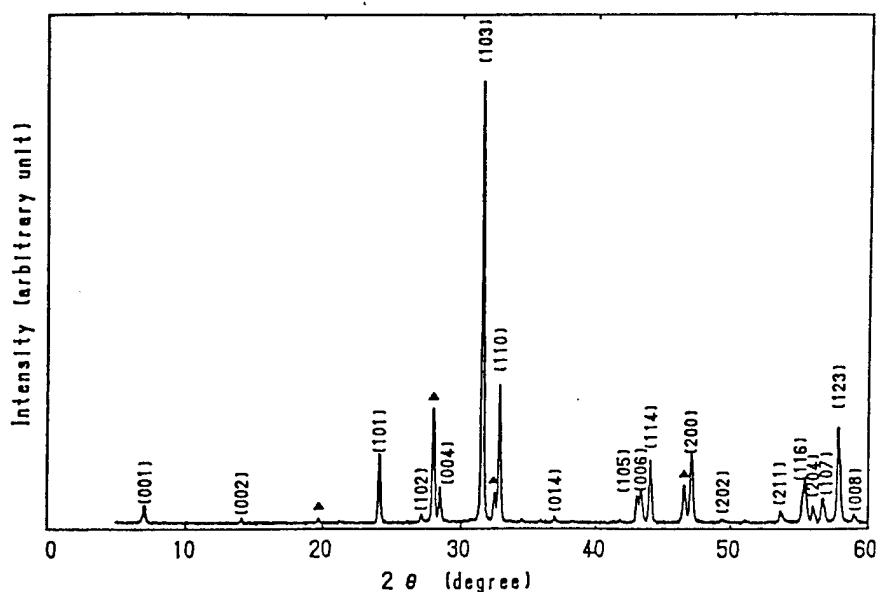


Figure 3. X-ray powder diffraction pattern of $Nd_2Sr_{0.5}Ce_{0.5}Cu_{1.2}O_z$. Δ indicate the peaks from $Nd_{1-x}Ce_xO_z$.

Based on these experimental results, Takayama-Muromachi et al. proposed the new model comprising of alternating slabs K_2NiF_4 - and Nd_2CuO_4 -type structures. We have finally determined the crystal structure of $(Nd_{1-x-y}Sr_xCe_y)_2CuO_{4-z}$ by using the TOF neutron powder diffraction technique.

A sample with the composition $(Nd_{0.66}Sr_{0.205}Ce_{0.135})_2CuO_{4-z}$ was given to be single phase. As has been pointed out by Takayama-Muromachi et al.[4] and Tokura et al.[6], both the superconducting volume fraction and T_C increased after long-term annealing under the oxygen atmosphere.

The sample used in the structure analysis experiment showed an onset of superconductivity at 22K in magnetization measurement. The Meissner signal reached about 12% at 8K.

XPS spectra were measured to determine the valence of Ce on a spectrometer equipped with a Mg X-ray source ($h\nu = 1253.5\text{eV}$) and a cylindrical-mirror analyzer[7]. As a result, we can safely conclude that Ce atoms in the superconducting sample are in a tetravalent state as in CeO_2 . It is interesting to note that, in the CaF_2 -type structures of CeO_2 and $Ce_{1-x}Nd_xO_{2-x/2}$, Ce^{4+} ions are surrounded by eight oxide ions disposed at the corner of a cube. Therefore, Ce^{4+} ions are preferentially situated at site of Nd_2CuO_4 -type slab in eight-fold coordination. The oxidation state of +4 is very common among Ce compounds, and the effective ionic radius, r , of $IXSr^{2+}$ (1.31\AA [8]) is about 30% larger than that of $IXCe^{4+}$ (ca. 1.0\AA), where roman numbers attached to cation names denote their coordination numbers. Therefore, the possibility can be ruled out that Ce ions share site in K_2NiF_4 -type slabs in nine-coordination with Sr^{2+} ions. Throughout this paper, a metal position other than Cu in the K_2NiF_4 -type unit is referred to as M, and that in the Nd_2CuO_4 -type unit as M'. The coordination number is 9 for site M and 8 for site M', which suggests that larger cations prefer site M to site M'.

Neutron diffraction data were taken on a high-resolution TOF neutron powder diffractometer, HRP, at the KENS pulsed spallation neutron source at the National Laboratory for High Energy Physics. Structure parameters were refined with a RIETAN program[9] for the Rietveld analysis of TOF neutron powder diffraction data. To determine the oxygen positions more precisely, atomic displacements in the [MO] sheets were taken into account. In the "ideal" model, O(2) atoms were located at a 2c position ($1/4, 1/4, z$; point symmetry : 4mm) of space group $P4/nmm$. In a new model, each O(2) atom was "split" into four atoms at an 8j site (x, x, z ; point symmetry : m) slightly off a fourfold rotation axis and two mirror planes parallel to ac and bc planes, which lowers the local symmetry.

Final structure parameters and their standard deviations are listed in Table I, and selected metal-oxygen distances are in Table II. Lattice parameters were refined to be $a = 3.8564(3)\text{\AA}$ and $c = 12.4846(9)\text{\AA}$. R factors were $R_{wp} = 5.64\%$, $R_p = 4.27\%$, $R_1 = 3.32\%$, $R_F = 2.57\%$ and $R_e = 4.76\%$. Figure 4 illustrates final profile fit and difference patterns. The good fit between the observed and calculated patterns strongly supports the present structural model.

The coordination numbers of M, M' and Cu are, respectively, 9, 8, and 5, which are reasonable from a crystallo-chemical point of view. The $[CuO_5]$ pyramid contains four short Cu-O(1) bonds (1.9355\AA) and one long Cu-O(2) bond (2.221\AA), as in $YBa_2Cu_3O_7$. The Cu-O(2) bond is evidently shorter than corresponding bonds in other superconductors with $[CuO_5]$ pyramids, e.g., $YBa_2Cu_3O_7$ and $Tl_2Ba_2CaCu_2O_8$. The bases of $[CuO_5]$ pyramids form a two-dimensional $[CuO_2]$ plane perpendicular to the [001] direction. The M-O(2) bond parallel to the [001] direction is as short as 2.268\AA , which is comparable to the Cu-O(2) distance.

Figure 5 shows the crystal structure of $(Nd_{1-x-y}Sr_xCe_y)_2CuO_{4-z}$. The unit cell consists of two parts: the upper part in Figure 5 is of the K_2NiF_4 -type where the M (Nd,Sr) ion is coordinated to 9 oxide ions, while the lower part is of the Nd_2CuO_4 type including M'(Nd,Ce) ion in 8-coordination. There is only one crystallographic site with pyramidal coordination for the Cu ion. From a structural point of view, high- T_C superconductors are classified into two groups: one contains copper in distorted octahedral coordination, e.g., $(La_{1-x}M_x)_2CuO_4$ (M:Ca, Sr and Ba) and $(Bi,Tl)_2(Sr,Ba)_2CuO_6$, and the other contains copper in pyramidal coordination, e.g., $LnBa_2Cu_3O_7$ (Ln:Y and various lanthanoid elements), $(Bi,Tl)_m(Sr,Ba)_2Ca_nCu_{n+1}O_{m+2(n+2)}$ and $Pb_2Sr_2ACu_3O_{8+z}$ ($A = Ln, Ln + (Sr \text{ or } Ca)$). $(Nd_{1-x-y}Sr_xCe_y)_2CuO_{4-z}$ has the simplest structure of superconductors that are composed of $[CuO_5]$ pyramids ever found. This material must be one of the best candidates for studying the origin of high- T_C superconductivity.

3. Ln-Ce-Ba-Cu-O system (Ln:Nd, Sm, Eu and Gd)

The samples were prepared by the solid state reaction of rare-earth metal oxides (Nd_2O_3 , Sm_2O_3 , Eu_2O_3 , Gd_2O_3 and CeO_2), $BaCO_3$ and CuO . The details are published elsewhere[3]. Single-phase samples were obtained at a nominal composition of Ln:Ba:Ce:Cu=6:4:2:9 for Ln=Eu atom. However, the solubility ratio is different for each rare earth oxides, nominal compositions are slightly different for the other rare earth compounds.

Figure 6 shows the temperature dependences of resistivities for $Ln_6Ba_4Ce_2Cu_9O_y$ with Ln:Nd, Sm, Eu. Although the samples are single-phased in the powder X-ray diffraction patterns, the semiconducting behaviors are observed at low

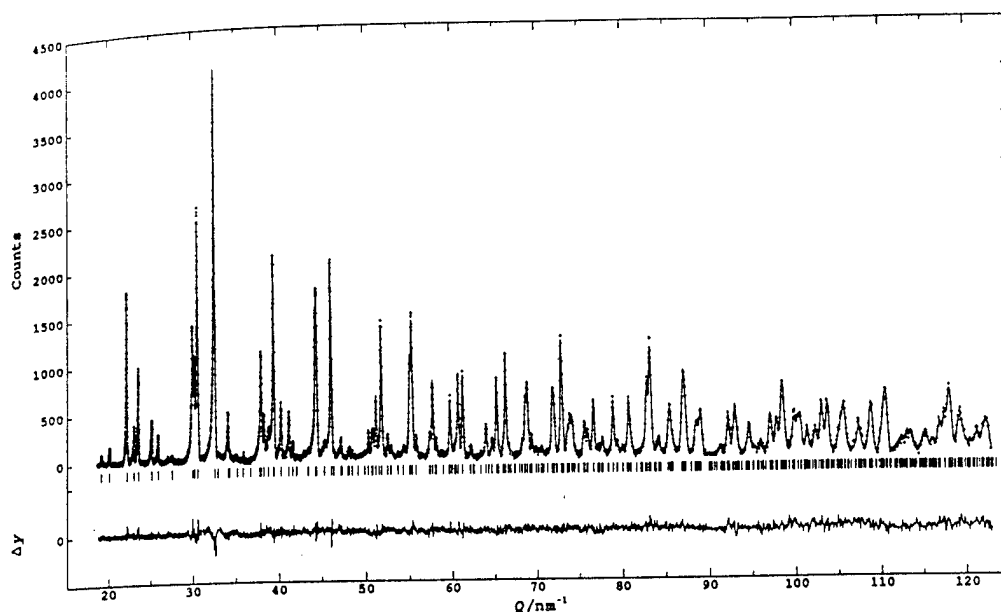


Figure 4. Rietveld refinement profiles for $\text{Nd}_{0.66}\text{Sr}_{0.205}\text{Ce}_{0.135})_2\text{CuO}_{4-x}$. Background was fit as part of the refinement but has been subtracted before plotting to show net intensities. Plus marks (+) are the raw neutron diffraction data, and the overlapped continuous line is the calculated profile. Tick marks below the profile indicate the positions of the 501 allowed reflections. The curve in the bottom is the difference between the observed and calculated intensities in the same scale.

Table I.
Structure parameters in $(\text{Nd}_{0.66}\text{Sr}_{0.205}\text{Ce}_{0.135})_2\text{CuO}_{4-x}$ ($Z=2$). Estimated standard deviations in parentheses refer to the last digit printed. B is isotropic thermal parameter. The occupation factors, g , of Nd, Ce and Sr are fixed at 0.59, 0 and 0.41 for site M, and at 0.73, 0.27 and 0 for site M'.

Atom	Site	x	y	z	g	$B/\text{\AA}^2$
M	2c	1/4	1/4	0.3893(3)	1	0.787
M'	2c	1/4	1/4	0.1035(3)	1	0.393
Cu	2c	1/4	1/4	-0.2510(3)	1	0.496
O(1)	4f	3/4	1/4	0.2378(3)	1	1.000
O(2)	8j	0.2958(58)	$=x$	-0.4291(6)	0.2304(40)	1.607
O(3)	2a	3/4	1/4	0	1	0.737

Table II.
Interatomic distances, ℓ , in $(\text{Nd}_{0.66}\text{Sr}_{0.205}\text{Ce}_{0.135})_2\text{CuO}_{4-x}$. N is the number of equivalent bonds.

Bond	ℓ \AA	N
M-O(1)	2.701(3)	4
M-O(2 ⁱ)	2.281(9)	4/4
M-O(2 ⁱⁱ)	2.53(3)	4/4
M-O(2 ⁱⁱⁱ)	2.783(3)	8/4
M-O(2 ^{iv})	3.02(3)	4/4
M'-O(1)	2.555(3)	4
M'-O(3)	2.321(2)	4
Cu-O(1 ⁱⁱⁱ)	1.9352(4)	4
Cu-O(2)	2.238(9)	4/4

- i) $x, y, z + 1$
- ii) $x - 1/2, y - 1/2, -z$
- iii) $x - 1/2, -y, -z$
- iv) $-x, -y, -z$

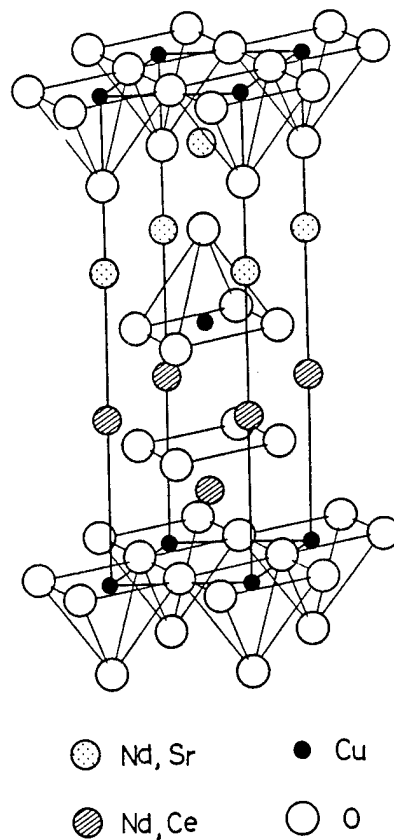


Figure 5. Crystal structure of $(\text{Nd}_{1-x-y}\text{Sr}_x\text{Ce}_y)_2\text{CuO}_{4-x}$.

temperature. This seems to be due to the oxygen vacancies, since such a tendency tends to disappear after the long-term annealing under the high-pressure oxygen as seen in the case of Eu-compound. The maximum onset superconducting transition temperature at present is about 48K. The superconducting characteristics of this materials strongly depend on the annealing conditions. Figure 7 shows the temperature dependences of the A.C. magnetic susceptibilities in $\text{Nd}_6\text{Ba}_4\text{Ce}_2\text{Cu}_9\text{O}_y$. The curve(2) for the sample annealed under O_2 atmosphere improved superconducting behavior with regard to both the Meissner volume fraction and transition temperature compared to the curve(1) for a non-annealed sintered sample.

Recently, Tamegai et al.[10] measured the Hall effect on the Eu and Nd compounds(Figure 8). Hall coefficients for these compounds are positive, indicating that carriers are holes. As shown in Figure 8, Hall coefficients are slightly temperature dependent, with a broad maximum at around 120K. Average hole number per copper ion in the Cu-O planes at just above T_C is estimated to be 0.09. This value is much smaller the value 0.23 in $\text{YBa}_2\text{Cu}_3\text{O}_{7-y}$. The difference in the carriers concentrations may be the reason why T_C in this system is as low as about 40K.

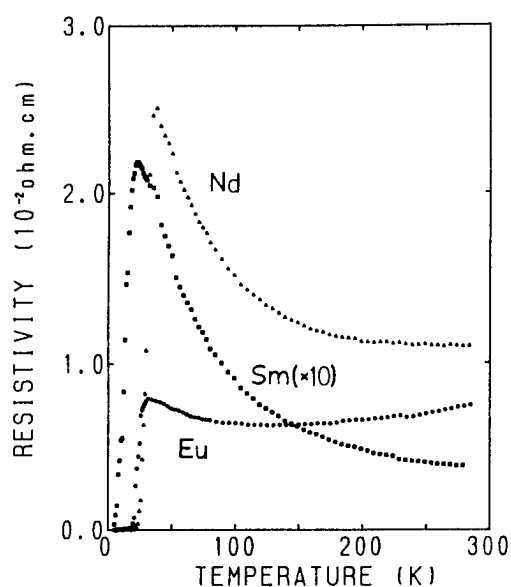


Figure 6. Temperature dependences of the resistivities in $\text{Ln}_6\text{Ba}_4\text{Ce}_2\text{Cu}_9\text{O}_y$ (Ln: Nd, Sm, Eu).

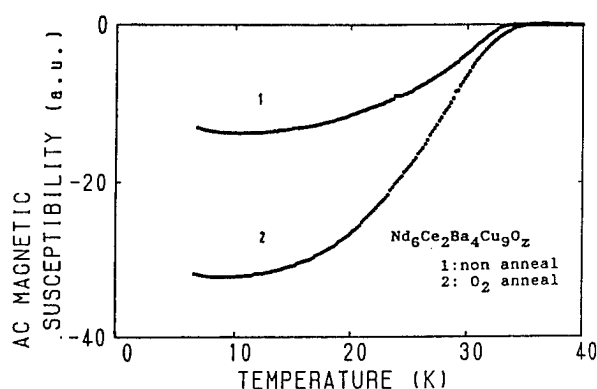
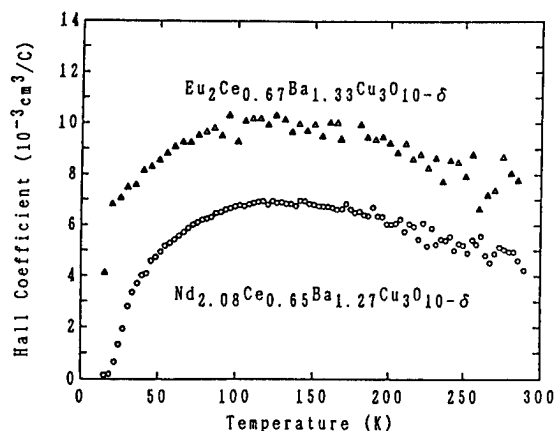


Figure 7. Temperature dependences of the A.C. magnetic susceptibilities in $\text{Nd}_6\text{Ba}_4\text{Ce}_2\text{Cu}_9\text{O}_y$. Curves (1) and (2) correspond to the non-annealed and the annealed samples, respectively.



T. Tamegai et al.

Figure 8. Temperature dependences of Hall coefficients for $\text{Eu}_6\text{Ba}_4\text{Ce}_2\text{Cu}_9\text{O}_y$ and $\text{Nd}_6\text{Ba}_4\text{Ce}_2\text{Cu}_9\text{O}_y$.

To determine the crystal structure of this system, we performed the Rietveld analysis of X-ray powder diffraction as well as high-resolution electron imaging technique.

Electron diffraction patterns and electron micrographs were taken by Matsui and Horiuchi. Electron diffraction patterns of the $\text{Eu}_6\text{Ba}_4\text{Ce}_2\text{Cu}_9\text{O}_y$ indicate that the unit cell is body-centered tetragonal ($a \sim 3.8\text{\AA}$ and $c \sim 28\text{\AA}$); hkl reflections with odd values of $h+k+l$ are systematically absent. Tsuda et al.[11] determined the space group to be $I4/mmm$ (No. 139) by using the convergent-beam electron diffraction.

The high-resolution image given in Figure 9 was taken with the incident beam parallel to $[100]$. Two types of arrangements were observed in the image. One is the large two dark dots marked with R. This may be R_2O_2 layers (Nd_2CuO_4 -type slabs). Between two R_2O_2 layers, zig-zag arrangement of three perovskite layers was observed. They are considered to be perovskite layers consisting of almost the same heavy ions (marked as R') and Cu ions. Local structure must be similar to that of the tetragonal $\text{YBa}_2\text{Cu}_3\text{O}_{7-y}$. The layer sequence in the structure of our new compounds is shown in Figure 10.

Based on the above lattice image and referring to cationic order in $\text{Nd}_{1.2}\text{Ba}_{1.8}\text{Cu}_3\text{O}_{7-y}$ [12] and $(\text{Nd,Ce,Sr})_2\text{CuO}_4$, the structural model was constructed. The R site (8-coordinated site in Nd_2CuO_4 -type) is occupied by Eu^{3+} and Ce^{4+} ions, because both ions have nearly the same radius (ionic radii in the 8-coordinated site are $^{\text{VIII}}\text{Eu}^{3+}$: 1.066\AA and $^{\text{VIII}}\text{Ce}^{4+}$: 0.97\AA). On the other hand, Ba^{2+} ionic radii are too large in the coordination ($^{\text{VIII}}\text{Ba}^{2+}$: 1.42\AA). The coordination number in the R' site is difficult to fix because of the oxygen vacancy. Analogous to $\text{YBa}_2\text{Cu}_3\text{O}_{7-y}$, this site is supposed to be 10-coordinated. We assume that the relatively large Ba^{2+} and Eu^{2+} ions prefer the R' site ($^{\text{X}}\text{Ba}^{2+}$: 1.52\AA and $^{\text{X}}\text{Eu}^{2+}$: 1.35\AA). Therefore, we assume the structural model to be $(\text{Eu}_{1-x}\text{Ce}_x)_2(\text{Ba}_{1-y}\text{Eu}_y)_2\text{Cu}_3\text{O}_{10-z}$ in a chemical formula for the Rietveld analysis.

Powder X-ray diffraction was performed on a Rigaku diffractometer RAD-rC with a rotating anode source and a graphite monochromator. The diffraction pattern indicates that the sample is single phased. The crystal structure was refined by Rietveld analysis with the RIETAN program.

Final structure parameters are listed in Table I. The refined lattice parameters are $a = 3.8504(6)\text{\AA}$ and $c = 28.4598(5)\text{\AA}$. The R factors are $R_{\text{wp}} = 6.6\%$, $R_p = 5.2\%$, $R_1 = 2.9\%$, $R_F = 2.8\%$ and $R_e = 4.2\%$. Figure 11 shows the final profile fit and difference patterns. Good agreement between the observed and calculated patterns strongly supports the proposed structural model. To obtain the reliable structure parameters for oxygens, a TOF neutron powder diffraction data has been made.

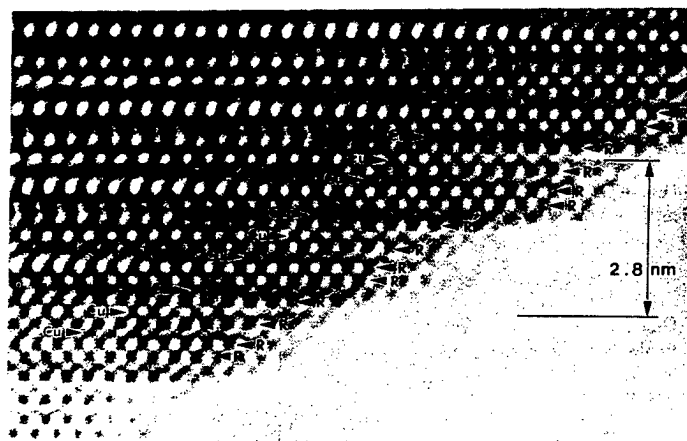


Figure 9. A high resolution electron microscope image of $\text{Eu}_6\text{Ba}_4\text{Ce}_2\text{Cu}_9\text{O}_y$ taken with an incident electron beam along the a axis. Dots indicated by R and R' correspond to the (Eu,Ce) and (Ba,Eu) sites, respectively.

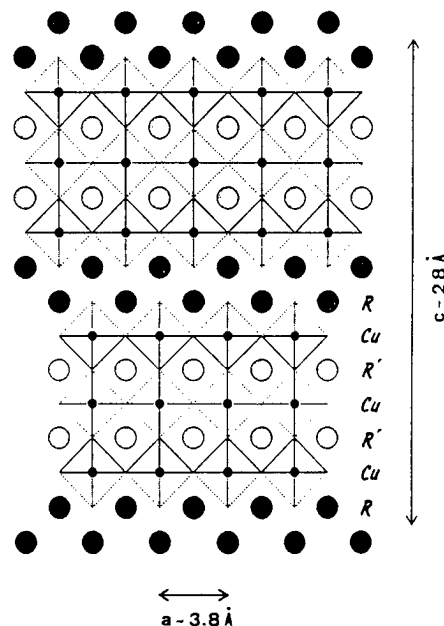


Figure 10. Schematic structural model of $\text{R}_2\text{R}'_2\text{Cu}_3\text{O}_x$. Circles indicated by R and R' correspond to the same construction in Figure 9.

Structural parameters of Oxygen atoms in $(\text{Eu,Ce,Ba})_4\text{Cu}_3\text{O}_{9-z}$ could not be determined, by the neutron diffraction, because the neutron diffraction is not applicable to the Eu-containing compound owing to a very large absorption cross section of Eu. Therefore, has $(\text{Nd,Ce,Ba})_4\text{Cu}_3\text{O}_{9-z}$ [13] isomorphous with $(\text{Eu,Ce,Ba})_4\text{Cu}_3\text{O}_{9-z}$ compound was used for the TOF neutron Rietveld analysis. The results confirm the basic structural features of $(\text{Ln,Ce,Ba})_4\text{Cu}_3\text{O}_{9-z}$ determined by X-ray Rietveld analysis.

The crystal structure of the Eu-Ce-Ba-Cu-O system is shown in Figure 12. The unit consists of two parts: the upper and lower slabs correspond to the Nd_2CuO_4 -type structure and the center part exhibits Cu-O pyramids and a deficient perovskite structure. In the Cu-O frame, the structure is very similar to tetragonal $\text{YBa}_2\text{Cu}_3\text{O}_{7-y}$.

We wish to thank Prof. K. Kitazawa and Dr. K. Kishio (The University of Tokyo) for the SQUID measurements. We also wish to thank Dr. Y. Matsui, Dr. S. Horiuchi and Dr. F. Izumi (National Institute for Research in Inorganic Materials) for their invaluable help and useful discussions. We also wish to thank Dr. H. Fujiki (Aoyama-Gakuin University) for useful discussions.

This work is supported by a Grant-in-Aid for Scientific Research on Priority Areas "Mechanism of Superconductivity"

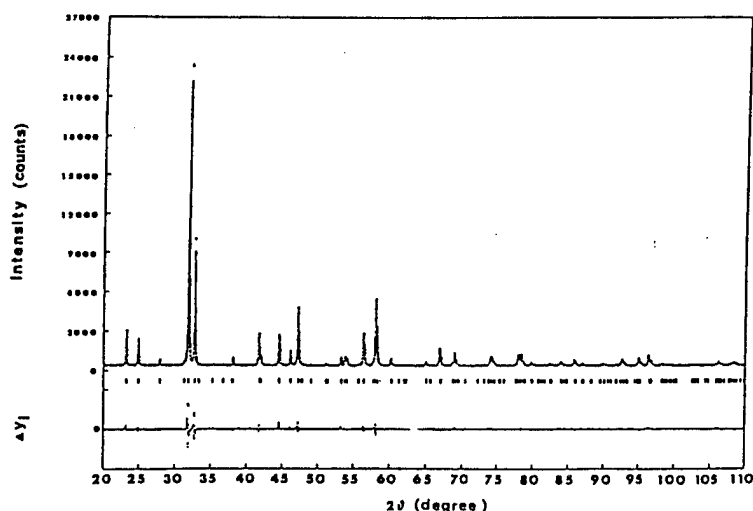


Figure 11. Rietveld refinement of an X-ray diffraction pattern of $(\text{Eu}_{0.67}\text{Ce}_{0.33})_2(\text{Ba}_{0.67}\text{Eu}_{0.33})_2\text{Cu}_3\text{O}_{9-z}$.

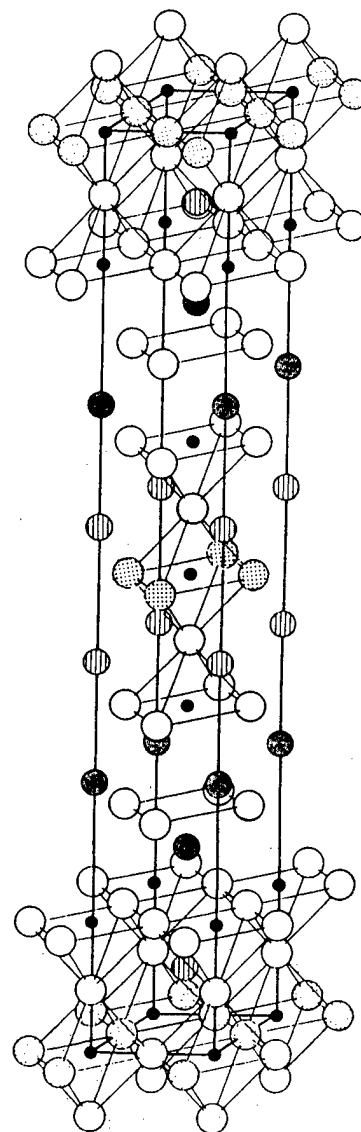
Figure 12 Crystal structure of the $(\text{Eu}_{0.67}\text{Ce}_{0.33})_2(\text{Ba}_{0.67}\text{Eu}_{0.33})_2\text{Cu}_3\text{O}_{9-z}$. 4c site is oxygen-deficient (see Table III).

Table III.

Structure parameters in $(\text{Eu}_{0.67}\text{Ce}_{0.33})_2(\text{Ba}_{0.67}\text{Eu}_{0.33})_2\text{Cu}_3\text{O}_{10-z}$ ($Z=2$). Estimated standard deviations in parentheses refer to the last digit printed. B is the isotropic thermal parameter. The occupation factors, g, of Eu and Ba are fixed at 0.67, 0.33 and 0 for site R, and at 0.33, 0.67 and 0.67 for site R'.

Atom	Site	x	y	z	g	$B/\text{\AA}^2$
R	4e	0	0	0.2942(2)	1	0.6(2)
R'	4e	0	0	0.4245(2)	1	1.1(2)
Cu(1)	2a	0	0	0	0.85(5)	2.2(12)
Cu(2)	4e	0	0	0.1423(8)	1	1.1(3)
O(1)	4c	0	1/2	0	0.27(15)	2.7(8)
O(2)	4e	0	0	0.0664(27)	1	2.7(8)
O(3)	8g	0	1/2	0.3535(19)	1	2.7(8)
O(4)	4d	0	1/2	1/4	1	2.7(8)

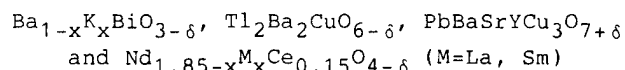
- Eu, Ce
- ◐ Ba, Eu
- Cu
- O
- ◑ O (4c)



References

1. J. Akimitsu, S. Suzuki, M. Watanabe and H. Sawa: Jpn. J. Appl. Phys. 27(1988)L1859.
2. H. Sawa, S. Suzuki, M. Watanabe, J. Akimitsu, H. Matsubara, H. Watabe, S. Uchida, K. Kokusho, H. Asano, F. Izumi and E. Takayama-Muromachi: Nature 337(1989)347.
3. H. Sawa, K. Obara, J. Akimitsu, Y. Matsui and S. Horiuchi: J. Phys. Soc. Jpn. 58(1989).
4. E. Takayama-Muromachi, Y. Matsui, Y. Uchida, F. Izumi, M. Onoda and K. Kato: Jpn. J. Appl. Phys. 27(1988)L2283.
5. K. Tsuda, M. Tanaka, J. Sakanoue, H. Sawa, S. Suzuki and J. Akimitsu: Jpn. J. Appl. Phys. 28(1989)L389.
6. Y. Tokura, H. Matsubara, H. Watabe, M. Sakai, H. Ikeda, S. Okuda, S. Tanaka, H. Takagi and S. Uchida: (preprint).
7. F. Izumi, E. Takayama-Muromachi, A. Fujimori, T. Kamiyama, H. Asano, J. Akimitsu and H. Sawa: Physica C 158(1989)440.
8. R. D. Shannon: Acta Crystallogr. A32(1976)751.
9. F. Izumi: J. Crystallogr. Soc. Jpn. 27(1985)23.
10. T. Tamegai, Y. Iye, M. Ogata, K. Obara and J. Akimitsu: Jpn. J. Appl. Phys. 28(1989)L1537.
11. K. Tsuda, M. Tanaka and J. Akimitsu: Jpn. J. Appl. Phys. 28(1989)L1552.
12. F. Izumi, S. Takekawa, Y. Matsui, N. Iyi, H. Asano, T. Ishigaki and N. Watanabe: Jpn. J. Appl. Phys. 26(1987)L1616.
13. F. Izumi, H. Kito, H. Sawa, J. Akimitsu and H. Asano: Physica C 160(1989)235.

Oxygen Contents and Superconductivity in Several High-Tc Oxides:



Y.Syono, M.Kikuchi, K.Ueki, A.Tokiwa, K.Oh-ishi, S.Nakajima*,
T.Suzuki**, M.Nagoshi**, N.Kobayashi and Y.Muto.

Institute for Materials Research, Tohoku University,
Katahira, Aoba-ku, Sendai 980

*Hachioji Research Center, CASIO Computer Co., Ltd. Hachioji 192,

**Steel Research Center, NKK Corporation, Kawasaki 210

Oxygen contents of several high Tc oxides were determined by thermo-gravimetry (TG) and iodometric titration method, and their effects on superconductivity were discussed. $\text{Ba}_{1-x}\text{K}_x\text{BiO}_{3-\delta}$ showed remarkable oxygen vacancy amounting to $\delta \sim 0.5$, if annealed in N_2 atmosphere. Tc observed for $0.35 \leq x \leq 0.5$ decreased with increasing 6s electron cocentration and Bi-O distance ($=a/2$), which were both increasing functions of δ , and a metal-insulator transition occurred at about $a=4.30$ Å. Non-superconductivity in $\text{Tl}_2\text{Ba}_2\text{CuO}_{6-\delta}$ ($\delta \sim 0$) due to over-doping of charge transfer $\text{Tl}^{3-t}-(\text{Cu-O})^p$ was turned into a superconducting state by formation of a small amount of oxygen vacancy. The highest Tc value of 85 K was achieved by an optimum value of $\delta \sim 0.15$. $\text{PbBaSrYCu}_3\text{O}_y$ with a structure derivative of $\text{Pb}_2\text{Sr}_2\text{YCu}_3\text{O}_8$ showed a reversible structural transition at about 580 C with oxygen content change from $y=7.0$ to $y=8.2$. Tc in La and Sm substituted $\text{Nd}_{1.85}\text{Ce}_{0.15}\text{CuO}_{4-\delta}$ was measured for the specimens with $\delta \sim 0.03$ and discussed in terms of Cu-O bond length.

1. Introduction

Importance of oxygen contents on the superconducting property, particularly on Tc, of high Tc oxides was first explicitly recognized in $\text{YBa}_2\text{Cu}_3\text{O}_{7-\delta}$ (YBCO) system, in which Tc of 90 K was found for $0 \leq \delta < 0.2$, and superconductivity vanished for $\delta > 0.8$ [1,2]. Conditions for superconductivity in YBCO were demonstrated in a more extensive fashion as oxygen content vs. carrier concentration diagram for the La(Ba) and Ca(Y) substituted system by Tokura et al. [3]. Simple stoichiometric compounds of the YBCO system, as far as cations are concerned, greatly help the development of such notion, because single phase materials can be prepared rather easily and precisely characterized with the oxygen content.

However, implication of oxygen contents on the superconductivity in the later found more complex compounds such as layered structure type Bi and Tl systems and $\text{Ba}_{1-x}\text{K}_x\text{BiO}_{3-\delta}$ (BKBO) system has not been fully elucidated so far, not to say being neglected, partly due to the complexity of composition and structure which makes the synthesis of single phase material rather difficult, and also partly due to difficulty in determining the oxygen content with sufficient precision for the discussion of its

significance on the superconductivity because of involvement of heavy atoms like Bi and Tl. Accordingly, the determination of oxygen contents with accuracy for the high T_c oxides is not easy task, although it is indispensable for the origin of superconductivity.

The aim of the present work is to establish reliable methods for the analysis of the oxygen content and to apply them to the actual determination of the oxygen content in several complex, but important systems such as Tl system or BKBO.

2. Experimental

Oxygen contents of the specimens are to be determined for the single phase material either by thermogravimetry or iodometric titration method. Desorption or absorption of oxygen can be measured as a small weight change by a thermobalance. Absolute value of oxygen contents can be determined by reducing the material in hydrogen atmosphere [4]. In most high- T_c Cu oxides only Cu components are reduced to Cu metal by heating to above 800°C, whereas other components generally remained as stable component oxides upon decomposition. However this method is not applicable, if multivalent elements are concerned or reduction products are not evaluated as simple metals or oxides. The method has not been successful in absolute determination of oxygen contents for the BKBO system, although relative change of oxygen contents can be rather easily evaluated in N_2 or O_2 atmosphere.

Iodometric titration is an alternative method for determining the absolute value of oxygen contents [5]. In this method, the oxide material is to be dissolved by hydrochloric acid under the presence of I^- . Since the ionic state of Cu in strong acidic solution is monovalent, higher valence Cu in solids contributes to the production of I_2 , in proportion to the difference with monovalent Cu. However, existence of other multivalent metal ions prevents unambiguous determination of Cu valence.

The method is successfully applied to BKBO, in which the trivalent Bi is stable in hydrochloric acid solution and excess valence of Bi can be detected by production of I_2 . In this case, rather strong yellow color of BiI^{4-} ions disturbs visual judgments of color change at the end point in titration of I_2 by sodium thiosulfate solution. This difficulty will be overcome by using autotitrator, by which potential change at the end point of titration is electrically detected.

3. Results and discussion

3.1 BKBO system

Discovery of a superconductor $Ba_{1-x}K_xBiO_{3-\delta}$ (BKBO) [6-8] with $T_c=30$ K opened another new route to high T_c oxides besides Cu-based oxides. There are marked similarities between BKBO and previously known BPBO ($BaPb_xBi_{1-x}O_3$) [9]. Both systems are three dimensional, s-electron superconductors with the perovskite structure. Semiconducting CDW state in $BaBiO_3$ is brought into cubic, metallic state by substitution of either Bi by Pb in BPBO or Ba by K in BKBO, thereby reducing the number of 6s electron and contracting Bi-O bond length. In BKBO, however, BiO_6 octahedral network in the perovskite structure is not disturbed by K substitution for Ba, in contrast to the Pb substitution for Bi in BPBO. This might be a cause for higher T_c in the former than in the latter. Another marked discrepancy lies in that BKBO has an easier tendency for oxygen loss because of monovalent K substitution, different from BPBO in which tetravalent Pb^{4+} is substituted for Bi. In the present study [10], oxygen contents of BKBO ($x=0.35, 0.40$ and 0.50) were carefully controlled by annealing at

370-546°C in N₂ atmosphere, and their effects on the unit cell dimension and T_c were studied in detail.

Figure 1 shows the variation of the unit cell dimension, *a*, with the amount of oxygen vacancy, δ , in BKBO, determined by iodometry and thermogravimetry. Bi-O bond length which is given by *a*/2 in the cubic perovskite structure linearly increased with δ . Such expansion with δ is reasonably understood by the increase in the s-electron concentration, or decrease in average Bi valence. T_c determined from susceptibility measurements showed a considerable decrease with increasing number of s-electrons and turns to 0 K around one s-electron per Bi atom, accompanied by a sudden transition to an insulator (Fig.2). Such decrease in T_c can be considered to be due to the expansion of unit cell dimension, *a*, and sudden disappearance of superconductivity as a result of metal-insulator transition was observed at *a*=4.30 Å, independent of the composition (Fig.3).

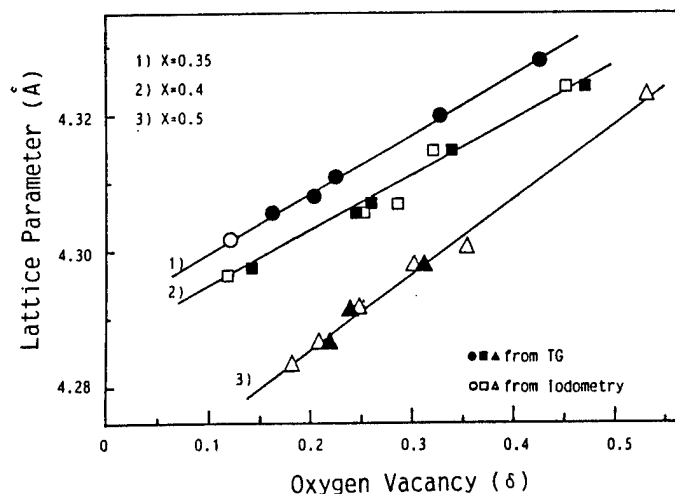


Fig. 1 Lattice parameters, *a*, versus oxygen vacancy, δ , of Ba_{1-x}K_xBiO_{3- δ} [10].

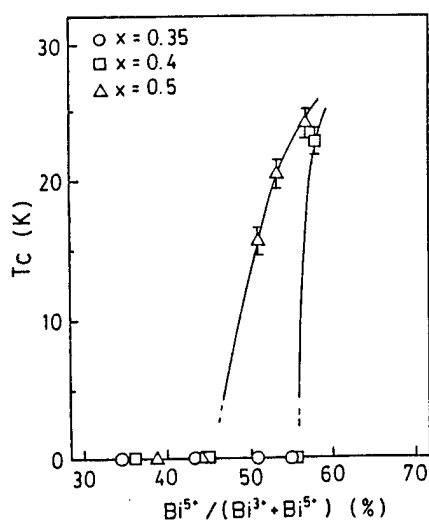


Fig. 2 Variation of T_c with oxidation state of Bi in Ba_{1-x}K_xBiO_{3- δ} [10].

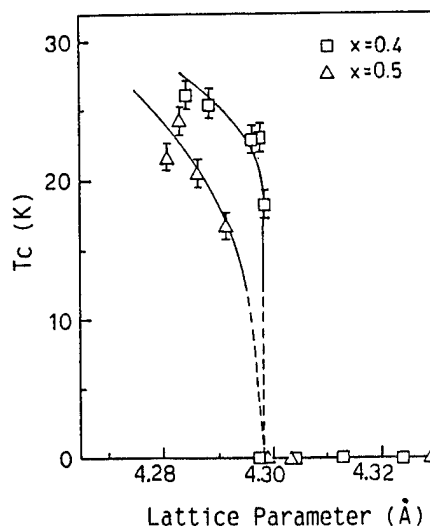


Fig. 3 Dependence of T_c on the lattice parameter, *a*, of Ba_{1-x}K_xBiO_{3- δ} [10].

3.2 $\text{Tl}_2\text{Ba}_2\text{CuO}_6$ (2201)

The simplest member, $\text{Tl}_2\text{Ba}_2\text{CuO}_6$, of the Tl layer structure oxides has shown a marked range of T_c from non-superconductivity to 90 K [11-14], depending on the preparation condition. The origin of such diversity in T_c was recently clarified, when the oxygen content was precisely determined [15-17].

The as-prepared specimen of $\text{Tl}_2\text{Ba}_2\text{CuO}_{6-\delta}$ in O_2 atmosphere, which has presumably no oxygen vacancy, is non-superconductor, owing to the over-doping arising from charge transfer mechanism between Tl^{3+} and Cu^{2+} . Such over-doping can be relieved by deletion of a small number of oxygen (or substitution of Ba^{2+} by La^{3+}), realizing optimum carrier concentration favorable for the appearance of superconductivity.

Figure 4 shows how T_c changes with the quenching temperature of the specimens annealed in O_2 and N_2 atmosphere. T_c monotonically increased with increasing quenching temperature and reached its maximum value of 75 K and 85 K at $T_q=800^\circ\text{C}$ in O_2 and 600°C in N_2 respectively. This change in T_c corresponded to the loss of oxygen during heat treatment in O_2 and N_2 atmosphere, which was determined by thermogravimetric analysis and shown in Fig.5. Weight change was very slight up to about 600°C , above which rapid decrease due to decomposition was observed.

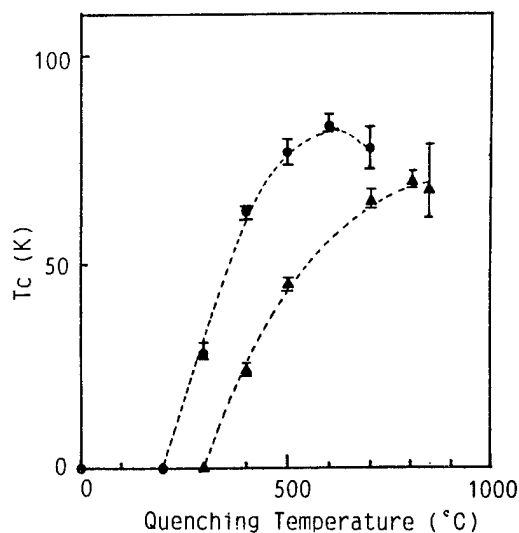


Fig. 4 Variation of T_c with quenching temperature of $\text{Tl}_2\text{Ba}_2\text{CuO}_{6-\delta}$ annealed in N_2 (●) and in O_2 (▲) [17].

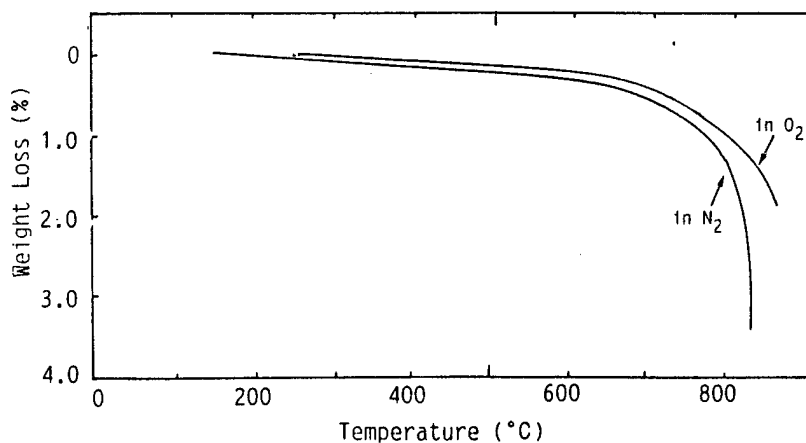


Fig. 5 Weight change of $\text{Tl}_2\text{Ba}_2\text{CuO}_{6-\delta}$ measured with increasing temperature at a rate of $5^\circ\text{C}/\text{min}$. Rapid change above 700°C was due to decomposition [17].

T_c versus loss of oxygen is plotted in Fig. 6. The maximum value of T_c was attained at about $\delta = 0.15$, which was considered to give an optimum carrier concentration in this compound. The over-doping state in the as-prepared oxygen-annealed 2201 specimen is probably ascribable to the charge transfer mechanism like $Tl^{3+} \rightarrow (Cu-O)^p$, as already found in the 2212 and 2223 specimen [18]. Judging from very similar XPS $Tl 4f$ core spectrum observed in 2201 (Fig. 7) [17] to those in 2212 and 2223, it would be natural to assume the same amount of positive charge transferred from Tl to Cu. If so, the effect of charge transfer is expected to be very large in the single Cu layer substance of 2201, compared with multi Cu layer substances of 2212 and 2223 specimens, leading to non-superconductivity due to over-doping. This situation explains why such remarkable over-doping is realized exclusively in the 2201 materials.

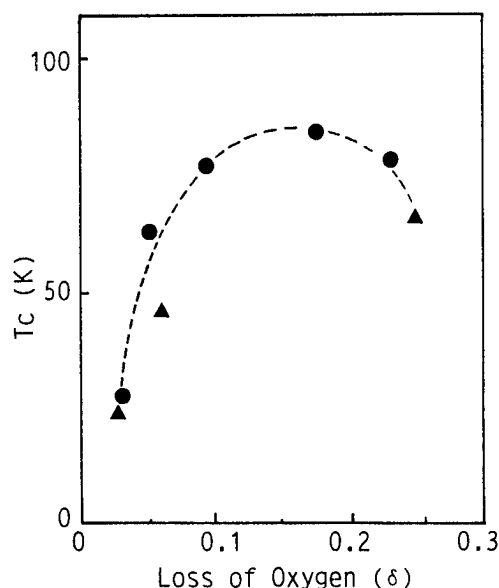


Fig. 6 Dependence of T_c on the oxygen loss, δ , of $Tl_2Ba_2CuO_{6-\delta}$ [17].

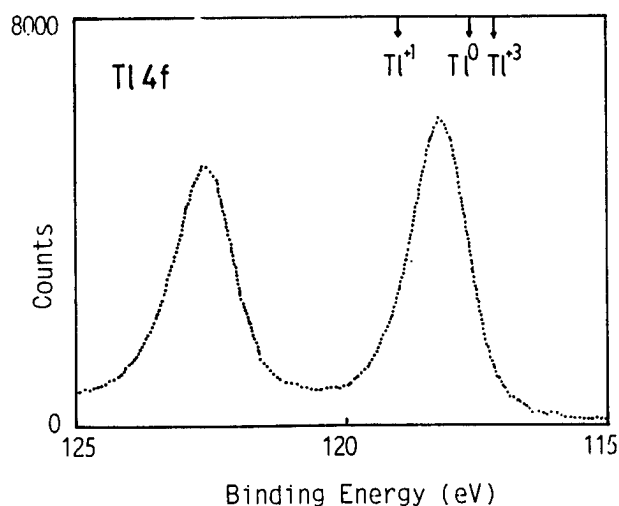


Fig. 7 XPS Tl 4f core spectrum of $Tl_2Ba_2CuO_{6-\delta}$ [19].

3.3 $PbBaSrYCu_3O_y$ ($y=7-8.4$)

The structure of a high T_c oxide $Pb_2Sr_2YCu_3O_8$, first reported by ATT Bell group [20], is different from the Bi and Tl layered system, in that PbO -Cu- PbO block layers interleave perovskite blocks. The tetragonal structure of $PbBaSrYCu_3O_7$ obtained by quenching from $830^\circ C$ in $1\% O_2-N_2$, was recently determined by high resolution electron microscopy and EPMA to be a derivative of $Pb_2Sr_2YCu_3O_8$, in which one of the PbO layers in the PbO -Cu- PbO block was missing, and Ba/Sr layers adjoined both sides, as shown in Fig. 8a [21]. Interestingly the remaining PbO -Cu block tends to form a two-dimensional short-range cluster, where small domains with several unit cell areas consisting of PbO -Cu pairwise block alternates with an anti-phase boundary.

$PbBaSrYCu_3O_y$ was found to show an abrupt phase transition around $580^\circ C$ by TG and high temperature XPD, as shown in Fig. 9. TG clearly indicated a reversible weight change due to desorption and absorption of 1.2 oxygen atom per formula unit upon heating and cooling respectively. The transition was shown to be accompanied by discontinuous change in lattice parameters of c and a . The structure of $PbBaSrYCu_3O_{8.2}$ was

proposed as shown in Fig. 8b, where no cation migration was assumed to occur during the transition.

Although neither $\text{PbBaSrYCu}_3\text{O}_7$ nor $\text{PbBaSrYCu}_3\text{O}_{8.2}$ showed superconductivity, Ca substitution for Y remarkably reduced electrical resistivity, and in some cases realized T_c up to 50 K. Further detailed study is now being carried out for achieving higher T_c .

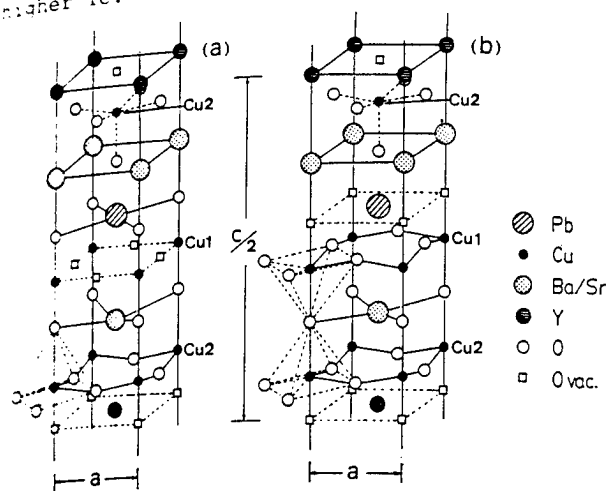


Fig. 8 Crystal structure of $\text{PbBaSrYCu}_3\text{O}_y$ [21].
(a) $y = 7.0$, (b) $y = 8 + \delta$.

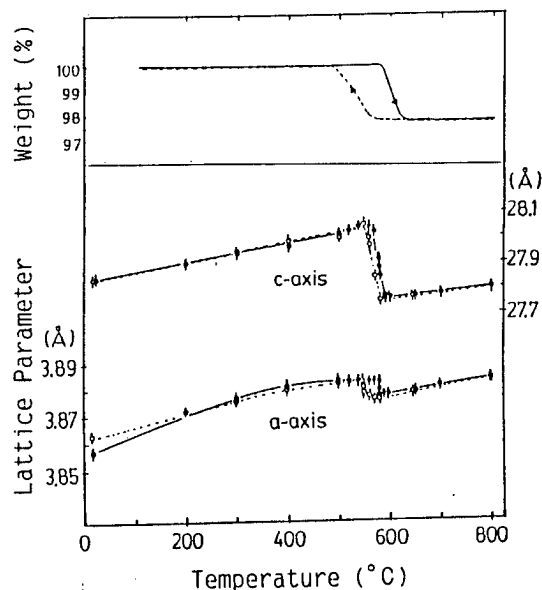


Fig. 9 Weight change (top) and variation of lattice parameters (bottom) of $\text{PbBaSrYCu}_3\text{O}_y$ [21].

3.4 $\text{Nd}_{1.85-x}\text{M}_x\text{Ce}_{0.15}\text{O}_{4-\delta}$ ($M=\text{La}, \text{Sm}$)

Electron superconductor of $\text{Nd}(\text{Ce})\text{-Cu-O}$ system [22] gave a strong impact on the study of high T_c oxides. However, no clear answer has been given yet to the question why only the specimens treated under reduced atmosphere show superconductivity.

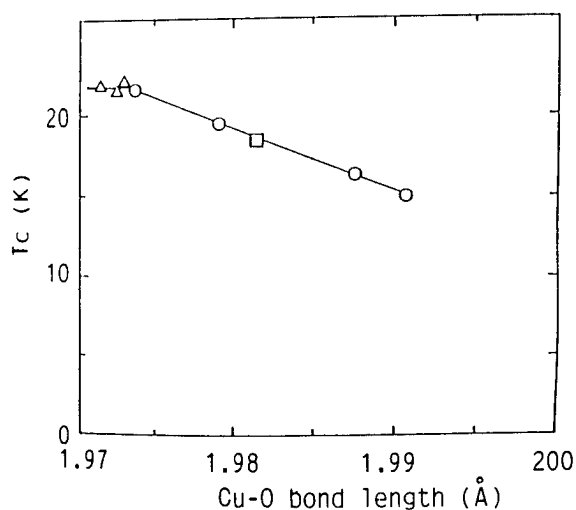


Fig. 10 Dependence of T_c on Cu-O bond length of $\text{Nd}_{1.85-x}\text{M}_x\text{Ce}_{0.15}\text{CuO}_{4-\delta}$ [23]. $M = \text{La}$ (o) and Sm (Δ). \square : $\text{Pr}_{1.85}\text{Ce}_{0.15}\text{CuO}_{4-\delta}$ [23].

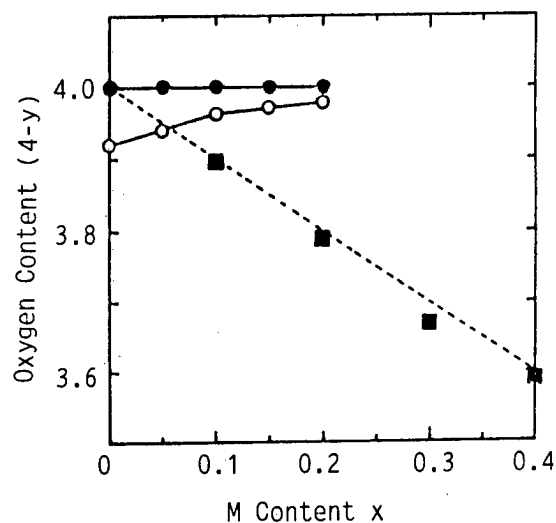


Fig. 11 Oxygen content versus M content of $\text{Nd}_{2-x}\text{M}_x\text{CuO}_{4-\delta}$. $M = \text{Ce}$ (circle) and Na (square). Closed and open symbols show specimens annealed in air and Ar [25].

In the present study [23], oxygen vacancy controlled specimens of the La or Sm substituted system for Nd were prepared, and the relation between Tc and Cu-O bond length was studied, as shown in Fig. 10. Substitution of Nd by La with larger ionic radius than Nd decreased Tc in accordance with the elongation of Cu-O bond, but small Sm substitution, which contracted Cu-O bond, did not change Tc substantially, consistent with the recent result of pressure effects on Tc [24].

An attempt to introduce holes in Nd_2CuO_4 by substituting Nd^{3+} by Na^+ was unsuccessful [25]. Charge compensation was completely made by formation of oxygen vacancy, as shown in Fig. 11, and Cu remained as divalent. This situation is probably related to longer Cu-O bond length in Nd_2CuO_4 than in La_2CuO_4 with the K_2NiF_4 type structure, as pointed out by Muromachi et al. [26].

References

1. M.Kikuchi, Y.Syono, A.Tokiwa, K.Oh-ishi, H.Arai, K.Hiraga, N.Kobayashi, T.Sasaoka and Y.Muto: Jpn.J.Appl.Phys.26(1987)L1066.
2. E.Takayama-Muromachi, Y.Uchida, M.Ishii, T.Tanaka, and K.Kato: Jpn.J.Appl. Phys.,26(1987)L1156.
3. Y.Tokura, J.B.Torrance, T.C.Huang and A.I.Nazzari: Phys.Rev.B 38(1988)7156.
4. M.Kikuchi, K.Oh-ishi: Oyo Buturi 59(1990)85, in Japanese.
5. T.Hasegawa, K.Kishio, K.Kitazawa: Oyo Buturi 59(1990)81, in Japanese.
6. L.F.Mattheiss, E.M.Gyorgy, D.W.Johnson Jr.: Phys Rev.B37(1988)3745.
7. R.J.Cava, B.Batlogg, J.J.Krajewski, R.C.Farrow, L.W.Rupp Jr., A.E.White, K.T.Short, W.F.Peck Jr., T.Y.Kometani: Nature 332(1988)814.
8. D.G.Hinks, B.Dabrowski, J.D.Jorgensen, A.W.Mitchell, D.R.Richards, Pei Shiyong, Shi Donglu: Nature 333(1988)836.
9. K.Kitazawa, M.Naito, T.Tanaka: Kotai Buturi 18(1983)535.
10. K.Ueki, A.Tokiwa, M.Kikuchi, T.Suzuki, M.Nagoshi, R.Suzuki, N.Kobayashi and Y.Syono: Proceedings of 2nd International Symposium on Superconductivity at Tsukuba, November 1989, in press.
11. T.C.Huang, V.Y.Lee, R.Karini, R.Beyer and S.S.P.Parkin: Mat.Res.Bull. 23(1988)1307.
12. C.C.Torardi, M.A.Subramanian, J.C.Calabrese, J.Gopalakrishnan, E.M.McCarron, K.J.Morrissey, T.R.Askew, R.B.Flippen, U.Chowdhry and W.Slright: Phys.Rev.B38(1988)225.
13. M.Kikuchi, N.Kobayashi, H.Iwasaki, D.Shindo, T.Oku, A.Tokiwa, T.Kajitani, K.Hiraga, Y.Syono and Y.Muto: Jpn.J.Appl.Phys. 27(1988)L1050.
14. Y.Shimakura, Y.Kubo, T.Manako, T.Satoh, S.Iijima, T.Ichihashi and H.Igarashi: Physica C 157(1989)279.
15. Y.Kubo, Y.Shimakura, T.Manako, T.Satoh, S.Iijima, T.Ichihashi and H.Igarashi: Proceedings of M2S-HTSC at Stanford Univ., July 1989, p.991.
16. S.Nakajima, M.Kikuchi, T.Oku, N.Kobayashi, T.Suzuki, K.Nagase, K.Hiraga, Y.Muto and Y.Syono: Physica C 160(1989)458.
17. M.Kikuchi, S.Nakajima, Y.Syono, K.Nagase, R.Suzuki, T.Kajitani, N.Kobayashi and Y.Muto, in preparation.
18. Y.Syono, M.Kikuchi, S.Nakajima, T.Suzuki, T.Oku, K.Hiraga, N.Kobayashi, H.Iwasaki and Y.Muto: MRS Symp. Proc., vol.156 eds. J.D.Jorgensen et al. (1989) p.229.

19. T.Suzuki, M.Nagoshi, Y.Fukuda, Y.Syono, M.Kikuchi, N.Kobayashi and M.Tachiki: Phys.Rev.B 40(1989)5184.
20. R.J.Cava, B.Batlogg, J.J.Krajewski, L.W.Rupp, L.F.Schneemeyer, T.Siegrist, R.B.van Dover, P.Marsh, W.F.Peck Jr., S.H.Glarrum, J.H.Marshall, R.C.Farrow, J.B.Wazzak, R.Hull and P.Trevor: Nature 336(1988)211.
21. A.Tokiwa, T.Oku, M.Nagoshi, M.Kikuchi, K.Hiraga and Y.Syono: Physica C 161(1989)459.
22. Y.Tokura, H.Takagi and S.Uchida: Nature 337(1989)345.
23. K.Oh-ishi, Y.Syono, M.Kikuchi N.Kobayashi and Y.Muto: Solid State Commun.,(1990) in press.
24. C.Murayama, N.Mori, S.Yomo, H.Takagi, S.Uchida and Y.Tokura: Nature 339(1989)293.
25. K.Oh-ishi, M.Kikuchi, Y.Syono, N.Kobayashi and Y.Muto: J.Solid State Chem. 83(1989)237.
26. E.Takayama-Muromachi, F.Izumi, Y.Uchida, K.Kato and H.Asano: Physica C (1990), in press.

Preparation and Superconducting Properties of $\text{Pb}_2\text{Sr}_2\text{Y}_{0.5}\text{Ca}_{0.5}\text{Cu}_3\text{O}_{8+\delta}$ with Zero Resistance at 75 K

Y.Saito, Y.Koike, T.Noji, M.Masuzawa, H.Sunagawa, H.Kawabe⁺, N.Kobayashi⁺⁺

Department of Applied Physics, Faculty of Engineering, Tohoku University,
Aramaki Aoba, Aoba-ku, Sendai 980.

⁺TATSUTA Electric Wire & Cable Co., Ltd., 2-3-1 Iwatacho, Higashi-Osaka, Osaka 578.

⁺⁺Institute for Materials Research, Tohoku University, Katahira, Aoba-ku, Sendai 980.

Good quality samples of $\text{Pb}_2\text{Sr}_2\text{Y}_{0.5}\text{Ca}_{0.5}\text{Cu}_3\text{O}_{8+\delta}$ have been prepared by solid-state reaction under low oxygen pressure and adequate post-annealing in flowing nitrogen gas. The best sample shows metallic temperature dependence of the resistivity above T_c , an onset of the superconducting transition at 83 K and zero resistance at 75 K. The superconducting transition curve becomes as broad in the parallel magnetic field to the current direction as in the perpendicular field, suggesting that the broadening is not simply attributed to the flux-flow resistance. The value of $-dH_{c2}/dT$ is estimated as 1.7 - 1.8 T/K. The resistive tail in the lower portion of the transition curve is well expressed as $\rho = \rho_0 \exp(-U_0/k_B T)$. The values of U_0 and $-dH_{c2}/dT$ are similar to those of Bi-Sr-Ca-Cu-O and Tl-Ba-Ca-Cu-O. The critical current density J_c shows hysteresis with respect to the magnetic field sweep, and is as low as 0.1 Acm^{-2} at 4.2 K in magnetic fields between 1 T and 13 T.

Since the discovery of high- T_c superconductivity in the La-Ba-Cu-O, many kinds of high- T_c superconductors with modified perovskite structures including two-dimensional sheets of CuO_2 have been found. The compound $\text{Pb}_2\text{Sr}_2\text{ACu}_3\text{O}_{8+\delta}$ discovered by Cave et al. [1] also belongs to the high- T_c superconductors with the CuO_2 sheets, where A is a lanthanide Ln, Y or a mixture of (Ln or Y) and (Ca or Sr). The crystal structure of this family of compounds is characterized by double CuO_2 pyramidal layers, and the layer sequence along the c-axis is expressed as $-\text{A-CuO}_2\text{-SrO-PbO-CuO}_8\text{-PbO-SrO-CuO}_2-$. Two kinds of Cu are considered to show different valences: one is +2 for the pyramidal CuO_2 layers and the other is almost +1 for the almost oxygen-free CuO_8 layers, as are observed in non-superconducting $\text{YBa}_2\text{Cu}_3\text{O}_6$. The structure can be regarded in the same light as those of $\text{YBa}_2\text{Cu}_3\text{O}_{7-\delta}$, $\text{Bi}_2\text{Sr}_2\text{CaCu}_2\text{O}_{8+\delta}$ and $\text{Tl}_n\text{Ba}_2\text{CaCu}_2\text{O}_{6+n}$ ($n=1,2$), when the $\text{PbO-CuO}_8\text{-PbO}$ triple layer is replaced by a $\text{CuO}_{1-\delta}$ layer, a BiO-BiO double layer and a TlO or a TlO-TlO double layer, respectively. In the $\text{Pb}_2\text{Sr}_2\text{ACu}_3\text{O}_{8+\delta}$ family, the optimal composition to attain high- T_c superconductivity is known to be $\text{Pb}_2\text{Sr}_2\text{Y}_{0.5}\text{Ca}_{0.5}\text{Cu}_3\text{O}_{8+\delta}$. The superconducting quality of ceramics samples reported so far, however, is not so good. The transition width is very broad, and the temperature-coefficient of the resistivity above T_c is negative in every ceramic sample. Here, we report our success in preparing ceramics samples of good quality with a positive temperature-coefficient of the resistivity and with $T_{c, \text{zero}}$ as high as 75 K [2]. We also report on measurements of the resistive transition for these samples, made in various magnetic fields up to 21 T. The upper critical field H_{c2} , the superconducting fluctuation, the resistive tail at the lower portion of the transition curve and the critical current density J_c are discussed [3].

Ceramic samples of the nominal composition $\text{Pb}_2\text{Sr}_2\text{Y}_{0.5}\text{Ca}_{0.5}\text{Cu}_3\text{O}_{8+\delta}$ were synthesized by a two-step solid-state reaction. In the first step, the precursor of $\text{Sr}_2\text{Y}_{0.5}\text{Ca}_{0.5}\text{Cu}_3\text{O}_y$ without PbO was prepared from a mixture of SrCO_3 , Y_2O_3 , CaCO_3 and CuO . The well-mixed powders were heated in air at 900°C for 5 h. In the next step, the precursor was pulverized, mixed with PbO , pelletized and sintered in flowing gas of 1% O_2 in N_2 at a temperature between 900°C and 930°C for 2 h (we call this process the first heat-treatment). Then it was cooled to a temperature between 750°C and 800°C and kept in the same flowing gas for 12 h, followed by quenching in liquid nitrogen (we call this process the second heat-treatment). Post-annealing was performed in flowing nitrogen gas at 500°C for various hours. After the second heat-treatment, samples of the single phase of the $\text{Pb}_2\text{Sr}_2\text{ACu}_3\text{O}_{8+\delta}$ structure are obtained as shown in Fig.1(b), but their superconducting quality is not so good. After the post-annealing at 500°C , the best result is attained as shown in Fig.2. As shown in the inset, the width of the superconducting transition becomes narrow, and the values of $T_{\text{C, onset}}$ and $T_{\text{C, zero}}$ are as high as 83 K and 75 K, respectively. These are the best record as far as we know. Moreover, it is noteworthy that positive temperature-coefficients of the resistivity ρ are observed above T_{C} for these samples. The resistivity in the normal state decreases with increasing the annealing time. These good behaviors are considered to be attributed to the decrease of crystalline disorder owing to the post-annealing. What is most plausible is the ordering of oxygen atoms in the PbO layer, for these oxygen atoms have been pointed out to occupy randomly one of four possible positions around the symmetric position [4]. Another reason is that the X-ray diffraction pattern shown in Fig.1(c) is almost similar to that of the single phase as shown in Fig.1(b), although an unknown small peak is observed. If anything, the good behaviours of T_{C} and ρ will be related to the ordering of oxygen atoms and/or lead atoms in the PbO layer.

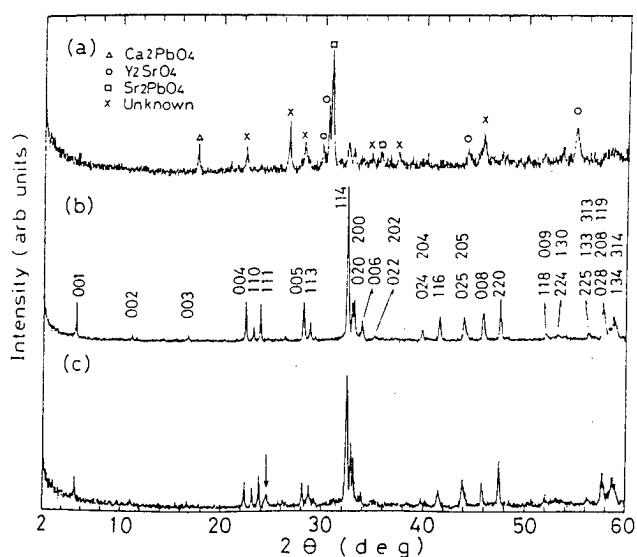


Fig.1. Powder X-ray diffraction patterns using $\text{CuK}\alpha$ radiation. (a) A sample quenched after the first heat-treatment. Marked peaks are due to impurity phases. (b) A sample after the second heat-treatment, succeeding the first heat-treatment. (c) A sample post-annealed in flowing nitrogen gas at 500°C for 12 h. A peak marked by an arrow is not identified.

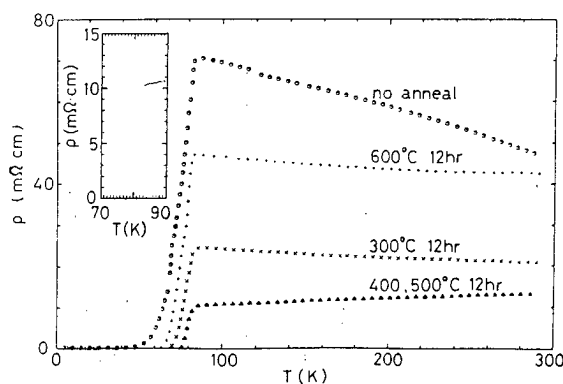


Fig.2. Temperature dependence of the resistivity ρ for samples post-annealed in flowing nitrogen gas at various temperatures for 12 h. The inset is for the sample post-annealed at 500°C .

Figure 3 shows the temperature dependence of ρ in various magnetic fields parallel to the current direction. As the applied field is increased, the transition curve becomes broad and the resistive tail extends to lower and lower temperatures. This behavior is similarly observed for the parallel and perpendicular fields to the current direction, suggesting that the broadening of the transition curve in magnetic fields is not simply attributed to the flux-flow resistance due to Lorentz force. Effects of the superconducting fluctuation in magnetic fields may be important [5]. $H_{C2}(T)$, defined at the midpoint of the transition curve, is shown in Fig.4. H_{C2} is found to be proportional to $T_C - T$, though it shows slight positive curvature near T_C . The value of $-dH_{C2}/dT$ is estimated as 1.7 - 1.8 T/K, which is comparable to those of $\text{Bi}_{2-x}\text{Pb}_x\text{Sr}_2\text{Ca}_2\text{Cu}_3\text{O}_y$ [6,7] and $\text{Tl}_2\text{Ba}_2\text{Ca}_2\text{Cu}_3\text{O}_y$ [8] and smaller than those of $\text{YBa}_2\text{Cu}_3\text{O}_{7-\delta}$ [9] and $\text{La}_{1.85}\text{Sr}_{0.15}\text{CuO}_{4-\delta}$ [10], as listed in Table I. $H_{C2}(T)$ defined at the end-point, namely zero-resistance temperature, is also shown in Fig.4. The upper critical field at 0 K, $H_{C2}(0)$, is roughly estimated using the relation $H_{C2}(0) = 0.69T_C |dH_{C2}/dT|_{T_C}$ given by the WHH theory [11]. $H_{C2}(0)$ is 85 - 96 T for H_{C2} defined at the midpoint. The Ginzburg-Landau coherence length at 0K, $\xi(0)$, is estimated from the following equation, $H_{C2}(0) = \phi_0 / 2\pi\xi^2(0)$, where ϕ_0 is the superconducting flux quantum. $\xi(0)$ is estimated as 19-20 Å. The values of $H_{C2}(0)$ and $\xi(0)$ are comparable

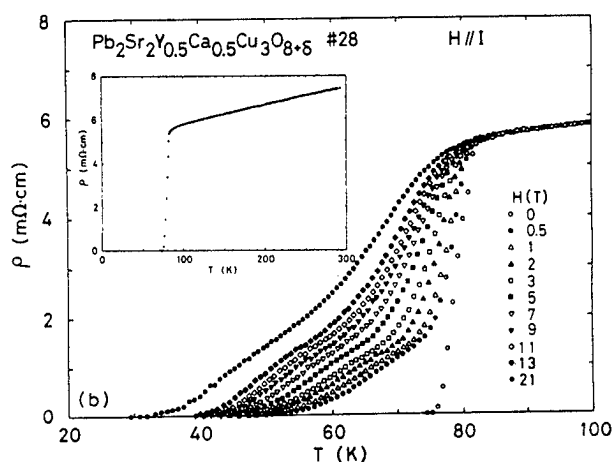


Fig.3. Temperature dependence of the resistivity ρ in various magnetic fields parallel to the current direction. The inset is the temperature dependence of ρ in zero field.

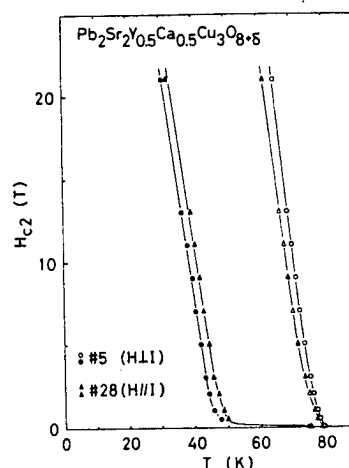


Fig.4 Temperature dependence of H_{C2} , defined at the midpoint of the transition curve of ρ vs. T in various magnetic fields (\circ, Δ), and also defined at the end-point, namely zero resistance (\bullet, \blacktriangle). Magnetic fields are parallel to the current direction for sample #28 and perpendicular for sample #5.

Table I. Superconducting parameters for various ceramic samples of high- T_C oxides. Symbols mid and end indicate that parameters are defined at the midpoint of the transition curve of ρ vs. T and at the zero-resistance temperature, respectively.

	T_C (K)		$-dH_{C2}/dT$ (T/K)		$H_{C2}(0)$ (T)		$\xi(0)$ (Å)	
	mid	end	mid	end	mid	end	mid	end
$\text{Pb}_2\text{Sr}_2\text{Y}_{0.5}\text{Ca}_{0.5}\text{Cu}_3\text{O}_{8.6}$ #5 (H⊥I)	79.2	74.8	1.83	1.45	96.2	45.4	18.5	26.9
#28 (H//I)	78.9	75.5	1.66	1.41	85.1	46.7	19.7	26.6
$\text{Bi}_{1.5}\text{Pb}_{0.5}\text{Sr}_2\text{Ca}_2\text{Cu}_3\text{O}_y$ [6]	105		1.5		110		17	
$\text{Bi}_{1.4}\text{Pb}_{0.6}\text{Sr}_2\text{Ca}_2\text{Cu}_3\text{O}_{9.60y}$ [7]	110		1.8		140		15	
$\text{Tl}_2\text{Ba}_2\text{Ca}_2\text{Cu}_3\text{O}_y$ [8]	117	114	1.3		100		18	
$\text{YBa}_2\text{Cu}_3\text{O}_{7-\delta}$ [9]	92	91.3	2.4	1.2	150	60	15	23
$\text{La}_{1.85}\text{Sr}_{0.15}\text{CuO}_{4-\delta}$ [10]	38.3	35	2.7		71		22	

to those of ceramic samples of other high- T_c oxides. The value of $\xi(0)$ can be estimated from the analysis of the superconducting fluctuation observed in the upper portion of the transition curve in the ρ vs. T plot in zero field, too. Just above T_c , the resistivity deviates from the T -linear dependence in the normal state, which is regarded as due to the superconducting fluctuation. The excess conductivity over the normal conductivity σ_n is shown as a function of reduced temperature in Fig.5. In the vicinity of T_c , the excess conductivity $\sigma - \sigma_n$ is proportional to $(T - T_c)^{-1/2}$, suggesting that the superconducting fluctuation is three-dimensional. According to the theory by Aslamazov and Larkin [12], the excess conductivity in the three-dimensional system is given by $\sigma - \sigma_n = \{e^2/32\pi\xi(0)\} \{(T - T_c)/T_c\}^{-1/2}$. From this equation, $\xi(0)$ is estimated to be 480 Å. This value is much larger than that estimated from $H_{c2}(0)$. This disagreement will be caused by the underestimation of $\sigma - \sigma_n$ in the ceramic sample, for the good agreement is attained for well-sintered samples of $\text{YBa}_2\text{Cu}_3\text{O}_{7-\delta}$ [13] and single-crystal samples of $\text{Bi}_2\text{Sr}_2\text{CaCu}_2\text{O}_{8+\delta}$ [14]. In other words, the value of ρ in our ceramic samples is not intrinsic and includes effects of grain boundaries. Better sintering will decrease the value of ρ .

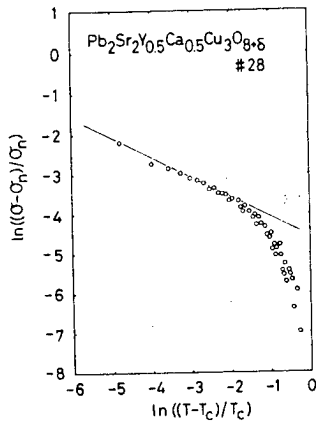


Fig.5. Temperature dependence of the excess conductivity. The solid line is the prediction of the theory for the three-dimensional superconducting system.

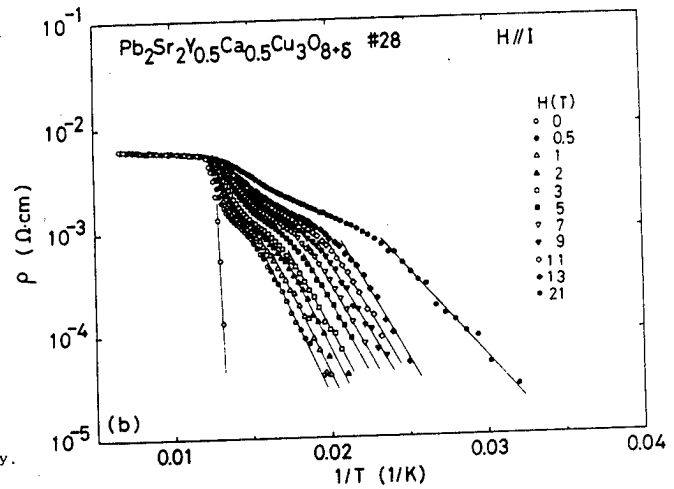


Fig.6. Plot of $\log \rho$ vs. T^{-1} for data shown in Fig.3.

The resistive tail in magnetic fields shown in Fig.3 is well expressed as $\rho = \rho_0 \exp(-U_0/k_B T)$, as shown in Fig.6. The thermal activation energy U_0 is not so dependent on the field direction to the current direction. As shown in Fig.7, U_0 decreases with increasing the magnetic field strength, and the magnetic field dependence of U_0 is given by $U_0 \propto H^{-0.1}$ for sample #5 and $U_0 \propto H^{-0.08}$ for sample #28, though data at 21 T deviate. The exponential temperature dependence of the resistive tail was first pointed out by Palstra et al. [15] in a single crystal of $\text{Bi}_2\text{Sr}_2\text{CaCu}_2\text{O}_{8+\delta}$. Later, this temperature dependence has been reported for many kinds of samples of high- T_c oxides, such as ceramic samples [16,17], highly oriented films [18] and single crystals [14,19,20]. The activation energy U_0 has been thought to be related to the potential energy of flux pinning and the resistive tail has been discussed using the model of flux creep and flux flow. This model, however, cannot be simply applied to our data, because the resistive tail and the value of U_0 are not so dependent on the field direction to the current direction, though the flux-flow resistance due to Lorentz force should be influenced by the configuration of the

magnetic field and the sample current. If the magnetic flux does not enter a sample straight in the vortex state and is bent by grain boundaries and/or the crystallographic anisotropy, the model of flux creep and flux flow may be essentially true to explain the resistive tail. The value of U_0 in $\text{Pb}_2\text{Sr}_2\text{Y}_{0.5}\text{Ca}_{0.5}\text{Cu}_3\text{O}_{8+\delta}$ is close to those of $\text{Bi}_2\text{Sr}_2\text{CaCu}_2\text{O}_{8+\delta}$ [14-16,18] and $\text{TlBa}_2\text{CaCu}_2\text{O}_y$ [20] and smaller than that of $\text{YBa}_2\text{Cu}_3\text{O}_{7-\delta}$ [18]. This may suggest that U_0 is related to the crystallographic anisotropy, for the anisotropy of $\text{Pb}_2\text{Sr}_2\text{Y}_{0.5}\text{Ca}_{0.5}\text{Cu}_3\text{O}_{8+\delta}$ is similar to those of $\text{Bi}_2\text{Sr}_2\text{CaCu}_2\text{O}_{8+\delta}$ and $\text{TlBa}_2\text{CaCu}_2\text{O}_y$ and larger than those of $\text{YBa}_2\text{Cu}_3\text{O}_{7-\delta}$.

Figure 8 shows J_c at 4.2 K in magnetic fields. J_c drastically decreases in the low field region and is almost constant, 0.1 Acm^{-2} , in magnetic fields between 1 T and 13 T. Hysteresis with respect to the magnetic field sweep is observed in low magnetic fields. These magnetic field dependence and hysteresis are often observed in ceramic samples of high- T_c oxides [21]. These are considered to be due to inhomogeneous superconductivity, namely weak superconducting regions in a ceramic sample. According to the theory by Tachiki and Takahashi [22], a large value of the intrinsic J_c is expected for layered high- T_c oxides with a larger lattice constant than $\xi(0)$ along the c-axis. That is, the complicated layer structure along the c-axis itself is thought to work as strong pinning centers of vortices. If this is true, a large J_c is expected in $\text{Pb}_2\text{Sr}_2\text{Y}_{0.5}\text{Ca}_{0.5}\text{Cu}_3\text{O}_{8+\delta}$ whose crystal structure along the c-axis is very complicated. As far as our samples are concerned, however, J_c is not large and is considered to be limited by grain boundaries and anisotropy rather than the intrinsic pinning force. In order to attain high J_c in $\text{Pb}_2\text{Sr}_2\text{Y}_{0.5}\text{Ca}_{0.5}\text{Cu}_3\text{O}_{8+\delta}$, it will be necessary to prepare highly oriented films or single crystals, as studied for other high- T_c oxides.

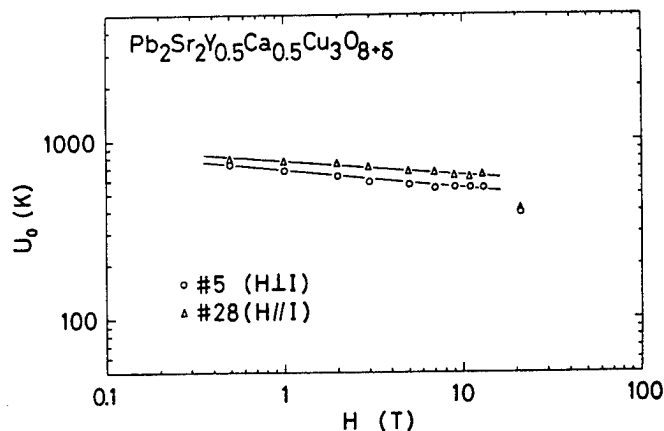


Fig.7. Magnetic field dependence of the activation energy U_0 . Magnetic fields are parallel to the current direction for sample #28 (Δ) and perpendicular for samples #5 (\circ).

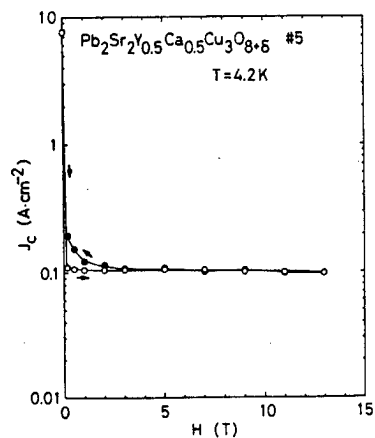


Fig.8. Magnetic field dependence of J_c on increasing field (\circ) and on decreasing field (\odot).

- [1] R.J. Cava et al.: Nature **336** (1988) 211.
- [2] M. Masuzawa et al.: Jpn. J. Appl. Phys. **28** (1989) L1524.
- [3] Y. Koike et al.: submitted to Jpn. J. Appl. Phys.
- [4] R.J. Cava et al.: Physica **C157** (1989) 272.
- [5] R. Ikeda et al.: J. Phys. Soc. Jpn. **58** (1989) 1377, 1906.
- [6] Y. Muto et al.: The Science of Superconductivity and New Materials, Nakajima (World Scientific, Singapore, 1989) p.98.
- [7] H. Kumakura et al.: Jpn. J. Appl. Phys. **27** (1988) L1514.
- [8] H. Iwasaki et al.: Jpn. J. Appl. Phys. **27** (1988) L1631.
- [9] Y. Muto et al.: Novel Superconductivity, ed. S.A. Wolfand and V.Z. Kresin (Plenum Publishing Co., New York, 1987) p.787.
- [10] N. Kobayashi et al.: Jpn. J. Appl. Phys. **26** (1987) L358.
- [11] N.R. Werthamer et al.: Phys. Rev. **147** (1966) 295.
- [12] L.G. Aslamazov and A.I. Larkin: Phys. Lett. **26A** (1968) 238.
- [13] P.P. Freitas et al.: Phys. Rev. **B36** (1987) 833.
- [14] Y. Koike et al.: Research Report on Mechanism of Superconductivity (1989) p.66.
- [15] T.T.M. Palstra et al.: Phys. Rev. Lett. **61** (1988) 1662.
- [16] Y. Jia and J.A. Wilson: Solid State Comm. **71** (1989) 191.
- [17] J.D. Hettinger et al.: Supercond. Sci. Technol. **1** (1989) 349.
- [18] N. Kobayashi et al.: Physica **C159** (1989) 295.
- [19] T.T.M. Palstra et al.: Appl. Phys. Lett. **54** (1989) 763.
- [20] H. Iwasaki et al.: Physica **C159** (1989) 301.
- [21] K. Watanabe et al.: Cryogenics **29** (1989) 263.
- [22] M. Tachiki and S. Takahashi: Solid State Comm. **70** (1989) 291.

Thallium-Substitution Effects
in Ferroelectric Bismuth Layer-Oxides

Masaaki TAKASHIGE, Fuminao SHIMIZU, Haruhiko SUZUKI,
and Shozo SAWADA

College of Science and Engineering, Iwaki Meisei University
5-5-1 Iino, Chuohdai, Iwaki-shi, Fukushima, 970

Thallium-substituted ferroelectric bismuth layer-oxides having nominal compositions such as $\text{PbBi}_{2-x}\text{Tl}_x\text{Nb}_2\text{O}_9$, were synthesized. The effect of substitution were pursued by measuring dielectric constants and the powder X-ray diffraction lines as a function of thallium concentration x .

1. INTRODUCTION

In the recent progress of oxides-superconductors researches, the bismuth layer-structure is one of stimulated interests. These materials[1-4] have structures with interleaved Bi_2O_2 layers and perovskite-like layers consists of CuO -pyramids or planes, and the materials with Tl_2O_2 or TlO layers instead of Bi_2O_2 have also been found [5,6].

These systems are similar in structure to the ferroelectric $\text{Bi}_4\text{Ti}_3\text{O}_{12}$ -family also having structures with interleaved Bi_2O_2 layers and various numbers of perovskite-like layers which consist of octahedron-networks such as TiO_6 , NbO_6 [7,8].

In the present report, our interest is put to investigate whether the Bi_2O_2 layer can be replaced by Tl_2O_2 layer in the series of $\text{Bi}_4\text{Ti}_3\text{O}_{12}$ -family ferroelectrics. For this purpose, we have synthesized systems having nominal compositions as $\text{MBi}_{2-x}\text{Tl}_x\text{Nb}_2\text{O}_9$, ($M=\text{Ba}, \text{Sr}, \text{Pb}, x < 2$). Here we wish to report X-ray powder diffraction and temperature characteristicity of dielectric constants of these Tl-substituted systems and to discuss potentiality of Tl-ion for the formation of these kinds of layer-oxide in connection with high- T_c superconducting Tl-layer materials.

2. MATERIAL SYNTHESSES

Materials synthesized here are listed in Table 1 [9]. All end-members have a structure with pseudo-perovskite layer of $\text{MNb}_2\text{O}_7^{2-}$ having two NbO_6 -octahedrons, interleaved between Bi_2O_2 layers, as schematically shown in Fig.1. The present purpose is to substitute Tl into the Bi-site in the Bi_2O_2 layers.

Starting materials are oxides and carbonates of each metal. Because of toxicity and high volatility of trivalent thallium oxides, the following firing condition was adopted. The pellets of starting mixture were wrapped with platinum foil and put into a fused-quartz tube filled with oxygen gas. This tube was pulled down into a furnace preheated at 950°C . After 2 hours firing, it was pulled up and rapidly cooled down to ambient temperatures. The loss of Tl was estimated to be less than 20 % from the weight-check before and after firing.

- #1-1 $\text{BaBi}_2\text{Nb}_2\text{O}_9$
 #1-2 $\text{BaBi}_{1.5}\text{Tl}_{0.5}\text{Nb}_2\text{O}_9$
 #1-3 $\text{BaBi}_{1.0}\text{Tl}_{1.0}\text{Nb}_2\text{O}_9$
 #1-4 $\text{BaTl}_{2.0}\text{Nb}_2\text{O}_9$
- #2-1 $\text{SrBi}_2\text{Nb}_2\text{O}_9$
 #2-2 $\text{SrBi}_{1.5}\text{Tl}_{0.5}\text{Nb}_2\text{O}_9$
 #2-3 $\text{SrBi}_{1.0}\text{Tl}_{1.0}\text{Nb}_2\text{O}_9$
 #2-4 $\text{SrTl}_{2.0}\text{Nb}_2\text{O}_9$
- #3-1 $\text{PbBi}_2\text{Nb}_2\text{O}_9$
 #3-2 $\text{PbBi}_{1.9}\text{Tl}_{0.1}\text{Nb}_2\text{O}_9$
 #3-3 $\text{PbBi}_{1.5}\text{Tl}_{0.5}\text{Nb}_2\text{O}_9$
 #3-4 $\text{PbBi}_{1.0}\text{Tl}_{1.0}\text{Nb}_2\text{O}_9$
 #3-5 $\text{PbTl}_{2.0}\text{Nb}_2\text{O}_9$

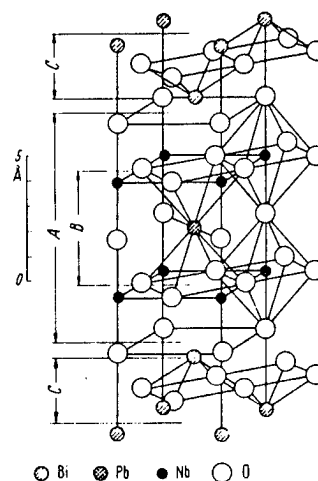


Fig.1 $\text{MBi}_2\text{Nb}_2\text{O}_9$ - structure
 (after ref.[8]).

Table 1. Nominal compositions synthesized [9].

3. X-RAY POWDER DIFFRACTION

The powder X-ray diffraction pattern was checked. As one example, the results for #2 are shown in Fig.2. For the concentration range $x < 1$, basically it showed the pattern similar to that of the end-member, but for $x=2$, some foreign phase seems to be realized. The same tendency was observed in #1, but in the #3, a foreign phase appeared in rather low concentration range. We have not yet performed full-identification of these diffraction patterns.

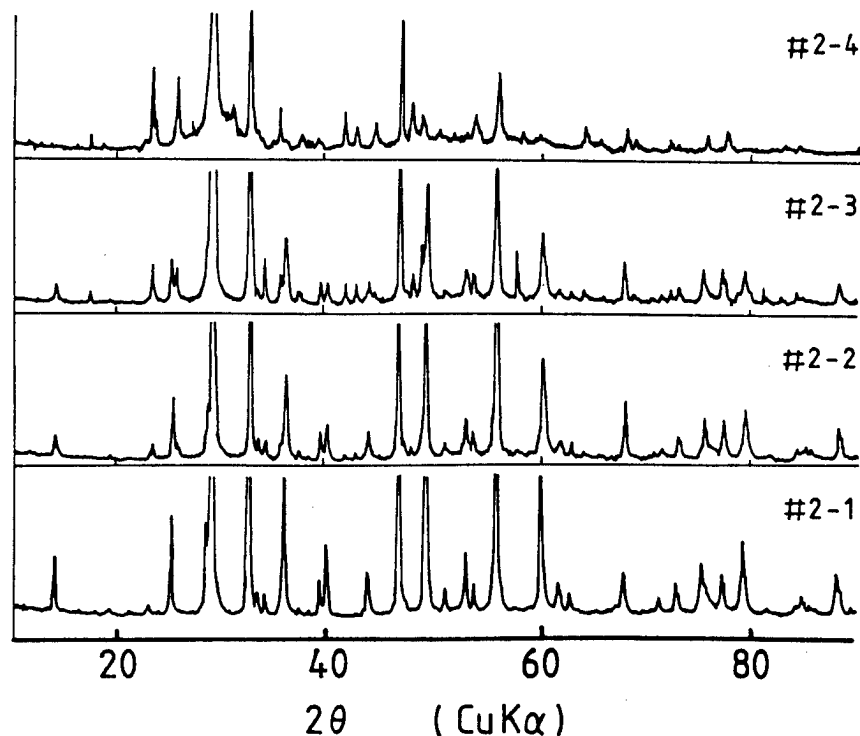
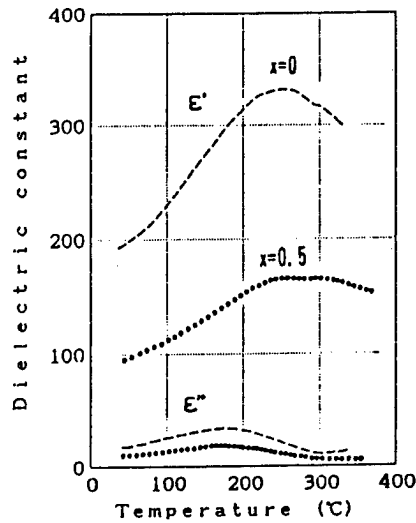


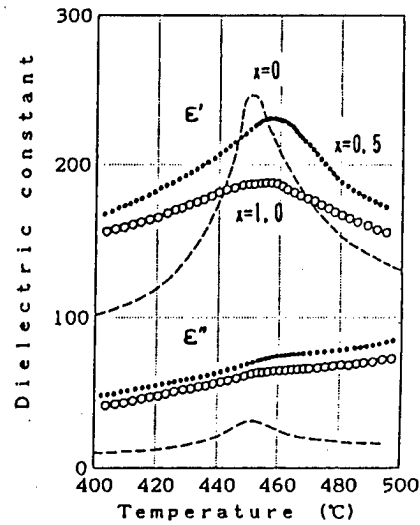
Fig.2 X-ray powder diffraction from the system $\text{SrBi}_{2-x}\text{Tl}_x\text{Nb}_2\text{O}_9$.

4. DIELECTRIC MEASUREMENTS

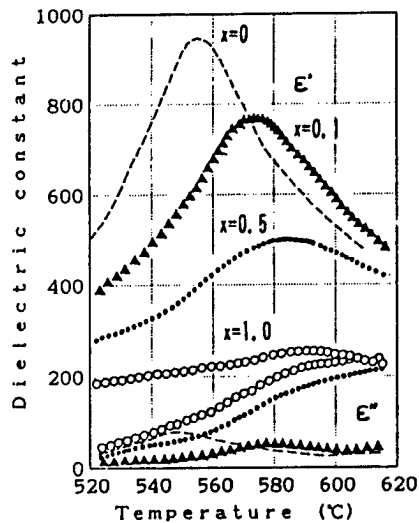
The dielectric constants measured at 1MHz for pellet samples electroded with silver paste are demonstrated in Fig.3(1)~(3). The peak temperature of the real part of the dielectric constants ϵ' correspond to ferroelectric Curie point T_C . With increase of Tl-concentration, ferroelectric T_C 's tend to shift higher temperatures as seen in these figures. At the same time, imaginary part of the dielectric constant ϵ'' increased and the dielectric measurement was not attainable in the high concentration range because of anomalous increase in loss tangent ϵ'/ϵ'' .



(1) #1 : $\text{BaBi}_{2-x}\text{Tl}_x\text{Nb}_2\text{O}_9$



(2) #2 : $\text{SrBi}_{2-x}\text{Tl}_x\text{Nb}_2\text{O}_9$



(3) #3 : $\text{PbBi}_{2-x}\text{Tl}_x\text{Nb}_2\text{O}_9$

Fig.3 Temperature dependence of the dielectric constants of Tl-substituted systems [9].

5. DISCUSSION

Much work has been conducted on the mixed systems of $\text{Bi}_4\text{Ti}_3\text{O}_{12}$ -family ferroelectrics [8]. However almost all efforts are to replace a site on pseudo-perovskite layers by other elements such as rare-earth [10]. For example, ferroelectric T_C -change in the system $\text{Pb}_{1-x}(\text{NaLa})_{x/2}\text{Bi}_2\text{Nb}_2\text{O}_9$ which corresponds to

the series here has also been reported by Takenaka [11]. The aim of these investigations is to lower ferroelectric T_C 's as a practical use of high dielectric constant materials around room temperature region. In such cases, the lowering of ferroelectric T_C with substitutions has been observed, in contrast to the tendency observed here. Although substantial amount of Tl-inclusion is still open, the present result gives a possibility to imply that an amount of Tl can be soluble into Bi_2O_2 layers.

However, within the present firing condition, it seems to be difficult to synthesize a layer-material like $\text{MTl}_2\text{Nb}_2\text{O}_9$, which is fully replaced by Tl_2O_2 layer. This situation is very different from the case of Tl-double layer high- T_C superconducting materials. Ideally the Tl_2O_2 layer has the charge of $+2e$ as well as Bi_2O_2 layer, but generally, trivalent Tl-ions tend to be reduced to monovalent during firing at high temperatures. If a certain amount of Tl reduced are introduced into Bi-sites in the present Bi-layered structure, the excess charge of the layer like $\text{Bi}_{2-x}\text{Tl}_x\text{O}_2$ deviates from ideal one. This deviation will lead to non-compensation of charges with the pseudo-perovskite layer.

On the other hand, this condition is not so crucial in Tl-double layer high- T_C superconductive materials. Because as a common nature of the high- T_C superconductive materials, the pseudo-perovskite structures of CuO are always accompanied with an oxygen-deficiency and a mixed valent state of Cu-ions. This obviously gives advantage to compensate such a deviated charge of the Tl_2O_2 layer, even if it is much reduced.

We need to conduct more detailed systematic works in further understanding of such a difference between Bi-layered ferroelectrics and superconductors.

We wish to thank Prof. K.Sakata and Dr. T.Takenaka of Science University of Tokyo for giving us valuable informations of Bi layered-oxides.

REFERENCES

1. H.Maeda, Y.Tanaka, M.Fukutomi and T.Asano: Jpn.J.Appl.Phys. 27 L201 (1988).
2. C.Michel, M.Hervieu, M.M.Borel, A.Grandin, F.Deslandes, J.Provost and B.Raveau: Z.Phys. B68 421 (1987).
3. J.Akimitsu, A.Yamazaki, H.Sawa and H.Fujiki: Jpn.J.Appl.Phys. 26 L2080 (1987).
4. E.Takayama-Muromachi, Y.Uchida, A.Ono, F.Izumi, M.Onoda, Y.Matsui, K.Kosuda, S.Takekawa and K.Kato: Jpn.J.Appl.Phys. 27 L556 (1988).
5. S.Kondoh, Y.Ando, M.Onoda, M.Sato and J.Akimitsu: Solid State Commun. 65 55 (1988).
6. Z.Z.Sheng and A.M.Hermann: Nature 332 138 (1988).
7. A.Aurivillius: Arkiv Kemi 1 463(1949).
8. For instance, see Landolt-Bornstein, *Ferroelectrics and Related Materials*, III/16, Subvolume a Oxides (Springer 1981) and references therein.
9. M.Takashige, F.Shimizu, H.Suzuki, S.Sawada and T.Yamaguchi: presented at the 7th International Meeting on Ferroelectricity (Sept. 1989, Saarbrücken), to be published in *Ferroelectrics*.
10. R.W.Wolfe and R.E.Newnham: J.Electrochem.Soc. 116 832 (1969).
11. For instance, T.Takenaka: *Doctor Thesis of Kyoto University*, (1985).

Preparation and Characterization of Certain Cu-Oxides Stabilized in Layered Structures by the Use of High Pressures and High Oxygen Pressures

M. Takano and *Y. Takeda

Institute for Chemical Research, Kyoto University
Uji, Kyoto 611, Japan

*Faculty of Engineering, Mie University
Tsu, Mie 514, Japan

(La, Nd)₂CuO_{4+δ}, ACuO₂ (A: Ba_{1/3}Sr_{2/3}), and R₂CuO₄ (R: Y, Dy, Ho, Er, Tm) crystallizing in the Nd₂CuO₄-type structure with or without using KClO₄ as an oxygen donor. Related layered oxides, Sr₂FeO₄, Sr₃Fe₂O₇, and (La,Sr)₂NiO₄, in which the metallic 3d levels almost overlap the oxygen 2p levels and "unusual" electronic states are realized, have also been studied.

All the "High-T_c" Cu-oxide superconductors commonly contain two-dimensional CuO₂ sheets. A pair of Cu ions neighboring each other within a sheet share a coordinating oxide ion, while a pair of Cu ions separated from each other in subsequent sheets are never connected in that way. Blocks like /SrO/BiO/BiO/SrO/ and sheets like /Ca/ intervene between successive CuO₂ sheets [1,2], and these play an essential role in controlling oxidation and reduction of the CuO₂ sheets. Magnetic coupling between subsequent CuO₂ sheets must be stronger, if the intervening blocks are thinner. It is a tempting idea to relate the well-known increase in T_c with m in Bi₂Sr₂Ca_{m-1}Cu_mO_z to development of three-dimensional magnetic correlation. On the other hand, Tl₂Ba₂CuO_z changes its T_c from 0K (normal metal state) to above 80 K as oxygen content is decreased only by Δz=-0.1 [3]. Since the increase in T_c is not terminated by saturation but by a structural instability due to oxygen reduction, the T_c-upon-m dependence in Tl₂Ba₂Ca_{m-1}Cu_mO_z is much less remarkable than that for the corresponding Bi-based series. It may be factors like energy gaps between Cu 3d_{z²}, Cu3d_{x²-y²}, and O2p_σ influenced by structural details that most strongly affects T_c, rather than the development of a three dimensional magnetic correlation with increasing m.

Thus, detailed studies of the composition and structure of the intervening blocks and sheets are very important from the viewpoint of solid state chemistry. And finding of new types of blocks should have great impact.

It is interesting to notice here that lattice mismatch between a CuO₂ sheet and an intervening block often modifies the composition and structure of the block. For example, La₂CuO₄ tends to be excess in oxygen, and this tendency may be caused by such a mismatch. The tolerance factor for this compound, $t = (r_{\text{La}^{3+}} + r_{\text{O}^{2-}}) / 2^{1/2} (r_{\text{Cu}^{2+}} + r_{\text{O}^{2-}})$, is considerably smaller than the ideal value of unity. Incorporation of excess oxygen into interstitial sites between a pair of LaO layers as suggested Jorgensen et al [4], may be interpreted to contribute to relaxing the mismatch by expanding the LaO lattice. If so, substitution of a smaller rare earth ion like Nd³⁺ for La³⁺ would enhance the above tendency. According to our experience, in fact, the Nd-for-La substitution strongly facilitates the oxygen incorporation, and a bulky superconductor with T_c=38K has been formed by treating La_{1.8}Nd_{0.2}CuO_z under 60 kb at 1050 °C for 0.5h [5]. The

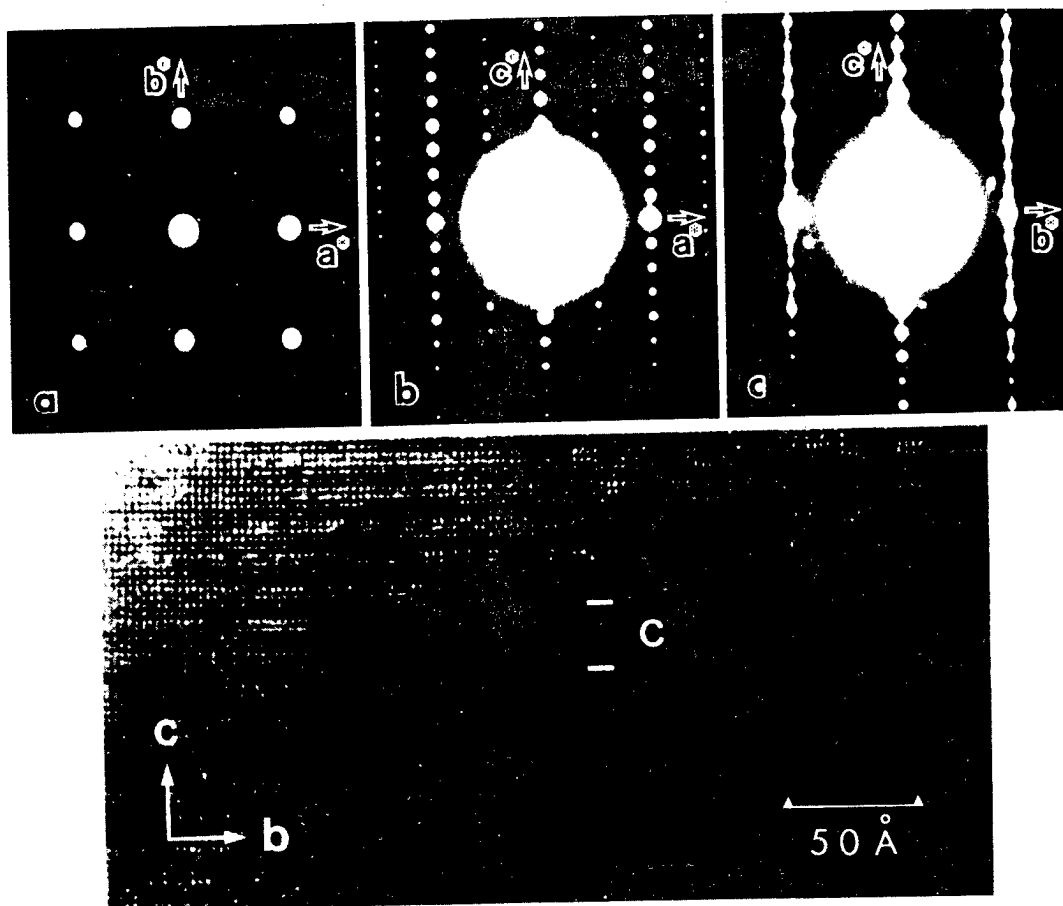


Fig. 1 ED patterns (upper) and a TEM image (lower) of $\text{Bi}_{2-x+y}\text{Pb}_x\text{Sr}_{2-y}\text{Cu}_{1+y/4}\text{O}_z$ with $(x, y) = (0.4, 0.125)$, a modulation-free superconductor with $T_c = 14$ K.

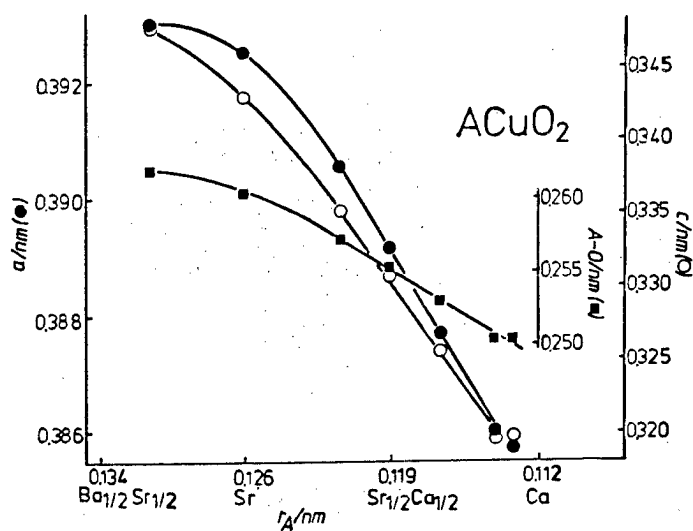


Fig. 2 Lattice constants ($a/2 = \text{Cu-O}$ bond length) and the A-O bond length of ACuO_2 stabilized under high pressure.

lattice constants before (as prepared in an oxygen stream of 1 atm) and after the treatment are $(a/A, b/A, c/A)=(5.349, 5.409, 13.112)$ and $(5.346, 5.389, 13.201)$, respectively. The elongation of the c axis due to oxygen incorporation is remarkable. On the other hand, $T_c=45K$ according to a preliminary study of La_2CuO_4 prepared in a similar way.

Quite similarly to the above, excess oxygen is incorporated in the superconductors in the Bi-Sr-Ca-Cu-O system, not randomly as above but in an ordered way in "Bi-dilute" sections [6]. And this causes a structural modulation. The $m=1$ phase has exact compositions of $Bi_{2+x}Sr_{2-x}Cu_{1+y}O_z$ ($0.1 < x < 0.6$ and $0 < y < x/2$), and superconductivity can be seen only for $0.1 < x \leq 0.13$ as reported already [7]. This means that the positive charge due to the Bi/Sr > 1 composition is overcompensated by excess oxygen. T_c is 7K, being only 1/15 that of the 2223 phase and only 1/12 that of $Tl_2Ba_2CuO_z$. One possibility of the great reduction may be assigned to the serious puckering of the CuO_2 sheet in the modulated structure. By substituting large Pb^{2+} for small Bi^{3+} , a modulation free phase has been found to be formed [8]. The ED patterns and TEM image shown in Fig. 1 reveal the absence of any modulation. T_c is raised, however, to only 16K at the present stage.

It was found by Tokura et al. [2] that CuO_2 sheets without any apical oxygen atoms show superconductivity if these are reduced and, therefore, carry excess electrons. Since before this finding the role of the central CuO_2 sheet having no apical oxygen atoms in the $m=3$ phase in the Bi- and Tl-based 2223 phases has long been puzzling for the present authors, and preparation and characterization of $ACuO_2$ (A: alkaline earth) have been tried. $SrCuO_2$, for example, can be obtained easily under ambient pressure but does not crystallize in layered structure. However, application of high pressure induces a structural transition to the desired structure in which single CuO_2 sheets and single Sr sheets are stacked alternatively. The high pressure phase has a higher density. The composition range stabilized in this structure under 60 kb ranges at least from

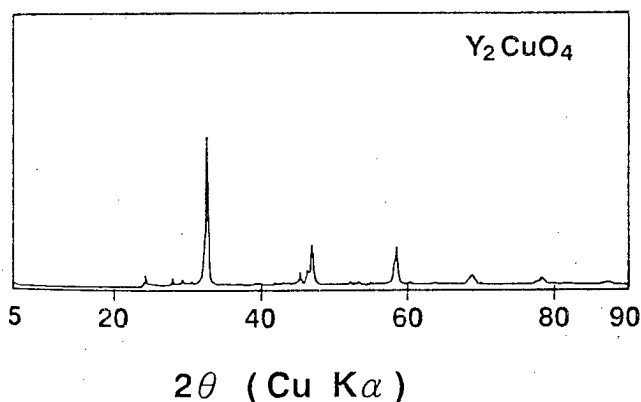


Fig. 3 XRD pattern of Y_2CuO_4 crystallizing in the Nd_2CuO_4 -type structure stabilized under high pressure.

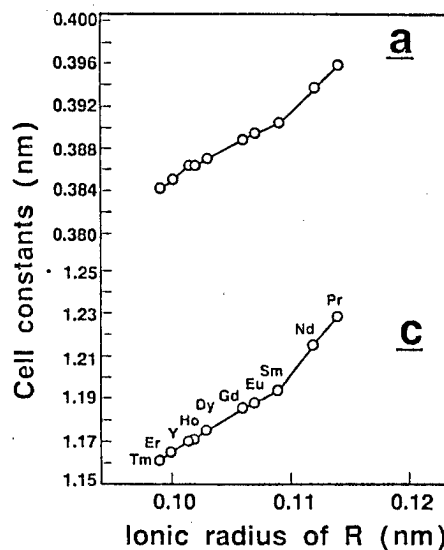


Fig. 4 Lattice constants ($a/2 = Cu-O$ bond length) of R_2CuO_4 crystallizing in the Nd_2CuO_4 -type structure.

$A = \text{Ba}_{1/3}\text{Sr}_{2/3}$ to $\text{Sr}_{2/3}\text{Ca}_{1/3}$. In the course of this study, Siegrist et al. and Yamane et al. [9,10]. reported that this structure can be formed around $A = \text{Sr}_{0.1}\text{Ca}_{0.9}$ even under ambient pressure. The composition dependence of the lattice constants is shown in Fig. 2.

Another result obtained by using high pressure concerns stabilization of the Nd_2CuO_4 -type structure for small rare earth ions, Y, Dy, Ho, Er, and Tm [11]. Under ambient pressure R_2CuO_4 with R ranging from Pr-Gd is stabilized in this structure. By treating under 6×10^4 atm at 950°C the range of R has been found to be widened. The XRD pattern of nearly monophasic Y_2CuO_4 is shown in Fig. 3, and the cell constants are plotted as a function of R in Fig. 4. In the Nd_2CuO_4 -type structure an R ion is in a cubic eight-fold coordination of oxide ions. From a simple geometrical consideration it is expected that there holds a relation of $r_R/r_O \geq 0.73$ between the ionic radii of R and oxygen. It ranges from 0.81 to 0.76 for R=Pr-Gd for which the Nd_2CuO_4 type structure can be stabilized under ambient pressure. The range can be extended under the high pressure used over 0.74 to 0.71 for R=Y-Tm. Thus, the simple rule for the eight-fold coordination of $r_R/r_O \geq 0.73$ may be considered to be slightly relaxed by using the high pressure. The tetragonal cell constants, a and c, decrease linearly with decreasing R ion size till Yb destabilizes this structure. It is remarkable that the Cu-O bond is shortened to 0.1922nm at R=Tm. This value is nearly the same as that in CaCuO_2 (see Fig. 2) and also as those in $\text{La}_2\text{SrCu}_2\text{O}_6$ (=0.193nm) and $\text{La}_{1.9}\text{Ca}_{1.1}\text{Cu}_2\text{O}_6$ (=0.191nm) in both of which the Cu ions are coordinated square pyramidally. Injection of carriers to these two kinds of high pressure phases is under way.

Another challenge to solid state chemists would be to find "High- T_c " superconductivity in compounds containing transition metals other than copper. It is interesting to notice that the metallic 3d levels decrease in energy as the atomic number increases. These approach and may overlap the oxygen 2p levels and, as a result, various unusual electronic states are realized. In perovskites containing Fe^{4+} like $\text{Ca}_{1-x}\text{Sr}_x\text{FeO}_3$ and $\text{Sr}_{1-x}\text{La}_x\text{FeO}_3$, a charge disproportionation formed as $2\text{Fe}^{4+}(t_{2g}^3 e_g^1) \rightleftharpoons \text{Fe}^{(4+\delta)}(t_{2g}^3 e_g^{1-\delta}) + \text{Fe}^{(4-\delta)}(t_{2g}^3 e_g^{1+\delta})$ generally occurs at low temperatures [12]. The degree of disproportionation, δ , strongly depends upon the kind of the "A" cation: $\delta=0$ for SrFeO_3 . More recently, the disproportionation has been found to occur in $\text{Sr}_3\text{Fe}_2\text{O}_7$ and Sr_2FeO_4 , suggesting that the lattice dimension can influence the ground state. In comparison with the similar case of $\text{BaBi}^{(4+\delta)}\text{Bi}^{(4-\delta)}\text{O}_3$ which remains diamagnetic, possible contribution of spin-spin interactions between the Fe ions and anions carrying holes should be examined in the future.

Structural transport, and magnetic data for the system $\text{La}_{2-x}\text{Sr}_x\text{NiO}_4$, $0 \leq x \leq 1.6$, have been studied [14]. The oxygen content of the system was controlled by annealing under various oxygen partial pressures below 150 atm. A Rietveld analysis of the room-temperature powder XRD data showed that the tetragonal distortion of the NiO_6 octahedra decreases monotonically with increasing x for $0 \leq x \leq 1.4$, but the La(Sr)-O(2) bond length increases anomalously in the interval $0 \leq x \leq 0.6$. A semiconductor-metal transition decreases monotonically with increasing x from about 675 K (x=0) to 20 K (x=1.2). Samples with $x > 1.0$ exhibited a weak ferromagnetic moment at 5 K and the onset of a positive component in the Hall effect. And metallic conduction persists down to 4 K for $x \geq 2$ as shown in Fig.5. Comparison of the $\text{La}_{2-x}\text{Sr}_x\text{CuO}_4$ and $\text{La}_{2-x}\text{Sr}_x\text{NiO}_4$ systems shows that the superconductive copper oxides have the equilibrium $\text{Cu}^{3+} + \text{O}^{2-} = \text{Cu}^{2+} + \text{O}^-$ shifted to the right and, for x=0, antiferromagnetic correlation in a half-filled $\sigma_{x^2-y^2}$ band whereas the weakly ferromagnetic nickel oxides have the equilibrium $\text{Ni}^{4+} + \text{O}^{2-} = \text{Ni}^{3+}$

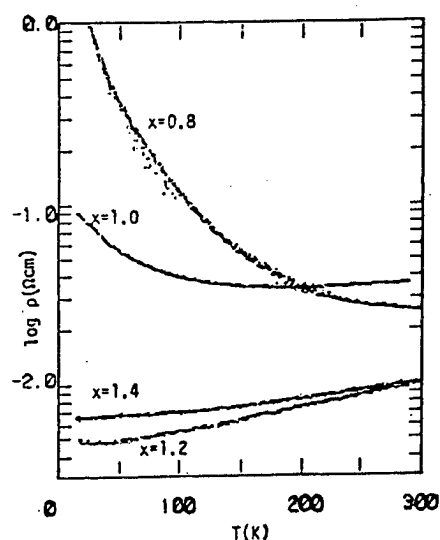


Fig. 5 Temperature dependence of electrical resistivity of $\text{La}_{2-x}\text{Sr}_x\text{NiO}_4$.

+0⁻ shifted to the right, but ferromagnetic correlations in a quarter-filled σ^* band.

In summary, both Fe^{4+} and Ni^{3+} allow ferromagnetic correlations due to the electronic states of e_g^1 parentage. Considerably strong antiferromagnetic correlations may be expected from Ni^{2+} with an electronic state of e_g^3 parentage, though studies of oxides containing this interesting cation have been little reported. The author's group has begun to prepare and characterize oxides containing Ni^{2+} .

The authors heartily thank his coworkers in Mie Univ., Kyoto Univ., Okayama Univ., and Kobe Steel, Ltd. for allowing him to summarize the experimental results.

Reference

- [1] J. B. Torrance, Y. Tokura, A. I. Nazzari, A. Bezingue, T. C. Huang, and S. S. P. Parkin, *Phys. Rev. Lett.* **61** (1988) 1127.
- [2] Y. Tokura, H. Takagi, and S. Uchida, *Nature* **337** (1989) 345.
- [3] Y. Shimakawa, Y. Kubo, T. Manako, and H. Igarashi, *Phys. Rev. B*, in press.
- [4] J. D. Jorgensen et al., *Phys. Rev. B* **38** (1988) 11337.
- [5] Y. Takeda and M. Takano, in preparation.
- [6] A. Yamamoto, M. Onoda, E. Takayama-Muromachi, F. Izumi, T. Ishigaki, and H. Asano, *Phys. Rev. B*, in press.
- [7] Y. Ikeda, H. Ito, S. Shimomura, Y. Oue, K. Inaba, Z. Hiroi, and M. Takano, *Physica C* **159** (1989) 93.
- [8] Y. Ikeda, Z. Hiroi, H. Ito, S. Shimomura, M. Takano, and Y. Bando, *Physica C*, in press.
- [9] T. Shiegt, S. M. Zahurak, D. W. Murphy, and R. S. Roth, *Nature* **334** (1988) 231.
- [10] H. Yamane, Y. Miyazaki, and T. Hirai, *J. Cer. Soc. Jpn.* **97** (1989) 143.
- [11] H. Okada, M. Takano, and Y. Takeda *Physica C*, in press.
- [12] Review: M. Takano and Y. Takeda, *Bull. Inst. Chem. Res., Kyoto Univ.* **61** (1983) 406.
- [13] M. Takano and Y. Takeda, in preparation.
- [14] Y. Takeda, R. Kanno, M. Sakano, O. Yamamoto, M. Takano, Y. Bando, H. Akinaga, K. Takita, and J. B. Goodenough, *Mat. Res. Bull.*, in press.

Absence of superconductivity in the $(\text{La}_{1-x}\text{Sr}_x)_2\text{NiO}_4$ system

M. Takahashi, H. Iwawaki, N. Kobayashi, S. Hosoya,
T. Fukuda and Y. Muto

Institute for Materials Research, Tohoku University
2-1-1 Katahira, Sendai, Japan

The $(\text{La}_{1-x}\text{Sr}_x)_2\text{NiO}_4$ system which is related to high- T_c superconductor $(\text{La}_{1-x}\text{Sr}_x)_2\text{CuO}_4$ has been studied. The electrical resistivity of samples ($0 \leq x \leq 0.4$) has been measured between 4.2 K and 300 K. All the samples showed semiconductor-like behavior and we could not find superconductivity. Structural and electrical properties are discussed on the basis of powder X-ray diffraction analysis and resistivity measurement.

The discovery of High- T_c superconducting oxides $(\text{La}_{1-x}\text{A}_x)_2\text{CuO}_{4-\delta}$ ^(1,2), where A is Ba or Sr, has initiated a considerable research effort on these and related compounds. The $(\text{La}_{1-x}\text{Sr}_x)_2\text{NiO}_4$ system, which has the K_2NiF_4 structure⁽³⁾, is structurally very similar to $(\text{La}_{1-x}\text{Sr}_x)_2\text{CuO}_{4-\delta}$, and so its physical properties are of much interest in contrast with $(\text{La}_{1-x}\text{Sr}_x)_2\text{CuO}_{4-\delta}$. Electrical transport and magnetic properties of the parent compound $\text{La}_2\text{NiO}_{4\pm\delta}$ have already been reported by various groups⁽⁴⁻⁶⁾. Their experiments show that $\text{La}_2\text{NiO}_{4\pm\delta}$ is semiconductor-like in the sense that at low temperature its resistivity rises with decreasing temperature and has a metal-semiconductor transition at about 500-600 K, and that it is also an antiferromagnet with Néel temperature sensitive to oxygen nonstoichiometry δ . On the other hand, the electrical transport of Sr-doped $(\text{La}_{1-x}\text{Sr}_x)_2\text{NiO}_4$ was studied by J. Gopalakrishnan et al.⁽³⁾ and M. Khairy et al.⁽⁷⁾. The temperature dependence of its resistivity, however, is not well-known. Recently, J. M. Honig et al.⁽⁸⁾ reported that the $(\text{La}_{1-x}\text{Sr}_x)_2\text{NiO}_4$ system became superconducting at temperatures as high as 70 K. If this discovery is verified by other researchers, it will become the first copperless superconductor with T_c greater than about 30 K. In the present work, we have studied the temperature dependence of the resistivity and the crystal structure of the $(\text{La}_{1-x}\text{Sr}_x)_2\text{NiO}_4$ system ($0 \leq x \leq 0.4$) in order to re-examine of the superconductivity in this system.⁽⁸⁾

All the samples were prepared by solid state reaction. The starting materials La_2O_3 , NiO and SrCO_3 of 4N purity were mixed in the appropriate ratio, pelletized, followed by pre-heating at 1100°C for 12 hours in air. After this treatment, the pre-heated samples were ground into powder again, pelletized and sintered at 1200°C ($x < 0.1$) or 1250°C ($0.1 \leq x \leq 0.4$) for 48 hours in air. Furthermore a part of the sample with $x = 0.1$ was annealed in oxygen gas at 500°C for 24 hours or CO/ CO_2 gas mixture at 1000°C for 20 hours. The flow ratio of CO to CO_2 is 1:100 or 5:100. The powder X-ray diffraction analyses were made at room temperature using $\text{CuK}\alpha$ radiation. Structural calculations were made with a least square method. For electrical measurements, the samples were cut into a shape of bars. Electrical

resistivity was measured by the four-probe method. The measurements on all the samples were carried out in the temperature range of 4.2-300 K.

The powder X-ray diffraction analyses showed that all the samples were crystallized in a single phase with the tetragonal K_2NiF_4 structure. The lattice parameters (a and c) calculated from the powder X-ray diffraction patterns are given in Fig.1. In Fig. 1, a decreases up to $x = 0.3$ with increasing x and becomes almost constant in the region of $x \geq 0.3$. On the other hand, as x increases, c increases in low concentrations and decreases after taking the maximum value near $x = 0.2$. These x -dependence of the lattice parameters are nearly consistent with the results of early works reported by J. Gopalakrishnan et al.⁽³⁾. The above results are explained as follows. If La^{3+} in La_2NiO_4 is substituted by Sr^{2+} , it is necessary for preserving electroneutrality that the valence of Ni changes from +2 to +3. The trivalent nickel produced by Sr substitution is considered to be in the low spin state $t_{2g}^6e_g^1$. Therefore, the Ni^{3+} -O octahedra are susceptible to Jahn-Teller effect. The increase of the c -axis and the decrease of the a -axis in the region of $x \leq 0.25$ show that a single e_g electron is in the $d_{3z^2-r^2}$ orbital, and that the Ni^{3+} -O bonds parallel to the c -axis become longer and those perpendicular to the c -axis become shorter. The decrease of the c -axis in the region of $x \geq 0.25$ may indicate that the orbital of the above e_g electron changes from the $d_{3z^2-r^2}$ to the $d_{x^2-y^2}$.

Fig.2 shows the temperature dependence of resistivity in $\log \rho$ versus $1000/T$ plot. In the temperature region of 4.2-300 K, all the samples show semiconductor-like behaviors. At lower temperature the resistivity of the samples with lower x diverges. $\log \rho$ of the sample without Sr^{2+} substitution ($x = 0$) is linear against $1/T$ above 100 K and shows an activation-type conductivity. The behaviors of Sr^{2+} -substituted samples, however, lose linearity at higher temperature. The activation energies calculated from the initial slope are shown in Fig.3. While in the region of $x \leq 0.25$ they show no remarkable change, above $x = 0.25$ they decrease suddenly, showing that samples become more conductive. This result supports the above explanations that near $x = 0.25$ the electronic configuration changes from $t_{2g}^6d_{3z^2-r^2}^1$ to $t_{2g}^6d_{x^2-y^2}^1$ and the c -axis takes the maximum value. It is different from the concentration dependence of the $(La_{1-x}Sr_x)_2CuO_4$ ⁽⁹⁾ system, which becomes more conductive as x increases.

Furthermore, the samples with $x = 0.1$ were annealed under three different conditions in order to change the amount of oxygen. Fig. 4 shows the resistivities of those samples. All of them remain semiconductor-like. It is found, however, that the more deficient sample in oxygen has lower activation energy, being more conductive. Taking this result into account, the above assumption that Sr substitution is not accompanied by oxygen defects but by oxidation of Ni.

In summary, we have studied electrical resistivity of the $(La_{1-x}Sr_x)_2NiO_4$ system. All the samples show semiconductor-like behavior ($4.2 \text{ K} < T < 300 \text{ K}$) and their x dependence can be explained in terms of the electronic configuration of Ni^{3+} . However, it would not be understood by the same picture as the $(La_{1-x}Sr_x)_2CuO_4$ system. More experiments are required for detailed discussions. In conclusion, we can not find any superconducting behavior in this system in concentrations below $x = 0.4$.

References

1. J. G. Bednorz and K. A. Müller, Z. Phys. **B46**, 189 (1986)
2. S. Uchida, H. Takagi, K. Kitazawa and S. Tanaka, Jpn. J. Appl. Phys. Lett. **26**, L1 (1987)
3. J. Gopalakrishnan, G. Colsmann and B. Reuter, J. Solid State Chem. **22**, 145 (1977)
4. M. Sayer and P. Odier, J. Solid State Chem. **67**, 26 (1987)
5. G. Aepli and D. J. Buttrey, Phys. Rev. Lett. **61**, 203 (1988)
6. D. J. Buttrey, J. M. Honig and C. N. R. Rao, J. Solid State Chem. **64**, 287 (1986)
7. M. Khairy, P. Odier and J. Choisnet, J. Phys. Colloq. C1 **47**, C1-831 (1986)
8. Z. Kakol, J. Spalek and J. M. Honig, J. Solid State Chem. **79**, 288 (1989)
9. Z. Kakol, J. Spalek and J. M. Honig, Solid State Commun. **71**, 283 (1989)

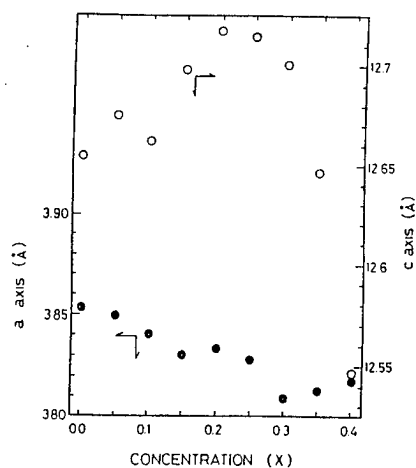


Fig.1 Concentration dependence of lattice parameters.

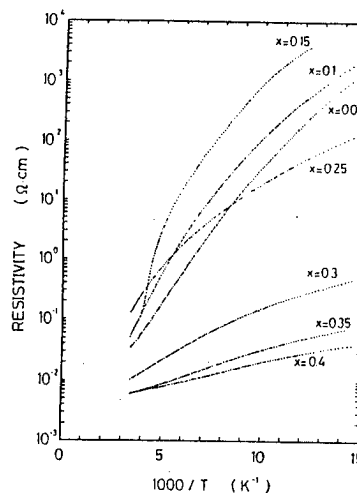


Fig.2 Semilogarithmic plot of R vs. 1/T.

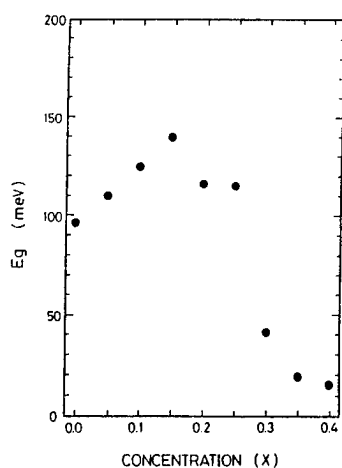


Fig.3 Concentration dependence of the activation energy.

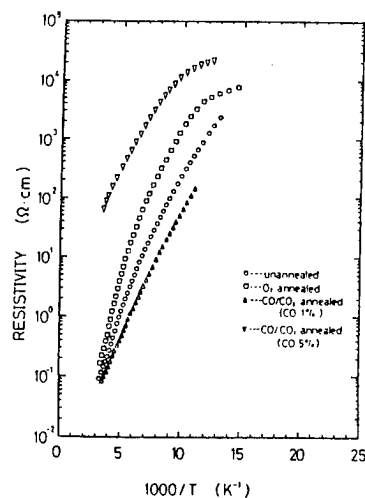


Fig.4 R vs 1/T plot of the samples annealed under various conditions.

Tsuyoshi TAMEGAI, Chiho OKADA, and Yasuhiro IYE

*The Institute for Solid State Physics, The University of Tokyo,
Roppongi, Minato-ku, Tokyo 106 Japan*

The effect of strontium and oxygen content variation on the transport properties of the $La_{2-x}Sr_{1+x}Cu_2O_{6+y}$ system was systematically studied. Discussion on the reason for the absence of superconductivity in this system is given.

1. Introduction

A vast accumulation of the experimental studies on the high T_c superconductors suggests the following empirical necessary condition for the occurrence of superconductivity; the presence of two-dimensional copper oxygen layers and the carrier density in the appropriate range. In the $La_{2-x}Sr_xCuO_4$ system [1], for instance, superconductivity occurs in the range of $0.05 < x < 0.3$, with highest transition temperature for $x \approx 0.15$. One may ask a question whether these conditions are necessary and/or sufficient for the occurrence of high temperature superconductivity. The former part of the question can be expressed alternatively, whether the mechanisms of high temperature superconductivity is same for the copper oxides and the bismuth oxides. Another class of systems relevant to this question are $La_4BaCu_5O_{13-y}$ [2], and $La_{8-x}Sr_xCu_8O_{20-y}$ [3], having three dimensional structure. Though these compounds show metallic behavior down to the lowest temperature, they do not show superconductivity. The $La_{2-x}Sr_{1+x}Cu_2O_{6+y}$ system [4], which has two dimensional copper oxygen double layers similar to those in $YBa_2Cu_3O_{7-y}$, may be relevant to the latter part of the question. Though it satisfies the above conditions and shows metallic behavior at least around room temperature, superconductivity is not found in this system down to 0.3K [5]. In this paper, we report a systematic study of the transport properties of this system by varying strontium and oxygen contents.

2. Structure and Synthesis

The ideal structure of $La_2SrCu_2O_6$ is shown in Fig. 1. This structure is realized in $La_{2-x}Sr_{1+x}Cu_2O_{6+y}$ for $0 < x < 0.2$. In the actual structure, excess oxygen atoms occupy the sites between two neighboring CuO_2 planes. La and Sr atoms, not shown in this figure, share their sites statistically. In an isostructural $La_{2-x}Ca_{1+x}Cu_2O_{6+y}$ system, the range of calcium content is much narrower, because La and Ca with their different ionic radii do not exchange their sites so easily as in the La and Sr case. The calcium layer do not readily accommodate the excess oxygen atoms, because of the small ionic radius of Ca.

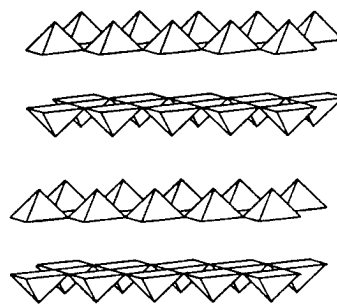


Fig. 1

Schematic view of the idealized structure of $La_2SrCu_2O_6$.

Samples were prepared by the standard solid state reaction of La_2O_3 , SrCO_3 and CuO . The final heat treatment was performed at 1060°C for all samples with different strontium contents. Single phased samples were obtained in the range of strontium content $0 < x < 0.20$. For samples with $x \leq 0$, X-ray peaks of $\text{La}_{2-x}\text{Sr}_x\text{CuO}_4$ became discernible as an impurity phase. On the other hand, with increasing the strontium content up to $x > 0.15$, the $\text{La}_{2-x}\text{Sr}_{1+x}\text{Cu}_2\text{O}_{6+y}$ structure gradually turns into another structure with ordered oxygen vacancies, $\text{La}_{1+x}\text{Sr}_{2-x}\text{Cu}_2\text{O}_{5.5+y}$ [6].

3. Effect of Oxygen Stoichiometry

For a systematic study of the effect of oxygen stoichiometry, a batch of samples with the strontium content $x = 0.1$, $\text{La}_{1.9}\text{Sr}_{1.1}\text{Cu}_2\text{O}_{6+y}$ were prepared. Samples with different oxygen content were prepared by quenching them from different temperatures, T_q . After fully oxygenized in an oxygen flow, samples were heated in a vertical furnace at different temperatures for 20 hours in air. Then they were quenched into liquid nitrogen. Figure 2 shows the temperature dependence of the resistivity of $\text{La}_{1.9}\text{Sr}_{1.1}\text{Cu}_2\text{O}_{6+y}$ quenched from different temperatures. All the samples show little temperature dependence around room temperature, but upturn of resistivity is seen at low temperatures. Samples quenched from higher temperatures show higher resistivities at room temperature and the upturn of the resistivity occurs from higher temperatures. It should be noted that the sample quenched from higher temperature have a positive slope around room temperature. The hole number per copper atom estimated from the Hall coefficient at room temperature assuming single carrier conduction is 0.056 for the sample quenched from 1000°C . This agrees well with the value, 0.05, expected when the hole is supplied only by the strontium. Thus, the excess oxygen content is $y \approx 0$ in this high temperature quenched sample. The behavior of this high T_q sample is very similar to that of $\text{La}_{1.9}\text{Ca}_{1.1}\text{Cu}_2\text{O}_6$, which has virtually no excess oxygen. On the other hand, for the furnace-cooled $\text{La}_{1.9}\text{Sr}_{1.1}\text{Cu}_2\text{O}_{6+y}$ sample, the oxygen content was determined by iodometry as $y = 0.25$. This corresponds to a hole number per copper of 0.30. Thus, this furnace cooled sample may be classified as an "overdoped" system in comparison with other copper oxide systems which show high temperature superconductivity.

Figure 3 shows the Hall coefficient of $\text{La}_{1.9}\text{Sr}_{1.1}\text{Cu}_2\text{O}_{6+y}$ at room temperature as a function of quenching temperature, T_q . The increase of Hall coefficient occurs for $T_q > \sim 500^\circ\text{C}$. Thermogravimetric analyses show that the oxygen loss takes place above 450°C in $\text{La}_{1.9}\text{Sr}_{1.1}\text{Cu}_2\text{O}_{6+y}$. The T_q -dependence shown in Fig. 3 is consistent with this result. The data in Fig. 3 prove that the high temperature quenching process indeed decreases the hole density in this system.

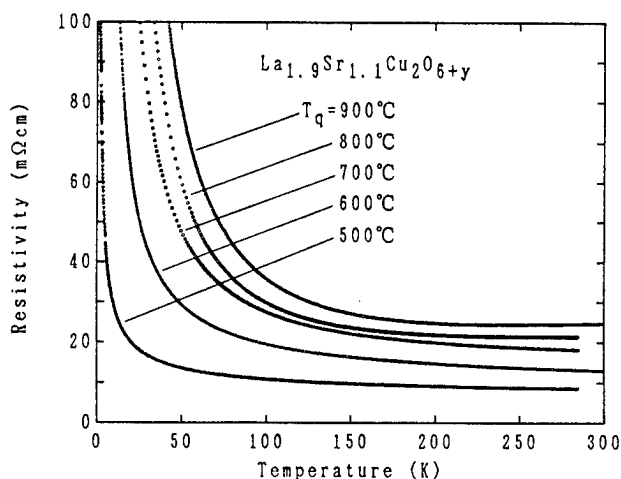


Fig. 2 Temperature dependence of resistivity of $\text{La}_{1.9}\text{Sr}_{1.1}\text{Cu}_2\text{O}_{6+y}$ samples with different y prepared by quenching from different temperatures.

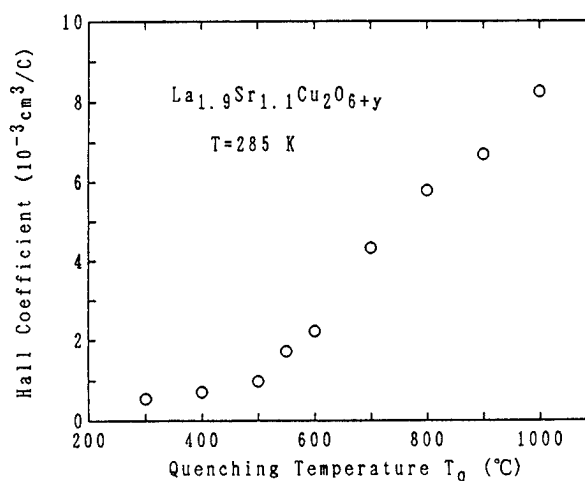


Fig. 3 The Hall coefficient of $\text{La}_{1.9}\text{Sr}_{1.1}\text{Cu}_2\text{O}_{6+y}$ at room temperature as a function of the quenching temperature, T_q .

Figure 4 shows the temperature dependence of the Hall coefficient for $La_{1.9}Sr_{1.1}Cu_2O_{6+y}$ having different T_q . The Hall coefficient is a smooth function of the temperature and slightly increases with lowering temperature as in the case for fully oxygenized sample [5].

Based on the chemical estimate and the Hall measurement, we can conclude that the present series of $La_{1.9}Sr_{1.1}Cu_2O_{6+y}$ samples with different T_q cover a rather wide (from "underdoped" to "overdoped") range and that the system does not undergo superconducting transition at any hole density.

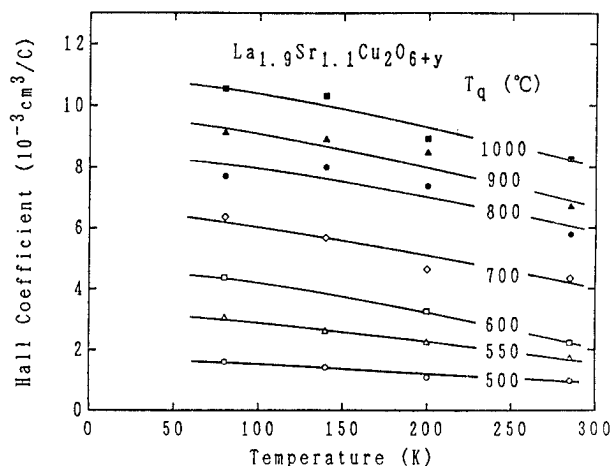


Fig. 4 Temperature dependence of Hall coefficient of $La_{1.9}Sr_{1.1}Cu_2O_{6+y}$ quenched from different temperatures.

4. Effect of Strontium Content Variation

Figure 5 shows the temperature dependence of resistivity of $La_{2-x}Sr_{1+x}Cu_2O_{6+y}$ having different strontium content. Samples were fully oxygenized by being furnace cooled in oxygen flow. Regardless of the strontium content, all the sample show similar metallic behavior around room temperature and slight upturn of the resistivity at low temperatures. An anomaly due to the presence of the superconducting phase of $La_{2-x}Sr_xCuO_4$ is evident around 20K for the sample with $x = -0.05$.

The temperature dependences of the Hall coefficients for $La_{2-x}Sr_{1+x}Cu_2O_{6+y}$ with different strontium content are shown in Fig. 6. Except for the sample with $x = -0.05$, the Hall coefficient is positive and its temperature dependence is weak. The drastically different behavior of the $x = -0.05$ sample should be taken with caution at the present stage, because we can not estimate the effect of the impurity phase of $La_{2-x}Sr_xCuO_4$ on the Hall coefficient. Elementary valence counting tells that the hole number per copper in $La_{2-x}Sr_{1+x}Cu_2O_{6+y}$ is given by $0.5x + y$. The roughly constant Hall coefficient for $0.05 \leq x \leq 0.15$ may suggest that the oxygen content changes to compensate the change in the strontium content.

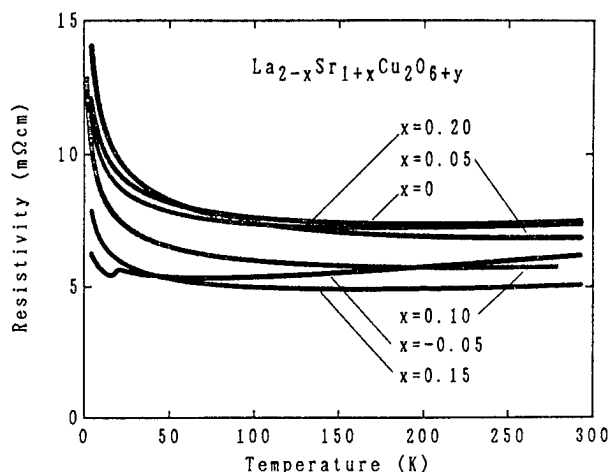


Fig. 5 Temperature dependence of resistivity of $La_{2-x}Sr_{1+x}Cu_2O_{6+y}$ samples with different strontium contents, x .

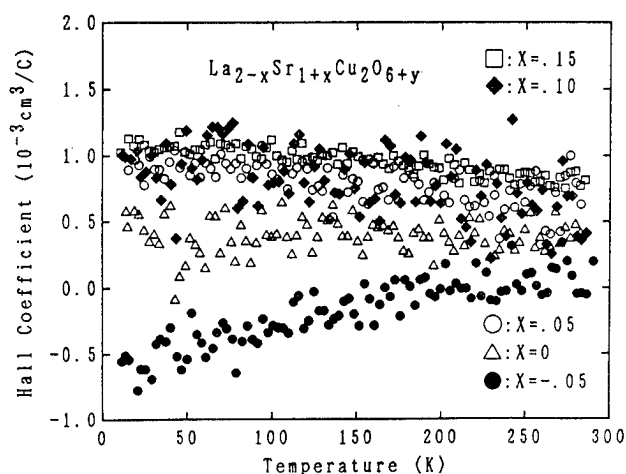


Fig. 6 Temperature dependence of Hall coefficient in the $La_{2-x}Sr_{1+x}Cu_2O_{6+y}$ system with different strontium contents, x .

The trend of the Hall coefficient toward negative sign with decreasing strontium content as seen in the $x = 0$ and -0.05 samples is opposite to what is expected from the apparent decrease of the hole number. This kind of behavior may be related with the fact that the sign of Hall coefficient is negative for the three dimensional copper oxide systems, $La_4BaCu_5O_{13-y}$ and $La_{8-x}Sr_xCu_8O_{20-y}$ [5]. The excess oxygen in the $La_{2-x}Sr_{1+x}Cu_2O_{6+y}$ system would make the system more three-dimensional by connecting two neighboring CuO_2 planes.

5. Conclusions

The $La_{2-x}Sr_{1+x}Cu_2O_{6+y}$ system is an outstanding exception among the layered copper oxides, in the sense that it does not show superconductivity despite the fact that it appears to satisfy the structural and carrier density requirements for the occurrence of high temperature superconductivity. The reason for the absence of superconductivity in the $La_{2-x}Sr_{1+x}Cu_2O_{6+y}$ system, is most likely to be sought in the detrimental effect of excess oxygen atoms inserted between two neighboring CuO_2 layers. One may compare this strong suppressing effect of the midplane oxygen atoms with the relatively mild suppression of transition temperature by copper site substitutions, or the lack of magnetic pair breaking in the rare earth substitution in the $YBa_2Cu_3O_{7-y}$ system. The characteristic low temperature upturn of resistivity in the $La_{2-x}Sr_{1+x}Cu_2O_{6+y}$ system seems to suggest that weak carrier localization is responsible in this temperature range. While the localization effect certainly acts to suppress the potential superconductivity, whether it explains the absence of superconductivity in the $La_{2-x}Sr_{1+x}Cu_2O_{6+y}$ remains to be seen. In this context, it would be interesting if one can dope the $La_{2-x}Sr_{1+x}Cu_2O_{6+y}$ system without introducing excess oxygen atoms.

References

- [1] J.B. Torrance, Y. Tokura, A.I. Nazzari, T.C. Huang, and S.S.P. Parkin, Phys. Rev. Lett. 61 1127 (1988).
- [2] C. Michel, L. Er-Rakho, and B. Raveau, J. Phys. Chem. Solids 49, 451 (1988).
- [3] J.B. Torrance, Y. Tokura, A.I. Nazzari, and S.S.P. Parkin, Phys. Rev. Lett. 60, 542 (1988).
- [4] N. Nguyen, L. Er-Rakho, C. Michel, J. Choisnet, and B. Raveau, Mat. Res. Bull. 15, 891 (1980).
- [5] T. Tamegai, and Y. Iye, Physica C 159, 181 (1989).
- [6] D.M. De Leeuw, C.A.H.A. Mutsaers, G.P.J. Geelen, and C. Langereis J. Solid State Chem. 80 276 (1989).

Anisotropic Properties of $\text{La}_{8-x}\text{Sr}_x\text{Cu}_8\text{O}_{20-\delta}$ Epitaxial Thin Films

T. Murakami, Y. Enomoto and K. Moriwaki

NTT Opto-Electronics Laboratories, Tokai-Mura, Ibaraki Ken 319-11

$\text{La}_{8-x}\text{Sr}_x\text{Cu}_8\text{O}_{20-\delta}$ thin films are epitaxially grown on SrTiO_3 single crystal substrates by rf magnetron sputtering. They exhibit anisotropic electrical properties but the degree of anisotropy is smaller than that found in usual high T_c superconductors. The resistivity in the [001] direction decreases monotonously with temperature decrease, but that in the [100] exhibits a broad peak at about 180K. Such anisotropic behavior can be explained by assuming that this matter has a quasi-one-dimensional electronic structure. Furthermore, the Hall coefficients are negative and decrease rapidly with temperature decrease.

Since the discovery of high T_c superconductivity in K_2NiF_4 type copper oxide,¹⁾ several high T_c copper oxides have been reported and a lot of effort has been devoted to understanding their high T_c mechanism. It is of significant interest that some copper oxides do not exhibit superconductivity even though their structures are similar to those of superconducting oxides. The physical properties of these oxides have been examined only with ceramic samples. Therefore, investigation of single crystalline samples may explain why superconductivity does not appear in these oxides and may also reveal important information about the mechanism of superconductivity.

We have examined the properties of $\text{La}_{8-x}\text{Sr}_x\text{Cu}_8\text{O}_{20-\delta}$ ($1.28 < x < 1.92$), which is a metallic, but nonsuperconducting, copper oxide. Its cubic perovskite structure with channels of oxygen vacancies running along the c-axis and with a sheet and chain Cu-O network was determined by Torrance and co-workers²⁾ and Er-Rakho and co-workers³⁾. Its crystal structure makes this oxide anisotropic three-dimensional. This is different from the strong two-dimensional overlap in high T_c superconducting systems and may take a certain role in suppressing superconductivity. This letter reports experimental results on the anisotropy of transport property of $\text{La}_{6.63}\text{Sr}_{1.33}\text{Cu}_8\text{O}_{20-\delta}$ ($\text{La}_5\text{Sr}_1\text{Cu}_6\text{O}_{15}$) thin films. Hereafter, we abbreviate this compound to L516 from the chemical composition.

Samples used here were L516 thin films grown epitaxially on a SrTiO_3 (110) substrate by the rf magnetron sputtering method. The sputtering target was a compound of $\text{La}_5\text{Sr}_1\text{Cu}_9\text{O}_{18}$ which had excessive Cu to assure correct film composition. Ceramic targets were prepared from an appropriate mixture of La_2O_3 , SrCO_3 , and CuO . The mixed powders were fired in air at 1030° for 10 hours in a Pt crucible, followed by 3 cycles of regrinding. The powders were then pressed into round plates and sintered at 1050° for 10 hours in air. Sputtering was carried out under the following conditions: substrate temperature 600°, atmosphere pressure ($\text{Ar}+10\%\text{O}_2$) 2×10^{-2} Torr, and rf power 100W. In addition, annealing was carried out at 850° in a gas flow of $\text{Ar}+10\%\text{O}_2$. Film composition was determined by electron-probe-microanalysis (EPMA). Film thickness, measured with a stylus profilometer, ranged from 200 nm to 600 nm and the deposition rate was about 2 nm/min. The films were patterned into a rectangular shape ($0.5 \times 5 \text{ mm}^2$) with 6

terminals to measure the resistivity ρ and Hall coefficient R_H . Electrodes were formed with evaporated Au and silver paste.

Film orientation was examined with the simple 4-axis x-ray diffraction method. Figure 1 shows typical X-ray diffraction patterns for an L516 thin film with surface orientations of 90° (Fig. 1(a)) and 45° (Fig. 1(b)) to the rotary axis ($\theta/2\theta$), where the film was deposited on a (110) SrTiO_3

substrate. Diffraction peaks in Fig. 1 (a) were indexed as the (100) planes of L516 and those in Fig. 1 (b) were indexed as the (110) plane, with a unit cell composed of a $\sqrt{8} \times \sqrt{8} \times 1$ cubic perovskite. These results indicate that the film grew with its [100] axis normal to the film surface. The lattice constants of the films are $a = b = 1.09$ nm, which agree with Er-Rakho's results³⁾. In these films, the unit length of the a-axis is $\sqrt{8}$ times the lattice constant of SrTiO_3 , a , within a 0.7 % misfit factor. An RHEED pattern for the film is shown in Figure 2. The streaky pattern indicates that the film is single-crystalline with a very smooth surface.

Figure 3 schematically describes the configuration of Cu-O planes and the crystal axis of L516 with respect to the substrate. Cu-O₆ octahedra align on crossing lines of two orthogonal groups of Cu-O planes, and Cu-O₅ pyramids lie on mid-lines between two neighbour octahedra lines. From the Cu-O plane configuration shown in Fig. 3, some anisotropy should exist for the two directions, [100] and [001], in the epitaxial film.

Temperature dependences of resistivity (ρ) along the [100] and [001] directions in L516 films are shown in Fig. 4. The values are close to those of ceramic samples previously reported²⁾. The resistivity along [100] is 4 or 5 times larger than that along [001]. The anisotropy is smaller than that for 2-dimensional high- T_c materials. In the [001]

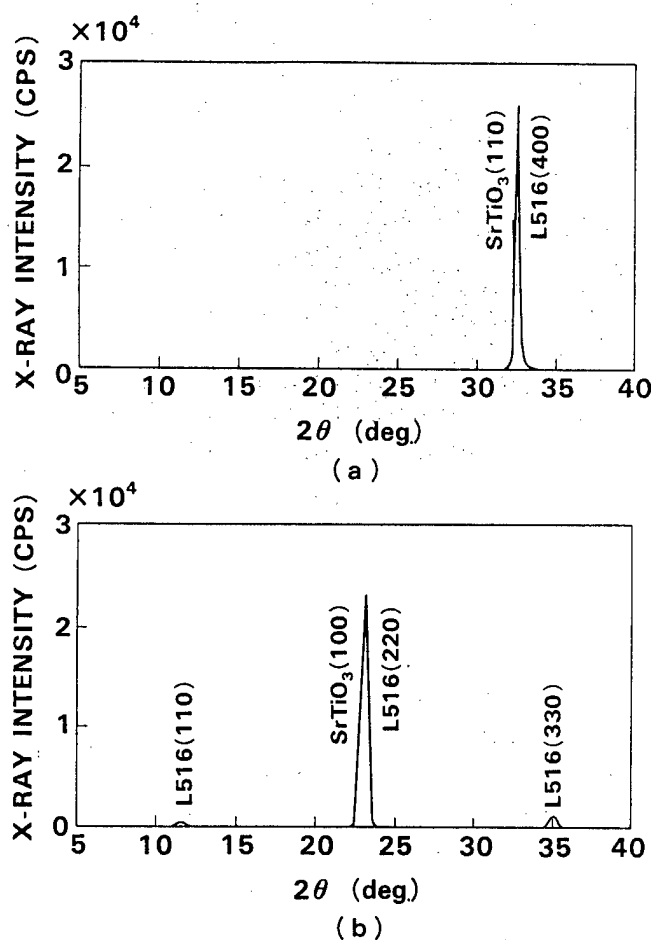


Fig.1: X-ray θ - 2θ diffraction patterns for L516 thin films on SrTiO_3 (110) face substrates. (a) film is set under a conventional method without tilt, and (b) film is tilted at 45° to the θ - 2θ axis. The peaks are reflections from the planes slanting film surface at 45° .



Fig. 2: RHEED patterns for the film.

direction, the resistivity decreases slightly with decreasing temperature in the whole region. On the other hand, the resistivity in the [100] direction has a broad, weak peak at about 180 K. Here, it should be noticed that such an anomaly can be observed only in the [100] direction. For ceramic samples²⁾⁴⁾⁵⁾, similar peaks were observed not only in their resistivity vs. temperature relations but also in their magnetic susceptibility vs. temperature relations. The same anomaly in the resistivity also can be seen in the result reported by Torrance and co-workers. Later, we will discuss this point as it relates to anisotropic properties.

Figure 5 shows the temperature dependences of Hall coefficients (R_H) for the same sample in Fig. 4. The Hall coefficients were measured under a magnetic field of 5T, perpendicular to the film surface, in the temperature range from 10K to 280K. The open circles denote the R_H values derived from induced voltages along [001], while the closed circles denote those from [100]. Both values were negative, but because the signs of the Seebeck coefficients for ceramic samples are positive below room temperature⁶⁾, the carriers cannot be determined to be electrons only from the sign of Hall coefficients. The anisotropy factor of R_H is about 2.5. This ratio corresponds to the resistivity anisotropy. The carrier densities (n) rapidly decrease with decreasing temperature. For comparison, corresponding data observed for $\text{La}_{1.7}\text{Sr}_{0.3}\text{CuO}_4$ are also shown (In this case, the Hall coefficients are positive)⁷⁾. This result implies that the carriers in L516 might localize at low temperatures. However, the resistivity shows a metallic temperature behavior. At the same time, the relation between $\ln(n - n_f)$ and $1/T$ is nonlinear, where n_f is the free carrier density remaining at a low temperature. Thus, the rapid decrease of Hall carriers is ascribed to another mechanism.

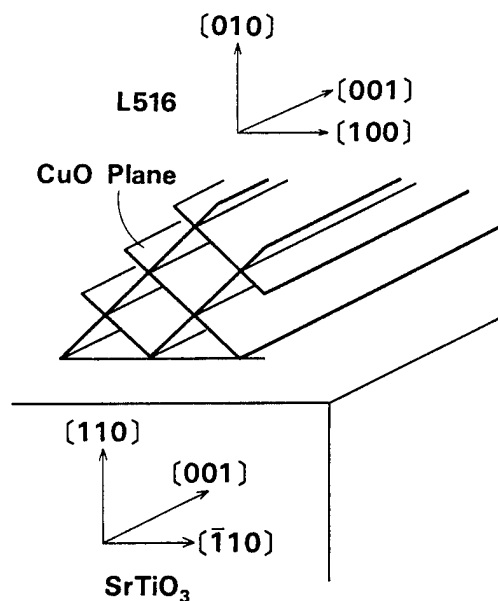


Fig. 3: Schematic configuration of Cu-O planes and a crystal axis with respect to the substrate.

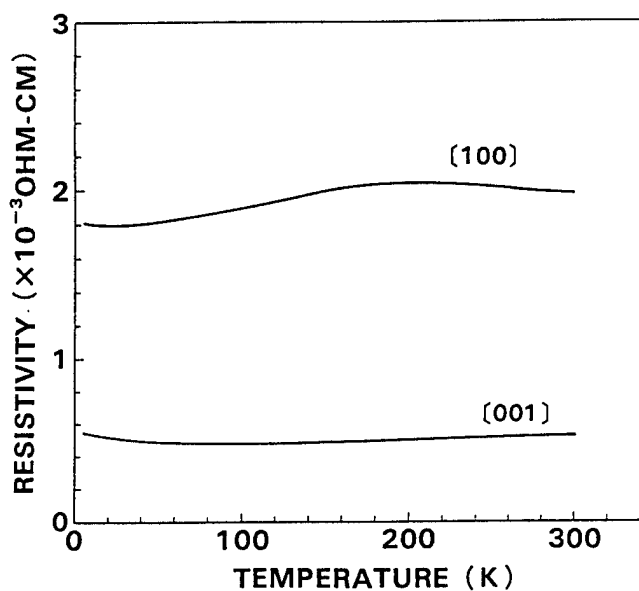


Fig. 4: Temperature dependence of resistivity (ρ) for [100] and [001] directions of L516 films.

The experimental results for resistivity and Hall coefficients showed anisotropic behaviors. Such anisotropy arises from the special crystal structure of L516, while those of high T_c copper oxides come from the two-dimensional structure of Cu-O. The structure of L516 is viewed as a compound consisting of three kinds of linear chains running along the c-axis^{2,3}. Each linear chain consists of octahedra, pyramids, or square sheets of Cu-O. Er-Rakho et al³ related that this matter has the geometry of the CuO₅ pyramids with four mean Cu-O distances (1.88-1.93 Å) and one longer (2.39 Å). These Cu-O distances are close to those observed in the super-conductor YBa₂Cu₃O_{7-x} and thus there can exist carriers in the pyramids. On the other hand, the CuO₆ octahedra are compressed along the c axis in contrast to the cases of the usual high T_c superconductors. With the short Cu(I)-O(I) length, no free carriers exist in the

In L516, linear chains of the pyramids and the octahedra run in parallel along the [001] direction and lie in series in the [100] direction. In the [001] direction, most of the current may flow along linear chains of pyramids, while in the [100] direction, carriers may flow by tunneling octahedra between pyramids. Therefore, this matter may have a quasi-one-dimensional electronic structure. The above assumption can completely explain the above anisotropic properties.

Previously, an anomaly in the resistivity vs. temperature curve in the [100] direction was described. Such an anomaly was not observed in the [001] direction. This can be explained as follows: In this direction, linear chains of pyramids and octahedra lie in parallel. Meanwhile, such spin order can not exist in the pyramids, because anti-ferromagnetic ordering disappears when free carriers exist⁸. Thus, such ordering should exist in the octahedra. The assumption can explain the anomaly only in the [100] direction. The change in the carrier scattering mechanism at the phase transition may induce such an anomaly.

In conclusion, we have studied the anisotropy of the electrical and optical properties of L516 thin films grown epitaxially on SrTiO₃ (110) substrates. The anisotropies are smaller than those observed for usual high- T_c superconductors. The resistivity along [001] is metallic and that along [100] has a broad peak at about 180 K, which may suggest anti-ferromagnetic ordering. The Hall coefficients are negative and decrease rapidly with decreasing temperature. The possibility of a quasi-one-dimensional electronic structure makes this matter extremely attractive.

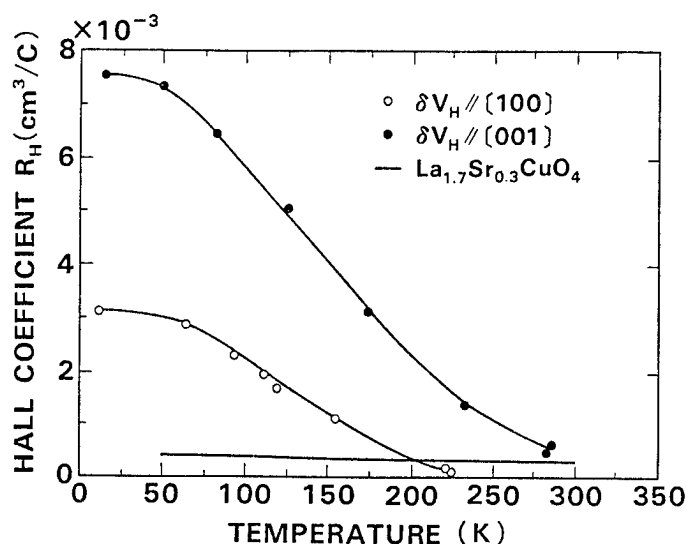


Fig. 5: Temperature dependence of Hall coefficients (R_H) for the same samples in Fig. 3. The open circles denote the R_H derived from the induced voltage along [001], while the closed circles denote those from [100]. For comparison, corresponding data for an $\text{La}_{1.7}\text{Sr}_{0.3}\text{CuO}_4$ single crystal thin film is shown inverting those signs.

References

- 1) J.G.Bednorz and K.A.Muller, Z.Phys., 64, 189, (1986).
- 2) J.B.Torrance, Y.Tokura, A.Nazzal and S.S.P.Parkin, Phys. Rev. Lett. 60 542 (1988). Y.Tokura, J.B.Torrance, A.I.Nazzal, T.C.Huang and C.Oritz, J.Am.Chem.Soc. 109 7555 (1987).
- 3) L.Er-Rakho, C.Michel, and B.Raveau, J.Solid State Chem. 73, 514, (1988).
- 4) T.Tamegai and Y.Iye, Physica C159 181 (1989).
- 5) T.Murakami and Y.Enomoto, to be submitted elsewhere.
- 6) C Michel, L. Er-Rakho and B.Raveau, J. Phys. Chem. Solids 49 451 (1988).
- 7) M.Suzuki, Phys. Rev. B39 2312 (1989).
- 8) R.J.Birgeneau, D.R.Gabbe, H.P.Jenssen, M.A.Kastner, P.J.Picone, T.R.Thurston, G.Shirane, Y.Endoh, M.Sato, K.Yamada, Y.Hidaka, M.Oda, Y.Enomoto, M.Suzuki and T.Murakami, Phys. Rev. B38, 6614 (1988).

Ba-Y-Cu-O Films Prepared by Various RF Sputtering Techniques and Their Structure and Superconducting Properties

H.Morita, H.Fujimori, Y.Koyanagi, K.Watanabe, K.Noto and Y.Muto.

Institute for Materials Research, Tohoku University, Sendai 980

We have examined various rf sputtering methods to find the best technique for preparation of the high- T_c superconducting oxide thin films. In this report, some significant phenomena found through this experiment are described, such as (A) Effect of dc magnetic field applied during sputtering, (B) Effect of an oblique incidence of sputtered atom-beam.

The relation between the crystalline microstructure and hysteresis of critical current density J_c against measuring magnetic field B (J_c - B hysteresis) was examined for the two Ba-Y-Cu-Oxide films which were prepared by rf sputtering method in dc magnetic field H of 10 and 30 Oe. It has been found that the application of H gives rise to a grain growth and to the regular alignment of the grains. The J_c - B hysteresis becomes small and the J_c value becomes large with increasing H . This field effect is considered as an important technique for preparation of good thin films. Therefore, we have investigated the effect of H on morphology and superconducting properties of films in detail.

(A) Sample preparation by sputtering in dc magnetic field

Thin film samples of Ba-Y-Cu-O superconductors were prepared by an rf sputtering method shown in Fig.1. A $Ba_{6.6}Y_{1.0}Cu_{8.3}O_x$ target 90 mm in diameter was prepared by a solid phase reaction method. The target was sputter-etched for 50 hs prior to film growth experiments in order to ensure thermal equilibrium for the alteration in composition of the target surface. Sputtering was carried out in an atmosphere of 50%Ar+50%O₂ with a total pressure of 35 mTorr. The discharge power was 70 W and the target-substrate distance was 55 mm. A dc magnetic field of 0~40 Oe parallel to the target (or to the substrate) was produced by a Helmholtz coil which is set outside the chamber. The substrate temperature was 440 °C. Since this temperature was too low for crystallization of oxide, the as-prepared sample was in the amorphous state and insulator. Therefore, a post-annealing of 890°C x1h was necessary for the transformation into a superconducting film.

Fig.2 shows the H dependence of the superconducting onset temperature T_c^{on} and zero resistance temperature T_c^{off} . T_c^{on} shows a little dependence on H , on the other hand, T_c^{off} shows a vague maximum around 30 Oe. The small change in

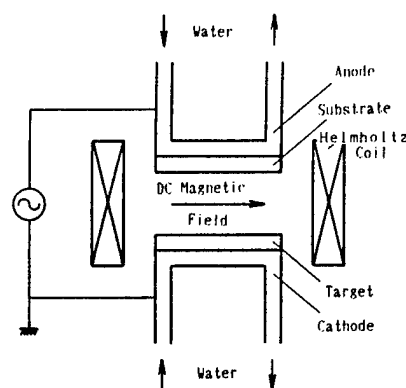
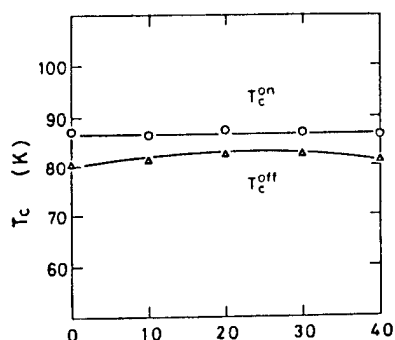
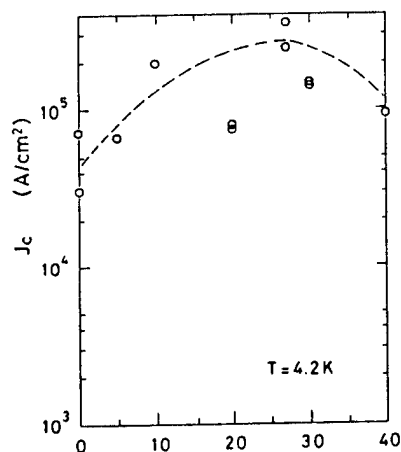


Fig.1 Sample preparation method in magnetic field



D.C. Magnetic Field (Oe)

Fig.2 Magnetic field dependences of superconducting transition onset T_c^{on} and off-set T_c^{off} temperatures



D.C. Magnetic Field (Oe)

Fig.3 Magnetic field dependence of critical current density measured at 4.2 K.

grains also becomes large. X-ray diffraction experiments have revealed that the c-axis orientation becomes clear with increasing H.

(B) Effect of an oblique incidence of sputtered atom-beam

As a most possible mechanism for the effect of H described above, the oblique incidence of the beam of electrified sputtered-atoms and oxides, coming from the target onto the surface of films, may be taken into account. In order to check this point, we have examined the effect of declination of the substrate against target in zero magnetic field. The method for this is shown in Fig. 5.

T_c^{on} suggests that the composition can not be changed very much by an application of H. EPMA experiments showed no appreciable change in composition, supporting above consideration. Nevertheless, T_c^{off} was appreciably changed by H. The change in T_c^{off} is, therefore, thought to be related to a change in the structure of films. Critical current density J_c measured at 4.2 K also depends strongly on H, suggesting that the film structure is changed by H (Fig.3).

A large difference in surface morphology was found between the samples prepared in H=0 and 30 Oe. Figure 4 shows the SEM photographs for the post-annealed films which were prepared in H = 0 and 30 Oe, respectively. In the case of H=0 (Fig.4 A), the grain shapes are somewhat round and similar to that of bulk samples prepared by a sintering method. On the other hand, as seen in Fig.4 B, the grain shapes become rectangular with increasing H, and the contacting area between

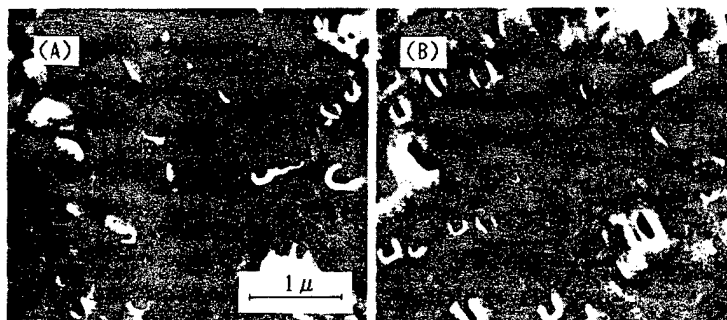


Fig.4 SEM photographs for the post-annealed films prepared in H=0 (A) and H=30 Oe (B).

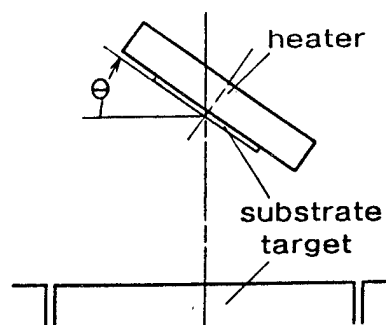


Fig.5 Sample preparation method by declining substrate

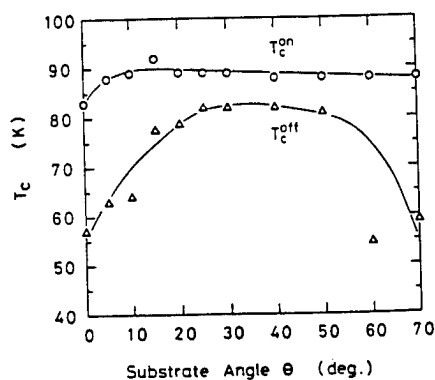


Fig.6 Substrate angle dependences of superconducting transition onset T_c^{on} and offset T_c^{off} temperatures

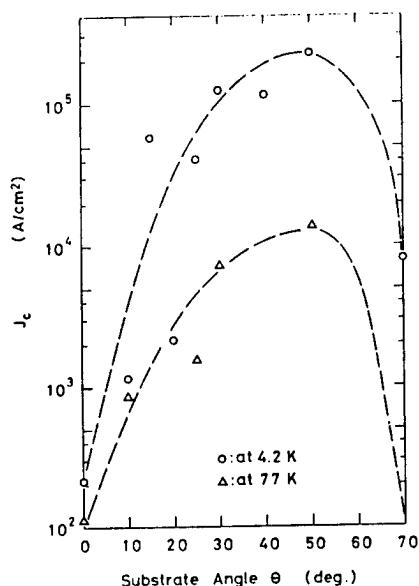


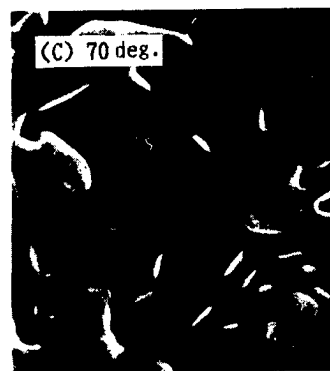
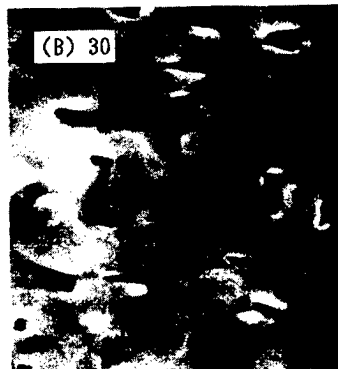
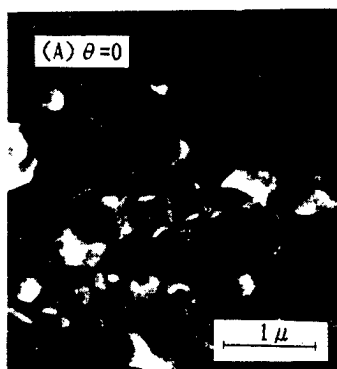
Fig.7 Substrate angle dependences of critical current densities measured at 4.2 and 77 K

Other sputtering conditions are the same as those for the experiment (A).

Figure 6 shows the substrate angle θ dependences of T_c^{on} and T_c^{off} . The θ dependence of T_c^{on} is small and T_c^{off} shows a maximum around $\theta = 50^\circ$. Fig.7 shows the θ dependence of J_c measured at 4.2 and 77 K. Both the curves show maximum around $\theta = 50^\circ$. The surface morphologies of these samples have been found to be similar to those of the samples made in magnetic field. The morphology of the film prepared with $\theta = 0^\circ$ (Fig.8A) looks like that of the bulk sample prepared by a sintering method. When $\theta = 10^\circ$, the grain growth is developed. The X-ray experiment shows that when $\theta = 30^\circ - 50^\circ$, c axis orientates perpendicular to film surface. In the Fig.8B, the preferential alignment of crystalites also indicates that a and b axes orientate preferentially in plane. When $\theta = 70^\circ$, the grains are grown so large that the net of grains is visible clearly (Fig.8C).

It is pointed out from the above experiments that the oblique incidence of the sputtered atom-beam to the substrate surface has the similar effect to the deposition in dc magnetic field, for the morphology of films. The mechanism that the films prepared by above two methods, which are in the amorphous state, memorize the oblique incidence of atoms and reflect it on surface morphology by an annealing at 900°C has not been made clear in the present work.

Fig.8 SEM photographs for post-annealed films prepared with substrate angles shown in the photographs



Preparation of $(\text{Bi}_{1-x}\text{Pb}_x)_2\text{Sr}_2\text{Ca}_3\text{Cu}_4\text{O}_y$ Superconducting Film
by a Single Composite Target Sputtering Method

Yoichiro Kawai, Toshifumi Terui⁺ and Yusei Maruyama

Institute for Molecular Science, Myodaiji, Okazaki, Aichi 444

⁺Department of Functional Molecular Science, The Graduate University
for Advanced Studies, Myodaiji, Okazaki, Aichi 444

Thin films of the $(\text{Bi}_{1-x}\text{Pb}_x)_2\text{Sr}_2\text{Ca}_3\text{Cu}_4\text{O}_y$ phase which is difficult to be realized in bulk specimens have been prepared by a single composite target sputtering method. Although the obtained film seems to be of a single phase by an X-ray analysis, the residual resistivity at low temperatures has still a semiconducting character after the sharp drop near 86K.

Since the discovery of the high- T_c oxide superconductors,¹⁻⁴⁾ many studies on corresponding superconducting thin films have been carried out. Such studies are very important especially for searching or synthesis for new superconductors, because of the possibility of stabilizing new stoichiometries and/or crystalline structures in a film which may not be formed in bulk specimens. Typical examples for the preparation of such superconducting thin films, $\text{Bi}_2\text{Sr}_2\text{Ca}_3\text{Cu}_4\text{O}_y$ (2234) or $\text{Bi}_2\text{Sr}_2\text{Ca}_4\text{Cu}_5\text{O}_y$ (2245), by using layer-by-layer deposition from multiple sources have been reported by Adachi et al.⁵⁾ and Tabata et al.,⁶⁾ respectively.

Our aim is to synthesize such new materials of higher- T_c superconductors that are difficult or impossible to obtain in bulk specimens. In this paper, we report the stabilization of a superconducting 2234 phase in the thin films prepared by a sputtering method which has the industrial advantage of using a single composite target. $\text{Bi}_2\text{Sr}_2\text{Ca}_2\text{Cu}_3\text{O}_y$ (2223) was also studied but preliminarily to find optimum sputtering conditions.

Thin films were prepared on (100) MgO single-crystal substrate (17mm ϕ ×1mm) by an rf-magnetron sputtering. Each target was made by simple mixing of the component powders (Bi_2O_3 (3N), PbO_2 (3N), SrCO_3 (4N), CaCO_3 (4N) and CuO (4N)) in appropriate ratio and then pressing into discs (100mm ϕ ×4mm). Lead was incorporated in order to make the synthesis of the 2234 phase easier. The separation, D, between target and substrate in the sputtering vessel was adjusted to 37mm, 40mm or 43mm, in each case. The composition of the sputtering gas was finally set to 40% argon and 60% oxygen under a constant total pressure of 1Pa. The substrate was heated by a Kanthal wire during deposition and cooled spontaneously in the bell-jar under 1 atmospheric pressure of oxygen after the deposition was completed. Thin films about 7000Å thick were obtained in 3 hrs. with an rf-power of 150W.

The chemical composition and crystal structure of the films were analyzed by ICP (Inductively Coupled Plasma) emission spectroscopy and X-ray diffractometry, respectively. The electrical resistivity was measured by a conventional four probe method.

In this equipment system, the film composition was very sensitive to the substrate temperature (T_s). The atomic ratio Bi/Ca, Sr/Ca and Cu/Ca decreased as T_s increased from 510°C to 630°C (Fig. 1), because the each deposited mass of Bi, Sr and Cu decreased but that of Ca increased as T_s increased. In addition, increasing of T_s

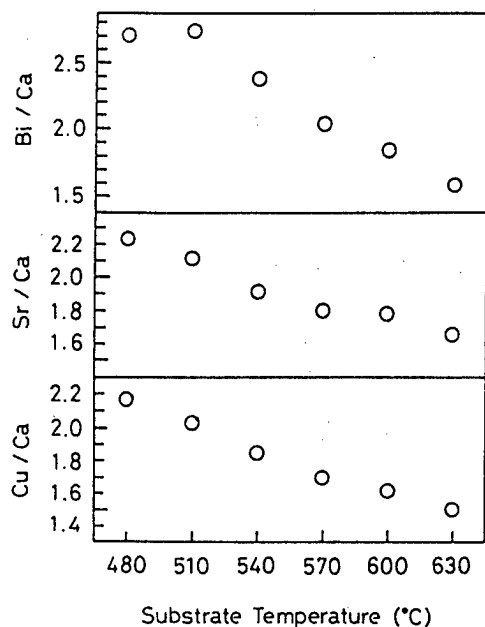


Fig. 1. The dependence of the composition on substrate temperatures. The target of Bi:Sr:Ca:Cu=4.3:1.9:2:3 was used.

caused whitening of the films. Since the degree of whitening was reduced by increasing the ratio of oxygen in the sputtering gas, the whitening is probably due to insufficiency of oxygen in the films (see Fig. 2). It was found that both 2223 and

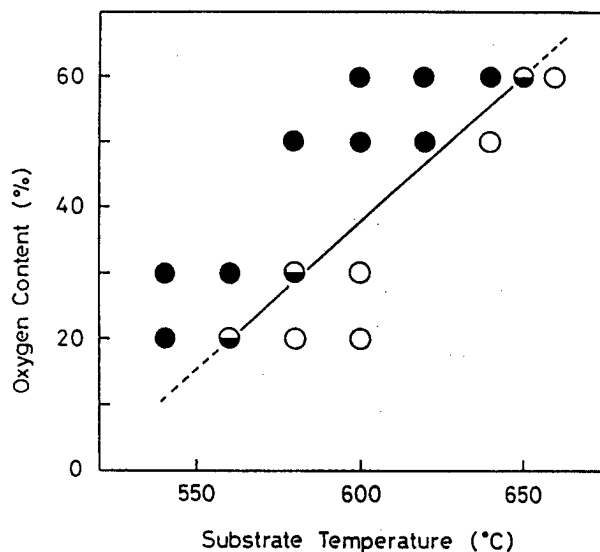


Fig. 2. The effects of substrate temperature and oxygen content in the sputtering gas on the color of the 2223 films, :black, :center white and edges black, :white.

2234 phases are easily formed under the condition that $T_s \geq 600^\circ\text{C}$. It was also found that the target-substrate separation of 40mm is the most favorable one to form both 2223 and 2234 phases.

A superconducting film of $(\text{Bi}_{0.8}\text{Pb}_{0.2})_{2.1}\text{Sr}_{2.1}\text{Ca}_{2.0}\text{Cu}_{3.1}\text{O}_y$ was obtained by adjusting the sputtering conditions as described above. Its X-ray diffraction pattern shown in Fig. 3 indicates that there are three different phases corresponding to $C_0=31\text{\AA}$, 37\AA and 42\AA in the film. Correspondingly, there seem to be three T_c^{onset} for

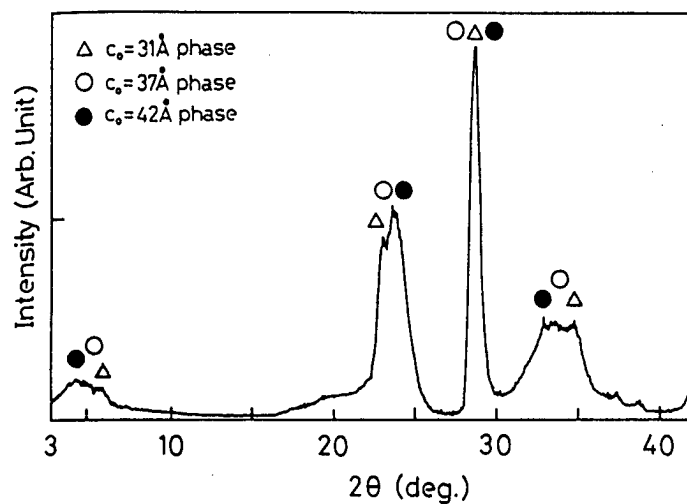


Fig. 3. The X-ray diffraction pattern of a $(\text{Bi}_{0.8}\text{Pb}_{0.2})_{2.1}\text{Sr}_{2.1}\text{Ca}_{2.0}\text{Cu}_{3.1}\text{O}_y$ film obtained at $T_s = 630^\circ\text{C}$.

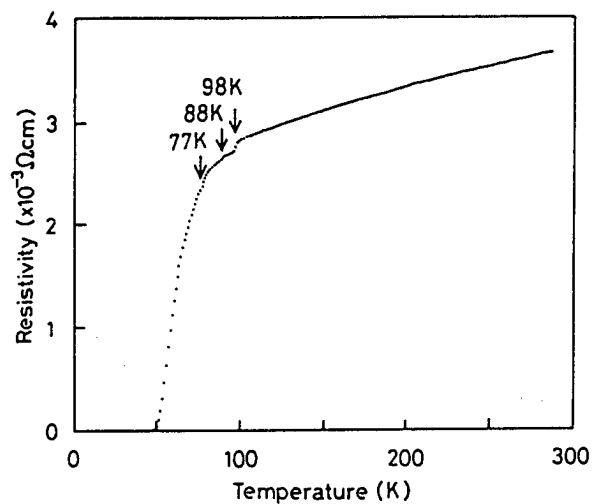


Fig. 4. The dependence of the resistivity on substrate temperature.

Table 1. The correlation among C_0 , T_s^{onset} and superconducting phase.

C_0 (Å)	T_c^{onset} (K)	superconducting phase
31	75	2212
37	98	2223
42	88	2234

superconduction, 77, 88 and 98K, in the resistivity-temperature curve (Fig. 4). These three phases are probably 2212, 2223 and 2234, as shown in Table 1. The X-ray diffraction patterns obtained from each different area in this film indicate that the 2234 phase is present mainly near the center of the film and 2212 is mainly near the edge.

The color-shifting of the film from all-black to all-white with increasing substrate temperature suggests that the substrate temperature at the center was approximately 15°C higher than that at the edge. In addition, the monitored substrate temperature fluctuated by $\pm 7^\circ\text{C}$ during the course of deposition. These two effects may result in the formation of three different phases in the film.

Figure 5 shows the X-ray diffraction patterns of the film of which monitored temperature fluctuation was controlled within $\pm 1^\circ\text{C}$. The phase-admixture in the

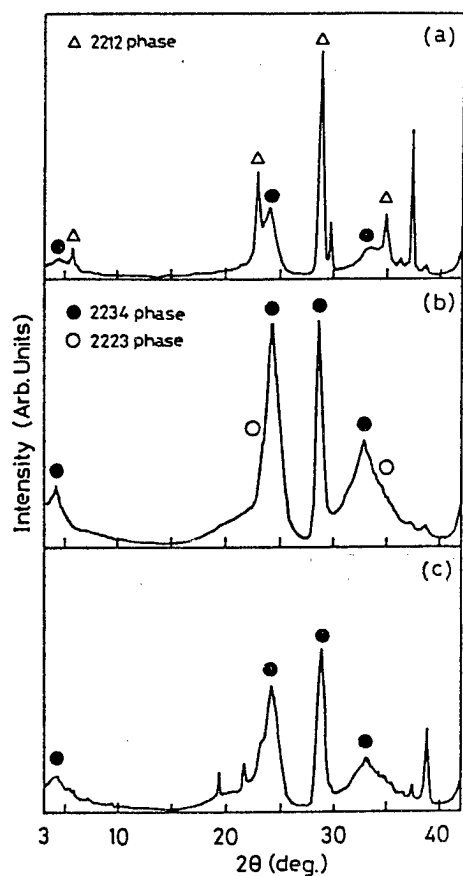


Fig. 5. The X-ray diffraction patterns of the films obtained at 630°C (a), 610°C (b), and 590°C (c), respectively.

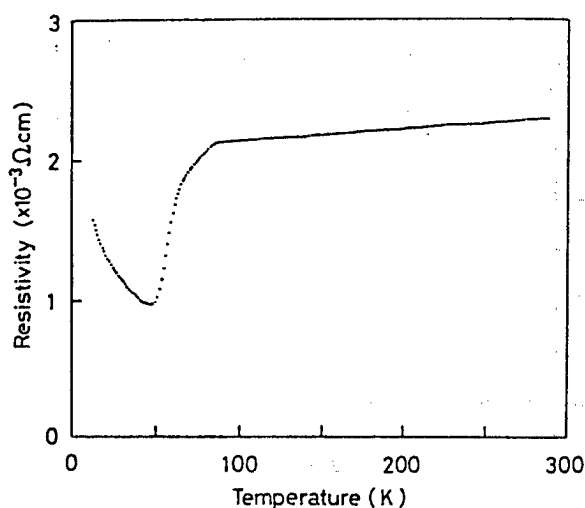


Fig. 6. The temperature dependence of the resistivity for the film of which nominal composition was $(\text{Bi}_{0.8}\text{Pb}_{0.2})_{2.1}\text{Sr}_{1.95}\text{Ca}_3\text{Cu}_{4.1}\text{O}_y$.

deposited film seems to be very sensitive to T_g , and the optimum T_g for 2234 phase formation proved to be 610°C.

The resistivity of the film of $T_g=610^\circ\text{C}$ suddenly dropped at 86K (Fig. 6), probably indicating the existence of the single high- T_c superconducting phase, but it did not fall down to zero at lower temperatures. This fact implies that some semiconducting phases might be present on the grain boundaries of the superconducting phase.

In conclusion, the superconducting 2234 phase in Bi-Sr-Ca-Cu-O system can be

stabilized in a film obtained by a single composite target sputtering method with finely controlled conditions. The most important two parameters are the substrate temperature and the target-substrate separation.

ACKNOWLEDGEMENTS

The authors would like to thank Dr. T. Inabe for his support and discussion, and also to Prof. R. J. Fleming of Monash University in Australia for his helpful advice. This work was partly supported by the Grand-in-Aid for Science Research on Priority Areas "Mechanism of Superconductivity" (No. 031) from the Ministry of Education, Science and Culture of Japan.

REFERENCES

- 1) J. G. Bednorz and K. A. Müller, Z. Phys., B64 (1986) 189.
- 2) M. K. Wu, J. R. Ashburn, C. J. Torng, P. H. Hor, R. L. Meng, L. Gao, Z. J. Huang, Y. Q. Wang and C. W. Chu, Phys. Rev. Lett., 58 (1987) 908.
- 3) H. Maeda, Y. Tanaka, M. Fukutomi and T. Asano, Jpn. J. Appl. Phys., 27 (1988) L209.
- 4) Z. Z. Sheng and A. M. Hermann, Nature, 332 (1988) 55.
- 5) H. Adachi, S. Kohiki, K. Setsune, T. Mitsuya and K. Wasa, Jap. J. Appl. Phys., 27 (1988) L1883.
- 6) H. Tabata, T. Kawai, M. Kanai, O. Murata and S. Kawai, Jap. J. Appl. Phys., 28 (1989) L430.

Preparation of Oxide Superconductors by Oxidation of Amorphous
Ln-Ce-Cu (Ln= Pr, Nd or Sm) Alloy Tapes

Kunio Matsuzaki, Koichi Shimizu*, Akihisa Inoue and Tsuyoshi Masumoto

Institute for Materials Research, Tohoku University
Katahira 2-1-1, Sendai 980, Japan

Ductile amorphous tapes in Ln-Ce-Cu (Ln=Pr, Nd or Sm) alloys ranging from 0 to 45 at%Ce and 25 to 40 at%Cu were prepared by melt spinning. The sequent annealing treatment of 573 K x 21.6 ks in O₂ followed by 1323 K x 10.8 ks in O₂ and then 1353 K x 21.6 ks in Ar for Ln_{1.85}Ce_{0.15}Cu alloys resulted in formation of oxides with a tetragonal (T') structure. Furthermore, their oxides were found to exhibit superconductivity with onset teperatures of 13 K for Ln=Pr, 22 K for Nd and 12 K for Sm. Thus, the process seems to be useful as an alternative method of obtaining the electron-doped superconducting oxides.

1. Introduction

After the discovery of a high T_c oxide superconductor by Bednorz and Muller [1], various kinds of oxides have been found to exhibit superconductivity at temperatures higher than the highest T_c value for metallic superconducting compounds. The first high- T_c oxide was found in $\text{La}_{2-x}(\text{Ca, Sr or Ba})_x\text{CuO}_y$ [2,3] systems with K_2NiF_4 -type structure and their maximum T_c value was about 40 K. Subsequently, a $\text{Y}_1\text{Ba}_2\text{Cu}_3\text{O}_y$ [4] with T_c at temperatures higher than the boiling temperature of liquid nitrogen was discovered, followed by (Bi,Pb)-Sr-Ca-Cu oxide [5] and then Tl-Ba-Ca-Cu oxide [6]. It is notable that the latter two oxides exhibit a zero resistance at temperatures above 100 K. It is generally known that these new oxide superconductors belong to a hole-doped type and the valence of Cu plays an important role in the appearance of high- T_c superconductivity. Recently, Tokura et al. [7] discovered a new superconducting oxide $\text{Nd}_{2-x}\text{Ce}_x\text{CuO}_y$ with T_c of 20 K, which has a Nd_2CuO_4 structure (T' phase). It is of interest that the $\text{Nd}_{2-x}\text{Ce}_x\text{CuO}_y$ is an electron-doped superconductor and the doping of electron is attributed to the substitution of Nd with a valence of +3 by Ce with a valence of +4. This result also led to a Th doping of Nd_2Cu oxide [8] as well as to a substitution of oxygen with a valence of -2 by fluorine with a valence of -1 [9]. These oxides synthesized by the doping method have been reported to exhibit T_c at 20 K for $\text{Nd}_{2-x}\text{Th}_x\text{CuO}_y$ and 27 K for $\text{Nd}_2\text{CuO}_{4-y}\text{F}_y$. The present authors have previously reported that melt-spun alloys in La-Sr-Cu [10], Yb-Ba-Cu [11] and Eu-Ba-Cu [12] systems have an amorphous or a nonequilibrium structure with good bend ductility and subsequent oxidation gives rise to the superconducting oxides with high T_c values. This paper is intended to present the formation range of amorphous phase in Ln-Ce-Cu

*On leave from Furukawa Kikai & Kinzoku Co., Ltd., Yoshima, Iwaki 970-11, Japan

(Ln=Pr, Nd or Sm) ternary alloys by melt spinning and the preparation of electron-type superconducting oxides by oxidation of their amorphous alloy tapes.

2. Experimental Procedure

The ternary Ln-Ce-Cu (Ln= Pr, Nd or Sm) alloy ingots were prepared by arc-melting a mixture of pure Ce, Cu and Pr, Nd or Sm metals in an argon atmosphere. The ingots were spun to a continuous tape with about 20 μm thickness and 0.1 mm width by a single roller melt spinning apparatus. Subsequently, the melt-spun tapes were heated in a flow of argon and oxygen mixture gas. The structure of as-quenched and oxidized tapes was examined by X-ray diffractometry with monochromated Cu K α . The changes in structure and weight of the melt-spun tape upon heating were also examined by differential thermal analysis (DTA) and thermogravimetric analysis (TGA). The resistive measurement was made by the DC four-probe technique.

3. Results and Discussion

Figure 1 shows the compositional ranges in which an amorphous phase is formed in rapidly solidified Pr-Ce-Cu, Nd-Ce-Cu and Sm-Ce-Cu ternary alloys. A mostly single amorphous phase is obtained in the range of 40 to 70 at% Pr and 0 to 30 at% Ce for Pr-Ce-Cu system, 35 to 70 at% Nd and 0 to 30 at% Ce for Nd-Ce-Cu system and 20 to 75 at% Sm and 0 to 45 at% Ce for Sm-Ce-Cu system. Thus, the formation range is much wider for Sm-Ce-Cu system than for the other two systems. All the amorphous alloys possess good ductility which is shown by a 180 degree bending without fracture.

As an example, Fig. 2 shows the compositional dependence of crystallization temperature (T_x) for the Sm-Ce-Cu amorphous alloys. T_x decreases from 425 to 371 K with an increase of Ce and Cu contents. A similar compositional dependence of T_x was also observed for Pr-Ce-Cu and Nd-Ce-Cu alloy systems and the T_x decreases from 397 to 372 K and 384 to 364 K, respectively. Thus, the T_x is also the highest for the Sm-Ce-Cu alloys with the largest glass-forming tendency.

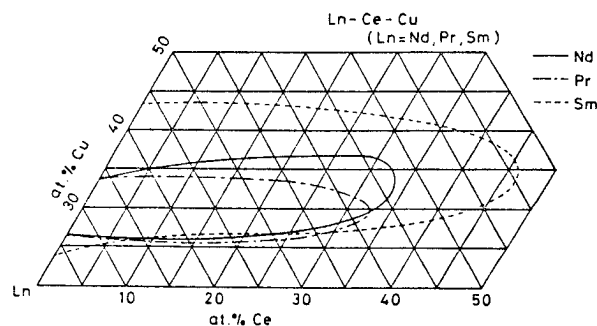


Fig. 1 Compositional ranges for the formation of amorphous phase in rapidly solidified Pr-Ce-Cu, Nd-Ce-Cu and Sm-Ce-Cu alloys.

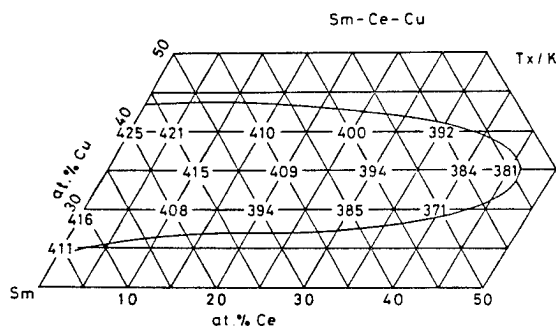


Fig. 2 Compositional dependence of crystallization temperature (T_x) for Sm-Ce-Cu amorphous alloys.

Figure 3 shows the DTA and TGA curves for the $\text{Ln}_{1.85}\text{Ce}_{0.15}\text{Cu}$ (Ln=Pr, Nd or Sm) amorphous alloys on heating at 10 K/min in air. For instance, the Nd-Ce-Cu alloy exhibits a sharp exothermic peak without any change in sample weight at 420 K followed by a large broad peak accompanied by a significant increase in sample weight in the

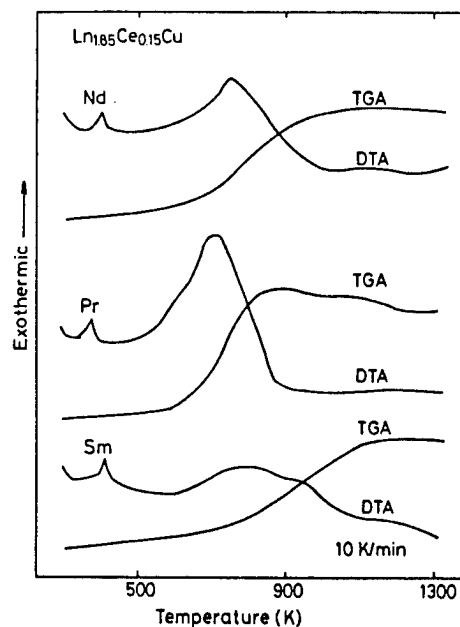


Fig. 3 DTA and TGA curves of $\text{Ln}_{1.85}\text{Ce}_{0.15}\text{Cu}$ ($\text{Ln}=\text{Pr}, \text{Nd}$ or Sm) amorphous alloys on heating at 10 K/min in air.

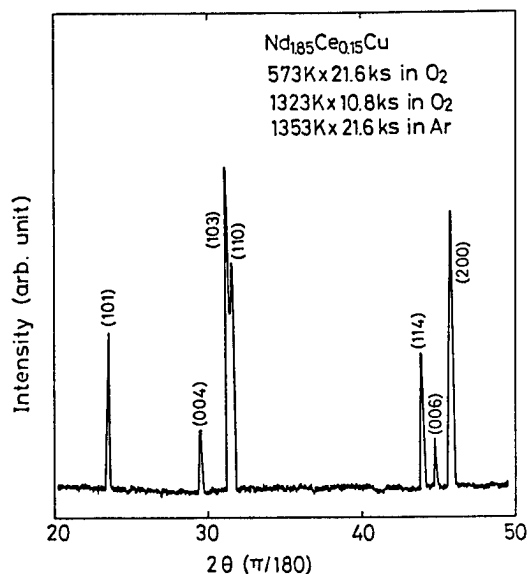


Fig. 4 X-ray diffraction pattern of an oxide prepared by annealing the melt-spun $\text{Nd}_{1.85}\text{Ce}_{0.15}\text{Cu}$ amorphous alloy in the condition of 573 K x 21.6 ks in O_2 followed by 1323 K x 10.8 ks in O_2 and 1353 K x 21.6 ks in Ar.

temperature range of 710 to 800 K. As is evident from the data shown in Fig. 2, the low-temperature peak is due to crystallization. On the other hand, the high-temperature peak with the increase in weight corresponds to the oxidation of the crystalline phase formed by crystallization.

Figure 4 shows the X-ray diffraction pattern of a $\text{Nd}_{1.85}\text{Ce}_{0.15}\text{Cu}_1$ oxide prepared by annealing treatment of 573 K x 21.6 ks in O_2 followed by 1323 K x 10.8 ks in O_2 and then 1353 K x 21.6 ks in Ar. All the diffraction peaks for the oxide sample can be identified to be the tetragonal T' phase with lattice parameters of $a=0.395$ nm and $c=1.209$ nm, in good agreement with those reported by Tokura et al. [7]. Accordingly, the annealing treatment of the melt-spun $\text{Nd}_{1.85}\text{Ce}_{0.15}\text{Cu}$ amorphous alloy is concluded to bring about the oxide consisting of a mostly single T' phase. In addition, $\text{Pr}_{1.85}\text{Ce}_{0.15}\text{Cu}$ and $\text{Sm}_{1.85}\text{Ce}_{0.15}\text{Cu}$ alloys were also confirmed to have the same oxide phase with the T' structure after the sequent annealing treatment.

Figure 5 shows the normalized electrical resistance, $R/R_{\text{R.T.}}$, as a function of temperature for the $\text{Ln}_{1.85}\text{Ce}_{0.15}\text{Cu}$ ($\text{Ln}=\text{Pr}, \text{Nd}$ or Sm) oxides prepared by the same annealing treatment shown in Fig. 4. Although the resistance of the Nd-Ce-Cu oxide increases slightly with a decrease of temperature from room temperature (R.T.) to 25 K, it begins to decrease at about 22 K through an appearance of superconductivity and becomes zero at 5 K. The $\text{Pr}_{1.85}\text{Ce}_{0.15}\text{Cu}$ and $\text{Sm}_{1.85}\text{Ce}_{0.15}\text{Cu}$ oxides behave like a semiconductor in the temperature range from R.T. to 15 K, followed by the small resistive drop due to the onset of superconductivity at about 13 K, as shown in Fig. 5. Although the three oxides have the same T' single phase, the temperature reaching zero resistance is significantly different in their oxides. Further optimization of

composition and annealing condition for the Ln-Ce-Cu oxides is under investigation with the aim of enhancing the zero-resistance temperature. The onset temperatures for the present oxides are nearly the same as those for the $\text{Nd}_{1.85}\text{Ce}_{0.15}\text{Cu}$ oxide prepared by conventional solid state reaction [7]. Accordingly, it may be concluded that the oxidation method of metallic precursor is useful to obtain the electron-doped superconducting oxides as well as the hole-doped superconducting oxides [10-12].

In conclusion, we have succeeded in preparing the electron-doped superconducting oxides in Ln-Ce-Cu-O (Ln=Pr, Nd or Sm) systems by oxidation of the melt-spun amorphous Ln-Ce-Cu alloy tapes. The onset temperature is 13 K for $\text{Pr}_{1.85}\text{Ce}_{0.15}\text{Cu}$ oxide, 22 K for $\text{Nd}_{1.85}\text{Ce}_{0.15}\text{Cu}$ oxide and 12 K for $\text{Sm}_{1.85}\text{Ce}_{0.15}\text{Cu}$ oxide. Preparation of a $\text{Ln}_2\text{CuO}_{4-y}\text{F}_y$ superconductor by annealing of amorphous alloys under a stream of oxygen and fluorine mixture gas is under trial.

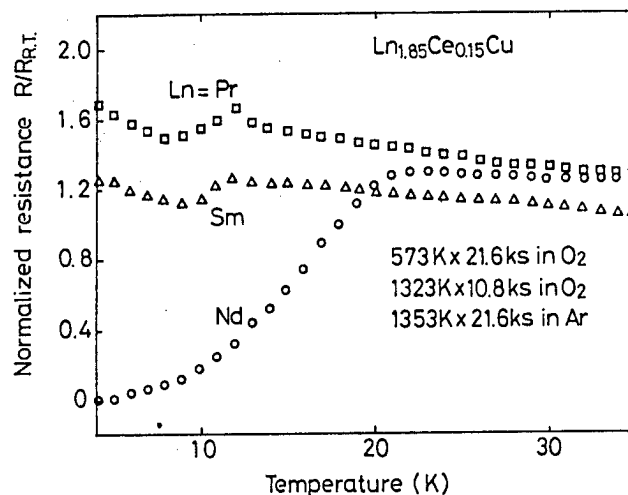


Fig. 5 Normalized electrical resistance $R/R_{R.T.}$ as a function of temperature for oxides prepared by annealing the melt-spun $\text{Ln}_{1.85}\text{Ce}_{0.15}\text{Cu}$ (Ln=Pr, Nd or Sm) amorphous alloys in the condition of 573 K x 21.6 ks in O_2 followed by 1323 K x 10.8 ks in O_2 and 1353 K x 21.6 ks in Ar.

References

- 1) J.G. Bednorz and K.A. Muller: Z. Phys. B 64 (1986) 189.
- 2) C.W. Chu, P.H. Hor, R.L. Meng, L. Gao, Z.J. Hung and Y.Q. Wang: Phys. Rev. Lett. 58 (1987) 405.
- 3) S. Uchida, H. Takagi, K. Kitazawa and S. Tanaka: Jpn. J. Appl. Phys. 26 (1987) L1.
- 4) M.K. Wu, J.R. Ashburn, C.J. Torng, P.H. Hor, R.L. Meng, L. Gao, Z.J. Huang, Y.Q. Wang and C.W. Chu: Phys. Rev. Lett. 58 (1987) 908.
- 5) H. Maeda, Y. Tanaka, M. Fukutomi and T. Asano: Jpn. J. Appl. Phys. 27 (1988) L209.
- 6) Z.Z. Sheng and A.M. Hermann: Nature 332 (1988) 138.
- 7) Y. Tokura, H. Tanaka and S. Uchida: Nature 337 (1989) 345.
- 8) J.T. Markert, E.A. Early, T. Bjornholm, S. Ghamaty, B.W. Lee, J.J. Neumeier, R.D. Price, C.L. Seaman and M.B. Maple: Physica C 158 (1989) 178.
- 9) A.C.W.P. James, S.M. Zakurak and D.W. Murphy: Nature 338 (1989) 240.
- 10) K. Matsuzaki, A. Inoue, H.M. Kimura, K. Moroishi and T. Masumoto: Jpn. J. Appl. Phys. 26 (1987) 1334.
- 11) K. Matsuzaki, A. Inoue, H.M. Kimura, K. Aoki and T. Masumoto: Jpn. J. Appl. Phys. 26 (1987) L1310.
- 12) K. Matsuzaki, A. Inoue, H.M. Kimura and T. Masumoto: Jpn. J. Appl. Phys. 26 (1987) L1610.

Ultrahigh-Pressure Study of High T_C Oxides

H. Aoki, M. Kumazawa*, K. Kurita*, S. Kobayashi, S. Ikehata, A. Nakamura, S. Katsumoto, F. Komori, T. Fujii**, T. Ishii[†], K. Kinoshita[†] and T. Yamada[†]

Department of Physics, University of Tokyo, Hongo, Tokyo 113,

*Department of Geophysics, University of Tokyo, Yayoi, Tokyo 113,

**Earthquake Research Institute, University of Tokyo, Yayoi, Tokyo 113

[†]NTT Basic Research Laboratories, Musashino, Tokyo 180,

Abstract Ultra-high pressure (25GPa) is applied to high T_C copper oxides ($\text{YBa}_2\text{Cu}_3\text{O}_{7-\delta}$ and CuO) to search for possible structural phase transitions.

The class of high- T_C copper oxides first discovered by Bednorz and Muller are reminiscent of rock-forming minerals both chemically and structurally. In fact, high- T_C materials all have crystal structures related to perovskite, which is a key structure for rock-forming minerals (silicates). It has been well established in geophysics that silicates such as Mg_2SiO_4 undergo a series of structural phase transitions when high pressure (of the order of 20GPa) is applied. The present study is motivated by an observation that such structural transitions can possibly be expected also for the copper oxides. Since they possess perovskite-related structures rather than perovskite itself, which is already the high-pressure form, we can expect structural flexibility under ultra-high pressure. We can also expect to fabricate new materials and structures, which is, solid state chemically, only possible under extreme conditions. The high-pressure phases tend to have higher coordination number and covalency in general, so that we can thereby probe the superconducting mechanism.

The high-pressure study on the high- T_C materials has been primarily focused on the in situ experiment[1], i.e., the change of structure and T_C during the application of pressure. By contrast, we look for new phases that are (meta)stable in normal pressure/temperature and thus can be quenched after the high pressure is turned off. As the ultra-high pressure facility, we employ the multiple-anvil high-pressure apparatus, which has been developed by Kumazawa and coworkers[2]. The multiple-anvil method has an advantage that (a)relatively large sample volumes can be accommodated and (b)well-defined high temperature can be applied. The control parameters we have varied include pressure ($p \leq 25\text{GPa}$ here), temperature ($T \leq 1350^\circ\text{C}$), duration of high p/T treatment, rapid or slow cooling, starting material (ceramics or ingredient powder mixture) and redox condition (including heater and capsule design).

This year we are trying to apply higher pressures (up to about 25GPa) with high-pressure apparatus at the Institute for Studies of the Earth's Interior, Okayama University, collaborating with E. Itoh. As for starting materials, we also give special attention to pure CuO (tenorite), which has an interesting (distorted PdO) crystal structure as well as antiferromagnetism with $T_N = 230\text{K}$.

We are indebted to Prof. Y. Tokura for providing us CuO samples. We also thank the Institute for Studies of the Earth's Interior, Okayama University, for hospitality.

references

- [1] See, e.g., S. Yomo et al., Jpn J. Appl. Phys. 26(1987), L603; T. Matsumoto et al., Jpn. J. Appl. Phys. 27(1988), L600.
- [2] M. Kumazawa and S. Endo in "Materials Science of the Earth's Interior" ed. by I. Sunagawa (Tera Scientific, 1984), p.587.

H.Kojima and I.Tanaka

Institute of Inorganic Synthesis, Faculty of Engineering,
Yamanashi University, Miyamae 7, Kofu 400, Japan

The attempts of single crystal growth of $\text{La}_{2-x}\text{Sr}_x\text{CuO}_4$ were carrying out through a year. $\text{La}_{1.86}\text{Sr}_{0.14}\text{CuO}_4$ and $\text{La}_{1.80}\text{Sr}_{0.20}\text{CuO}_4$ crystals were grown. These crystals were characterized by back Laue X-ray method and magnetization measurement. In addition the phase relation which helps to crystal growth was investigated in La_2O_3 - SrO - CuO system and the phase diagram of system above mentioned was made.

We have succeeded to grow the sizable and high quality single crystals of $\text{La}_{2-x}\text{Sr}_x\text{CuO}_4$ (LSCO) by TSFZ method[1]. Now we are trying to grow different contents of Sr in this system. However, there were reported to find such several compounds as $\text{La}_x\text{Sr}_{14-x}\text{Cu}_{24}\text{O}_{41}$ ($0 \leq x \leq 5$), $\text{La}_{1.28-x}\text{Sr}_x\text{Cu}_8\text{O}_{20-8}$ ($1.28 \leq x \leq 1.92$), $\text{La}_{2-x}\text{Sr}_{1+x}\text{Cu}_2\text{O}_{6+x}$ ($0 \leq x \leq 0.15$) and $\text{La}_{1+x}\text{Sr}_{2-x}\text{Cu}_2\text{O}_{5.5+x}$ addition to $\text{La}_{2-x}\text{Sr}_x\text{CuO}_4$ ($0 \leq x \leq 1.5$) in the La_2O_3 - SrO - CuO system[2-5]. It is not obvious whether these compounds may form from molten state or not, because these compounds were formed by sintering process.

In this study, we have investigated what kinds of crystal could be formed from molten liquids of La_2O_3 - SrO - CuO system by using Slow Cooling Floating Zone method(SCFZ method) and DTA-TG analysis. Also, we are growing the single crystals of $\text{La}_{1.86}\text{Sr}_{0.14}\text{CuO}_4$ and $\text{La}_{1.80}\text{Sr}_{0.20}\text{CuO}_4$ and offering grown crystals to other researcher to measure physical properties.

La_2O_3 , SrCO_3 and CuO were used as the starting raw materials. The starting powders were combined in appropriate proportions to prepare mixtures with desired composition and calcined at 850°C for 24 hr.. These calcined materials were pressed at 1 ton/cm^2 to form cylindrical shape rods. These rods were sintered at $1,000$ - $1,100^\circ\text{C}$ in an atmosphere of oxygen gas for 24 hr.. The apparatus for fused experiments was an infrared heating furnace of double ellipsoidal type(Nichiden Machinery Ltd.) with 1.5 kw halogen lamps as the heat source. The sample rods were solidified by slow cooling after the molten zone was formed under a pressure of 0.2MPa of oxygen gas. The composition of solidified samples was analyzed by EPMA(JEOL, model JXA-8600M). Both melting and solidified temperatures were determined by DTA-TG analysis.

The procedure of SCFZ method is followed. The sintered rod of certain composition was placed inside an infrared heating furnace and then melted to form molten zone. The molten zone was separated to top and down by mechanically and slow cooling. Then the compounds having high melting temperature were started to solidified, and finally the compound of eutectic composition was solidified. The variation of com-

position depending on the solidified temperature could be obtained by EPMA analysis.

The phase relation of La_2O_3 - SrO - CuO system

Fig.1 shows the composition image of end part of grown La_2CuO_4 crystal. From the contrast of photo, there were three different phases whose composition were La_2CuO_4 , $\text{LaCuO}_{2.5}$ and CuO in order of brightness. Also, both CuO and Cu_2O were mixed in the darker part. $\text{LaCuO}_{2.5}$ is corresponded to $\text{La}_{1-x}\text{Sr}_x\text{Cu}_8\text{O}_{20-3}$ when $x=0$ and a new phase which was not reported before. Fig.2 shows the results of DTA analysis of sintered material whose composition was $\text{La}:\text{Cu}=1:1$. These results showed that the profiles of DTA were different when temperature was up and down. This could be due to that some of CuO were changed to Cu_2O . From both results of DTA and EPMA analysis, the peaks at 990°C , at $1,050^\circ\text{C}$ and at $1,075^\circ\text{C}$ were due to fusion and solidification of cuprous oxide, cupric oxide and $\text{LaCuO}_{2.5}$, respectively. Fig.3 shows the XRD pattern of $\text{LaCuO}_{2.5}$. We did not analyze this pattern in detail, but this pattern was clearly different from the solid phase obtained at latest. From these results, it was



Fig.1 Composition image of end part of grown crystal

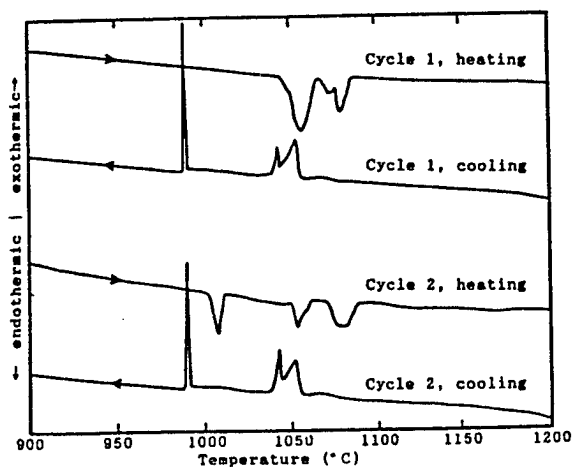


Fig.2 Results of DTA-TG analysis

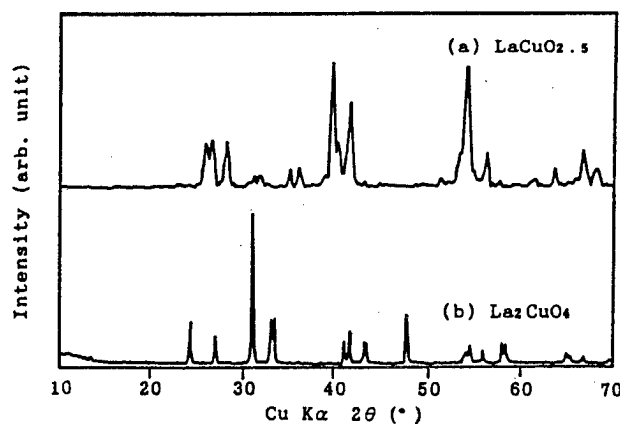


Fig.3 XRD pattern of $\text{LaCuO}_{2.5}$

revealed that $\text{LaCuO}_{2.5}$ was decomposed to La_2CuO_4 and liquids phase at the peritectic temperature of $1,075^\circ\text{C}$. The phase diagram of $\text{LaO}_{1.5}$ - CuO system is shown in fig.4. It was proved that another $\text{LaCuO}_{2.5}$ phase beside La_2CuO_4 phase exists in $\text{LaO}_{1.5}$ - CuO system and this $\text{LaCuO}_{2.5}$ was decomposed to La_2CuO_4 and liquid phase above $1,075^\circ\text{C}$. The dashed line in this phase diagram showed the eutectic temperature when Cu_2O was considered.

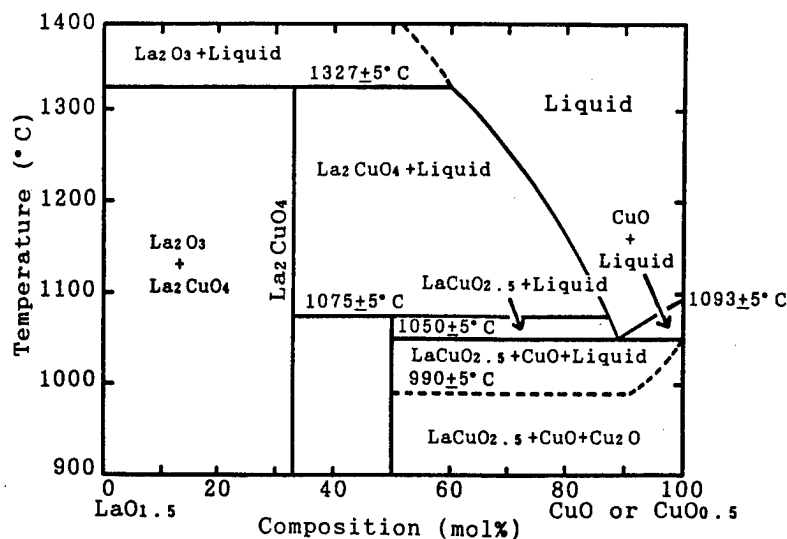


Fig.4 Phase diagram of the $\text{LaCuO}_{1.5}$ -CuO system

In order to investigate the phase relation in La_2O_3 -SrO-CuO system, SCFZ method was applied to fuse the sintered rods of solvent composition ($\text{La}:\text{Sr}:\text{Cu}=2-x:x:4$, $x=0.4, 0.8, 1.2, 1.6$) which would be used for growth experiments of LSCO by TSFZ method. The composition of end part of LSCO solidified crystal grown by TSFZ method was analyzed by EPMA. It made clear from the composition image that existing phases were La_2CuO_4 , $\text{La}_x\text{Sr}_{14-x}\text{Cu}_{24}\text{O}_{38+8}$, CuO and Cu_2O . These results are collectively shown in fig.5 and table 1. Several phases, such as (201) phase, (101) phase, (212) phase, (0,14,24) phase, CuO and Cu_2O were formed depending on the composition of starting materials, and these composition were quite different from the values reported already. Concerning (201) phase, it was reported that solid solution was possible to form until $x=1.5$ of Sr(x) content by sintering method. However, it made clear that solid solution was possible to form until $x=0.32$ of Sr(x) content when it was formed from molten state. The range of Sr contents to form solid solution for other phases, such as (101) and (212) phases, was wider from molten state than from sintering process. This difference could be due to the decomposition reaction of CuO to form Cu_2O . Also it could be due to the presence of Cu^{2+} and Cu^+ in molten state in La_2O_3 -SrO-CuO system. The larger \square and \triangle symbols in fig.5 were represented the composition of sample used for crystal growth and fusion experiments. The produced phases from molten state were shown by smaller symbols in fig.5. From these results, it could be estimated two following important

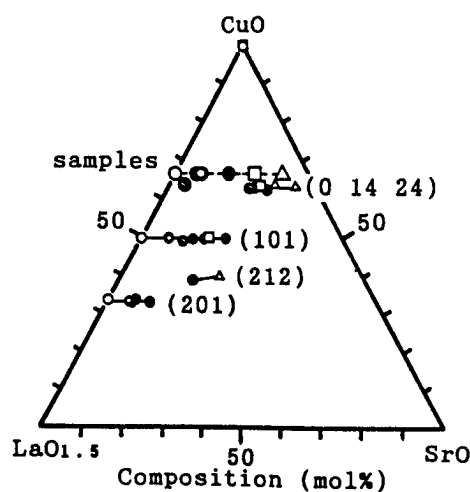


Fig.5 The ternary diagram of $\text{LaO}_{1.5}$ -SrO-CuO system

points for growth of LSCO single crystals.

(1) The composition range of Sr content was $0.0 \leq x \leq 0.32$ which was possible to grow LSCO single crystal.

(2) The Sr content of solvent for growth of LSCO single crystal was $x \leq 0.8$. When the solvents of $x \geq 1.2$ were used (\square and \triangle in fig.5), LSCO crystal did not form and another (212) and (101) phases were crystallized.

Table 1 Compounds and their composition range in La_2O_3 - SrO - CuO system

crystalline phase	chemical composition	composition range	reported values ²⁻⁵
(2 0 1)	$\text{La}_{2-x}\text{Sr}_x\text{CuO}_4$ -	$0.00 \leq x \leq 0.32$	$0.00 \leq x \leq 1.5$
(1 0 1)	$\text{La}_{1-x}\text{Sr}_x\text{CuO}_{2.5}$ -	$0.00 \leq x \leq 0.42$	$0.16 \leq x \leq 0.24$
(2 1 2)	$\text{La}_{2-x}\text{Sr}_{1+x}\text{CuO}_6$ -	$0.09 \leq x \leq 0.22$	$0.00 \leq x \leq 0.15$
(0,14,24)	$\text{La}_x\text{Sr}_{14-x}\text{Cu}_{24}\text{O}_{38}$ +	$1.9 \leq x \leq 6.2$	$0.0 \leq x \leq 5.0$

The crystal growth of LSCO single crystals

We are still growing single crystals of $\text{La}_{2-x}\text{Sr}_x\text{CuO}_4$ by TSFZ method. The single crystals of $\text{La}_{1.86}\text{Sr}_{0.14}\text{CuO}_4$ were offered to several researchers to measure physical properties. Now we are trying to grow $\text{La}_{1.80}\text{Sr}_{0.20}\text{CuO}_4$ single crystal and succeeded to get this composition and this crystal was offered already and measuring the value of T_c .

References

- [1] I.Tanaka, K.Yamane and H.Kojima, J.Crystal Growth, **96**, 711(1989).
- [2] J.Hahn et al., Chemtronics, **2**, 126(1987).
- [3] N.Nguyen et al., Mat.Res.Bull., **15**, 891(1980).
- [4] L.Er-Rakho et al., J. Solid State Chem., **73**, 514(1988).
- [5] D.M.De Leeuw et al., J. Solid State Chem., **80**, 276(1989).

Crystal Growth and Characterization of Oxide Superconductors and Related Compounds

H. Takei, H. Takeya, F. Sakai, M. Koike and J. Akimoto

Institute for Solid State Physics, the University of Tokyo,
7-22-1, Roppongi, Minato-ku, Tokyo 106, Japan

The present investigation has been performed along the three courses: [1] crystallization from glassy states of the Bi-Sr-Ca-Cu-O system, [2] growth of Bi-Sr-Ca-Cu-O film crystals by a newly developed method "solvent-evaporation epitaxy(SEE)" and [3] growth and characterization of the two dimensional, triangle crystal NaTiO_2 .

Because of the high superconducting transition temperature in the Bi-Sr-Ca-Cu-O compounds, much attention to this system has been devoted during the past two years. Many investigators have tried to obtain single-crystal specimens of this system by using various kinds of techniques. It becomes clear that there exist some difficulties for obtaining less-imperfect, high quality crystals with conventional techniques. These difficulties are considered to be come from a lack of the fundamental knowledge among the growth features of Bi-Sr-Ca-Cu-O crystals. We thus performed the observation of crystallization process from a glassy state of Bi-Sr-Ca-Cu-O by high resolution electron microscope, and found out that the crystallization of the superconductive phases with $T_c=30$ and 80K starts even below 600°C and stably progresses up to above 900°C . This fact suggests that the stable phases between 600°C and 900°C are the superconductive ones ($T_c=30$ and 80K).

In section [II], we describe a new method for growing crystal films of the Bi-Sr-Ca-Cu-O superconductors. Apparently, film growth technique is one choice for obtaining two dimensionally large and high quality crystals. Though considerable efforts have been paid, complete single-crystal films have not yet been prepared. No single-crystal film of the high $T_c(110\text{K})$ phase have also been obtained. Quite recently we found an epitaxial film formation with an evaporation of solvent KCl during the experiments of liquid phase epitaxy. We applied this technique to the Bi-Sr-Ca-Cu-O superconductors, and the (001)-oriented films with $T_c=80\text{K}$ and 110K were obtained.

The final section [III] represents growth of NaTiO_2 single crystals which are believed to be one of the key materials for clarifying the mutual interaction of spins in Ti^{3+} ions on the two dimensionally oriented triangle lattice. We succeeded to prepare the single-crystals from high-temperature solutions of sodium metal. The crystals, however, contain a considerable amount of Na-defect, which was introduced by a migration of sodium ions from the layered lattice. Such defects would affect the magnetic susceptibility at low temperatures.

[I] Crystallization from a Glassy State in the Bi-Sr-Ca-Cu-O System

The Bi-Sr-Ca-Cu-O system involves at least three types of superconducting compounds: $\text{Bi}_2(\text{Sr,Ca})_2\text{CuO}_x$ ($T_c=30\text{K}$, A-phase, $\text{Bi}_2(\text{Sr,Ca})_3\text{Cu}_2\text{O}_x$ ($T_c=80\text{K}$, B-phase) and $\text{Bi}_2(\text{Sr,Ca})_4\text{Cu}_3\text{O}_x$ ($T_c=110\text{K}$, C-phase). Many investigators have suggested that the phase relations between the three are complicated and no complete data on the stability field of these compounds have been reported. Kuwahara et al.[1] and Kitazawa et al.[2] have suggested that the stoichiometric B-phase is only stable

between 800°C and its melting point of about 1000°C, and tends to decompose into the A- and C-phases below 800°C by the supposed solid state disproportionation reaction.

The present section describes the initial process of crystallization from Bi-Sr-Ca-Cu-O glass which was prepared by rapid cooling of the melt. The reason why the glass specimens were adopted as a starting material is that the glassy state is considered to be superior in homogeneity to sintered materials. Our observations have revealed that both the A- and B-phases crystallize stably from a glassy medium at 600°C which is above the crystallization temperature, T_x , of about 450°C, [3,4] whereas the C-phase was not observed at this temperature range. This fact means that at 600°C, the A- and B-phases are stable but C is not.

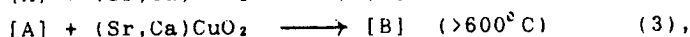
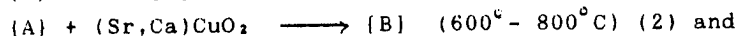
The glassy specimens of the Bi-Sr-Ca-Cu-O system were obtained by dropping the melt on a cold copper plate. X-ray powder diffraction (XPD) analysis showed only a very broad peak around 30° in 2θ of CuK radiation (see Fig. I-1). This result closely resembles those reported previously [5,6]. Annealing of as-prepared specimen was carried out in a resistance furnace in air at a maximum temperature between 400°C and 900°C, and the specimens were quenched to room temperature. Complete melting was observed above 940°C. In the DTA experiments, the as-quenched specimens displayed two large peaks, exothermic and endothermic, the patterns of which were almost the same as that reported by Yoshimura et al. [6]. The exothermic peak, which appeared sharply at about 450°C, corresponded to the glass-to-crystal transition while the broad endothermic one, which started near 800°C and ended above 900°C, corresponded to the melting of crystallized materials. This melting behavior is almost the same as that reported for sintered specimens [7].

The XPD results of the annealed specimens indicated that a clear change appeared between 400°C and 600°C, as shown in Fig. I-1. The specimens annealed at temperatures up to 400°C showed no significant change in the XPD patterns from the as-quenched glassy state, whereas those annealed above 600°C changed into a crystalline state. The XPD peaks of the crystalline state were assigned as a mixture of $\text{Bi}_2(\text{Sr,Ca})_2\text{CuO}_x$ (A-phase) and $\text{Bi}_2(\text{Sr,Ca})_3\text{Cu}_2\text{O}_x$ (B-phase). The specimens annealed at 800°C were mainly of the B-phase and the superconducting transition was observed at 84K as an onset T_c , and at 80K as a mid T_c . The residual resistivity completely disappeared at 55K.

The 500°C annealed specimens were in an intermediate state between the glassy and crystalline states. Figure I-2 shows the changes of the XPD patterns with annealing time at 500°C. It is clear that the diffraction peaks became sharper with an increase in the annealing time. The XPD lines of the specimens annealed at 500°C for 120 h, however, are much broader than those of the 600°C-annealed specimen (see also Fig. 1). This means that the annealing at 500°C is very critical for crystallization in the glassy Bi-Sr-Ca-Cu-O media. The microscope and SEM observations clarified within their degree of resolution that no apparent change occurred in the bulk part of the specimens by annealing at this temperature.

Figures I-3(a)-(c) show the high resolution electron micrographs of the annealed specimens at 500°C and 600°C. Clear lattice images are observed in the specimen annealed at 500°C for 12 hr. It should be noted that two types of lattice spacings, 1.30nm and 1.55nm, are observed in a single photograph, as shown in Fig. I-3(a). The former value corresponds to the (1/2)c-spacing of the A-phase and the latter to that of the B-phase. The patterns, which were thought to be due to a stacking disorder caused by a compositional fluctuation in the glassy media, were commonly observed in the present TEM photographs of the 500°C annealed specimens. Figures I-3(b) and 3(c), which show the specimens annealed at 600°C for 12 h, indicate that both the A- and B-crystals grow stably as a result of this heat treatment.

The results of the low-temperature annealing is expressed by the formulae:



where A is $\text{Bi}_2(\text{Sr,Ca})_2\text{CuO}_x$ and B is $\text{Bi}_2(\text{Sr,Ca})_3\text{Cu}_2\text{O}_x$, and the marks {} and [] represent the glassy and crystalline states, respectively. With an increase of the annealing temperature above 600°C , the reactions (2) and (3) proceed, and finally, the major part of the reaction product becomes the B-phase. Precipitation of the C-phase, whose (1/2)c-spacing was reported to be about 1.8nm^2 , was not observed in the temperature range between 500° and 600°C .

Kuwahara et al.[1] and Kitazawa et al.[2] have presented a tentative phase diagram of the pseudobinary system $\text{Bi}_2\text{Sr}_2\text{CaCuO}_x$ and CaCuO_2 near the melting, and suggested the occurrence of the solid-state disproportionation reaction between the phases A, B and C below 800°C . The reaction can be expressed by the formula,



where the B-phase is unstable and changes into [A] and [C] at this temperature range. This formula(4) is completely opposite to our formulae(1)-(3), because the most stable phase between 600° and 800°C is [B]. Similar results have been reported by Kanai et al.[8], where the formation of the B-phase was observed by XPD analyses on the quenched and then annealed Bi-Sr-Ca-Cu-O samples between 650° and 874°C . Many studies have pointed out that the C-phase appears from [B] in a partially molten condition in a shallow temperature range between 840° and 900°C and easily decomposes above 900°C .

The stability field of the phase [C] has not been completely clarified. Ono et al.[9] have reported that the C-phase only appears between 870° and 900°C in air with a small amount of liquid. The present experiments partly support the above results because an origination of the C-phase could not be observed in the TEM photographs of the specimens annealed between 500° and 600°C .

References:

- [1] K. Kuwahara, S.Yaegashi, K. Kishio, T. Hasegawa and K. Kitazawa; Progress in High Temp. Supercond., 9(1988)38.
- [2] K.Kitazawa, S.Yaegashi, K.Kishio, T.Hasegawa, N.Kanazawa, K.Park and K.Fueki; presented at Amer.Cer.Soc. 90th Annual Meeting, Cincinnati, Ohio, May 1988, to be published in Adv. Cer. Materials.
- [3] R.A.Vaile, S.Bosi, T.Puzzer, A.Bailey, J.Cochrane, N.Mondinos, K.Sealey, G. J. Russell, D.N.Matthews, M.Aristides and K.N.R.Taylor; J.Crystal Growth, 91(1988)450.
- [4] Y.Oka, N.Yamamoto, H.Kitaguchi, K.Oda and J.Takada; Jpn.J.Appl.Phys., 28(1989)L213.
- [5] T.Minami, Y.Akamatsu, M.Tatsumisago, N.Tohe and Y.Kowada; Jpn.J.Appl.Phys., 91(1988)L777.
- [6] M.Yoshimura, T.Sung, Z.Nakagawa and T.Nakamura; Jpn.J.Appl.Phys., 27(1988)L1877.
- [7] J.M.Tarascon, Y.Le Page, P.Barboux, B.G.Bagley, L.H.Greene, W.R.Mackinnon, G. W. Hull, M. Giroud and D. M. Hwang; Phys.Rev.B., 37(1988)9382.
- [8] T.Kanai, T.Kumagai, A.Soeta, T.Suzuki, K.Aihara, T.Kamo and S.Matsuda; Jpn.J.Appl. Phys., 27(1988)L1435.
- [9] A.Ono, K.Kosuda, S.Sueno and Y.Ishizawa; Jpn.J.Appl.Phys., 27(1988)L1007.

[II] Preparation of Oxide Superconductor Films by the Solvent-Evaporation Epitaxy

Solvent evaporation is one of the most common technique for obtaining crystals. However, its application to epitaxy has not been tried yet. The present section deals with the first trial for epitaxial growth of the Bi-type oxide superconductor films by the solvent evaporation.

Thin films of Bi-Sr-Ca-Cu-O system superconductors have been studied for fundamental research and for microelectronics applications. Our group tried to prepare high T_c Bi-Sr-Ca-Cu-O films on MgO substrates by the liquid phase epitaxy [1], where various kinds of fluxes were used, and $\text{Bi}_2\text{Sr}_2\text{CaCu}_2\text{O}_x$ films were grown only from a KCl flux. The films prepared by a dipping technique were rough in their surfaces and showed a superconducting transition with the onset T_c at 95K, but had a residual resistivity at 50K by 1/10 to 95K in an as-grown state.

Recently, we found that a smooth film was formed on the MgO(100) substrate when the mixture of Bi-Sr-Ca-Cu-O powder with KCl was plastered on the substrate, and then heated around 900 C. The solvent KCl was removed by evaporation and the film growth of Bi-Sr-Ca-Cu-O advanced. The fact that no residual KCl was detected by EPMA means that the solvent was completely evaporated during heating. The film formation is supposed to be made in the liquid phase by concentrating the solution after the evaporation of the solvent. Thus we name this process "solvent evaporation epitaxy (SEE)".

The three starting compositions were selected in this study: Bi:Sr:Ca:Cu = 2:2:1:2, 2:2:2:3 and 2:2:2:4 in atomic ratios. The sintered materials were ground and passed through the mesh(#325) into fine powders. The powder was mixed with KCl as a flux using acetone, where the solvent KCl was added from ten to four hundred times to the solute in mol ratio, and the mixture was spread on the MgO substrate($5 \times 10 \times 1 \text{ mm}^3$) at a thickness of about 1-2mm. After the acetone had dried naturally, the sample was placed in an alumina boat and heated in a resistance furnace kept between 825 °C and 915 °C for 2 h or 10 h and then cooled in air. It was observed that KCl was gradually evaporated and removed completely during the heating cycle.

We here report successful results on the three samples, where the films were prepared in the following conditions: film #1 (KCl/ $\text{Bi}_2\text{Sr}_2\text{CaCu}_2\text{O}_x$ =300, 850 °C for 2 h), film #2 (KCl/ $\text{Bi}_2\text{Sr}_2\text{CaCu}_2\text{O}_x$ =300, 850 C for 10 h) and film #3 (KCl/ $\text{Bi}_2\text{Sr}_2\text{Ca}_2\text{Cu}_4\text{O}_x$ = 300, 900 °C for 10 h). Typical X-ray diffraction patterns of films #2 was shown in Fig.II-1. These films consisted of two phases which gave only 001($l=2n$) Bragg reflections corresponding to $\text{Bi}_2\text{Sr}_2\text{CuO}_x$ ($c=24\text{\AA}$) and $\text{Bi}_2\text{Sr}_2\text{CaCu}_2\text{O}_x$ ($c=31\text{\AA}$). This indicates that the c-axis of the film is oriented along [001] of the MgO substrate, as reported previously [1]. The oriented over-growth was also confirmed by X-ray precession photographs taken together with the film and the substrate, as shown in Fig.II-2. The orientation relationship between the two has already been reported elsewhere [5]. In films #2 and #3, $\text{Bi}_2\text{Sr}_2\text{CaCu}_2\text{O}_x$ appeared as a major phase. The mean compositions of the films were determined by EPMA to be Bi:Sr:Ca:Cu=2.3:1.9:1.0:2.0 (#1), 2.1:1.8:0.9:2.0(#2) and 1.9:1.8:0.7:2.0 (#3). With film #1, $\text{Bi}_2(\text{Sr,Ca})_2\text{CuO}_x$ and Ca_2CuO_x were observed by point analysis of EPMA. The difference between films #1 and #2 was considered to be caused by different annealing processes. Figure II-3 shows a typical SEM photograph of the film, which indicates that the film was much more dense and smooth than the film reported in our previous paper [1]. No film formation was observed without KCl in the same growth condition as used in film #1 or #2.

Owing to the high density and the smoothness, better results on superconductivity were obtained. Figure II-4 shows the electrical resistance in the as-grown state measured for films #1, #2 and #3. Films #1 and #2 exhibit a double transition at 111K and 88K for onset T_c , whereas film #3 has a single transition around 90 K for onset T_c . Zero resistances were measured at 81K on films #1 and #3 and at 85 K on film #2. The results suggest that there was a small amount of 110K superconducting phase in films #1 and #3. Since the measured thickness of film #1 was about 5 μm , the resistivity was estimated to be 300 $\mu\Omega\text{cm}$ at 88K. Although film #1 apparently had inclusions of $\text{Bi}_2(\text{Sr,Ca})_2\text{CuO}_x$, the so-called 20K superconducting phase

shown in fig. 1, it had no residual resistivity below 81K. SEM-EPMA revealed that the $\text{Bi}_2(\text{Sr,Ca})_2\text{CuO}_x$ phase appeared as small islands of about $10\text{ }\mu\text{m}$ size and occupied about 5% of the entire film area. It is possible that a superconducting path was constructed in between the $\text{Bi}_2\text{Sr}_2\text{Ca}_2\text{Cu}_3\text{O}_x$ and $\text{Bi}_2\text{Sr}_2\text{CaCu}_2\text{O}_x$ phases, and consequently, the resistivity due to $\text{Bi}_2(\text{Sr,Ca})_2\text{CuO}_x$ was not detected. Figure II-5 shows an anisotropic behaviour in resistivity under an externally applied magnetic field at 72.5K. When the external field was applied parallel to the c-plane (relative angle:0 degree), the resistivity change showed minimum, and the maximum value was observed when the field was perpendicular to the c-plane (angle:90 degree). From these values, the upper critical field H_{c2} can be estimated to be: above 10T for field $H \parallel$ ab-plane and below 1T for $H \parallel$ c-plane at 72.5K.

The present SEE technique also produced a small amount of $\text{Bi}_2\text{Sr}_2\text{Ca}_2\text{Cu}_3\text{O}_x$, the so-called 110 K phase, in spite of the short period for preparing the film at 850°C . The preparation of the 110 K phase in the powder-metallurgical method needs a long annealing time or partial melting around 900°C [6,7]. On the other hand, Honda et al.[8] have reported an appearance of the high- T_c phase in the Bi-Sr-Ca-K-Cu-O system even at 860°C for 5 h, where the partial melting occurred by an addition of potassium ions to the system. This and our results suggest that potassium ions play a considerable role in producing the 110 K superconductor through the liquid phase.

References

- [1] H.Takeya and H.Takei;Jpn.J.Appl.Phys.,28(1989)L229.
- [2] A.Katsui and H.Ohtsuka;J.Crystal Growth,91(1988)261.
- [3] A.Katsui;Jpn.J.Appl.Phys.,27(1988)L844.
- [4] L.F.Schneemeyer, R.B.van Dover, S.H.Glarum, S.A.Sunshine, R.M.Fleming, B.Batlogg, T.Siegrist, J.H.Marshall, J.V.Waszczyk and L.W.Rupp; Nature,332(1988)420.
- [5] H.Takeya and H.Takei;Jpn.J.Appl.Phys.28(1989)L1571.
- [6] H.Nobumasa, K.Shimizu, Y.Kitano and T.Kawai;Jpn.J.Appl.Phys.,27(1988)L846.
- [7] A.Ono; Jpn.J.Appl.Phys.,27(1988)L1213.
- [8] T.Honda, T.Wada, M.Sakai, M.Miyajima, N.Nishikawa, S.Uchida, K.Uchinokura and S. Tanaka;Jpn.J.Appl.Phys.,27(1988)

[III] Growth and Structure Analysis of Nonstoichiometric Single Crystal Na_xTiO_2 ($x \sim 0.5$)

Hirakawa et al.[1] first pointed out that NaTiO_2 and LiNiO_2 were promising candidates of two dimensional triangular lattice antiferromagnet with $S=1/2$. To clarify the physical properties of NaTiO_2 , they successfully prepared NaTiO_2 powder samples using the reaction of Na_2O with Ti_2O_3 at 1273K under high-pressure Ar gas atmosphere. NaTiO_2 was originally described by Hagenmuller et al.[2]. They prepared powder samples using a redox reaction of metal sodium and titanium dioxide at 1173K, and revealed from the result of X-ray powder diffraction that this compound had a rhombohedral unit cell, and the $-\text{NaFeO}_2$ type structure. Recently, Maazaz et al.[3] examined the structures of the Na_xTiO_2 system ($0.46 \leq x \leq 1$) by the electrochemical deintercalation from the stoichiometric NaTiO_2 powder. In this paper, we describe the crystal growth and crystal structure of the nonstoichiometric $\text{Na}_{0.5}\text{TiO}_2$, and further, we discuss the decrease of the intersheet distance with the Na-defects in comparison with the Na_xTiO_2 system ($0.46 \leq x \leq 1$) previously reported [4].

Starting materials were TiO_2 powder (99.9%) and excess sodium metal blocks with 99% purity. They were placed in a sealed iron vessel, heated in a resistance furnace at $1200\text{--}1400^\circ\text{C}$ in an argon gas flow for several hours and slowly cooled to room temperature. In many cases, no apparent leakage of sodium vapor from the vessel was observed. After cooling, the vessel was opened by sawing in air, and the products of

black crystal grains were taken out as soon as possible, and were kept in a vacuum.

The black Na_xTiO_2 crystals having a violet tone, maximum $5 \times 3 \times 3 \text{ mm}$ in size, were grown together with needle-shaped NaTi_2O_6 crystals. Under air atmosphere, the bubbling caused by a reaction with moisture, oxygen or CO_2 gas, was observed on the surfaces of the Na_xTiO_2 crystals, and white powder which was supposed to be NaOH or Na_2CO_3 was precipitated on the crystal surfaces.

Figure III-1 is a SEM photograph of the as-grown Na_xTiO_2 crystal indicating that it grows with a developed (0001) habit. The data of EPMA represented that the bulk composition of the block crystals was almost uniform with an approximate molar ratio $\text{Na}/\text{Ti}=0.5/1.0(x=0.5)$. This result suggested that the crystals contained a considerable amount of Na-defect. Small crystals of $\text{Na}_{0.5}\text{TiO}_2$ were held in evacuated glass capillaries of 0.3 mm diameter with 0.01 mm thickness, and were used for the following X-ray diffraction study. Laue and precession photographs indicate that the crystal belongs to the trigonal system with the possible space group $R\bar{3}2$, $R3m$, or $R\bar{3}m$ and has the hexagonal cell parameters $a=3.0\text{\AA}$ and $c=16.9\text{\AA}$.

A small block crystal with the approximate chemical formula of $\text{Na}_{0.5}\text{TiO}_2$, $\sim 0.15 \times 0.10 \times 0.05 \text{ mm}$ in size, which was held in an evacuated glass capillary, was used for the crystal structure determination. The space group of highest symmetry $R\bar{3}m$, confirmed by successful refinement, was adopted. The refinement was initiated with the atomic coordinates given by Hagenmuller et al.[2]. The final difference Fourier map showed no significant residual electron density, and the sodium site occupancy with the equivalent isotropic temperature factor of 5.48, was refined to 0.54(1). The final atomic parameters are given in Table III-I.

The crystal structure of $\text{Na}_{0.5}\text{TiO}_2$, as shown in Fig.III-2 is a typical layer structure of Na, Ti and O atoms. Na atom is octahedrally coordinated by six oxygen atoms with the Na-O bond distance of $2.460(3)\text{\AA}$, which is well consistent with the average 6-fold distance of 2.44\AA reported in the literature [5]. The arrangement of oxygen ions is divided by the sodium layers into the two close-packed oxygen layers surrounding Ti cations. The shortest O-O distance across the Na layer is $3.916(8)\text{\AA}$, which is much longer than the O-O distance of the average value 2.856\AA forming a TiO_6 octahedron. In addition, the thermal ellipsoids for the Na-site with an occupancy 0.54 are spread out over the (0001) plane (Fig.III-2). Accordingly, the long distance between the oxygen layers across the Na layer would provide an easy migration of Na ions to the crystal surface through the gap between the two oxygen layers.

The TiO_6 octahedra are connected each other by sharing the six edges in the (0001) plane, and form a sheet structure. The sharing O-O distance is $2.733(7)\text{\AA}$. The intrasheet Ti-Ti distance is 2.9791\AA , while the intersheet distance, which is equal to one third of the c-axis length, is 5.634\AA . Moreover, the shortest intersheet Ti-Ti distance is $5.899(1)\text{\AA}$, which is expected to be too far to interact with each other. This means that Ti cations in $\text{Na}_{0.5}\text{TiO}_2$ form the triangular lattice outstanding two-dimensionality. The 6-fold Ti-O distance is $2.021(2)\text{\AA}$. From the calculation of the valence bond sums using the Zachariasen's curve, the valence charge of titanium is 3.3, which is well consistent with the result of average titanium valency 3.5 from an estimation by the chemical formula with the sodium site occupancy of 0.54.

Microscope observation revealed that the clean crystal surface of the present $\text{Na}_{0.5}\text{TiO}_2$ was stable only for a few minutes in air atmosphere, then they covered with the vigorous bubbling of, probably, H_2 gas. The bulk part of $\text{Na}_{0.5}\text{TiO}_2$ crystal is, however, stable in air for several hours. The precession photographs of this bulk crystal held in the evacuated capillary represented the lattice parameters $a=3.0\text{\AA}$ and $c=16.9\text{\AA}$. A prolonged exposure to air for more than several days changed the chemical

composition of the bulk part to $\text{Na}_{0.3}\text{TiO}_2$, determined by EPMA analyses. The Laue and precession photographs showed that the $\text{Na}_{0.3}\text{TiO}_2$ crystal had the trigonal symmetry remained unchanged. No obvious changes in both chemical composition and the lattice parameters were observed with further exposures to air.

The lattice contraction process with decreasing Na-content was continuously monitored by the automated four-circle diffractometer (MoK radiation) using a small crystal of $\text{Na}_{0.3}\text{TiO}_2$ in air, after the determination of crystal orientation. No other reflections, indicating the distortion from the trigonal symmetry were observed using the peak search method in every 20 hours. The typical lattice parameters, determined by the least-squares method, were listed in Table III-II with their exposure time to air atmosphere. The chemical composition of each specimen could not be determined because of their rapid lattice contractions. The most contracted lattice parameters with the chemical formula $\text{Na}_{0.3}\text{TiO}_2$ are $a=2.9665(5)\text{\AA}$, $c=15.755(9)\text{\AA}$, and $V=120.07(8)\text{\AA}^3$.

The intrasheet Ti-Ti distance in Na_xTiO_2 crystals, which is identical to the a-axis length, decreases with decreasing Na-content from 2.9791\AA ($x=0.54$) to 2.9665\AA ($x=0.3$) (Table III-II). This can be explained by a decrease in the ionic radius of Ti with changing the oxidation state from $3+$ to $4+$, because of decreasing Na-content. Similar feature was observed in the Na_xTiO_2 powder specimens [3], as well as in Na_xMO_2 , where M is Ni, Cr, or Co [6,7]. On the other hand, the intersheet distance of 5.643\AA in the present $\text{Na}_{0.3}\text{TiO}_2$ crystal, which is equal to one third of the c-axis length, is much longer than 5.408\AA in the stoichiometric NaTiO_2 powder [3]. The increase in the intersheet distance with decreasing Na-content is also observed in other Na_xMO_2 systems with deintercalation [6,7].

The present rhombohedral lattice contraction process of Na_xTiO_2 crystal with the range of $0.3 \leq x \leq 0.54$ revealed that the intensities of all reflections decreased together with the Na-content. This suggests that some structural damage occurred during the exposure to air atmosphere. In addition, changes in diffraction intensities of the 107, 003, and 006 reflections between $\text{Na}_{0.3}\text{TiO}_2$ and $\text{Na}_{0.54}\text{TiO}_2$ crystals were considerably large in comparison with those of the corresponding 104 reflections. Similar feature was reported by Vidyasagar and Gopalakrishnan [8] in the Li_xVO_2 system, where the intensity of the 003 line decreased steadily with decreasing lithium content.

We have succeeded in preparation of the nonstoichiometric Na_xTiO_2 ($x \sim 0.5$) single crystals from high-temperature solutions of sodium metal and titanium dioxide. The triangular lattice of titanium cations outstanding two-dimensionality in $\text{Na}_{0.54}\text{TiO}_2$ was confirmed from the single crystal X-ray structure analysis. However, these crystals are strongly attacked by the moisture, oxygen or CO_2 in air atmosphere. This causes a decrease in the Na-contents from $x=0.54$ to $x=0.3$ with a remarkable lattice contraction of about 1.2\AA towards the c-axis direction in the rhombohedral Na_xTiO_2 crystals.

References

- [1] K.Hirakawa, H.Kadowaki and K.Ubukoshi; J.Phys.Soc.Jpn., 54(1985)3526.
- [2] P.Hagenmuller, A.Lecerf and M.Onillon; C.R.Acad.Sci.Paris, 255(1962)928.
- [3] A.Maazaz, C.Delmas and P.Hagenmuller; J.Inclusion Phenomena, 1(1983)45.
- [4] J.Akimoto and H.Takei; J.Solid State Chem., 79(1989)212.
- [5] D.T.Cromer and J.B.Mann; Acta Crystallogr., A24(1968)321.
- [6] C.Fouassier, C.Delmas and P.Hagenmuller; Mat.Res.Bull., 10(1975)443.
- [7] J.J. Braconnier, C.Delmas and P.Hagenmuller; Mat.Res.Bull., 17(1982)993.
- [8] K.Vidyasagar and J.Gopalakrishnan; J.Solid State Chem., 42(1982)217.

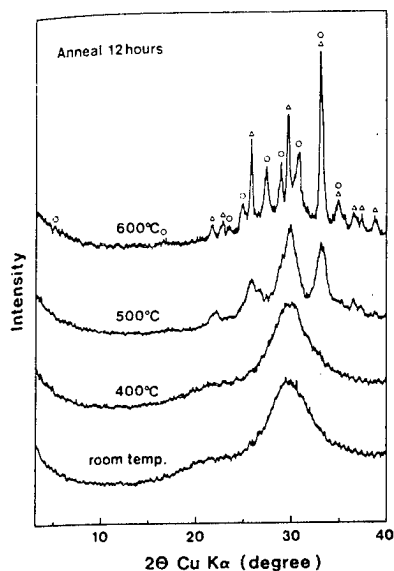


Fig.I-1. Changing of the X-ray powder diffraction (XPD) patterns of the glassy specimen by annealing at 400°, 500° and 600°C for 12 h in air. The analytical composition at the glassy state is $\text{Bi}_{2.0}\text{Sr}_{1.4}\text{Ca}_{0.9}\text{Cu}_{2.2}\text{O}_x$. The marks Δ and \circ on the peaks of the 600°C annealed specimen correspond to the A- and B-phases, respectively.

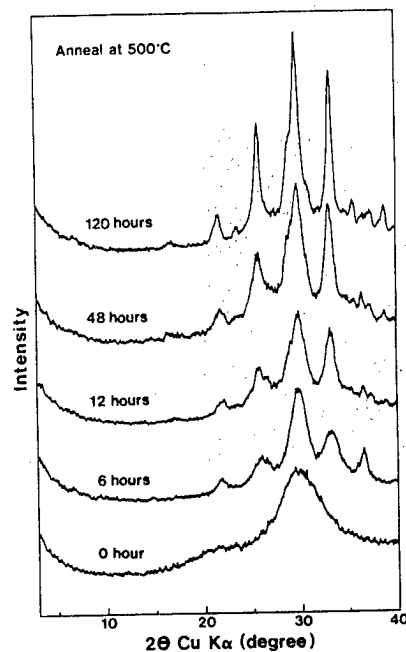


Fig.I-2. Change in the XPD patterns with annealing time at 500°C in air.

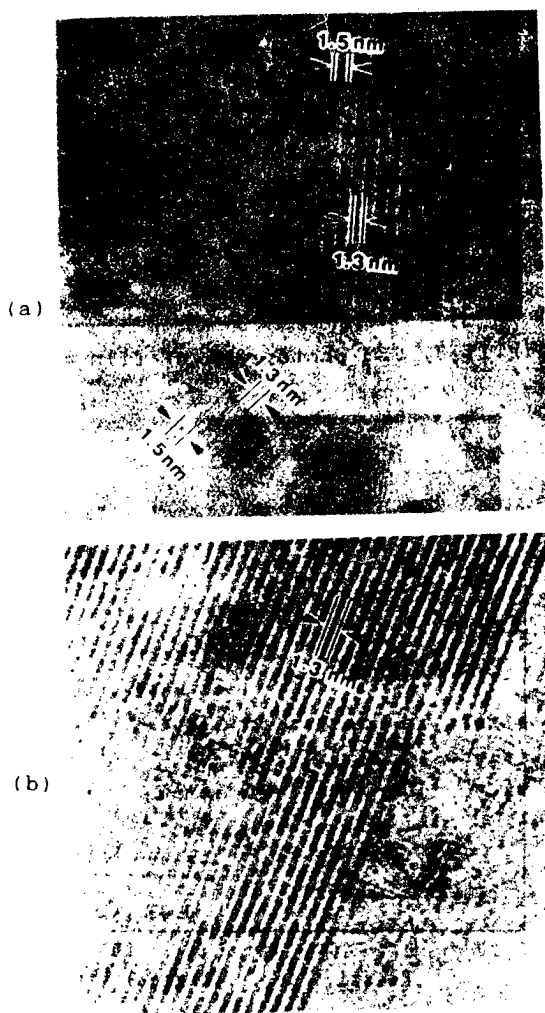
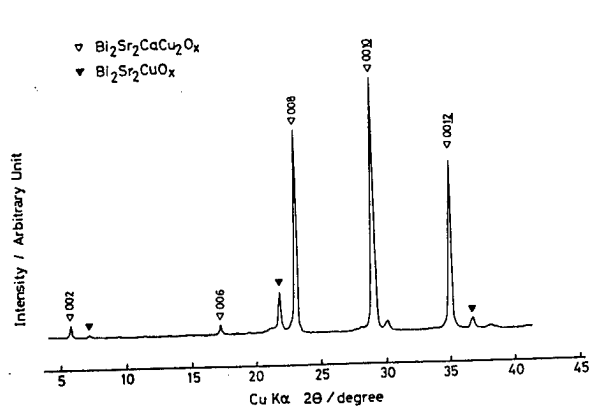
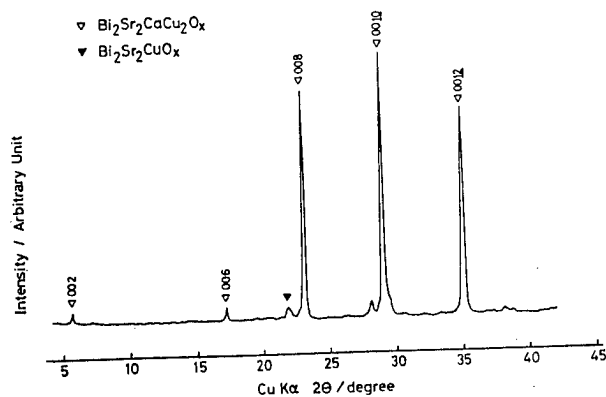


Fig.I-3. Electron micrographs of the annealed specimens, (a) represent the annealed specimens at 500°C in air for 120 h, (b) and (c) are the 600°C annealed specimens for 12 h in air.



(a)



(b)

Fig.II-1. The X-ray diffraction patterns of film #2(a) and film #3(b).

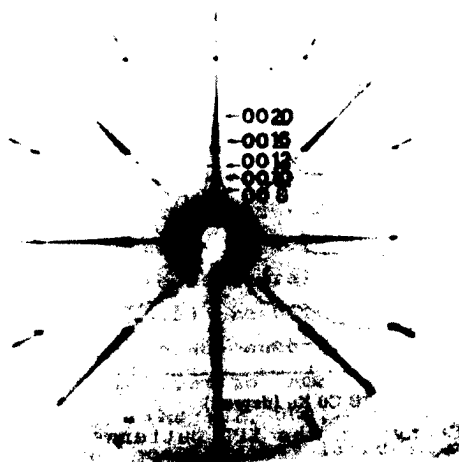


Fig.II-2. A precession photograph of the Bi-Sr-Ca-Cu-O film (weak spots) with MgO(001) substrate (strong spots).

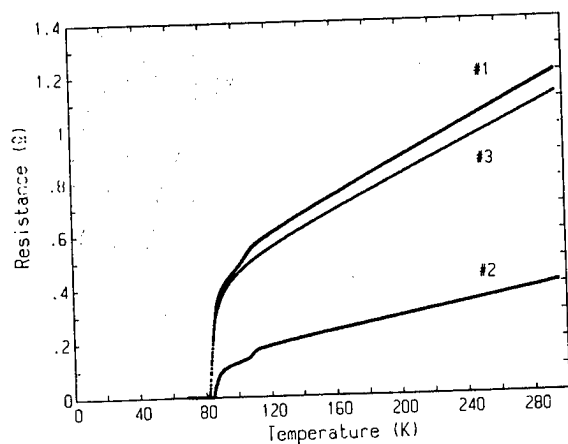


Fig.II-4. The temperature dependences of the resistance for films #1, #2 and #3 in an as-grown state.

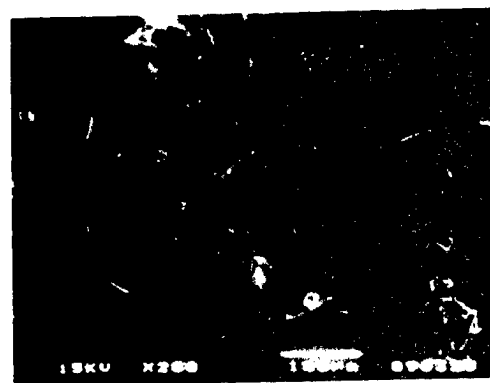


Fig.II-3. SEM photograph of film #2.

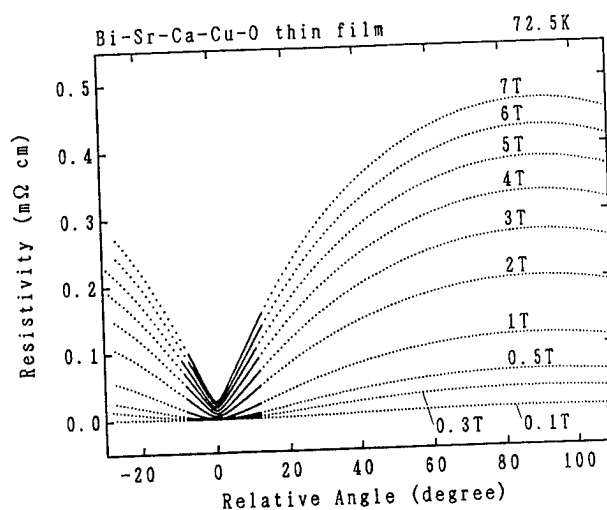


Fig.II-5. Resistivity changes of the SEE films with external magnetic field. The horizontal axis is an angle to the ab-plane.

Table III-I. Positional parameters, site occupancy and temperature factors for $\text{Na}_{0.54}\text{TiO}_2$

atom	site	z	occupancy	β_{11}	β_{33}	$B_{\text{eq.}} (\text{\AA}^2)$
Na	3a	0.0	0.54	0.28(3)	0.0015(4)	5.48
Ti	3b	0.5	1.0	0.021(1)	0.00111(5)	0.79
O	6c	0.229	1.0	0.022(4)	0.0009(1)	0.73

Table III-II. Lattice parameters of Na_xTiO_2 crystals with exposure time to the air

time(h)	a (\AA)	c (\AA)	V (\AA^3)	x ^{a)}
0	2.9791(6)	16.928(3)	130.11(5)	0.54
15	2.9786(8)	16.900(5)	129.83(6)	--
25	2.9749(5)	16.662(9)	127.70(7)	--
39	2.9744(5)	16.335(7)	125.16(6)	--
69	2.9723(4)	16.045(9)	122.76(7)	--
91	2.9714(4)	15.973(9)	122.13(7)	--
137	2.9702(4)	15.844(10)	121.36(8)	--
>1000	2.9665(5)	15.755(9)	120.07(8)	0.3

a) The value $x=0.54$ was determined by structure analysis, and of 0.3 was by chemical analysis.



Fig.III-1. SEM photograph of single crystal Na_xTiO_2 ($x \sim 0.5$), where the developed surface is (0001).

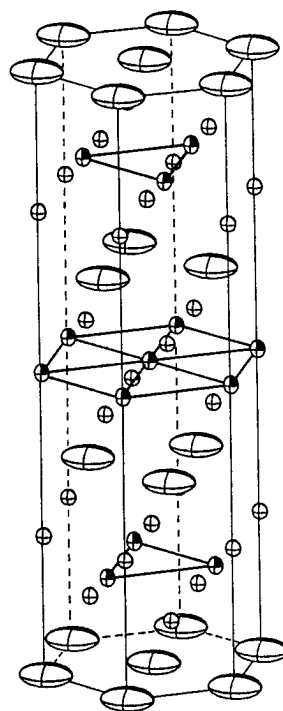


Fig.III-2. An ORTEP drawing of $\text{Na}_{0.54}\text{TiO}_2$. The Ti-Ti interactions forming regular triangles are indicated by the bold lines. Ellipsoids are scaled in 75% probability

Single crystal growth of superconducting oxides and related compounds by the flux, floating zone and other methods

T. Fukuda, T. Shishido, S. Hosoya, M. Toyota, K. Ukei,
T. Kajitani, D. Shindo, H. Iwasaki, M. Takahashi, H. Kikuchi,
S. Nakajima, K. Ohishi, T. Sasaki and Y. Saito

Institute for Materials Research, Tohoku University, Katahira 2-1-1,
Aoba-kur, Sendai 980, Japan

Abstract

Growth of $\text{Bi}_2\text{Sr}_2\text{CaCu}_2\text{O}_x$, $\text{R}_2\text{Ba}_2\text{CuPtO}_8$ ($\text{R}=\text{Er}, \text{Ho}, \text{Y}$), $\text{R}_2\text{Ba}_3\text{Cu}_2\text{PtO}_{10}$ ($\text{R}=\text{Er}, \text{Ho}, \text{Y}$) and $\text{Ba}_4\text{CuPt}_2\text{O}_9$ were performed by the flux method using CuO and alkali halides as solvent. R_2MO_4 ($\text{M}=\text{Cu}, \text{Ni}$), $\text{Bi}_2\text{Sr}_2\text{CaCu}_2\text{O}_x$ and $\text{Tl}_2\text{Ba}_2\text{Ca}_2\text{Cu}_3\text{O}_x$ were grown by the floating zone and high pressure Bridgman method, respectively. Single crystals with dimension up to mm^3 order have been successfully obtained. Fundamental electrical and magnetic properties as well as crystal structure have been investigated.

In order to elucidate the superconducting mechanism, single crystals with high quality and large dimension are essentially required. Furthermore, it is also important to crystallize the related compounds around the superconducting oxides. Almost all the copper-complex superconducting oxides known so far are regarded as incongruent melting compounds, therefore appropriate technique such as Flux, TSFZ are employed for the growth of the single crystals. In this report we describe single crystal growth of the superconducting oxides and related compounds by the flux, floating zone and other methods.

I. Flux growth

1-1 $\text{Bi}_2\text{Sr}_2\text{CaCu}_2\text{O}_x$

Recently, Balestrino et. al have been grown films of $\text{Bi}_2\text{Sr}_2\text{CaCu}_2\text{O}_x$ from KCl solution on gadolinium gallium garnet substrate.¹⁾ This technique is particularly promising in view of the possibility to grow large epitaxial films of both $\text{Bi}_2\text{Sr}_2\text{CaCu}_2\text{O}_x$ and the $\text{Bi}_2\text{Sr}_2\text{Ca}_2\text{Cu}_3\text{O}_x$ phases. Thus, KCl is important intermediate for synthesis of the single crystals of this system.

We have been reported that single crystals of $\text{Bi}_2\text{Sr}_2\text{CaCu}_2\text{O}_x$ have been grown by the KCl flux method.^{2,3)} In this section we report on the crystal growth of $\text{Bi}_2\text{Sr}_2\text{CaCu}_2\text{O}_x$ using another alkali halide KBr ($d_{20}=2.756\text{gcm}^{-3}$, m. p.=748°C, b. p.=1393°C) as a solvent. The solute was prepared from nitrates of Bi, Sr, Ca and Cu. Weighed nitrates were dissolved in water and stirred to mix well. Water was exclude by heating, the resultant residue was heated furthermore at low temperature (below 500°C) in order to calcine. The solvation of this solute to the KBr solvent proceeded very smoothly. In a typical experiment, a 30 wt% mixture of the solute ($\text{Bi}:\text{Sr}:\text{Ca}:\text{Cu}=2:2:2:3$) in KBr was heated to 880°C at 300°C^{-1} , held at that temperature for 3h, and then cooled at 5°C^{-1} to 740°C. Fig.1. shows the surface of the $\text{Bi}_2\text{Sr}_2\text{CaCu}_2\text{O}_x$. The magnetization as a function of the temperature of the single crystal $\text{Bi}_2\text{Sr}_2\text{CaCu}_2\text{O}_x$ ($H=20\text{G}$) are shown in Fig. 2. Details will be presented elsewhere.⁴⁾

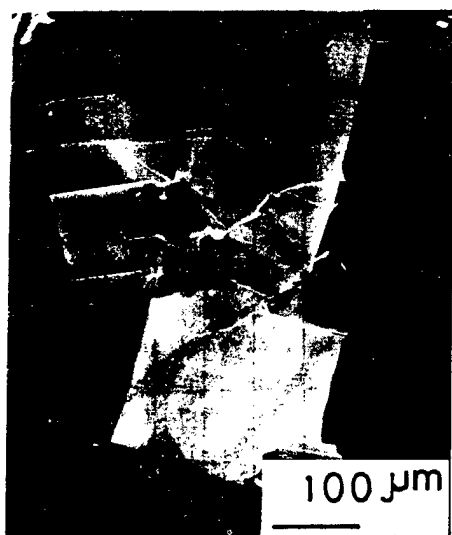


Fig. 1 $\text{Bi}_2\text{Sr}_2\text{CaCu}_2\text{O}_x$ single crystal

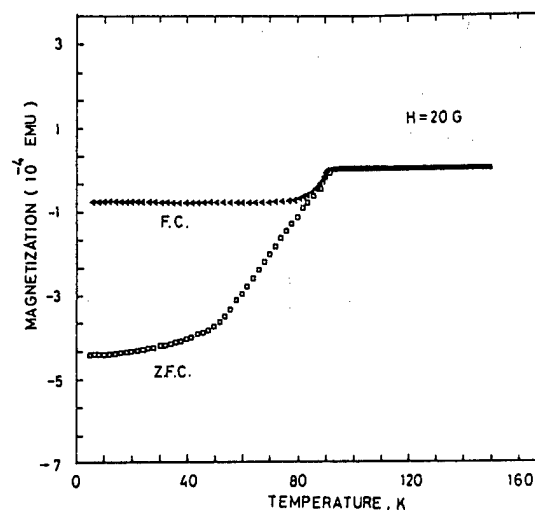


Fig. 2 Magnetization vs temperature ($H=20\text{G}$)

1-2 New Pt complex oxides

Three types of new Pt complex oxides have been found out.

1-2-1 $\text{R}_2\text{Ba}_2\text{CuPtO}_8$ ($\text{R}=\text{Er}, \text{Ho}, \text{Y}$)⁵⁻¹²

As shown in Fig. 3, rectangular prism crystals of black luster were obtained. Crystallographic investigations revealed an orthorhombic symmetry (space group: Pcmn) and had a characteristic one-dimensional zig-zag chain- $\{\text{Cu}^{2+}\text{-O-Pt}^{4+}\text{-O}\}$ structure^{9,10}. Fig. 4 shows the relationship between the electric conductivity and the temperature of these compounds. All compounds were clarified to be semiconductors with conductivity proportional to $\exp(T^{-1/2})$. These results are explained by a usual activation-type mechanism with a thermal lattice-vibration effect in the Mott-Hubbard model for $\{\text{Cu}^{2+}\text{-O-Pt}^{4+}\text{-O}\}$ zig-zag chains¹¹. $\text{Er}_2\text{Ba}_2\text{CuPtO}_8$ shows successive antiferromagnetic orderings at 7K (Fig. 5), while $\text{Ho}_2\text{Ba}_2\text{CuPtO}_8$ shows antiferromagnetic one at 2K, and $\text{Y}_2\text{Ba}_2\text{CuPtO}_8$ shows the antiferromagnetic ordering¹².

1-2-2 $\text{R}_2\text{Ba}_3\text{Cu}_2\text{PtO}_{10}$ ($\text{R}=\text{Er}, \text{Ho}, \text{Y}$)^{8,13}

These compounds were black luster platelets. Fig. 6 shows the appearance of the $\text{Er}_2\text{Ba}_3\text{Cu}_2\text{PtO}_{10}$. Crystallographic investigations showed monoclinic symmetry (space group C2/m). Measurement of the physical properties are in progress.

1-2-3 $\text{Ba}_4\text{CuPt}_2\text{O}_9$ ^{8,14}

This compound of transparent green was obtained as rectangular prism crystals (Fig. 7) and was free from R elements. Satellite reflections typical for a modulated structure were observed in the X-ray diffraction experiments: trigonal, P_{111}^{321} , $a=10.081(3) \text{ \AA}$, $c_0=4.224(5) \text{ \AA}$, $q=0.519c_0^*$, $V=371.7 \text{ \AA}^3$, $Z=1.5$. The structure is built of columns parallel to the c axis consisting of Pt_2O_9 and Cu linked alternatively. There are two variants of the position of the column related by vector shift c_0 . A superlattice is formed by a periodic alternation of the two variants in one dimension. Ba ions are located between the columns. Further characterization of this compound is currently under way.



Fig. 3 $\text{Er}_2\text{Ba}_2\text{CuPtO}_8$ single crystal

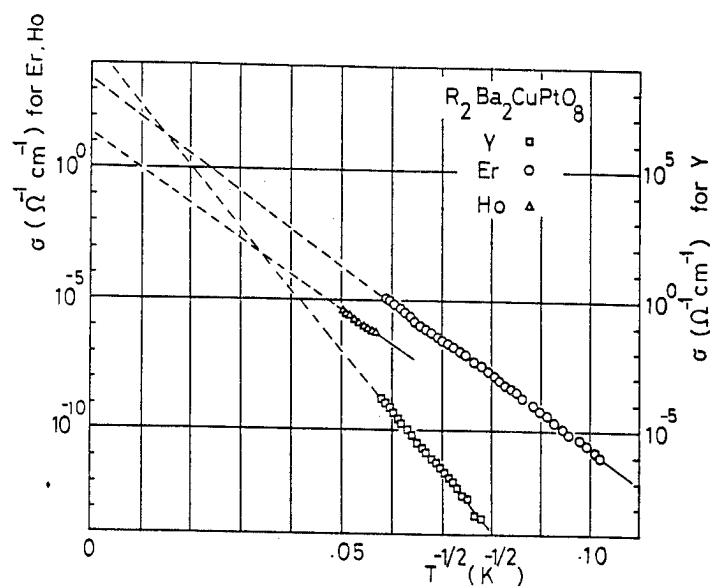


Fig. 4 Electrical conductivity vs temperature

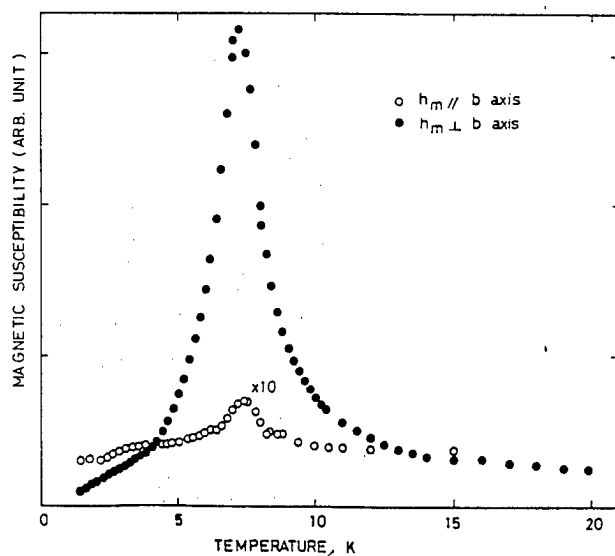


Fig. 5 Magnetic susceptibility vs temperature

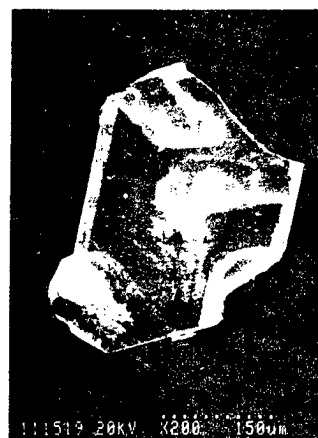


Fig. 6 $\text{Er}_2\text{Ba}_3\text{Cu}_2\text{PtO}_{10}$ single crystal



Fig. 7 $\text{Ba}_4\text{CuPt}_2\text{O}_9$ single crystal

II. Floating zone and other growth techniques

2-1 Summary of growth trials

In this section, we summarize brief results of growth runs for several superconductors and the related compounds first, which have been carried out using both lamp-image floating zone and a high pressure-inductive furnace under controlled condition of oxygen partial pressure, and describe growths and structure analyses of as-grown, annealed single crystals of Nd_2CuO_4 : Ce in relation to their properties.

As most of all the compounds tend to melt incongruently, the growths have been done from appropriately nonstoichiometric melt. Atmospheric $p\text{O}_2$ would be the most influential factor since it affects melting behavior, crystallizing phases and etc. The compounds, growth methods and atmospheric $p\text{O}_2$ ranges are listed in Table 1 together with some remarks and typical dimensions of obtained crystal. Different methods have been tried in order to determine suitable growth technique for the growth of La_2CuO_4 : Sr and Nd_2CuO_4 : Ce single crystals. Sealed soft capsule technique were employed for La_2CuO_4 : Sr and Tl-compounds. The capsules were pressurized at 30 atm by gaseous Ar to compensate inner pressure increase with increasing temperature due to oxygen release. Growth runs by means of direct-inductive heating with 200 kHz-high frequency by the high pressure FZ method has not been succeeded because of melt instability. Even under 6atm of $p\text{O}_2$, inductively heated Pt-Rh crucible was attached by the Nd_2CuO_4 : Ce melt with excess CuO and finally ruptured.

Compound	growth method (furnace)	atmosphere	single crystal dimension(order)/ remarks
La_2NiO_4	FZ (L.I)	$10^{-2} \sim 2 \text{ atm O}_2$ (N_2/O_2)	cm^3
La_2CoO_4	FZ (L.I)	$10^{-4} \sim 10^{-2} \text{ atm O}_2$ (CO/CO_2)	cm^3
La_2CuO_4 : Sr	FZ (L.I)	$10^{-1} \sim 2 \text{ atm O}_2$ (N/O_2)	cm^3
	H. P. BM in sealed capsule	20 atm Ar (external pressure)	- crucible reacted
	H. P. FZ(direct induction)	6 atm O_2 (Ar/ O_2)	- growth unstable
Nd_2CuO_4 : Ce	FZ (L.I)	$0.2 \sim 2 \text{ atm O}_2$ (N_2/O_2)	mm^3
	H. P. SC in PtRh crucible	6 atm O_2 (Ar/ O_2)	- crucible reacted
	H. P. FZ(direct induction)	6 atm O_2 (Ar/ O_2)	- growth unstable
	H. P. FZ(ring susceptor radiation)	6 atm O_2 (Ar/ O_2)	mm^3
Pr_2CuO_4 : Ce	FZ(L.I)	$1 \sim 2 \text{ atm O}_2$	mm^3
Bi-comp.	FZ(L.I)	$10^{-2} \sim 1 \text{ atm O}_2$	mm^3
Tl-comp.	H. P. BM in sealed capsule	30 atm Ar (external pressure)	$\sim 0.1 \text{ mm}^3$

* FZ(L.I.): Floating zone(lamp image furnace) H. P. BM; High pressure Bridgman
H. P. SC; High pressure slow cooling, H. P. FZ; High pressure floating zone

Table. 1 Summary of growth trials for superconductors and related compounds

2-2 $(\text{Nd}_{1-x}\text{Ce}_x)_2\text{CuO}_4$

Single crystals of Nd_2CuO_4 :Ce have been successfully obtained by the travelling solvent floating zone method using excess CuO as solvent. Several compositions of the solvent was chosen as shown in Fig. 8. Nd_2CuO_4 :Ce crystallized from the melt with composition ranging a to f. Intrusion of the solvent component toward low temperature region of nutrient rod and additional bubbling of the melt caused by the oxygen release interfered with stable zone-travel in case of those using composition a and f, respectively. It can be seen shiny and flat cleavage plane(001). Typical boule cut parallel to the growth direction grown under the conditions; 1 atm O_2 , solvent comp. c, travelling rate 0.7mm/h, is shown in Fig. 9. Preferred growth occurs along to one of the equivalent a tetra direction, consequently, crystal segments exhibit elongated, columnar morphology. Though trace impurity phase, $(\text{Nd}, \text{Ce})_x\text{O}_y$ was recognized inbetween the segments, single crystals with dimensions up to $2 \times 3 \times 7 \text{ mm}^3$ could be cut from the boule. Effective distribution coefficient, C_S/C_L , for Ce was suggested to be close to unity.



Fig. 9 $(\text{Nd}_{1-x}\text{Ce}_x)_2\text{CuO}_4$ single crystals.

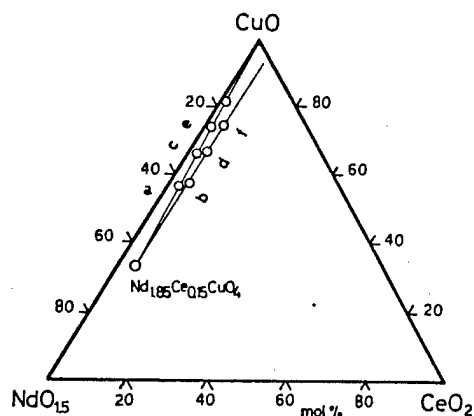


Fig. 8 Solvent compositions for growth of Nd_2CuO_4 :Ce single crystals by TSFZ method.

The as-grown crystals did not show superconducting transition, whereas the crystals annealed in Ar at 900 C for several hours exhibited superconductivity, as shown in Fig. 10. Fig. 11 represents an ORTEP drawing of the as-grown single crystal at R. T. analysed by 4-circle X-ray diffractometry, which belongs tetragonal phase with space group $I4/mmm$. Occupancy factor for O_1 site is equal to unity while O_2 site is calculated to be 0.92. The Ce content x in the formula $(\text{Nd}_{1-x}\text{Ce}_x)_2\text{CuO}_4$ was estimated to be 0.07 by the determined lattice parameters, $a=b=3.9428$ and $c=12.068\text{\AA}$.

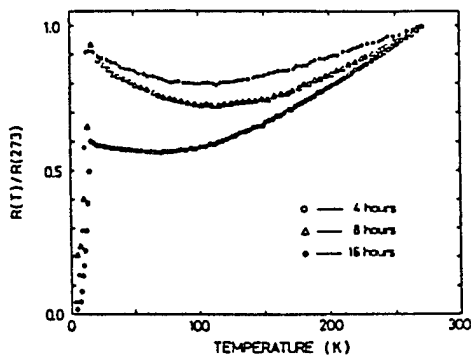


Fig. 10 Annealing-time dependency on electrical resistivity as a function of temperature

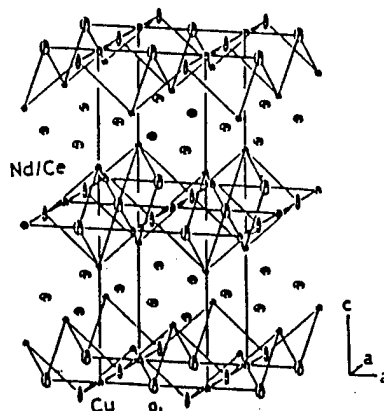


Fig. 11 ORTEP drawing for single crystal $(\text{Nd}_{1-x}\text{Ce}_x)_2\text{CuO}_4$

Fig.12 shows the result of high temperature X-ray powder analyses for pulverized as grown single crystals, which have been done in air. Sharp spectrum of tetragonal symmetry can be seen at 100°C, while split of 101 reflection into two peaks suggesting orthorhombic distortion has been detected at 800°C. The phase transition temperature was diffusive and have not been determined clearly. To clarify the phase transition, measurements in He atmosphere have been made using air-sintered specimen. Fig. 13 indicates the time dependency of the powder pattern. The lowest pattern a), measured at 700°C in air using non-superconductor $\text{Nd}_{1.85}\text{Ce}_{0.15}\text{CuO}_4$ shows tetragonal symmetry. 101 reflection also splits into two peaks by annealing at 900 C for 5h in He as in the former case. Pattern e) for as-quenched specimen from 900°C in He seems to be tetragonal. Those evidence suggest that the phase transition occurs depending both on temperature and oxygen vacancy content. It should be also noted that $\text{Nd}_{1.85}\text{Ce}_{0.15}\text{CuO}_4$ crystals grown under 1 atm O_2 suffer orthorhombic-tetragonal phase transition during cooling process. 2) The phase transition takes place in the preparation process of superconducting sintered specimens of $\text{Nd}_{1.85}\text{Ce}_{0.15}\text{CuO}_{4-\delta}$. Further studies on the structural analyses at high temperature region are required.

Fig. 13 Variation of x-ray powder patterns vs annealing time at 900°C in He for air-sintered specimen.

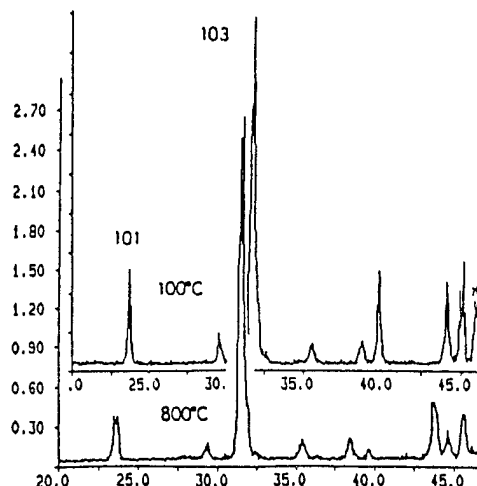
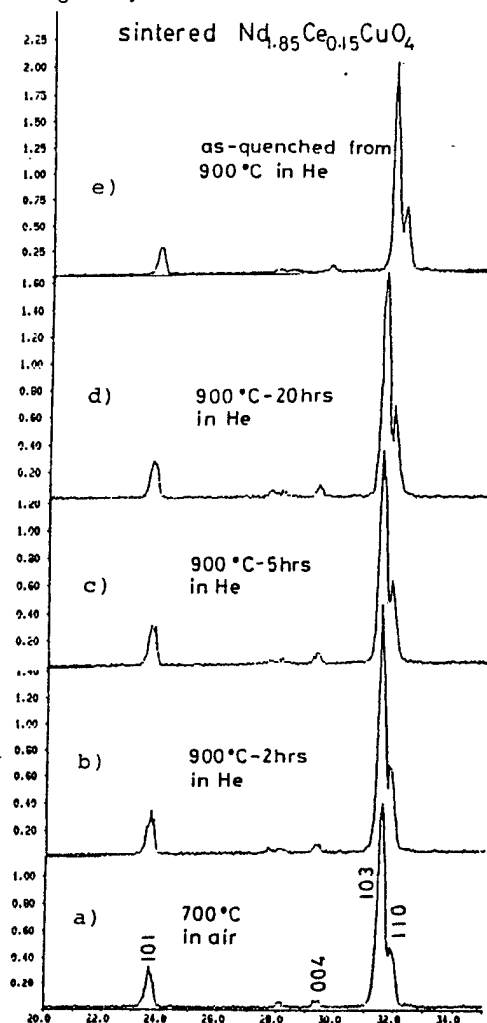


Fig. 12 X-ray powder patterns at high temperatures for pulverized $(\text{Nd}_{1-x}\text{Ce}_x)_2\text{CuO}_4$ single crystal



References

- 1) G. Balestrino, A. Paoletti, P. Paloli and P. Pomano: Appl. Phys. Lett. 54(20), 15 May 1989, 2041.
- 2) T. Takahashi, H. Matsuyama, H. Katayama-Yoshida, Y. Okabe, S. Hosoya, K. Seki, H. Fujimoto, M. Sato and H. Inokuchi: Nature 334 (1988) 691.
- 3) T. Shishido, D. Shindo, K. Ukei, T. Sasaki, N. Toyota and T. Fukuda: Jpn. J. Appl. Phys. 28, 1989, 1791.
- 4) T. Shishido, N. Toyota, D. Shindo, T. Sasaki, K. Ukei and T. Fukuda, in preparation.
- 5) T. Shishido, T. Fukuda, N. Toyota, K. Ukei and T. Sasaki: J. C. G. 85(1987)599.
- 6) T. Shishido, T. Fukuda, N. Toyota, K. Ukei and T. Sasaki: Jpn. J. Association of Crystal Growth 14 (1987) 199.
- 7) T. Shishido, Y. Saito, T. Fukuda, N. Toyota, T. Sasaki, H. Iwasaki and K. Ukei: Jpn. J. Appl. Phys. 27 (1988) 11926.
- 8) T. Shishido, Y. Saito, N. Toyota, K. Ukei, T. Sasaki and T. Fukuda: Submitted to Mol. Cryst. Liq. Cryst., Gordon and Breach Science Publishers.
- 9) K. Ukei, T. Shishido and T. Fukuda: Acta Cryst. (1988) C44, 958.
- 10) Y. Saito, K. Ukei, T. Shishido and T. Fukuda: submitted to Acta Cryst. C.
- 11) N. Toyota, P. Koorevaar, J. van der Berg, P. Kes, J. A. Mydosh, T. Shishido, Y. Saito, N. Kuroda, K. Ukei, T. Sasaki and T. Fukuda, J. Phys.: Condens. Matter(1989)3721.
- 12) N. Toyota, C. van den Beek, J. A. Mydosh, P. Koorevaar, J. van den Berg, P. Kes, Y. Nishihara, K. Murata, T. Shishido, Y. Saito, K. Ukei, T. Sasaki, H. Iwasaki and T. Fukuda, submitted to Yamada Conference XXV on Magnetic Phase Transition(April, 1990, Osaka).
- 13) Y. Saito, K. Ukei, T. Shishido and T. Fukuda; submitted to Acta Cryst. C.
- 14) K. Ukei, Y. Watanabe, T. Shishido and T. Fukuda; submitted to Acta Cryst. C.

Cross sectional observation of Bi-O and Cu-O layers by STM/STS in $\text{Bi}_2\text{Sr}_2\text{CaCu}_2\text{O}_y$

K. Kitazawa, T. Hasegawa, K. Kishio, M. Nanto and H. Suzuki

Department of Industrial Chemistry, University of Tokyo
Bunkyo-ku, Tokyo 113, Japan

The a-c plane of the single crystal $\text{Bi}_2\text{Sr}_2\text{CaCu}_2\text{O}_y$ was observed by scanning tunneling microscopy (STM)/spectroscopy (STS) at room temperature. The STM image obtained clearly showed the atomic corrugations corresponding to both Cu-O and Bi-O layers, depending on the tip bias voltage. Furthermore, the tunneling spectrum on $(\text{CuO}_2)_2$ layer showed a pseudo-gap near the Fermi level, possibly due to the strong electron correlation.

The cleaved surface (a-b plane) of Bi-Sr-Ca-Cu-O has previously been investigated by scanning tunneling microscopy (STM)/spectroscopy (STS) [1-5]. In terms of the correlation between the low-dimensionality of the electronic structure and the high- T_c in the cuprate superconductors, extension of the observation to the cross section of the layered structure should be of great interest. However, this has not been performed to date probably because of the difficulties in obtaining a stable and sufficiently wide surface for STM measurement. Here, we report the first results of atomic resolution STM/STS observations for the b-c plane on a large single crystal $\text{Bi}_2\text{Sr}_2\text{CaCu}_2\text{O}_y$ (BSCCO), clearly showing the sandwiched structure of Bi-O and Cu-O layers. The bias voltage dependence of the STM images and the STS spectrum at room temperature on each of the layers have revealed the presence of insulative band gap in the Bi-O layer. Also a large and gradual dip in the density of states near the Fermi level has been observed in the Cu-O layer, supporting the presence of pseudo-gap due to the strong correlation among electrons on the layer.

The "single crystal" boule ($10 \times 5 \times 5 \text{ mm}^3$) composed of many thin but long single crystalline platelets was grown by a traveling solvent floating zone (TSFZ) method [6]. Since all the crystals grew with the c-axis perpendicular to the growth axis, the boule was suited to probe both a-b and b-c planes. Here we refer to the direction of the modulation as the b-axis. The STM/STS apparatus was hand-made with a special soft ware so that the STS spectra could be obtained by accumulating the signal on many equivalent atomic positions on the surface to achieve the high S/N ratio. The atomic resolution STS was actually performed intermittently during the STM observation by sweeping the tip voltage in a short period of a few ms, while the tip position and the tip-sample distance were held constant. Just prior to the STM measurement, fresh surfaces of the a-b or b-c planes were prepared by cleaving with a Scotch tape or by scratching with a diamond file, respectively. The measurements were performed under a dry N_2 atmosphere.

Figures 1 and 2 show the STM image of the a-b and b-c planes, respectively, taken at the tip bias voltage of -1.5 V. The negative bias voltage implies the

electron tunneling into the electronic states of the sample above the Fermi level (E_F). In Fig. 2, two kinds of paired rows with different brightness run along the direction labeled "b". The paired rows repeat with a periodicity of 1.53 nm, in good agreement with half the c-spacing of the unit cell, 1.54 nm [7]. In addition, atomic corrugations in each of the rows along "b" are also seen from the figure, and the averaged interval between the corrugation, 0.26 nm, is consistent with half the a-spacing of the pseudo-tetragonal structure, 0.54 nm [7]. According to the transmission electron microscope (TEM) observations [8,9], atoms sinusoidally deviate from their ideal position in tetragonal configuration along b-axis. Considering the modulated structure along b-direction seen in the STM image, we assigned the observed plane in Fig. 2 as the b-c plane. The surface atomic corrugation which is disordered in Fig. 2 is also similar to the reported TEM image of the b-c plane [11,12].

In Fig. 3, the STM image taken at the bias voltage of +0.1 V was shown, where the tunneling occurred from the electronic states below E_F to the tip. The difference in brightness between adjacent paired rows



Fig. 1 STM image of a cleaved surface of the a-b plane in single crystalline $\text{Bi}_2\text{Sr}_2\text{CaCu}_2\text{O}_y$ observed at a tip bias voltage of -1.5 V relative to the sample. The tunneling current was 0.2 nA.

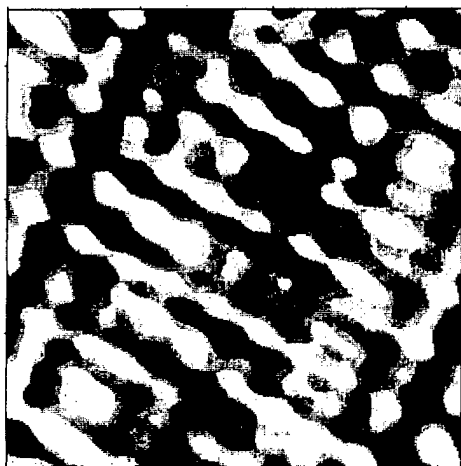


Fig. 2 STM image of a scratched surface of the b-c plane in single crystalline $\text{Bi}_2\text{Sr}_2\text{CaCu}_2\text{O}_y$ observed at a tip bias voltage of -1.5 V relative to the sample. The tunneling current was 0.7 nA.



Fig. 3 STM image of a scratched surface of the b-c plane in single crystalline $\text{Bi}_2\text{Sr}_2\text{CaCu}_2\text{O}_y$ observed at a tip bias voltage of +0.1 V relative to the sample. The tunneling current was 0.6 nA.

in Fig. 3 is substantially enhanced in comparison with that in Fig. 2, indicating that the local density of states (DOS) near E_F , $N(0)$, in the brighter rows along the b-axis (BR) is much higher than that in the darker rows (DR). Recent STS works on the a-b plane of BSCCO in a ultra high vacuum [4,5] reported the Bi-O layer to be essentially insulating. Considering the metallic nature of BSCCO as a whole, it is reasonable to assume that BR and DR correspond to $(\text{CuO}_2)_2$ and $(\text{BiO})_2$ layers, respectively.

In Fig. 4(a) and 4(b) are plotted the normalized conductance values, $(dI/dV)/(I/V)$, against tip voltage. The quantity is experimentally [10] and theoretically [11] known to be a good measure of local DOS independent of the tip-sample distance. The signal is averaged along $(\text{BiO})_2$ and $(\text{CuO}_2)_2$ layers. Here we should note that the normalized conductance is defined to be unity at zero bias, and $(dI/dV)/(I/V)$ -V curve hence represents the DOS profile only in a relative manner at the tip position. In other words, it is impossible so far to compare the absolute DOS values between the two different locations by the STS technique.

The DOS profile on the edge of the $(\text{BiO})_2$ layer (Fig. 4(a)) showed a steep trough at $V=0$ with a rather flat bottom with width about 0.1 eV. This suggests that the electronic structure on the $(\text{BiO})_2$ layer has band gap as has been reported for STS observations on the a-b plane which is supposed to be covered with the BiO layer on the top [4,5].

Even in the DOS profile on the edge of the $(\text{CuO}_2)_2$ layer (Fig. 4(b)), where $N(0)$ should be finite to make it a metallic layer, the "dip" around $V=0$ is also seen. Besides, the STM image at small bias voltages such as in Fig. 3 shows that $(\text{CuO}_2)_2$ area is much brighter than the $(\text{BiO})_2$ area. Since a clear Fermi edge has been observed in BSCCO by photoemission spectroscopy [12-15], we presume the observed dip to be related to a pseudo-gap with a finite $N(0)$ in $(\text{CuO}_2)_2$ layer. The presence of a pseudo-energy gap has been a matter of main interest in the electronic structure of the cuprate superconductors and has first been clearly observed by the combination of UPS and inverse UPS measurements [12-14]. But the present observation of the pseudo-gap is the first experimental observation specifically performed in the $(\text{CuO}_2)_2$ layer. This unique feature of the CuO_2 layer is quite a contrast to a rather flat DOS spectrum expected for a typical metal in which the band width is large compared to the correlation interaction among electrons. Band calculations [16,17], in which the electron correlation is not

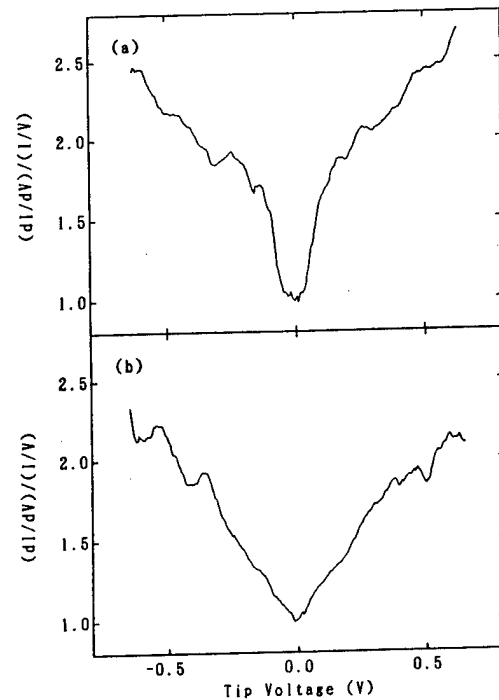


Fig. 4 The normalized conductivity values on the darker rows (DR) (a) and brighter rows (BR) (b) on the b-c plane as a function of tip bias voltage. The DR and BR were assigned to $(\text{BiO})_2$ and $(\text{CuO}_2)_2$ layers, respectively (see text).

incorporated, do not predict the "dip" structure in Fig. 4(b).

Furthermore, the relative brightness of the STM and STS images on the $(\text{CuO}_2)_2$ and $(\text{BiO})_2$ rows has been found to vary significantly with the tip voltage, reflecting the variation of relative contributions from the two layers to the local DOS depending on the difference in energy from E_F . Detail will be reported elsewhere.

In conclusion, it was directly confirmed from the bias voltage-dependent STM and STS measurements that the local DOS in the $(\text{CuO}_2)_2$ layer is much higher than that in $(\text{BiO})_2$ layer near E_F , reflecting the highly anisotropic electronic structure in $\text{Bi}_2\text{Sr}_2\text{CaCu}_2\text{O}_y$ that conduction electrons pass through the two-dimensional $(\text{CuO}_2)_2$ layers sandwiched by insulating $(\text{BiO})_2$ layers with a finite energy gap. However, even in the tunneling spectrum in the $(\text{CuO}_2)_2$ layer, a pseudo-gap is also recognized, suggesting the essential importance of the strong electronic correlation in the CuO_2 layer.

References

- [1] S. L. Tang, R. V. Kasowski, M. A. Subramanian and W. Y. Hsu, *Physica* **C156**, 177 (1988).
- [2] M. D. Kirk, C. B. Eom, B. Oh, S. R. Spielman, M. R. Beasley, A. Kapitulnik, T. H. Geballe and C. F. Quate, *Appl. Phys. Lett.* **52**, 2071 (1988).
- [3] M. D. Kirk, J. Nogami, A. A. Baski, D. B. Mitzi, A. Kapitulnik, T. H. Geballe and C. F. Quate, *Science* **242**, 1673 (1988).
- [4] M. Tanaka, T. Takahashi, H. Katayama-Yoshida, S. Yamazaki, M. Fujinami, Y. Okabe, W. Mizutani, M. Ono and K. Kajimura, *Nature* **339**, 691 (1989).
- [5] C. K. Shih, R. M. Feenstra, J. R. Kirtley and G. V. Chandrashekar, *Phys. Rev.* **B40**, 2682 (1989).
- [6] N. Motohira, K. Kuwahara, T. Hasegawa, K. Kishio and K. Kitazawa, *J. Cer. Soc. Jpn. Int. Ed.*, **97**, in press.
- [7] J. M. Tarascon, Y. Le Page, P. Barboux, B. G. Bagley, L. H. Greene, W. R. McKinnon, G. W. Hull, M. Giroud and D. M. Hwang, *Phys. Rev.* **B37**, 9382 (1988).
- [8] Y. Matsui, H. Maeda, Y. Tanaka and S. Horiuchi, *Jpn. J. Appl. Phys.* **27**, L372 (1988).
- [9] Y. Matsui, H. Maeda, Y. Tanaka, E. Takayama-Muromachi, S. Takekawa and S. Horiuchi, *Jpn. J. Appl. Phys.* **27**, L827 (1988).
- [10] J. A. Stroscio, R. M. Feenstra and A. P. Fein, *Phys. Rev. Lett.* **57**, 2579 (1986).
- [11] N. D. Lang, *Phys. Rev.* **B34**, 5947 (1986).
- [12] T. Takahashi, H. Matsuyama, H. Katayama-Yoshida, Y. Okabe, S. Hosoya, K. Seki, H. Fujimoto, M. Sato and H. Inokuchi, *Nature* **334**, 691 (1988).
- [13] W. Drube, F. J. Himpsel, G. V. Chandrashekar, M. W. Shafer, *Phys. Rev.* **B39**, 7328 (1989).
- [14] H. Ohta, *Phys. Rev.* **B39**, 7354 (1989).
- [15] M. Onellion, M. Tang, Y. Chang, G. Margaritondo, J. M. Tarascon, P. A. Morris, W. A. Bonner and N. G. Stoffel, *Phys. Rev.* **B38**, 881 (1988).
- [16] L. F. Mattheiss and D. R. Hamann, *Phys. Rev.* **B38**, 5012 (1988).
- [17] S. Massidda, J. Yu and A. J. Freeman, *Physica* **C152**, 251 (1988).

H. Asano

Institute of Materials Science, University of Tsukuba
Tsukuba 305, Japan

Crystal structures of oxide superconductors $(\text{Ba}_{1-x}\text{Nd}_x)_2(\text{Nd}_{1-y}\text{Ce}_y)_2\text{Cu}_3\text{O}_{8+z}$, $\text{Bi}_2\text{Sr}_2(\text{Ln}_{1-x}\text{Ce}_x)_2\text{Cu}_2\text{O}_{10}$ and $\text{Bi}_2(\text{Sr,Ca})_3\text{Cu}_2\text{O}_{8+x}$ have been investigated by neutron and X-ray diffraction. $(\text{Ba}_{1-x}\text{Nd}_x)_2(\text{Nd}_{1-y}\text{Ce}_y)_2\text{Cu}_3\text{O}_{8+z}$ is a hybrid of Nd_2CuO_4 and tetragonal $\text{YBa}_2\text{Cu}_3\text{O}_{7-y}$ structures. $\text{Bi}_2\text{Sr}_2(\text{Ln}_{1-x}\text{Ce}_x)_2\text{Cu}_2\text{O}_{10}$ is a derivative of $\text{Bi}_2\text{Sr}_2\text{CaCu}_2\text{O}_8$, where the Ca layer is replaced by a Nd_2CuO_4 -type slab $(\text{Ln,Ce})_2\text{O}_2$. An incommensurate structure of $\text{Bi}_2(\text{Sr,Ca})_3\text{Cu}_2\text{O}_{8+x}$ has also been clarified.

I. Crystal structure of $(\text{Ba}_{1-x}\text{Nd}_x)_2(\text{Nd}_{1-y}\text{Ce}_y)_2\text{Cu}_3\text{O}_{8+z}$ [1]

Recently, Sawa et al. [2] discovered a new superconductor $(\text{Ba}_{1-x}\text{Ln}_x)_2(\text{Ln}_{1-y}\text{Ce}_y)_2\text{Cu}_3\text{O}_{8+z}$ ($\text{Ln} = \text{Nd, Sm, Eu and Gd}$) with T_c of 40K and determined a crystal structure of $(\text{Ba}_{0.67}\text{Eu}_{0.33})_2(\text{Eu}_{0.67}\text{Ce}_{0.33})_2\text{Cu}_3\text{O}_{8+z}$ by Rietveld analysis of X-ray powder diffraction. The structure is a hybrid of $\text{Nd}_2\text{CuO}_4(\text{NCO})$ and tetragonal $\text{YBa}_2\text{Cu}_3\text{O}_{7-y}(\text{YBCO})$ structures (see Fig. 1). However, location and occupation factor of oxygen cannot be determined very precisely by X-ray diffraction. Therefore, neutron powder diffraction was applied to refine structure parameters of an isomorphic compound $(\text{Ba}_{0.63}\text{Nd}_{0.37})_2(\text{Nd}_{0.68}\text{Ce}_{0.32})_2\text{Cu}_3\text{O}_{8.92}$. A neutron diffraction experiment was carried out on a high-resolution neutron powder diffractometer HRP at KEK. Observed intensity data were analyzed by Rietveld method.

Final structure parameters based on space group $I4/mmm$ are listed in Table I. Tetragonal lattice parameters were refined to be $a = 3.8747(4)$ and $c = 28.599(3)$ Å. R-factors are $R_w = 4.9$, $R_p = 3.7$, $R_1 = 3.9$ and $R_f = 3.1\%$. Figure 1 shows the crystal structure of $(\text{Ba}_{0.63}\text{Nd}_{0.37})_2(\text{Nd}_{0.68}\text{Ce}_{0.32})_2\text{Cu}_3\text{O}_{8.92}$. The structure contains two kinds of slabs: $(\text{CuO}_2)(\text{MO})(\text{CuO}_2)(\text{MO})(\text{CuO}_2)$ of a YBCO-type slab and $(\text{CuO}_2)(\text{M}')(\text{O}_2)(\text{M}')(\text{CuO}_2)$ of an NCO-type slab. Ba with a larger ionic radius locates at a 12-coordinate M site of the YBCO slab, while Ce with a smaller radius at an 8-coordinate M' site of the NCO slab. Nd with an intermediate ionic radius occupies both the M and M' sites. An oxygen site O(1) on a CuO_2 plane of the YBCO slab is deficient and the occupation factor $g = 0.46(2)$. Atomic arrangement in the YBCO slab is just the same as that of a tetragonal form of a solid-solution compound $\text{Nd}_{1-x}\text{Ba}_x\text{Cu}_3\text{O}_{7-y}$.

II. Crystal structure of $\text{Bi}_2\text{Sr}_2(\text{Ln}_{1-x}\text{Ce}_x)_2\text{Cu}_2\text{O}_{10}$ [3,4]

A new oxide superconductor $\text{Bi}_2\text{Sr}_2(\text{Ln}_{1-x}\text{Ce}_x)_2\text{Cu}_2\text{O}_{10}$ (Bi-2222; $\text{Ln} = \text{Sm, Eu and Gd}$) with T_c of 30K was recently discovered by Tokura et al. [3]. The material is single phase for Ce concentration x ranging from 0.03 to 0.25. The crystal structure was investigated by X-ray and electron diffraction. The structure is tetragonal with lattice parameters $a = 3.88$ and $c = 17.9$ Å. Figure 2 shows the crystal structure of

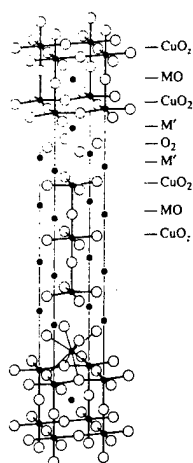


Fig. 1. Crystal structure of $(\text{Ba}_{1-x}\text{Nd}_x)_2(\text{Nd}_{1-y}\text{Ce}_y)_2\text{Cu}_3\text{O}_{8+z}$.
 $M = (\text{Ba}, \text{Nd})$ and $M' = (\text{Nd}, \text{Ce})$.

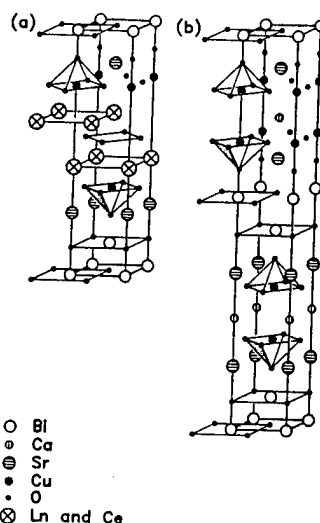


Fig. 2. Crystal structures of
 (a) $\text{Bi}_2\text{Sr}_2(\text{Ln}_{1-x}\text{Ce}_x)_2\text{Cu}_2\text{O}_{10}$
 and (b) $\text{Bi}_2\text{Sr}_2\text{CaCu}_2\text{O}_8$.

Table I. Structure parameters of
 $(\text{Ba}_{0.63}\text{Nd}_{0.37})_2(\text{Nd}_{0.68}\text{Ce}_{0.32})_2\text{Cu}_3\text{O}_{8.92}$.

Atom	Site	x	y	z	g	B/Å ²
M	4e	0	0	0.4244(2)	1	1.3
M'	4e	0	0	0.2956(1)	1	0.3
Cu(1)	2a	0	0	0	1	0.4
Cu(2)	4e	0	0	0.1418(1)	1	0.5
O(1)	4c	0	1/2	0	0.46(2)	2.3
O(2)	4e	0	0	0.0639(2)	1	1.9
O(3)	8g	0	1/2	0.3525(1)	1	0.8
O(4)	4d	0	1/2	1/4	1	0.9

Bi-2222 in comparison with $\text{Bi}_2\text{Sr}_2\text{CaCu}_2\text{O}_8$ (Bi-2212). The structure of Bi-2222 is closely related to that of Bi-2212. A Ca layer in Bi-2212 is replaced by an XCO -type slab $(\text{Ln}, \text{Ce})(\text{O}_2)(\text{Ln}, \text{Ce})$. As a result, opposed bases of the CuO_5 pyramid in Bi-2222 are displaced to each other by $(a + b)/2$. X-ray Rietveld analysis on compounds of $\text{Ln} = \text{Sm}$ ($x = 0.15, 0.20$ and 0.25) and $\text{Ln} = \text{Gd}$ ($x = 0.25$) supports the structure model (space group $P4/nmm$) shown in Fig. 2. The same structure was also found by electron diffraction in $\text{Tl}_2\text{Ba}_2(\text{Ln}_{1-x}\text{Ce}_x)_2\text{Cu}_2\text{O}_{10}$ (Tl-2222), although this compound is semiconducting.

In contrast to Tl-2222, electron diffraction patterns of Bi-2222 revealed that the compound shows a superstructure. The unit cell of the superstructure is defined as $A = 9\sqrt{2}a$, $B = \sqrt{2}a$ and $C = 2c$, where a and c refer to the tetragonal lattice of Fig. 2. It should be noted that modulation along the A axis in Bi-2222 is commensurate, which is distinctive from incommensurate Bi-based superconductors Bi-2201 ($\text{Bi}_2\text{Sr}_2\text{CuO}_8$), Bi-2212 and Bi-2223 ($\text{Bi}_2\text{Sr}_2\text{Ca}_2\text{Cu}_3\text{O}_{10}$). In order to clarify the modulated structure, single crystal X-ray diffraction work was carried out on

$\text{Bi}_2\text{Sr}_2(\text{Gd}_{0.85}\text{Ce}_{0.15})_2\text{Cu}_2\text{O}_{10}$. Precession and Weissenberg photographs confirmed the commensurate superstructure found in electron diffraction. Then, intensity data were collected on a 4-circle diffractometer using $\text{Mo K}\alpha$ radiation. A total of 1260 independent reflections were measured, out of which 640 reflections with $F_o \geq 3\sigma$ were regarded as observed and used in structure refinement.

As an initial step, an average structure (space group Cmma) with a unit cell of $\sqrt{2}a \times \sqrt{2}a \times c$ was determined using only fundamental reflections. The result supports the structure model shown in Fig. 2. Resultant structure parameters are listed in Table II. It is worth noting that thermal parameters of Bi, O(2) and O(3) are unusually large, where O(2) is an oxygen atom in the BiO layer and O(3) is in the SrO layer and coordinated to Bi. This indicates that superlattice modulation occurs mainly in the BiO layer and the atoms in this layer suffer considerable displacement from the average positions. Complete understanding of the modulated structure, however, must await full analysis of superlattice reflections, which is currently in progress.

Table II. Structure parameters in the average structure of $\text{Bi}_2\text{Sr}_2(\text{Gd}_{0.85}\text{Ce}_{0.15})_2\text{Cu}_2\text{O}_{10}$.

Atom	Site	x	y	z	B/ \AA^2
Bi	4g	0	1/4	0.5861(1)	4.3
Sr	4g	0	1/4	0.2656(2)	2.8
Gd,Ce	4g	0	1/4	0.0692(1)	1.7
Cu	4g	0	1/4	0.8322(3)	2.0
O(1)	8l	1/4	0	0.1610(8)	2.0
O(2)	4g	0	1/4	0.404(2)	14.8
O(3)	4g	0	1/4	0.704(2)	9.8
O(4)	4a	1/4	0	0	2.6

III. Incommensurate structure of $\text{Bi}_2(\text{Sr,Ca})_3\text{Cu}_2\text{O}_{8+x}$ [5]

It is well known that Bi-based superconductors Bi-2201, Bi-2212 and Bi-2223 show incommensurate superstructures. In this work, incommensurate modulation of $\text{Bi}_2(\text{Sr,Ca})_3\text{Cu}_2\text{O}_{8+x}$ was investigated by a newly developed Rietveld program for modulated structures. Structure analysis was carried out by simultaneous refinement of X-ray and neutron powder diffraction data.

An average structure of Bi-2212 is shown in Fig. 2(b). Modulation occurs along the $[110]$ direction of the tetragonal lattice of Fig. 2(b). This direction is defined as the b axis of the modulated structure. Figure 3 shows a projection of the modulated structure on the b-c plane. It is seen that all the atoms are displaced from the average positions. In particular, displacement of Bi occurs mainly along the b axis, forming Bi-condensed and Bi-dilute regions. This result is in accordance with a high-resolution electron-microscopic image (Fig. 4) by Matsui et al. [6]. Figure 5 shows a projection of the modulated structure on the a-b plane. As shown in Fig. 5(a), extra oxygen atoms are incorporated into the BiO layer and expand a Bi-Bi distance to form the Bi-dilute region. Due to these extra oxygen atoms, oxygen content is given as $x = 1.0$. Atomic arrangement in SrO, CuO_2 and Ca layers is rather regular as seen in Fig. 5(b)-(d).

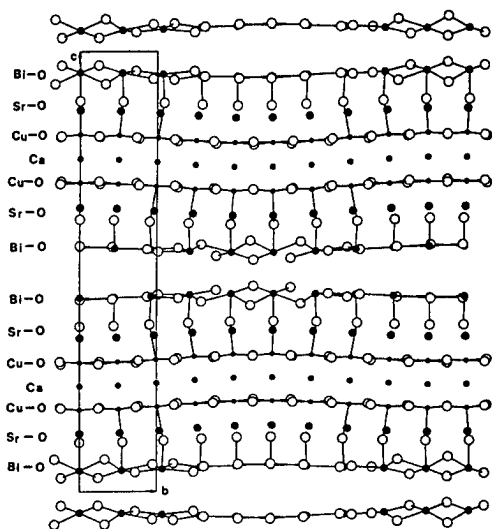


Fig. 3. Projection of the modulated structure on the b-c plane. Solid and open circles represent metal and oxygen atoms, respectively.

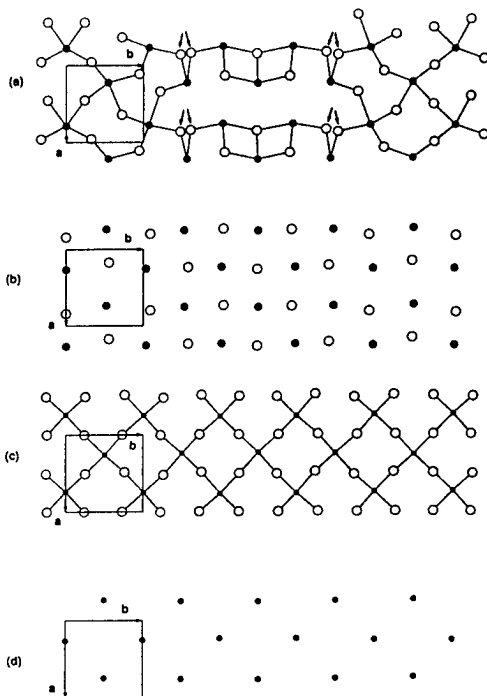


Fig. 5. Projection of the modulated structure on the a-b plane. (a)-(d) corresponds to BiO, SrO, CuO₂ and Ca layers. Oxygen atoms in the BiO layer show occupational modulation, and oxygen with occupation factor greater than 0.4 is drawn. Arrows show statistically occupied two positions with occupation factor near 0.5.

From examination of occupation factors, followings are concluded; (1) the Bi site is occupied only by Bi, (2) the Sr site adjacent to the Bi-dilute region is occupied partly by Bi and Ca, while the site adjacent to the Bi-condensed region is occupied mostly by Sr and (3) the Ca site is randomly occupied by Ca and Sr. From these results, chemical composition of the present sample is determined to be Bi_{2.3}Sr_{1.4}Ca_{1.3}Cu₂O_{9.0}, which is consistent with a nominal composition Bi₂Sr_{1.5}Ca_{1.5}Cu₂O₉ taking existence of a small amount of impurities Ca₂CuO₃ and CaO

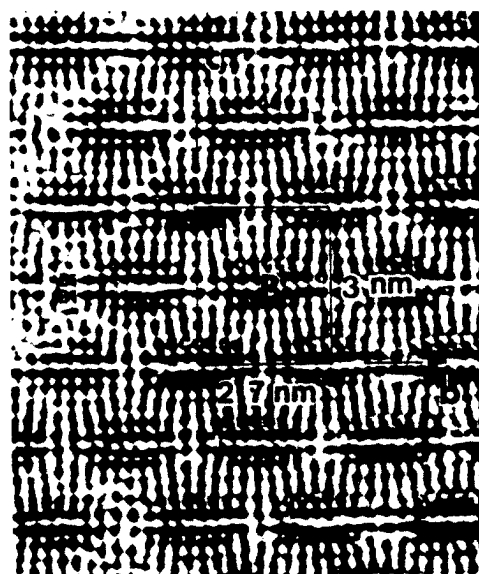


Fig. 4. High-resolution electron-microscopic image of Bi₂(Sr,Ca)₃Cu₂O_{8+x} [6]. The image shows existence of Bi-condensed (marked as B) and Bi-dilute regions, and the resultant lattice distortion.

into account.

References

- [1] F. Izumi, H. Kito, H. Sawa, J. Akimitsu and H. Asano: *Physica C* 160 (1989) 235.
- [2] H. Sawa, K. Obara, J. Akimitsu, Y. Matsui and S. Horiuchi: *J. Phys. Soc. Jpn.* 58 (1989) 2252.
- [3] Y. Tokura, T. Arima, H. Takagi, S. Uchida, T. Ishigaki, H. Asano, R. Beyers, A. I. Nazzari, P. Lacorre and J. B. Torrance: submitted to *Nature*.
- [4] I. Nakai, K. Imai, T. Arima, Y. Tokura, H. Asano, H. Takagi, S. Uchida, R. Beyer and J. B. Torrance: submitted to *Jpn. J. Appl. Phys.*
- [5] A. Yamamoto, M. Onoda, E. Takayama-Muromachi, F. Izumi, T. Ishigaki and H. Asano: submitted to *Phys. Rev. B*.
- [6] Y. Matsui, H. Maeda, Y. Tanaka and S. Horiuchi: *Jpn. J. Appl. Phys.* 27 (1988) L372.

Oxygen Deficiency in 1-2-3-Type Oxide Superconductors

E. Takayama-Muromachi

National Institute for Research in Inorganic Materials

1-1 Namiki, Tsukuba, Ibaraki 305, Japan

In a 1-2-3-type oxide superconductor, oxygen defects usually give a negative effect on superconductivity, but in different degrees for different systems. The superconductivity of $\text{La}_{1+x}\text{Ba}_{2-x}\text{Cu}_3\text{O}_y$ (LBCO) or an impurity-doped system $\text{YBa}_2\text{Cu}_{3-x}\text{M}_x\text{O}_y$ ($\text{M}=\text{Fe}, \text{Co}$) is much more sensitive to oxygen defects than the case of $\text{YBa}_2\text{Cu}_3\text{O}_y$ (YBCO). In this article, we suggest that this enhancement of oxygen-deficiency effect in the former two systems is associated with the oxygen disordering within the Cu1-O plane. Preliminary results of Monte Carlo simulation is presented for the oxygen disordering in the impurity-doped YBCO system.

INTRODUCTION

One of the most striking aspects of 1-2-3-type oxides is a very high level of oxygen defects which is introduced at a high temperature and/or in a low oxygen fugacity atmosphere. With increasing oxygen defects, difference between a - and b -dimensions in a orthorhombic cell becomes smaller and at some oxygen content, the compound is transformed to tetragonal structure. In YBCO, oxygen content at the transition point is ca. 6.4 [1]. In the case of LBCO [2] or some impurity-doped YBCO systems [3], the orthorhombic-to-tetragonal transition is induced not only by oxygen defects but also by increasing x -value in $\text{La}_{1+x}\text{Ba}_{2-x}\text{Cu}_3\text{O}_y$ or in $\text{YBa}_2\text{Cu}_{3-x}\text{M}_x\text{O}_y$, i.e., by substitution of the Ba or Cu1 site with foreign elements. In these systems, oxygen ions in the Cu1-O layer are, more or less, disordered compared with YBCO.

Though the oxygen deficiency in a 1-2-3 compounds generally suppresses its superconductivity, degree of suppression is widely different from system to system. In the above-mentioned LBCO and impurity-doped systems, dependence of T_c on the amount of oxygen defects is far more pronounced than the case of YBCO [2,4]. In this article, we propose that this large suppression of T_c is associated with oxygen disordering within the Cu1-O layer. In the latter half of this paper, we report preliminary results of Monte Carlo simulation of an impurity-doped YBCO system which shows satisfactorily that

impurity doping induces orthorhombic to tetragonal transition.

T_C SUPPRESSION BY OXYGEN DEFECTS

Figure 1 indicates dependence of T_C on oxygen deficiency for $YBa_2Cu_3O_y$ and $La_{1.1}Ba_{1.9}Cu_3O_y$ [2] where oxygen defect concentration is expressed by $\Delta y = y_{\max} - y$ (y_{\max} means maximum oxygen content in one atm O_2 , 6.93 for $YBa_2Cu_3O_y$ and 7.10 for $La_{1.1}Ba_{1.9}Cu_3O_y$). The dramatic decrease of T_C in $La_{1.1}Ba_{1.9}Cu_3O_y$ by small amount of oxygen defects should be emphasized: the superconductivity is completely suppressed near $\Delta y = 0.2$ while T_C is still as high as 70 K in the YBCO at that point.

In Fig. 2, T_C vs. Δy relations are shown for Fe-doped YBCO system with $x = 0.0, 0.05$ and 0.1 in $YBa_2Cu_{3-x}Fe_xO_y$. T_C is not suppressed substantially in this Fe-concentration range if the sample is well oxidized. However, dependence of T_C on oxygen defect concentration varies very largely depending on the Fe-concentration. Superconductivity is much more sensitive in the sample with higher Fe-concentration.

EFFECT OF OXYGEN DISORDERING IN Cu1-O LAYER

As described above, partial substitution of Ba or Cu1 site with some foreign elements causes orthorhombic-to-tetragonal transition. Takayama-Muromachi et al. explained this transition by extra oxygen ions in the Cu1-O layer which are located

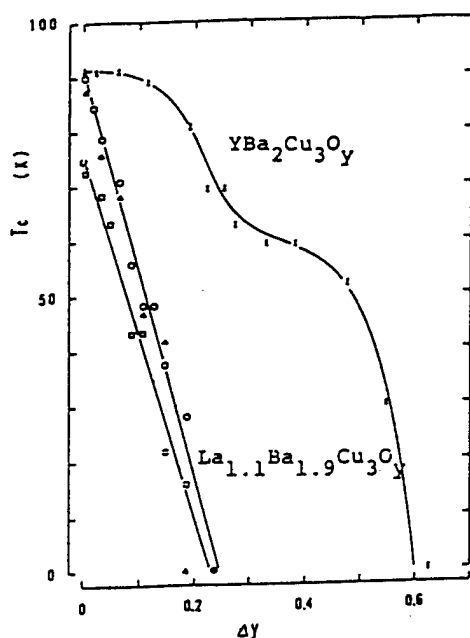


Fig. 1. Dependence of T_C on oxygen deficiency Δy in $YBa_2Cu_3O_y$ and $La_{1.1}Ba_{1.9}Cu_3O_y$.

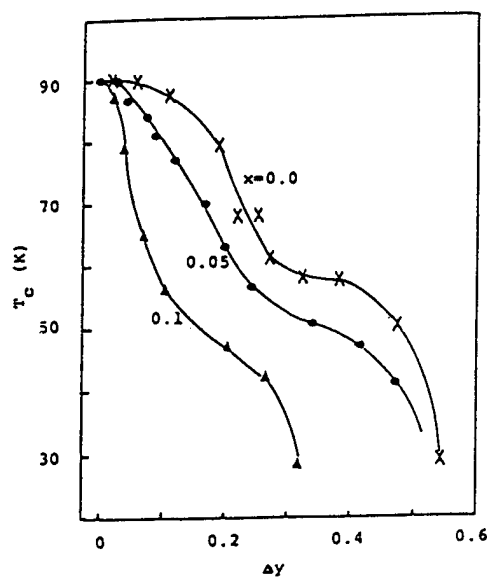


Fig. 2. Dependence of T_C on oxygen deficiency Δy in $YBa_2Cu_{3-x}Fe_xO_y$ ($x = 0.0, 0.05, 0.1$).

around the substitute Cu1 (or Ba) site [2,5]. According to them, if the Cu in the Cu1 site is, for instance, substituted by Fe, two additional oxygen ions should be introduced around the Fe ion due to its octahedral site preference and such additional oxygen ions disturb the 1-D Cu-O chain to cause averaged tetragonal symmetry. The large suppression of T_c in LBCO or Fe-doped YBCO seems to be associated with the oxygen disordering within the Cu1-O layer.

To discuss the effect of the oxygen disordering, let us first consider completely ordered state in an oxygen-deficient YBCO. For instance, figure 3 shows the completely ordered Cu1-O layer of the YBCO with $y=6.5$. In the figure, every two Cu line is completely filled with oxygen ion while other line is completely vacant. The Cu ions in the former line take a square coplanar coordination whereas those in the latter line take a linear two coordination. It seems reasonable from the crystal chemical feature of the Cu ion to assume that the Cu in the square coplanar coordination is divalent and that in the linear two coordination is monovalent. Then we can calculate concentration of "free" holes by assuming that Cu in the Cu2 site is divalent and Ba and Y ions are divalent and trivalent, respectively. Figure 4 shows variation of number of Cu^+ ions ($n(\text{Cu}^+)$) and "free" holes (n_h) per unit cell as functions of y value. When the completely ordered state is assumed, both $n(\text{Cu}^+)$ and n_h change linearly with y and n_h is, of course, larger than the case in which all Cu ions are assumed to be divalent.

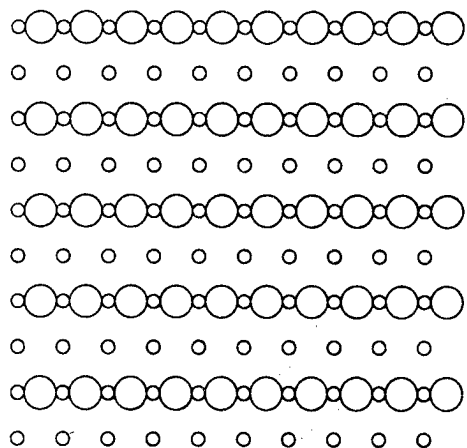


Fig.3. Completely ordered Cu1-O layer for $\text{YBa}_2\text{Cu}_3\text{O}_{6.5}$.

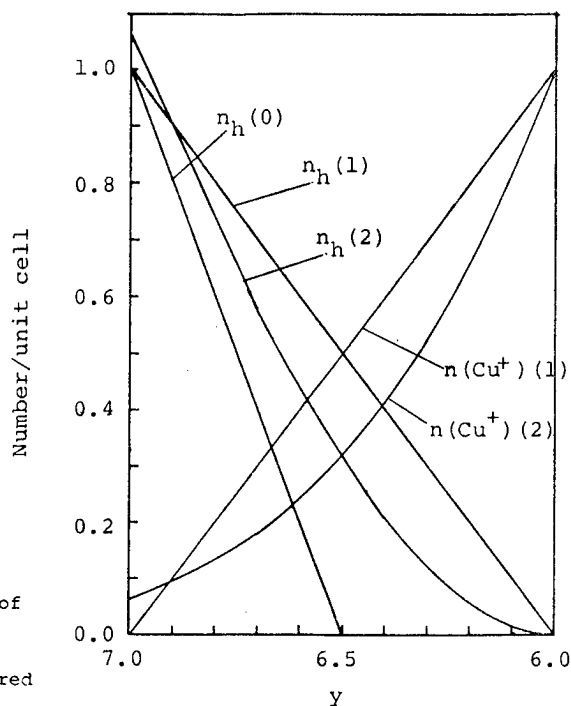


Fig.4. Hole and Cu^+ concentration as functions of y . $n_h(0)$ is hole concentration assuming no Cu^+ , $n_h(1)$ or $n_h(2)$ is hole concentration for ordered and disordered state, respectively. $n(\text{Cu}^+)(1)$ or $n(\text{Cu}^+)(2)$ is Cu^+ concentration for ordered and disordered state, respectively

Let us consider the other simple case, i.e., the completely disordered state. If the oxygen ions are randomly distributed in the Cu1-O layer, $n(\text{Cu}^+)$ and n_h varies as shown in Fig. 4. (Here, we assume that only Cu ions with the linear two coordination are monovalent and other Cu ions are divalent.) The value of $n(\text{Cu}^+)$ of the disordered state is smaller than that of the ordered state except for the range of y value near 7.0 and n_h decreases more steeply with increasing oxygen defects. We suggest that this steep decrease of n_h causes the very large suppression of T_c by a small amount of oxygen defects found in the LBCO and impurity-doped YBCO.

MONTE CARLO SIMULATION OF IMPURITY-DOPED YBCO

Oxygen order-disorder phenomena in the Cu1-O layer was simulated using Monte Carlo method. In our model, energy of the system is determined by the coordination of the Cu ion or a doped-impurity ion: if a Cu ion in the Cu1 site takes square planar coordination or linear two coordination, it is assumed to have a lower energy $V_1 < 0$ while if it takes other coordination, it has a higher energy $V_2 > 0$. On the contrary, an impurity ion such as a Fe ion prefers octahedral coordination, so that energy V_3 of the impurity ion in an octahedral coordination is low and that of other coordination (V_4) is high. In the present study, we took the following parameters: $-V_1/k_B T = V_2/k_B T = 1.3$ and $-V_3/k_B T = V_4/k_B T = 3.0$. The Monte Carlo simulation was performed on a 30x30 square network of metal sites (total number of oxygen sites is 2x30x30) at fixed number of oxygen ions and fixed number of impurity ions.

We first simulated the system without impurity ions. A random configuration was made using random numbers as an initial configuration and the iteration was pursued 500 Monte Carlo steps per oxygen site. The resulting structure is shown in Fig. 5 (a large open circle indicates a oxygen ion and small one indicates a Cu ion). It is seen that 1D Cu-O chain is formed giving an almost perfect orthorhombic structure. It was confirmed that orthorhombic-to-tetragonal transition occurred by removing oxygen ions at $y \sim 6.4$.

Figure 6 shows a structure simulated for the system including impurity ions (an impurity ion is expressed by a small filled circle). Oxygen content y was fixed to be 7.0 and concentration of the impurity ions at the Cu1 sites was also fixed to 0.06. In this simulation, oxygen and metal ions were both allowed to change their sites. 1-D Cu-O chains of one direction are seen in Fig. 6 and tetragonal structure was not obtained. Here we should note that an impurity doped compound is usually synthesized at higher temperatures where oxygen content of the product is much less than 7.0 and oxidation is done at lower temperatures after syntheses. To simulate this heat

Fig.5-8 Monte Carlo simulation of CuI-O layer (see text).

Fig.5

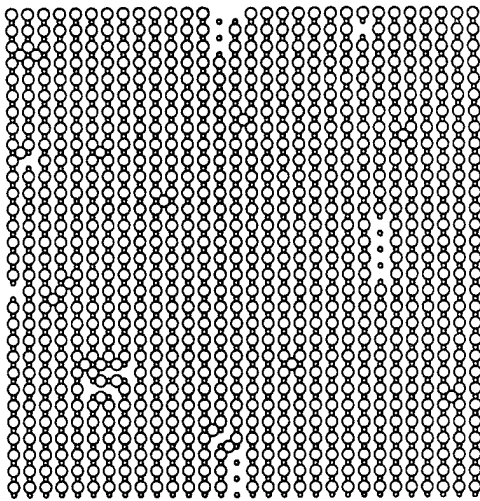


Fig.6

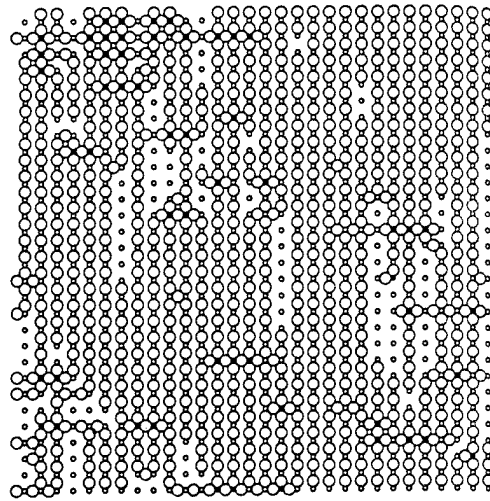


Fig.7(a)

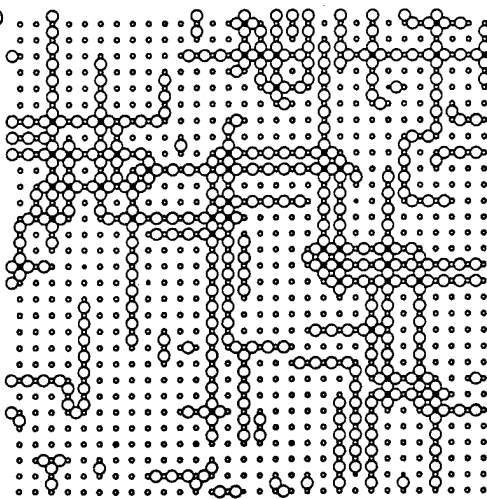


Fig.7(b)

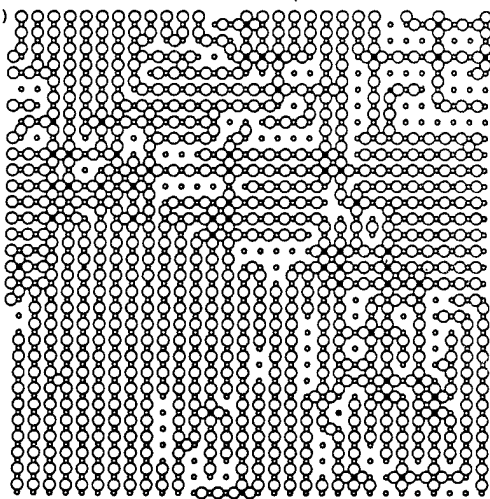


Fig.8(a)

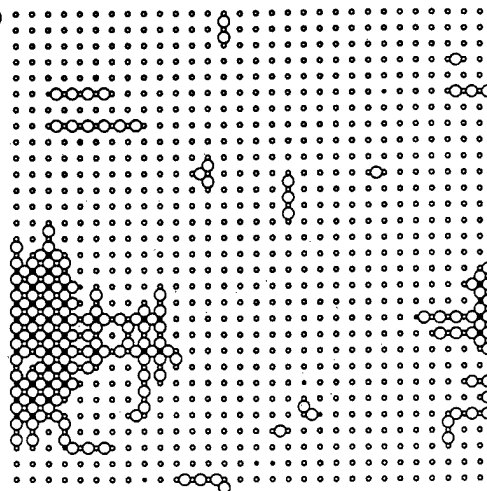
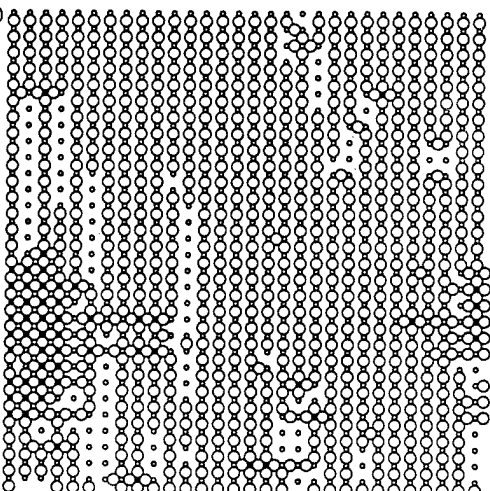


Fig.8(b)



process, two-step simulation was performed: at the first simulation, oxygen content was fixed at 6.5 and both metal and oxygen ions were allowed to change their sites (the resulting structure is shown in Fig. 7(a)) then at the second step, additional oxygen ions were introduced randomly until $y=7.0$ and iteration was pursued by fixing positions of impurity ions (only oxygen ions were allowed to change their sites). A "twin structure" is obtained as a final structure (Fig. 7(b)). If each domain of the twin structure is small enough (micro twin structure), such structure will be recognized to be tetragonal by the X-ray analysis. Thereby, the present simulation shows satisfactorily the orthorhombic-to-tetragonal transition by impurity doping.

Figures 8(a-b) are the results of the same two-step simulation. But the oxygen content is fixed to be 6.2 at the first-step simulation. In the resulting structure of the first-step simulation (Fig. 8(a)), a large cluster of impurity ions is seen to be formed and final structure (Fig. 8(b)) is not tetragonal but orthorhombic. This is consistent with a experimental results. It has been reported that orthorhombicity is recovered in a Fe-doped sample if the tetragonal compound is annealed in a low oxygen fugacity atmosphere and then is oxidized again at a lower temperature [4].

ACKNOWLEDGMENT

The present author expresses his sincere thanks to Drs. A. Yamamoto, F. Izumi and K. Kato for their helpful suggestions on computer programing of Monte Carlo method.

REFERENCES

- [1] For instance, E. Takayama-Muromachi, Y. Uchida, M. Ishii, T. Tanaka and K. Kato, Jpn. J. Appl. Phys. **26**, L1156 (1987).
- [2] E. Takayama-Muromachi, Y. Uchida, A. Fujimori and K. Kato, Jpn. J. Appl. Phys. **27**, L223 (1988).
- [3] For Instance, Y. Maeno, T. Tomita, M. Kyougoku, S. Awaji, Y. Aoki, K. Hoshino, A. Minami and T. Fujuta, Nature, **328**, 512 (1987).
- [4] E. Takayama-Muromachi, Y. Uchida, A. Fujimori and K. Kato, Proc. MRS Int'l. Mtg. on Adv. Mats. Vol. **6**, p467 (1988).
- [5] E. Takayama-Muromachi, Y. Uchida, A. Fujimori and K. Kato, Jpn. J. Appl. Phys. **26**, L2087 (1987).

Anomalous Properties of 2-1-4 Compounds

Y. Maeno, M. Kato, T. Suzuki, M. Kurisu* and T. Fujita

Faculty of Science, Hiroshima University, Hiroshima 730, Japan

*Present Address : Faculty of Engineering, Iwate University, Morioka 020, Japan

A few topics on the properties of compounds in the K_2NiF_4 (2-1-4) structure are presented. In $(La_{1-x}Ba_x)_2CuO_4$, a first-order structural transition from orthorhombic to low-temperature tetragonal phase occurs at x around 0.08. The strong suppression of superconductivity in this tetragonal phase is further characterized by resistivity measurements under hydrostatic pressure up to 18 kbar and by partial substitution for Ba by Sr. The system $(La_{1-x}Sr_x)_2NiO_4$ exhibits anomalous behavior at $x = 0.3$, associated with the transition from high-spin to low-spin configuration. Unusual magnetic and transport behavior near $x = 0.50$ is compared with that of $(La_{1-x}Sr_x)_2CuO_4$ near $x = 0$.

1. Superconductivity and the low-temperature tetragonal phase in $(La_{1-x}Ba_x)_2CuO_4$

The crystal symmetry of $(La_{1-x}Ba_x)_2CuO_4$ (LBCO) at room temperature is known to be tetragonal ($I4/mmm$) for $x > 0.05$ and orthorhombic ($Cmca$) for $x < 0.05$. In the early stage of the research in high- T_c superconductors, we reported a crystallographic, magnetic and superconductive phase diagram of this system [1]. As the temperature is reduced, LBCO with $x < 0.10$ undergoes a structural change from tetragonal high-temperature phase (THT) to the orthorhombic phase (OMT) at an x -dependent transition temperature, T_{d1} , which decreases from 530 K for $x = 0$ with increasing x . Fleming et al. [2] reported a similar structural change in $(La_{1-x}Sr_x)_2CuO_4$. Recently, Axe et al. [3] performed both X-ray and neutron diffraction experiments on LBCO with $x = 0.05$ and reported a transition to a new tetragonal low-temperature phase (TLT) with $P4_2/nm$ symmetry below 52 K. Such a sequence of transition as THT-OMT-TLT is quite peculiar because apparent symmetry restoration is involved in the second transition to TLT. It should be noted that the same sequence of transitions has been known in the K_2NiF_4 -type compound $(CH_3NH_3)_2FeCl_4$ (MAFeC) [4].

The structures of OMT and TLT differ in a subtle way in the ordering of the tilted oxygen octahedra [3]. However, this subtle difference in the structure results in a drastic change in the superconducting properties. The transition temperature T_c is sharply depressed in the range of x in which the transition to TLT occurs. A precise characterization of both the structural and superconductive anomaly in LBCO would thus give us a clue to understand the pairing mechanism in the cuprate superconductors.

Samples used in this study were prepared by solid-state reaction as described in Ref. 5. The Ba concentration of the samples was $x = 0, 0.019 (0.016 \pm 0.001), 0.035$

(0.028 ± 0.001), 0.039 (0.032 ± 0.001), 0.047 (0.041 ± 0.002), 0.059 (0.051 ± 0.004), 0.071 (0.065 ± 0.004), 0.079 (0.068 ± 0.003), 0.10 (0.087 ± 0.001) and 0.12 (0.106 ± 0.001), where values in the parentheses were determined by electron-probe microanalysis. Note that the variation of the Ba concentration within a sample is systematically greater for x around 0.06 .

Powder X-ray diffraction measurements were carried out by using a conventional diffractometer with $\text{CuK}\alpha$ radiation. A continuous-flow cryostat (Oxford Instruments CF1108) was used for the measurements at reduced temperatures. Since a first-order transition was expected, temperature variation was controlled to be slower than 5 K per hour. In Fig. 1 (a), the relative variation of the lattice parameters (using the notations for the THT phase a and b , which are related to the OMT parameters a^* and b^* by $a = a^*/\sqrt{2}$ and $b = b^*/\sqrt{2}$) with temperature are plotted for $x = 0.059$. The lattice parameters at room temperature are $a = 3.78$ Å and $c = 13.27$ Å. As is clearly seen, changes in a and b are gradual at $T_{d1} = 210$ K (THT to OMT), whereas they are abrupt at $T_{d2} = 49$ K. Moreover, as in Fig. 1 (b) hysteresis over 5 K on cooling and warming exists in the OMT-TLT transition. These results strongly suggest that the THT-OMT transition is of the second order, whereas the OMT-TLT transition is of the first order. These are consistent with the group theoretical arguments which state that the OMT-TLT transition should be of the first order, since the TLT symmetry ($P4_2/n\text{cm}$) is not a subgroup of the OMT symmetry (Cmca).

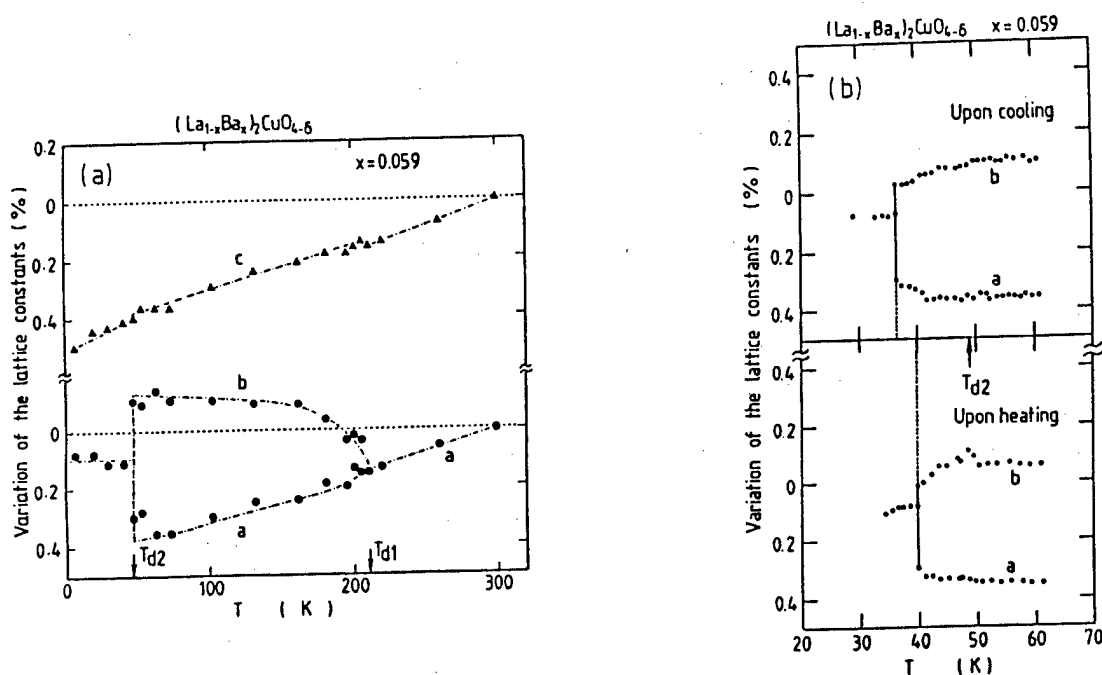


Fig. 1(a) Relative variation of the lattice parameters with temperature for the sample of $(\text{La}_{1-x}\text{Ba}_x)_2\text{CuO}_4$ with $x=0.059$. (b) The lattice parameters a and b for the same sample. The measurement in (b) was performed both on cooling and heating at a rate slower than 5 K per hour.

The phase diagram illustrated in Fig. 2 summarizes the results of our X-ray studies on various LBCO samples. When temperature is very slowly reduced, the structure sequence of the THT-OMT-TLT phases is found for samples with $0.035 \leq x \leq 0.10$. The transition temperature T_{d1} appears to depend almost linearly with x . As in Fig. 3, the superconducting transition temperature T_c shows an anomalous dip around $x = 0.06$, where the TLT transition temperature T_{d2} attains its maximum.

Figure 4 shows the temperature dependence of the electrical resistivity of the sample with $x = 0.06$ at various measurement pressures up to 18 kbar. At ambient pressure, the resistivity shows a minimum at 62 K, which is more than 10 K higher than T_{d2} , and the resistivity drop associated with superconductivity occurs in two steps. These three characteristic features are commonly seen in samples with x around 0.06 prepared under various heat treatments, including the post-annealing in oxygen at 100 bar. No hysteresis was observed in the temperature dependence of these features whether the samples were quickly cooled or annealed at temperatures slightly below T_{d2} for a few days before resistivity measurements. By applying pressure, the lower T_c for the second superconducting transition increases at a rate of 0.8 K/kbar up to 10 kbar, which is about four times the rate for the orthorhombic sample with $x = 0.08$. We have not carried out any structural study at high pressure, but we expect T_{d2} to decrease with increasing pressure. In this connection, it is interesting to note that in MAMC with $M = Fe$ mentioned above, T_{d2} (OMT-TLT) decreases from 233 K at 0 kbar to 216 K at 5 kbar [4].

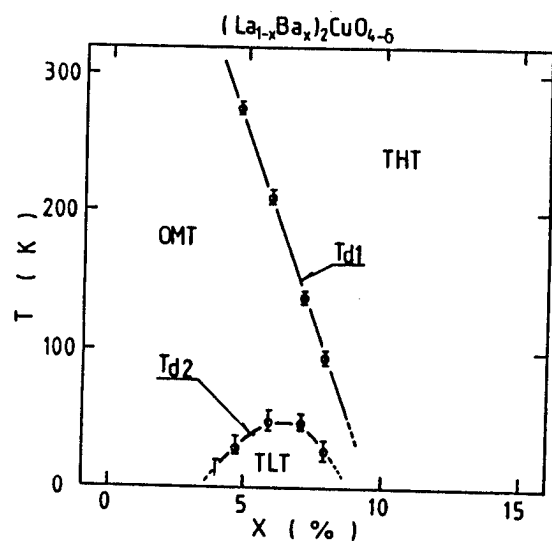


Fig. 2. Phase diagram of $(La_{1-x}Ba_x)_2CuO_4$. The transition temperatures T_{d1} and T_{d2} were determined by X-ray diffraction.

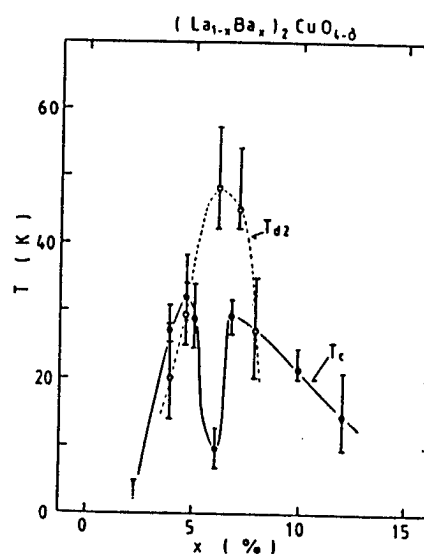


Fig. 3. T_{d2} determined by X-ray diffraction and T_c determined by resistivity as functions of x in $(La_{1-x}Ba_x)_2CuO_4$. An anomalous dip in T_c is clearly seen around $x=0.06$.

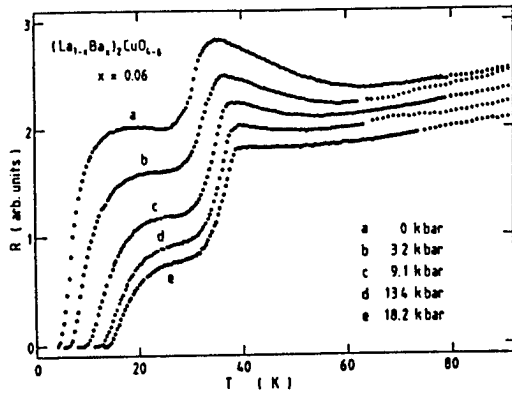


Fig. 4. Pressure dependence of the electrical resistivity for $(\text{La}_{1-x}\text{Ba}_x)_2\text{CuO}_{4-x}$ with $x=0.06$.

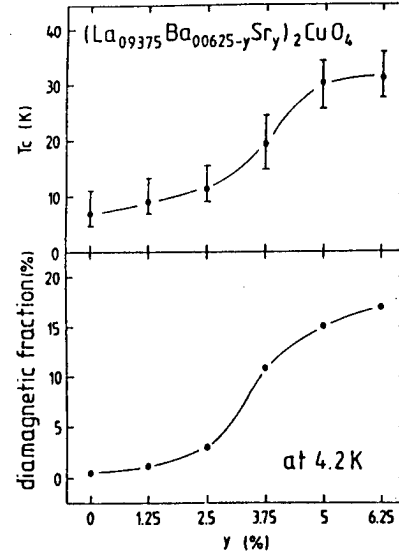


Fig. 5. The variations of T_c determined by the resistivity and the diamagnetic volume fraction at 4.2 K as functions of the Sr concentration y in $(\text{La}_{0.9375}\text{Ba}_{0.0625-y}\text{Sr}_y)_2\text{CuO}_4$.

Anomalous dip in T_c also exists in $(\text{La}_{1-x}\text{Sr}_x)_2\text{CuO}_4$ [7], although structural change to TLT phase has never been reported in this system. In order to examine a connection between superconductivity and T_{d2} in a different way, we prepared $(\text{La}_{0.9375}\text{Ba}_{0.0625-y}\text{Sr}_y)_2\text{CuO}_4$ with $0 \leq y \leq 0.0625$. The value 0.0625 was chosen so that exactly 1/16 of the La-site is occupied by the divalent atoms as discussed below. The variations of T_c determined from the resistivity and the diamagnetic fraction at 4.2 K for samples field-cooled under 24 Oe are presented as functions of the Sr content y in Fig. 5 (a) and (b), respectively. For small y , the mid-point T_c remains below 10 K, and at the same time the diamagnetic fraction is an order of magnitude smaller than that for greater Sr content. From the temperature dependence of the diamagnetic susceptibility, it is concluded that the component which is responsible for the first onset at about 33 K is not a bulk superconductor. As y is increased above 0.025, a sharp increase in both T_c and the diamagnetic fraction occur, and they tend to saturate for y close to 0.0625. We are currently investigating the variations of T_{d2} of these samples.

We have described anomalous structural and superconducting properties of LBCO with $x \approx 0.06$. It is interesting to consider why the anomaly exists at this particular range of x . Since the anomaly in T_c also appears in LSCO, it is unlikely that change in the average ionic radius of the La site by doping plays an essential role. The unit cell of the TLT phase is twice as large as that of the THT phase ($a^* = \sqrt{2}a$ and $c^* = c$) but the cell which contains one complete rotation of the spiral of the tilted oxygen octahedra contains 16 equivalent La sites. It is natural to speculate that the presence of a foreign ion with different valency or ionic radius from those of La in one of these 16 La sites would promote the stability of the TLT phase. In reality, the transition to the TLT phase occurs not only in the intimate vicinity of $x = 0.0625$.

but in a much wider range of x , $0.035 \leq x \leq 0.10$. The width of the (110) X-ray diffraction peak for TLT is noticeably wider than the corresponding one for THT [5]. There is an intrinsic reason for a large degree of structural disorder in the TLT phase. Because of the presence of a pair of anti-phase domains with opposite signs of rotation of the spiral of ordered oxygen octahedra, the size of the coherent domains in the TLT phase is expected to be greatly reduced compared to that in the OMT phase. In addition, even the possibility of the coexistence of both TLT and OMT domains within the samples cannot be ruled out. As noted above, the variation in x within the samples were systematically greater for x around 0.06 already at room temperature. It is not known whether there is any intrinsic reason for this variation.

Let us now consider the relation between the structural change and the superconducting and normal-transport properties. We argued above that the presence of the minimum in the resistivity at about 60 K is unlikely to be a direct consequence of the OMT-TLT structural change, although they may well originate from the same physical mechanism. It cannot be concluded whether the superconductivity with T_c at about 10 K is an intrinsic property of the TLT phase. Because of the very short coherence length of the cuprate superconductivity, it is expected that not only T_c but also the Meissner fraction is strongly reduced in the presence of a great degree of structural disorder, which is, as discussed above, is in practice inevitable in the TLT phase. Another intriguing possibility is that the superconductivity is very sensitive to a particular phonon mode which is expected to change substantially at the OMT-TLT transition. The fact that LSCO without phase change to TLT also exhibits the anomaly in T_c suggests that the anharmonicity in the particular mode of lattice vibrations, which leads to stabilize TLT in the case of LBCO, may play an important role in superconductivity. Quite recently, it is reported [8] that the oxygen isotope effect in both LSCO and LBCO shows a dramatic enhancement in up to 0.6 for x around 0.06. These results point to the essential involvement of phonons in the mechanism of superconductivity in these systems. Both high pressure and the introduction of Sr in place of Ba act to suppress the stability of TLT, and both lead to enhance T_c of the anomalous state with $x \approx 0.06$. Thus, competition between the original T_c in the OMT phase and T_{d2} for the structural change is quite important in order to understand the anomalous behavior in superconductivity in these compounds.

2. High-spin and low-spin configurations in $(\text{La}_{1-x}\text{Sr}_x)_2\text{NiO}_4$

In this section, we will describe anomalous physical properties of $(\text{La}_{1-x}\text{Sr}_x)_2\text{NiO}_{4+\delta}$ (LSNO), another compound in the K_2NiF_4 structure. We focus on the following two aspects involved in this system. One is the anomalies in the x -dependences of various physical properties at $x \approx 0.3$, originating from the change from the high-spin to the low-spin state of the d-electrons. The other is unusual magnetic behavior at x around 0.5, which is compared with that of LSCO at small x (Sr).

The crystal structure of $\text{La}_2\text{NiO}_{4+\delta}$ at room temperature is known to be orthorhombic if $\delta \approx 0$, but is transformed to tetragonal by a small amount of excess oxygen $\delta > 0.05$ [9]. Both the transport and magnetic properties for $x = 0$ are consistent with that for the localized $3d^8$ electron system of Ni^{2+} in the high-spin configuration with $S = 1$. On the other hand, an EPR spectrum of LSNO with $x = 0.5$ indicates that Ni^{3+} is in the low-spin configuration [10].

Polycrystalline samples of LSNO were prepared by heating the mixture of the powders of La_2O_3 , SrCO_3 and NiO at $1100 \sim 1290^\circ\text{C}$ in air for a total of 5 days with several intermediate grindings. Unless specified, the data shown below are taken on samples furnace-cooled in air in about 12 hours. Powder X-ray diffraction spectra indicate that the samples with $x \leq 0.6$ were of single-phase in the K_2NiF_4 structure. Figure 6 shows the variations of the lattice parameters at room temperature and their ratio, c/a , with x . Samples with $x = 0$ did not show any orthorhombic distortion. Although we have not determined the amount of off-stoichiometric oxygen, δ , this is expected because they were prepared in air and contain excess interstitial oxygen. With increasing x , a sharp change in the x -dependence of the lattice parameters takes place at $x = 0.25 \sim 0.30$, consistent with the results of Takeda et al. [11]. This change is reflected in both the resistivity and magnetic susceptibility.

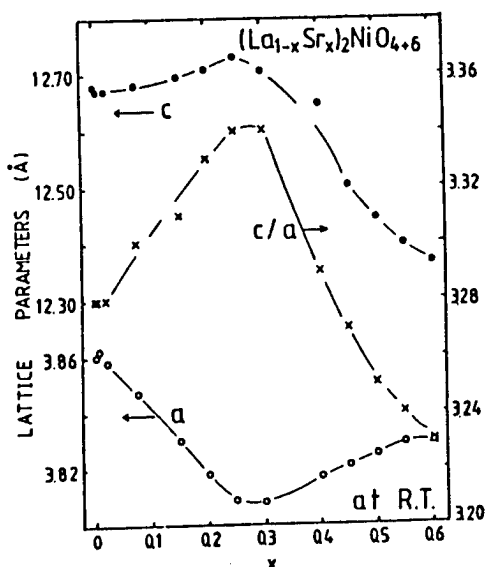


Fig. 6. Variation of the lattice parameter and their ratio, c/a , in $(\text{La}_{1-x}\text{Sr}_x)_2\text{NiO}_{4+\delta}$.

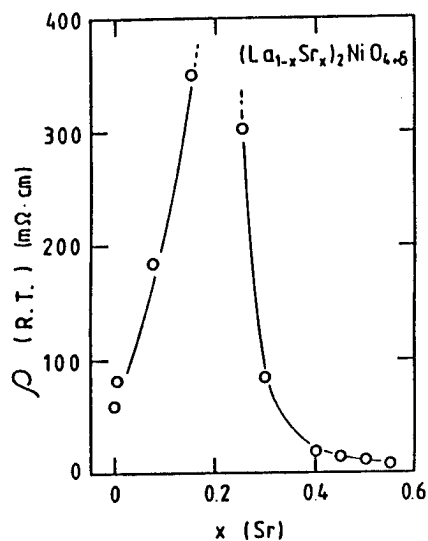


Fig. 7. Resistivity ρ at room temperature as a function of x in $(\text{La}_{1-x}\text{Sr}_x)_2\text{NiO}_{4+\delta}$.

The resistivity ρ at room temperature, shown in Fig. 7, attains maximum at $x \approx 0.2$. Relatively small resistivity at room temperature for $x = 0$ might be due to the carriers doped excess oxygen. The temperature dependence of ρ is semiconductive for small x . By increasing x further above 0.3, the temperature coefficient of ρ tends to become positive. Above $x = 0.45$, the conduction becomes metallic near room temperature and shows a transition from itinerant to localized behavior at $T_0 = 200$ K for $x = 0.45$ and 100 K for $x = 0.55$. Below T_0 , the temperature dependence of the resistivity could not be fitted very well either with the form for variable-range hopping in two or three dimension or an activated form.

Figure 8 shows the magnetic susceptibility below room temperature for selected values of x . For $x = 0$, χ is quite sensitive to the amount δ , and thus the way samples were heat treated [12]. As shown by the closed circles in Fig. 8, the sample furnace-cooled in air exhibited a pronounced, sharp peak in χ at the Neel temperature $T_N = 110$ K, whereas the sample rapidly cooled in air from 1000°C , as represented by the open circles, shows much smaller peak at $T_N = 60$ K. Unlike La_2CuO_4 , stoichiometric ($\delta=0$) crystal of La_2NiO_4 in the orthorhombic structure does not show such a clear anomaly in χ , because the magnetic moments of Ni^{2+} ions are not canted in the antiferromagnetic state. In any case, the molar susceptibility at room temperature is about twenty times greater than that for La_2CuO_4 . The value of χ at room temperature decreases with x , but the rate of decrease with x shows anomaly at $x \approx 0.3$ and becomes two times more rapid for x above 0.3. At the same time, the Curie-Weiss component

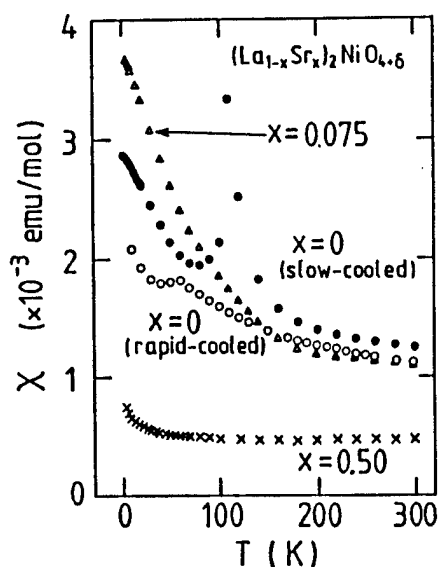


Fig. 8. Variation of the magnetic susceptibility with temperature for $(\text{La}_{1-x}\text{Sr}_x)_2\text{NiO}_{4+\delta}$.

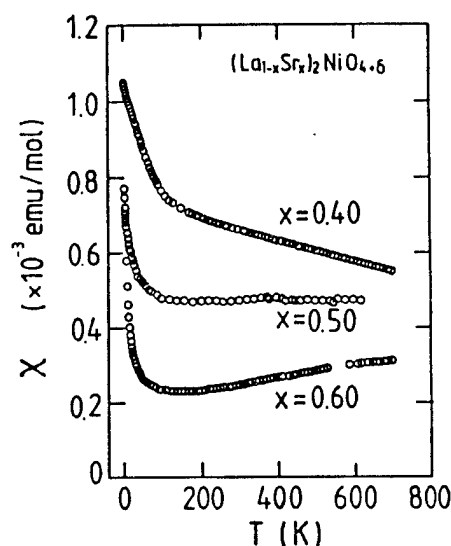


Fig. 9. Magnetic susceptibility up to 700 K for samples of $(\text{La}_{1-x}\text{Sr}_x)_2\text{NiO}_{4+\delta}$ with x close to 0.5. The temperature coefficient of χ increases with x and becomes positive for $x \geq 0.5$.

decreases with x , and for $x \geq 0.50$ the temperature coefficient of χ even changes sign and becomes positive for temperature down to about 100 K, below which the upturn in χ is observed, probably due to localized 3d electrons which amounts to a few percent of the total Ni atoms.

Figure 9 shows the susceptibility up to 700 K for selected samples with x around 0.5. Because the samples are exposed to He gas in the SQUID magnetometer and are expected to release oxygen at high temperatures, special care was paid to check the reversibility of χ during the temperature excursions. The temperature coefficient of the susceptibility above about 200 K systematically increases with x and becomes positive for $x \geq 0.5$. For $x = 0.60$, χ tends to saturate above 600 K, suggestive of the presence of a broad maximum. Such behavior is quite similar to the susceptibility of $(\text{La}_{1-x}\text{Sr}_x)_2\text{CuO}_4$ with $x < 0.1$ [13]: with decreasing x from above 0.1, the temperature coefficient of χ changes sign from negative to positive, and the broad maximum in χ appears at temperature which increases toward $x = 0$. This behavior is interpreted as due to the two-dimensional antiferromagnetic correlation between Cu spins, with the correlation length increasing toward $x = 0$.

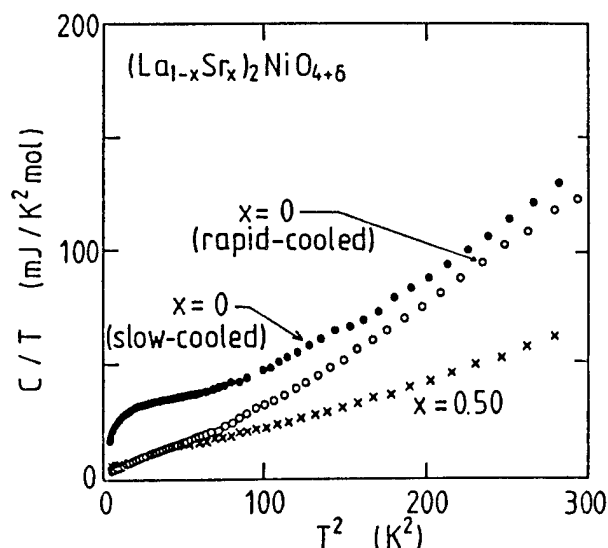


Fig. 10. Variation of the ratio of the molar specific heat to temperature, C/T , with T^2 for $(\text{La}_{1-x}\text{Sr}_x)_2\text{NiO}_{4+\delta}$. The sample with $x = 0$ furnace-cooled in air (slow-cooled) shows a pronounced hump in C/T at low temperature.

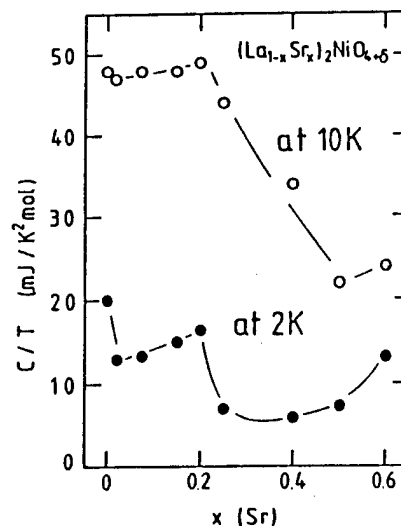


Fig. 11. Values of the molar specific heat divided by temperature, C/T , at 2 and 10 K for $(\text{La}_{1-x}\text{Sr}_x)_2\text{NiO}_{4+\delta}$. Furnace-cooled samples were used for the measurements.

The specific heat was measured between 1.8 and 20 K by using an adiabatic calorimeter with a mechanical heat switch. In Fig. 10, the molar specific heat divided by temperature, C/T , is plotted against T^2 for the samples used in the measurements of the magnetic susceptibility shown in Fig. 8. The lattice is significantly hardened for large x , as indicated by the decrease in the slope of C/T against T^2 , from which the Debye temperature is estimated to increase from 345 K for $x = 0$ to 450 K for $x = 0.50$.

Samples slowly cooled in air, presumably with a greater amount of excess oxygen especially for small x , show pronounced humps in C/T at low temperatures. In order to characterize the relative magnitude of these humps, the values of C/T at 2 and 10 K are plotted against x in Fig. 11. A clear correlation exists between the variation of the magnitude of the humps with x and the anomalies at $x = 0.2 \sim 0.3$ observed in other physical quantities, which are ascribed to the transition from the high-spin to low-spin state. It is not likely that the anomalous hump in the specific heat is an intrinsic properties of the stoichiometric LSNO, because it depends heavily on the conditions of the heat treatment as shown in Fig. 10 for the two samples with $x = 0$. The temperature dependence of the specific heat is fitted with $C = \gamma T + \beta T^3 + \alpha C_4$, which contains, in addition to the standard electronic and lattice contributions, the Schottky term, C_4 , for the two-level system with the energy separation Δ . A satisfactory fit is obtained if a broad distribution for the energy separation centered at Δ is introduced in the analysis. The values of Δ are between 15 and 20 K and do not depend in any systematic way on x . From the curve for the slowly cooled sample with $x = 0$ in Fig. 8, we obtain $\Delta = 17$ K, the width $W = 9$ K and $\alpha = 0.05$. If the two-level system originates from the resonant tunneling of an excess oxygen atom between equivalent interstitial sites, it is inferred that α is equivalent to the amount of excess oxygen contained in each formula unit. It is interesting to note the qualitative correlation between the magnitude of the Curie-Weiss component in the susceptibility and of the hump in C/T , since interstitial oxygen atoms also create impurity levels for the d-electrons of Ni ions and give rise to localized moments. It is not clear why the strong suppression of the Schottky hump in C/T occur for x greater than 0.2, because it is reported that the amount of oxygen varies little in this range of x [11].

We have described various physical properties of LSNO which depend anomalously on x . Below x of about 0.3, the electrons are in the high-spin configuration and localized, resulting in the negative temperature coefficient of the resistivity and the Curie-Weiss susceptibility. For greater values of x , the d-electrons tend to be delocalized and provide metallic conductivity for $x \geq 0.40$ down to a certain temperature which decreases with increasing x . At the same time, the susceptibility becomes Pauli-like and the positive temperature coefficient in χ is realized for $x \geq 0.50$.

Because of the low-spin configuration, the system $(\text{La}_{1-x}\text{Sr}_x)_2\text{NiO}_4$ with x around 0.5 have common features to $(\text{La}_{1-x}\text{Sr}_x)_2\text{CuO}_4$ with x close to 0. Both are spin $1/2$ systems ($3d^7$ for Ni and $3d^9$ for Cu) and show positive temperature coefficient of χ , which for LSCO is ascribed to the two-dimensional antiferromagnetic correlation between the spins. By doping, both systems exhibit metallic conductivity. There are, however, significant differences. We have not found any antiferromagnetic ordering for $x = 0.50$ in LSNO, whereas in LSCO with $x = 0$, $T_N = 250$ K and disappears rapidly by doping with x as small as 0.01 [1,13]. In LSNO with $x = 0.50$, the electrons occupy quarter-filled σ^* band because of the orbital degeneracy of the $3d_{z^2}$ and $3d_{x^2-y^2}$, whereas in LSCO with $x = 0$, they are in the half-filled σ^* band. For better comparison with the superconductive Cu system, it is desired to study related Ni oxide compounds in which the orbital degeneracy is relaxed.

The authors are grateful to A. Odagawa and N. Kakehi for their contributions in this work.

REFERENCES

- [1] T. Fujita, Y. Aoki, Y. Maeno, J. Sakurai, H. Fukuba and H. Fujii: Jpn. J. Appl. Phys. **26** (1987) L368.
- [2] R. M. Fleming, B. Batlogg, R. J. Cava and E. A. Rietman: Phys. Rev. **B35** (1987) 7191.
- [3] J. D. Axe, H. Moudden, D. Hohlwein, D. E. Cox, K. M. Mohanty, A. R. Moodenbaugh and Y. Xu: Phys. Rev. Lett. **62** (1989) 2751.
- [4] T. Goto, M. Yoshizawa, A. Tamaki and T. Fujimura: J. Phys. **C15** (1982) 3041.
- [5] T. Suzuki and T. Fujita: J. Phys. Soc. Jpn. **58** (1989) 1883.
- [6] T. Suzuki and T. Fujita: Physica **C159** (1989) 111.
- [7] M. Oda, T. Ohguro, N. Yamada and M. Ido: J. Phys. Soc. Jpn. **58** (1989) 1137.
- [8] M. K. Crawford: presented at the 2nd International Symposium on Superconductivity, Nov. 14-17 (1989), Tsukuba, Japan.
- [9] J. D. Jorgensen, B. Dabrowski, S. Pei, D. R. Richards and D. G. Hinks: Phys. Rev. **B40** (1989) 2187.
- [10] G. Demazeau, J. L. Marty, B. Buffat, J. M. Dance, M. Pouchard, P. Dordor and B. Chevalier: Mat. Res. Bull. **17** (1982) 37.
- [11] Y. Takeda, R. Kanno, M. Sakano, O. Yamamoto, M. Takano, Y. Bando, H. Akinaga, H. Takita and J. B. Goodenough: Mat. Res. Bull., in press.
- [12] D. J. Buttrey, J. M. Honig and C. N. R. Rao: J. Solid State Chem. **64** (1986) 287.
- [13] H. Takagi, T. Ido, S. Ishibashi, M. Uota, S. Uchida and Y. Tokura: Phys. Rev. **B40** (1989) 2254.

Ultrasonic Properties in $\text{La}_{2-x}\text{M}_x\text{CuO}_{4-\delta}$ (M=Ba and Sr) and Correlation between T_c and Hole Concentration in the Cation-Substituted $\text{Bi}_2\text{Sr}_2\text{CaCu}_2\text{O}_{8+\delta}$ System

T. Fukase, Y. Koike*, T. Goto, T. Nomoto, Y. Iwabuchi, and T. Hanaguri

Institute for Materials Research, Tohoku University,
Katahira, Aoba-ku, Sendai 980

Ultrasonic attenuation and velocity have been measured down to 1.5 K in $\text{La}_{2-x}\text{Ba}_x\text{CuO}_{4-\delta}$ and $\text{La}_{2-x}\text{Sr}_x\text{CuO}_{4-\delta}$ with 7 MHz longitudinal waves. On cooling from room temperature, pronounced softening of the lattice is observed for $0.09 \leq x \leq 0.20$ down to the transformation temperature from the tetragonal high-temperature phase to the orthorhombic phase, T_{d1} , and a large attenuation peak is observed at T_{d1} . Below T_{d1} the lattice remains soft. The further low-temperature transformation from the orthorhombic phase to the tetragonal low-temperature phase is observed with partial lattice stiffening and a small attenuation peak not only for $\text{La}_{2-x}\text{Ba}_x\text{CuO}_{4-\delta}$ but also for $\text{La}_{2-x}\text{Sr}_x\text{CuO}_{4-\delta}$. Correlation between superconducting T_c and hole concentration has been investigated in the $\text{Bi}_2\text{Sr}_2\text{CaCu}_2\text{O}_{8-\delta}$ system. The hole concentration is varied by substituting cations with different valences for Sr or Ca. We find that T_c increases, takes a maximum at the hole concentration corresponding to 0.2 - 0.3 holes per CuO_2 unit, and then decreases, with increasing hole concentration, similarly to those in the $\text{La}_{2-x}\text{Sr}_x\text{CuO}_{4-\delta}$ and $\text{YBa}_2\text{Cu}_3\text{O}_{7-\delta}$ systems.

1. Ultrasonic Properties in $\text{La}_{2-x}\text{Ba}_x\text{CuO}_{4-\delta}$ and $\text{La}_{2-x}\text{Sr}_x\text{CuO}_{4-\delta}$

In spite of subsequent finding of new materials with higher superconducting transition temperature T_c , the doped La_2CuO_4 (LCO) system discovered by Bednorz and Müller^[1] has continued to receive special interest, because this system has a relatively simple crystal structure and is believed to share a common superconducting mechanism to other high- T_c copper-oxide-based systems. The crystal structure of $\text{La}_{2-x}\text{Ba}_x\text{CuO}_{4-\delta}$ (LBCO) and $\text{La}_{2-x}\text{Sr}_x\text{CuO}_{4-\delta}$ (LSCO) is a layered perovskite of K_2NiF_4 type. As the temperature is lowered, a structural phase transformation from the tetragonal high-temperature phase (THT; space group $I4/mmm$) to the orthorhombic phase (OMT; space group Cmca) takes place.^[2-4] The transformation temperature, T_{d1} , about 515 K in the undoped material ($x=0$), decreases with increasing Ba or Sr concentration x .

For LBCO X-ray and neutron scattering experiments confirmed a further low-temperature phase transformation to the tetragonal phase (TLT; space group $\text{P4}_2/\text{ncm}$) in a narrow region around $x = 0.12$.^[5,6] The low-temperature phase diagram was presented by several authors^[5-7] and the close relation between the structural transformation (transformation temperature is expressed as T_{d2}) and the depression of T_c around $x = 0.12$ was pointed out. In this paper, we report our ultrasonic experiments of $\text{La}_{2-x}\text{Ba}_x\text{CuO}_{4-\delta}$ and $\text{La}_{2-x}\text{Sr}_x\text{CuO}_{4-\delta}$ with $0 \leq x \leq 0.20$ and drastic anomalies observed at the structural transformation temperatures mentioned above not only for LBCO but also for LSCO. The relationship of this structural transformation

to the unusual depression of the superconductivity near $x = 0.12$ is briefly discussed.

The polycrystalline ceramic samples were prepared using La_2O_3 (4N-purity), BaCO_3 (4N), SrCO_3 (4N) and CuO (4N) as starting materials. The mixtures were first fired at 1000°C in air for 24h, and then finely ground using a ball mill, pressed into ingots using hydrostatic pressure of 70 kg/mm^2 with the rubber press method, sintered in air at 1050°C for 50h, and finally annealed in flowing oxygen at 500°C for 50h. X-ray powder diffraction showed the specimens to be a single phase. The samples were of cylindrical shaped, 9 mm in diameter, and with lengths ranging from 10 to 12 mm. The density was more than 90 % of that calculated from X-ray data. The attenuation of ultrasonic waves and the velocity change of the longitudinal waves of 7 MHz were simultaneously measured using the pulse echo method and the pulse-superposition method, respectively. A Z-cut lithium niobate transducer was bonded to the samples with Nonaq stopcock grease. A good echo train with more than 10 echoes was observed for most samples. All measurements were performed on the first and second echoes. The ac susceptibility of the samples was also monitored simultaneously to measure T_c .

Figure 1 shows the temperature dependences of the sound velocity $V_s(T)$ and the ultrasonic attenuation coefficient $\alpha(T)$ for $\text{La}_{1.90}\text{Ba}_{0.10}\text{CuO}_{4-\delta}$. The sound velocity shows large decrease with decreasing temperature from room temperature down to T_{d1} . This lattice softening remains on further cooling. Partial stiffening occurs below T_{d2} . A large attenuation peak and a small attenuation peak are observed at T_{d1} and T_{d2} , respectively. The magnitude of attenuation peaks seems to depend on the order of the phase transformations, that is, a large attenuation peak is observed at the second-order phase transformation while a small peak is observed at the first order phase transformation. Similar behavior is observed in a Ba-concentration region of $0.09 \leq x$ as shown in Fig. 2. The low-temperature phase diagram obtained in these experiments is shown in Fig. 3. T_{d2} obtained by the present experiments does not decrease so rapidly in a large Ba-concentration region as those obtained by Sera et al.^[7] or Suzuki et al..^[6] Figure 3 also illustrates the Ba-concentration

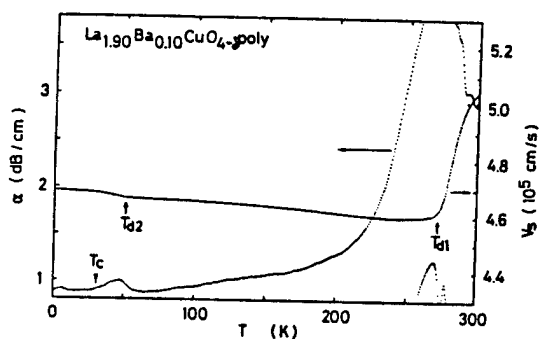


Fig. 1 Temperature dependence of the sound velocity and attenuation coefficient of 7MHz longitudinal waves in $\text{La}_{1.90}\text{Ba}_{0.10}\text{CuO}_{4-\delta}$.

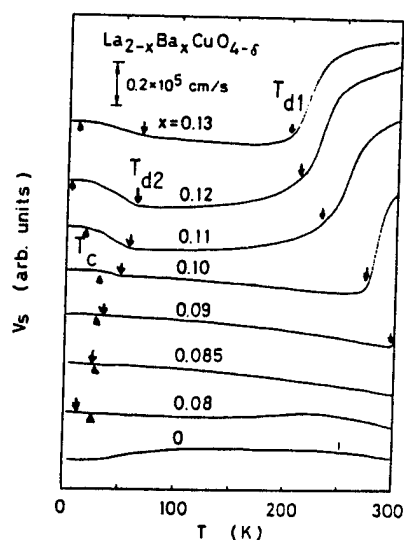


Fig. 2 Temperature dependence of the sound velocity change in $\text{La}_{2-x}\text{Ba}_x\text{CuO}_{4-\delta}$.

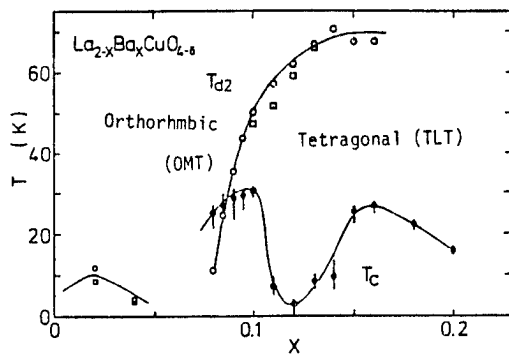


Fig. 3 Experimental phase diagram of $\text{La}_{2-x}\text{Ba}_x\text{CuO}_{4-\delta}$. Open circles indicate the structural transformation-temperature T_{d2} which is defined at the temperature of the beginning of the increase of the sound velocity. Open squares indicate T_{d2} defined at the temperature of the attenuation peak. Solid circles indicate T_c defined at the middle point of the ac susceptibility change.

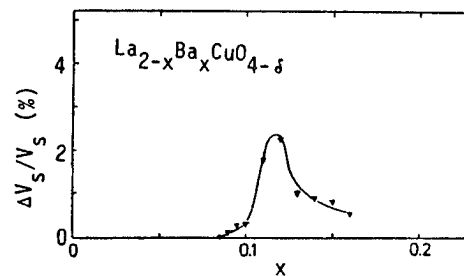


Fig. 4 Ba concentration dependence of the sound velocity change below T_{d2} .

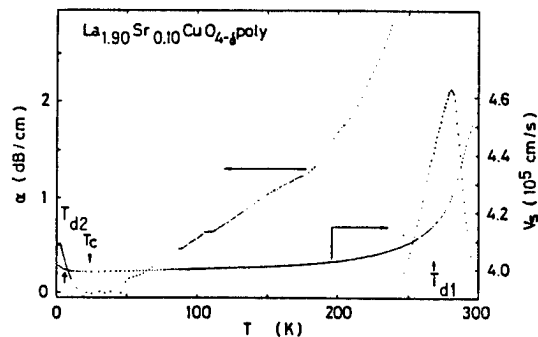


Fig. 5 Temperature dependence of the sound velocity and attenuation coefficient of 7MHz longitudinal waves in $\text{La}_{1.90}\text{Sr}_{0.10}\text{CuO}_{4-\delta}$.

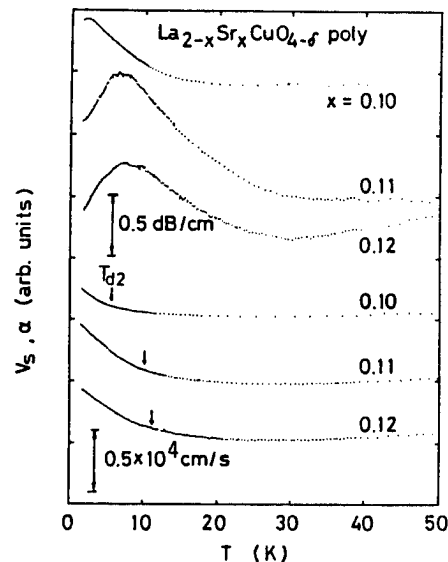


Fig. 6 Temperature dependence of the sound velocity change and attenuation coefficient of 7MHz longitudinal waves in $\text{La}_{2-x}\text{Sr}_x\text{CuO}_{4-\delta}$.

dependence of T_c , determined by the ac susceptibility measurements, which shows an anomalous dip around $x = 0.12$. Figure 4 shows the Ba-concentration dependence of the amount of stiffening ($\Delta V_s/V_s$) below T_{d2} . There seems to be some correlation between the amount of stiffening below T_{d2} and the suppression of T_c .

Figure 5 shows the temperature dependences of the sound velocity and the ultrasonic attenuation coefficient for $\text{La}_{1.90}\text{Sr}_{0.10}\text{CuO}_{4-\delta}$. The sound velocity shows large decrease with decreasing temperature from room temperature down to T_{d1} and the attenuation coefficient takes a peak value at T_{d1} in the similar way to that of LBCO. It is emphasized that the lattice stiffening and the small attenuation peak observed at T_{d2} for LBCO, are also observed for LSCO near 6 K. This low-temperature anomaly is observed in a Sr-concentration region of $0.10 \leq x \leq 0.12$ as shown in Fig. 6. On

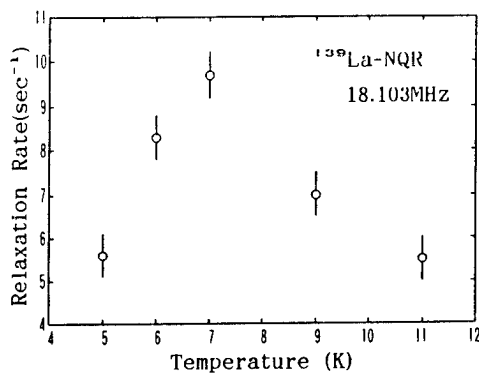


Fig. 7 Temperature dependence of nuclear relaxation rate T_1^{-1} of ^{139}La in $\text{La}_{1.88}\text{Sr}_{0.12}\text{CuO}_{4-\delta}$.

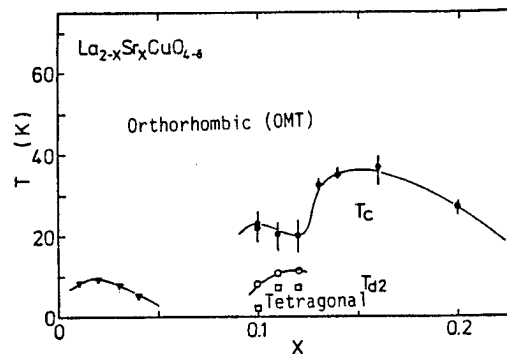


Fig. 8 Experimental phase diagram of $\text{La}_{2-x}\text{Sr}_x\text{CuO}_{4-\delta}$. Open circles indicate the structural-transformation temperature T_{d2} defined at the temperature of the beginning of the increase of the sound velocity. Open squares indicate T_{d2} defined at the temperature of the attenuation peak. Solid circles indicate T_c defined at the middle point of the ac susceptibility change.

the analogy of LBCO, the temperature where the lattice stiffening begins can be considered T_{d2} . Nuclear relaxation time T_1 of ^{139}La in $\text{La}_{1.88}\text{Sr}_{0.12}\text{CuO}_{4-\delta}$ takes a minimum value around 7 K as shown in Fig. 7. This result consists with the occurrence of the structural transformation at the temperature. Low temperature x-ray diffraction experiments are in progress. The low-temperature phase diagram obtained in our ultrasonic experiments is shown in Fig. 8. Figure 8 also illustrates the Sr-concentration dependence of T_c determined by the ac susceptibility measurements. In the case of LSCO, however, T_{d2} is lower than T_c and T_c vs x curve shows a small dip around $x = 0.12$. Therefore, it seems that the low-temperature structural transformation does not directly depress T_c but the origin of the low-temperature structural transformation and the origin of the depression of T_c have a common factor.

2. Correlation between T_c and hole concentration in the cation-substituted $\text{Bi}_2\text{Sr}_2\text{CaCu}_2\text{O}_{8+\delta}$ system^[8]

Correlation between T_c and hole concentration was investigated for $\text{Bi}_2\text{Sr}_2\text{Ca}_{1-x}\text{Lu}_x\text{Cu}_2\text{O}_{8+\delta}$, $\text{Bi}_2\text{Sr}_2\text{Ca}_{1-x}\text{Na}_x\text{Cu}_2\text{O}_{8+\delta}$, $\text{Bi}_2\text{Sr}_{2-x}\text{La}_x\text{CaCu}_2\text{O}_{8+\delta}$ and $\text{Bi}_2\text{Sr}_{2-x}\text{K}_x\text{CaCu}_2\text{O}_{8+\delta}$ within the range of solid solubility. As shown in Fig. 9 and 10, the hole concentration estimated from the Hall coefficient at 290 K decrease with increasing substitution concentration of Lu^{3+} and La^{3+} for Ca^{2+} and Sr^{2+} , respectively. On the other hand, it does not change for Na- and K-substituted samples, suggesting that oxygen atoms are deficient due to the substitution. The hole concentration for Na- and K-substituted samples could be increased by annealing at 600 °C in 1 bar of oxygen and by annealing at 430 °C in 250 bar of oxygen. Dependence of T_c on the hole concentration is described in Fig. 11. We find that T_c shows universal correlation with the hole concentration. That is, T_c increases, takes a maximum, and then decreases with increasing hole concentration. Judging from

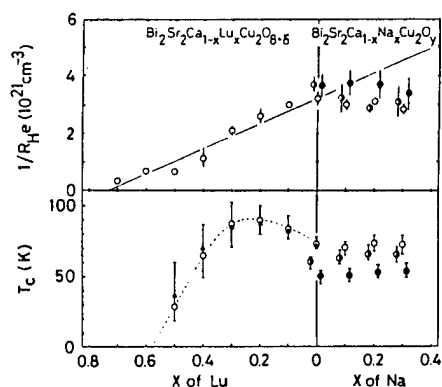


Fig. 9 Variations with x of T_c and hole concentration $1/R_{He}$ at 290 K estimated from the Hall coefficient R_H in the $\text{Bi}_2\text{Sr}_2\text{Ca}_{1-x}\text{Lu}_x\text{Cu}_2\text{O}_{8+\delta}$ and $\text{Bi}_2\text{Sr}_2\text{Ca}_{1-x}\text{Na}_x\text{Cu}_2\text{O}_{8+\delta}$ systems. Circles in the figure of T_c vs. x are T_c 's defined at the midpoint of the transition curve in the ρ vs. T plot. Bars in the figure of T_c vs. x indicate the temperatures where ρ drops to 90 % and 10 % of the normal-state resistivity. Triangles indicate T_c 's defined at the onset temperature of the Meissner effect. Open, half-closed and fully closed circles correspond to samples made by no additional annealing, by annealing at 600 °C in 1 bar of oxygen and by annealing at 430 °C in 250 bar of oxygen, respectively. The solid line is calculated, assuming that one Lu atom and one Na atom substituted for a Ca atom compensates and supplies one hole, respectively.

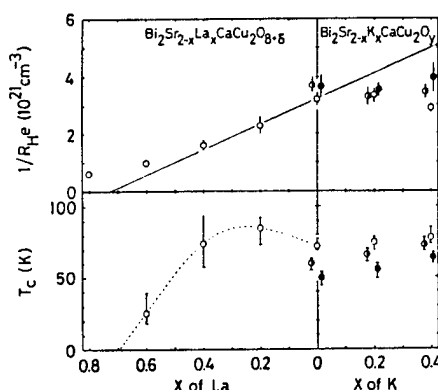


Fig. 10 Variations with x of T_c and hole concentration $1/R_{He}$ at 290 K estimated from the Hall coefficient R_H in the $\text{Bi}_2\text{Sr}_{2-x}\text{La}_x\text{CaCu}_2\text{O}_{8+\delta}$ and $\text{Bi}_2\text{Sr}_{2-x}\text{K}_x\text{CaCu}_2\text{O}_{8+\delta}$ systems. Symbols are defined similarly to those in fig. 9. The solid line is calculated, assuming that one La atom and one K atom substituted for a Sr atom compensates and supplies one hole, respectively.

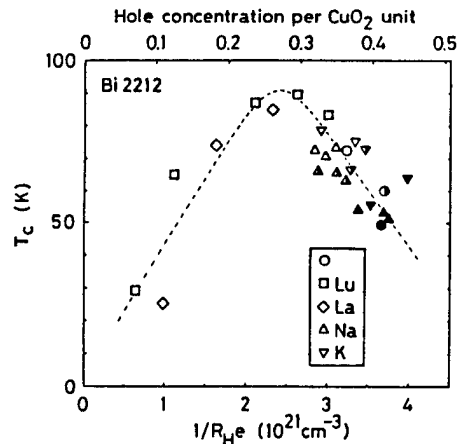


Fig. 11 Correlation between T_c and hole concentration $1/R_{He}$ in the $\text{Bi}_2\text{Sr}_2\text{Ca}_{1-x}\text{Lu}_x\text{Cu}_2\text{O}_{8+\delta}$ (\square), $\text{Bi}_2\text{Sr}_2\text{Ca}_{1-x}\text{Na}_x\text{Cu}_2\text{O}_{8+\delta}$ (\triangle , \blacktriangle , \triangle), $\text{Bi}_2\text{Sr}_{2-x}\text{La}_x\text{CaCu}_2\text{O}_{8+\delta}$ (\diamond), $\text{Bi}_2\text{Sr}_{2-x}\text{K}_x\text{CaCu}_2\text{O}_{8+\delta}$ (∇ , \blacktriangledown , \triangledown) and $\text{Bi}_2\text{Sr}_2\text{CaCu}_2\text{O}_{8+\delta}$ (\circ). Open, half-closed and fully closed symbols correspond to samples made by no additional annealing, by annealing at 600 °C in 1 bar of oxygen and by annealing at 430 °C in 250 bar of oxygen, respectively.

the universal curve, the fact that T_C of non-substituted $\text{Bi}_2\text{Sr}_2\text{CaCu}_2\text{O}_{8+\delta}$ is a little lower than those of Lu- and La-substituted samples with the composition of $x = 0.2$ is reasonably understood as due to too many holes to take a maximum. The maximum of T_C is realized at the hole concentration corresponding to 0.2-0.3 holes per CuC_2 unit. This correlation of T_C with the hole concentration is markedly similar to those in the $\text{La}_{2-x}\text{Sr}_x\text{CuO}_{4-\delta}$ [9] and $\text{YBa}_2\text{Cu}_3\text{O}_{7-\delta}$ [10] systems. It seems beyond doubt that the hole concentration in the CuO_2 sheets is essential to the high- T_C superconductivity.

references

- 1) J. G. Bednorz and K. A. Müller: Z. Phys. B64 (1986) 189.
- 2) R. M. Fleming et al.: Phys. Rev. B35 (1987) 7191.
- 3) T. Fujita et al.: Jpn. J. Appl. Phys. 26 (1987) L368.
- 4) R. J. Birgeneau et al.: Phys. Rev. Lett. 59 (1987) 1392.
- 5) J. D. Axe et al.: Phys. Rev. Lett. 62 (1989) 2751.
- 6) T. Suzuki and T. Fujita: J. Phys. Soc. Jpn. 58 (1989) 1883, Physica C159 (1989) 111.
- 7) M. Sera et al.: Solid State Commun. 69 (1989) 851.
- 8) Y. Koike, Y. Iwabuchi, S. Hosoya, N. Kobayashi and T. Fukase: Physica C159 (1989) 105.
- 9) J. B. Torrance, Y. Tokura, A. I. Nazzal, A. Bezing, T. C. Huang and S. S. P. Parkin: Phys. Rev. Lett. 61 (1988) 1127.
- 10) Y. Tokura, J. B. Torrance, T. C. Huang and A. I. Nazzal: Phys. Rev. B38 (1988) 7156.

* Present address; Faculty of Engineering, Tohoku University, Aramaki Aoba, Aoba-ku, Sendai 980

Comparison of High Pressure Effects on Transition Temperature
in the Electron- and Hole-Doped Oxide Superconductors

S.Yomo^{*}, C.Murayama^{**}, N.Mōri^{**}, H.Takagi⁺,
S.Uchida⁺ and Y.Tokura⁺⁺

* Department of Electronic and Information Engineering and Research Institute for Higher Education Programs, Hokkaido Tokai University, Minami-ku, Sapporo 005, Japan

** Institute for Solid State Physics, University of Tokyo, Roppongi, Minato-ku, Tokyo 106, Japan

+ Engineering Research Institute, University of Tokyo, Hongo, Bunkyo-ku, Tokyo 113, Japan

++ Department of Physics, University of Tokyo, Hongo, Bunkyo-ku, Tokyo 113, Japan

Electron-doped superconductors $\text{Nd}_{2-x}\text{Ce}_x\text{CuO}_{4-y}$ exhibit almost no pressure effect on the superconducting transition temperature (T_c). However, a structurally related hole-doped superconductor $\text{Nd}_{1.3}\text{Ce}_{0.2}\text{Sr}_{0.5}\text{O}_{4-z}$ shows a remarkably large pressure effect on T_c . A comparison with the pressure effects in the other hole-doped systems indicates an importance of the bond between copper and apical oxygens in the Cu-O pyramids, which is missing in the electron-doped oxides.

Recently, electron-doped oxide superconductors $\text{Ln}_{2-x}\text{Ce}_x\text{CuO}_{4-y}$ ($\text{Ln} = \text{Pr}, \text{Nd}$ and Sm) have been discovered by Tokura, et al. [1]. These are the first examples which have electrons as carriers, among the family of high T_c oxide superconductors most of which have hole carriers, and therefore are important for elucidating the mechanism of high T_c superconductivity. The superconducting transition temperature of almost all the hole-doped copper oxide compounds increases with increasing pressure [2]. The pressure coefficient has a large positive value compared with a typical conventional (BCS) superconductor. The systematic survey of the T_c s of Y-Ba-Cu-O and La-Sr-Cu-O compounds has shown that T_c is strongly correlated with hole concentration [3-5], but the Hall coefficient is only weakly dependent on pressure [6,7]. These results indicate that the large change in T_c with pressure is caused, not by a change in hole concentration, but by other factors related to changes in the interatomic distances. In this report, we describe that the newly discovered electron-doped superconductor $\text{Nd}_{2-x}\text{Ce}_x\text{CuO}_{4-y}$ and $\text{Pr}_{1.85}\text{Ce}_{0.15}\text{CuO}_{4-y}$ exhibit almost no pressure effect on the T_c up to 2.5 GPa, in remarkable contrast to the hole-doped superconductor $\text{Nd}_{1.3}\text{Ce}_{0.2}\text{Sr}_{0.5}\text{O}_{4-z}$. The Cu-O pyramids characteristic of the hole-doped compounds lose their apical oxygens to become square planes in the electron-doped materials. If the pressure effect on T_c does arise from changes in bond lengths, the difference in behaviour of the two compounds points to the involvement of the bond between copper and apical oxygen, which is missing in the electron-doped material. Part of the result has been published elsewhere[14].

The polycrystalline samples used in this study were prepared by the solid state reaction technique as described in ref.1 and 8. In the $\text{Nd}_{2-x}\text{Ce}_x\text{CuO}_{4-y}$ solid solution having the Nd_2CuO_4 type structure, the so called T' phase, superconductivity appears abruptly at a Ce composition near $x=0.14$, with a T_C of about 20 K, and disappears at about $x=0.18$. The largest Meissner signal and the highest T_C were obtained at $x=0.15$. The negative Hall and Seebeck coefficients observed¹ in the normal state showed that the charge carriers are electrons, introduced by the substitution of Ce^{4+} for Nd^{3+} . On the other hand, for $\text{Nd}_{2-x-y}\text{Ce}_x\text{Sr}_y\text{CuO}_{4-z}$ compounds, which have the T^* structure (see inset of Fig.2), the carriers are holes and superconductivity occurs in the composition range $x=0.15-0.2$ and $y=0.4-0.5$ (ref.9 ,10).

The electrical resistivities of $\text{Nd}_{2-x}\text{Ce}_x\text{CuO}_{4-y}$ ($x=0.13, 0.15, 0.16, 0.17, 0.18$), $\text{Pr}_{1.85}\text{Ce}_{0.15}\text{CuO}_{4-y}$ and $\text{Nd}_{1.3}\text{Ce}_{0.2}\text{Sr}_{0.5}\text{O}_{4-z}$ were measured at pressures up to 2.5 GPa using the four-lead method. Gold wires of 20 micron in diameter acted as electrodes; these were attached to the specimen with rectangular shape (about 5mmx1mmx1mm) using indium solder. The resistance at the contact was less than few ohm. The pressure was generated by means of a Cu-Be clamp type piston-cylinder apparatus, using a Teflon cell with fluid pressure medium, Fluorinert #FC70. Pressure was applied at room temperature and the apparatus was immersed into liquid He. The pressure was determined at temperatures near T_C by interpolating between the value given as load per area at room temperature and the value obtained by using a lead manometer. The temperature was measured by using a calibrated platinum resistance thermometer in the range from 20K to 300K and a germanium one below 100 K.

Figure 1 shows the temperature dependence of resistivities obtained in $\text{Nd}_{1.85}\text{Ce}_{0.15}\text{CuO}_{4-y}$ near T_C at various pressures. The resistivity shows a semiconducting behavior, which seems not to be intrinsic but due to inhomogeneities in the samples. The normal state resistivity decreases with increasing pressure with a rate of $R^{-1}dR/dp = -0.089 \text{ GPa}^{-1}$, while the superconducting transition temperature T_C determined at the midpoint of the transition is found to shift very little for pressures up to at least 2.5 GPa. This is remarkable, in view of the results obtained

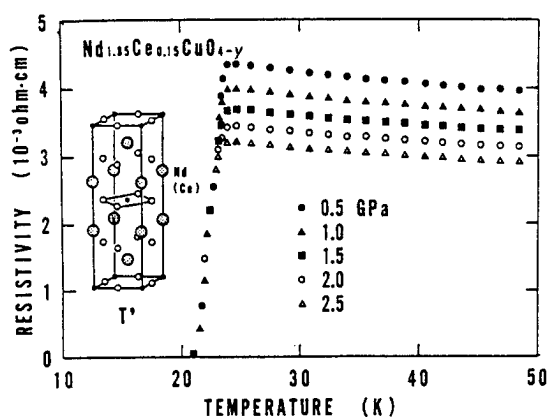


Fig.1 The temperature dependence of the resistivity of $\text{Nd}_{1.85}\text{Ce}_{0.15}\text{CuO}_{4-y}$ under high pressure. Inset, the T' structure.

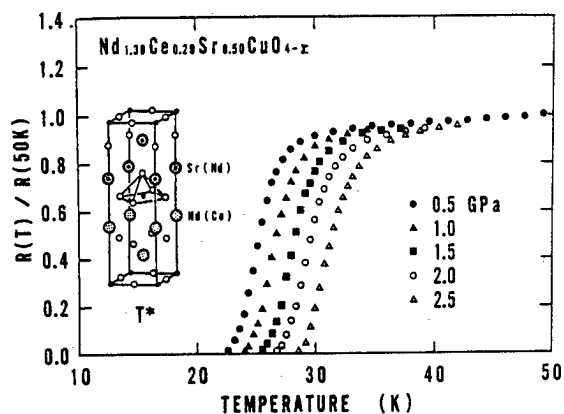


Fig.2 The temperature dependence of the resistance of $\text{Nd}_{1.3}\text{Ce}_{0.2}\text{Sr}_{0.5}\text{CuO}_{4-z}$ normalized to that at 50 K under pressure. Inset, the T^* structure.

so far for many other copper oxide superconductors, as mentioned above. Figure 1 shows that not only the the midpoint but also both the onset and zero resistivity points of the transition do not change by more than ± 0.05 K, which is much smaller range than was obtained by Markert et al.[11].

Similar results were obtained in other compositions $x=0.16$ and 0.17 in $\text{Nd}_{2-x}\text{Ce}_x\text{CuO}_{4-y}$, and $\text{Pr}_{1.85}\text{Ce}_{0.15}\text{CuO}_{4-y}$. The specimens of $x=0.13$ and 0.18 in $\text{Nd}_{2-x}\text{Ce}_x\text{CuO}_{4-y}$ which are non-superconducting at ambient pressure were not converted into superconducting state by high pressure in the present experimental pressure ($p < 2.5$ GPa) and temperature ($4.2 < T < 300$ K) range.

In Fig.2, the relative resistance normalized at 50 K is shown as a function of temperature for $\text{Nd}_{1.3}\text{Ce}_{0.2}\text{Sr}_{0.5}\text{CuO}_{4-z}$ at various pressures in the temperature range between 10 K and 50 K. At ambient pressure the resistivity is about 3.7×10^{-3} ohmcm at room temperature; with increasing pressure, it decreases at a rate of $R^{-1}dR/dp = -0.054 \text{ GPa}^{-1}$. The T_C is seen to depend strongly on pressure, in contrast to the behaviour observed for $\text{Nd}_{1.85}\text{Ce}_{0.15}\text{CuO}_{4-y}$. Both of the transition-onset and zero resistivity temperatures shift with pressure at the same rate as the 'midpoint' T_C .

The T_C s of these compounds are plotted as a function of pressure in Fig.3. A clear difference is demonstrated between the pressure effects on T_C of these two cuprate superconductors. The pressure coefficients, dT_C/dp , for $\text{Nd}_{1.85}\text{Ce}_{0.15}\text{CuO}_{4-y}$ and $\text{Nd}_{1.3}\text{Ce}_{0.2}\text{Sr}_{0.5}\text{CuO}_{4-z}$ are 0 ± 0.05 and $3.0 \pm 0.1 \text{ K GPa}^{-1}$, respectively. The pronounced increase of T_C with increasing pressure for $\text{Nd}_{1.3}\text{Ce}_{0.2}\text{Sr}_{0.5}\text{CuO}_{4-z}$ is typical of hole-doped superconductors. The anomalous behaviour of $\text{Nd}_{2-x}\text{Ce}_x\text{CuO}_{4-y}$ relative to the other compounds is illustrated more clearly in Fig.4, where we plot $d \ln T_C / dp$ against T_C . The value of $d \ln T_C / dp$ for $\text{Nd}_{1.3}\text{Ce}_{0.2}\text{Sr}_{0.5}\text{CuO}_{4-z}$ (Nd-Ce-Sr-Cu-O) is located near that for oxygen-deficient $\text{YBa}_2\text{Cu}_3\text{O}_{6.3}$, both of which have almost the same T_C . The value for $\text{Nd}_{1.85}\text{Ce}_{0.15}\text{CuO}_{4-y}$ (Nd-Ce-Cu-O , $T_C=22$ K), however, is located

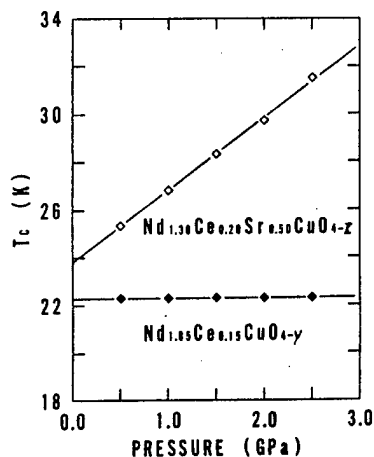


Fig.3 The pressure dependence of the superconducting transition temperatures (T_C) of $\text{Nd}_{1.85}\text{Ce}_{0.15}\text{CuO}_{4-y}$ and $\text{Nd}_{1.3}\text{Ce}_{0.2}\text{Sr}_{0.5}\text{CuO}_{4-z}$.

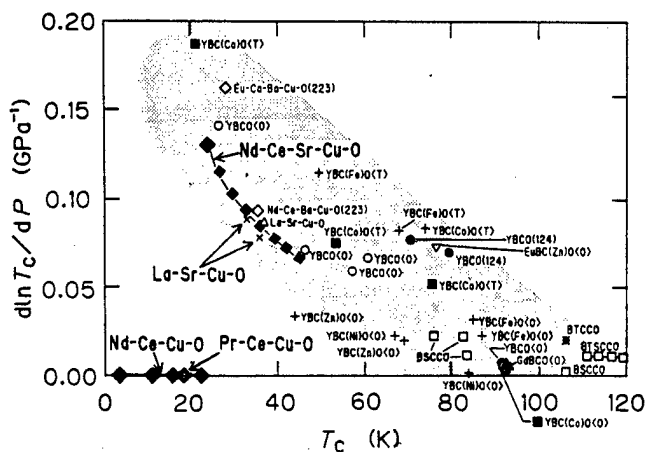


Fig.4 The pressure coefficient of the logarithm of T_C as a function of T_C . (C.Murayama et al., manuscript in preparation). Shaded region denotes the approximate field for all compounds except Nd-Ce-Cu-O and Pr-Ce-Cu-O .

far below that for $\text{Nd}_{1.3}\text{Ce}_{0.2}\text{Sr}_{0.5}\text{CuO}_{4-z}$, despite the fact that the two compounds have almost the same T_c .

It has been suggested (ref.2 and C.M. et al., manuscript in preparation) that there might exist a general trend of increasing $\text{dln}T_c/\text{dP}$ values with decreasing T_c , on the basis of the properties of hole-doped superconductors. Recently Neumeier et al.[12] showed that pressure coefficients of the T_c s of $(\text{Y}_{1-x}\text{Pr}_x)\text{Ba}_2\text{Cu}_3\text{O}_{7-y}$ compounds change sign from positive to negative with increasing Pr concentration. This result was ascribed to the effect of hybridization between the localized Pr 4f state and valence band states which was very sensitive to applied pressure. The decrease in T_c could be due to the weakening of superconducting electron pairs through the strong Coulomb repulsion between electrons in the Pr 4f state. In the case of the Nd-Ce-Cu-O and Nd-Ce-Sr-Cu-O compounds, on the other hand, Ce was confirmed to be tetravalent by photoemission spectroscopy irrespective of their carriers (ref.10 and A.Fujimori et al., preprint). This implies that the Ce 4f state is not as important as the Pr state in controlling the effect of pressure, although further studies will be required to clarify this point. Rather, it seems plausible that the valence electrons donated by Ce affect the electronic structures of valence or conduction bands near the Fermi level as suggested by A.Fujimori et al.(preprint).

From the structural view point, it is interesting to note that $\text{Nd}_{2-x}\text{Ce}_x\text{CuO}_{4-y}$ has only Cu-O squares whereas in $\text{Nd}_{1.3}\text{Ce}_{0.2}\text{Sr}_{0.5}\text{CuO}_{4-y}$ there exist pyramidal Cu-O squares with an apical oxygen. High pressure X-ray studies[13] reveal that the linear compressibilities do not differ for the different crystallographic axes in $\text{YBa}_2\text{Cu}_3\text{O}_{7-y}$ and $(\text{La}_{0.9}\text{Sr}_{0.1})_2\text{CuO}_{4-y}$. We suggest, therefore, that a change in the apical Cu-O distance in the pyramids may play a major part in determining the change of T_c under pressure. Indeed, all of the cuprate superconductors which follow the general trend with respect to the pressure effect on T_c have Cu-O pyramids without exception. In a recent neutron experiments[15] of $\text{YBa}_2\text{Cu}_4\text{O}_8$ which has Cu-O pyramid structure, pressure of 1GPa shortened a bond length between the apical O and in-plane Cu by about 2.5%, whereas the positions of other atoms and the unit cell changed little. This oxide has a large pressure effect[16,17] and is located in the shaded region in Fig.4 (YBCO(124)). We know, moreover, many experimental results which show the broadening of the superconducting transition under high pressure, especially in the cases using an opposed-anvil device. The pressure induced broadening is partly due to a pressure distribution, but it may also be caused partly by a uniaxial stress affecting the Cu-O distance between the apical oxygen and the copper atom in the pyramids. In these respects, it is desirable to investigate the effect on T_c of a uniaxial stress.

Recently, calculations of Madelung energy (Y.Ohta et al., preprint) showed that the optimum T_c s of all the known hole-doped superconductors are scaled by the Madelung potential of apical oxygens relative to that of CuO_2 planes. The trend of the pressure effect on T_c given in the shaded region in Fig.4 is qualitatively explained by this model. On the other hand, it was demonstrated theoretically (H.Matsukawa & H.Fukuyama, preprint) that apical oxygens have an important role in controlling the antiferromagnetic coupling between Cu and O-hole spins and the modification of the O-hole Bloch band. The reduction in the bond length between the apical oxygen and in-plane copper, which will be caused by pressure, enhances T_c in this model. These two theories are qualitatively consistent with our experimental results and will be helpful to clarify the mechanism of high T_c superconductivity.

In conclusion, we have shown that the newly discovered electron-doped superconductor $\text{Nd}_{2-x}\text{Ce}_x\text{CuO}_{4-y}$ and $\text{Pr}_{1.85}\text{Ce}_{0.15}\text{CuO}_{4-y}$ exhibits no pressure effect on the T_c , which is in great contrast to the pressure effect for the hole-doped superconductor $\text{Nd}_{1.3}\text{Ce}_{0.2}\text{Sr}_{0.5}\text{CuO}_{4-z}$. These results suggest that a change in the distance between the apical oxygen and the copper atom in the Cu-O pyramids dominates the effect of pressure on the superconducting transition temperatures of the cuprate compounds.

The authors thank H.Matsubara and H.Watabe for the help in sample preparation. This work was supported partially by Grant-in-Aid for Scientific Research and that for Scientific Research on Priority Areas, Mechanism of Superconductivity, from the Ministry of Education, Science and Culture, Japan.

References

- [1] Tokura, Y., Takagi, H. & Uchida, S. *Nature* **337**, 345-347(1989).
- [2] Griessen, R. *Phys. Rev.* **B36**, 5284-5290(1987).
- [3] Torrance, J.B., et al. *Phys.Rev.Lett.* **61**, 1127-1130(1988).
- [4] Tokura, Y., et al. *Phys.Rev.* **B38**, 7156-7159(1988).
- [5] Tokura, Y., et al., in "Mechanisms of High-Temperature Superconductivity" ed.by Kamimura, H. & Oshiyama (Springer, Berlin, in the press).
- [6] Parker, I.D. & Friend, R.H. *J. Phys.* **C21**, L345-L352(1988).
- [7] Tanahashi, N., et al. *Jpn. J.Appl.Phys.* **28**, L762(1989).
- [8] Takagi, H., Uchida, S. & Tokura, Y. *Phys.Rev.Lett.* **62**, 1197-1200(1989).
- [9] Akimitsu, J., et al. *Jpn. J. Appl.Phys.* **27**, L1859-L1860(1988).
- [10] Tokura, Y. et al. *Phys. Rev.B*(in the press)
- [11] Markert, J.T., et al. *Physica C* (in the press)
- [12] Neumeier, J.J., Maple, M.B. & Torikachvili, M.S. *Physica C* **156** 574-578(1988).
- [13] Takahashi, H., et al., *Jpn. J. Appl. Phys. Suppl.* **26-3**, 1109-1110(1987).
- [14] Murayama, C. et al. *Nature*, **339**, 293(1989).
- [15] Kaldis, E. et al. *Physica C* **159**, 668(1989).
- [16] Bucher, B. et al. *Physica C* **157**, 478(1989).
- [17] Yamada, Y. et al. *Jpn.J.Appl.Phys.* (in the press).

Characteristics of Electronic Properties of High- T_c Oxides

Masatoshi Sato, Masafumi Sera, Shin-ichi Shamoto, Masashige Onoda,
Shin-ichi Yamagata and Hideshi Fujishita[†]

Institute for Molecular Science, Myodaiji, Okazaki 444

[†]College of Liberal Arts, Kanazawa University, Kanazawa 920

Recent results of various kinds of experimental studies carried out to clarify the characteristics of the electronic nature of high- T_c oxides are presented.

1. Introduction

Various experimental studies of high- T_c oxides have revealed that they have quite unusual physical properties in their normal states, which stem from their very strong electron correlations, their low carrier densities and the low dimensional nature of the systems. Then, a fundamental question has arisen in the course of the works if the carriers in the systems which exhibit superconductivity can be described by the usual Fermi liquid picture or not. To answer it, has been one of the important issues for the understanding of the superconductivity with the surprisingly high T_c . On the other hand, the rough features of the high- T_c superconductivity have been found not to be inconsistent with the consequence of the BCS's mean field type theory with s-wave symmetry, where most behaviors in the superconducting state do not reflect the direct information on the microscopic origin of the Cooper pair formation. Then, it seems to be another important issue to clarify, through careful and detailed studies, if the superconducting behaviors of the high- T_c oxides have certain characteristic difference from those of ordinary superconductors. If any difference exists, it may become a useful clue to elucidate the mechanism of the superconductivity. Keeping these things in mind, we have continuously carried out the extensive studies and added further information to the results described in the previous report [1].

2. On the y -Dependence of the Carrier Nature in $\text{La}_{2-y}\text{Sr}_y\text{CuO}_4$

The phase diagram of $\text{La}_{2-y}\text{Sr}_y\text{CuO}_4$ has been studied by many authors [2,3]. The superconductivity appears in the y region of $0.05 \leq y \leq 0.30$. As discussed in the previous report [1], the Hall coefficient [4,5], magnetic susceptibility [4-6], Seebeck coefficient [5] and EPR relaxation rate of the doped Mn [7] exhibit anomalous y -dependence at the superconductor-normal metal phase boundary of $y=y_c \approx 0.30$, suggesting that there exists certain distinction of the carrier natures between the two phases. Here, we present new results which add further information on the electronic nature of this system.

At first, we would like to make a brief comment on the nature of holes in the insulating region ($y < 0.04$). Fig. 1(A) shows the spin canted structure of the antiferromagnetic $\text{La}_{2-y}\text{M}_y\text{CuO}_4$ ($\text{M}=\text{Sr}$ or Ba). Under the magnetic field H applied perpendicular to the CuO_2 plane and larger than certain critical value $H_c(T)$, a sudden change from the structure (A) to (B) occurs, showing the metamagnetic behavior in the

M-H curve [8]. These were first found by the authors' group and confirmed by neutron scattering experiment in collaboration with BNL and MIT groups [9]. The MIT group found the significant increase of the conductivity ($\Delta\sigma/\sigma \sim 1$) accompanied with the change of the spin structure [10]. Their recent work under the very strong magnetic field within the CuO_2 plane revealed that $\Delta\sigma$ was proportional to the fraction of the spin structure (B) [11].

Only the model which seems to be able to explain why the conductivity is largely influenced by the spin structure, is the one proposed by Jarrell et al. [12]. The essential point of their model is that the spin directions of the holes in CuO_2 planes are determined by the direction of the ferromagnetic component of the plane induced by the spin canting. It is very interesting to note here that if holes can be considered to form local singlets with neighboring Cu spins, the spin directions of the holes cannot be specified by the direction of the ferromagnetic component. Then, the result seems to support the spatially extended picture of holes.

To see the y -dependence of other physical quantities around y_c , we have studied the low temperature specific heat of $\text{La}_{2-y}\text{Sr}_y\text{CuO}_4$ up to $y \approx 0.50$, where samples sintered at 1080°C under 300 atm O_2 pressure are used.

Fig. 2(a) shows the C/T vs. T^2 curves for several samples and 2(b) shows the coefficient r of the observed T -linear term as a function of y , where the solid line for $y < 0.3$ is drawn by using the data reported by Wada et al. [13]. The figure suggests rather smooth variation of the r -value through y_c . For the samples prepared simultaneously with the present ones, x-ray absorption experiment was also carried out by Takahashi et al. [14], which showed the smooth growing, through y_c , of the number of the electronic states near ϵ_F . The effective mass of these electronic states should decrease rather rapidly with y in the region $y > y_c$ to explain the observed decrease of r and the observed increase of the number of the electronic states.

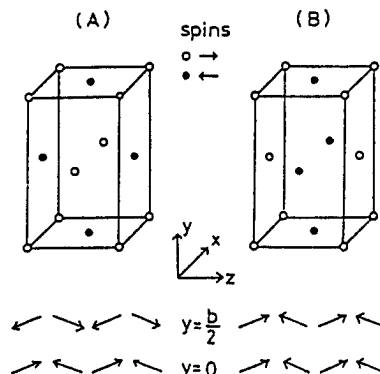


Fig. 1. (A) Spin structure of the antiferromagnetic phase of $\text{La}_{2-y}\text{Sr}_y\text{CuO}_4$. Under the magnetic field perpendicular to the CuO_2 plane and larger than the critical field H_c , the structure (B) becomes stable. In each structure, the directions of the Cu spins are shown in the yz plane with the canting angle being exaggerated.

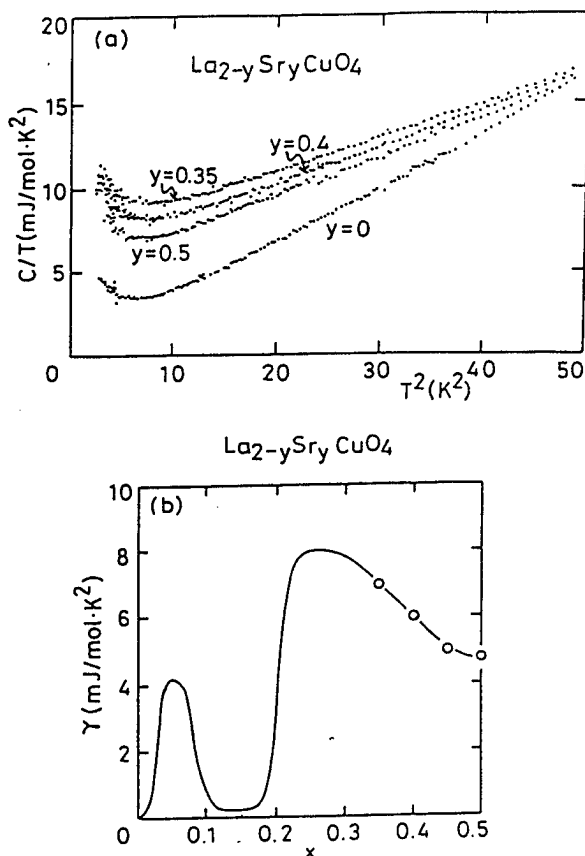


Fig. 2. (a) Experimental results of C/T of $\text{La}_{2-y}\text{Sr}_y\text{CuO}_4$ are shown as a function of T^2 for various values of y . (b) The coefficients of the T -linear term determined at low temperatures are shown. Details are in the text.

The y -dependence of the doping effect has also been studied [15] by using the system of $\text{La}_{2-y}\text{Sr}_y\text{Cu}_{1-x}\text{Ni}_x\text{O}_4$ for various values of x and y , where the carrier numbers and the degree of randomness can be independently changed by changing y and x , respectively. Here, for the y values of 0.10, 0.15, 0.22, 0.32 and 0.45, the doping effect of Ni was studied by changing the x values.

Figs. 3(a)-3(c) show the example results of the resistivity measurements, where for larger values of x , the resistivity exhibits upturn or σ decreases linearly in $\log T$ with decreasing T , which indicates the electron localization occurs at low temperatures. If we define the critical concentration x_c as the x value where the resistivity upturn becomes appreciable, the value of T_c for $y < y_c$, goes to zero at $x \geq x_c$ as shown in Fig. 4. Then, the superconductivity can be considered to be suppressed by the electron localization. At the concentration x , where the superconductivity disappears, the Hall coefficient was found to remain positive without showing any anomalous x -dependence. The magnetic susceptibility χ seems to undergo the gradual change in its temperature derivative $d\chi/dT$; that is, the existence of the temperature region where the positive value of $d\chi/dT$ is found, seems to characterize the superconducting phase.

The value of x_c are shown in Fig. 5 as a function of y or the carrier concentration. It shows smooth increase through $y_c \approx 0.30$, suggesting that any significant change of the electronic nature cannot, at least, be detected by this experiment. The curve is simply understood by assuming the fact the x_c values are determined as the concentration where $\epsilon_F \tau \approx 1$, where τ is the electron life time and ϵ_F is the Fermi energy or the kinetic energy of the carriers. This also supports that the resistivity upturn is due to the electron localization.

As we have already mentioned, the y -dependence of the magnetic susceptibility, Hall coefficient and Seebeck coefficient of $\text{La}_{2-y}\text{Sr}_y\text{CuO}_4$ have quite significant

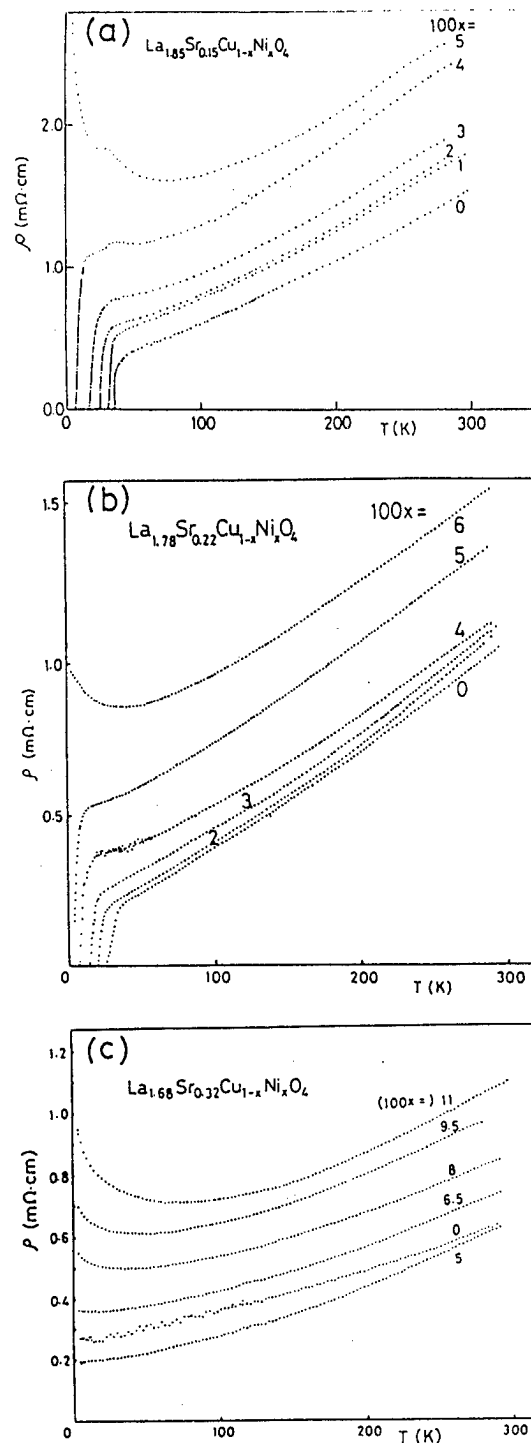
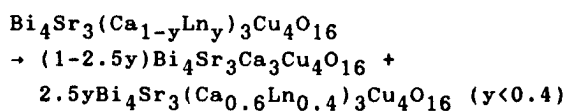


Fig. 3. Resistivity data of $\text{La}_{2-y}\text{Sr}_y\text{Cu}_{1-x}\text{Ni}_x\text{O}_4$ systems with $y=0.15$ (a), 0.22(b) and 0.32(c).

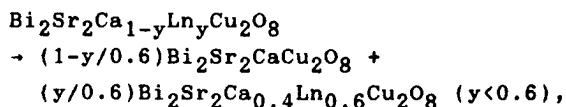
anomaly at $y=y_c$. However, the r value and the critical concentration x_c of the metal (superconductor)-insulator transition due to the randomness introduced by the doping do not show the appreciable anomaly at $y=y_c$.

It is interesting to note that the observed y -dependence of the $|dT_c/dx|$ seems to exclude the proposal made by several researchers that the superconducting phase of $\text{La}_{2-y}\text{Sr}_y\text{CuO}_4$ is confined to the very narrow region of y , because $|dT_c/dx|$ should be, if the proposal is true, constant for all values of y . This carrier concentration dependence of $|dT_c/dx|$ gave us the additional means of checking the phase separation, the existence of which had been presumed [16] in $\text{Bi-Sr-(Ca,Ln)-Cu-O}$ system (Ln=lanthanide atoms). As is

discussed in the paper by Yamagata et al. [17], there are many experimental data on the compounds with the nominal formula of $\text{Bi}_4\text{Sr}_3\text{Ca}_{3-y}\text{Ln}_y\text{Cu}_4\text{O}_{16}$ or $\text{Bi}_2\text{Sr}_2\text{Ca}_{1-y}\text{Ln}_y\text{Cu}_2\text{O}_8$ which indicate the possible existence of the phase separation into the Ln-poor and Ln-rich phases as shown below.



or



where the first ones in the right hand sides of the equations are superconducting and the seconds are insulating. For example, the width of the Gd EPR signal in the samples nominally described as $\text{Bi}_4\text{Sr}_3\text{Ca}_{3-y}\text{Gd}_y\text{Cu}_4\text{O}_{16}$ is independent of y and very broad, indicating that the Gd-Gd spin interaction is y -independent or the local Gd concentration is constant which can be understood by the segregation model described above. Fig. 6 shows the Ni concentration dependence of T_c of $\text{Bi}_2\text{Sr}_2\text{Ca}_{1-y}\text{Y}_y\text{Cu}_{2-x}\text{Ni}_x\text{O}_8$ for several values of x . Although due to the very complicated formula of the initial mixtures, the data are

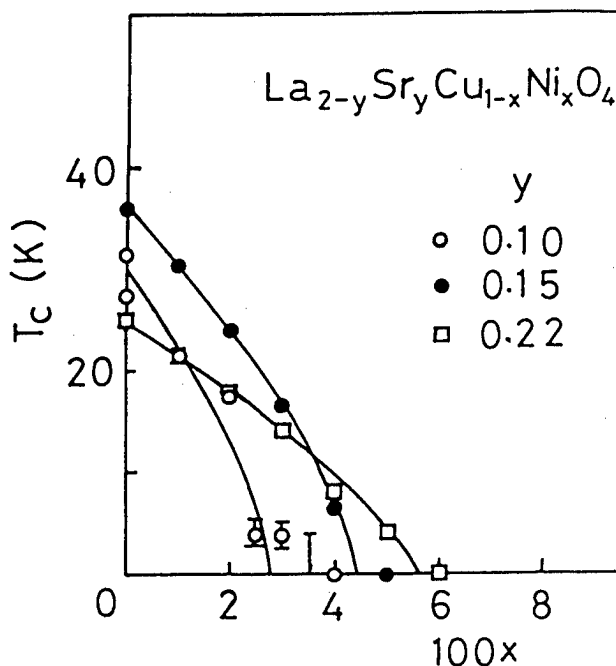


Fig. 4. Superconducting transition temperatures of $\text{La}_{2-y}\text{Sr}_y\text{Cu}_{1-x}\text{Ni}_x\text{O}_4$ are plotted as a function of the Ni concentration x for various fixed values of y .

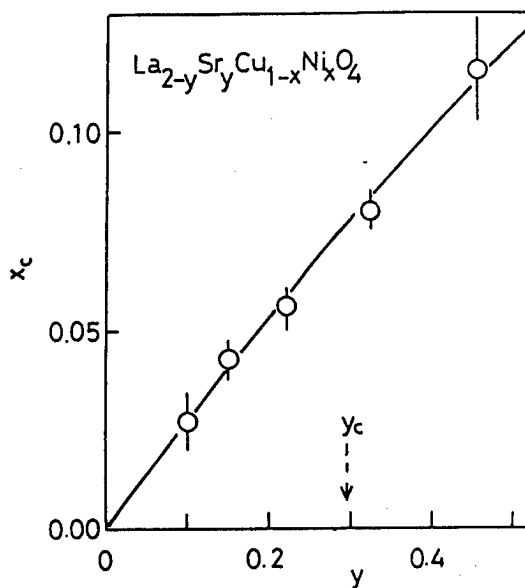


Fig. 5. The critical Ni concentrations x_c of the metal (superconductor)-insulator transition induced by the randomness in $\text{La}_{2-y}\text{Sr}_y\text{Cu}_{1-x}\text{Ni}_x\text{O}_4$ are shown as a function of y , where y_c indicates the superconducting-normal metallic phase boundary.

rather largely scattered, the essential feature that the values of $|dT_C/dx|$ in the region of x smaller than the solubility limit are constant for all y values, can be seen, which supports the existence of the phase separation.

A possible objection to this conclusion might be based on the experimental fact that the y -dependence of lattice parameters does not have any indication of the existence of two phases. However, it can be understood by considering intergrowth type structure or epitaxially grown phases. Here, we would like to point out that the phase separation problem should be carefully avoided in the study of the doping effect.

3. Electronic Specific Heat of $\text{Ln}_{2-y}\text{Ce}_y\text{CuO}_4$

Specific heats of the electron doped systems, $\text{Nd}_{1.85}\text{Ce}_{0.15}\text{CuO}_4$ and $\text{Pr}_{2-y}\text{Ce}_y\text{CuO}_4$ ($0 \leq y \leq 0.25$) have been measured to compare them with those of the hole doped systems. In the case of Nd-system, there exists the large contribution to the specific heat from the spin degree of freedom at low temperatures. Therefore, the attention was focused around T_C . The result is shown in Fig. 7, where the jump of the specific heat at T_C , ΔC , is found to be very small even for the sample with about 40% Meissner volume fraction. If we assume the relation $\Delta C = 1.43rT_C$, the value of r is estimated to be $(1.2 \pm 1.4) \text{ mJ/mol} \cdot \text{K}^2$, which is much smaller than the cases of $\text{La}_{2-y}\text{Sr}_y\text{CuO}_4$ and $\text{YBa}_2\text{Cu}_3\text{O}_{6+x}$.

Because Pr-system does not have the spin contribution to the specific heat at low temperatures, the electronic contribution of the system could be measured. Although the coefficients r of the T -linear term were not zero even for the samples with $y=0$ (insulator) and $y=0.15$ (superconductor) possibly due to certain extrinsic effect and due to the incomplete volume fraction of the superconductivity, respectively, the intrinsic value of r in the normal state of $\text{Pr}_{1.85}\text{Ce}_{0.15}\text{CuO}_4$ could be guessed from the detailed analyses [18] to be about $2 \text{ mJ/mol} \cdot \text{K}^2$, which is consistent with the above result obtained for the Nd system.

The present observations indicate that the electronic density of states or the effective mass of the carriers in $\text{Ln}_{2-y}\text{Ce}_y\text{CuO}_4$ is rather small as compared with those of the hole carrier systems. Therefore, the carriers in $\text{Ln}_{2-y}\text{Ce}_y\text{CuO}_4$ seem to have the character of the extended type, which does not seem to support the picture that the doped carriers go into the upper Hubbard band mainly with the $\text{Cu}3d_{x^2-y^2}$ character.

4. Neutron Scattering Study of $\text{YBa}_2\text{Cu}_3\text{O}_{6+x}$ Crystals

In $\text{YBa}_2\text{Cu}_3\text{O}_6$ and La_2CuO_4 , for example, each Cu atom in CuO_2 plane is in d^9 state and then expected to have one electron in its highest atomic level, usually resulting

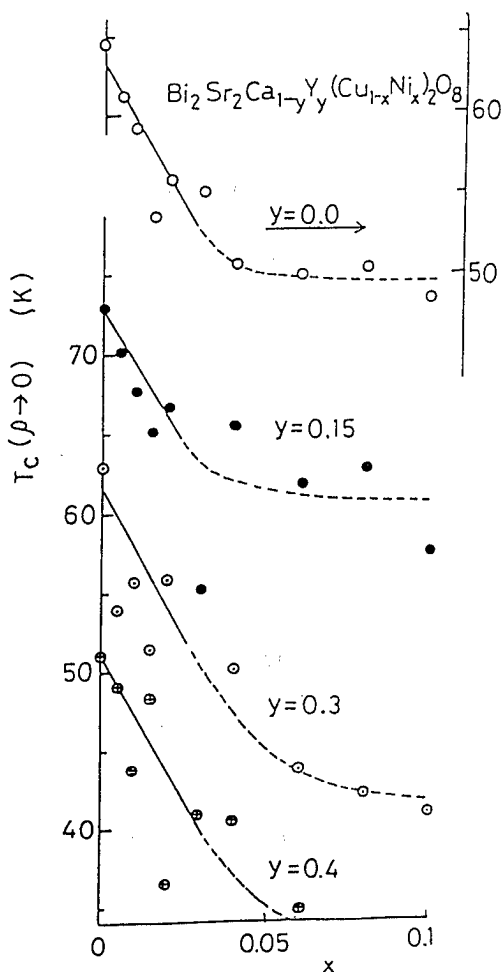


Fig. 6. Superconducting transition temperatures of the samples with the nominal formula of $\text{Bi}_2\text{Sr}_2\text{Ca}_{1-y}\text{Y}_y\text{Cu}_{1-x}\text{Ni}_x\text{O}_8$ are shown as a function of x for various fixed values of y .

in the metallic behavior. However, due to the strong electron correlation, it is insulating and has the localized spin of $1/2$. The very large antiferromagnetic coupling J between the nearest neighbor spins is one of the most significant features of these Cu oxides. Very small amount of doping of holes can suppress the antiferromagnetic ordering, realizing the high- T_c superconductivity. The main purpose of the neutron experiment is to see the magnetic fluctuations in the samples which exhibit the high- T_c superconductivity, and finally to clarify what kind of roles the fluctuation has, in the Cooper pair formation.

In case of $\text{La}_{2-y}\text{Sr}_y\text{CuO}_4$, the observation of the magnetic fluctuation has been reported in the superconducting phase [19] and there has been discussed the possible existence of the pseudo gap structure in the magnetic excitation spectra, which may have certain connection with the unconventional metallic state of strongly correlated carriers [20].

The present authors' group have been making much effort to grow large single crystals of $\text{YBa}_2\text{Cu}_3\text{O}_{6+x}$ which can be used in neutron inelastic scattering. In the previous report [1], the existence of the large spin excitations with two dimensional character similar to those in $\text{La}_{2-y}\text{Sr}_y\text{CuO}_4$ was reported in the antiferromagnetic phase. For crystals with $T_c \approx 90\text{K}$, however, we did not succeed in observing the spin fluctuation. Then, a number of crystals near the antiferromagnetic-superconducting phase boundary were prepared and finally the magnetic excitations in the superconducting phase could be observed [21,22]. Here, we discuss only on the results for the crystals with $x=0.45$ and 0.50 , for which, the value of T_c were determined as 45K and 50K , respectively, by the ac susceptibility measurements. It should also be noted that for the former crystal, although no magnetic Bragg reflection was detected at 10K , we cannot exclude the existence of the nonsuperconducting parts within it, while the whole volume of the latter crystal can be considered to be superconducting, because it is experimentally confirmed that only the orthorhombic phase exists within it. The main results are as follows. (i) For the crystal with $x=0.45$, the intensity of the magnetic excitation at 3meV increases significantly with decreasing T as the ordinary nearly-antiferromagnetic materials, which is in clear contrast to the case of $\text{La}_{2-y}\text{Sr}_y\text{CuO}_4$. (ii) As shown in Figs. 8 and 9, the intensity of the magnetic fluctuation in $\text{YBa}_2\text{Cu}_3\text{O}_{6.50}$ ($x=0.50$) increases with the excitation energy, while the result for $\text{YBa}_2\text{Cu}_3\text{O}_{6.45}$ exhibits quite different behavior. This increase of the intensity with ΔE , may be understood in two ways. First, the pseudo gap as observed in $\text{La}_{2-y}\text{Sr}_y\text{CuO}_4$ can also be observed in $\text{YBa}_2\text{Cu}_3\text{O}_{6.50}$ or second, the overdamping of the fluctuation modes with the wavelength longer than the magnetic correlation length

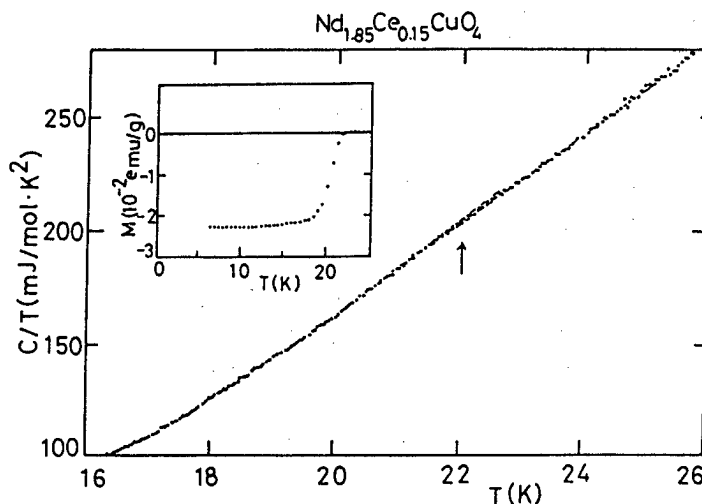


Fig. 7. Specific heat divided by T of $\text{Nd}_{1.85}\text{Ce}_{0.15}\text{CuO}_4$ are shown as a function of T . At the temperature indicated by the arrow, very small anomaly due to the superconducting transition can be seen. The insert shows the temperature dependence of the Meissner diamagnetism taken with field cooled condition. At low temperatures, the volume fraction is about 40%.

YBa₂Cu₃O_{6.5} $T_c = 50$ K

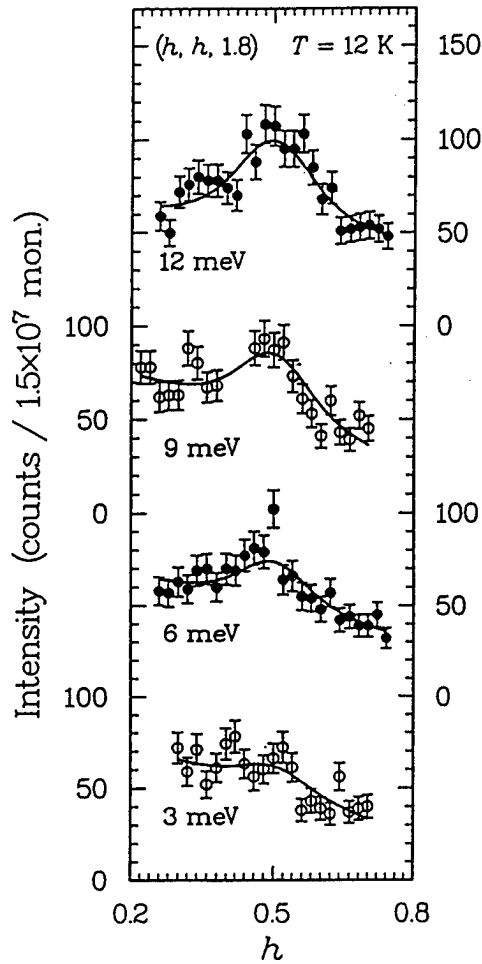


Fig. 8. Results of the constant-E scan taken for YBa₂Cu₃O_{6.50} with various transfer energy ΔE .

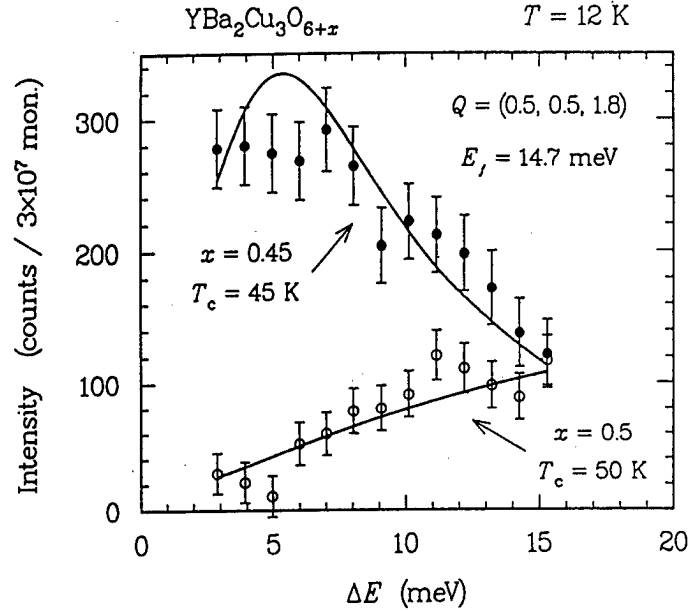


Fig. 9. Results of the energy scan at fixed Q-point (0.5, 0.5, 1.8) of YBa₂Cu₃O_{6.45} and YBa₂Cu₃O_{6.50}. Solid lines are the results of the theoretical fittings with the damped excitation mode model.

reduces the intensity of the low energy excitations. By the latter model, the theoretical fit was carried out, where rather satisfactory results were obtained as shown by the solid curves in Fig. 9.

The overdamped excitation model is often introduced to treat the fluctuations in usual materials above their phase transition temperatures and does not seem to have a connection with the idea discussed in ref. 20, for example, for the arguments on the unconventional metallic state of the strongly correlated electrons. Then, to distinguish which of the two models stated in (ii) truly describes the real phenomena may be one of the important keys in the study on the nature of the carrier system. It remains as a future problem. We have to see the detailed temperature dependence of the spectra to achieve this goal.

Now, we know that the intensity of the excitation at lower energy becomes weaker for samples with higher T_c . It suggests that if we choose the larger neutron energy transfer at low temperatures, we may be able to see the magnetic fluctuations even for crystals with $T_c \approx 90$ K.

In this section, we have described the present status of our neutron scattering experiments.

5. On the Anomalous Magnetic Behaviors in the Superconducting State of the High- T_C Oxides

We have, so far, presented our experimental results mainly on the normal state properties to see the characteristics of the high- T_C oxides. Here, preliminary results of the studies on the properties in the superconducting states are given. As stated in the introduction, most of the superconducting properties can roughly be described by the classical BCS theory. The existing exceptions seem to be (i) the absence of the enhancement of $\text{NMR-}T_1^{-1}$ just below T_C and (ii) the anomalous temperature dependence of H_{C1} [23] and the anomalous M-H curve taken for $H < H_{C2}$ [24].

The anomaly in (i) might indicate the d-wave symmetry of the order parameter with no gap near T_C , while at low temperatures, the T-dependence of the magnetic penetration depth λ clearly indicates the existence of the finite energy gap in the electronic excitations. Then, it is quite attractive to imagine that there exist certain change in the symmetry of the order parameter in the superconducting state [25]. The anomalous behaviors stated in (ii) seem to be interesting, because the observed anomalies might be the evidence for the symmetry change. We have been studying these behaviors by using sintered pellets and pulverized samples of $\text{La}_{2-y}\text{Sr}_y\text{CuO}_4$ and $\text{YBa}_2\text{Cu}_3\text{O}_{7-\delta}$ [26].

The values of H_{C1} were basically defined as the fields, where the magnetization M vs. field H line taken with increasing H for samples cooled in zero field begins to deviate from the straight line. To get the unambiguous value of this H_{C1} , the square root of the absolute value of the deviation, $|\Delta M|^{1/2}$ is plotted as a function of H [27] and the smooth extrapolation of the plotted line to the abscissa was used. Fig. 10 shows the results for the pulverized sample of $\text{La}_{1.85}\text{Sr}_{0.15}\text{CuO}_4$. Up to now, our results always show the anomalous temperature dependence.

In ref. 26, we also showed the anomalous behavior of the M-H curves. In the experiments, M was measured with fixed fields H and with increasing temperature after cooling the sample in the applied H and then, the M values were replotted as a function of H at constant temperatures. Further experiments with controlled sample cooling rates, have revealed the fact that the M-H curve depends on the cooling rate of the samples, although the whole behaviors of the magnetization are quite anomalous and cannot easily be understood.

Considering the possibility that these anomalous behaviors are related with certain dynamical phenomena such as the vortex motion, we decided to study if any anomalous behavior can be observed in the static quantities as the thermal conductivity or in the specific heat (we know that many anomalous behaviors have been observed in the dynamical quantities like the microwave absorption [28], internal friction [29] and the NMR T_2^{-1} [30]). However, the experimental accuracy of our

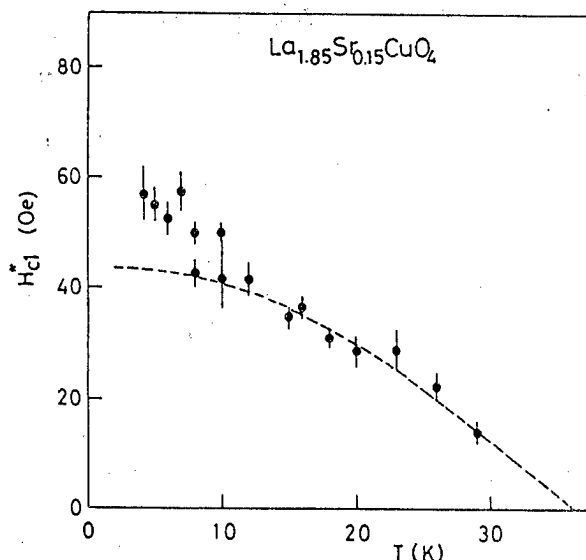


Fig. 10. Values of H_{C1} are shown as a function of H. The dashed line shows the temperature dependence expected by the BCS theory. See text for details.

specific heat measurement was not satisfactory to detect the anomaly even if it exists. Fig. 11 shows the example of the observed temperature dependence of the thermal conductivity of $\text{YBa}_2\text{Cu}_3\text{O}_{7-\delta}$, where we do not see any anomaly except the one at T_c . The magnitude of the anomaly should be smaller, if any, than 1/10 of the one observed at T_c .

6. Summary

Results of our recent works are described from the view point that to clarify the characteristics of the high- T_c oxides is primarily important. We believe that the essential points are now getting much clearer.

The authors are grateful to their collaborators, especially to the neutron scattering group at BNL.

References

1. M. Sato, M. Sera, M. Onoda, S. Shamoto, S. Kondoh, K. Fukuda, Y. Ando and S. Yamagata: Research Report on Mechanism of Superconductivity p114 March 1989
2. For examples, J. B. Torrance, Y. Tokura, A. I. Nazzari, A. Beziinge, T. C. Huang and S. S. P. Parkin: Phys. Rev. Lett. 61 (1988) 1127
3. T. Fujita, Y. Aoki, Y. Maeno, J. Sakurai, H. Fukuba and H. Fujii: Jpn. J. Appl. Phys. 26 (1987) L368
4. H. Takagi, Y. Tokura and S. Uchida: Mechanisms of High Temperature Superconductivity edited by H. Kamimura and A. Oshiyama Springer Verlag, p238, October 1988
5. Y. Ando, M. Sera, S. Yamagata, S. Kondoh, M. Onoda and M. Sato: Solid State Commun. 70 (1989) 303
6. M. Oda, T. Ohguro, N. Yamada and M. Ido: J. Phys. Soc. Jpn. 58 (1989) 750
7. M. Onoda and M. Sato: Solid State Commun. 70 (1989) 309
8. K. Fukuda, M. Sato, S. Shamoto, M. Onoda and S. Hosoya: Solid State Commun. 63 (1987) 811 and K. Fukuda, S. Shamoto, M. Sato and K. Oka: Solid State Commun. 65 (1988) 1323
9. M. A. Kastner, R. J. Birgeneau, T. R. Thurston, P. J. Picone, H. P. Jenssen, D. R. Gabbe, M. Sato, K. Fukuda, S. Shamoto, Y. Endoh, K. Yamada and G. Shirane: Phys. Rev. B38 (1988) 6636
10. T. Thio, T. R. Thurston, N. W. Preyer, P. J. Picone, M. A. Kastner, H. P. Jenssen, D. R. Gabbe, C. Y. Chen, R. J. Birgeneau and A. Aharony: Phys. Rev. B38 (1988) 905
11. T. Thio, C. Y. Chen, B. S. Freer, D. R. Gabbe, H. P. Jenssen, M. A. Kastner, P. J. Picone, N. W. Preyer and R. J. Birgeneau: preprint

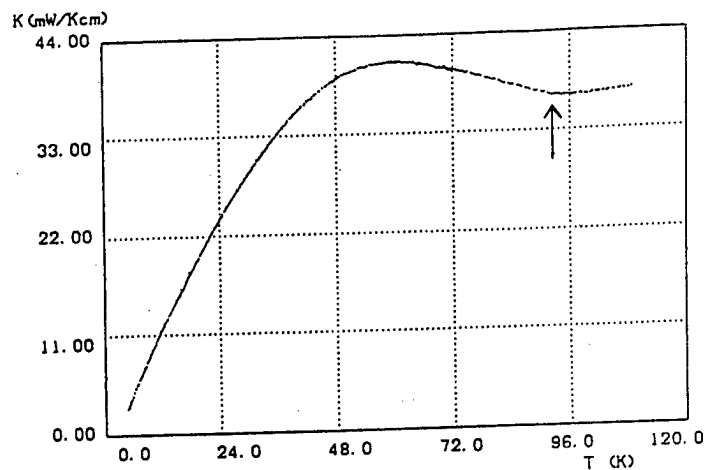


Fig. 11. Temperature dependence of the thermal conductivity of a sintered specimen of $\text{YBa}_2\text{Cu}_3\text{O}_{7-\delta}$. The anomaly at T_c is indicated by the arrow.

12. M. Jarrell, D. L. Cox, C. Jayaprakash and H. P. Krishnamurty: Phys. Rev. B40 (1989) 8899
13. N. Wada, H. Muro-oka, Y. Nakamura and K. Kumagai: Physica C157 (1989) 453
14. T. Takahashi: private communication
15. H. Fujishita and M. Sato: Solid State Commun. 72 (1989) 529
16. K. Fukuda: Thesis
17. S. Yamagata, K. Adachi, M. Onoda, H. Fujishita, M. Sera, Y. Ando and M. Sato: Solid State Commun. submitted
18. M. Sera, S. Shamoto and M. Sato: Solid State Commun. 72 (1989) 749
19. G. Shirane, R. J. Birgeneau, Y. Endoh, P. Gehring, M. A. Kastner, K. Kitazawa, I. Tanaka, T. R. Thurston and K. Yamada: Phys. Rev. Lett. 63 (1989) 330
20. R. B. Laughlin: Mechanism of High Temperature Superconductivity edited by H. Kamimura and A. Oshiyama Springer Verlag p76 October, 1988
21. G. Shirane, J. Als-Nielsen, M. Nielsen, J. M. Tranquada, H. Chou, M. Sato and S. Shamoto: Phys. Rev. B to be published
22. J. M. Tranquada, W. J. L. Buyers, H. Chou, T. E. Mason, M. Sato, S. Shamoto and G. Shirane: Phys. Rev. Lett. submitted
23. J. P. Stöbel, B. Hensel, H. Adrian and G. Saemann-Ischenko: Physica C153-155 (1988) 1537
24. M. Takigawa, P. C. Hammel, R. H. Heffner, Z. Fisk, J. P. Thompson and M. Maley: Proc. Int. Conf. on M²S, Stanford July 1989
25. D. Hirashima and T. Matsuura: J. Phys. Soc. Jpn.
26. M. Sato, S. Shamoto, M. Sera and H. Fujishita: Solid State Commun. 72 (1989) 689
27. M. Naito and K. Kitazawa: preprint
28. R. Karim, H. How, R. Seed, A. Widom, C. Vittoria, C. Balestrino and P. Paroli: Solid State Commun. 71 (1989) 983
29. C. Durán, P. Esquinazi, C. Fainstein and N. Reguerio: Solid State Commun. 65 (1988) 957
30. M. Tei, H. Takai, K. Mizoguchi and K. Kume: Proc. ISNQRS Takayama, August 1989 to be published in Z. Naturforsch. (a)

Specific Heat Study of $\text{Ba}_2\text{YCu}_3\text{O}_y$ ($6 \leq y < 7$) and Ni/Zn Substituted Samples

Y. Nakazawa, J. Takeya and M. Ishikawa

Institute for Solid State Physics, University of Tokyo
Roppongi, Minato-ku, Tokyo 106 Japan

The specific heat of $\text{Ba}_2\text{YCu}_3\text{O}_y$ ($6 \leq y < 7$) and $\text{Ba}_2\text{Y}(\text{Cu}_{1-x}\text{M}_x)_3\text{O}_{\sim 7}$ ($\text{M} = \text{Ni}$ and Zn) has been measured in the temperature range of 0.5 and 120 K to clarify origins and nature of specific heat anomalies in the superconducting state such as finite γ values and upturn in C_p/T as well as the double peak around T_c . The results on the Ni or Zn substituted samples suggest that the finite γ and the upturn are related to disorder on CuO_2 planes and CuO chains, respectively. The double peak was found to be extremely sensitive to the oxygen concentration on CuO chains, the higher temperature peak being dominant at a little less oxygen concentration. For some Ni substituted samples we discovered low temperature magnetic ordering of short range type at 0.8 K in the superconducting state.

Although a considerable number of specific heat measurements has been performed on high T_c oxide superconductors [1], there still remain several unanswered important questions to distinguish theories proposed for the mechanism of high T_c superconductivity. In order to clarify some of these questions we performed specific heat measurements on well annealed samples prepared as previously reported [2]. For this study we modified our adiabatic heat pulse calorimeter for high temperature (30 K \sim 300 K) such that a small (0.5 \sim 1 gram) YBCO sample could be measured within one percent of precision and with about 0.5 percent of random errors. This modification was motivated to discern small anomalies on the specific heat curves of YBCO samples below T_c as previously seen by us [3].

In Fig. 1, we present the specific heat curves for $\text{Ba}_2\text{YCu}_3\text{O}_y$ ($6.80 \leq y \leq 6.92$) between 50 and 120 K, which show a discontinuity at T_c , $\Delta C_p/T_c$ as high as 60 mJ/mol-K². The curve for $y = 6.92$ has a broad peak at 89 K and a shoulder at 92 K. We believe that these features around T_c correspond to the distinct double peak discerned by our previous ac calorimetry [4], being simply broadened here by the present calorimetry of heat pulse type. It is more interesting to note that for the samples of $y = 6.84$ and 6.88 the higher temperature peak becomes dominant, while the lower temperature peak is broadened and shifted to a lower temperature. It seems to be reasonable to assume that this variation of the specific heat peaks results primarily from the change in the ordering of oxygen atoms around the Cu1 sites, i.e. the detailed structure of CuO chains. Very similar behavior has also been observed in our preliminary study on $\text{Ba}_2\text{ErCu}_3\text{O}_y$ ($6.87 \leq y \leq 6.92$). It is further noted here that $\Delta C_p/T_c$ for the higher temperature peak is always only about two thirds of that for the lower temperature peak. At the moment we are not sure about the origins of these two peaks, but we may attribute the lower temperature peak, which appears to be more sensitive to the oxygen content, to the superconductivity related to the CuO chains and the other to the CuO_2 planes, or alternatively attribute both to different ordered states of CuO chains like the proposed ordered homologous structures of $\text{Ba}_2\text{YCu}_3\text{O}_{7-n/(2n+1)}$ [5].

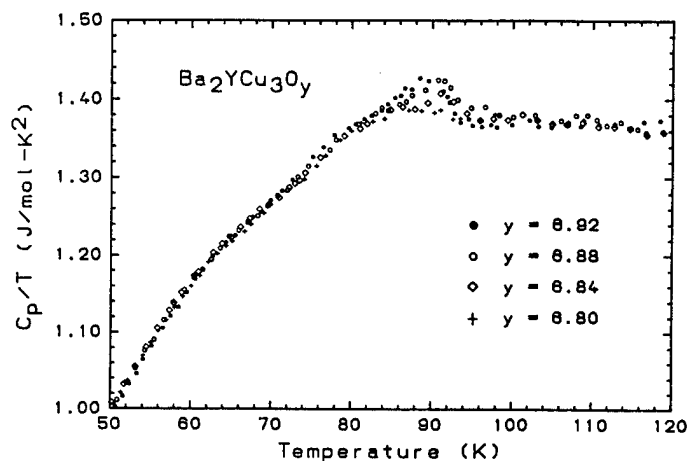


Fig. 1 High temperature specific heat of $\text{Ba}_2\text{YCu}_3\text{O}_y$, showing variation of double peak.

If the latter model is correct, we must consider these YBCO samples as a mixture of some of those homologous structures with different order of CuO chains, even if they are well annealed samples. In this regard it is interesting to note the small but manifest anomaly around 65 K, as can be seen in Fig. 1, which seems to correspond to the anomaly in the ortho-II ($y = 6.5$) phase with an ordered double-cell structure [6]. To settle the question more careful experiments such as magnetic field dependence of these anomalies would be necessary. Along this line, we began to study effects of substitution of magnetic (Ni) or non-magnetic (Zn) atoms onto the CuO_2 planes. Specific heat curves of $\text{Ba}_2\text{Y}(\text{Cu}_{1-x}\text{Zn}_x)_3\text{O}_{\sim 7}$ are shown in Fig. 2 for $x = 0.5, 1.0$ and 2.0 .

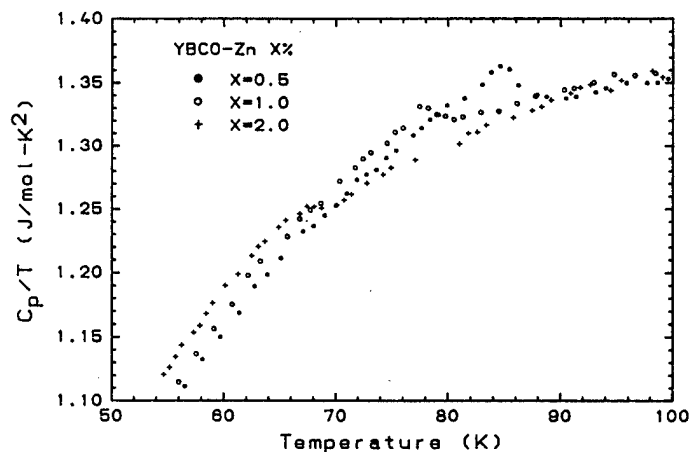


Fig. 2 High temperature specific heat of $\text{Ba}_2\text{Y}(\text{Cu}_{1-x}\text{Zn}_x)_3\text{O}_{\sim 7}$.

It is important to remember here that both nickel and zinc atoms replace Cu_2 atoms on the CuO_2 plane without disturbing CuO chains much. One of the most important differences between the curves for YBCO and YBCO-Zn in Figs. 1 and 2 is that the peak of the former broadens very rapidly with a slight decrease of T_c , while the peak of YBCO-Zn remains discernible even if T_c is decreased by more than 20 K. It would be then reasonable to attribute this to less disturbed CuO chains in the latter system. This is also true for the Ni substituted samples, although the peaks are slightly broader than those for the Zn samples probably because of more inhomogeneous distribution of nickel atoms on the CuO_2 planes. This difference between oxygen depleted YBCO and the substituted samples strongly suggests the important role of CuO chains for the superconductivity in the $\text{Ba}_2\text{YCu}_3\text{O}_y$, although more direct evidence would be awaited.

We now turn ourselves to the low temperature anomalies in these systems. We have already reported the variation of γ^* as a function of oxygen concentration in $\text{Ba}_2\text{YCu}_3\text{O}_y$ [3]. We present in Fig. 3 more recent result, where the γ^* remains approximately constant ($\sim 4 \text{ mJ/mol-K}^2$) except for the region of normal metal around $y = 6.3$. Contrary to this, γ^* of the Zn substituted samples dramatically increases with the zinc substitution, as can be seen in Fig. 4. The actual C_p/T vs T^2 curves are shown in Fig. 5 for $x = 0, 0.5, 3$ and 5.

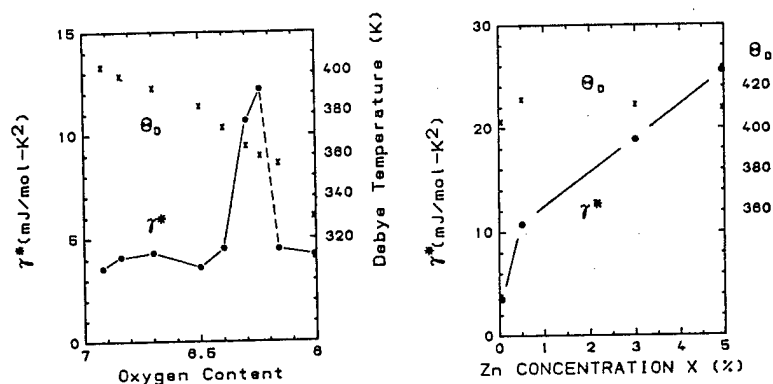


Fig. 3 (left) γ^* and θ_D of $\text{Ba}_2\text{YCu}_3\text{O}_y$.

Fig. 4 (right) γ^* and θ_D of $\text{Ba}_2\text{Y}(\text{Cu}_{1-x}\text{Zn}_x)_3\text{O}_{7.7}$.

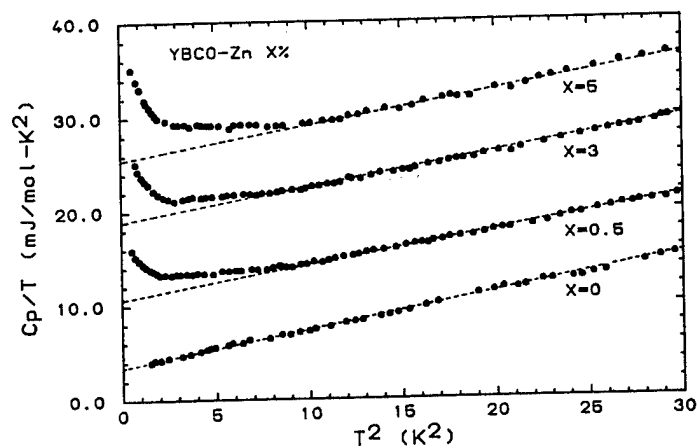


Fig. 5 Low temperature specific heat of $\text{Ba}_2\text{Y}(\text{Cu}_{1-x}\text{Zn}_x)_3\text{O}_{7.7}$.

It is clear from the Figure that the upturn of C_p/T at low temperatures and the γ^* are of different origin, because the γ^* increases without accompanying a noticeable change of the upturn. It is more important to note here that the discontinuity at T_c is not much affected by such a large increase of γ^* (see Fig. 2). These facts point to a tentative conclusion that the finite γ in the superconducting state of these systems is intrinsic and associated somehow with a disorder on CuO_2 planes, as previously conjectured [3]. We are now trying to test this conjecture by investigating effects of disorder, particularly on the magnetic properties of the zinc substituted system. A similar increase of γ^* has been observed also for the nickel substituted system, but in this case it was not so obvious as in the former system because of the presence of the magnetic order around 0.8 K, as can be seen in Fig. 6.

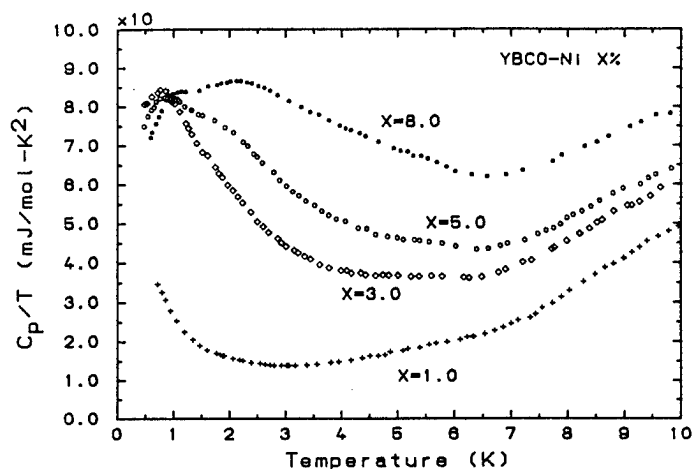


Fig. 6 Low temperature specific heat of $\text{Ba}_2\text{Y}(\text{Cu}_{1-x}\text{Ni}_x)_3\text{O}_{\sim 7}$, showing magnetic order.

It is obvious from the curves that the magnetic order is not of long range but of short range type, probably like spin-glass or small clusters. This is consistent with the broader specific heat peak at T_c in this system, as commented above. This is the first observation of magnetic order by specific heat measurements on substituted samples of YBCO, and similar short range magnetic order is expected to occur also for Fe substituted samples, as previously conjectured by us [7]. We also measured low temperature specific heat of $\text{Ba}_2\text{Dy}(\text{Cu}_{0.95}\text{M}_{0.05})_3\text{O}_{\sim 7}$ ($\text{M} = \text{Ni}$ and Zn) to study effect of magnetic and non-magnetic atoms on the Néel temperature, T_N and found that the nickel substitution reduces and broadens T_N but the zinc substitution does not affect it.

In summary, we measured low and high temperature specific heat of $\text{Ba}_2\text{YCu}_3\text{O}_y$ ($6 \leq y \leq 7$), $\text{Ba}_2\text{ErCu}_3\text{O}_y$ ($6.88 \leq y \leq 6.92$) and $\text{Ba}_2\text{Y}(\text{Cu}_{1-x}\text{M}_x)_3\text{O}_{\sim 7}$ ($\text{M} = \text{Ni}$ and Zn) in an attempt to clarify several important questions concerning specific heat anomalies. The double peak around T_c was reaffirmed for the two former systems and the higher temperature peak at 92 K is associated with a state of slightly less oxygen (~ 6.88) and the other peak around 89 K rapidly broadens and disappears with decreasing oxygen concentration. From low temperature results we determined the variations of the residual γ^* and the upturn of C_p/T as a function of oxygen and Ni/Zn concentration, which suggest that both γ^* and the upturn are of different origin and due to disorder on CuO_2 planes and CuO chains, respectively. In this sense, both low temperature anomalies are primarily intrinsic to this type of compound, not due to foreign impurity phases as suspected by some workers. Finally it is pointed out that all the present results are consistent with the idea of the essential role of CuO chains for the superconductivity in the YBCO system.

We would like to thank the other members of our group at I.S.S.P., K. Hirota, N. Shirakawa and T. Shibuya for their collaboration.

References

- [1] For a recent review, see the paper by A. Junod in Physical Properties of High Temperature Superconductors I, edited by D.M. Ginsberg, World Scientific, Singapore (1990).
- [2] Y. Nakazawa and M. Ishikawa; Physica C 158 (1989) 381.
- [3] Y. Nakazawa and M. Ishikawa, to be published in; Physica C, Proc. of Int. M^2S -HTSC Conf., Stanford(USA), July 23-28, 1989.
- [4] M. Ishikawa, Y. Nakazawa, T. Takabatake, A. Kishi, R. Kato and A. Maesono; Solid State Commun. 66 (1988) 201.
- [5] A.G. Khachaturyan and J.W. Morris Jr.; Phys. Rev. Lett. 61 (1988) 215.
- [6] T. Takabatake, M. Ishikawa, Y. Nakazawa and K. Koga; Physica C 152 (1988) 424.
- [7] M. Ishikawa, T. Takabatake, A. Tohdake, Y. Nakazawa, T. Shibuya and K. Koga; Physica C 153-155 (1988) 890.

K. Mori, K. Noto*, Y. Ogiso**, T. Igarashi**, Y. Isikawa, and K. Sato**

College of Liberal Arts, Toyama University, 3190 Gofuku, Toyama 930, Japan

*Department of Electrical Engineering, Iwate University, Morioka 020, Japan

**Faculty of Science, Toyama University, 3190 Gofuku, Toyama 930, Japan

The temperature dependences of the thermal conductivity and electrical resistivity of $\text{La}_{1.85}\text{Sr}_{0.15}\text{CuO}_4$ superconductor have been measured in the temperature range from 1.8K to 260K in order to investigate the scattering mechanism of conduction. Although the thermal conductivity does not exhibit a striking increase below T_c , such as in the systems Y-Ba-Cu-O(1-2-3 type) and Bi-Pb-Sr-Ca-Cu-O, the lattice thermal conductivity was dominant. The T^2 -dependence of the thermal conductivity was also observed below 10K, like as those of Y-Ba-Cu-O and Bi-Pb-Sr-Ca-Cu-O. The low temperature specific heat has been also measured in the temperature range from 1.8K to 43K and it turned out that the electronic specific heat coefficient, γ , was very small and the Debye temperature, θ_D , was about 221K.

We have already reported the thermal conductivity, κ , of high temperature superconductors in the systems of Y-Ba-Cu-O(1-2-3 type, YBCO) and Bi-Pb-Sr-Ca-Cu-O(BPSCCO)[1,2]. The sudden increase of the thermal conductivity of these superconductors near T_c was observed and interpreted as the results of electron correlation to Cooper pairs. Therefore the phonons are no more scattered by electrons and thermal conductivity increases. These superconductors showed the T^2 -dependence in $\kappa(T)$ below 10K. However, the explanation of the T^2 -dependence has not been established yet[3].

In this paper, we report the results of the temperature dependences of thermal conductivity and electrical resistivity on $\text{La}_{1.85}\text{Sr}_{0.15}\text{CuO}_4$ superconductor in the temperature range from 1.8K to 260K, and also report the result of the low temperature specific heat in the temperature range from 1.8K to 43K.

The sample was prepared by the conventional powder sintering method. X-ray diffraction pattern of this sample showed K_2NiF_4 type crystal structure. A steady heat flow method was used to measure the thermal conductivity. Detail of measurement technique was described elsewhere[4]. The electrical resistivity was measured by DC method with four terminals. The low temperature specific heat was measured by an adiabatic heat pulse method[5].

Figure 1 shows the temperature dependence of the electrical resistivity, ρ , on $\text{La}_{1.85}\text{Sr}_{0.15}\text{CuO}_4$. The sharp superconducting transition is observed and the superconducting transition temperature, T_c , was

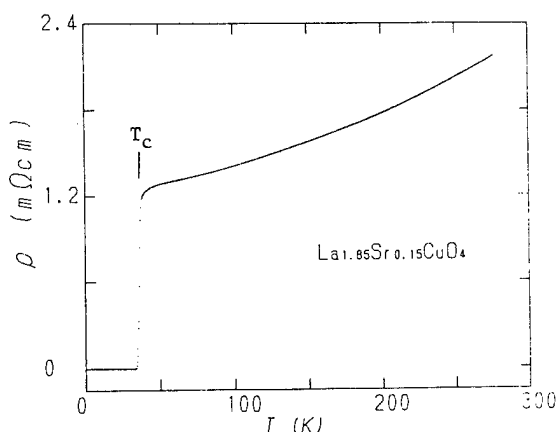


Fig.1 Temperature dependence of electrical resistivity, ρ .

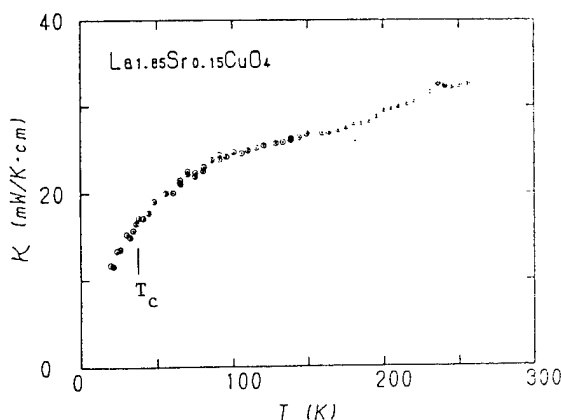


Fig.2 Temperature dependence of thermal conductivity, κ .

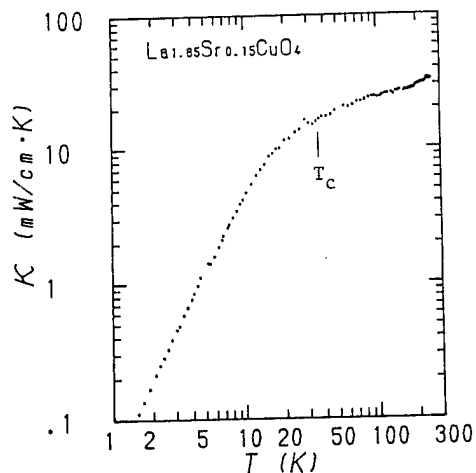


Fig.3 Temperature dependence of thermal conductivity by log-log plots.

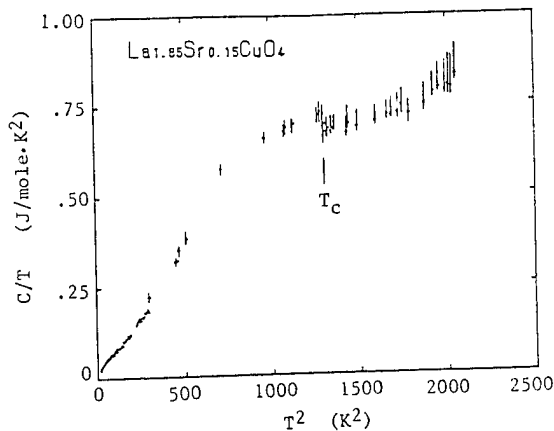


Fig.4 Specific heat divided temperature, C/T vs T^2 in the temperature range from 4.2K to 43K.

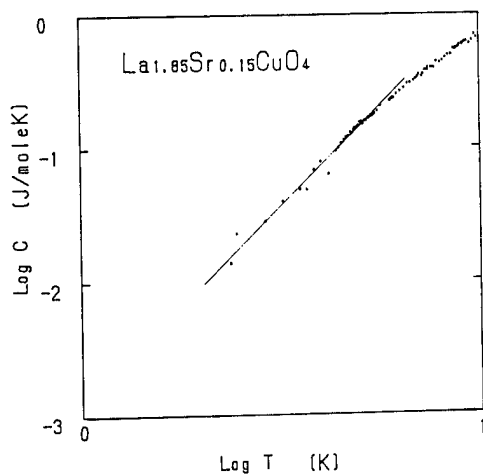


Fig. 5 Log-log plots of C vs T below 10K.

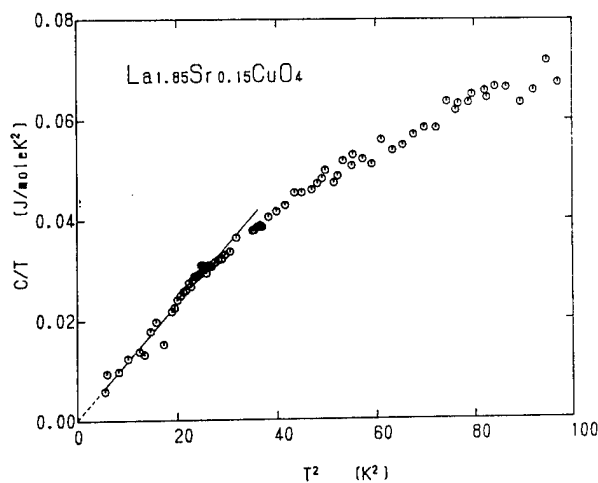


Fig.6 C/T vs T^2 between 1.8K and 10K.

34K, at which $\rho=0$. The transition width, ΔT_c , was about 3K. The value of ρ at $T=0K$ was $1.15m\Omega\cdot cm$, which was obtained by extrapolating $\rho(T)$ in the normal state into $T=0K$ smoothly.

Figures 2 and 3 show the temperature dependence of the thermal conductivity, κ , on $La_{1.85}Sr_{0.15}CuO_4$. As seen in figures, the thermal conductivity decreases with decreasing temperature monotonically. No sudden increase of κ was observed below $T_c=34K$. The contribution of thermal conductivity, κ_c , from the charge carrier was estimated by using the Wiedemann-Franz law, $L=\kappa_c\rho/T$ in terms of the electrical resistivity data just above T_c , where $L=2.45\times 10^{-8}W\Omega/K^2$ is the Lorenz number. The estimated value of κ_c is $5mW/cm\cdot K$ at $T=260K$, and it amounts about 30% of the total conduction. Therefore, the main part of thermal conduction is considered due to the phonons similar to the other high- T_c superconductors, YBCO and BPSCCO[1,2].

Figure 4 shows the results of the specific heat, C , divided temperature, T , against T^2 in the temperature range from 4.2K to 43K. The specific heat jump at T_c is barely seen; $\Delta C/T_c \approx 24mJ/mole\cdot K^2$. Using the BCS theory[8], the electronic specific heat coefficient, γ , is estimated as about $17mJ/mole\cdot K^2$.

Figure 5 shows the results of the specific heat, C , vs. temperature, T , by log-log plots between 1.8K and 10K. Solid line shows the T^3 -dependence, which corresponds to the lattice specific heat. Figure 6 shows the results of C/T vs T^2 below 10K in detail. C/T is expressed by the straight line through zero point; $C/T=1.26T^2 mJ/mole\cdot K^2$ below 4.2K. However, since we have no data below 1.8K, it cannot be concluded whether $\gamma T=0$ or not. The Debye temperature, θ_D , was estimated as about 221K. The simple kinetic

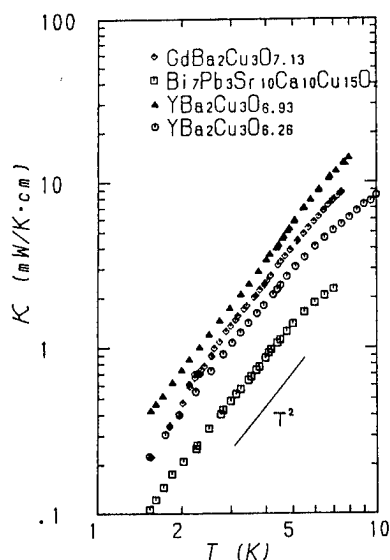


Fig. 7 Log-log plots of κ vs T in the systems YBCO and BPSCCO.

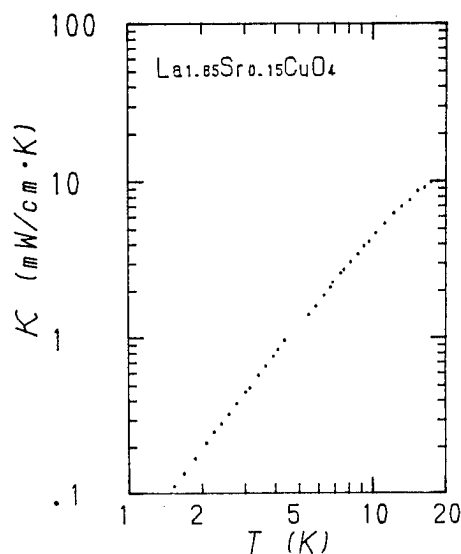


Fig. 8 Log-log plots of κ vs T below 20K. T^2 -dependence is observed below 10K.

formula, $\kappa_p = (1/3)C_L v L$, relates the phonon thermal conductivity, κ_p , to the phonon specific heat, C_L , the phonon velocity, v , and the phonon mean free path, L . Using our data, κ and C_L at $T = 1.8K$ and $v = 4.64 \times 10^5$ cm/sec obtained by Horie et al.[9], the value of L is calculated as $0.24 \mu m$.

Finally, We describe the temperature dependence of thermal conductivity at low temperatures. Figure 7 shows the temperature dependence of thermal conductivity for the systems of YBCO and BPSCCO by log-log plots below 10K. All samples show the T^2 -dependence. Figure 8 shows the results of $La_{1.85}Sr_{0.15}CuO_4$ below 20K. As seen in Fig. 8, the T^2 -dependence of thermal conductivity is also observed on this sample. It seems that the T^2 -dependence of thermal conductivity at low temperatures in high- T_c oxide superconductors is common characteristic features. Although there are a few explanation for this T^2 -dependence, it is not known clearly[6,7].

We would like to thank Dr. S. Nishijima for the preparation of sample, which is the round-robin test sample(BL5) of the Multicore-Project-Data Base Group conducted by the Ministry of Science and Technology.

References

- [1] K. Mori, K. Noto, M. Sasakawa, Y. Isikawa, K. Sato, N. Kobayashi, and Y. Muto; *Physica C* 153-155 (1988) 1515.
- [2] K. Mori, M. Sasakawa, T. Igarashi, T. Isikawa, K. Sato, K. Noto and Y. Muto; *Proc. M²S-HTSC* (1989, Stanford) to be published.
- [3] M. Nunez Regueiro, D. Castello, M. A. Izbizky, D. Esparza and C. D'Ovidio; *Phys. Rev. B* 36 (1987) 8813.
- [4] K. Mori, M. Sasakawa, Y. Isikawa, K. Sato and K. Noto; *J. Coll. Lib. Arts, Toyama Univ.* 22 (1989) 1.
- [5] K. Mori, Y. Muto, T. Fukuroi and H. Watanabe; *Sci. Rep. Rits, A-vol.19* (1968) 304.
- [6] M. Nunez Regueiro, M. A. Izbizky and P. Esquinazi; *Solid State Comm.* 67 (1988) 401.
- [7] A. Jezowsky, J. Klamut, R. Horyn and K. Rogacki; *Supercond. Sci. Technol.* 1 (1989) 296.
- [8] J. Bardeen, L. N. Cooper and J. R. Schrieffer; *Phys. Rev.* 108 (1957) 1175.
- [9] Y. Horie, T. Fukami and S. Mase; *Solid State Commun.* 63 (1987) 653.

Study of High-Temperature Superconductors in La-Sr-Cu-O
and Pb-doped Bi-Sr-Ca-Cu-O Systems

R.Yoshizaki

Institute of Applied Physics and Cryogenics Center,
University of Tsukuba, Ibaraki 305, Japan

Nearest-neighbor spin-correlation energy J was estimated from the peak temperature of the normal state susceptibility in the $\text{La}_{2-x}\text{Sr}_x\text{CuO}_{4-y}$ system. The energy J decreases linearly with increasing x in the range of $x > 0.08$. However, J deviates from the linear dependence to the higher energy side for $x < 0.08$. This behavior of J was interpreted from the role of localized holes and itinerant ones. The superconducting phase diagram of the 2223-phase was studied in the $n=3$ Bi-Sr-Ca-Cu-O system. The experimental result suggests the holes are preferably populate in the outer two CuO_2 sheets of the three.

I. The La-Sr-Cu-O System

Enormous efforts have been made to clarify the mechanisms of the high-temperature oxide superconductivity, but they are still controversial. On the phonon mechanism, nonlinear dependence of isotope effect on the hole concentration in the $\text{La}_{2-x}\text{Sr}_x\text{CuO}_{4-y}$ (LSCO) system by Crawford et al. [1] makes the mechanism turn about to the frontier of the discussion. However, the spin fluctuation mediated superconductivity is the most attractive mechanism of high T_c as well as the charge fluctuation mediated one [2]. The behaviors of the Cu spins have been studied extensively in the LSCO system against hole concentration or in the relation to the superconducting phase diagram by means of neutron scattering ($J=1400$ K for the sample $x=0$) [3], Raman scattering ($J=1700$ K= 1200 cm^{-1} for $x=0$) [4] and magnetic susceptibility measurements [5-8], where J is the nearest-neighbor spin-correlation energy. In all the measurements, no experiment covers whole range of x where J remains finite value. In the present work, the correlation energy J has been studied in the LSCO system by means of the magnetic susceptibility measurement of the normal state in the wide range of the temperature up to 1200 K. The results will be discussed in the relation to the itinerancy of holes and the superconducting phase diagram.

The LSCO ceramic samples were sintered by employing hot-press technique [9]. The hot-pressed ceramics are dense enough and have good quality in the superconducting profiles [10]. Magnetic transition temperature T_c and the volume fraction of the superconductivity were estimated from ac-susceptibility measurement. The magnetic susceptibility of the normal state was measured by employing a magnetic balance ($1200 > T > 300$ K) and a SQUID magnetometer ($T < 400$ K). In both experiments, the samples were exposed to the low-pressure He exchange-gas. In this circumstances, oxygen atoms desorb from the sample with small x above 1000 K and, in consequence, the magnetic susceptibility decreases [10]. Then, a special attention was paid to monitor the oxygen content of the sample whether it changes during the magnetic measurement. Oxygen content was checked by means of iodometry and observing the degradation of the superconducting properties of T_c and fractional volume.

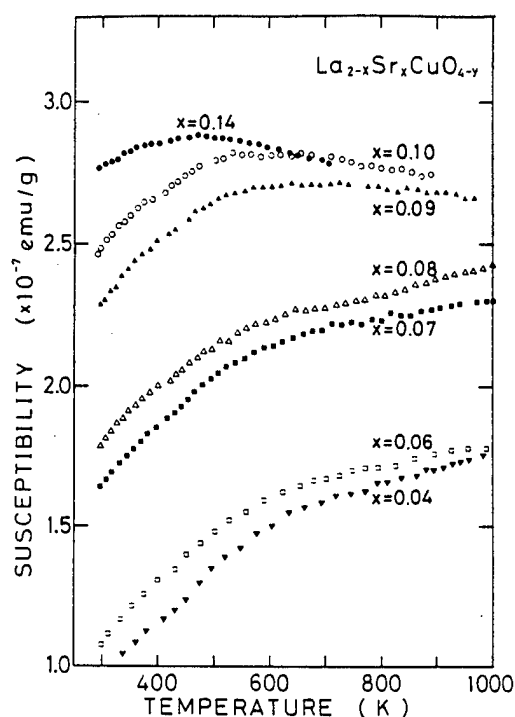


Fig. 1 Temperature dependence of the magnetic susceptibility of the normal state in the La-Sr-Cu-O system for the various concentration of x . (from Reference 11).

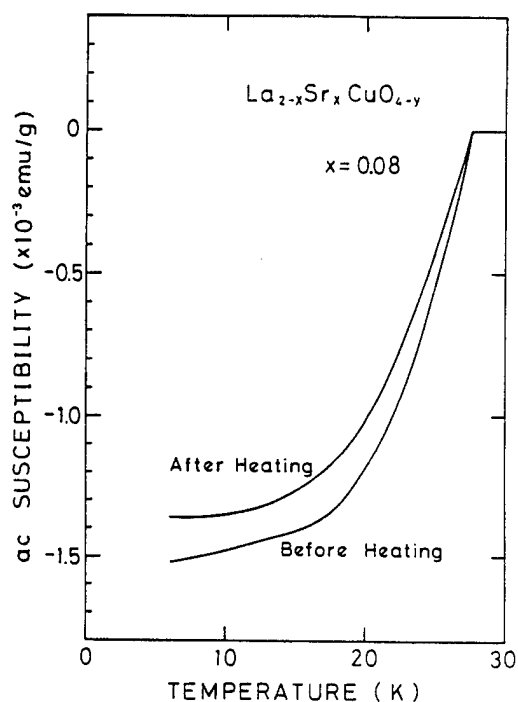


Fig. 2 Superconducting diamagnetism for the sample $x=0.08$ measured before and after the high temperature magnetic measurement. (from Reference 11).

The experimental results of the high-temperature susceptibility without the correction of the core diamagnetism are shown in Fig. 1 [11]. It is evident that the susceptibility for the sample with $x=0.09$ slightly decreases as increasing temperature above 800 K, showing a broad maximum as well as those for the samples $x>0.09$. In contrast, the susceptibility for the sample $x=0.08$ does not saturate nor decreases as increasing temperature up to 1200 K. Thus the temperature corresponding to the maximum of the susceptibility, T_{max} , shifts to the higher temperature side as decreasing Sr concentration x and jumps up like step-wise from $x=0.08$ to 0.09. Concerning to the magnitude of the maximum susceptibility, it increases with increasing hole densities or, accordingly, with decreasing of T_{max} . Those behaviors are consistent with the results of the earlier works [5-8].

Before the high-temperature magnetic measurement, the carrier densities were determined from the iodometric analysis. The results showed the excellent linear correlation of hole densities to the Sr concentrations in the present range of x up to 0.18 as reported by Torrance et al. [12]. After the magnetic measurement, the carrier densities obtained from iodometry show a little lower values for the samples experienced the temperature higher than 800 K. For such samples, however, the superconducting properties hardly change through the thermal cycle. A typical example is shown in Fig. 2 for the sample with $x=0.08$. As seen in the figure, the magnetic onset temperature is identical within the experimental error of 0.1 K, although the sample experi-

enced 1200 K, and the magnitude of the low temperature superconducting diamagnetism χ decreases slightly of about 10 %. Referring to the x dependence of T_c and χ in this LSCO system [10], the change of hole concentrations, dx , is estimated from the shift of T_c and the magnitude of χ at low temperature, which is $dx < 0.01$.

It should be noted that the desorption of oxygen atoms resulted in the decrease of the magnetic susceptibility as indicated in Fig. 1 of Ref. 10. Then, if the oxygen atoms desorbed at high temperatures for the sample $x=0.08$ or $x < 0.08$, the susceptibility would decrease and show a maximum at high temperature, contrary to the experimental results in Fig. 1. Thus that T_{\max} is higher than 1200 K for the samples $x \leq 0.08$ is true, even though the oxygen atoms would desorb at the higher temperature. The highest temperature measured for the samples $x \geq 0.09$ is lower than 1000 K and we believe that the influence of the oxygen desorption must be negligibly small for those samples.

The T_{\max} is plotted against the Sr concentration x in Fig. 3. The present results ($0.09 \leq x < 0.2$) indicate good coincidence with the results of the other magnetic measurements ($0.15 \leq x$); That is, T_{\max} exhibits linear dependence on the Sr concentration x in the range of $x \geq 0.09$. If we extrapolate the linear dependence to the lower x , T_{\max} at $x=0$ is expected to be 1000-1200 K as suggested by Oda et al. [6]. In the results of the present experiment, however, T_{\max} shows up-turn at $x=0.08$ as described above and it is indicated by the solid curve in Fig. 3. We have measured eight samples with different x in the range of $0 \leq x \leq 0.08$, and it is ensured that the T_{\max} exceeds 1200 K.

From the theoretical point of view, T_{\max} is calculated for $S=\frac{1}{2}$ system in a linear chain model by Bonner and Fischer [13], and the result is $kT_{\max}=1.3J$, where k is the Boltzman constant. In the two dimensional system, $kT_{\max}=0.95J$ was obtained for the simplest model by Line [14]. In any way we can put roughly $kT_{\max}-J$. Then the ordinate of Fig. 3 expresses J in Kelvin units. The observed J values other than the magnetic measurements are also plotted in Fig. 3; They are obtained from neutron scattering [3] (denoted by a solid circle) and Raman scattering [4] (denoted by open rectangulars). If we extrapolate the step-wise increase of J at $x=0.08$ to the lower x , the solid curve seems to approach to the upper branch of J , that is observed in neutron or Raman scattering experiments. The upper branch of J observed by Raman experiment shows the moderate decrease of J as increasing x , comparing to the lower branch observed by the magnetic measurements. The moderate decrease at small x region is due to the localized character of the doped holes, as well as due to the enhancement of J ex-

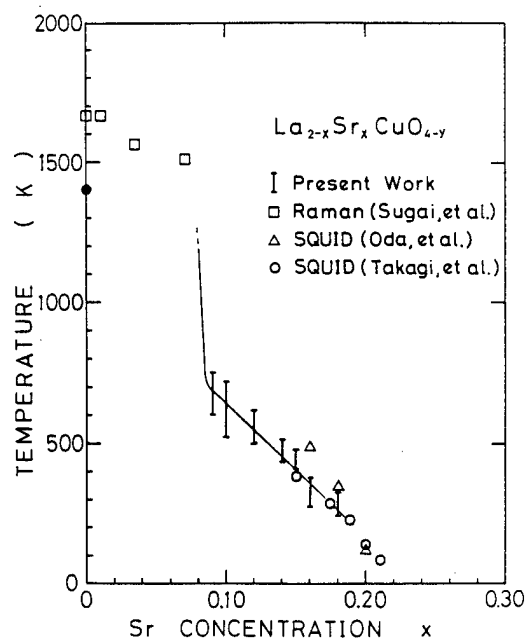


Fig. 3 T_{\max} is plotted as a function of x . T_{\max} expresses J in Kelvin units assuming $kT_{\max}=J$. The solid curve is guide for eyes to the behavior of J against x . J observed by other experiments are also plotted for neutron (a solid circle) and Raman (open rectangulars) experiments. (from Reference 11).

pected from the shrinkage of the lattice constant of the plane as pointed by Torrance et al. [8]. The transition from upper to lower branches occurs as increasing of the itinerant character of holes. When we estimate the itinerancy of holes from the conductivity at 300 K in Fig. 1 of Ref. 8, the conductivity starts to increase from $x=0.08$, that is in good agreement with the present results.

II. Pb-doped Bi-Sr-Ca-Cu-O System

Superconducting phase diagram against the hole density per a CuO_2 plane, p , has been studied extensively in many superconducting cuprate systems [15]. In particular, it is indicated experimentally that the phase diagram for the $n=2$ cuprate system in the BSCCO system nearly coincided with that for the $n=1$ cuprate system of LSCO when the T_c was normalized by the maximum T_c in each system, where n is the number of CuO_2 sheets in a chemical formula [16]. This result suggests the possibility that the normalized phase diagram is universal for the CuO_2 -based superconductors as pointed out firstly by Tokura et al. [17]. For the case of $n=3$, the situation is a little different, since the carrier population in the mid sheet of the three CuO_2 planes is still in question [18]. In order to clarify this problem, we have synthesized a single-phase $n=3$ cuprate (the 2223 phase) in the Pb-doped BSCCO system [19], and the hole concentration was varied by introducing La substitution for Sr or Ca atoms.

The magnetic properties of the superconductivity was measured by employing an ac- and a SQUID magnetometer. Hole densities were estimated from iodometry, assuming the chemical formula determined by electron probe microscope analysis. The compositions of the formula is close to the nominal one except the content of Pb due to vaporization in firing process. The results are summarized in Fig. 4. When we assume the holes are distributed only in the equivalent two sheets other than the mid sheet, the results are denoted by solid circles. On the other hand, assuming that the holes are equally distributed in the three sheets (denoted by open circles), the phase diagram moves to the lower hole-density side as shown in the figure. The phase diagram for the $n=2$ system (the 2212 phase) [16] is expressed by solid curves and triangles for comparison. We need the experiments at higher hole densities. However, the results in Fig. 3 suggest the holes are distributed preferably to the outer two sheets of the three.

III. SUMMARY

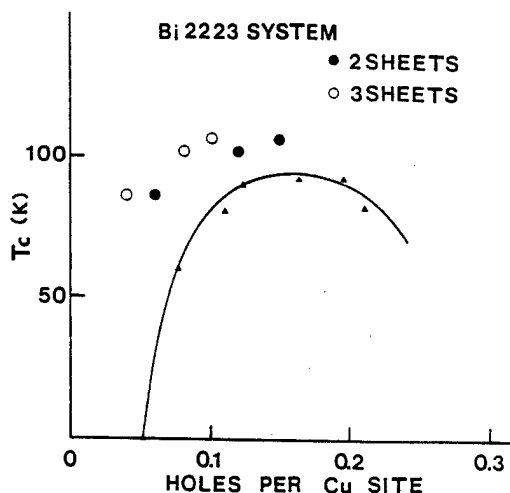


Fig. 4 Phase diagram of the superconductivity for the 2223 phase of BSCCO. Assuming holes are distributed only in the outer two sheets, the results are indicated by solid circles, and open circles denote the results for the equally distributed case. The phase diagram for the 2212 phase is expressed by a solid curve and triangles.

We have observed the magnetic susceptibility of the normal state in the LSCO system up to 1200 K. The temperature corresponding to the maximum of the magnetic susceptibility decreases almost linearly to the Sr concentration x in the range of $x > 0.09$. From $x = 0.09$ to 0.08 , T_{\max} increases abruptly and exceeds the experimental limit of 1200 K. Assuming $kT_{\max} - J$, we have discussed the present results with the relation to the J values observed in the lower x region by neutron or Raman experiments. We propose the presence of two branches of J : The upper branch is in the small x region where the conductivity is small, the lower branch is in the large x region where the conductivity is large, and the transition between the two branches occurs at about $x = 0.08$. Then we believe that we have observed the T_{\max} phase diagram from the transition region to the lower branch.

We have synthesized a single phase 2223-BSCCO and reduced the hole densities from the substitution of La for Sr or Ca. The obtained superconducting phase diagram indicates the preferable population of holes to the outer two CuO_2 -sheets of the three.

The author would like to express his gratitude to A. Tasaki and E. Kita for a help of the magnetic balance measurement and discussion. He also thanks to all the member of his colleagues for technical assistance. The works are supported by Grant-in-Aid for Scientific Research on Priority Areas, "Mechanisms of Superconductivity" from the Ministry of Education, Science and Culture.

REFERENCES

- [1] M.K.Crawford, W.E.Farneth, and E.M.McCarron III, Abstract of the 2nd Intern. Symposium on Superconductivity (ISS'89) (Tsukuba, 1989) p.28.
- [2] "Mechanisms of High Temperature Superconductivity" eds. H.Kamimura and A.Oshiyama, Springer-Verlag, Berlin Heiderberg, 1989.
- [3] Y.Endoh et al., *ibid.* p.129.
- [4] K.B.Lyon et al., *Phys. Rev. B* **37**, 2353 (1988); S.Sugai et al., *Phys. Rev. B* **38**, 6436 (1988).
- [5] D.C.Johnston et al., *Phys. Rev. B* **36**, 4007 (1987).
- [6] M.Oda et al., *J. Phys. Soc. Jpn.* **58**, 1137 (1989); M.Oda et al., to be published in *Phys. Rev. B*.
- [7] H.Takagi et al., *Phys. Rev. B* **40**, 2254 (1989).
- [8] J.B.Torrance et al., *Phys. Rev. B* **40**, 8872 (1989).
- [9] R.Yoshizaki et al., *Jpn. J. Appl. Phys.* **26**, L311 (1987).
- [10] R.Yoshizaki and I.Nakai, Research Report on Mechanism of Superconductivity, Science Research on Priority Areas No. 031 Ministry of Education, Science and Culture, (1989) p.89.
- [11] R.Yoshizaki, N.Ishikawa, H.Sawada, E.Kita and A.Tasaki, to be published.
- [12] J.B.Torrance et al., *Phys. Rev. Lett.* **61**, 1127 (1988).
- [13] J.C.Bonner and M.E.Fischer, *Phys. Rev.* **135**, A640 (1964).
- [14] M.E.Lines, *J. Phys. Chem. Solids* **31**, 101 (1970).
- [15] See for example, Abstracts of Intern. Conf. on M^2S HTSC, Stanford 1989.
- [16] R.Yoshizaki et al., Proc. of the Tsukuba Seminar on High T_c Superconductivity, eds. Masuda et al. (Tsukuba, 1989) p.21.
- [17] Y.Tokura et al., *Phys. Rev. B* **38** 7156 (1988).
- [18] J. Kondo et al., *J. Phys. Soc. Jpn.* **57** 4334 (1988).
- [19] H.Ikeda et al., to be published in *Jpn. J. Appl. Phys.*

Hole Concentration Dependences of T_c in Cuprate Oxide Superconductors

K. Takita, H. Akinaga, T. Ohshima, Y. Orimoto, Y. Takeda^a and M. Takano^b

Institute of Materials Science, University of Tsukuba
Tsukuba, Ibaraki 305, Japan

^aDepartment of Chemistry, Faculty of Engineering, Mie University
Tsu 514, Japan

^bInstitute for Chemical Research, Kyoto University
Uji, Kyoto-fu 611, Japan

By changing of two parameters of x and δ , in $\text{Nd}_{1+x}\text{Ba}_{2-x}\text{Cu}_3\text{O}_{7-\delta}$, it is found that the superconducting transition temperature T_c is determined uniquely by the hole concentration p_H , where p_H is the effective hole concentration deduced from the Hall coefficient R_H ($p_H=1/R_H e$). p_H shows almost the same value to p_s which is a mobile hole concentration in the sheet of CuO_2 plane deduced from chemical analysis. T_c increases with p_H almost linearly up to 95K. Furthermore, the relations between T_c vs. p_H and T_c vs. p_s are investigated in the higher concentration range using the samples of YBCO-like system, $\text{Nd}_{0.80}\text{Ca}_{0.22}\text{Ba}_{1.98}\text{Cu}_3\text{O}_{7-\delta}$ with various amount of oxygen, which were prepared by the annealing in high pressure oxygen. p_H shows larger values than p_s , and T_c shows a trend of decreasing with increasing hole concentration, which is qualitatively similar to but quantitatively different from the case of $\text{La}_{2-x}\text{Sr}_x\text{CuO}_4$.

INTRODUCTION Using single-phase solid solution system $\text{Nd}_{1+x}\text{Ba}_{2-x}\text{Cu}_3\text{O}_{7-\delta}$ and changing the two parameters of x and δ by the annealing in high pressure oxygen, it has been confirmed by the present authors that the superconducting transition temperature T_c in the system is determined uniquely by the hole concentration p_H , where p_H is the effective hole concentration deduced from the Hall coefficient R_H just above T_c ($p_H=1/R_H e$) [1]. Furthermore, p_H shows almost the same value to p_s which is a mobile hole concentration in the sheet of CuO_2 plane deduced from chemical analysis based on an assumption proposed by Tokura et al. [2]. T_c increases with p_H almost linearly up to 95K, i.e. $T_c \propto (p_H - p_{H0})$, showing a contrast to the case of $\text{La}_{2-x}\text{Sr}_x\text{CuO}_4$ system.

On the other hand, according to the chemical analysis performed by Tokura et al. for Ca-substitution system $\text{Y}_{1-x}\text{Ca}_x\text{Ba}_2\text{Cu}_3\text{O}_{7-\delta}$ where Y is expected to be substituted partially by Ca, it was suggested that in the higher hole concentration region T_c has a trend of decreasing with increasing hole concentration.

Thus it seems to be imperative to investigate the relation between T_c and the hole concentrations p_H in the higher hole concentration region of the Ca-substitution system, together with the relation between p_H and p_s . In the present paper, we report the result of such investigation performed by using Ca-substitution system $\text{Nd}_{0.80}\text{Ca}_{0.22}\text{Ba}_{1.98}\text{Cu}_3\text{O}_{7-\delta}$ with various values of $7-\delta$.

EXPERIMENTAL The method to obtain the single phase samples of Ca-substitution systems such as $Y_{1-x}Ca_xBa_2Cu_3O_{7-\delta}$ and $Nd_{1-x}Ca_xBa_2Cu_3O_{7-\delta}$ has not been confirmed for significant amount of x . Furthermore, according to comparison between X-ray diffraction and neutron diffraction data of the same samples, it is shown that the inclusion of Ca_2CuO_3 and $CaCu_2O_3$ can not be detected by X-ray diffraction up to 10% or so, because of the small X-ray scattering cross section of the lighter elements[3].

Considering these facts, we prepared the samples which all have the same composition, i.e. $Nd_{0.80}Ca_{0.22}Ba_{1.98}Cu_3O_{7-\delta}$ with various amounts of oxygen ($7-\delta$). The samples with largest amounts of ($7-\delta$) were obtained by the annealing in high pressure oxygen up to 1000atm. (at 350°C, for 60hrs). Some samples were prepared by the reduction of oxygen from high-pressure-annealed samples. The reduction process was monitored by TGA analyzer.

RESULTS AND DISCUSSION As proposed by Tokura et al.[2] the superconducting properties of YBCO-like systems can be described by a kind of phase diagrams as shown in Fig.1. The abscissa represents 3 times of an average charge of [Cu-O] i.e. the hole concentration per unit cell, and the ordinate represents oxygen content. The triangles represent the points of investigated samples of $Nd_{1+x}Ba_{2-x}Cu_3O_{7-\delta}$. The plotted points along the solid line A, represent the samples of the present experiments. The point denoted by double circle represents the sample annealed in oxygen at high pressure. The open circle represents the sample sintered in oxygen at 1atm. The dot-dashed line represents the boundary between insulating samples and samples with a certain amount of mobile holes in the case of $Nd_{1+x}Ba_{2-x}Cu_3O_{7-\delta}$. In the case of $Nd_{0.80}Ca_{0.22}Ba_{1.98}Cu_3O_{7-\delta}$, this boundary should be shifted to left hand side, because the average charge of so-called Y-site is about 2.8 instead of 3 in YBCO. The solid line parallel to the broken line is the boundary which has been determined experimentally in the present experiment.

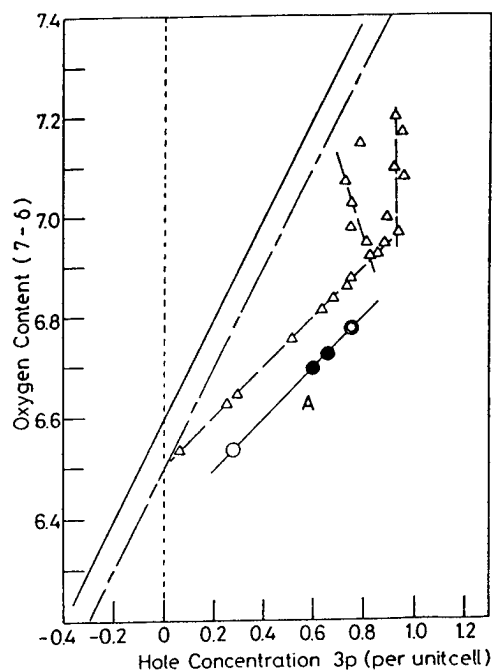


Fig.1. Phase diagram of YBCO-like systems against the oxygen content ($7-\delta$) and the hole concentration. The dot-dashed line represents the boundary between the superconducting samples and the insulating samples, proposed by Tokura et.al.[2]. The triangles represent the points for the investigated samples of $Nd_{1+x}Ba_{2-x}Cu_3O_{7-\delta}$.

For $Nd_{0.80}Ca_{0.22}Ba_{1.98}Cu_3O_{7-\delta}$, the points are plotted along the solid line A. Single and double open circles represent the points of the samples annealed in 1atm. oxygen and in oxygen at high pressure of about 1000atm., respectively. The points for the samples whose oxygen contents are reduced after annealing in high pressure oxygen, are shown by closed circles. The solid line parallel to the dot-dashed line is the boundary for $Nd_{0.80}Ca_{0.22}Ba_{1.98}Cu_3O_{7-\delta}$ samples proposed in the present experiment.

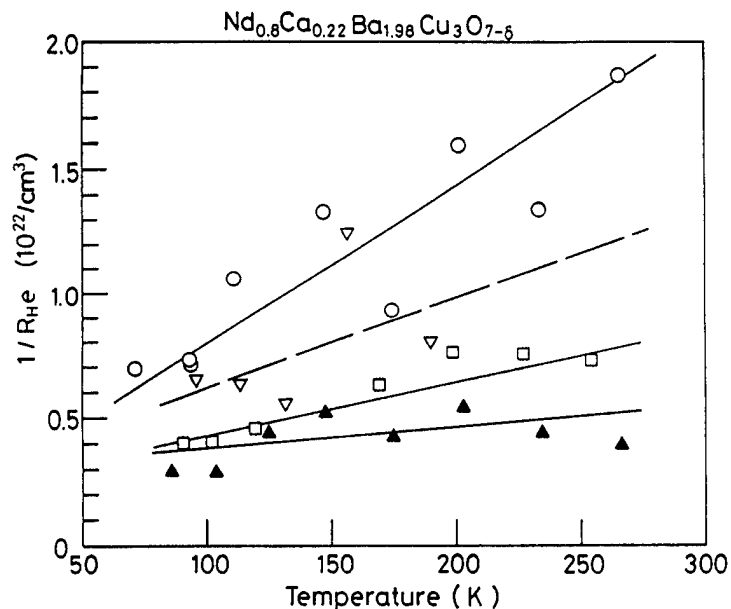


Fig.2. Temperature dependences of the effective hole concentration p_H ($=1/R_{He}$) for $Nd_{0.80}Ca_{0.22}Ba_{1.98}Cu_3O_{7-\delta}$ with various oxygen content. $(7-\delta)=6.78$; [\bigcirc]: $(7-\delta)=6.73$; [∇]: $(7-\delta)=6.70$; [\square]: $(7-\delta)=6.54$; [\blacktriangle]

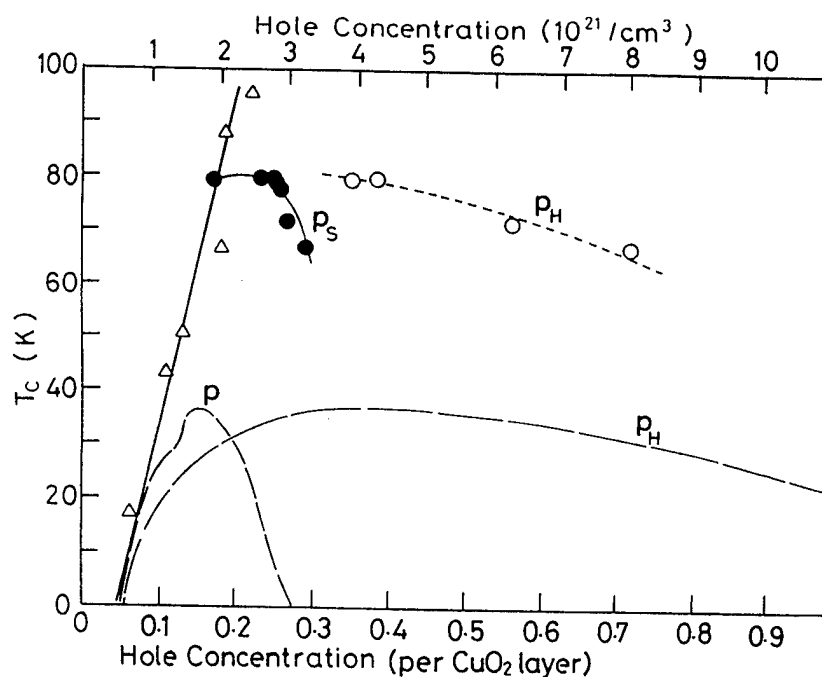


Fig.3. T_c - p_H and T_c - p_s relations of $Nd_{0.80}Ca_{0.22}Ba_{1.98}Cu_3O_{7-\delta}$ are plotted by open and closed circles, respectively. T_c - p_H relation of $Nd_{1+x}Ba_{2-x}Cu_3O_{7-\delta}$ samples annealed in oxygen at high pressure is also plotted by open triangles. For comparison, T_c - p_H and T_c - p relations of $La_{2-x}Sr_xCuO_4$ are shown by broken lines, where p is the chemical hole concentration calculated from the composition x [4]. The scale of the abscissa shown in the bottom is common for all systems, while that in the top is valid for only 1-2-3 systems.

In Fig. 2, the effective hole concentrations p_H (in the unit of cm^{-3}) are plotted against temperature for various samples with different oxygen content (7- δ). Although the observed data are rather scattered, a systematic variation is evident as seen in the figure.

In Fig. 3, the relation of T_c with the hole concentrations deduced from the Hall coefficient p_H ($p_H = 1/R_{HE}$) are plotted by the open circles. They are compared with T_c - p_S relation plotted by closed circles, where p_S are obtained as the hole concentration per CuO_2 layer through chemical analysis using the diagram of Fig. 1.

As already mentioned and plotted by triangles in Fig. 3, the T_c - p_H (or T_c - p_S) relation obtained in $\text{Nd}_{1+x}\text{Ba}_{2-x}\text{Cu}_3\text{O}_{7-\delta}$ system are expressed approximately as $T_c \propto (p_H - p_{H0})$. On the other hand, the result obtained in Ca-substitution system obtained in the present experiment is as shown in Fig. 3. It seems that the effective hole concentration p_H is much larger than the chemically determined mobile hole concentration (p_S) in the higher concentration range. This is qualitatively similar behaviors to those obtained in $\text{La}_{2-x}\text{Sr}_x\text{CuO}_4$ [4]. Quantitatively, however, the behavior shows difference as is seen in Fig. 3. Especially, in the highest T_c region around $T_c = 80 \sim 95\text{K}$, the result suggests a complicated situation.

To our knowledge, reported data of T_c in Ca-substitution systems with 1-2-3 structure with significant amount of Ca showed always T_c of about 80K or less than this. Even in the result of the present experiment, the highest T_c of $\text{Nd}_{0.80}\text{Ca}_{0.22}\text{Ba}_{1.98}\text{Cu}_3\text{O}_{7-\delta}$ is about 80K at the hole concentration around 0.2 per CuO_2 layer, as shown in Fig. 3. In $\text{Nd}_{1+x}\text{Ba}_{2-x}\text{Cu}_3\text{O}_{7-\delta}$ system, however, T_c is about 95K for the same value of the hole concentration. This complication may be related to the problem of oxygen ordering in the samples. The importance of the ordering of oxygen in the hole doping mechanisms is demonstrated by the Madelung energy calculation by J. Kondo et al. [5]. Although further detailed experimental investigation seems to be necessary for T_c above 80K, it should be pointed out that we have obtained p_H value for 2223 Bi-system ($T_c = 110\text{K}$), which is just corresponding on the straight line obtained in the $\text{Nd}_{1+x}\text{Ba}_{2-x}\text{Cu}_3\text{O}_{7-\delta}$ system shown in Fig. 3. Thus we may say that an universal relation between T_c and p_H or p_S exist at least in the lower hole concentration region below that of the highest T_c of each cuprate oxide systems, although the relation is different for the higher concentration region.

REFERENCES

- [1] K. Takita, H. Akinaga, K. Masuda, H. Asano, Y. Takeda, M. Takano, K. Nishiyama and K. Nagamine, Proc. Tsukuba Seminar on High T_c Superconductivity, University of Tsukuba (1989) p.11.
- [2] Y. Tokura, J. B. Torrance, T. C. Huang and A. I. Nazzari, Phys. Rev. B38 (1989) 7156.
- [3] K. Takita and H. Asano, unpublished data.
- [4] H. Takagi, T. Ido, S. Ishibashi, M. Uota and S. Uchida, Phys. Rev. B40 (1989) 2254.
- [5] J. Kondo, Y. Asai and S. Nagai, J. Phys. Soc. Jpn. 57 (1988) 4334.

RESISTIVITY, HALL COEFFICIENT AND TRANSITION TEMPERATURES IN Ag DOPED Bi-Sr-Ca-Cu-O
AND Sb DOPED (Bi,Pb)-Sr-Ca-Cu-O SUPERCONDUCTORS

K. Oto, K. Murase and S. Takaoka

Department of Physics, Faculty of Science, Osaka University
1-1 Machikaneyama, Toyonaka, 560 Japan.

The temperature dependences of the resistivity and Hall coefficient have been investigated in Ag doped $(\text{Bi}_{1-x}\text{Ag}_x)_2\text{Sr}_2\text{CaCu}_2\text{O}_y$ system. The superconductive phase is dominant within $0 \leq x < 0.4$, and the structure of the formed 80K phase was not changed by Ag doping. The resistivity increases exponentially with increasing x . The Hall coefficient does not change in the samples, where the 80K phase is dominant. By partial substitution of Pb and Sb for Bi, the 110K phase is well stabilized. The electrical transport properties of the Sb and Pb doped sample are almost the same as those of the only Pb doped 110K phase. Our observed superconducting transition temperature is at most 108K in the Sb and Pb doped Bi-Sr-Ca-Cu-O system.

Introduction

The high T_c superconductors have strong correlations between their T_c and hole concentrations[1-3]. In the Bi-Sr-Ca-Cu-O superconductor, it was reported that the carrier concentration could be varied by substitution of Y[3] or alkaline metals[4] for Sr or Ca, and the T_c correlated with its carrier concentration. Torardi et al.[5] reported that the excess oxygen was involved in the Bi-O sheets. It may be expected that the status of the Bi-O sheets affects the carrier concentration by substitution for Bi. We have observed the correlation between carrier concentration and T_c in the doped 80K phase[6]. Here, we studied whether the carrier concentration could be varied by the substitution of Ag for Bi.

It was reported that partial substitution of Pb for Bi is effective to stabilize the 110K phase[7]. To investigate the role of Pb, we have tried to stabilize the 110K phase by substitution of Ge, In, Sn and Sb other than Pb. However, we could not stabilize the 110K phase like Pb substitution. Especially, 30% substitution of Sb for Bi made the sample insulator. It was reported that T_c of the Sb and Pb doped Bi-Sr-Ca-Cu-O system is above 130K[8]. We reinvestigated this system and its transport properties.

Experimental

The samples were prepared by usual solid-state reaction from the oxides and carbonates powders with purities of 99.9%. Samples were examined by a powder X-ray diffraction method (Cu $K\alpha$, Rigaku RAD-ROC). The electrical resistivity was measured by a four-probe method using an AC resistance meter. The measuring current was 0.3mA and the detection limit was $0.1\text{m}\Omega$ ($\sim 60\text{mA}/\text{cm}^2$ and $\sim 2 \times 10^{-6} \Omega \cdot \text{cm}$ in this study). The Hall coefficient was measured at a magnetic field 1.3 Tesla and the current was 100mA. During the Hall measurement, the temperature was stabilized within 0.05K.

1. Ag doped Bi-Sr-Ca-Cu-O system

We made eight samples of nominal composition $(\text{Bi}_{1-x}\text{Ag}_x)_2\text{Sr}_2\text{CaCu}_2\text{O}_y$ ($x=0\sim 0.7$). Appropriate amount of Bi_2O_3 , Ag_2O , SrCO_3 , CaCO_3 and CuO powders were mixed and heated at 800°C for 12 hours in air. The calcined mixture was reground and pressed into pellets. The pellets were sintered at 850°C for 12 hours in air, then the furnace was cooled to room temperature.

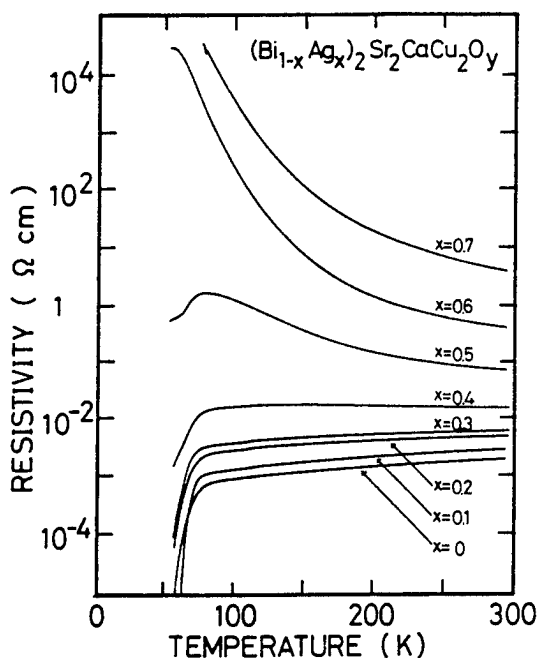


Fig. 1 Temperature dependences of the resistivity for $(\text{Bi}_{1-x}\text{Ag}_x)_2\text{Sr}_2\text{CaCu}_2\text{O}_y$ system.

The temperature dependences of the resistivity are shown in Fig. 1. The samples of $x=0\sim 0.4$ exhibit metallic conductivity and superconductivity. The T_{c0} (offset) are 58K ($x=0$), 62K ($x=0.1$), 55K ($x=0.2$) and 54K ($x=0.3$) respectively. In the samples of $x \geq 0.5$, the normal state resistivity showed thermal activation type semiconducting properties in the temperature 100K~300K. In Fig. 2, the powder X-ray diffraction patterns are shown for the samples with various amount of Ag substitution, $x=0, 0.1, 0.2, 0.4$ and 0.7 respectively. In the samples $x < 0.4$, the 80K phase (noted ●) is dominant and their estimated lattice parameters show no change. It is probable that the doped Ag does not occupy the sites of Sr, Ca and Cu, since the diffraction pattern of the 80K phase is not changed by Ag doping. The Hall coefficient (R_H) and the resistivity at 300K vs. the amount of the Ag substitution x is shown in Fig. 3. With increasing x , the resistivity also increases nearly exponentially. On the other hand, R_H change is very small in the samples that show superconductivity ($x=0\sim 0.4$). Although it is not clear whether the replacement of Bi by Ag occurs or not, both the substitution of Ag^+ for Bi^{3+} and Bi deficiency may cause to exhaust excess oxygen in Bi-O layer for the charge neutrality. Thus carrier density may be compensated.

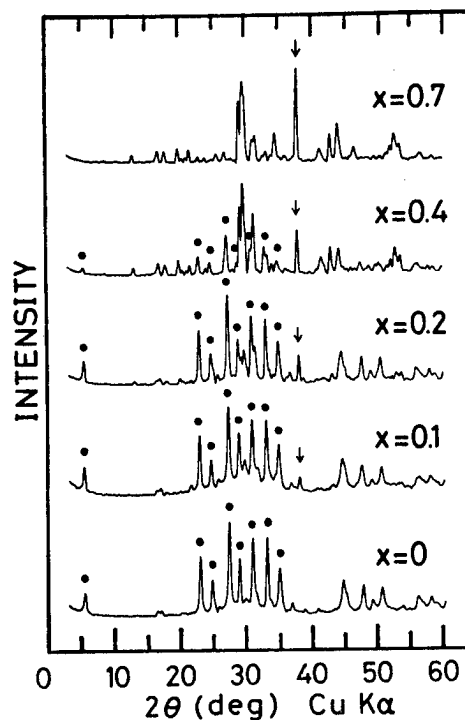


Fig. 2 Powder X-ray diffraction patterns of $(\text{Bi}_{1-x}\text{Ag}_x)_2\text{Sr}_2\text{CaCu}_2\text{O}_y$ system. The ● marked peaks are from the 80K phase. Peaks indicated by the arrow is from Ag.

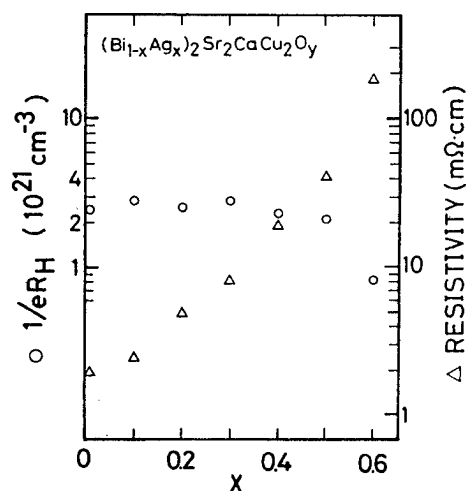


Fig. 3 Hall coefficient (marked ○) and the resistivity (marked △) vs. the amount of the substitution of Ag (x) at 300K.

2. Sb doped Bi,Pb-Sr-Ca-Cu-O system

The samples were prepared from Bi_2O_3 , PbO , Sb_2O_3 , SrCO_3 , CaCO_3 and CuO powders. These were mixed with the cation ratio of $\text{Bi:Pb:Sb:Sr:Ca:Cu} = 1.5:0.4:0.1:2:2:3$ and heated 820°C for 12 hours in air, then reground and pelletized[8]. The samples were sintered under several conditions (Temp. 842°C $\sim 890^\circ\text{C}$, sintered 12 \sim 566 hours, air-quenched or cooled slowly).

In Fig. 4, the temperature dependences of the resistivity are shown. In the sample A (sintered at 875°C for 20 hours and air-quenched[8]), the resistivity is higher than that of the other samples which were cooled in the furnace after sintering. A little drop of the resistivity appears at 110K and T_{c0} is 55K. We could not obtain the sample of the 110K phase dominance with sintering temperature above 870°C . The samples B and C (sintered at 845°C for 65 and 450 hours, respectively and cooled in the furnace) show metallic conductivity and their T_{c0} are 102K and 108K, respectively. It is noted that the 110K phase dominates after shorter sintering time by Pb and Sb doping, in comparison with the only Pb doped sample needed about 200 hours with sintering temperature at 845°C [6].

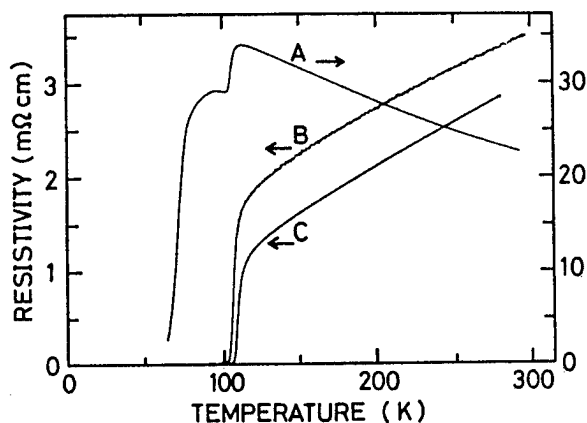


Fig. 4 Temperature dependences of the resistivity for the samples of various sintering conditions. (A: sintered 875°C /20h and air-quenched[7], B: sintered 845°C /65h, C: sintered 845°C /450h, sample B and C were cooled in furnace after sintering.)

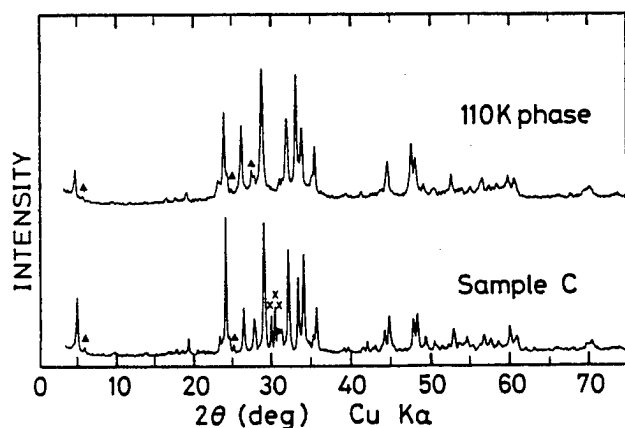


Fig. 5 Powder X-ray diffraction patterns of the sample C and the sample of the only Pb doped 110K phase[8]. ▲: 80K phase, X: impurity phase.

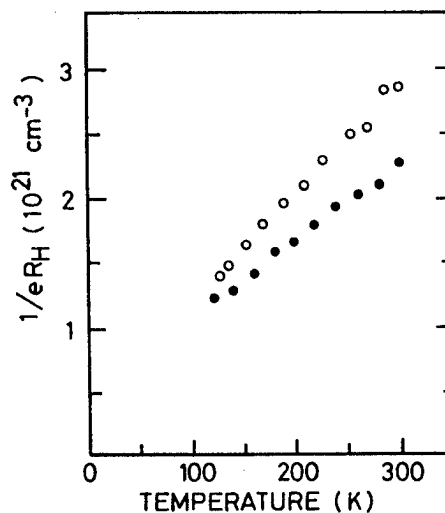


Fig. 6 Temperature dependences of the Hall coefficient of the sample C (marked ●) and the sample of the only Pb doped 110K phase[8] (marked ○) shown in Fig. 5.

In Fig. 5, the powder X-ray diffraction patterns are illustrated for the samples C and Pb doped 110K phase[6] for comparison. In the sample C, though a small amount of the 80K phase (marked \blacktriangle) and impurity phase (marked \times) are detected, almost all the diffraction peaks are coincident with those of the 110K phase. The intensity of (0 0 2n) peaks are stronger and sharp, both lattice parameters a and c are about 0.4% smaller than those of the only Pb doped sample. The structure of the 110K phase may be more stabilized by the substitution of Pb and Sb. The temperature dependence of the Hall coefficient (R_H) for the sample C and the only Pb doped sample are shown in Fig. 6. In both samples, the $1/eR_H$ is proportional to temperature. Such a behavior is observed in the 110K phase. The value of $1/eR_H$ in the sample C is a little smaller than that of the only Pb doped sample. It is probably due to multiphase in the sample C.

Summary

In Ag doped $(\text{Bi}_{1-x}\text{Ag}_x)_2\text{Sr}_2\text{CaCu}_2\text{O}_y$ system, the superconductive phase is dominant within the amount of substitution (x) of Ag for Bi below 0.4. The structure of the 80K phase shows no change by Ag doping. The resistivity increases exponentially with increasing x. The value of the R_H does not change with the amount of the substitution of Ag (x) in the samples in which the 80K phase is dominant.

By partial substitution of Pb and Sb for Bi, the 110K phase is well stabilized. The electrical transport properties are not so different from those of the only Pb doped 110K phase. Our observed T_{c0} is at most 108K.

Acknowledgments

The X-ray powder diffraction measurement was performed at the X-ray Diffraction Service of the Department of Chemistry, Faculty of Science, Osaka University. This work was supported by a Grant-in-Aid for Scientific Research on Priority Areas "Mechanism on Superconductivity" from the Ministry of Education, Science and Culture, Japan.

References

- (1) J.B. Torrance, Y. Tokura, A.I. Nazzari, A. Bezinge, T.C. Huang and S.S.P. Parkin: Phys. Rev. Lett. 61 1127 (1988).
- (2) Y. Tokura, J.B. Torrance, T.C. Huang and A.I. Nazzari: Phys. Rev. B38 7156 (1988).
- (3) T. Tamegai, K. Koga, K. Suzuki, M. Ichihara, F. Sakai and Y. Iye: Jpn. J. Appl. Phys. 28 (1989) L112-115.
- (4) Y. Koike, Y. Iwabuchi, S. Hosoya, N. Kobayashi and T. Fukase: Physica C 159 (1989) 105-110.
- (5) C.C. Torardi, J.B. Parise, M.A. Subramanian, J. Gopalakrishnan and A.W. Sleight: Physica C 157 (1989) 115-123.
- (6) K. Oto, K. Murase and S. Takaoka: Solid State Commun. 71 (1989) 819.
- (7) M. Takano, J. Takada, K. Oda, H. Kitaguchi, Y. Miura, Y. Ikeda, Y. Tomii and H. Mazaki: Jpn. J. Appl. Phys. 27 (1988) L1041.
- (8) Liu Hongbao, Gao Liezhao, Zhou Ling, Mao Zhigiang, Li Xiaoxian, Yu Zhidong, Xue Bai, Mao Xianglei, Zhou Guien, Run Yaozhong, Chen Zhaojia, Zhang Yuheng: Solid State Commun. 69 (1989) 867.

Kiichi OKUDA, Satoru NOGUCHI, and Masatoshi YOSHIKAWA

College of Engineering, University of Osaka Prefecture,
4-804 Mozu-Umemachi, Sakai, Osaka 591

Magnetic properties of high- T_c superconducting oxides were investigated by ac-complex magnetic susceptibility. The magnetic penetration depth $\lambda(T)$ is measured for various superconducting oxides and its temperature dependence is satisfactorily explained by using BCS gap parameter $\Delta(T)$ in the case of dirty limit. Strong correlation between T_c and $[1/\lambda]^2$ was found. The loss peak of ac-susceptibility in the bulk sample near T_c was measured as a function of field amplitude and frequency of oscillating field. Frequency dependence of the peak temperature was explained by the flux-creep model of Anderson and Kim, and the activation energy of flux in YBCO was estimated to be $U_0 \sim 2.9\text{eV}$.

Study of Magnetic response in high- T_c superconducting oxides under ac and dc magnetic fields is important for understanding the mechanism of superconductivity. In the present study we investigated the magnetic response by ac-complex magnetic susceptibility $\chi(\omega, T) = \chi'(\omega, T) - j\chi''(\omega, T)$. A typical example of ac-complex susceptibility in YBCO system is shown in Fig.1 for both sintered bulk and powdered samples. A broad peak of χ'' and the second step increase of diamagnetic susceptibility χ' at the corresponding temperature for the bulk sample are attributed to the Josephson coupling among grain boundaries [1]. No such anomaly is found in the powdered sample with decoupled superconducting grains. In the present work a systematic study of such measurements were done for the superconducting oxides developed so far, and (1) the magnetic penetration depth $\lambda(T)$ and (2) the magnetic irreversibility of bulk sample near T_c are discussed from the real part χ' and the imaginary part χ'' of the magnetic susceptibility, respectively.

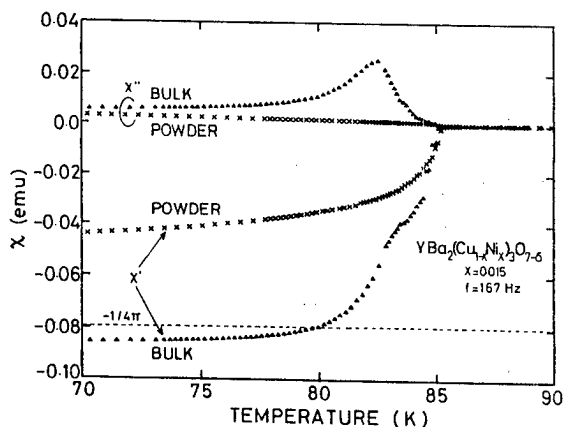


Fig.1. An example of ac-complex magnetic susceptibility $\chi = \chi' - j\chi''$ for YBCO system.

1. Magnetic penetration depth $\lambda(T)$

The samples used in the present experiments, $(\text{La}_{1-x}\text{Sr}_x)_2\text{CuO}_4$, $\text{YBa}_2\text{Cu}_3\text{O}_y$ (ortho I and ortho II), $\text{Bi}_2\text{Sr}_2\text{CaCu}_2\text{O}_8$ and $(\text{Bi,Pb})_2\text{Sr}_2\text{Ca}_2\text{Cu}_3\text{O}_{10}$, were prepared by usual sintering method. For the present purpose of the estimation of magnetic penetration

depth, they were ground and screened by the standard mesh to make a uniform grain size. It was checked by a microscope to range from 6 to 9 μ m. Then, they were mixed with highly purified alumina of 67wt.% so as to decouple the superconducting grains electrically. AC-complex magnetic susceptibility was measured by using Hartshorn type of mutual inductance bridge operating at 167Hz and two phase lock-in amplifier.

For the sample composed of the superconducting spheres with radius R, the diamagnetic susceptibility in the Meissner state is given by solving London equations as

$$-4\pi\chi' = (3/2)P(x) \quad (1),$$

$$\text{where} \quad P(x) = 1 - (3/x)\coth(x) + 3/x^2 \quad (2),$$

with $x=R/\lambda$, λ being the penetration depth. By applying the equations (1) and (2) to the obtained value of χ' at each temperature and using the observed value of radius R the magnetic penetration depth $\lambda(T)$ was estimated. An example of the temperature dependence of $\lambda(T)/\lambda(0)$, where $\lambda(0)$ is the extrapolation of $\lambda(T)$ to $T=0$, is shown as a function of $(T/T_c)^2$ in Fig.2 for $\text{YBa}_2\text{Cu}_3\text{O}_y$ (ortho I phase). In the figure the experimental data are given by dots and a broken line $\lambda_L(T)$ shows the theoretical curve in the dirty limit given by [2].

$$\lambda(T)/\lambda(0) = [(\Delta(T)/\Delta(0))\tanh(\Delta(T)/2k_B T)]^{-1/2} \quad (3),$$

where $\Delta(T)$ is the BCS gap parameter. The agreement with the experimental results is rather good. Similar results were obtained for all other compounds. In the figure 3 the superconducting transition temperature T_c is plotted as a function of $[1/\lambda(0)]^2$ for typical compounds whose crystallography were well established so far. It is noted that T_c has strong correlation with $[1/\lambda(0)]^2 = 4\pi n_s e^2 / m^* c^2$.

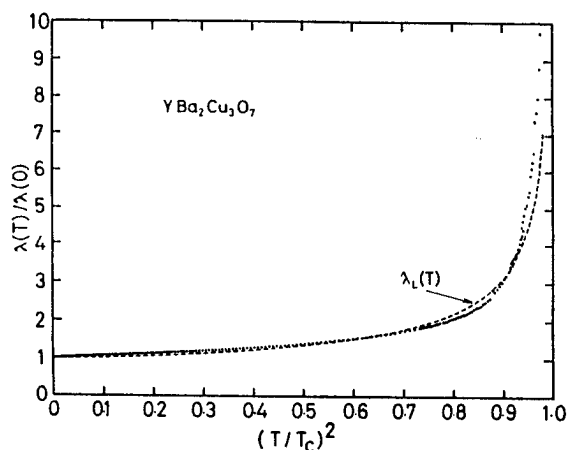


Fig.2. Temperature dependence of magnetic penetration depth $\lambda(T)$. A broken line $\lambda_L(T)$ is the theoretical curve given in the text.

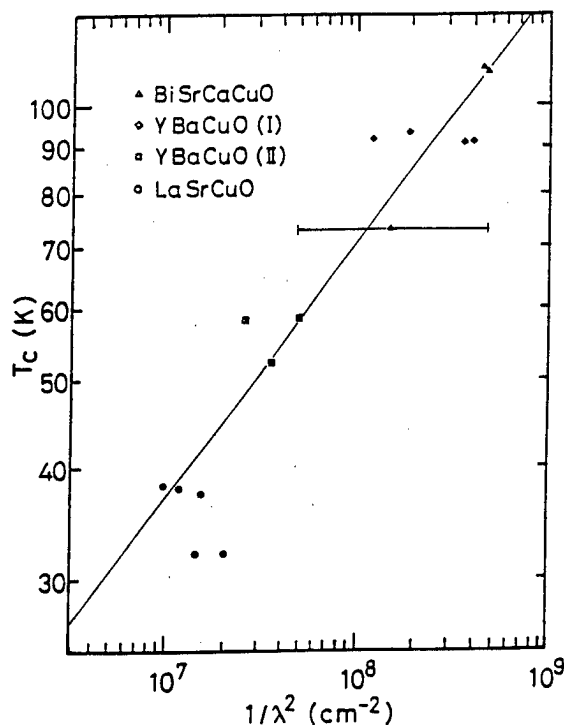


Fig.3. T_c vs. $(1/\lambda(0))^2$. A strong correlation is found.

2. Magnetic irreversibility

To investigate the magnetization dynamics of sintered bulk sample the ac-complex magnetic susceptibility $\chi = \chi' - j\chi''$ was measured. An example of χ', χ'' vs. T for a sintered bulk sample of $\text{YBa}_2(\text{Cu}_{1-x}\text{Ni}_x)_3\text{O}_y$ with $x=0.060$ is shown in Fig.4. The measuring frequency is 167Hz and the amplitude of oscillating field h_0 is varied from 0.02 to 4 Oe. When the amplitude is increased, the peak of χ'' is shifted to lower temperatures and the width is broadened. At the peak temperature (T_p) of χ'' the real part of the susceptibility χ' shows the second-step increase as shown in the figure.

The temperature T_p is reduced by T_c as $1-T_p/T_c$ and plotted as a function of $h_0^{2/3}$ for the various samples in Fig.5. A good linear relation was obtained for each samples. One of the idea to explain the linear relation is the flux-creep model of Anderson and Kim [3] based on the G-L theory. According to the model the relation near T_c is given as

$$1-t = p[kT_c \text{Bln}(f_0/f)]^{2/3} \quad (4),$$

where $t = T_p/T_c$, p the experimentally determined factor, f , f_0 being the measuring and characteristic frequency for the flux trapped well, respectively. In the model, the peak of χ'' is dominated near the onset point of irreversible behavior in the magnetization, where the vortex lines are thermally activating very rapidly across the pinning barriers and the critical current drops rapidly. For the small value of p in eq.(4) large critical current is expected. For instance, the results in two samples $(\text{Bi,Pb})_2\text{Sr}_2\text{Ca}_2\text{Cu}_3\text{O}_x$ and Au-composited $(\text{Bi,Pb})_2\text{Sr}_2\text{Ca}_2\text{Cu}_3\text{O}_x$ with the bulk critical current $J_c = 500$ and 1100 A/cm^2 respectively, are compared in Fig.6 [4]. The line for Au-composited sample with large J_c shows a slow increase with $h_0^{2/3}$ and the large value of $h_0^{2/3}$ for the same temperature ($1-t$) compared to the pure

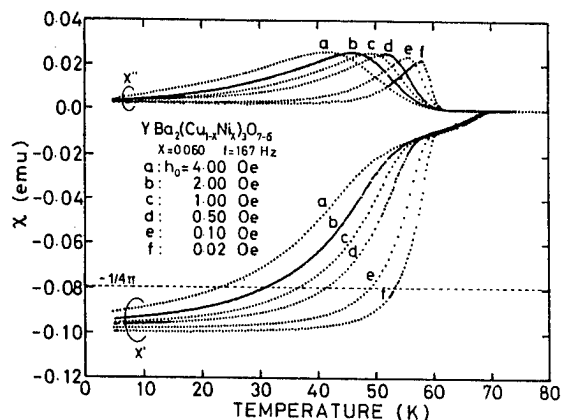


Fig.4. A Typical example of the ac-complex susceptibility for the bulk sample.

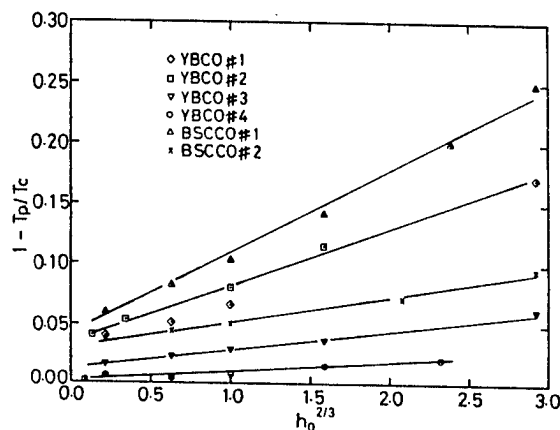


Fig.5. $1-T_p/T_c$ vs. $h_0^{2/3}$ for YBCO and BSCCO system.

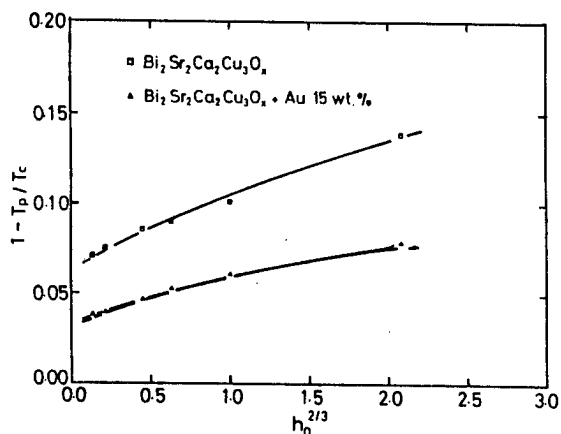


Fig.6. $1-T_p/T_c$ vs. $h_0^{2/3}$ for Au-composited and pure $\text{Bi}_2\text{Sr}_2\text{Ca}_2\text{Cu}_3\text{O}_x$.

sample.

From the relation (4) it is expected that the loss peak is shifted to higher temperature with increasing the measuring frequency. The results in YBCO is shown in Fig.7. The relation between the measuring frequency f and the peak temperature T_p is given by the theory of Anderson and Kim [3] as

$$f = f_0 \exp[-U_0/kT_p] \quad (5),$$

where U_0 is the activation energy of the flux. An example of the experimental results, $1/T_p$ vs. f , is shown in Fig.8 for YBCO sample. From the tangent the activation energy U_0 is estimated to be 2.94eV.

References

- [1] S.Noguchi, J.Inoue, K.Okuda, Y.Maeno and T.Fujita: Jpn.J.Appl.Phys.27(1988) L390.
- [2] A.A.Abrikosov, L.P.Gorkov and I.E.Dzyaloshinski: Method of Quantum Field theory in Statistical Physics (Dover New York, 1963)
- [3] P.W.Anderson: Phys.Rev.Lett. 9(1962) 309, Y.B.Kim: Rev.Mod.Phys. 36(1964)39
- [4] K.Okuda, M.Yoshikawa, M.Imai, N.Imanaka and G.Adachi: to be published in Jpn.J.Appl.Phys.

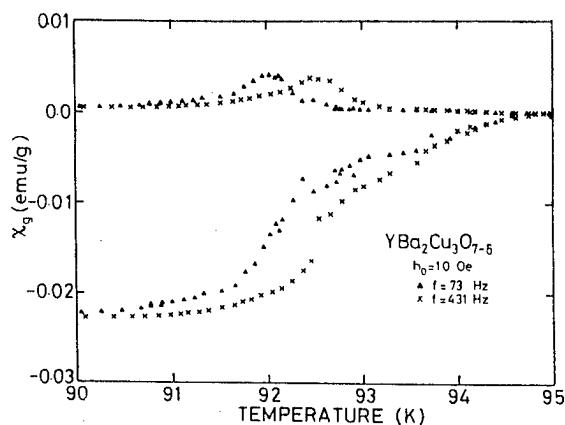


Fig.7. Ac-complex susceptibility YBCO as a parameter of measuring frequency. When the frequency is increased, the loss peak is shifted to higher temperature.

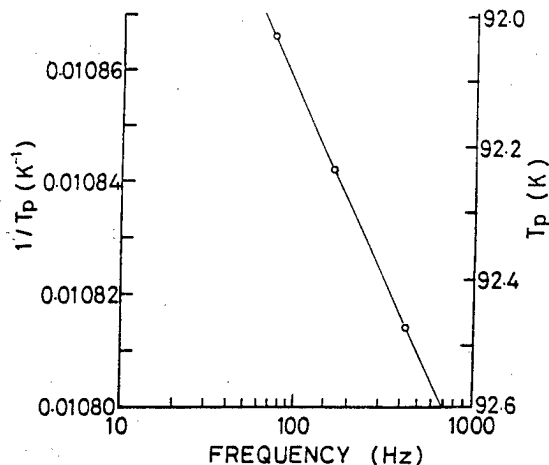


Fig.8. The inverse temperature of loss peak as function of measuring frequency.

Anomalous Behaviors of Resistive Transition in High T_c -Phase
Bi-Pb-Sr-Ca-Cu-O Thin films in Magnetic field

S. Mase, T. Fukami, Y. Horie and A. A. A. Youssef

Department of Physics, Kyushu University, Fukuoka 812, Japan

Almost purely single phase and c-axis-oriented $(\text{Bi}_{1-x}\text{Pb}_x)_2\text{Sr}_2\text{Ca}_2\text{Cu}_3\text{O}_{10+y}$ films were prepared with the excimer laser evaporation method. The resistive transition behaviors of this substance in high magnetic fields were investigated. The coherence length was derived from the $\rho(T, H)$ versus T curves above and below T_c . The anomalous $\rho(T, H)$ versus H curves below T_c were analyzed with a proposed empirical formula. A discussion is made of the anomalous behaviors in resistive transition in magnetic field.

1. Introduction

It is known that the resistive transition width in high T_c superconductors under magnetic field is quite broad as compared with that in ordinary type II superconductors. The resistivity pattern is different from that of the so-called flux flow resistivity. These anomalous behaviors have been interpreted by Tinkham in terms of phase slippage [1] and by Ikeda et al. [2] in terms of one-dimensional fluctuation theory. The theories are too complicated to be easily digestible, but it seems that the applicability of the theories is still limited to some conditions. For example, for the latter the temperature range may be limited to a narrow range below T_c .

Since we could prepare almost single phase and c-axis oriented $(\text{Bi}_{1-x}\text{Pb}_x)_2\text{Sr}_2\text{Ca}_2\text{Cu}_3\text{O}_{10+y}$ (BPSCCO) thin films with the excimer laser evaporation method, we have investigated the behaviors of the resistive transition under rather high fields. As in the case of low T_c phase $\text{Bi}_2\text{Sr}_2\text{CaCu}_2\text{O}_{8+y}$, high T_c phase BPSCCO shows much broader resistive transition than the case of $\text{YBa}_2\text{Cu}_3\text{O}_7$. A detailed study of these properties will be valuable to investigate the mechanism of high T_c superconducting transition.

2. Anomalous Behaviors of Resistive Transition in Magnetic Field

2.1 Coherence lengths from $\rho(T, H)$ vs. T curves above and below T_c

In Fig. 1 we show the experimental results of the electrical resistivity $\rho(T, H)$ versus T curve as a parameter of magnetic field H [3]. The notation of the crystal axes follows the conventional one. Remarkable characteristics in the $\rho(T)$ curve of oxide superconductors are the linear relationship in $\rho(T)$ versus T curve and the succeeding rounding out in the curve near T_c . Some people considered that all of the rounding out in the $\rho(T, H=0)$ versus T curve should be ascribed to the fluctuation effect. However, if this rounding out is all due to the fluctuation effect, this must be affected by applying magnetic fields. We investigated this problem intensively under magnetic fields up to $H = 10$ T. In Fig. 1 it is to be noted about the followings. First, the bundle of $\rho(T, H)$ curves is appreciably separated from about $T \sim 120$ K in both figures (a) and (b). Secondly, there is no appreciable drastic change

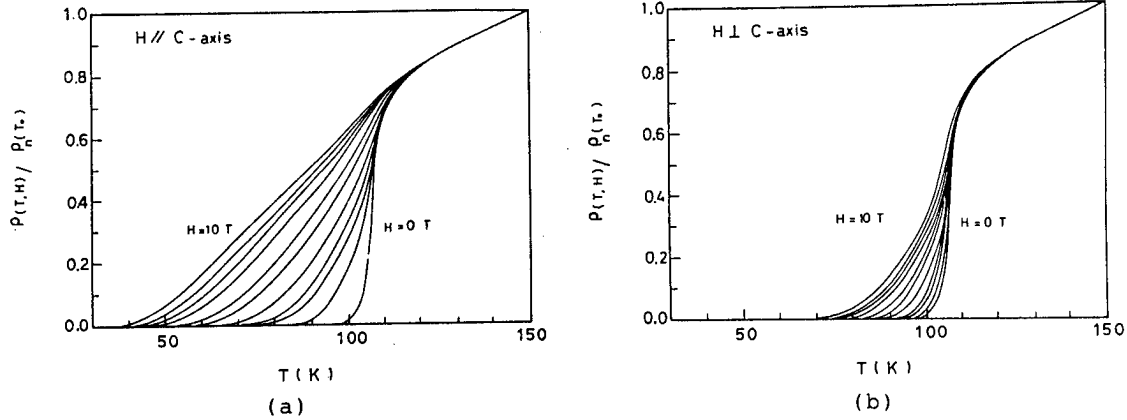


Fig. 1. Experimental data on $\rho(T,H)/\rho_n(T_0)$ versus T in BPSCCO [3]:
 (a) $\vec{H} // c\text{-axis}$, $\vec{\tau} // ab\text{-plane}$ ($\vec{H} \perp \vec{\tau}$); (b) $\vec{H} \perp c\text{-axis}$, $\vec{\tau} // ab\text{-plane}$ ($\vec{H} \perp \vec{\tau}$).
 H in each curve is taken at 10, 8, 6.5, 5, 3, 2, 1, 0.5, 0.3, 0.1 and 0 T from left to right.

of curvature in the $\rho(T,H)$ versus T in the neighborhood of $T_c(0)$ deduced from the $\rho(T)$ versus T curve at $H = 0$. The transition width is quite broad.

(a) Fluctuation conductivity

According to classic theories of fluctuation conductivity in the absence of magnetic field, the fluctuation contribution to the conductivity in a 2-dimensional system, $\sigma'(T)^{(2)}$, consists of two terms, the Aslamazov-Larkin term $\sigma'_{AL}(T)^{(2)}$ and the Maki-Thompson term $\sigma'_{MT}(T)^{(2)}$. In the presence of magnetic field these are suppressed. Recently some sophisticated theories were presented, but as far as the temperature region above T_c is concerned, probably classic theories given by Maki and Aoi may be enough in the object of derivation of the coherence length. We based our analyses on the above well known classic theories.

Differently from some of previous papers, we consider that the real fluctuation effect becomes appreciable from a temperature T' (~ 120 K) below which the bundle of $\rho(T,H)$ curves is separated appreciably with increasing H . We define a fluctuation contribution to the conductivity, $\Delta\sigma'(T,H)$, purely experimentally:

$$\begin{aligned} \Delta\sigma'(T,H)/\sigma_n(T_0) &= [\sigma(T,0) - \sigma(T,H)]/\sigma_n(T_0) \\ &= \rho_n(T_0)[1/\rho(T,0) - 1/\rho(T,H)]. \end{aligned} \quad (1)$$

Here, T_0 is a reference temperature above which the fluctuation effect is certainly negligibly small. The relation $\sigma(T,H) = 1/\rho(T,H)$ is well satisfied in HTSC with a much smaller antisymmetric part of conductivity than the symmetric part. It is to be noted that in this formula we did not use any linear extrapolation procedure to derive the normal part of the conductivity, $\sigma_n(T)$, which becomes rather ambiguous in the case of strongly rounding curve of $\rho(T)$ versus T .

We describe only the results of the analyses on BPSCCO. All of the present analyses show that the dependence of $\Delta\sigma'(T,H)/\sigma_n(T_0)$ on ϵ ($= (T - T_c)/T_c$) is much

neener to that of the 2-dimensional system. From the fitting of curves we obtained the best fitting values of T_c and the coherence lengths $\xi_{ik}(0)$ at $T = 0$ ($\xi_{ab}(T)$ for $\vec{H} // c$ -axis and $\xi_{ac}(T)$ for $\vec{H} \perp c$ -axis). These are shown in Table I, together with the results for YBCO by us [4] and by Matsuda et al. [5] in comparison. These results are compared with those from $(dH_{c2}(T)/dT)$ at $T < T_c$ mentioned below. The very short coherence lengths $\xi_{ik}(0)$'s are common properties of high T_c superconductors.

Table I. $T_c(H=0)$ and $\xi_{ik}(0)$'s derived from the comparison between experiments on the fluctuation contribution to $\sigma(T,H)$ above T_c and theory, together with $\xi_{ik}(0)$'s obtained from $H_{c2}(T)$. The quantities in the first line were derived from the measurements of those in the second line denoted as From. The values of the pair breaking parameter, $\delta = 0.037$ (BPSCCO) and $\delta = 0.022$ (YBCO), are taken in the calculation of $\Delta\sigma'(T,H)$.

From	$T_c(H=0)$ (K)	$\xi_{ab}(0)$ (Å)	$\xi_{ac}(0)$ (Å)	$\xi_{ab}(0)$ (Å)	$\xi_{ac}(0)$ (Å)
	$\Delta\sigma'$	$\Delta\sigma'$	$\Delta\sigma'$	$H_{c2}(T)_{//}^{\dagger}$	$H_{c2}(T)_{\perp}^{\dagger}$
BPSCCO[3]	107	11.3	6.0	~ 11	~ 5.4
YBCO[4]	89.5	12.5	—	12.1	6.8
YBCO[5]	85.5	11.5	4.2	—	—

\dagger $-dH_{c2}(T)/dT$ at $T \lesssim T_c$ was derived from the point of $\sim \rho_{100\%}$ for BPSCCO[3] and that of $\sim \rho_{80\%}$ for YBCO[5] in $\rho(T,H)$ versus T curve.

(b) $H_{c2}(T)$ versus T

The upper critical field $H_{c2}(T)$ is defined as the field at which the fluxoids begin to overlap. This is given by the formula

$$H_{c2}(T) = \phi_0 / 2\pi\xi(T)^2 = (\phi_0 / 2\pi\xi(0)^2) \cdot \epsilon. \quad (2)$$

As seen from Fig. 1, the phase transition point can not be definitely defined from $\rho(T,H)$ versus T curves, in particular in the case of $\vec{H} // c$ -axis. Nevertheless, as will be found from a later exhibited figure of $\rho(T,H)$ versus H curves at several $T < T_c(0)$, the nature of a partial destruction of superconducting state is largely involved in the data in the region of $T < T_c(0)$. Therefore, instead of fixing the threshold level of $\rho(T,H)$ as in the conventional manner of $\rho_{50\%}$, we evaluated $H_{c2}(T)$ from several threshold levels. The results are shown in Fig. 2. From this figure the slope $-dH_{c2}(T)/dT$ is also evaluated: since the intersection of the $\rho(T,H)$ versus T curve and the threshold level $\rho_{x\%}$ exceeds the value of $T_c(0)$ in the case of low field and high $x\%$, only the slope of $H_{c2}(T)$ versus T has a physical meaning in such a case.

The calculated value of $\xi_{ik}(0)$'s from each threshold level is shown in Fig. 3. From the figure one can see that $\xi_{ab}(0)$ decreases rapidly with increasing $x\%$ above 80%, while $\xi_{ac}(0)$ decreases very slowly and almost saturates above 80%. The value of $\xi_{ik}(0)$ from $\sim \rho_{100\%}$ is nearly in agreement with that from the analysis of the fluctuation conductivity above T_c . It is to be noted that an approximate agreement of $\xi_{ik}(0)$'s from two different temperature regions can be obtained only in the case of a large magnitude of x in $\rho_{x\%}$.

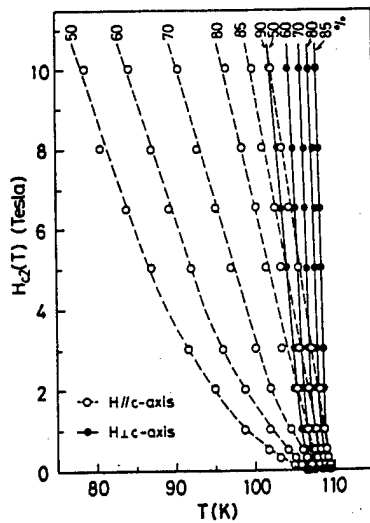


Fig. 2. $H_{c2}(T)$ versus T in the cases of $\vec{H} // c$ -axis (broken lines) and $\vec{H} \perp c$ -axis (solid lines) [3].

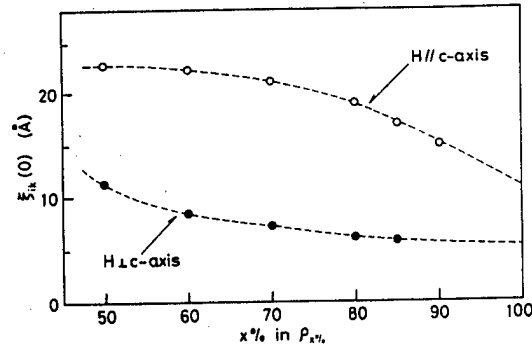


Fig. 3. $\xi_{ik}(0)$ versus $x\%$ in $\rho_{x\%}$ in the cases of $\vec{H} // c$ -axis and $\vec{H} \perp c$ -axis [3].

2.2 Anomalous $\rho(T, H)$ versus H below T_c

In the so-called flux flow state in the case of $\vec{H} \perp \vec{I}$, the flux flow resistivity ρ_f is defined as $dV(T, H, I)/dI$ in the linear region of the voltage $V(T, H, I)$ versus the current I curve. Let us rewrite the experimental results of $\rho(T, H)$ versus T curves in the region of $T < T_c$ in Fig. 1 into $\rho(T, H)$ versus H curves, as shown in Fig. 4. (Here, the normal resistivity $\rho_n(T, H=0)$ is defined as an extrapolation of the curve of the region from $T \sim T_0$ (~ 150 K) to $T \sim T'$ (~ 120 K)). As seen from the figure thus obtained, the curves near $T \lesssim T_c$ are far from the ordinary pattern of the flux flow resistivity. Main characteristics of $\rho(T, H)$ versus T and $\rho(T, H)$ versus H are as follows:

(i) One remarkable characteristic is the angular dependence of $\rho(T, H)$ versus T curve at $T < T_c$. Namely, the pattern of $\rho(T, H)$ versus T curves in the case of $\vec{H} // \vec{I}$ is nearly the same as the case of $\vec{H} \perp \vec{I}$, as shown in Fig. 5. The pattern is essentially the same as in the case of low T_c phase Bi-system [6]. The Lorentz force must not appear in the former case so that the mechanism of the flux flow resistivity is not applicable to this case. Thus, the experimental result suggests us a necessity of a different mechanism of resistivity under \vec{H} at $T < T_c$ from that of the flux flow resistivity.

(ii) $V(T, H, I)$ versus I curves in the present oxide superconductors show the ohmic nature, except for the region of very small $\rho(T, H)$. There is no remarkable sign to show where the phase transition occurs in the $\rho(T, H)$ versus T curves. When we want to derive the $H_{c2}(T)$ versus T , we should focus our attention on the upper nonlinear region in $V(T, H, I)$ versus I curve in the case of usual type II superconductors. However, in the high T_c superconductors there does not exist such nonlinear region. Namely, the linear region of the so-called flux flow type resistivity region invades the upper nonlinear region to be ascribed to a true thermal destruction of superconductivity.

(iii) As seen from $\rho_f(T,H)/\rho_n(T)$ versus H at $T < T_c$ in Fig. 4, though the definition of $\rho_f(T,H)$ in the figure is different from that of the flux flow resistivity ρ_f , the curves in a low temperature region are rather similar to the flux flow pattern, but those above about 80 K are far from it. The latter reminds us the pattern observed in the midway in change from the typical flux flow resistivity pattern to the complete normal state resistivity in ordinary type II superconductors. The phase transition point is not definitely defined from the original $\rho(T,H)$ versus T curves, but it must exist in a limiting case at higher temperatures in the extremely nonlinear region of $\rho_f(T,H)/\rho_n(T)$ against H in Fig. 4.

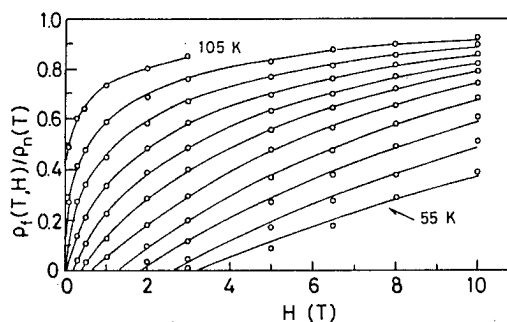


Fig. 4. $\rho_f(T,H)/\rho_n(T)$ versus H at $T < T_c$ in the case of $\vec{H} \parallel c$ -axis, $\vec{I} \parallel ab$ -plane ($\vec{H} \perp \vec{I}$). The curves are arranged by every temperature interval of 5 K from 105 K (left) to 55 K (right).

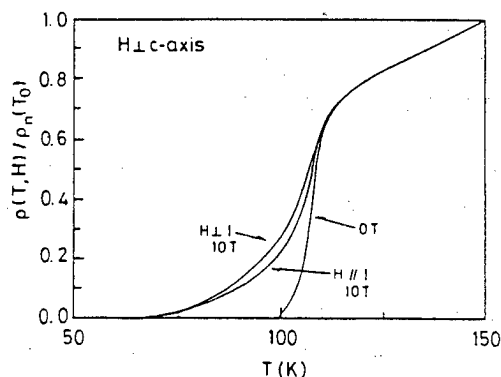


Fig. 5. $\rho(T,H)/\rho(T_0)$ versus T curves in the cases of $\vec{H} \perp \vec{I}$ ($\vec{H} \perp c$ -axis, $\vec{I} \parallel ab$ -plane) and $\vec{H} \parallel \vec{I}$ ($\vec{H} \perp c$ -axis, $\vec{I} \parallel ab$ -plane).

2.3 Flux Creep

In a low resistivity region, the character of the resistivity under the presence of magnetic field may change from the flux flow type to the flux creep one in the case of $\vec{H} \perp \vec{I}$. As in the case of the problem of the flux flow resistivity we have rather similar $\rho(T,H)$ versus T curves in a low resistivity region in both cases of $\vec{H} \perp \vec{I}$ ($\vec{H} \parallel ab$ -plane) and $\vec{H} \parallel \vec{I}$ ($\vec{H} \perp c$ -axis, $\vec{I} \parallel ab$ -plane). Let us express the resistivity due to the flux creep as

$$\rho_{cr}(T,H)/\rho_n(T) \approx \exp[-U(T,H)/k_B T]. \quad (3)$$

It is found from Fig. 6 that $U(T,H)$ is expressed as

$$U(T,H) \propto (1 - t)/H^n \quad (t = T/T_c; 1 > n > 0). \quad (4)$$

The term $(1 - t)$ is certainly required to get a linear relationship in the plotting of $\ln \rho(T,H)$ versus $(1 - t)/T$, as in the case of low T_c -phase Bi-system [6]. As for the value of n , it depends on the orientations of \vec{H} ($\vec{H} \parallel c$ -axis or $\vec{H} \perp c$ -axis) and also on the magnetic field region in a complicated manner.

The temperature and field dependences of $U(T,H)$ is still in controversy. In particular, for $YBa_2Cu_3O_7$ some papers suggest that $U(T,H)$ is independent of T [7,8].

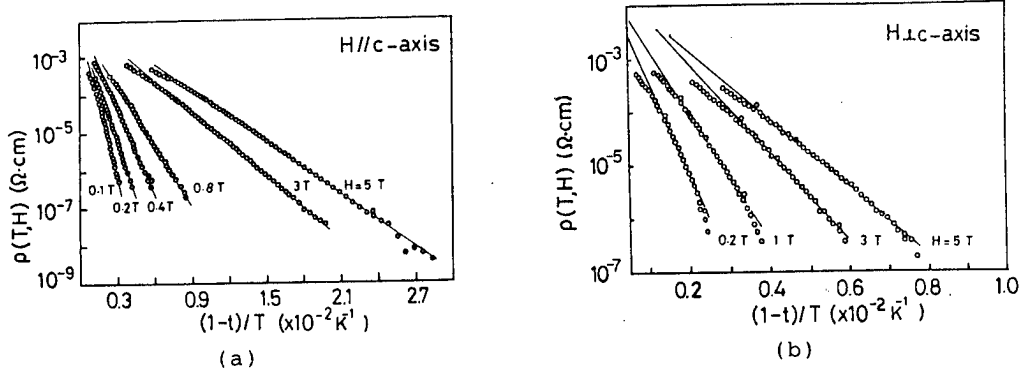


Fig. 6. $\ln(\rho(T,H))$ versus $(1-t)/T$ in the cases of $\vec{H} // c$ -axis (a) and $\vec{H} \perp c$ -axis (b).

however, any data show that $U(T,H)$ decrease as T approaches toward the region of the above-mentioned so-called flux flow resistivity region.

3. Analyses and Discussions

3.1 $H_{C2}(T)$ versus T and $T_C(H)$

The derived value of $-dH_{C2}(T)/dT$ in the case of $\vec{H} // c$ -axis is much larger than that from the conventional $\rho_{50\%}$ criterion. Nevertheless, the $H_{C2}(T)$ versus T curve in Fig. 2 shows that even for the $\rho_{90\%}$ criterion the $T_C(H)$ at $H = 10$ T should be suppressed by about 7 K relatively to $T_C(0)$. It seems that the 7 K suppression is still too large, as one can guess from the following results. According to the specific heat measurements [9-11] and the sound velocity measurements [12,13], the shift of $T_C(0)$ due to applying H is quite small. For example, in the sound velocity measurements the shifts of T_C derived from the shift of the jump position, i.e. $\Delta T_C(H)$, in the sound velocity versus T curve is ≈ 0.9 K for both $YBa_2Cu_3O_7$ and $(La_{1-x}Sr_x)_2CuO_4$ polycrystals under $H = 10$ T [13]. Because of this insensitivity of the $T_C(H)$ value to the magnetic field, it is quite natural that the agreement of the values of $\xi(0)$'s from $\rho(T,H)$ above T_C and from $\rho(T,H)$ below T_C can be obtained for only $-dH_{C2}(T)/dT$ in the case of a large x in $\rho_{x\%}$.

3.2 Analysis of $\rho(T,H)$ below T_C

In order to explain systematically the peculiar features of $\rho(T,H)$ versus T and $\rho(T,H)$ versus H below T_C , we consider that the resistivity mechanism below T_C is different from the flux flow resistivity type. Namely, the resistivity in the mixed state under high magnetic fields and near T_C appears when the applied current passes through many walls in the normal state. We assume the following empirical formula:

$$\rho_f(T,H)/\rho_n(T) = 1 - \exp[-\{(H - H_0)/H_{C2}^*(T)\}^n]. \quad (5)$$

The second term stands for a local percolation rate of supercurrent. The $H_{C2}^*(T)$ is a quantity similar to $H_{C2}(T)$ in the subsection 2.1 but not necessarily equal to it. H_0 is a field above which $\rho(T,H)$ becomes appreciable in Fig. 1, and n is a number as $n \leq 1$. The H is higher, then the effective volume of the fluxoids in the normal state is

larger. Furthermore, the temperature exceeds the flux creep region described in the subsection 2.3, the effective volume of the fluxoids may become much larger, in particular in the case of $\vec{H} // c$ -axis, because of a smaller flux potential barrier. These temperature and field dependences of the effective volume of the normal part may be taken into account by choosing a smaller $H_{c2}^*(T)$ than $H_{c2}(T)$ and smaller n than 1.

The numerical results of eq. (5) by making use of suitable values of $H_{c2}^*(T)$ and n were already shown in Fig. 4 in comparison with the experiments. The experimental results are well reproduced by eq. (5). According to eq. (5), the $\rho_f(T, H)/\rho_n(T)$ versus T curve depends only the field orientation, i.e., on $H/H_{c2}^*(T)$, so that this formula can explain naturally the result of the similarity in both cases of $\vec{H} \perp \vec{I}$ ($\vec{H}, \vec{I} // ab$ -plane) and $\vec{H} // \vec{I}$ ($\vec{H}, \vec{I} // ab$ -plane).

The present analysis is completely phenomenological. If the microscopic theories mentioned before [1,2] are extended in their applicability range, of course, the present explanation must retire.

4. Summary

We have shown that the coherence length derived from the fluctuation conductivity above T_c is approximately equal to that from $-dH_{c2}(T)/dT$ just below T_c only the case of a large magnitude of x in ρ_{xx} . In the derivation of $H_{c2}(T)$ versus T curves we have relied on an inference that T_c is only slightly affected by the presence of magnetic field even at $H = 10$ T. Some experimental evidences for this inference were presented in the text.

In order to explain the anomalous behaviors in $\rho(T, H)$ versus T and $\rho(T, H)$ versus H , we proposed a new mechanism of resistive transition at $T_c(H)$ which is largely different from that in the ordinary type II superconductors. The proposed empirical formula for the resistivity below T_c is a natural manifestation of the proposed mechanism of the resistive transition, so that the fact that the formula can well reproduce the experimental data is a strong support to the proposal.

Acknowledgement

This work is supported by a Grant-in-Aid for Scientific Research on Priority Areas "Mechanism of Superconductivity" from the Ministry of Education, Science and Culture.

References

- [1] M. Tinkham: Phys. Rev. Lett. 61 (1988) 1658.
- [2] R. Ikeda, T. Ohmi and T. Tsuneto: J. Phys. Soc. 58 (1989) 1377; R. Ikeda: J. Phys. Soc. Jpn. 58 (1989) 1906.
- [3] A. A. A. Youssef, Y. Horie and S. Mase: to be published in Solid State Commun; A. A. A. Youssef, T. Fukami and S. Mase: submitted to Solid State Commun.
- [4] B. Zhao, K. Shiraki, Y. Horie, S. Mase, L. Li, Z. Y. Zhang, Y. Y. Zhao and L. F. Chen: to be submitted to Physica C.
- [5] Y. Matsuda, T. Hirai, S. Kojima, T. Terashima, Y. Bando, K. Iijima, K. Yamamoto and K. Hirata: Phys. Rev. B 40 (1989) 5176.
- [6] T. Fukami, T. Kamura, T. Yamamoto and S. Mase: Physica C 160, (1989) 391.
- [7] T. T. M. Palstra, B. Batlogg, L. F. Schneemeyer and J. V. Waszczak: Phys. Rev. Lett. 61 (1988) 1662.

- [8] T. Kobayashi, H. Iwasaki, H. Kawabe, K. Watanabe, H. Yamane, H. Kurosawa, H. Masumoto, T. Hirai and Y. Muto: Physica C 159 (1989) 295.
- [9] R. A. Fisher, J. E. Gordon, S. Kim, N. E. Phillips and A. M. Stacy: Physica C 153 (1988) 1092.
- [10] S. E. Inderhees, M. B. Salamon, N. Goldenfeld, J. P. Rice, B. G. Pazol, D. M. Ginzberg, J. Z. Liu and G. W. Crabtree: Phys. Rev. Lett. 60 (1988) 1178.
- [11] M. B. Salamon, S. E. Inderhees, J. P. Rice, B. G. Pazol, D. M. Ginzberg and N. Goldenfeld: Phys. Rev. B 38 (1988) 885.
- [12] Y. Horie, and S. Mase: Solid State Commun. 69 (1989) 535.
- [13] Y. Horie, Y. Terashi, T. Fukami and S. Mase: to be published in Physica C.

Kazuko Sekizawa and Yoshiki Takano

Department of Physics, College of Science and Technology, Nihon University,
Kanda-Surugadai 1-8, Chiyoda-ku, Tokyo 101, Japan

The effects of Ni and Zn substitutions for Cu on the superconducting transition temperature T_c have been investigated on $\text{LaBa}_2\text{Cu}_3\text{O}_y$. The sample of $\text{LaBa}_2\text{Cu}_3\text{O}_y$ with T_c of 90 K was obtained by a particular process of heating and cooling in flowing nitrogen and the final annealing at 310 °C in flowing oxygen. The decrease rate of T_c with x in $\text{LaBa}_2\text{Cu}_3\text{-xM}_x\text{O}_y$ ($\text{M}=\text{Ni and Zn}$) was reduced by the prolongation of the final annealing (40h \rightarrow 80h), while T_c of pure $\text{LaBa}_2\text{Cu}_3\text{O}_y$ was not affected by the prolonged final annealing. This reduced decrease rate of T_c in La compounds was still twice as large as that in heavy rare earth compounds. The analysis of oxygen content showed that this improvement of superconductivity in substituted samples was not due to the increase in oxygen content but due to the progress of oxygen ordering. The magnetization in the presence of the crystal electric field (CEF) splitting and the applied field was calculated for $\text{NdBa}_2\text{Cu}_3\text{O}_y$ and $\text{ErBa}_2\text{Cu}_3\text{O}_y$. A large apparent paramagnetic Curie temperature is introduced by the CEF effects in $\text{NdBa}_2\text{Cu}_3\text{O}_y$.

1. Introduction

In $\text{RBa}_2\text{Cu}_3\text{O}_y$ compounds with magnetic rare earth (R) ions, information about the electronic structure of [Cu-O] layer can be obtained by investigating the crystal electric field (CEF) splitting of R ion and the interaction between R ions. We have previously studied the effects of Ni and Zn substitutions for $\text{RBa}_2\text{Cu}_3\text{O}_y$ ($\text{R}=\text{Y, Nd, Gd, Dy and Er}$) on the superconducting transition temperature T_c and paramagnetic properties of R ions above T_c .^{1,2)}

In the course of our study on $\text{RBa}_2\text{Cu}_3\text{O}_y$ superconductors, we have noticed the following two results. One is the fact that the effects of Cu site substitution in Nd compound are larger than those in Y and heavy rare earth compounds. The other is the fact that the paramagnetic Curie temperature θ_p of $\text{NdBa}_2\text{Cu}_3\text{O}_y$ takes a large negative value in spite of its relatively small de Gennes factor. In order to investigate whether the former result is originated in the effect of the ionic radius of R ion, we have prepared Ni and Zn substituted $\text{LaBa}_2\text{Cu}_3\text{-xM}_x\text{O}_y$, which contains nonmagnetic La ion with a large ionic radius, and studied the substitution effects on the superconducting transition temperature T_c . In order to clarify the origin of large θ_p , we have calculated the magnetization of $\text{NdBa}_2\text{Cu}_3\text{O}_y$ and $\text{ErBa}_2\text{Cu}_3\text{O}_y$ using a Hamiltonian which includes the crystal field term and Zeeman term.

2. Substitution and Annealing Effects of $\text{LaBa}_2\text{Cu}_3\text{-xM}_x\text{O}_y$ ($\text{M}=\text{Ni and Zn}$)

An orthorhombic $\text{LaBa}_2\text{Cu}_3\text{O}_y$ with T_c of ~ 90 K is difficult to be obtained. A tetragonal $\text{LaBa}_2\text{Cu}_3\text{O}_y$ with T_c of ~ 60 K is obtained by ordinary annealing in oxygen atmosphere. We have succeeded to obtain $\text{LaBa}_2\text{Cu}_3\text{O}_y$ with T_c of ~ 90 K using a following procedure. Powders with stoichiometric ratio were thoroughly mixed and calcined at 930 °C for 20 hours in air. Then, they were pressed into bars

and sintered at 930 °C for 20 hours in air. The sintered bars were reground and pressed into bars again, and sintered and annealed under the condition in Fig. 1. A gas flow rate of nitrogen and oxygen was 140 ml/min. In the first series, a final annealing time T_a at 310 °C was 40 hours. Same process was performed for all samples. The change of T_c with x is shown in Fig. 2 (a).

In substituted samples, T_c raises as T_a is prolonged. However, in pure $\text{LaBa}_2\text{Cu}_3\text{O}_y$, even if T_a is prolonged, T_c scarcely change. The change of T_c of the samples with T_a of 80 hours is shown in Fig. 2 (b). Lattice parameters for all samples are shown in Table 1. The T_a dependence of the lattice parameter ratio b/a (orthorhombicity) is shown in Fig. 3. While this ratio decreases with T_a in pure $\text{LaBa}_2\text{Cu}_3\text{O}_y$, it increases with T_a in substituted samples, indicating the improvement of oxygen ordering. Oxygen content of pure and Zn substituted samples determined by the inert gas fusion non-dispersive infrared absorption method is shown in Table 2. This indicates that a long time annealing improves the oxygen ordering in Zn substituted samples, while the prolonged annealing increases the oxygen content but deteriorates the oxygen ordering in pure $\text{LaBa}_2\text{Cu}_3\text{O}_y$.

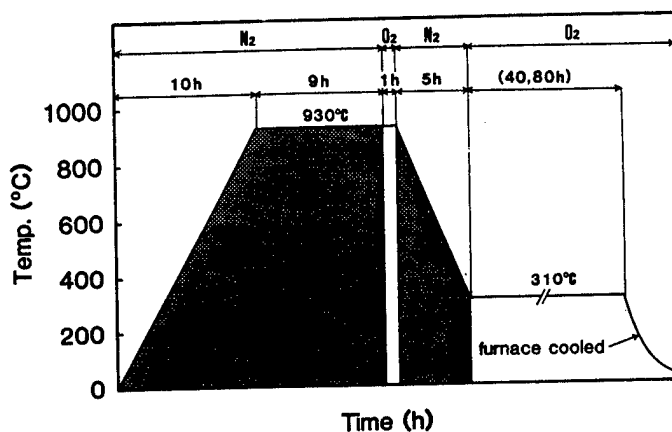


Fig. 1 Synthetic procedure for $\text{LaBa}_2\text{Cu}_3\text{O}_y$ with T_c of ~ 90 K.

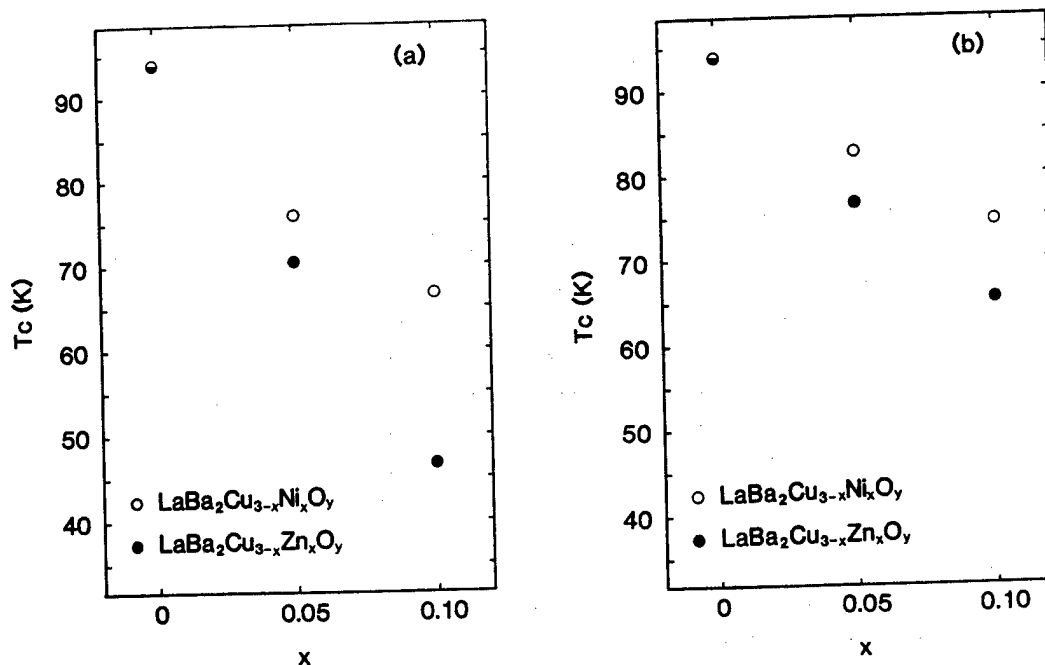


Fig. 2 The temperature dependence of T_c on the substituent concentration x for (a) samples annealed for 40 hours and (b) samples annealed for 80 hours.

Table 1 Lattice parameters for all the samples investigated in this study.

M	T _a (h)	x	a(Å)	b(Å)	c(Å)
Ni	40	0.0	3.890	3.934	11.82
		0.05	3.888	3.929	11.81
		0.1	3.894	3.929	11.80
	80	0.0	3.887	3.927	11.80
		0.05	3.885	3.929	11.81
		0.1	3.886	3.928	11.81
Zn	40	0.0	3.890	3.934	11.82
		0.05	3.888	3.926	11.81
		0.1	3.895	3.929	11.81
	80	0.0	3.887	3.927	11.80
		0.05	3.887	3.927	11.80
		0.1	3.897	3.937	11.83

Table 2 Oxygen content of LaBa₂Cu₃O_y and LaBa₂Cu_{2.9}Zn_{0.1}O_y

T _a (h)	LaBa ₂ Cu ₃ O _y	LaBa ₂ Cu _{2.9} Zn _{0.1} O _y
40	6.80	6.78
80	6.91	6.79

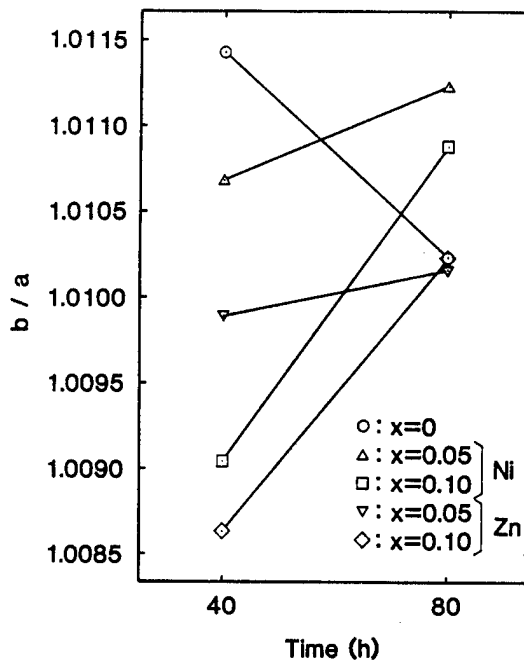


Fig. 3 The annealing time dependence of the lattice parameter ratio b/a.

3. Magnetization of NdBa₂Cu₃O_y and ErBa₂Cu₃O_y

The high temperature part of magnetic susceptibility χ can be fitted to the Curie-Weiss formula in both NdBa₂Cu₃O_y and ErBa₂Cu₃O_y. The effective magnetic moment derived from the Curie constant was in good agreement with the trivalent free ion value. The paramagnetic Curie temperature θ_p of Er compound was small, but that of Nd compound was large and negative (~ 30 K). Recently, many researchers reported the results which indicated the importance of the crystal electric field (CEF) effects; the reduced magnetic moment from the free ion value in an antiferromagnetic state at low temperature, the Schottky anomaly in the specific heat and crystal field levels observed through inelastic neutron scattering (INS).³⁻⁵ We have calculated the magnetization of both Nd and Er compounds using a Hamiltonian which includes the crystal field term and Zeeman term.

A Hamiltonian used here is given as follows:

$$H = H_{\text{cry}} + H_{\text{Zeeman}},$$

where

$$H_{\text{cry}} = B_2^0 O_2^0 + B_2^2 O_2^2 + B_4^0 O_4^0 + B_4^2 O_4^2 + B_4^4 O_4^4 + B_6^0 O_6^0 + B_6^2 O_6^2 + B_6^4 O_6^4 + B_6^6 O_6^6$$

and

$$H_{\text{Zeeman}} = g\mu_B (J_x H_x + J_y H_y + J_z H_z).$$

The B_n^m are crystal field parameters, O_n^m the Stevens' operator equivalents, g the Lande factor and μ_B the Bohr magneton. J_i and H_i ($i=x, y$ and z) are total angular momentum operators and external magnetic fields for respective axes, respectively. The values of crystal field parameters of Nd and Er compounds are estimated from those of Ho compound which were determined by INS experiments, under the assumption that the geometrical factor of these compound is unchanged.⁵⁾ The calculated temperature dependence of the magnetization of these compounds is shown in Fig. 4 with experimental one. Our calculation indicates that a large apparent θ_p is introduced by the CEF effects in NdBa₂Cu₃O₇, even if an antiferromagnetic interaction between Nd ions is absent.

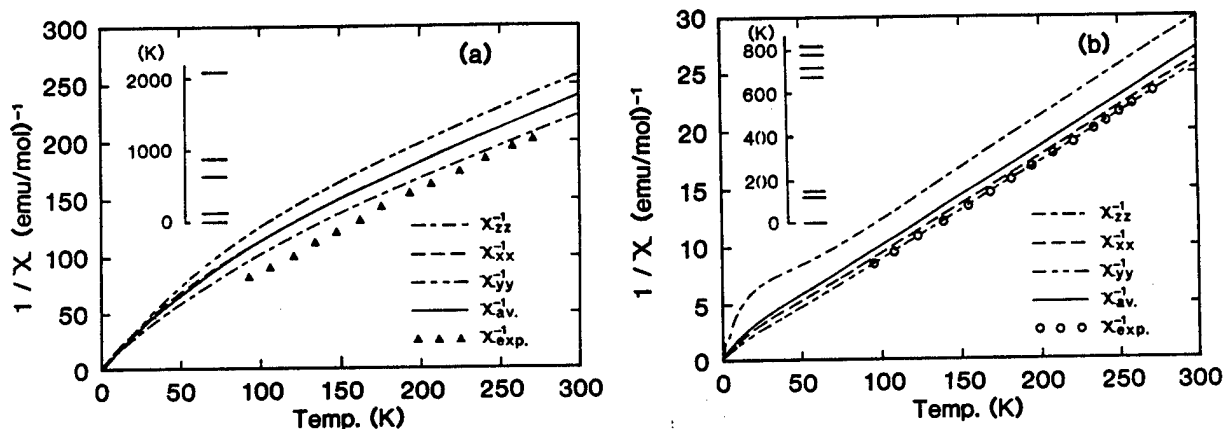


Fig. 4 Calculated and experimental temperature dependence of reciprocal magnetization of (a) Nd compound and (b) Er compound. An energy level splitting is shown in the respective inset.

References

- 1) T. Inaba, Y. Takano and K. Sekizawa, Solid State Commun. 70 (1989) 725.
- 2) K. Sekizawa, Y. Takano and T. Inaba, Physica C in print.
- 3) A. I. Goldman, B. X. Yang, J. Tranquanda, J. E. Crow and Chan-Soo Jee, Phys. Rev. B 36 (1987) 7234.
- 4) B. W. Lee, J. M. Ferreira, Y. Dalichaouch, M. S. Torikachvili, K. N. Yang and M. B. Maple, Phys. Rev. B 37 (1988) 2368.
- 5) A. Furrer, P. Bruesch and P. Unternahrer, Phys. Rev. B 38 (1988) 4616.

Dependence of Meissner Effect on the Shape of the Specimens and Magnetic Field

K. Kitazawa, T. Matsushita*, O. Nakamura**, Y. Tomioka, N. Motohira,
T. Tamura, T. Hasegawa, K. Kishio, I. Tanaka***, and H. Kojima***

Department of Industrial Chemistry, University of Tokyo
7-3-1 Hongo, Bunkyo-ku, Tokyo 113

* Department of Electronics, Kyushu University
6-10-1 Hakozaki, Higashi-ku, Fukuoka 812

** Tonen Ltd., R&D Laboratory
1-3-1 Nishitsurugaoka, Oimachi, Iruma-gun, Saitama 354

*** Institute of Inorganic Synthesis, Yamanashi University
7 Miyamae, Kofu 400, Japan.

The Meissner effect was systematically examined on cuprate superconductors $(\text{La}_{1-x}\text{Sr}_x)_2\text{CuO}_4$ ($x=0.06$) and $\text{Bi}_2\text{Sr}_2\text{CaCu}_2\text{O}_y$ in the form of single-crystal with various size, poly-crystal and powder under various magnetic field. The sample form was found to be an important factor to determine the Meissner fraction. A new model has been presented, applying the Bean's critical state model to the flux expulsion process in the type 2 superconductors.

Introduction

The quality of the oxide superconducting specimens has been frequently evaluated [1,2] by the Meissner curve in terms of the sharpness of the transition at T_c and the Meissner fraction, i.e., the ratio of the largest diamagnetism attained at the lowest temperature to the perfect diamagnetism. Because of the relative difficulties in preparing pure and homogeneous specimens of the cuprate superconductors in the early stage of the studies, the two indications: the sharpness of the change in the curve and the Meissner fraction, have been discussed in relation with the compositional homogeneity and the volume fraction of the superconducting phase in the specimens, respectively. In some cases, studies on the copresence of the superconductivity and magnetic ordering have been cast with some doubt for the possible presence of magnetic impurity phase, because the Meissner fraction observed on the specimen employed has been significantly lower than 100% [3].

This paper, however, intends to point out that the two indications are sharply dependent on how pinning force of vortices develops below the critical temperature as well as the shape of the equilibrium magnetization curve of the type 2 superconductors. As the result, the shape of the Meissner curve exhibit significant dependencies on the field of measurements and the granularity or size of specimens rather than their compositional qualities. Namely, it is pointed out that the criteria based on the Meissner measurement is very misleading unless a special precaution is taken. On the other hand, if certain required measurements are performed, the Meissner signal should be able to give a tool to evaluate the strength of the superconducting weak links in polycrystalline specimens and the development of pinning force of vortex lines as a function of temperature and magnetic field.

Experimental

The Meissner curves were taken by a Hoxan HSM-2000X SQUID susceptometer under constant magnetic

field by lowering the temperature at a speed about 2K/min. The susceptometer was equipped with a metallic Nb shielding tube around the specimen chamber inside the superconducting magnet. The intensity of the field in the range below 10 Oe was determined with the aid of the standard Pb metal. This was done because the hysteresis of the magnet was found to give a small error to estimate the field from the direct reading of the current. The setting procedure of the new magnetic field was repeated in the low field region until a symmetrical signal current was obtained for the pick up coils while the sample was moved up and down with a span about 50mm through the coils. The two pick up coils are asymmetrically wound and a symmetrical signal current has to be assured for the measurements in the homogeneous field.

The specimens employed were single-crystalline $(\text{La}_{1-x}\text{Sr}_x)_2\text{CuO}_4$ (LSCO) with $x=0.06\pm0.005$ prepared by the traveling solvent floating zone (TSFZ) method [4]. Specimens were shaped into platelets with about the same area but with different thicknesses among the series of the comparative studies. The specimens showed resistive critical temperature $T_c(R=0) = 35\text{K}$. The specimens were cut out of two different single-crystalline boules, A and B which gave nearly the same Sr content x . Sample A was cut into a platelet with a-b plane as the two faces and sample B with a-c plane as the faces with various thicknesses. Crystals grown by the same method and of the similar compositions have been characterized by the neutron scattering [5], resistive transition under magnetic field [6] and Hall measurement [7]. For comparison, measurements were made on polycrystalline sintered body of the same composition prepared by the standard solid state reaction [8]; fired at 1100°C in flowing oxygen atmosphere and cooled slowly down to room temperature at 35°C/hr . In addition to LSCO, single-crystal [9], poly-crystalline and powder specimens of $\text{Bi}_2\text{Sr}_2\text{CaCu}_2\text{O}_y$ were used for part of the comparative measurements.

Results

Figure 1 shows the Meissner curves obtained on a single-crystalline specimen A-1 in the field cooling processes under various magnetic fields. This immediately tells us that the final Meissner fraction attained at the lowest temperature is strongly dependent upon the intensity of the magnetic field. The perfect diamagnetism line should be at the level of $1.15 \times 10^{-2} \text{emu/g}$. Hence it is interpreted that the observed Meissner fraction is approaching towards 100% of the perfect diamagnetism as the field intensity is lowered.

The Meissner measurements of oxide superconductors in general have been performed under a magnetic field of typically several to several tens of Oersteds without paying any attention to the field dependency. The above observation tells us that the Meissner fraction observed under an arbitrary chosen magnetic

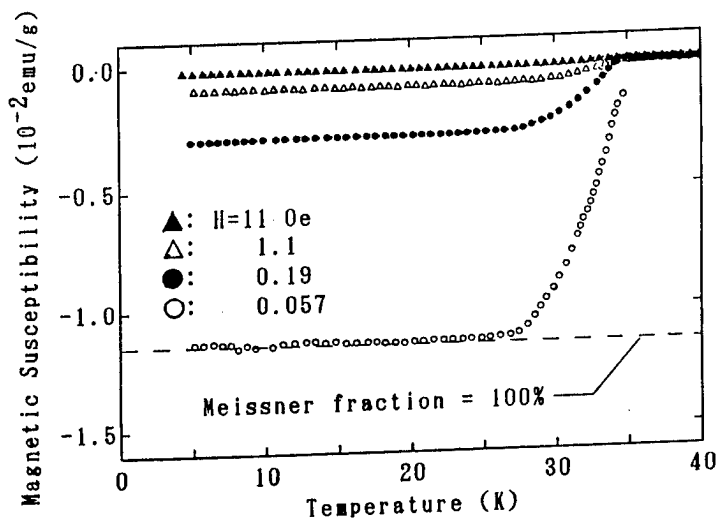


Fig. 1 The Meissner curves observed for a single-crystalline platelet of $(\text{La}_{0.94}\text{Sr}_{0.06})_2\text{CuO}_4$ (sample A-1) under different magnetic fields applied along the a-axis.

field cannot be used for any meaningful evaluation.

The dependence of the Meissner fraction on the measurement field has first been pointed out by Krusin-Elbaum, Malozemoff et al. [10] for $\text{Ba}_2\text{YCu}_3\text{O}_y$ single-crystalline specimens. The present measurement confirms their results also in LSCO. According to the Ginzburg-Landau theory, they predicted the $H^{-1/3}$ dependence of the Meissner fraction. Figure 2 shows the log-log plot of the Meissner fraction against the field. From the figure, one may approximate the dependence as $H^{-\alpha}$ but the power α has turned out to the range over $0.3 \sim 0.7$ in case of LSCO single-crystals depending on the field direction and on the shape of the specimen. Therefore, some other or additional mechanism must be sought in order to explain the dependence quantitatively.

Figure 3 shows the dependence of the Meissner fraction on the thickness of the specimen. It is clear that the Meissner fraction increases as the sample thickness decreases. This is perhaps the first observation to demonstrate the effect of sample size on the Meissner fraction, indicating the surface effect must be involved in the determining mechanism of the effect.

In order to further delineate the effect of sample size, the Meissner fraction vs. magnetic field relationships are compared for single-crystalline, poly-crystalline and powder specimens of $\text{Bi}_2\text{Sr}_2\text{CaCu}_2\text{O}_y$ in Fig. 4. The following three statements may be made from the figure. First of all, the powder specimen keeps quite a high level of the Meissner fraction up to a magnetic field about 10 Oe whereas both single- and poly-crystalline specimens show decrease in their Meissner fraction with increasing the field even in the lowest field range. Secondly, in the case of the poly-crystalline specimen, there is an intermediate range where the Meissner fraction stays nearly constant (about 30% in Fig. 4) with the increase in the magnetic field over about 0.3 to 40 Oe, while that of the single-crystal goes further down. Thirdly, the single-

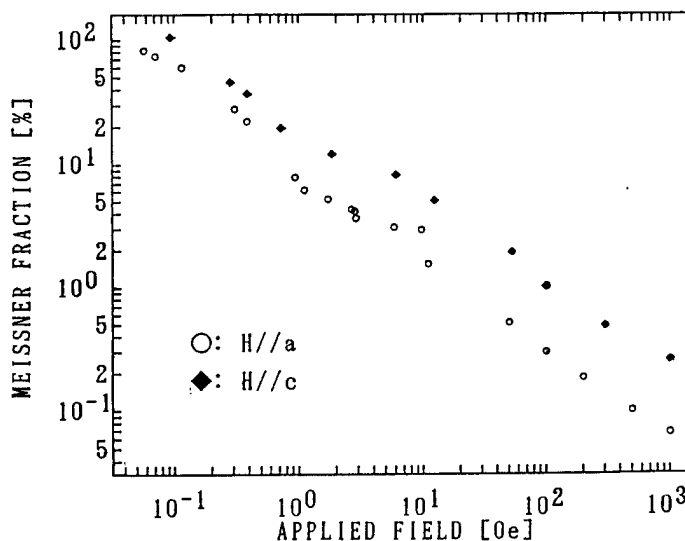


Fig. 2 The Meissner fraction f_M observed as a function of the field for a single-crystalline specimen of $(\text{La}_{0.94}\text{Sr}_{0.06})_2\text{CuO}_4$ (sample A-1) without considering the demagnetizing factor. The field direction was along the a or c axis.

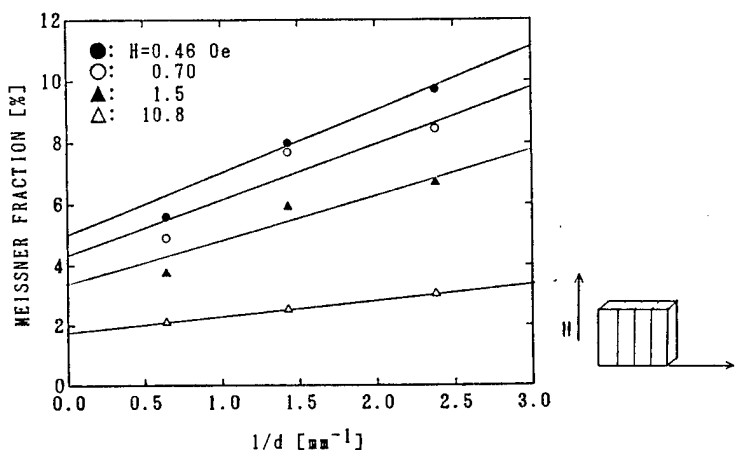


Fig. 3 Meissner fraction f_M of $(\text{La}_{0.94}\text{Sr}_{0.06})_2\text{CuO}_4$ single crystal samples B-1, B-2 and B-3 under various magnetic fields as a function of the thickness of the specimens.

crystalline specimen exhibits the lowest Meissner fraction over the whole range, although in the lowest field range, both single- and poly-crystalline specimens attain nearly 100% of the Meissner fraction. It is quite remarkable that the behavior of poly-crystalline specimen is quite similar to the single-crystal under the lowest field, while it resembles to the powder under the highest field, leaving the flat cross-over region in the intermediate range.

Figure 5 further supplements the above observation in the case of LSCO. The flat region is clearly observed in the poly-crystalline specimen in the intermediate field range over 0.1 to 10 Oe, while the single-crystalline specimen decreases in the Meissner fraction in this range as well. It is seen in the figure that the two curves cross each other at about 0.3 Oe. This is probably because the thickness of the poly-crystalline sample (ca. 0.55mm) is larger than that of the single-crystalline sample (ca. 0.2mm) in case of Fig. 5 as will be discussed later.

Therefore, the appropriate model of the flux expulsion process to give the Meissner signal must be able to explain the above stated unique features of the shape effect as well as the field dependence.

Model of Flux Expulsion

Oxide superconductors is known to be the type 2 superconductors. Schematically the equilibrium

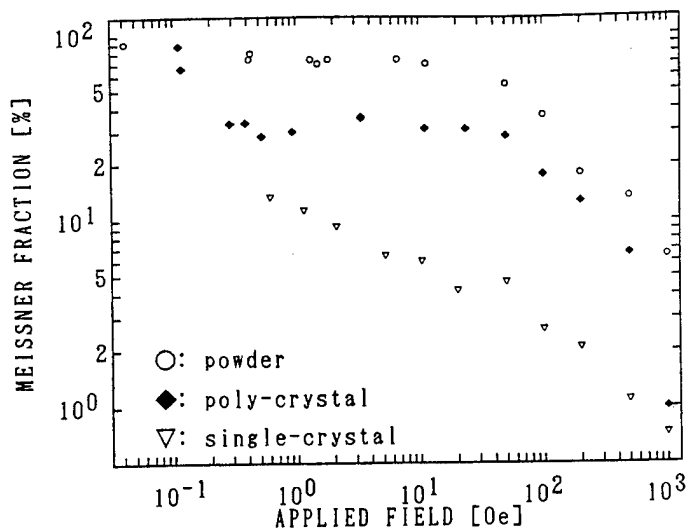


Fig. 4 Dependence of Meissner fraction f_M of single-crystal ($H//a$), poly-crystal (grain size 2-50 μm) and powder (1-20 μm) specimens of $\text{Bi}_2\text{Sr}_2\text{CaCu}_2\text{O}_y$ on the intensity of magnetic field.

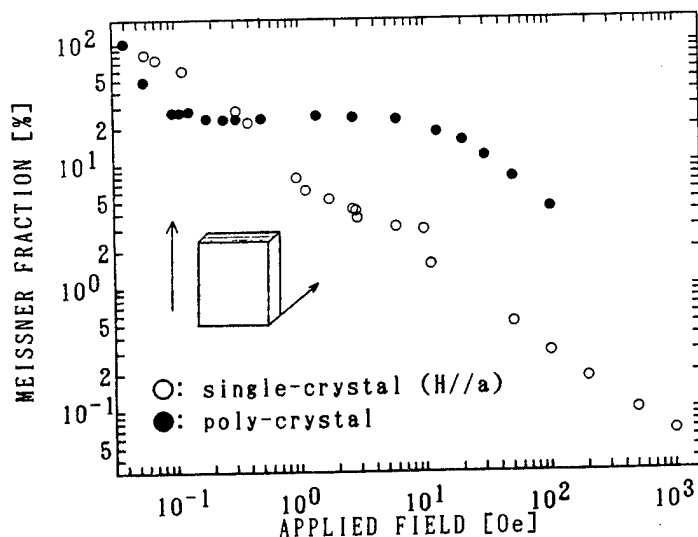


Fig. 5 Dependence of Meissner fraction f_M of single-crystal (sample A-1) and poly-crystal specimens of $(\text{La}_{0.94}\text{Sr}_{0.06})_2\text{CuO}_4$ as a function of the applied magnetic field. The orientation of the sample and field direction is shown.

magnetization curve of a type 2 superconductor can be illustrated as shown in Fig. 6. The straight line is the portion of the perfect diamagnetism, $-4\pi M = H$. The equilibrium magnetization curve becomes larger as the temperature T is lowered below T_c . Therefore when the external field H is set at C in the figure as an example, the expected Meissner fraction will be equal to BC/AC at $T=T_1$ and it will become larger as T is lowered further to T_2 and T_3 , finally become 100% at the temperature where $H_{c1}(T) = H$.

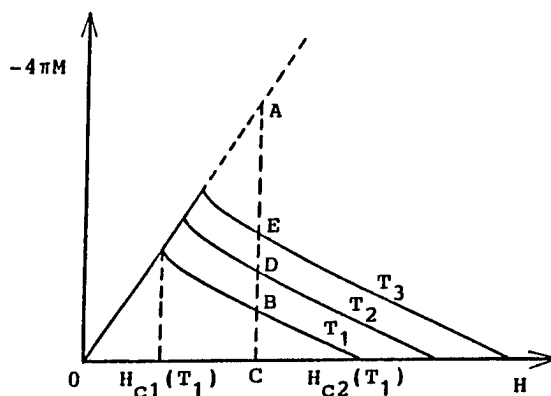


Fig. 6 Equilibrium magnetization curves of the type 2 superconductor at various temperatures : $T_1 > T_2 > T_3$.

Therefore if H is set higher than $H_{c1}(T=0K)$, the Meissner fraction will be smaller than 100% even at the lowest temperature. However, this cannot be the reason for the incomplete diamagnetism observed in the usual experiments (H is set several to several tens of Oersted) because $H_{c1}(T=0K)$ is known to be more than 50 Oe in the typical cuprate superconductors, such as LSCO and YBCO.

Krusin-Elbaum, Malozemoff et al. assumed that the flux expulsion process during the manifestation of the Meissner effect in the type 2 superconductor takes place reversibly down to a temperature when the vortex motion becomes irreversible, $T^*(H)$ and stops below this temperature due to the strengthened pinning force [10]. Therefore, if T_2 is set equal to $T^*(H)$, then the Meissner fraction attained by the process down to $T=T^*(H)$ can be expressed as DC/AC . It has been noticed in the cuprate superconductors that the irreversibility temperature T^* depends on the magnetic field as $(1-T^*/T_c) \propto H^{2/3}$. According to the GL theory, one may approximate the M - H curve in the vortex state (mixed state) by a straight line as $-M \propto (1-T/T_c)$. Then the Meissner fraction $f_M (= -4\pi M/H)$ can be expressed as $f_M(T, H) \propto (1-T/T_c)/H$ and hence $f_M(T^*)$ is proportional to $H^{2/3}/H = H^{-1/3}$. This is the essential process how Krusin-Elbaum et al. has predicted the $H^{-1/3}$ dependence of f_M .

The experimental observations described above, however, have given a rather stronger dependence on the field, $H^{-\alpha}$ with α up to about 0.7. Besides, Krusin-Elbaum et al's model cannot explain the size effect i.e., the surface effect. Therefore we will pay our attention to the fact that the flux expulsion must proceed via the escape process of vortices out of the sample surface. We assume that there is an additional expulsion of vortices in the vicinity of the surface even after the bulk motion of vortices have stopped due to irreversibility below T^* .

A) Model for a semi-infinite solid

Figure 7 illustrates our model. For simplicity, we take a slab of infinite area as the specimen with semi-infinite thickness. We assume the following processes to occur successively as T is lowered below T_c .

1) $T_c > T > T^*$

The flux expulsion proceeds reversibly and hence the internal flux density $B(T, x)$ decreases homogeneously in the slab down to $B_{eq}(T^*, H)$

2) $T^* > T$

2-1) A decreasing gradient will develop in $B(T, x)$ towards the surface below $T=T^*$. For simplicity, let us assume that we have lowered T from T^* stepwise to T_1 . Then the surface flux density $B(T_1, H, x=0)$ should become equal to the equilibrium value $B_{eq}(T_1, H)$ as given by the scheme in Fig.6. The vortices in the vicinity of the surface should then be expelled until a flux density

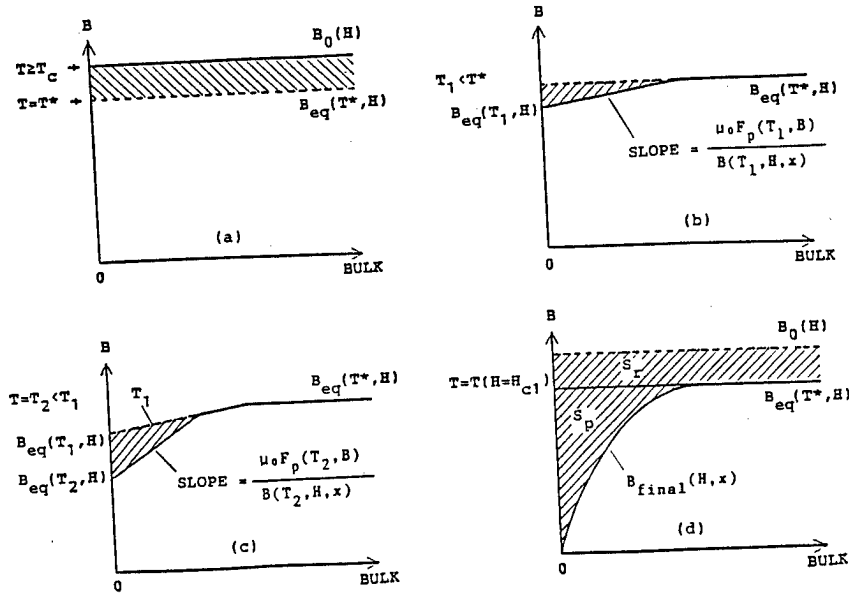


Fig. 7 The distribution of magnetic flux density B expected in a type 2 superconductor of a semi-infinite thickness according to the proposed model in the field-cooling process when the temperature is lowered down to (a) T^* (see text), (b) then step-wise to T_1 , (c) then again step-wise to T_2 ($< T_1$) and (d) for the case when T is lowered continuously from above T_c down below $T = T(H = H_{c1})$. the shaded area stands for the amount of vortices expelled during each of cooling processes.

gradient develops to balance the pinning force according to the Bean's critical state model [11],

$$dB(T_1, H, x)/dx = \mu_0 F_p(T_1, B)/B(T_1, H, x) \quad (1)$$

where F_p is the pinning force per unit volume and μ_0 is the permeability of vacuum. The final distribution of the flux density is expected to be as illustrated as in Fig. 7b. The shaded area stands for the amount of vortices expelled during this process. Strictly speaking, eq.(1) does not give a straight line because B is a function of x . But for the sake of simplicity, we approximate a constant gradient in this argument. A more rigorous treatment is given in the appendix.

2-2) Let us now suppose that we further lower T again step-wise down to $T_2 < T_1$. Then it is expected that $B(T_2, H, x=0) = B_{eq}(T_2, H) < B_{eq}(T_1, H)$ and vortices will further be expelled to attain $dB(T_2, H, x)/dx = \mu_0 F_p(T_2, B)/B(T_2, H, x)$ as the gradient of the flux density in the vicinity of the surface. No vortex motion is expected in the deeper region than $x = x_2$ where the two curves $B(T_1, H, x)$ and $B(T_2, H, x)$ cross as shown in Fig. 7c.

2-3) In the case if we gradually lower T , we can treat it just by repeating the infinitesimally small step-wise processes as 2-2) down to the lowest temperature of the measurements. The final distribution of flux density is then expected to become as illustrated in Fig. 7d. The shaded area S_r corresponds to the amount of flux expelled during the reversible expulsion process down to $T = T^*(H)$ and S_p to that expelled in the vicinity of the surface against the increasing pinning force below $T = T^*(H)$. Therefore, we expect an additional contribution, S_p to the Meissner effect according to this model than predicted by Krusin-Elbaum et al's model which considers contribution to the Meissner fraction only from the shaded area, S_r .

B) Model for a thin slab

We now extend our model to the case when the sample thickness is finite and equal to L as shown in Fig. 8. In this case, the vortex expulsion occurs on both sides and the expected distribution of flux density is shown in the figure. If the flux in the unshaded area S_u were expelled, the perfect

diamagnetism would result. Therefore the actual Meissner fraction f_M at the lowest temperature should be expressed as

$$\begin{aligned}
 f_M &= \frac{S_r + 2S_p}{S_r + 2S_p + S_u} \\
 &= \frac{[B_0(H) - B(T^*, H)] L}{B_0(H) L} + \frac{2S_p}{B_0(H) L} \\
 &= \left[1 - \frac{B(T^*, H)}{B_0(H)} \right] + \frac{2S_p}{B_0(H) L} \\
 &= C H^{-1/3} + \frac{2S_p}{B_0(H) L} \quad (2)
 \end{aligned}$$

where C is a constant. The first term in the last equation is the same as predicted by Krusin-Elbaum and is proportional to $H^{-1/3}$.

Therefore, if the second term gives us a significant contribution, a plot of f_M vs. $1/L$ should give a straight line unless L is too small and the two shaded areas of S_p 's overlap on each other. This is because both the quantities S_p and $B_0(H)$ are independent of L . The straight line should extrapolate to $CH^{-1/3}$ at $1/L = 0$. In Fig. 3, the straight lines have been drawn through the data points so that $H^{-1/3}$ relation to hold at $1/L=0$. Although the data have not been extensive enough, they appear to essentially support the prediction.

It is noticed in Fig. 3 that the relative contribution from the second term increases as the field is decreased and as the thickness of the sample decreases. It is about equal to that from the first term for the thinnest sample ($L=0.42\text{mm}$) under the field $H=0.46$ Oe. Therefore a dominant contribution is expected from the second term in case of a fine-grained powder specimen. From fig. 3, we can roughly estimate the thickness of the specimen at which nearly 100% Meissner fraction is achievable by extrapolating the straight line to $f_M = 100\%$. Under $H=10.8$ Oe for example, the estimate gives $6 \mu\text{m}$ while it is estimated to be $23 \mu\text{m}$ under $H=0.46$ Oe. This estimation can explain why the Meissner fraction is nearly 100% in the powder specimen up to a rather high magnetic field. In the case of $\text{Bi}_2\text{Sr}_2\text{CaCu}_2\text{O}_y$ (the anisotropic grain size ranging over $2\text{--}50 \mu\text{m}$), the Meissner fraction decays only slightly up to the field about 50 Oe. We have not succeeded in the corresponding measurements on LSCO powders. But the arguments here seem to be justifiable because f_M is only slightly larger for single-crystalline $\text{Bi}_2\text{Sr}_2\text{CaCu}_2\text{O}_y$ (thickness 0.1mm) than for single-crystalline LSCO (thickness 0.2mm) to allow the similar estimation in both of the materials.

C) Model for polycrystalline specimens

It has been known that poly-crystalline boundaries in the cuprates raise weak coupling of superconductivity between the grains. Under a weak field, however, the coupling should appear to be still strong enough and hence the poly-crystalline specimen should behave like a single body against the vortex motion. On the other hand, it should appear to be weak under a strong magnetic field and then grain boundaries should become the easy paths for vortices. Then a poly-crystalline body should be equivalent to an assembly of many isolated particles.

In this line, the cross-over behavior in the f_M - H curves in Figs. 4 and 5 of the poly-crystalline specimens can readily be explained. The cross-over is taking place over the field range

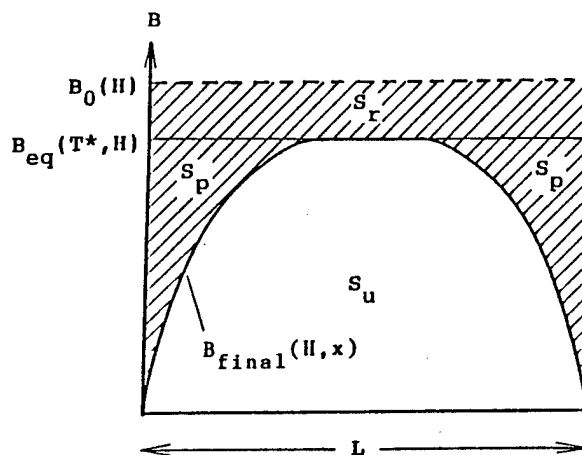


Fig. 8 The final distribution of flux density after the field cooling process of a slab with a finite thickness, L . The Shaded area represents the amount of the flux expelled during the whole process. The unshaded area corresponds to the amount of flux trapped.

from about 0.3 Oe to 40 Oe in the case of $\text{Bi}_2\text{Sr}_2\text{CaCu}_2\text{O}_y$. It can then be expected that the Meissner fraction in the flat cross-over region should become the larger if the boundary coupling is the weaker. This argument suggests us that the f_M -H curve of a poly-crystalline specimen should be able to be utilized to evaluate the superconducting coupling strength of the grain boundaries.

Summary

As has been described, the development of diamagnetism due to the flux expulsion during the field cooling process can be systematically understood if the pinning force is taken into account which intensifies as the temperature is lowered. In the field range frequently used for the Meissner signal measurement, the Meissner fraction is in the order : powder > poly-crystal > single-crystal for the cuprate superconductors provided that the thicknesses of the poly- and single-crystals are the same. A systematic study can provide informations on pinning force and on the weak link of superconductivity. A semi-quantitative model has been presented.

Appendix

$B_{\text{final}}(H, x)$ is the distribution of magnetic flux density after field cooling process: $T (\geq T_c) \rightarrow T_0 (H = H_{c1}(T_0))$. Generally, S_p in the Eq.(2) is given as

$$S_p = \int_0^\infty [B_{\text{eq}}(T^*, H) - B_{\text{final}}(H, x)] dx. \quad (\text{A-1})$$

It is possible to determine $B_{\text{final}}(H, x)$, if pinning force $F_p(T, B)$ is known as a function of T and B , and $B_{\text{eq}}(T, H)$ as a function of T and H . At present time, however, $F_p(T, B)$ is not known in detail. So, we simply assume here that $J_c(T, B) = F_p(T, B)/B(T, H, x)$ is independent of B in the limit of small B as in this case of Meissner measurements. Then,

$$\mu_0 F_p(T, B)/B(T, H, x) = \partial B(T, H, x)/\partial x = \mu_0 J_c(T). \quad (\text{A-2})$$

And hence, the magnetic flux density is expressed as

$$B(T + \Delta T, H, x) = \mu_0 J_c(T + \Delta T)x + B(T + \Delta T, H, 0) \quad (\text{A-3})$$

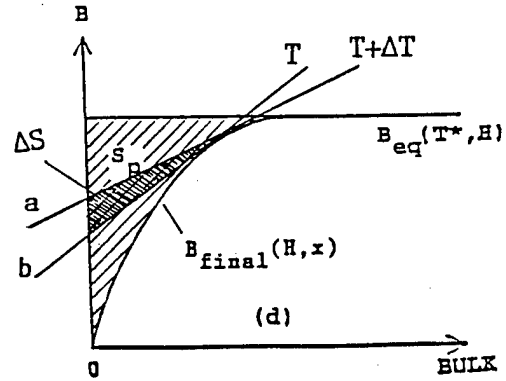
for $0 \leq x \leq x(T)$ at $T = T + \Delta T$, and

$$B(T, H, x) = \mu_0 J_c(T)x + B(T, H, 0) \quad (\text{A-4})$$

for $0 \leq x \leq x(T)$ at $T = T$. $x(T)$ is the crossing point for two straight lines a and b obtained by Eqs. (A-3) and (A-4), respectively, and is expressed as:

$$x(T) = -[B(T + \Delta T, H, 0) - B(T, H, 0)] / \mu_0 [J_c(T + \Delta T) - J_c(T)]. \quad (\text{A-5})$$

Then we can estimate the amount of vortices expelled in this process, ΔS :



$$\Delta S = (1/2)[B(T+\Delta T, H, 0) - B(T, H, 0)]x(T) . \quad (A-6)$$

And hence,

$$\begin{aligned} S_p &= \lim_{\Delta T \rightarrow 0} \sum \Delta S \\ &= \lim_{\Delta T \rightarrow 0} \sum \frac{1}{2} [B(T+\Delta T, H, 0) - B(T, H, 0)]x(T) \\ &= \lim_{\Delta T \rightarrow 0} \sum \frac{1}{2} [B(T+\Delta T, H, 0) - B(T, H, 0)] \frac{[-\partial B(T, H, 0)/\partial T]}{\mu_0[dJ_c(T)/dT]} \\ &= -\frac{1}{2} \int_{T_0}^{T^*} \frac{[\partial B_{eq}(T, H)/\partial T]^2}{\mu_0 dJ_c(T)/dT} dT . \end{aligned}$$

References

- [1] S.H. Bloom, M.V. Kuric, Y.S. Yao, R.P. Guertin, D. Nichols, C. Tee, A. Kebede, J.E. Crow, T. Mihalisin, G.N. Myer and P. Shulottmann, "High-Temperature Superconductors", Eds, M.B. Brodsky, R.C. Dynes, K. Kitazawa, H.L. Tuller, MRS (1988) p.19.
- [2] R.B. van Dover, R.J. Cava, B. Batlogg and E.A. Rietman, Phys. Rev. B35, 5337 (1987).
- [3] R.J. Bigeneau, D.R. Gabbe, H.P. Jenssen, M.A. Kastner, P.J. Picone, T.R. Thurston, G. Shirane, Y. Endoh, M. Sato, K. Yamada, Y. Hidaka, M. Oda, Y. Enomoto, M. Suzuki and T. Murakami, Phys. Rev. B38, 7316 (1989).
- [4] I. Tanaka, K. Yamane and H. Kojima, J. Crystal Growth 96, 711 (1989).
- [5] G. Shirane, R.J. Birgeneau, Y. Endoh, M.A. Kastner, K. Kitazawa, H. Kojima, I. Tanaka, T.R. Thurston and K. Yamada, Phys. Rev. Lett. 63, 330 (1989).
- [6] S. Kambe, M. Naito, K. Kitazawa, I. Tanaka and H. Kojima, Physica C160, 243 (1989).
- [7] K. Kitazawa, S. Kambe, A. Fukuoka, M. Naito, I. Tanaka and H. Kojima, Mater. Res. Soc. Symp. Proc. May 31 - June 3, Tokyo (1988).
- [8] K. Kishio, N. Sugii, K. Kitazawa and K. Fueki, Jpn. J. Appl. Phys. 26, L466 (1987).
- [9] M. Motohira, K. Kuwahara, T. Hasegawa, K. Kishio and K. Kitazawa, J. Ceram. Soc. Jpn. 97, 1009 (1989).
- [10] L. Krusin-Elbaun, A.P. Malozemoff, Y. Yeshurun, D.C. Cronemeyer and F. Holtzberg, Physica C153, 1469 (1988).
- [11] C.P. Bean, Phys. Rev. Lett. 8, 250 (1962).

Experimental and Theoretical High- T_c Research at Ibaraki University

Takekazu ISHIDA, Shokichi KANNO, and Toku SASAKI

Department of Physics, Faculty of Science, Ibaraki University, Mito 310, Japan

(Received January 10, 1990)

I. Quenching and phenolization: We investigated the effect of quenching and phenolization on T_c of three Bi-based compounds $\text{Bi}_2\text{Sr}_2\text{Ca}_n\text{Cu}_{1+n}\text{O}_{6+2n}$ ($n = 0, 1, 2$). By quenching, T_c of 2201 phase was raised from 6 K to 16 K and T_c of the 2212 phase increased from 69 K to 96 K. The 2223 phase remained to be 110 K superconductor when a quenching temperature T_q was less than 650°C. This suggests that hole concentration is in surplus in the as-prepared 2201 and 2212 compounds. Comparable T_c enhancement was observed by phenolization for the 2201 and 2212 phases.

II. Nonlinear susceptibility: The complex harmonic magnetic susceptibility $\chi_n' - i\chi_n''$ of sintered $\text{YBa}_2\text{Cu}_3\text{O}_{7-\delta}$ has been investigated as a function of superimposed dc magnetic field. The intergrain characteristics were qualitatively reproduced from the Kim critical state model. This indicates that the intergrain property belongs to the standard type II.

III. Interacting hole-spin model of CuO_2 plane: A model describing the high- T_c superconductivity has been proposed. The Hamiltonian contains the exchange and superexchange interactions. We present the phase diagram of the CuO_2 system as a function of hole density. The domain structure is essential to explain the superconductivity and the magnetic structure. The model predicts the singlet superconductivity.

I. Critical Temperature Control of Bi-Based Oxides by Quenching and Phenolization

The Bi-based cuprous oxide superconductors can be classified into three types depending on the number of CuO_2 stackings. T_c is known to increase as the number of stackings increases, but it is not known what discriminates T_c of the Bi compounds. We examined the effect of the high temperature quenching on T_c of the Bi-based compounds.¹⁻⁶

The samples were prepared by a solid state reaction from Bi_2O_3 , Pb_2O_3 , SrCO_3 , CaCO_3 and CuO . After pelletizing, the 2201 phase ($\text{Bi}_2\text{Sr}_2\text{CuO}_x$) was reacted at 760°C for 96 h, the 2212 phase was reacted at 840°C for 114 h, the 2212 phase ($\text{Bi}_2\text{Sr}_2\text{CaCu}_2\text{O}_x$) was reacted at 840°C for 17 h and at 850°C for 24 h, and the 2223 phase ($\text{Bi}_{1.92}\text{Pb}_{.48}\text{Sr}_2\text{Ca}_2\text{Cu}_{3.2}\text{O}_x$) was reacted at 845°C for 180 h. The X-ray analyses showed that the 2212 and 2223 samples were almost single phase but the 2201 sample contains the smaller amount of the second phase.

The samples were quenched from a high temperature (T_q) into liquid nitrogen. The resistivity was measured by the dc four terminal method. In the followings, we present T_c by temperatures of 10, 50, 90% resistive changes. In Fig. 1, we show T_c of the 2201 phase as a function of T_q . The midpoint T_c increased from 6 K to 16 K. In Fig. 2, we show T_c of the 2212 phase as a function of T_q . Above 300°C, the midpoint T_c increases from 69 K to 96 K.³ We first confirmed that the zero-resistivity temperature exceeded 90 K.⁵ This demonstrated that practically the 2212

phase is not inferior to the Y-Ba-Cu-O system. In Fig. 3, we show T_c of the 2223 phase as a function of T_q . Below 650°C, T_c is almost constant while T_c decreases above that temperature.⁴ This is in contrast with those of 2201 and 2212 phases.

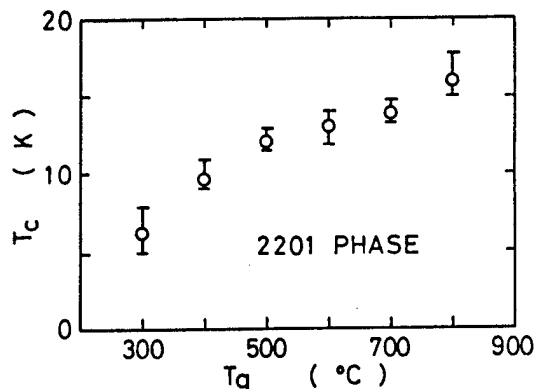


Fig. 1 T_c vs. T_q (2201 phase).

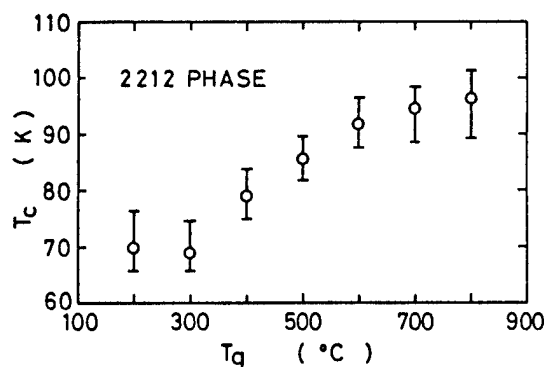


Fig. 2 T_c vs. T_q (2212 phase).

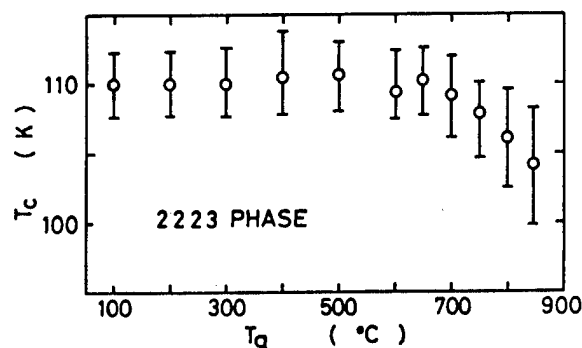


Fig. 3 T_c vs. T_q (2223 phase).

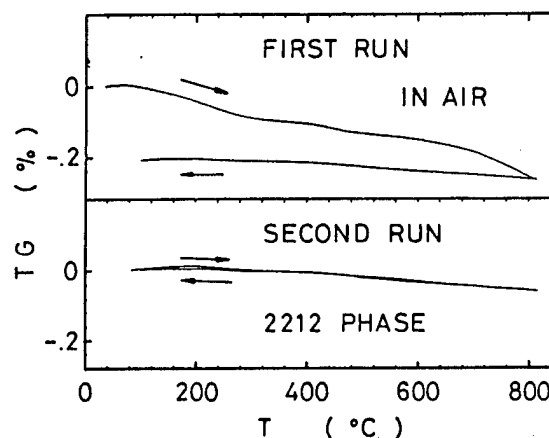


Fig. 4 TG data (2212 phase).

In Fig. 4, we show the thermogravimetric (TG) analyses of the 2212 sample measured in air flow of 200 ml/min. We minimized the effect of the ambient temperature fluctuation on the TG balance. The first run is not reversible for temperature increase and decrease of rate 20°C/min. This is probably due to the water vapor adsorbed during pulverization of the sample. Therefore, from the second reversible run, we estimated the change in the oxygen number by assuming the standard formula $\text{Bi}_2\text{Sr}_2\text{CaCu}_2\text{O}_8$. The oxygen number decreased only by 0.037 when the temperature increased from 200°C to 800°C. This smallness rules out the possibility to explain the T_c alteration solely by the oxygen stoichiometry.

We speculate that holes for the CuO_2 layer are supplied by the $(\text{BiO})_2$ layer. Quenching controls the amount of charge transfer presumably by inducing atomic disorder, resulting in changes in the superconducting and normal-state properties.⁶

Our results suggest that holes are overdoped in the as-prepared 2201 and 2212

compounds. Later, it was reported that hydrogen absorption in powdered 2212 sample also results in an increase of T_C .⁷ Hydrogen may decrease hole concentration in BSCCO. We examine a simple alternative method that controls the hole concentration of BSCCO. Hydrogen ions exist in an acid solution, but a strong acid would dissolve the sample of superconductor. The acidity of phenol is more moderate. We examined phenol as the simplest example of the phenolic acids.⁸ The 2201 sample was soaked in an ethanol solution of phenol for 15 h, reacted at a certain temperature $T_a = 150^\circ\text{C}$ for 24 h, and then quenched into room temperature in air. The midpoint T_C was found to increase from 6 K to 14 K. In Fig. 5, we show T_C of the 2212 phase as a function of T_a . Below 300°C , T_C is enhanced due to the effect of the phenolization while the effect of quenching becomes dominant above 300°C (compare Figs. 2 and 5). A heat treatment of the phenolized 2212 sample at 200°C resulted in the T_C increase from 72 K to 93 K.

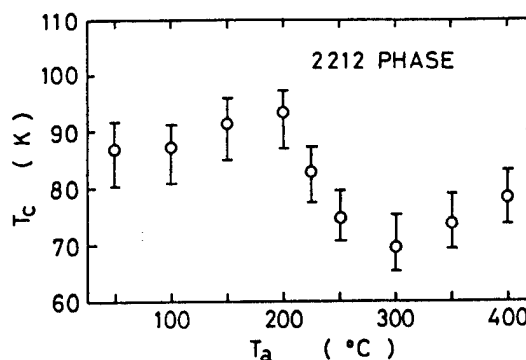


Fig. 5 Effect of phenolization.
 T_C vs. T_a (2212 phase).

1. T. Ishida and T. Sakuma, Jpn. J. Appl. Phys. 27, L1237 (1988).
2. T. Ishida, H. Mazaki, and T. Sakuma, Jpn. J. Appl. Phys. 27, L1626 (1988).
3. T. Ishida, Jpn. J. Appl. Phys. 27, L2327 (1988).
4. T. Ishida, Jpn. J. Appl. Phys. 28, L197 (1989).
5. T. Ishida, Jpn. J. Appl. Phys. 28, L573 (1989).
6. T. Ishida, S. Nakamura, Y. Iye, K. Koga, S. Okui, K. Kanoda, and T. Takahashi, Proceedings of M²S-HTSC (Stanford Univ., 1989) (to be published).
7. T. Takabatake et al., Physica C157, 263 (1989).
8. T. Ishida, Appl. Phys. Lett. 55, 1457 (1989).

II. Nonlinear Susceptibility of $\text{YBa}_2\text{Cu}_3\text{O}_{7-\delta}$

The ac susceptibility is useful for characterizing high- T_C superconductors.¹ A sintered oxide superconductor can be modeled as a system in which the superconducting grains are weakly coupled. In such materials, the susceptibility has both intrinsic and coupling components. The coupling component is very sensitive to both T and H_{ac} . This can be explained by the Ishida-Mazaki model, which predicted the appearance of the odd harmonic susceptibilities.²

The complex harmonic magnetic susceptibility $\chi_n' - i\chi_n''$ of sintered canonical oxide, $\text{YBa}_2\text{Cu}_3\text{O}_{7-\delta}$, has been investigated. The experimental variables for the measurement of χ_n were the sample temperature T ($10 < T < 110$ K), the ac magnetic field amplitude H_{ac} ($14 \text{ mOe} < H_{ac} < 85 \text{ Oe}$) and frequency f ($7.3 < f < 1460$ Hz), and the magnitude of a superimposed dc field H_{dc} ($0 < H_{dc} < 85 \text{ Oe}$). Details of our results will be published elsewhere.³

We compared the experimental harmonic susceptibilities with the theoretical ones. The calculation is based on the Kim critical state model for the critical

current density.⁴ We also used the analytic formula of the sample magnetization derived by Ji et al.⁵ We numerically obtained the harmonic susceptibilities by the Fourier transformation. The T - and H_{dc} - dependences of intergrain characteristics agreed well with the calculation from the simplified Kim model. As typical examples, we present the harmonic susceptibilities as a function of H_{dc} . In Fig. 1, we show the odd harmonics for $H_{ac} = 21.21$ Oe and -45 Oe $< H_{dc} < 45$ Oe. The theoretical curves in Fig. 2 are similar to the experimental ones. Figures 3 and 4 show the experimental and theoretical even harmonics. Good qualitative agreement was obtained for $n < 5$.

An important implication of the results is that the type of the intergrain superconductivity is conventional type II. Since the method probes the motion of flux quanta, it should be useful as a sensitive probe of vortex dynamics.

This work has been done in collaboration with R. B. Goldfarb (NIST, Boulder).

1. T. Ishida, T. Sakuma, T. Sasaki, and Y. Kawada, Jpn. J. Appl. Phys. 28, L559 (1989).
2. T. Ishida and H. Mazaki, J. Appl. Phys. 52, 8798 (1981).
3. T. Ishida and R. B. Goldfarb, Phys. Rev. B (submitted to).
4. Y. B. Kim et al, Phys. Rev. Lett. 9, 306 (1962).
5. L. Ji et al., Phys. Rev. B (to be published).

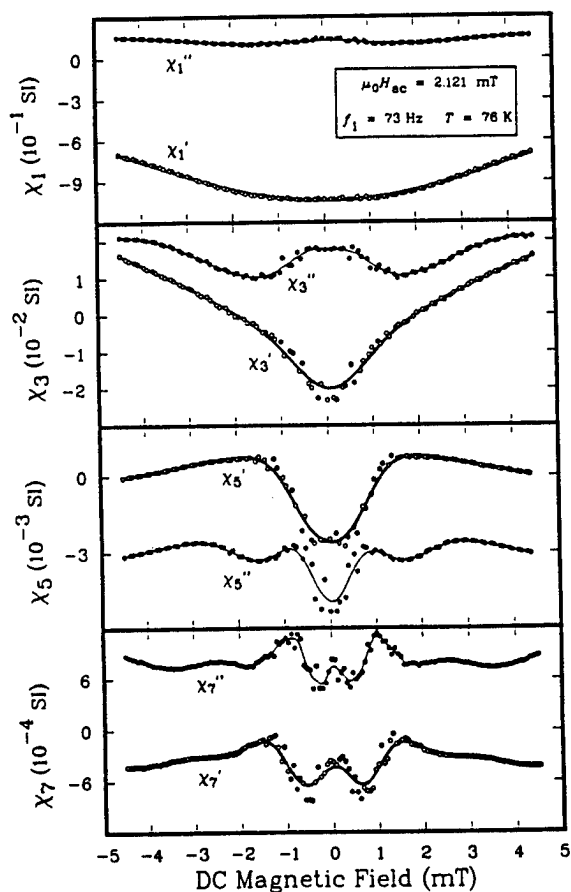


Fig. 1 Odd harmonics (experimental)

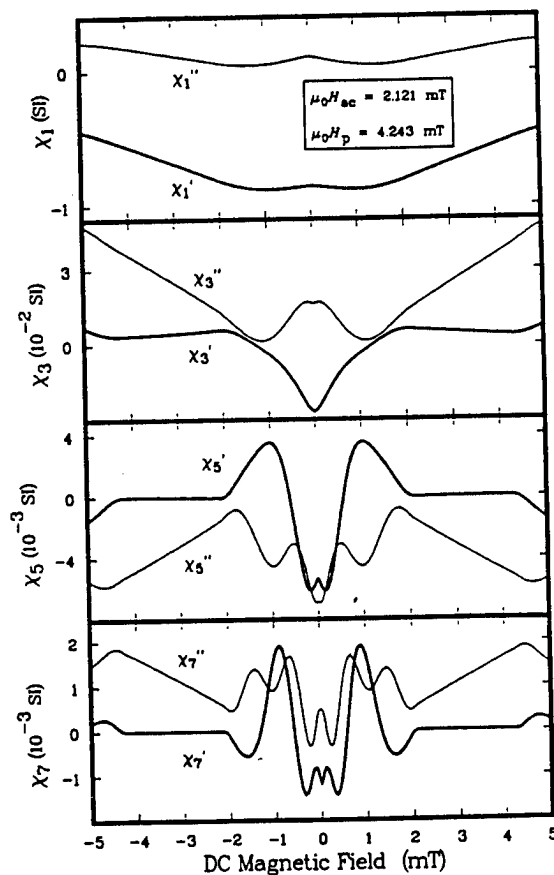


Fig. 2 Odd harmonics (theoretical)

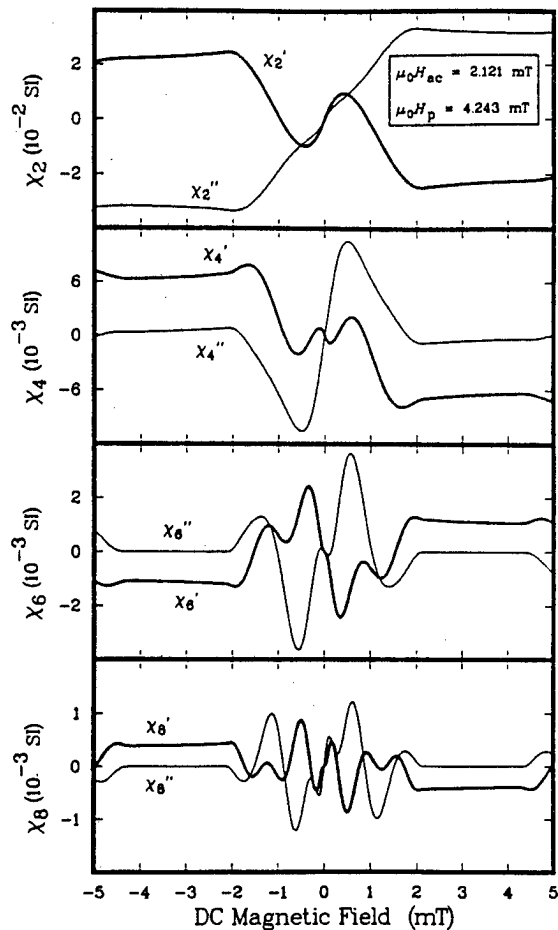
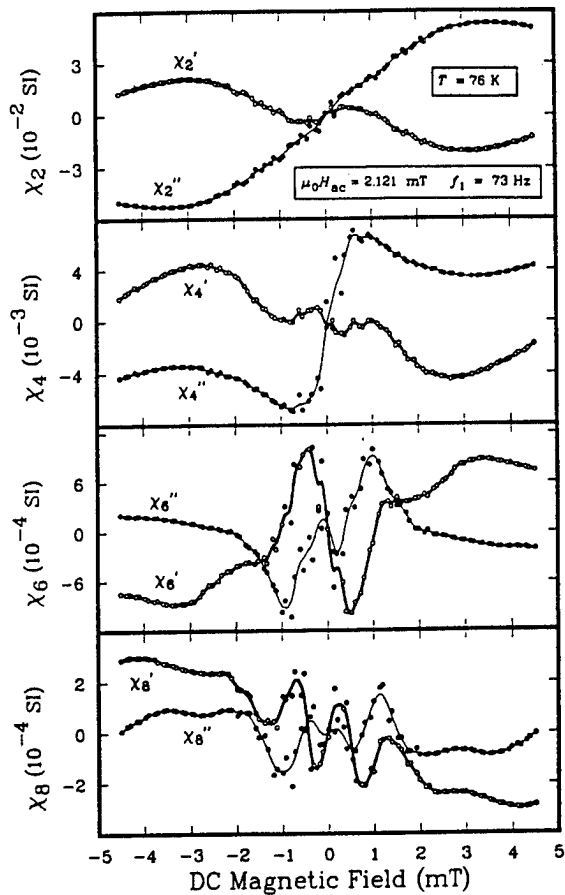


Fig. 3 Even harmonics (experimental). Fig. 4 Even harmonics (theoretical).

III. Magnetic Structure and Superconductivity in Interacting Hole-Spin Model for CuO₂ plane

Model Hamiltonian

The CuO₂ plane contained in cuprous oxides is believed to play a crucial role in superconductivity. Besides, the certain amount of holes is necessary to achieve the high-T_c superconductivity. Photoemission experiments have insisted that the oxygen 2p orbitals carry conductive holes while the copper 3d orbitals are well localized due to the strong Coulomb correlation.¹ Our picture is as follows: Holes are doped into oxygen 2p levels, travel around by quantum mechanical hopping, and work the Cu localized spins through the exchange interaction. Localized spins are correlated with each other through the antiferromagnetic superexchange interaction. We start from the following two dimensional Hamiltonian²

$$H = H_h + H_s + H_I \quad (1)$$

with

$$H_h = t_0 \{ a_{j+\delta}^\dagger a_j + \text{h.c.} \} \quad (2)$$

$$H_s = J \{ \mathbf{S}_j \cdot \mathbf{S}_{j+d} \} \quad (3)$$

$$H_I = (K/2) \{ \mathbf{S}_j \cdot (a_{j+\delta}^\dagger \boldsymbol{\sigma} a_{j+\delta}) \} \quad (4)$$

where H_h is the Hamiltonian for free holes, H_s expresses the antiferromagnetic

interaction between localized Cu^{2+} spins, and H_I represents the interaction between holes and localized spins. j denotes the Cu site of two dimensional CuO_2 plane. d and δ connect Cu^{2+} at j with its nearest neighbor Cu^{2+} and O^{2-} , respectively. $a_{j+\delta}^+ = (a_{j+\delta,+}^+, a_{j+\delta,-}^+)$ is two component spinor creating a hole at site $j+\delta$. S_j denotes the localized spin at j ($S = 1/2$). $\sigma = (\sigma_x, \sigma_y, \sigma_z)$ is the Pauli spin matrices. The antiferromagnetic superexchange coupling constant J , the exchange integral K , and the hopping integral t_0 are roughly given by

$$J = \epsilon^4 e^2 / a, K = \epsilon^2 e^2 / a, \text{ and } t_0 = \epsilon e^2 / a \quad (5)$$

where a is the nearest neighbor distance between Cu^{2+} 's, ϵ is the overlapping integral, and e is the electron charge. From Eq. (5) and $\epsilon \ll 1$, we obtain

$$J \ll K^2 / t_0 \ll K \ll t_0 \quad (6)$$

Since the unit cell contains two O^{2-} 's, one gets the "acoustic" and "optical" holes. The excitation of "optical" holes can be neglected if the hole density is not so high. Note that the energy of "optical" holes is higher than that of "acoustic" holes. The Hamiltonian (1) can be written as

$$H = \sum_p \epsilon_p a_p^+ a_p + KN^{-1/2} [S_{p-p'} \cdot (a_p^+ \sigma a_{p'})] + H_S \quad (7)$$

with

$$\epsilon_p = 2t_0[1 - \cos(ap_x/2)\cos(ap_y/2)] \quad (8)$$

$$S_k = N^{-1/2} \sum_j e^{ik \cdot r_j} S_j \quad (9)$$

where N is the total number of Cu^{2+} 's, and $a_p^+ = (a_{p,+}^+, a_{p,-}^+)$ is the spinor creating an "acoustic" hole with momentum p . For simplicity, we deal with the low energy excitation of holes (the Fermi momentum $p_F \ll 1/a$). Eq. (8) is reduced to $\epsilon_p = (1/4)t_0 a^2 p^2$.

Magnetic structure

We apply the variational method to evaluate the energy of the Hamiltonian (7). First, if Cu^{2+} spins are in antiferromagnetic state and holes are degenerated, the expectation value of energy per unit cell is

$$E/N = (2/N) \sum_{p < p_F} \epsilon_p - \alpha J = (t_0^2 / 16\pi) (ap_F)^2 - \alpha J = (\pi t_0 / 4) n_h^2 - \alpha J \quad (10)$$

where n_h is the hole number per unit cell, and $-\alpha J$ is the ground state energy of H_S (α is a constant of order unity).

Next, we consider the configuration where all localized Cu^{2+} spins are aligned in the same direction. That is, the system energy for H_S becomes maximum. The interaction between holes and localized spins is equivalent to the problem that the external magnetic field K is applied to the holes of magnetic moment 1. As is well known, the energy is given by³

$$E/N = (\pi t_0 / 2) n_h^2 - K n_h + J \quad \text{for } n_h \leq 2K / \pi t_0 \quad (11)$$

$$E/N = (\pi t_0 / 2) n_h^2 - K^2 / \pi t_0 + J \quad \text{for } n_h \geq 2K / \pi t_0 \quad (12)$$

where NJ is the possible maximum energy of H_S . When $n_h \leq 2K / \pi t_0$, all spins of the holes are aligned in the same direction. When $n_h \geq J/K$, the ferromagnetically aligned configuration is preferential than the antiferromagnetic configuration for localized spins because $J \ll K^2 / t_0$.

The system energy can be lowered further by introducing a domain structure of the localized spins. The domain is the compact region where all the localized spins are aligned in the same direction. In the followings, we explain the different phases as a function of hole density n_h .

Case: $n_h \lesssim (J/t_0)^{1/2}$ When localized spins are completely ordered in an antiferromagnetic manner, the number of domain is equal to that of holes. Each

domain contains a hole, of which the spin is antiparallel to the aligned localized spins in the domain. The linear domain size D_0 is given by $D_0/a = (t_0/J)^{1/4}$. The energy per unit cell is $E/N = (-K + (Jt_0)^{1/2})n_h - \alpha J$. The term $(-K + (Jt_0)^{1/2})$, the hole-domain "binding energy", is negative because $K \gg (Jt_0)^{1/2}$. The hole could not travel from the original domain because it is difficult to sweep away the whole domain in a time $-D_0/v$ (v ; the hole velocity). We reasonably conclude that the system is of the insulator nature. If the hole density increases to $n_h = (a/D_0)^2 = (J/t_0)^{1/2}$, then the localized spin system is perfectly covered with the domains. This means the disappearance of the antiferromagnetic state at that hole density.

Case: $(J/t_0)^{1/2} \lesssim n_h \leq 2K/\pi t_0$ The localized spin system forms the domain structure; there are no antiferromagnetic coupling between spins except the boundaries of the domains. Holes are trapped in the domains. All spins of the holes contained in a domain are aligned in the opposite direction to the aligned localized spins in the domain. The average linear size D_1 of the domains is given by $D_1/a = (t_0/J)n_h$. The energy correction to Eq. (11) is $\Delta E/N = -J^2/t_0 n_h$. In order that a hole travels from a domain to the next domain, the hole must have sufficiently large kinetic energy or must flip both its own spin and the localized spins; this process accompanies magnetic excitations. Since conductive holes should have energy larger than a definite value, the number of carriers should be limited. Thus, the hole system seems to behave like a semiconductor.

Case: $n_h > 2K/\pi t_0$ Again the system has the domain structure similar to the preceding case. The linear domain size D_2 is $D_2/a = K/J$. The energy correction to Eq. (12) is $\Delta E/N = -J^2/K$. There are enough untrapped holes of kinetic energy larger than K . In this case, the system becomes a hole conductor.

It is essential that the localized spin system goes from the antiferromagnetic ground state to "the state with nearly maximum energy of H_S " as n_h increases.

Superconductivity

In Fig. 1, the diagram gives the lowest hole-hole interaction, where the dashed line denotes the "magnon propagator". Assuming the spatial homogeneity, we have the effective interaction

$$H'_{eff} = K^2/12N \{ (a_{p1}^\dagger a_{p3})(a_{p2}^\dagger a_{p4}) \times [D(\epsilon_{p1} - \epsilon_{p3}, p_1 - p_3) + D(\epsilon_{p2} - \epsilon_{p4}, p_2 - p_4)] \} \quad (13)$$

with

$$D(\omega, k) = -i \int_{-\infty}^{\infty} dt e^{i\omega t} \langle \chi | TS_k(t) \cdot S_{-k}(0) | \chi \rangle \quad (14)$$

where $|\chi\rangle$ is the wave function of the localized spin. It is known that particles near Fermi surface play an important role in generating superconductivity. Our results are: (1) If $|\chi\rangle$ is the ground state of H_S , then the excitation energy is always positive and $D(\omega, k)$ becomes negative for small ω . Thus, from Eq. (13), the particles in singlet state interact repulsively with each other. (2) If $|\chi\rangle$ denotes the state with higher energy of H_S so that the "excitation energy" becomes negative, then $D(\omega, k)$ becomes positive for small ω ; the particles in "singlet" state interact attractively. The items (1) and (2) are true for any H_S and S_j as far as the interaction H_I (see Eq. (4)) is retained.

As stated before, the localized spins are of "nearly maximum energy for H_S " in hole-conducting regime. An important implication from the present model is, therefore, that the Cooper pairs are "singlet".

We apply the ferromagnetic magnon theory to calculation of $D(\omega, k)$. Bearing in

mind that the localized spin system has the domain structure, and taking the average of $D(\omega, \mathbf{p}_1 - \mathbf{p}_3)$ with respect to the angle between \mathbf{p}_1 and \mathbf{p}_3 , we have

$$H_{\text{eff}} = -(g/N) \sum_i a_{p1}^\dagger a_{p2}^\dagger a_{p3} a_{p4} \quad (15)$$

with

$$g = K^2/2Ja^2 p_F q - V_C \quad (16)$$

where $q = 1/D_2 = J/Ka$ and the Coulomb repulsion V_C is first introduced. The summation of momenta \mathbf{p}_i is restricted within $|\epsilon_{\mathbf{p}} - \epsilon_{\mathbf{F}}| \leq Ja^2(2p_F)^2$. Since the holes with kinetic energy higher than K can contribute to formation of the Cooper pairs, the mean-field transition temperature T_C is

$$T_C = (2\gamma/\pi k_B)(4Ja^2 p_F^2) \exp(-1/gN(0)) \text{ when } 2K/\pi t_0 \leq n_h \leq (K^2/2V_C Jaq)^2/2\pi \\ = 0 \quad \text{otherwise} \quad (17)$$

where $\ln \gamma = 0.577 \dots$ is the Euler constant, and $N(0) = 1/t_0$ denotes the energy density per oxygen atom at the Fermi level. T_C varies discontinuously from zero to the value given by Eq. (17) at $n_h = 2K/\pi t_0$. A more detailed analysis shows that T_C rises in the narrow range $\Delta n_h = JK/t_0$ at $n_h = 2K/\pi t_0$.

From the argument of magnetic structure and the T_C expression, we obtain the phase diagram for $T \ll T_N$ (Neel temperature) shown in Fig. 2, where AF, C, and S represent antiferromagnetic, conductive, and superconductive states, respectively. The phase diagram of Fig. 2 shows a qualitative agreement with the experimental one.

Our model shows that the high- T_C superconductivity is well described within the framework of the conventional BCS theory. Moreover, the Cu^{2+} localized spin system has the domain structure rather than the antiferromagnetic state. This is required to realize the singlet Cooper pairs. The experimental confirmation of the domain structure offers a check of our model. The present conclusions hold not only to hole superconductors but also to electron superconductors. The requirement for the latter is that conductive electrons of the kinetic energy $-t_0 a^2 p^2$ interact with antiferromagnetic spin system through spin coupling under the assumption of Eq. (6).

1. See for example, T. Takahashi et al., Nature 334, 691 (1988).
2. S. Kurihara, Phys. Rev. B39, 8600 (1989).
3. K. Huang, Statistical Mechanics (John Wiley, New York, 1963).

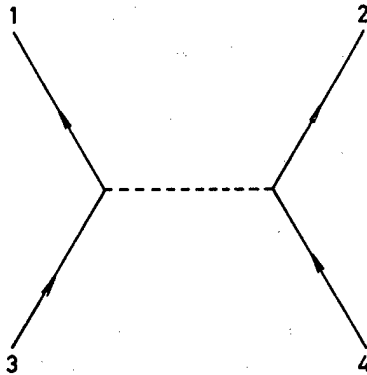


Fig. 1 Diagram of hole-hole interaction.

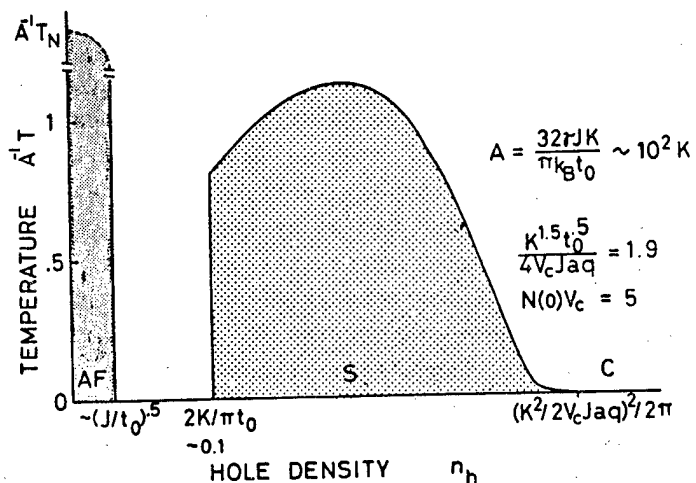


Fig. 2 Phase Diagram.

Thermally Activated Behavior in Resistive Transition and Magnetic
Relaxation of $\text{YBa}_2\text{Cu}_3\text{O}_x$ Films

N. Kobayashi, H. Kawabe*, K. Miyoshi, K. Watanabe, H.
Yamane, H. Kurosawa†, T. Hirai and Y. Muto

Institute for Materials Research, Tohoku
University, 2-1-1 Katahira, Sendai 980, Japan

*TATSUTA Electric Wire & Cable Co. LTD., 2-3-1

Iwatacho, Higashi-Osaka, Osaka 578

†RIKEN Co., 810 Kumagaya, Kumagaya 360

Electrical resistance and magnetic relaxation measurements have been performed on the $\text{YBa}_2\text{Cu}_3\text{O}_{7-\delta}$ films prepared by the chemical vapor deposition. The thermally activated behavior was observed in both measurements. The activation energy is estimated according to the simple flux creep model. However the activation energy obtained from the resistance measurement is about one order of magnitude as large as that from the magnetic relaxation.

Introduction

In high- T_c superconducting oxides, the characteristic properties have been observed in magnetic fields, such as the large logarithmic relaxation of magnetization [1-4] and the thermally activated dissipation in the resistive transition [5]. As a possible explanation of the logarithmic relaxation, Yeshurun and Malozemoff [4] proposed a "giant" flux creep model based on the anomalously small pinning energy for the flux line and the relatively large thermal energy kT , because of the high- T_c superconductor. The notable flux creep may lead to serious reduction of the critical current density J_c . However, several groups [6,7] reported that $\text{YBa}_2\text{Cu}_3\text{O}_{7-\delta}$ films had very high critical current density even at liquid nitrogen temperature. We do not yet know why the $\text{YBa}_2\text{Cu}_3\text{O}_{7-\delta}$ films exhibit such high- J_c property in spite of small pinning potentials.

We measured the electrical resistance near the superconducting transition and the relaxation of the magnetization in order to investigate the characteristics of the flux motion of the $\text{YBa}_2\text{Cu}_3\text{O}_{7-\delta}$ films with high- J_c value. In this report, the temperature and magnetic field dependences of pinning energies estimated from both electrical and magnetic measurements are presented. Brief reports on this investigation have been published in refs. 8 - 11.

Experimental

The $\text{YBa}_2\text{Cu}_3\text{O}_{7-\delta}$ films were epitaxially grown on $\text{SrTiO}_3(100)$ single crystal substrates ($10 \times 10 \text{ mm}^2$) by a chemical vapor deposition (CVD) technique at a deposition temperature of 850°C , where β -diketonate chelates of Y, Ba and Cu were used as source materials [12]. While the X-ray diffraction patterns indicated a strongly

preferred orientation of the c-axis perpendicular to the substrate, these patterns also suggest that the existence of a small amount of grain with the a-axis orientation and Cu-rich precipitates [12,13]. As typical examples for the critical current density of these samples, the J_c values at 77.3K for three samples are shown in Fig.1. Two samples have high- J_c values above $5 \times 10^5 \text{ A/cm}^2$ in the absence of magnetic field. When the magnetic fields were applied perpendicular to the c-axis, the J_c values of these samples decreases gradually at $B > 3 \text{ T}$ and are retained above $1 \times 10^4 \text{ A/cm}^2$ even at high magnetic field at 27T. On the other hand, one sample exhibits a relatively lower- J_c property of about $1 \times 10^5 \text{ A/cm}^2$. The magnetic field dependence of the J_c value is also stronger than that for the high- J_c samples.

For the resistance measurement, a narrow bridge with the dimension of 0.3mm wide, 2mm long and about 1 μm thick was formed by masking a part of the substrate. Current and voltage leads were attached by In pressure contact to sputtered Au electrodes. The electrical resistance measurement for both magnetic fields perpendicular and parallel to the c-axis was performed by a usual four-probe method with a dc current of 0.05mA (15A/cm²) along the a,b-axis (parallel to the sample layer). The data were taken by varying temperature in constant magnetic fields up to 25T using a hybrid magnet or a superconducting magnet.

The magnetic relaxation of the CVD films was measured in magnetic field up to 2T by using a commercial SQUID magnetometer. After zero field cooling to 5K, the sample was again warmed up to the objective temperature and subsequently the external field was applied. The magnetization data were taken as a function of time after the field sweep was stopped.

Results and Discussion

Figure 2 shows the electrical sheet resistance of the film H-64B as a function of temperature in various fields. The resistive transition at zero field is sharp with a width of 2-3K, while those in magnetic fields are pretty broad. In this figure, it should be noticed that each resistive transition has a knee near about 6 Ω at high fields above 13T. This means that the temperature dependence of resistance changes near this point. The low-resistance portion of the electrical sheet resistance is plotted as a function of T^{-1} in various magnetic fields in Fig. 3 for the magnetic field parallel to the c-axis. It can be seen that the resistance

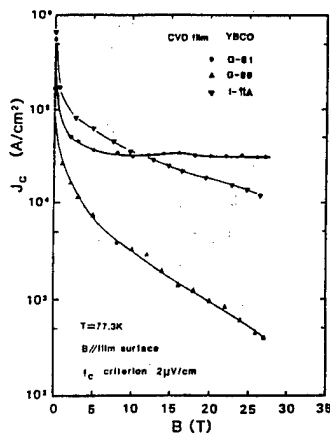


Fig.1 Critical current density at 77.3K

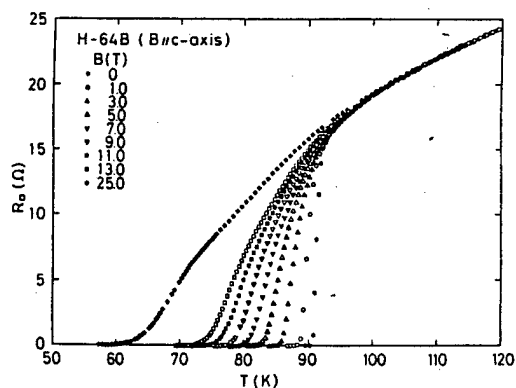


Fig.2 Resistance vs. temperature curves.

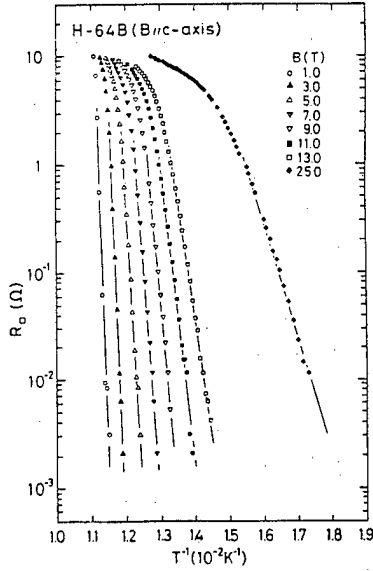


Fig.3 Semilogarithmic plot of R vs. 1/T.

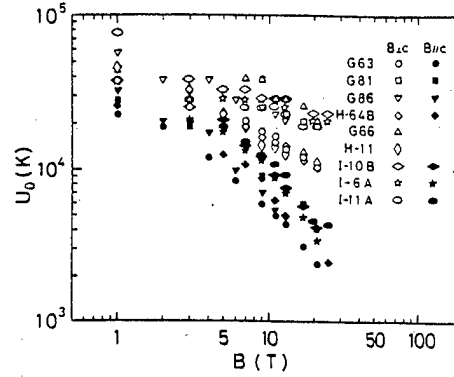


Fig.4 Activation energy estimated from the resistance measurement.

depends exponentially on T^{-1} over a wide resistance range, showing a thermally-activated behavior, as follows ;

$$\rho = \rho_0 \exp(-U_0/k_B T). \quad (1)$$

Then the activation energy U_0 is estimated from the linear part.

Figure 4 shows the magnetic field dependence of U_0 for many $\text{YBa}_2\text{Cu}_3\text{O}_{7-8}$ films studied. The U_0 values for the magnetic field perpendicular to the c-axis are much larger than those for B//c-axis. It seems that U_0 is proportional to B^{-1} for B//c-axis and to $B^{-1/2}$ for B⊥c-axis in higher fields. However, the U_0 values for both directions tend to saturate at lower fields.

In a simplified flux creep model, the activation energy U_0 depends on temperature and magnetic field by a form

$$U_0(T, B) = H_c^2(T) a_0^2 \xi(T) / 8\pi f^2 \\ = U_0(0, B) (1-t^2)^2 (1-t)^{-1/2}, \quad (2)$$

where $t = T/T_c$, $H_c(T)$ is the thermodynamic critical field, U_0 the flux lattice spacing, $\xi(T)$ the coherence length and f a scaling factor. We reanalyzed our data by replotting the resistance as a function of $(1-t^2)^2/t(1-t)^{1/2}$. Then the values of $U_0(0, B)$ are estimated from the linear relation between the resistance and $(1-t^2)^2/t(1-t)^{1/2}$. However, no serious difference is found between the $U_0(0, B)$ values and the U_0 ones shown in Fig. 4. This means that the analysis based on eq.(1) gives a good approximation for the $\text{YBa}_2\text{Cu}_3\text{O}_{7-8}$ films with relatively narrower resistive transition compared with those of Bi and Tl systems.

The logarithmic time decay of magnetization, as noticed by the previous reports [1-4], at a field of 0.1T for field parallel to the c-axis is shown in Fig. 5. While the magnetization at low temperature decays only a few percent for first one hour, the decay at 80K amounts to 25%. The magnetization decays logarithmically in time and can be expressed as

$$M(t) = M(0) \{1 - (k_B T / E_0) \ln t\}. \quad (3)$$

Here, E_0 is an activation energy obtained from magnetization and t is time. The E_0 values estimated from the present results are shown in Fig. 6 as a function of temperature. As temperature increases, the E_0 value of the two samples (G-81 and I-

11A) with high- J_c value increases at low temperature, take a maximum value at about 60K and then decreases rapidly. On the other hand, the E_0 value of the sample (G-86) with relatively smaller- J_c value does not depend on temperature up to about 60K. When the magnetic field is applied perpendicular to the c-axis, the activation energy behaves the similar temperature dependence to that for B//c-axis. However, the magnitude of the activation energy for B1c-axis is about four times as large as that for B//c-axis. The anisotropic property for the E_0 value is consistent with that obtained from the resistance measurement.

The anomalous temperature dependence of the E_0 value for the higher- J_c samples can not be understood by the simplified flux creep model based on the Anderson-Kim model, because the activation energy of each individual pinning center must decrease with increasing temperature. It may be explained by taking into account a distribution of activation energies as pointed out by Hagen and Griessen [14].

Figures 7(a) and (b) show the field dependence of the E_0 values for B//c-axis and B1c-axis, respectively. For B1c-axis, the E_0 value varies in proportion to $B^{-1/2}$ in whole field range studied. On the other hand, the E_0 value for B//c-axis and at 10K increases with increasing field at $B > 0.2T$, though at lower field it decreases similarly as that for B1c-axis. The field dependence proportional to $B^{-1/2}$ was also reported by Matsushita et al. [15] on a sintered bulk sample and they analyzed

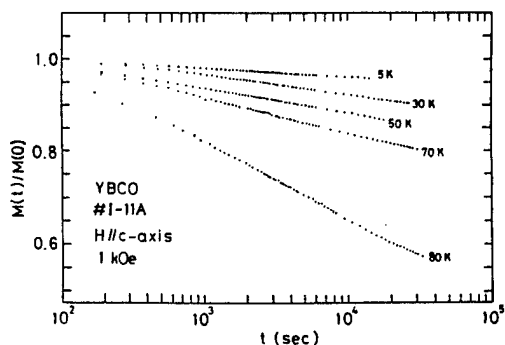


Fig.5 Logarithmic relaxation of the magnetization.

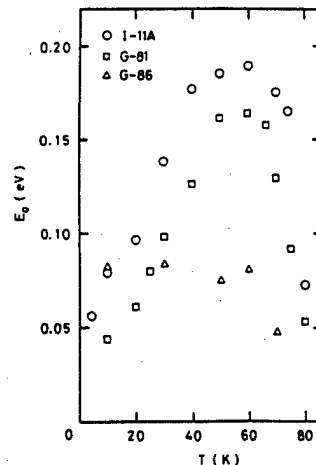


Fig.6 Temperature dependence of the activation energy estimated from the magnetic relaxation.

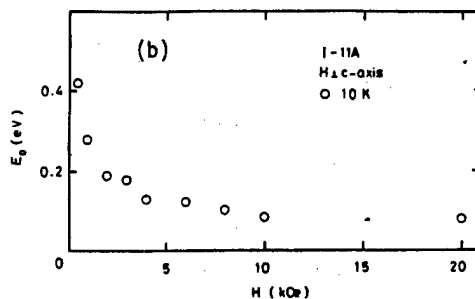
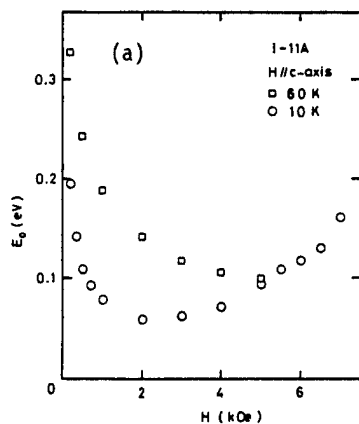


Fig.7 Magnetic field dependence of the activation energy estimated from the magnetic relaxation for B//c (a) and B1c (b).

their result by assuming the flux pinning by twinning planes. Our result does not consistent with their assumption, because the flux pinning by twinning planes is considered to be less effective for B_{1c}-axis.

Finally, it should be noted that the activation energies obtained from the two measurements are different by about one order of magnitude. It is necessary to understand the situation of the flux motion in each measurement in order to explain these different results.

Acknowledgements

The authors thank Professor T. Matsushita (Kyushu Univ.) for useful discussions. This work is supported by Grant-in-Aid for Scientific Research on Priority Areas "Mechanism of Superconductivity" from the Ministry of Education, Science and Culture, Japan.

References

- [1]. K. A. Müller, M. Takashige and J. G. Bednorz, Phys. Rev. Lett. 58, 1143 (1987)
- [2]. A. C. Mota, A. Pollini, P. Visani, K. A. Müller and J. G. Bednorz, Phys. Rev. B36, 401 (1987)
- [3]. T. K. Worthington, W. J. Gallapher and T. R. Dinger, Phys. Rev. Lett. 59, 1160 (1987)
- [4]. Y. Yeshurun and A. P. Malozemoff, Phys. Rev. Lett. 60, 2202 (1988)
- [5]. T. T. M. Palstra, B. Batlogg, L. F. Schneemeyer and J. V. Waszczak, Phys. Rev. Lett. 61, 1662 (1988)
- [6]. K. Watanabe, H. Yamane, H. Kurosawa, T. Hirai, N. Kobayashi, H. Iwasaki, K. Noto and Y. Muto, Appl. Phys. Lett. 54, 575 (1989)
- [7]. X. X. Xi, G. Linker, O. Meyer, E. Nold, B. Obst, F. Ratzel, R. Smithey, B. Strehlan, F. Weschenfelder and J. Geerk, Z. Phys. B74, 13 (1989)
- [8]. N. Kobayashi, H. Iwasaki, H. Kawabe, K. Watanabe, H. Yamane, H. Kurosawa, H. Masumoto, T. Hirai and Y. Muto, Physica C159, 295 (1989)
- [9]. H. Iwasaki, N. Kobayashi, M. Kikuchi, T. Kajitani, Y. Syono, Y. Muto and S. Nakajima, Physica C159, 295 (1989)
- [10]. N. Kobayashi, H. Kawabe, H. Iwasaki, K. Watanabe, H. Yamane, H. Kurosawa, H. Masumoto, T. Hirai, T. Matsushita and Y. Muto, Proc. M²S-HTSC (Stanford 1989).
- [11]. Y. Muto, N. Kobayashi and K. Watanabe, Proc. Honda Int. Symp. on the Application of High Magnetic Field to Materials Science (Sendai 1989).
- [12]. H. Yamane, H. Kurosawa, T. Hirai, K. Watanabe, H. Iwasaki, N. Kobayashi and Y. Muto, Supercond. Sci. Technol. 2, 115 (1989)
- [13]. H. Yamane, T. Hirai, H. Kurosawa, A. Suhara, K. Watanabe, N. Kobayashi, H. Iwasaki, E. Aoyagi, K. Hiraga and Y. Muto, Proc. ISS'89, (Tsukuba 1989).
- [14]. C. W. Hagen and R. P. Griessen, Phys. Rev. Lett. 62, 2857 (1989)
- [15]. T. Matsushita, S. Funaba, Y. Nagamatsu, B. Ni, K. Funaki and K. Yamafuji, Jpn. J. Appl. Phys. 28, L1508 (1989)

Neutron, Xray Scattering and Neutron Depolarization Studies on Magnetism and Superconductivity in Cuprous Oxides Materials

Yasuo Endoh

Department of Physics, Tohoku University
Aramaki Aoba, Aoba-ku Sendai, Japan

We report our research activities in 1989 by using mainly neutron scattering method under the research project of the investigation of the high T_c superconducting mechanism.

We continue to search the intimate relation between magnetism and superconductivity in a 'hole' doped system of $\text{La}_{2-x}\text{Sr}_x\text{CuO}_4$ along the line of the past two years studies. We also start to elucidate a newly discovered 'electron' doped system of $(\text{Nd,Pr})_{2-x}\text{Ce}_x\text{CuO}_4$.

1 Introduction

After the past two years' extensive investigations on the high T_c superconductivity, the role of magnetism in such novel superconductors is understood deeply and their intimate relation has been occasionally discussed. La_2CuO_4 which is the progenitor of the so-called 214 superconductors is now recognized to be an ideal model system of the $S=1/2$, 2 dimensional (2D-) Heisenberg antiferromagnet¹⁾. The first neutron scattering experiments from La_2CuO_4 revealed fascinating features including the absence of any appreciable enhancement of the quasielastic component near the Neel temperature (T_N) and an enormous energy scale for the spin fluctuations above T_N ²⁾. The former seems to be much akin to the quantum fluctuations in the $S=1/2$, Heisenberg antiferromagnetic quantum linear chain³⁾ and the latter seems to be an important factor to the high T_c superconducting mechanism.

Nevertheless these experiments motivated many theoretical studies to elucidate the fundamental subject of the quantum effect in two dimension which is still left unsolved. Furthermore the intimate relation between magnetism and superconductivity has been focused recently since the RVB mechanism was proposed⁴⁾. Thus we are approaching from the complete survey of the quantum fea-

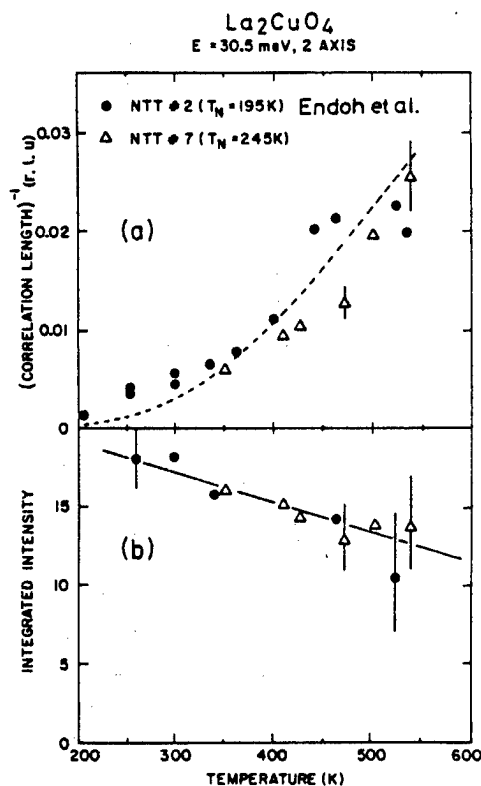


Fig.1 Temperature dependence of (a) inverse correlation length k and (b) integrated intensity measured by two-axis focusing scan.

tures in La_2CuO_4 to the elucidation of spin dynamics in the superconducting state by mainly using neutron scattering method.

Our research project has included more than thirty scientists in total for three years. Three major institutions, Brookhaven National Laboratory (headed by G. Shirane), Massachusetts Institute of Technology (headed by R. J. Birgeneau) and Tohoku University (headed by myself) have continuously organized this large collaboration team. More importantly, excellent single crystals have constantly been supplied by NTT Opto Electronics Laboratories (Y. Hidaka and T. Murakami) and Inorganic Material Research Facility, Yamanashi University (I. Tanaka and H. Kojima). Without their crystal growing skills and enthusiasms any success could be made in our investigations.

Neutron scattering measurements reported here have been carried out mainly at the HFBR at Brookhaven National Laboratory and partly at the JRR-2 at the Tokai Establishment of JAERI. Neutron depolarization measurements have been performed at the spallation pulsed neutron source at the Booster Synchrotron Facility of KEK. The work is not covered in this report but will be described in near future.

2 Quantum 2D antiferromagnet of $\text{La}_2\text{CuO}_{4+x}$ ⁵⁾

This section is devoted to the brief description of the quantum features of spin correlations in $\text{La}_2\text{CuO}_{4+x}$ which has the 3D long range order (LRO) below T_N . Note that T_N varies with x and the highest T_N of 320K corresponds to the stoichiometric oxygen content of La_2CuO_4 ($x=0$)⁶⁾. As mentioned in the preceding section, the spin correlation function for the 2D, quantum Heisenberg antiferromagnet was derived theoretically. Specifically the model developed by Chakravarty, Halperin and Nelson (CHN model)⁷⁾ is ready to implement and thus the direct comparison was made with the neutron scattering results which are the extension of the previous experiments from $\text{La}_2\text{CuO}_{4+x}$ ($T_N=250\text{K}$). The important conclusion in the CHN model is that the quantum Heisenberg antiferromagnet possesses the long range order at $T=0$ like the classical antiferromagnet. Now this conclusion seems to be widely accepted, which differs from the RVB conjecture.

The temperature dependence of the correlation length (ξ) in the 2D plane has been studied utilizing the energy integrated focusing scans of the 2-axis mode. The result is summarized in Fig.1, where two sets of data are shown with the fitted curve by the CHN model.

$$\xi^{-1} = \kappa = \left(\frac{1+T/2\pi\rho_s}{Da} \right) e^{-2\pi\rho_s/T}$$

$$D = 0.5$$

$$2\pi\rho_s = 0.576 \text{ hc/a} \quad (\text{c: spin wave velocity} \quad \text{a: lattice constant} = 3.79\text{\AA})$$

The best fitted curve was given with $C=850\text{meV}\text{\AA}$ which is consistent with the estimate by the Raman data⁸⁾. Thus the CHN model accounts for the experiments quite well and now the short correlation length observed is understood as the result of quantum fluctuations in spite of the strong exchange interaction.

Let us describe the results of the 3 axis inelastic scans. Because of the very

steep dispersion surface of the spin wave in this crystal with our finite resolution, it was extremely difficult to observe the proper function of $S(q, \omega)$ at a fixed q . We performed therefore exclusively q scans with the fixed energy (the constant E scans). However, for the same reason of the resolution effect, these scans across a 2D magnetic ridge could not resolve the $\pm q_{2D}$ contributions from the symmetric dispersion surface but gave a single peaked response cantered at the ridge.

At low temperatures well below T_N , the experimental data of the constant E scans is well fitted to the normal spin wave model. The resolution convolved calculation gives the spin wave velocity of 650-850 meVA assuming a sharp excitation. Above T_N , the dynamical structure factor, $S(q_{2D}, \omega)$ is given by the CHN model as follows

$$S(q_{2D}, \omega) = \omega_0^{-1} S(q_{2D}) \phi(k, v)$$

$$\omega_0^{-1} = c\xi^{-1} (T/2\pi\rho_s)^{1/2}$$

, where k and v are respectively $q_{2D}\xi$ and, ω/ω_0 . $S(q_{2D})$ must be properly scaled from $S(q_{2D}=0)$, which is written as $S(q_{2D}=0) = 125\xi^2 N_0^2 / 2\pi\rho_s [T+1]^2$.

$\phi(k, v)$ is assumed to be a two-Lorentzian form including the adjustable parameters, which were determined by the model calculation. In order to compare the experimental data with the dynamical structure factor in this model, we used the result by Tyc. Halp Chakravarty as well as the experimental values of C , $\xi(T)$, and the intensity scale factor.

Although the survey was limited in low energies up to 12 meV transfer, the quantum effect is quite obvious. One way to present the result is the energy dependence of the intensities integrated over q scanned with the fixed energy transfer as shown in Fig.2. The inset of the figure is the calculated intensities on the basis of the CHN model, which includes the resolution effect. The overall agreement between the experiment and the calculation is quite good except the quasielastic region near $E=0$. The fact of the broad peak appeared at the finite energy which eventually becomes flat at the elevated temperature

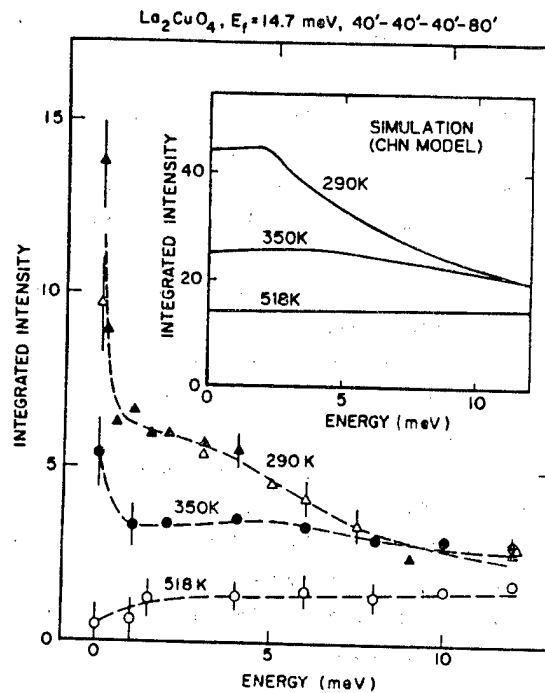


Fig.2 Energy dependence of integrated intensities of constant energy scans across the magnetic rod at different temperatures. The data at 290K are taken from two crystals NTT-7(open triangle) and NTT-8(solid triangle). The inset is the results of calculations utilizing the CHN model(see the text).

is the most unusual but significant features. This is the remarkable contrast to the Lorentzian form centered at $E=0$ given by any conventional theory for the interacting paramagnets. Even the normal spin wave formula must exhibit the monotonically decrease in intensities integrated over q with increase of energy. This unique feature predicted by CHN, which is revealed by this experiment, is mainly originated by the extremely short correlation length due to the quantum fluctuations. With this context the excitations are heavily overdamped at high temperatures.

This result reminds us the spin dynamics in the quantum linear chain where magnetic excitations spread above the bound spin wave, hence they obey the Fermi statistics⁹⁾. In other words, the inelastic neutron scattering intensities are like an ice cream filled in the cone which is an illustration of the quantum spin-wave dispersion surface in a q, ω space. There is no theory to prove what extent the similar view is valid for the case of the quantum planer Heisenberg antiferromagnet at this moment.

3 Magnetic State in superconducting $\text{La}_{2-x}\text{Sr}_x\text{CuO}_4$ ^{10,11)}

We have extended neutron scattering work to explore the spin dynamic in mostly superconducting $\text{La}_{2-x}\text{Sr}_x\text{CuO}_4$. In order to compare the features directly, we also made inelastic neutron scattering measurements on nonsuperconducting light doped crystals. Both the energy and temperature dependences of the scattering have been mapped out using 3 axis method.

One remarkable feature in the spin dynamics of superconducting crystals is an incommensurate, double peaked structure in the inelastic neutron scattering spectra. Since the incommensurability appears in the superconducting crystals, a new magnetic state is suggested in the superconducting materials, which may gain the kinetic energy to favor the occurrence of superconductivity. Although further experiments are necessary to elucidate in detail, numbers of interesting theoretical models are already proposed to interpret this fact. However these models should include the fact that Cu moments are well localized and also the strong antiferromagnetic interaction persists.

It is also suggestive that nonsuperconducting, light doped crystals show very weak temperature as well as energy dependences in $S(Q, \omega)$, although the 2D antiferromagnetic structure is unchanged. This smeared feature is just interpreted to be the reflection of the shortening of spin correlation length due to the increase of hole concentration which frustrates to the 2D antiferromagnetic ordered state.

Another feature is the fact that the integrated intensities over q must be divided by the quantum statistic factor of $\omega(1-e^{-\hbar\omega/k_B T})^{-1}$ to compare directly with the dynamical function of $S(Q, \omega)$.

This unusual temperature dependence occurs below a certain threshold value in energy only in the superconducting sample. It is also very important that the temperature dependence of the scattering intensities is not interpreted by the simple Bose statistics. Though the coupling between localized spins and quasiparticles of super currents and even a dynamical scattering function of $S(Q, \omega)$ for such spins in doped materials are not known, the sudden decrease of intensities for 6meV transfer suggests a formation of the energy gap in spin excitations¹²⁾. If

we estimate this energy gap around 10meV for this particular crystal with $T_C=33K$, this energy coincides with the estimate within the frame work of the weak coupling BCS theory. Note that the gap energy in the $T_C=12K$ crystal is also estimated to be around 5meV.

At this moment further discussions to connect to the superconductivity is too speculative and therefore much extended work is highly required.

4 Spin correlations in $(Nd,Pr)_{2-x}Ce_xCuO_4$ ^{13,14,15)}

Soon after the discovery of the 'electron' doped superconductors, the single crystal grow was initiated by Hidaka et al., at NTT.¹⁶⁾ Then experimental studies on the spin correlations were also started by using these single crystals. Although the detailed crystal structure and bulk properties are slightly different, the basic mechanism for the appearance of superconductivity is speculated to be considered in the same view of the 'hole' doped system.

Therefore it is very significant to study the spin correlations and fluctuations in $La_{2-x}Ce_xCuO_4$ and to make a detailed comparison with those for $La_{2-x}Sr_xCuO_4$ in order to find any intimate relation between magnetism and superconductivity in our point of view. When we discuss the spin correlations in these crystals, we must point out that Lanthanide atoms like Pr, Nd and Ce are all magnetic atoms unlike La and Y in the 'hole' doped system. It should also be pointed out that the local structure of oxygen atom is different with each other. There is no apical oxygen in the 'electron' doped compounds, although the chemical formula is represented in the same form.

First the 3D LRO antiferromagnetic structure in both Nd_2CuO_4 and Pr_2CuO_4 was determined exactly. In Nd_2CuO_4 the multiple magnetic phase transition was observed but the mechanism for the phase transition is not completely understood yet. In particular, the sharp transition around 70K is still mysterious since no associated anomaly other than the change in the magnetic structure is found. The participation of the lanthanide moments into the anti-ferromagnetic LRO was also observed at low temperatures suggesting the coupling to

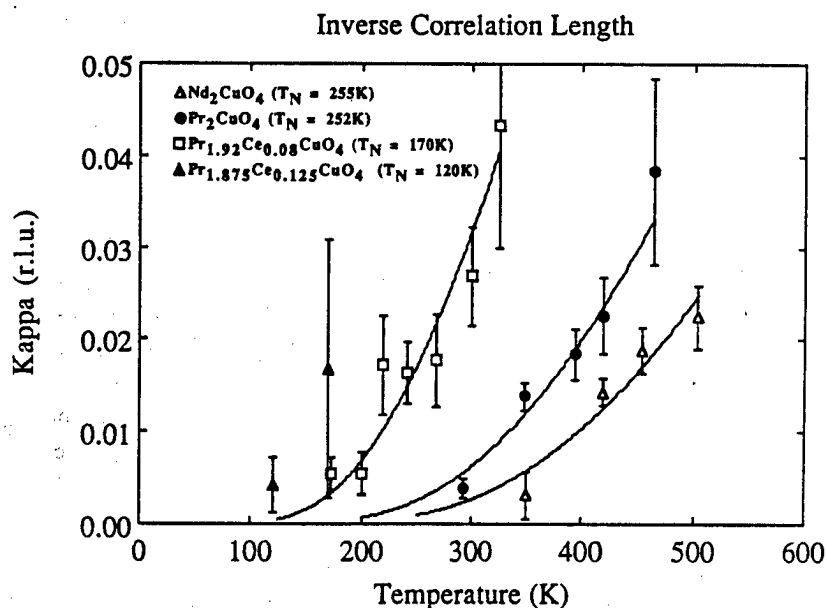


Fig.3 Temperature dependence of inverse correlation length in $(Nd,Pr)_{2-x}Ce_xCuO_4$.

the Cu moments is rather weak.

Above the Neel temperature, the strong as well as highly inelastic 2D spin correlations exist which is regarded as the common features associated with the crystal structure of the stacking of CuO_2 layers. The exchange energy is estimated from the temperature dependence of correlation length by using the Chakravarty, Halperin, Nelson model which turns out to be comparable to that of La_2CuO_4 .

The doping effect of spin correlations is just in the process of collecting the data. The difficulty arises mostly in the sample preparation. However the significant difference between the 'electron' and 'hole' doped systems in spin correlations is observed as was expected. As is seen in Fig.3, the temperature dependence in the correlation length is appreciable in the 'electron' doped systems, while as almost flat feature is characteristic in the 'hole' doped systems. The difference is understood qualitatively that the latter evinces primarily the frustration effect by doping, but the former does the dilution effect. The present result is consistent to the recent experimental results of photo emissions showing that the doped charges never go into either the Cu d or oxygen p orbital.

Acknowledgment

The author thanks all of his colleagues, but specifically, K. Yamada, K. Kakurai, T. R. Thurston and M. Matsuda in Tohoku University, R. J. Birgeneau and G. Shirane in United States for their continuous and restless enthusiasms.

The work is supported by the Ministry of Education, Science and Culture as the Special Project Research of the Grant In Aid for Scientific Research.

It is partly supported as the US-Japan Cooperative Neutron Scattering Program. The work in United States is supported by the U.S. National Science Foundation and the Division of Materials Science, the office of Basic Energy Science of the US, DOE.

References

- 1) R.J.Birgeneau and G.shirane, in Physical properties of high temperature superconductors, edited by D.M.Ginzburg (World Scientific, 1989), Y.Endoh, Phase Transitions, 15 223 (1989)
- 2) G. Shirane et al., Phys.Rev.Lett. 59 1613(1989), Y.Endoh et al., Phys.Rev.B37 7443(1988)
- 3) Y.Endoh et al., Phys.Rev.Lett 32 170 (1974)
- 4) P.W.Anderson, Science 235 1196 (1987)
- 5) K.Yamada et al., Phys.Rev.B40 4457 (1989)
- 6) M.A.Kastner et al, Phys.Rev.38 6636 (1988)
- 7) S.Chakravarty, B.I.Halperin and E.R.Nelson, Phys.Rev. B39 2344 (1989)
- 8) S.Sugai et al., Phys.Rev.B40 2686 (1989)
- 9) T.Yamada, Prog.Theor.Phys. 41 4585 (1989)
- 10) T.R.Thurston et al., Phys.Rev. 40 4585 (1989)
- 11) G.Shirane et al., Phys.Rev. B40 4585 (1989)
- 12) T.Imai et al., Phys.Rev. 40 (1989)
- 13) M.Matsuda et al., unpublished work
- 14) Y.Endoh et al., Phys.Rev.B40 7023 (1989)
- 15) T.Thurston et al., unpublished work
- 16) Y.Hidaka and M.Suzuki Nature 388 635 (1989)

Nuclear Spin-Lattice Relaxation in Highly Correlated Metallic and Superconducting Copper Oxides

H. Yasuoka, T. Shimizu, T. Imai and Y. Yoshinari
Institute for Solid State Physics, University of Tokyo,
Roppongi, Tokyo 106, JAPAN

Abstract

In order to understand the exotic Cu spin dynamics in the normal (metallic) state of the high- T_c and related metallic Cu oxides, the measurements of the ^{63}Cu and ^{17}O nuclear spin-lattice relaxation have been utilized. From the temperature dependence of the relaxation rate $1/T_1$ in the CuO_2 plane sites, it is found that highly enhanced relaxation process due to antiferromagnetic Cu spin fluctuations exists in the Cu sites of high- T_c oxides. The data are also exhibiting of the opening of a gap in the low-lying excitations with an energy comparable to the superconducting gap. In contrast to this, $1/T_1$ in the oxygen sites shows the Korringa type temperature dependence reflecting only the $q=0$ component of the dynamical susceptibility.

1. Introduction

It is well recognized by now that the understanding of the normal metallic state properties of high- T_c Cu oxides is the most essential part of the problem to make up a theoretical model for the mechanism of their superconductivity. The major question here is how we can describe the magnetism associated with the highly correlated Cu 3d electrons in the metallic state. The magnetic susceptibility has quite characteristic signatures, in most of the cases it has essentially no temperature dependence, in contrast to other metallic oxides like vanadium oxides where the amplitude of longitudinal spin fluctuations is saturated and the Curie-Weiss like temperature dependence has been observed at finite temperatures. Therefore, any experimental and theoretical arguments must be conformed to this most fundamental magnetic property. It should be also recalled that most of the superconducting Cu oxides are located at just near the insulating phase and the metallic state is realized by doping a small amount of holes or electrons under alloying. This alloying produces chemically several Cu valence states in the metallic phase and transfer of charge between sites of different valence should be of lower energy to invoke the metallic nature. Then the copper-oxygen interatomic Coulomb interaction would appear to be an important driving force for the transition to the superconducting state.

The NMR and NQR techniques offer an attractive way to investigate the microscopic magnetic properties since the response of inequivalent sites can, in principle, be resolved in the nuclear-resonance spectra and the dynamical properties of those can be studied by the nuclear magnetic relaxation at respective sites. Particularly, it is quite important for understanding the low-lying elementary excitations to make a systematic measurement of the nuclear spin-lattice relaxation time T_1 . Among variety of our NMR/NQR investigations, we restrict ourselves in this report to review and to discuss the work related to T_1 measurements for both the ^{63}Cu and ^{17}O in the CuO_2 plane sites. The unprecedented behavior of the temperature dependence of ^{63}Cu relaxation rate $1/T_1$ in a series of high- T_c Cu oxides has been observed, while $1/T_1$ for the oxygen sites exhibits the conventional Korringa temperature dependence. The results are compared with those for non-superconducting but metallic oxides, $\text{La}_4\text{BaCu}_5\text{O}_{13}$ and $\text{La}_{1.7}\text{Sr}_{0.3}\text{CuO}_4$.

2. Temperature dependence of ^{63}Cu nuclear spin-lattice relaxation

A great number of data for the temperature dependence of T_1 in high- T_c Cu oxides has been published already [1-9]. The following qualitative characteristics for the planar Cu sites are generally accepted by now. (1) $1/T_1$ in the normal state is highly enhanced and its temperature dependence is not accord with the Korringa process, which is due to the electron hole pair excitations at the Fermi surface. (2) There exist no "isotropic BCS" characteristics in $1/T_1(T)$ just below T_c . Irrespective of the system, $1/T_1(T)$ has been found to decline much more steeply,

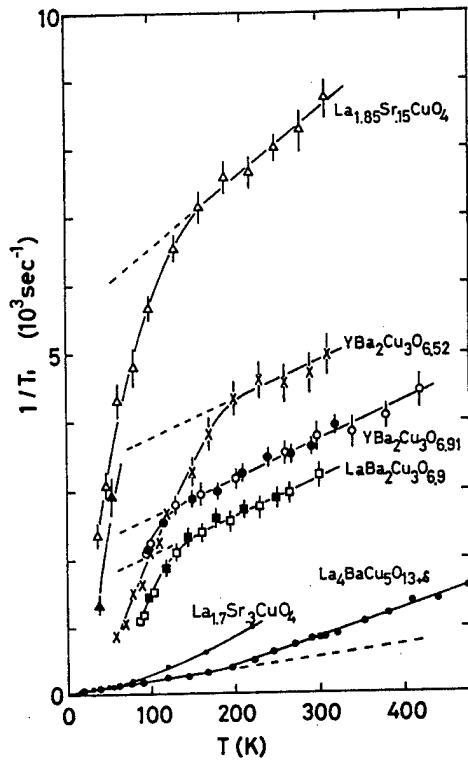


Fig. 1 Temperature dependence of ^{63}Cu spin-lattice relaxation rate $1/T_1$ in the normal state of high- T_c oxides for the CuO_2 plane sites. For comparison, data for metallic Cu oxides are also shown.

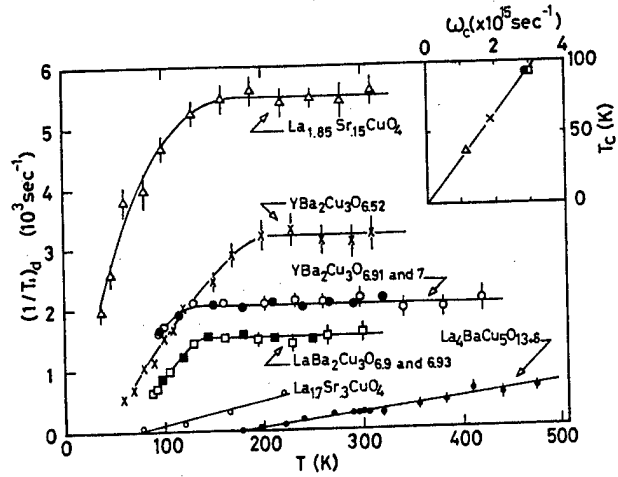


Fig. 2 Temperature dependence of the Cu d-spin contribution $(1/T_1)_d$ to the relaxation rate. Inset shows a relation between the T_c and the characteristic correlation frequency of the d-spin fluctuations.

without any peak, just below T_c than the BCS prediction. (3) The low temperature behavior ($T < 20\text{K}$) is still sample dependent where the relaxation process is limited by a small amount of magnetic impurities.

We have been pointing out that, before arguing the properties of the superconductivity from T_1 measurements, we must understand the normal state behaviors. Hence, we have made a systematic investigation on the temperature and material dependences of T_1 at the normal state, including non-superconducting but metallic Cu oxides.

In Fig. 1, $1/T_1(T)$ associated with the planar Cu sites is presented for the normal state. To make this plot, we have selected materials which exhibit "homogeneous" relaxation process, except for $\text{La}_{1.7}\text{Sr}_{0.3}\text{CuO}_4$ case where the longest relaxation component has been extracted from non exponential recovery of the nuclear magnetization. It has also been confirmed at several temperatures that the dominant relaxation process is to be "magnetic" from the measurements of isotope effect of T_1 (the ratio of $1/T_1$ for the two Cu isotopes being nearly equal to the square of the ratio of their γ_n values).

In general, the quantity $1/T_1$ may be defined in terms of autocorrelation function of the fluctuating local field, δH , acting on the nucleus in concern [10],

$$(1/T_1) = (\gamma_n/2) \int_{-\infty}^{+\infty} \langle \delta H^+(t) \cdot \delta H^-(0) \rangle \exp[i\omega_0 t] dt, \quad (1)$$

where γ_n and ω_0 are the nuclear gyromagnetic ratio and the frequency for resonance, respectively. If we assume the hyperfine field operator, $H = A(q)S$, and make use of the fluctuation and dissipation theorem, $1/T_1$ can be reduced to,

$$(1/T_1) = (1/2) \sum_q [\gamma_n A(q)]^2 \cdot S_{\perp}(q, \omega_0) \quad (2)$$

$$= 2 k T \sum_q [\gamma_n A(q)]^2 \cdot \text{Im}[\chi_{\perp}(q, \omega_0)] / \omega_0. \quad (3)$$

where $A(q)$ is the wave vector dependent hyperfine coupling constant, and $S_{\perp}(q, \omega_0)$ and $\chi_{\perp}(q, \omega_0)$ are the transverse components of the spin correlation function and the dynamical susceptibility, respectively. Then the problem is reduced to how we can describe the $\chi(q, \omega)$ in our system. Unfortunately, however, we can not rely on any kind of existing theory to describe $\chi(q, \omega)$ at present. Therefore, only phenomenological interpretations for the experimental results are given here.

The following characteristic features are immediately extracted from Fig. 1. (1) For the non-superconducting materials, the Korringa process is really seen at low temperatures, the rate of which can roughly be accounted for the estimated Cu site density of states. (2) With increasing temperature, an excess relaxation process starts to develop at around 100 K for all the cases. This is particularly remarkable for the superconducting materials. Since the uniform static susceptibility, $\chi(0,0)$, has essentially no enhancement in these systems and does not vary so much with material to material, the excess relaxation process is considered to be due to a peak in $\chi(q, \omega)$ at the finite value of q with negligible enhancement near $q=0$. This case arises when there are antiferromagnetic correlations, that seem appropriate for high- T_c oxide system because of the antiferromagnetic phase being present for the materials with zero or small carrier densities. (3) In the temperature well above T_c , $1/T_1(T)$ for the superconducting materials has an asymptotic functional form on temperature, i.e. $1/T_1 = aT + b$. Here, we associate the first and the second terms with the Korringa, $(1/T_1)_K$, and the process characteristic to the Cu spin dynamics, $(1/T_1)_d$, at finite temperatures, respectively.

There may be several ways to interpret the above characteristic features, ranging from localized to itinerant picture for the Cu 3d holes. We start to discuss the results from a localized regime, since some of the resonance experiments have indicated the existence of exchange coupled localized moments on the Cu sites in the normal state [11,12]. In this case, the temperature dependence of the d-spin contribution, $(1/T_1)_d$, to the relaxation process may be extracted by subtracting the Korringa term from the observed value. This is shown in Fig. 2. Here, we have assumed the Korringa term is due to the contact interaction with the conduction holes and does not depend on temperature. It is clearly seen in Fig. 2 that the temperature independent $(1/T_1)_d$ tends to diminish below about 150 K which is well above T_c . The high temperature value of $(1/T_1)_d$ may be analyzed by the same analogy of purely local moment limit with a characteristic correlation frequency, ω_c , for the local spin fluctuations. If we assume that the local field spectra have a Gaussian distribution centered about zero frequency, hence $S(q, \omega)$ in eq. (2) has a Gaussian decay with ω , we have [13],

$$(1/T_1)_d = (\pi/2)^{1/2} (A)^2 S(S+1) / (3\omega_c). \quad (4)$$

Using reasonable estimates of A from hyperfine fields observed in the antiferromagnetic phases [14,15], ω_c is estimated from the high temperature values of $(1/T_1)_d$. In the inset of Fig. 2, ω_c thus obtained is plotted against T_c . It is seen interestingly that T_c is proportional to the correlation frequency of the d-spin fluctuations within this model. It is also noted that the estimated ω_c is by an order of magnitude larger than the exchange frequency $\omega_{ex} = 1.3 \times 10^{14}$ (rad/sec) estimated from generally accepted value of $J \sim 1000$ K. This means that the frequency spectrum of $S(q, \omega)$ extend much higher frequency than the ω_{ex} , hence high energy excitations may be playing an important role on the Cu spin dynamics.

An alternative interpretation can be given from the basis of itinerant picture for the 3d holes. In this model, $\chi(q, \omega)$ in eq. (3) may be treated by the self-consistent renormalization theory of spin density fluctuations [16]. For nearly itinerant antiferromagnetic cases with two dimensional character of the Fermi surface, as is the present materials, this theory predicts a temperature independent relaxation process if χ_Q (Q being the antiferromagnetic wave vector) obeys the Curie-Weiss like temperature dependence. Although the quantitative account is

rather difficult to make since it depends on the detailed nature of the Fermi surface and degree of the enhancement of $\chi(Q, \omega_0)$. the high temperature behavior may be explained in this regime.

The remaining question having arisen even within the two limited discussions above is how we can interpret the drastic decrease of $1/T_1$ below $T \sim 150$ K. We believe this is one of the most important findings in the present relaxation studies. Irrespective of the model, the experimental data are exhibiting of the opening of a gap in the low-lying excitation spectrum with an energy comparable to the value of BCS gap. It should be stressed, however, that this gap is not directly due to the superconducting gap, since a sharp decrease of $1/T_1$ associated with the superconducting gap opening does exist at T_c for all the superconducting materials (see Fig. 3). The similar gap opening at around 150 K has recently been observed in the Cu^{2+} -hole spin excitation spectrum in $\text{La}_{1.85}\text{Sr}_{0.15}\text{CuO}_4$ by the neutron scattering experiments [17].

Finally, we should comment on the possible interpretation based on the proposed quasi-particle excitations (e.g. Spinons in the RVB picture) in these system [18,19]. If these particles obey Fermi statistics, the value of $1/T_1 T$ is a good measure of the density of states at the Fermi level, $N(E_f)$, in such excitations. The temperature dependence of $1/T_1 T$ is shown in Fig. 3. It is seen for the cases of $\text{YBa}_2\text{Cu}_3\text{O}_{6.5}$ and $\text{LaBa}_2\text{Cu}_3\text{O}_{6.9}$ that $N(E_f)$ increases with decreasing temperature having a plateau around 150 K and decreases with farther decreasing temperature. The latter is again suggestive of the opening of a gap in the density of states.

3. Temperature dependence of ^{17}O nuclear spin-lattice relaxation

For the ^{17}O spin lattice relaxation study in $\text{YBa}_2\text{Cu}_3\text{O}_7$, at least three groups have published different results for the temperature dependence. Ishida et al. have reported that $1/T_1(T)$ in the CuO_2 plane sites, O(2) and O(3), behaves like a Korringa process at the normal state and has a distinct enhancement just below T_c characteristic of BCS superconductors [20]. From these findings they made a statement that the superconductivity is realized by formation of p-hole pairing with dominant s-wave like symmetry. However, Hammel et al. have published completely

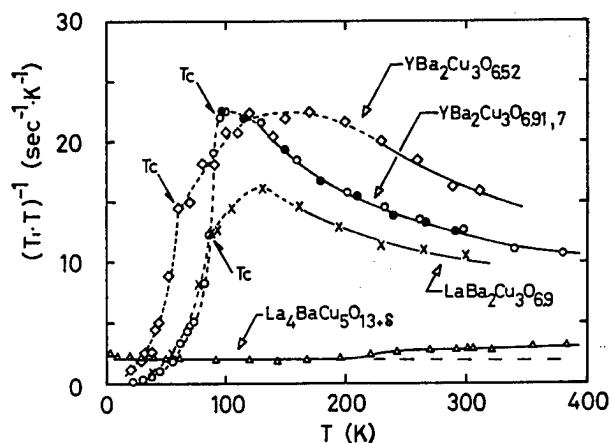


Fig. 3 Temperature dependence of $1/T_1 T$ in $\text{YBa}_2\text{Cu}_3\text{O}_7$, $\text{LaBa}_2\text{Cu}_3\text{O}_{6.9}$ and $\text{YBa}_2\text{Cu}_3\text{O}_{6.5}$. For comparison, the data in the non-superconducting $\text{La}_4\text{BaCu}_5\text{O}_{13.8}$ are also shown.

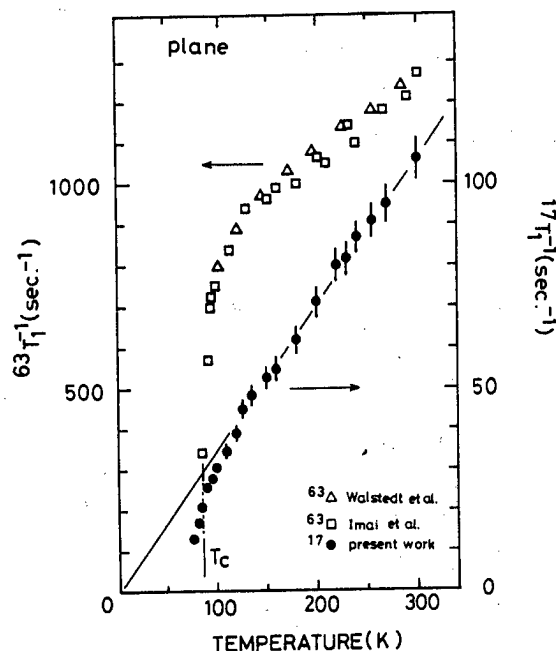


Fig. 4 Temperature dependence of ^{17}O spin-lattice relaxation rate in the plane sites of $\text{YBa}_2\text{Cu}_3\text{O}_{6.96}$. For comparison, the data for the Cu sites are also shown.

different version of the experimental results. Particularly, they have pointed out that any BCS enhancement at any Oxygen site does not exist in $\text{YBa}_2\text{Cu}_3\text{O}_7$ [21]. Another complication has appeared in the work by Wzieteh et al. where they found a shortening of the relaxation in the chain Oxygen sites in a limited temperature domain slightly below T_c [22]. They associate this hump to the absence of zeros of the superconducting order parameter over the Fermi surface and the s-symmetry for the pair wave function.

Having above complication in mind, we have decided to re-examine the relaxation study for the oxygen sites. In Fig. 4, we show our first result for $1/T_1(T)$ at the oxygen sites in the CuO_2 planes in $\text{YBa}_2\text{Cu}_3\text{O}_{6.96}$. It is clearly seen that the high temperature Korringa process is depressed to some extent below about 120 K and there exists no enhancement just below T_c . From the geometrical argument, the oxygen sites can probe the spin dynamics associated with only the $q=0$ component of the $\chi(q, \omega)$, while the relaxation at the Cu sites is predominantly manifested by the $q=Q$ component. Therefore, the present result suggests a Fermi liquid type of picture for the oxygen sites. In order to discuss more detail, we need to have the temperature dependence of the Knight shift for respective sites. Such experiments are now in progress and we will publish those with full discussion in a separate paper.

4. Summary

The temperature dependence of copper spin dynamics has been investigated by T_1 measurements for high- T_c and related oxides. Highly enhanced Cu relaxation process with a characteristic temperature dependence was found in the normal state of high- T_c oxides. This has been discussed by the manifestation of either antiferromagnetic Cu spin fluctuations or quasi-particle excitations. The experimental data are also exhibiting of the opening of a gap in the low-lying excitation spectrum with an energy comparable to the value of superconducting gap. The oxygen relaxation measurement in the CuO_2 plane sites of $\text{YBa}_2\text{Cu}_3\text{O}_{6.95}$ has been re-examined. It is found that $1/T_1(T)$ above 120 K shows the Korringa process and there exists no relaxation anomaly just below T_c which is characteristic of BCS superconductors.

Acknowledgments.

We thank Professors T. Moriya and H. Fukuyama for valuable theoretical discussions, and Professors Y. Ueda, K. Kosuge and Dr. K. Yoshimura for the material synthesis. This work is partially supported by a grant in aid for scientific research on priority areas from the Ministry of Education, Science and Culture of Japan.

References

- [1] M. Mali, D. Brinkmann, L. Pauli, J. Roos, H. Zimmermann and H. Hulliger: *Physic Letters A* **124**, 112 (1987)
- [2] W. W. Warren, Jr., R. E. Walstedt, R. F. Bell, G. F. Brennert, R. J. Cava, G. P. Espinosa, J. P. Remeika and E. A. Rietmann: *Phys. Rev. Lett.* **59**, 186 (1987)
- [3] Y. Kitaoka, S. Hiramatsu, T. Kondo and K. Asayama: *J. Phys. Soc. Jpn.* **57**, 30 (1988)
- [4] T. Imai, T. Shimizu, T. Tsuda, H. Yasuoka, T. Takabatake, Y. Nakazawa and M. Ishikawa: *J. Phys. Soc. Jpn.* **57**, 1771 (1988)
- [5] T. Imai, T. Shimizu, H. Yasuoka, Y. Ueda and K. Kosuge: *J. Phys. Soc. Jpn.* **57**, 2280 (1988)
- [6] R. E. Walstedt, W. W. Warren, Jr., R. F. Bell, G. F. Brennert, G. P. Espinosa, R. J. Cava, L. F. Schneemeyer and J. V. Waszczak: *Phys. Rev.* **B38** 9299 (1988)
- [7] W. W. Warren, Jr., R. E. Walstedt, G. F. Brennert, R. J. Cava, R. Tycko, R. F. Bell and G. Dabbagh: *Phys. Rev. Lett.* **62** 1193 (1989)
- [8] K. Ishida, Y. Kitaoka and K. Asayama: *J. Phys. Soc. Jpn.* **58**, 36 (1989)
- [9] T. Imai, T. Shimizu, H. Yasuoka, Y. Ueda, K. Yoshimura and K. Kosuge: submitted to *J. Phys. Soc. Jpn.* (1990)
- [10] T. Moriya: *J. Phys. Soc. Jan.* **18**, 516 (1963)

- [11] M. Horvatic, P. Segransan, C. Berthier, P. Butaud, J. Y Henry, M. Couach and J. P. Chaminade: Phys. Rev. B39, 7332 (1989)
- [12] C. P. Pennington, D. J. Durand, C. P. Slichter, J. P. Rice, E. D. Bukowski and D. M. Ginsberg: Phys. Rev. B39, 274 (1989)
- [13] T. Moriya: Prog. Theor. Phys. (Kyoto), 16, 641 (1956)
- [14] H. Yasuoka, T. Shimizu, Y. Ueda and K. Kosuge:
J. Phys. Soc. Jpn. 57, 2659 (1988)
- [15] T. Tsuda, T. Shimizu H. Yasuoka, K. Kishio and K. Kitazawa:
J. Phys. Soc. Jpn. 57, 2908 (1988)
- [16] T. Moriya: Springer Series in Solid-State Sciences 56,
Spin Fluctuations in Itinerant Electron Magnetism, (Springer-Verlag, 1985)
- [17] G. Shirane, R. J. Birgeneau, Y. Endoh, P. Gehring, M. A. Kastner, K. Kitazawa, H. Kojima, I. Tanaka, T. R. Thurston and K. Yamada:
Phys. Rev. Lett. 63, 330 (1989)
- [18] P. W. Anderson: Science 235, 1196 (1987)
- [19] P. W. Anderson, G. Baskaran, Z. Zou and T. Hsu:
Phys. Rev. Lett. 58, 2790 (1987)
- [20] K. Ishida, Y. Kitaoka, K. Asayama, H. Katayama-Yoshida, Y. Okabe and T. Takahashi: J. Phys. Soc. Jpn. 57, 2897 (1988)
- [21] P. C. Hammel, M. Takigawa, R. H. Heffner, Z. Fisk and K. C. Ott
Phys. Rev. Lett. 63, 1922 (1989)
- [22] P. Wzietek, D. Kongeter, D. Jerome, J. M. Bassat, J. P. Coutures, B. Dubois and Ph. Odier: Europhys. Lett. 8, 363 (1989)

NQR and NMR Studies of Hole- and Electron-Doped $\text{Ln}_{2-x}\text{M}_x\text{CuO}_4$

K. Kumagai, Y. Nakamura, I. Watanabe, M. Abe and H. Nakajima

Department Physics, Faculty of Science, Hokkaido University, Sapporo 060

Nuclear quadrupole resonance (NQR) and of ^{139}La and $^{63/65}\text{Cu}$ have been investigated in the wide range of x in hole-doped $\text{La}_{2-x}\text{M}_x\text{CuO}_4$ ($\text{M}=\text{Sr}, \text{Ba}$). We confirmed antiferromagnetic order of Cu moments in electron-doped $\text{Ln}_{2-x}\text{Ce}_x\text{CuO}_4$ ($\text{Ln}=\text{Nd}, \text{Pr}, \text{Sm}$). Unexpected observation of nuclear magnetic resonance (NMR) with vanishingly small quadrupole interactions in the Ce-doped samples suggests that the local electronic properties at Cu sites in electron-doped oxides differs from those of the hole-doped ones.

1. Introduction.

While many superconducting families differing in structure and constituent elements are discovered in copper based oxides, they all share Cu-O planes. The one striking feature is that antiferromagnetism is commonly situated near superconducting phase in both n-(electron-doped) and p-(hole-doped) type oxides. Therefore, it is important to understand strong antiferromagnetic spin fluctuations of CuO_2 sheets for the high- T_c superconductivity. It is highly necessary to accumulate experimental data on various properties and reveal the resemblance and difference of the electronic properties at Cu and O sites between n- and p-type superconductors.

In this report we summarize briefly our ^{139}La - and $^{63/65}\text{Cu}$ -NQR and NMR measurements of the hole-doped $\text{La}_{2-x}\text{M}_x\text{CuO}_4$ ($\text{M}=\text{Sr}, \text{Ba}$) and the electron-doped $\text{Ln}_{2-x}\text{Ce}_x\text{CuO}_4$ ($\text{Ln} = \text{Nd}, \text{Pr}, \text{Sm}$).

2. Experimental.

All samples were prepared by solid state reaction from mixed powder of appropriate amounts of SrCO_3 , BaCO_3 , La_2O_3 , CuO , Nd_2O_3 , Pr_2O_3 , Sm_2O_3 and CeO_2 [1,2]. The pellets were crushed in to powder of 350mesh for NQR and NMR measurements. A conventional phase coherent pulsed NMR apparatus was used for the NQR and NMR measurements of spectra and nuclear spin-lattice, T_1 , and spin-spin relaxation time, T_2 .

3. Results and Discussion.

3-1. NQR of hole-doped $\text{La}_{2-x}\text{M}_x\text{CuO}_4$.

We have investigated electrical resistivity and Cu and La-NQR in the wide range of Sr(Ba)-substitution in $\text{La}_{2-x}\text{M}_x\text{CuO}_4$ [3]. The concentration dependence of resistivity of $\text{La}_{2-x}\text{Sr}_x\text{CuO}_4$ is shown in Fig. 1. The resistivity have minimum near $x=0.3$. The system remains to be insulating up to

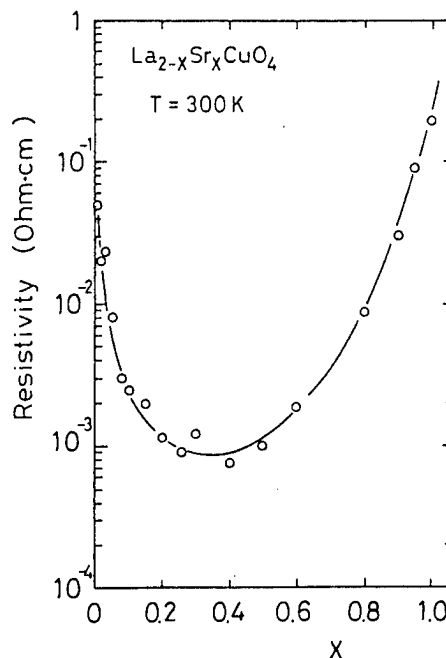


Fig. 1. Concentration dependence of electrical resistivity of $\text{La}_{2-x}\text{Sr}_x\text{CuO}_4$ at room temperature.

$x=0.05$ and the insulator-metal transition takes place near $x=0.05$. Superconductivity appears for appropriate hole-doping ($0.06 < x < 0.3$) [3]. The system undergoes again metal-insulator transition for near $x=0.8$ where the localization of the electronic state is demonstrated by the variable range hopping conduction [3].

As reported in the previous paper [1], the divergence of the nuclear spin relaxation rate of ^{139}La at $T_C^* \sim 10\text{K}$ indicates the existence of the peculiar frustrated magnetic phase between the 3D-antiferromagnetic and superconducting phases. The resonance frequencies between the nuclear $\pm 3/2 \leftrightarrow \pm 5/2$ transition of ^{139}La are shown as a function of temperature in Fig. 2. The anomalous shifts of the resonance frequency are observed at T_C^* , but not at 3D-AF transition temperature, T_N [1,4]. The difference of the frequency between above and below T_C^* is the largest at near $x=0.02$. From the detailed investigation of the resonance frequencies including $\pm 1/2 \leftrightarrow \pm 3/2$ and $\pm 5/2 \leftrightarrow \pm 7/2$ transition of ^{139}La , we obtain the parameters of electric quadrupole interaction and internal magnetic field by the fitting with numerical solution of the following Hamiltonian $H = H_Q + H_{hf}$,

$$H_Q = \frac{e^2 q Q}{4I(2I-1)} [3I_z^2 - I(I+1) + 1/2 n(I_+^2 + I_-^2)]$$

$$H_{hf} = -\gamma h H_0 [I_z \cos \theta + \frac{1}{2} \sin \theta (I_+ \exp(-i\phi) + I_- \exp(i\phi))],$$

where ν_Q is the quadrupole frequency, n is the asymmetry parameter and θ and ϕ are the angles between principal axis of electric field gradient (EFG) and internal field, H_0 . Figure 3 shows the x -dependence of the ν_Q and n above and below T_C^* . The ν_Q decreases gradually with x , but does not change at T_N and T_C^* . The n values in the antiferromagnetic phase are smaller than the ones in the paramagnetic phase above T_N . This fact implies that the magnetic order of Cu moments below T_N is associated with an anomalous change of electric quadrupole interactions.

Figure 4 shows the temperature dependence of the internal fields at La site. The saturated internal field at La site decreases with x , but exists at least up to $x=0.08$, which is consistent with the results of μSR [5] and heat capacity measurement [6,7]. The internal field changes discontinuously at T_C^* . The spin reorientation

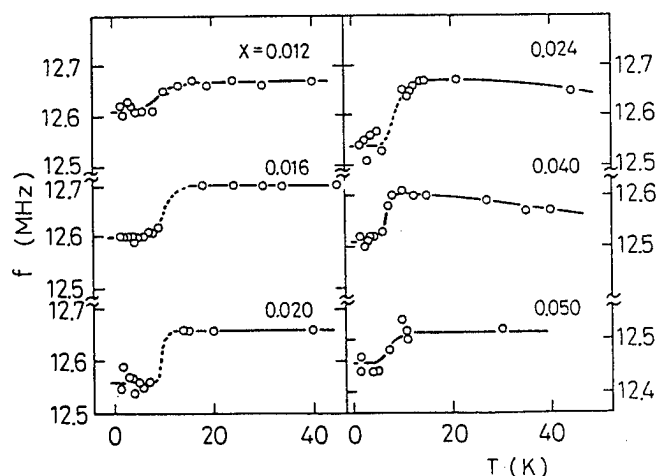


Fig. 2. Temperature dependence of resonance frequency of ^{139}La of the $\pm 3/2 \leftrightarrow \pm 5/2$ transition in $\text{La}_{2-x}\text{Ba}_x\text{CuO}_4$.

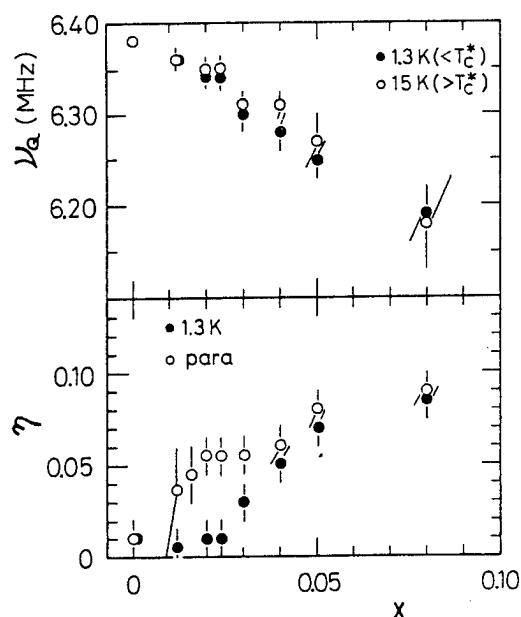


Fig. 3. Concentration dependence of the resonance frequency ν_Q and asymmetry parameter, n , of electric quadrupole interaction in the antiferromagnetic and the paramagnetic phase in $\text{La}_{2-x}\text{Ba}_x\text{CuO}_4$.

such as the La_2CuO_4 to the La_2NiO_4 type or the transition from the collinear to non-collinear spin structure can be considered to interpret the ^{139}La -NQR anomalies at T_c^* [8]. The present La-NQR results suggests the existence of successive magnetic transition for $x < 0.02$. The low temperature magnetic phase extends up to $x = 0.08$ where the superconducting phase appears.

The spin echo signals of $^{63}/^{65}\text{Cu}$ are observed between 30 and 50 MHz in zero external fields for $x \geq 0.12$ [3,9,10]. The failure of the observation of the Cu-NQR signals for $x < 0.1$ is caused by their very shortened T_2 . The spectra consist of two components of Cu-NQR spectra for $x < 0.4$ of which origin is not still unclear. The distribution of the electric quadrupole interaction due to oxygen vacancies and/or random distribution of Sr and La around Cu can be considered [11]. The effect of the charge differentiation on EFG is proposed [12].

The temperature dependence of $1/T_1$ in the superconducting samples of $x < 0.25$ is similar to those of Cu in CuO_2 plane of $\text{YBa}_2\text{Cu}_3\text{O}_7$ [13]. $1/T_1$ is much enhanced in the normal state for $x < 0.3 \sim 0.4$. For $x > 0.3$ where the electrical resistivity shows metallic behavior, the temperature dependence of $1/T_1$ obeys the Korringa relation $T_1 T = \text{const.}$ between 1.5 and 100 K. Figure 5 shows the x -dependence of the $T_1 T$ in the normal state. $T_1 T$ decreases dramatically with x up to $x = 0.3$ and attains the constant value of about $2.0 (\text{s} \cdot \text{K})^{-1}$ for $x > 0.4$ [3].

In addition to the remarkable change of T_1 , the spin-spin relaxation rate, $1/T_2$, decreases rapidly with increasing x , as seen in Fig. 5. The rapid decreases of T_1^{-1} and T_2^{-1} with increasing x suggest the suppression of the antiferromagnetic fluctuations with hole-doping and that the suppression of relaxation can be considered to result from the diminution of effective moments by hole-doping for $x > 0.4$.

The temperature dependence of T_2 is shown in Fig. 6. For the non-superconducting region

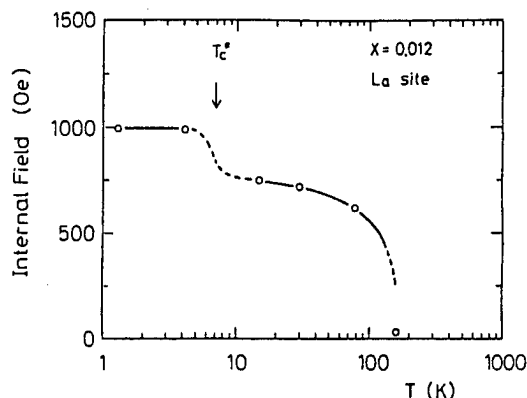


Fig. 4. Temperature dependence of internal fields at La sites in $\text{La}_{1.988}\text{Ba}_{0.012}\text{CuO}_4$.

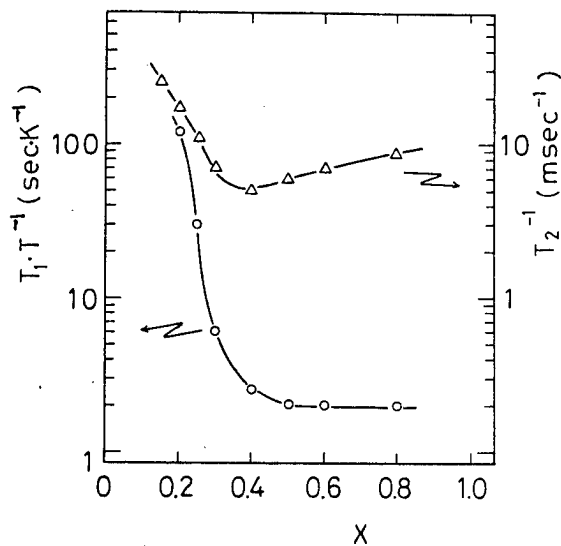


Fig. 5. Concentration dependence of $T_1 T^{-1}$ and $1/T_2$ of ^{63}Cu -NQR in $\text{La}_{2-x}\text{Sr}_x\text{CuO}_4$.

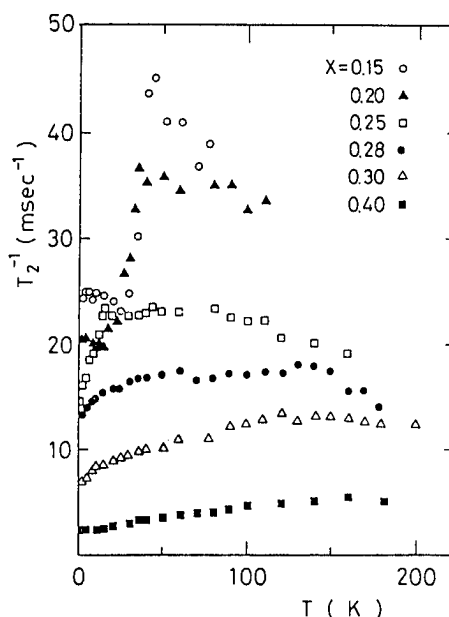


Fig. 6. Temperature dependence of $1/T_2$ of ^{63}Cu in $\text{La}_{2-x}\text{Sr}_x\text{CuO}_4$.

of $x > 0.3$, $1/T_2$ increases monotonously with increasing temperature up to 200K. For the superconducting region, however, $1/T_2$ decreases with increasing temperature in the normal state. (The abrupt decrease of $1/T_2$ below T_c is attributed to the change of the contribution from T_1 due to superconductivity.)

3-2. Cu-NQR and NMR of electron-doped $\text{Ln}_{2-x}\text{Ce}_x\text{CuO}_4$.

The zero field NMR signals were obtained in electron doped $\text{Ln}_{2-x}\text{Ce}_x\text{CuO}_4$ ($\text{Ln}=\text{Nd}, \text{Pr}, \text{Sm}$) [2,14]. The spectrum of Nd_2CuO_4 shown in Fig. 7 have six narrow peaks. They are explained as the superposition of six $^{63}/^{65}\text{Cu}$ lines which are originated from the quadrupole split Zeeman transition. The Larmor and quadrupole frequencies of ^{63}Cu are determined to be $\nu_L=117\text{MHz}$ and $\nu_Q=14\text{MHz}$, respectively. The hyperfine field of 103.7kOe is of the same order but somewhat large compared to the values of 78.8kOe of

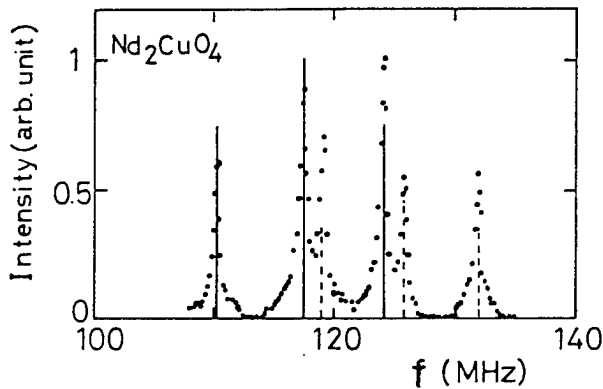


Fig. 7. Spin echo spectra of Cu in Nd_2CuO_4 .

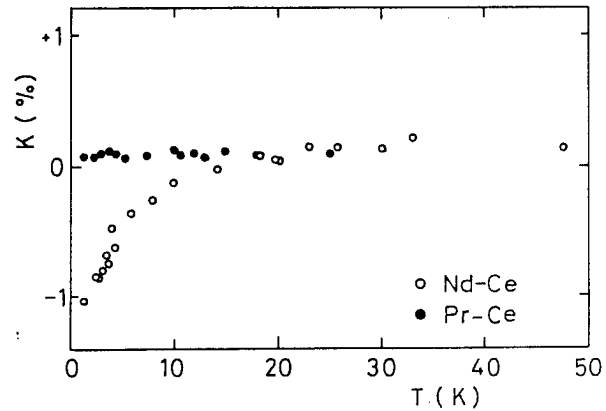


Fig. 9. Knight shift of Cu as a function of temperature for $\text{Nd}_{1.85}\text{Ce}_{0.15}\text{CuO}_4$ (\circ) and $\text{Pr}_{1.85}\text{Ce}_{0.15}\text{CuO}_4$ (\bullet).

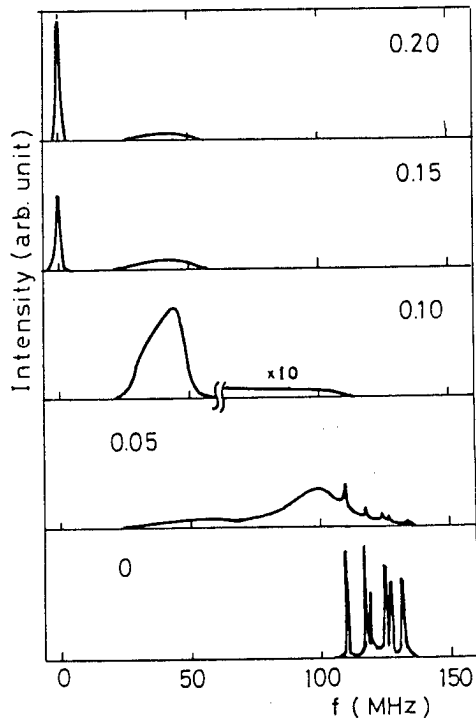


Fig. 8. Zero field Cu-NMR spectra as a function of external field in $\text{Nd}_{2-x}\text{Ce}_x\text{CuO}_4$. The line profiles at $f = 0\text{MHz}$ are obtained by NMR under external field.

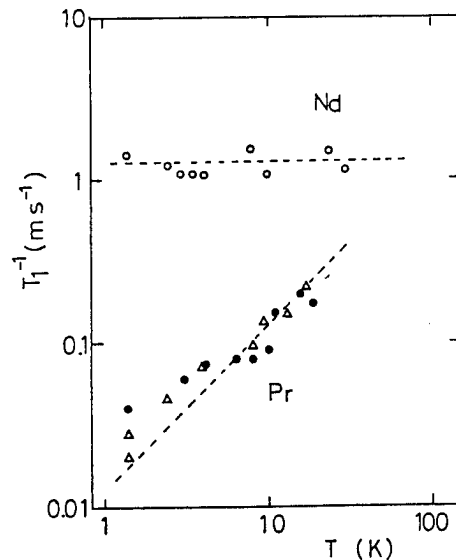


Fig.10. $1/T_1$ of Cu as a function of temperature for $\text{Nd}_{1.85}\text{Ce}_{0.15}\text{CuO}_4$ (\circ) and $\text{Pr}_{1.85}\text{Ce}_{0.15}\text{CuO}_4$ (\bullet)

La_2CuO_4 and 76.65kOe of $\text{YBa}_2\text{Cu}_3\text{O}_6$. The comparable values ν_L and ν_Q to those of hole-doped high- T_c superconductors suggest that Cu moments result from the electronic configuration of $3d^9$ of Cu orbital in the parent Nd_2CuO_4 . The similar antiferromagnetism of Cu moments are confirmed in Pr_2CuO_4 and Sm_2CuO_4 [15].

The zero field Cu-NMR spectra shift to lower frequency side with increasing x in $\text{Nd}_{2-x}\text{Ce}_x\text{CuO}_4$ [2,14]. The similar results are obtained for the system with $\text{Ln}=\text{Pr}$ and Sm [15]. The x -dependence of the resonance frequency is not interpreted only by a unique electric quadrupole interaction of $\nu_Q=14\text{MHz}$ as observed in the parent Nd_2CuO_4 . We consider that the hyperfine field at Cu site due to the ordering of Cu moments decreases with x but remains finite for $x>0.14$. The monotonous decrease of the hyperfine field with Ce-doping is a distinct feature which differs qualitatively from that obtained in the hole-doped ones.

We obtained Cu-NMR with extremely small EFG at Cu sites for $x>0.14$ where the antiferromagnetic order of Cu moments is absent. Figure 8 shows the Cu-NMR spectra as a function of external field. The unexpected and anomalous absence of the EFG at Cu sites is hard to explain at present time. The partial conversion of $3d^9$ electron configuration to $3d^{10}$ by electron-doping and the particular electronic state may mask the EFG at Cu sites in the T' -structure of $\text{Ln}_{2-x}\text{Ce}_x\text{CuO}_4$. Another origin for the cancellation of EFG at Cu site can be considered as a result from the increasing of hybridization of d and s character electrons with Ce-doping.

Figures 9 and 10 show the temperature dependence of Knight shift and $1/T_1$ of Cu-NMR at 12MHz. For the Nd-system, $1/T_1$ is much enhanced to the order of $1-2(\text{ms})^{-1}$ and is almost temperature-independent. The positive Knight shift at high temperatures decreases with decreasing temperature. The contribution of paramagnetic Nd moments to the local magnetic susceptibility is so large that we can not obtain information of superconducting energy gap through temperature dependence of $1/T_1$ and Knight shift. For the Pr-system, $1/T_1$ is less enhanced and is nearly proportional to temperature. The Knight shift has temperature-independent positive values below 20K. As Pr moments is of singlet ground state of J multiplet due to crystalline field effect, Pr moments behaves as nonmagnetic one at low temperature, which give difference of the Cu-NMR between the Nd- and Pr-systems.

Acknowledgements.

The authors would like to thank Prof. T. Fujita for his stimulating discussion. A part of the studies (for Nd-Ce-Cu-O system) are performed in collaboration with A. Awaji and T. Fujita.

References.

- [1] K.Kumagai, I.Watanabe, H.Aoki, Y.Nakamura, T.Kimura, Y.Nakamichi, H.Nakajima, Physica B148 (1987) 480.
- [2] M.Abe, K.Kumagai, S.Awaji and T.Fujita, Physica, C160 (1989) 8.
- [3] Y.Nakamura and K.Kumagai, Physica C161 (1989) 265.
- [4] K.Kumagai, Y.Nakamura, I.Watanabe and H.Nakajima, to be published in Z. Naturforsch (1990).
- [5] A.Weidinger, et al., Phys. Rev. Lett. 62 (1989) 102.
- [6] N.Wada, H.Muro-oka, Y.Nakamura and K.Kumagai, Physica C157 (1989) 453.
- [7] N.Wada, H.Muro-oka, Y.Nakamura and K.Kumagai, to be published in Physica C162-164 (1989).
- [8] I.Watanabe and K. Kumagai, in preparation.
- [9] K.Kumagai and Y.Nakamura, Physica C157 (1989) 307.
- [10] Y.Nakamura and K.Kumagai, to be published in Physica C162-164 (1989).
- [11] K.Ishida, et al., J. Phys. Soc. Jpn. 58 (1989) 36, and J. Phys. Soc. Jpn. 58 (1989) 2638.
- [12] K.Yoshimura, et al., J. Phys. Soc. Jpn. 58 (1989) 3057.
- [13] T.Imai, et al., J. Phys. Soc. Jpn. 57 (1988) 2280.
- [14] K.Kumagai, M.Abe, S.Awaji and T.Fujita, to be published in Physica C162-164 (1989).
- [15] K. Kumagai, S. Tanaka and M. Abe, in preparation.

1. NMR

Y. Kitaoka, K. Ishida, K. Fujiwara, G-q. Zheng, T. Kondo and K. Asayama

2. Susceptibility and Resistivity

Y. Oda and M. Yamada

Department of Material Physics, Faculty of Engineering Science, Osaka University, Toyonaka, Osaka 560

Abstract

1. ^{63}Cu NQR and ^{17}O NMR in $(\text{La}_{1-x}\text{Sr}_x)_2\text{CuO}_4$, $\text{YBa}_2\text{Cu}_3\text{O}_7$ and $\text{YBa}_2\text{Cu}_3\text{O}_{6.65}$, ^{205}Tl in $\text{Tl}_2\text{Ba}_2\text{Ca}_2\text{Cu}_3\text{O}_{10-y}$ ($T_c=116$ K) and $\text{Tl}_2\text{Ba}_2\text{CuO}_{6-y}$ ($T_c=0-90$ K), and Cu NMR in $\text{Nd}_{1.85}\text{Ce}_{0.15}\text{CuO}_{4-y}$ have been systematically investigated. From the hole content dependence of La system, $1/T_1$ in the superconducting sample is strongly enhanced as compared to that of the non-superconducting sample. Within the framework of RPA approximation, the temperature dependence of $(T_1T)^{-1}$ is related to that of the staggered susceptibility $\chi_Q(T)$. On the other hand, the Knight shift and $(T_1T)^{-1}$ of ^{17}O reflect the uniform susceptibility $\chi_0(T)$ which is temperature-dependent except for $\text{YBa}_2\text{Cu}_3\text{O}_7$. $(T_1T)^{-1}$ of ^{205}Tl behaves like a constant in wide temperature region above T_c , while it becomes temperature dependent at higher temperature like that of Cu. As in the case of La system, $(T_1T)^{-1}$ in the non-superconducting $\text{Tl}_2\text{Ba}_2\text{CuO}_{6-y}$ is markedly suppressed as compared to the superconducting materials, being temperature independent in whole temperature range. For the hole-doped compound, the enhanced behavior of χ_Q is a necessary condition for the occurrence of the superconductivity. For Nd system, the drastic change of the electronic state has been observed, accompanied with the diminish of the electric field gradient at the Cu site. $1/T_1$ is dominated by the fluctuation of Nd^{3+} moments and the intrinsic Cu relaxation is expected to be smaller compared with those of the hole-doped superconductor

2. The magnetic and the superconducting phase diagram is presented for $(\text{La}_{1-x}\text{Sr}_x)_2\text{CuO}_{4+y}$ annealed in high pressure oxygen gas up to 400 bar.

1. NMR Study

(1) Cu NQR in $(\text{La}_{1-x}\text{Sr}_x)_2\text{CuO}_4$ system

Since the finding of Cu NQR in this system (1), $1/T_1$ has been measured systematically for the various Sr contents. The most striking feature is that $(T_1T)^{-1}$, which is related to the staggered susceptibility $\chi_Q(T)$ as discussed below, decreases with increasing hole content and after the disappearance of the superconductivity, it is by one order of magnitude depressed being temperature independent, as shown in Fig. 1 (b) (2,3). Here $(T_1T)^{-1}$ in $(\text{La}_{1-x}\text{Sr}_x)_2\text{CuO}_4$ of $x=0.075$ with $T_c=38$ K (solid circles), $x=0.1$ with $T_c=30$ K (rectangle mark) and $x=0.15$ with $T_c=0$ (triangle marks) are shown. With increasing Sr content, T_1 is distributed due to the random mixture of Sr and La around Cu. For $x=0.1$ and $x=0.15$, $(T_1T)^{-1}$ extracted from the longer component of T_1 is plotted in Fig. 1 (b), all components of T_1 for $x=0.1$ show a marked reduction below T_c .

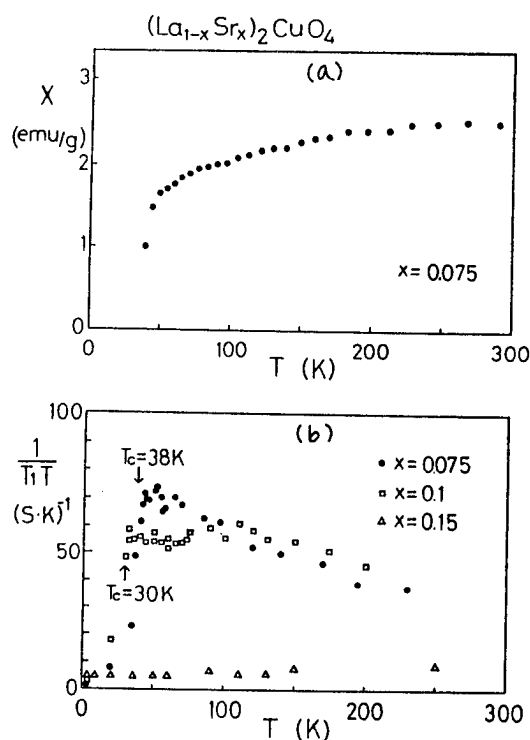


Fig. 1. (a) The magnetic susceptibility of the well annealed sample of $x=0.075$ with $T_c = 38$ K in $(La_{1-x}Sr_x)_2CuO_4$. (b) Temperature dependence of $(T_1T)^{-1}$ for $x=0.075$ (solid circles), $x=0.1$ (rectangle marks) and $x=0.15$ (triangle marks).

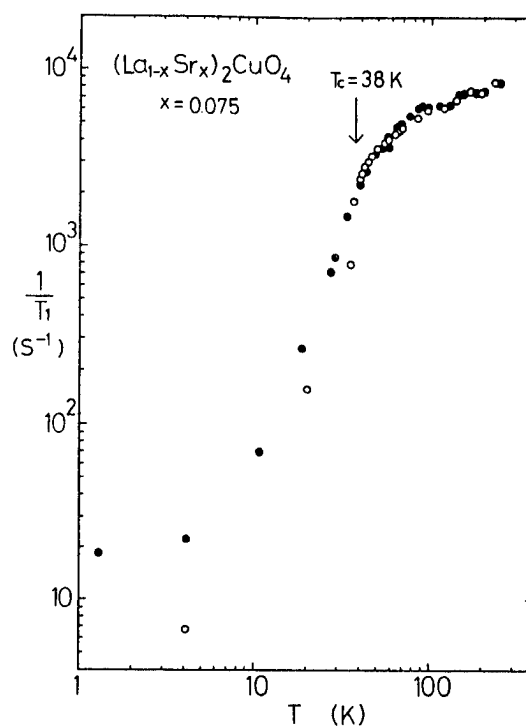


Fig. 2. Temperature dependence of $1/T_1$ in $(La_{1.85}Sr_{0.075})_2CuO_4$ with $T_c = 38$ K. Open circles indicate the data of the well annealed sample.

However, for the superconducting materials with Sr content more than $x=0.1$, the larger distribution of T_1 has been observed and then T_1 undergoes no appreciable variation below T_c even if the diamagnetism was observed (2,4). It is expected from the microscopic point of view that there exists no bulk superconductivity between $x=0.1$ with $T_c = 30$ K and $x=0.15$ with $T_c = 0$. Hence the superconducting phase diagram is considered to be not continuous between $x=0.1$ and 0.15 in consistent to a recent phase diagram proposed by the bulk measurements (5). We have also experienced the small distribution of T_1 even for $x=0.075$ with highest T_c depending on the sample preparation (4). However, by improving the sintering and annealing processes of the sample preparation, a good sample in which T_1 is not distributed has been synthesized. The temperature dependence of the susceptibility χ_0 of this sample is shown in Fig. 1(a). As seen in the figure, it should be noted that χ_0 starts to decrease around 50 K far above T_c . This type of behavior has also been observed for Y system, which is ascribed to the superconducting fluctuation. In order to see the sample-dependence of $1/T_1$ in $x=0.075$, we plotted $1/T_1$ for the well annealed sample (open circles) and the previous sample (closed circles) in Fig. 2. $1/T_1$ in the good sample decreases more rapidly below T_c compared to the previous data (1,2). As seen in Fig. 1(b), $(T_1T)^{-1}$ in $x=0.075$ is by more than one order magnitude enhanced as compared to that for the non-superconducting sample with $x=0.15$. In contrast to the decrease of the uniform

susceptibility $\chi_0(T)$ with decreasing temperature, $(T_1 T)^{-1}$ increases with decreasing temperature and ceases the increase below around 60 K, being nearly constant. This relaxation behavior tells us that the system cannot be interpreted in terms of a usual non-magnetic Fermi liquid picture, but strongly affected by the Cu d-spin fluctuations, which is considered to possess highly localized character.

Here we consider an origin of the temperature dependence of $(T_1 T)^{-1}$ for the superconducting material (4). In general, $(T_1 T)^{-1}$ is described by the formula as

$$(T_1 T)^{-1} = 2 \gamma_n^2 A_{hf}^2 \sum_q \text{Im} \chi(q, \omega_n) / \omega_n \quad (1)$$

where A_{hf} is the hyperfine coupling constant and $\chi(q, \omega)$ is the dynamical susceptibility and ω_n is the resonance frequency. In case when the q -dependence of $\chi(q, \omega)$ is negligible as in the localized moment system, eq. (1) is expressed with the use of the correlation time τ_{eff} of electron spin

$$(T_1 T)^{-1} = 2 \gamma_n^2 A_{hf}^2 \chi_0(T) \tau_{eff} \quad (2)$$

Thus $(T_1 T)^{-1}$ is proportional to the uniform susceptibility $\chi_0(T)$. As seen in Figs. 1 (a) and (b), eq. (2) is, however, not applicable to the Cu oxides, although the Cu-d spin moment is known to possess localized character from various measurements. Accordingly, the q -dependence should be taken into account to explain consistently the difference of the temperature dependence between the $\chi_0(T)$ and $(T_1 T)^{-1}$ as shown in Figs. 1 (a) and (b). We expect that $\chi(q, \omega)$ is enhanced by the antiferromagnetic spin fluctuation coming from the short-range A.F. spin correlation. In this case, within the framework of R.P.A. approximation, $\chi(Q+q, \omega)$ is derived as

$$\chi(Q+q, \omega) = \chi_0(\omega) / (1 - J_{Q+q} \chi_0(\omega)) \quad (3)$$

with $\chi_0(\omega)$, the dynamical susceptibility at single site, i.e.

$$\chi_0(\omega) = \chi_0 \omega / (\omega - i\Gamma) \quad (4)$$

where Γ is the magnetic relaxation rate of Cu spins. We expect that $\Gamma \sim \delta J_K / \hbar$ where δ is the hole concentration of doped holes and J_K is the exchange interaction between the Cu spins and the doped hole spins. J_{Q+q} is the Fourier component of the exchange constant between sites J_{ij} , i.e. $J_{Q+q} = 1/N \sum_{ij} J_{ij} \exp(i(Q+q)(r_i - r_j))$. From eq. (3), the imaginary part which is related to $(T_1 T)^{-1}$ is given by

$$\text{Im} \chi(Q+q, \omega) = \frac{\chi_0 \Gamma \omega}{\omega^2 + \Gamma^2 (1 - J_{Q+q} \chi_0)^2} \quad (5)$$

Hence we have

$$(T_1 T)^{-1} = 2 \gamma_n^2 A_{hf}^2 (\chi_0 / \Gamma) \sum_q \frac{1}{(1 - J_{Q+q} \chi_0)^2} \quad (6)$$

and since J_{Q+q} is reasonably expanded like $J_{Q+q} = J_Q - Cq^2 + \dots$, we have a relation of

$$(T_1 T)^{-1} \propto \chi_Q(T) / (C \chi_0 T) \quad (7)$$

Here eq. (6) is q -integrated by taking account of two dimensional character of the Cu oxides. It is thus considered that $(T_1 T)^{-1}$ of the superconducting compound reflects the enhanced behavior of the staggered susceptibility $\chi_Q(T)$ which is naturally temperature-dependent. On the other hand, it is evident that χ_Q for the non-superconductor is suppressed and becomes temperature independent. Consequently, the $T_1 T = \text{constant}$ law characteristic of the Fermi liquid is observed for the non-superconducting material. This feature has been confirmed for Tl (2201) systems which form a single Cu sheet without Ca layers as shown later. We conclude that there is a strong correlation between the high- T_c superconductivity and the enhancement of the staggered susceptibility χ_Q (4).

Next we comment about the relation between the present NMR result and the neutron experiment which has observed the decrease of the scattering intensity integrated over the wave vector q below around 120 K (6). As seen in Fig. 1 (b), there has, however, been observed no anomaly in the temperature variation of $(T_1 T)^{-1}$ around 120 K. The reason of the difference is not yet clear. From the NMR experiment which is capable of detecting the low energy excitation, we do not have any evidence of the gap formation in the spin excitation as suggested by the neutron experiment as far as the La system is concerned (4).

Here, we pay our attention to the behaviors that $(T_1 T)^{-1}$ is nearly temperature independent below 60 K and begins to decrease near above T_c . Together with the result of the susceptibility which also starts to reduce below 50 K as shown in Fig. 1(a), the reduction of both the uniform (χ_0) and the staggered (χ_Q) susceptibilities just above T_c may be associated with the 2-D superconducting pair correlation or the precursor of the 3-D superconducting transition.

(2) ^{205}Tl NMR in $\text{Tl}_2\text{Ba}_2\text{CuO}_{6-y}$ ($T_c = 0$ K, 12 K and 90 K) and $\text{Tl}_2\text{Ba}_2\text{Ca}_2\text{Cu}_3\text{O}_{10-y}$ ($T_c = 116$ K)

Now, Tl-Ba-Ca-Cu-O compounds have been well established. Among them, $\text{Tl}_2\text{Ba}_2\text{CuO}_{6-y}$ (Tl(2201)) with a single CuO_2 sheet is of great advantage to investigate systematically the relation between the T_c and the microscopic electronic state because T_c in this system with the same crystal structure is ranging from 0 to 90 K depending on the sample preparation. Apart from the CuO_2 sheet, Tl NMR is expected to provide new information on the electronic state different from those of Cu and oxygen in CuO_2 plane (7).

The temperature dependence of ^{205}Tl Knight shifts for $\text{Tl}_2\text{Ba}_2\text{CuO}_{6-y}$ are shown in Fig. 3. The positive shift becomes smaller with decreasing T_c . Since the chemical shift of Tl is considerably large, it is difficult to connect the variation of the Knight shift to the concentration of the doped hole. On the other hand, $(T_1 T)^{-1}$ exhibits a marked change as shown in Fig. 4. The striking feature is that $(T_1 T)^{-1}$ for the non-superconducting sample is temperature-independent and is strongly suppressed as compared to those of the superconducting materials. This behavior of $(T_1 T)^{-1}$ in Tl compounds is quite similar to the case of La system (see Fig. 1 (b)). As demonstrated by the nuclear magnetization recovery of ^{205}Tl in Fig. 5, T_1 of Tl is uniquely defined for the superconducting materials. This point is different from La system in

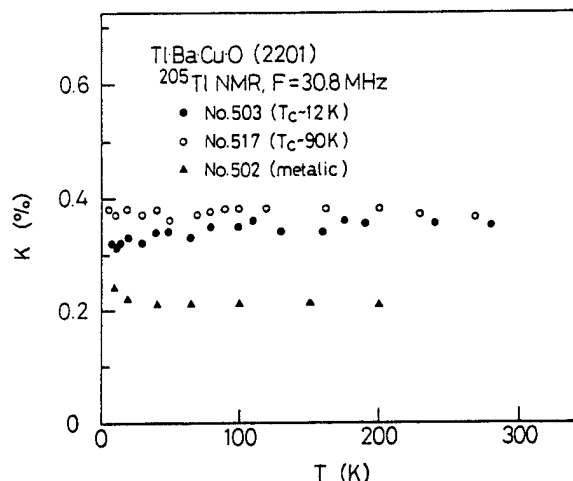


Fig. 3. Knight Shifts of ^{205}Tl in $\text{Tl}_2\text{Ba}_2\text{CuO}_{6-y}$. open circles: $T_c = 90$ K, closed circles: $T_c = 12$ K, triangle marks: $T_c = 0$ K.

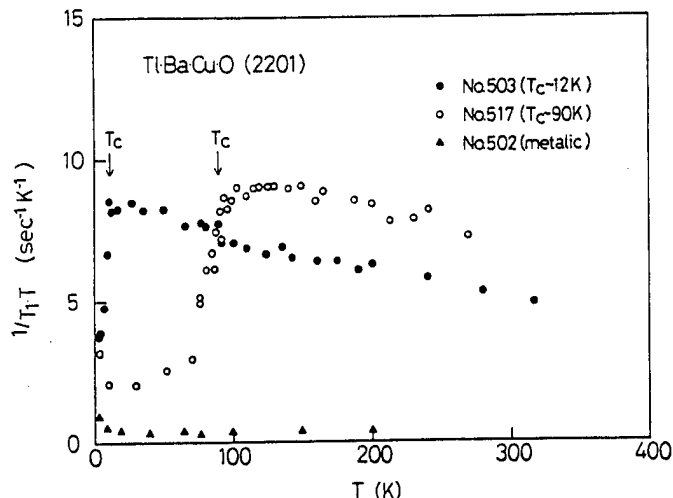


Fig. 4. Temperature dependence of $(T_1T)^{-1}$ of ^{205}Tl in $\text{Tl}_2\text{Ba}_2\text{CuO}_{6-y}$. open circles: $T_c = 90$ K, closed circles: $T_c = 12$ K, triangle marks: $T_c = 0$.

which T_1 of Cu is distributed due to the inhomogeneity in the LaO layer introduced by increasing Sr content. The relaxation behavior of $(T_1T)^{-1}$ in the Tl(2201) with $T_c = 12$ K and 90 K are similar to each other. Namely, $(T_1T)^{-1}$ stays constantly near T_c and decreases with increasing temperature. Again, this feature is quite similar to the behavior of La compound for $x = 0.075$ with $T_c = 38$ K (see Fig. 1(b)). From this similarity, the nuclear relaxation behavior of Tl site is expected to be relevant to that of Cu site. Hence it is plausible that $(T_1T)^{-1}$ of ^{205}Tl reflects the staggered susceptibility $\chi_Q(T)$.

Next we present the result of Tl NMR for $\text{Tl}_2\text{Ba}_2\text{Ca}_2\text{Cu}_3\text{O}_{10-y}$ (Tl(2223)). In this compound, two Tl NMR signals have been observed (7). The temperature dependence of both Knight shifts are presented in Fig. 6. From the comparison of NMR spectra between Tl(2201) with no Ca layer and Tl(2223), the Tl site with negative Knight shift is assigned to the Tl site in Ca layers where Ca ions are substituted by the Tl atoms.

T_1 of ^{205}Tl has been measured for TlO_2 layers with positive shift. $(T_1T)^{-1}$ for Tl(2223) is indicated in Fig. 7 together with the result of Tl(2201) with $T_c = 90$ K. As seen in the figure, $(T_1T)^{-1}$ keeps nearly a constant value up to room temperature. The magnitude of $(T_1T)^{-1}$ for Tl(2223) including three CuO_2 sheets is smaller, than that for Tl(2201) including one CuO_2 sheet. This sort of tendency has been found in $(T_1T)^{-1}$ of Cu in $(\text{La}_{1-x}\text{Sr}_x)_2\text{CuO}_4$ and $\text{YBa}_2\text{Cu}_3\text{O}_7$ (1).

(3) Cu NMR in electron-doped superconductor $\text{Nd}_{1.85}\text{Ce}_{0.15}\text{CuO}_{4-y}$

We have observed an anomalous Cu NMR signal with extremely small nuclear quadrupole frequency in contrast to the hole-doped Cu oxides discovered so far (8). In addition to this NMR signal, zero-field NMR or NQR signals have been reported by several groups (8,9). However, this type of zero-field signals which are believed to be sample-dependent are considered to be not intrinsic for the superconducting sample (9,10). It is interesting to compare the microscopic property of the electron doped

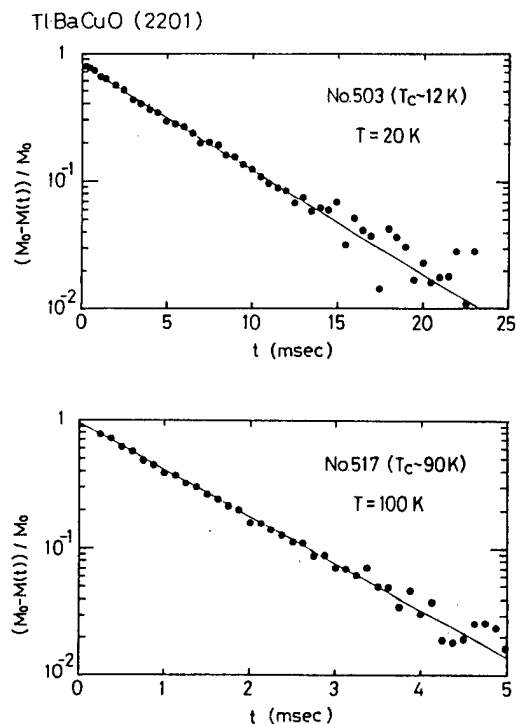


Fig. 5. The recovery curves of nuclear magnetization of ^{205}Tl above T_c in $\text{Tl}_2\text{Ba}_2\text{CuO}_{6-y}$. These nuclear relaxation behaviors demonstrate that the sample is homogeneous independent on T_c . This is different from the La system where T_1 is distributed with decreasing T_c .

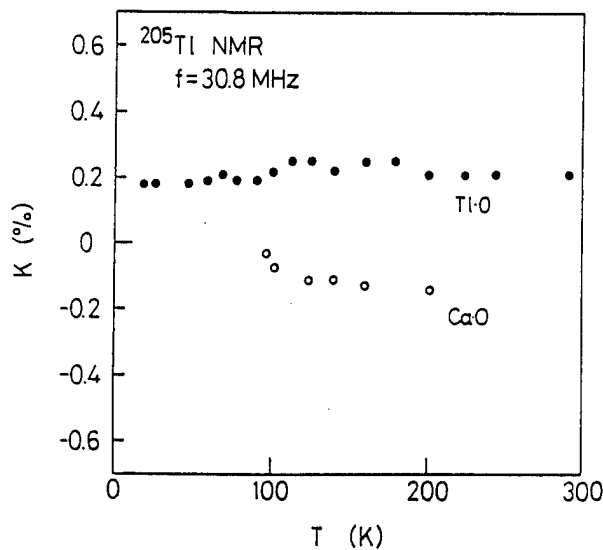


Fig. 6. Knight shifts of ^{205}Tl in $\text{Tl}_2\text{Ba}_2\text{Ca}_2\text{Cu}_3\text{O}_{10-y}$ with $T_c = 116$ K. The solid and open circles correspond to the Tl sites in TlO_2 and Ca layers, respectively.

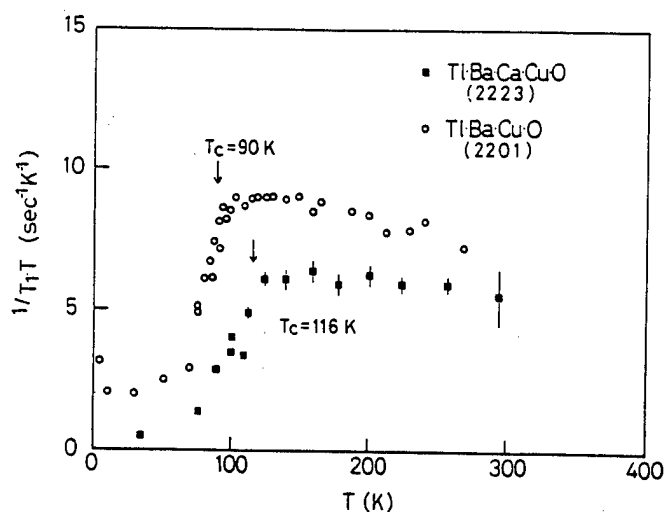


Fig. 7. Temperature dependence of $(T_1T)^{-1}$ of ^{205}Tl in $\text{Tl}_2\text{Ba}_2\text{CuO}_{6-y}$ (open circles) and $\text{Tl}_2\text{Ba}_2\text{Ca}_2\text{Cu}_3\text{O}_{10-y}$ (rectangle marks).

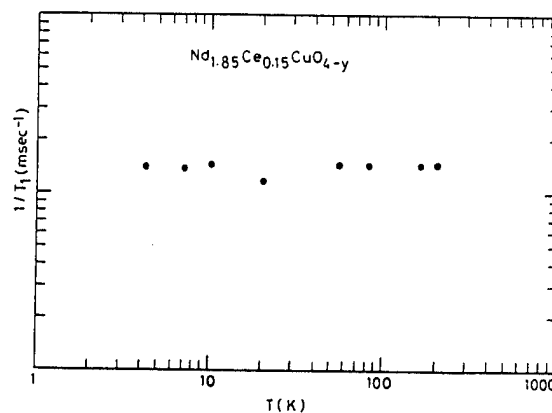


Fig. 8. Temperature dependence of $1/T_1$ of ^{63}Cu in the electron doped superconductor $\text{Nd}_{1.85}\text{Ce}_{0.15}\text{CuO}_{4-y}$.

system with that of the hole-doped system as presented above. However, T_1 of ^{63}Cu is temperature independent in the temperature range of 4.2 K - 200 K without any change below $T_c=23$ K. The result is shown in Fig. 8. This result shows that T_1 of Cu is dominated by the spin fluctuation of the local moments of Nd^{3+} and hence the intrinsic relaxation process is masked. When comparing the magnitude of $1/T_1$ for Nd system to that of La compound with $T_c=38$ K in high temperature region, we notice that $1/T_1$ for La compound is larger than that of Nd system. If the intrinsic relaxation rate of Cu in Nd system were of the same order as $1/T_1$ of La system, $1/T_1$ could be deviated from the behavior shown in Fig. 8 with increasing temperature. This is not the case. The intrinsic $1/T_1$ of Cu due to Cu spin fluctuations appears to be smaller compared with that of La and Y systems. Accordingly, together with the finding of extremely small nuclear quadrupole frequency, we speculate from the T_1 results that the electronic state of Cu d-electron in the electron-doped superconductor is quite different from the case of the hole-doped superconductor.

(4) ^{17}O NMR in High- T_c Superconductor

Since the doped holes are mainly introduced to the oxygen sites, the NMR of oxygen is expected to give important informations (3,11,12,13,14,15,16,17). We present here the ^{17}O NMR results of $(\text{La}_{0.925}\text{Sr}_{0.075})_2\text{CuO}_4$ ($T_c=38$ K) (3), $\text{YBa}_2\text{Cu}_3\text{O}_7$ ($T_c = 91$ K) (12,13,14,15) and $\text{YBa}_2\text{Cu}_3\text{O}_{6.65}$ ($T_c=61$ K) (17). The detailed sample preparation was published elsewhere (11).

(i) Knight Shift

The measurement was carried out with the use of the powder mixed with a low weight polymer which was oriented along the c-axis in situ in NMR coil set in the magnetic field. The temperature dependence of the Knight shifts K_c in CuO_2 and BaO or LaO layers with the c-axis parallel to the magnetic field are shown in Fig. 9, 10, and 11 for $(\text{La}_{0.925}\text{Sr}_{0.075})_2\text{CuO}_4$ ($T_c=38$ K) (3), $\text{YBa}_2\text{Cu}_3\text{O}_7$ ($T_c = 91$ K) (13) and $\text{YBa}_2\text{Cu}_3\text{O}_{6.65}$ ($T_c=61$ K) (17), respectively. As for $\text{YBa}_2\text{Cu}_3\text{O}_7$, both shifts K_c above T_c stay nearly a constant except for the slight decrease of the shift in CuO_2 plane below 100 K. Below T_c , K_c decreases dramatically and then becomes temperature-independent below about 30 K with negative value. This negative value of the shift at low temperatures is owing to the diamagnetic shift arising from the diamagnetic shielding by the supercurrent. The decreasing behavior has been found to be more rapid than the BCS prediction indicated by the dashed line in Fig. 10. The strong reduction of the Knight shift of ^{17}O in CuO_2 plane provides a strong evidence that the high- T_c superconductivity is formed by the singlet pairing with the strong coupling feature.

In $(\text{La}_{0.925}\text{Sr}_{0.075})_2\text{CuO}_4$ ($T_c=38$ K) and $\text{YBa}_2\text{Cu}_3\text{O}_{6.65}$ ($T_c=61$ K), the temperature dependence of K_c in CuO_2 plane becomes substantial, reflecting the temperature dependence of the uniform susceptibility (see Fig. 9 and 11), while the shifts in LaO and BaO layers are invariant above T_c . Actually, as demonstrated in the inset of Fig. 11, K_c in CuO_2 plane of $\text{YBa}_2\text{Cu}_3\text{O}_{6.65}$ is proportional to the susceptibility $\chi_o(T)$ with the hyperfine coupling constant of $35.5 \text{ kOe}/\mu_B$ (17). Furthermore, such relation between K_c and $\chi_o(T)$ has been also found for La system and the hyperfine coupling constant was estimated to be $137 \text{ kOe}/\mu_B$ (3). Here we note that the Knight shift in CuO_2 plane is predominated by the isotropic term of the hyperfine interaction which comes from the Fermi contact interaction with the spin density of s-symmetry. This isotropic term yields the difference of the microscopic electronic state at the oxygen

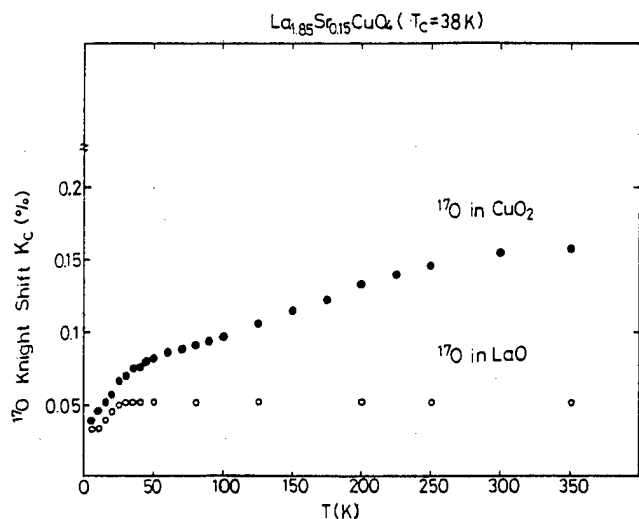


Fig. 9. Temperature dependence of Knight shifts of ^{17}O in $\text{La}_{1.85}\text{Sr}_{0.15}\text{CuO}_4$ with $T_c = 38$ K. Solid and open circles correspond to the data in CuO_2 and LaO layers, respectively.

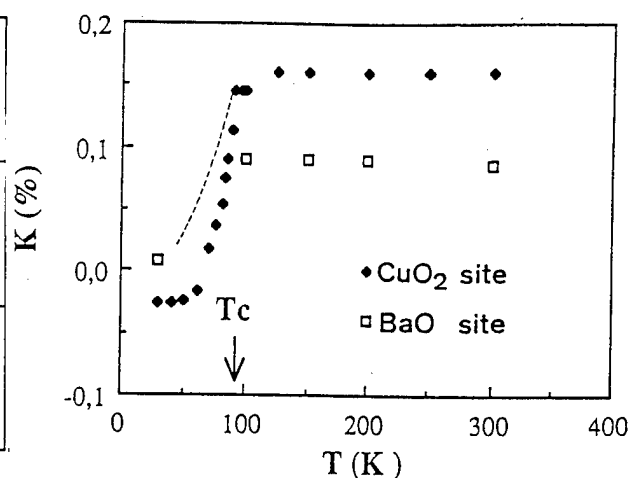


Fig. 10. Temperature dependence of Knight shifts of ^{17}O in $\text{YBa}_2\text{Cu}_3\text{O}_{7-y}$ with $T_c = 91$ K. Solid and open rectangle marks indicate the data in CuO_2 and BaO layers, respectively.

sites between CuO_2 plane and BaO or LaO layers. Hence we should take account of not only $\text{O}(2p)\text{-Cu}(3d)$ hybridization, but also the $\text{O}(2s)$ or $\text{Cu}(4s)\text{-Cu}(3d)$ hybridization in order to gain further insight into the electronic structure in high- T_c compound (3,13).

(ii) T_1 of Oxygen

We have first measured the temperature dependence of T_1 in $\text{YBa}_2\text{Cu}_3\text{O}_7$ and reported the enhancement just below T_c (11). In our previous report, this enhancement was considered to be associated with the oxygen site in CuO_2 . Takigawa, et al (12) and Horvatic, et al. (13) have shown that the various oxygen sites such as $\text{O}(2,3)$ in CuO_2 plane, $\text{O}(1)$ in CuO chain and $\text{O}(4)$ in BaO layer possess different electronic states. In fact, Takigawa et al. have reported that T_1 of $\text{O}(2,3)$ in CuO_2 is by two orders of magnitude shorter than T_1 of $\text{O}(4)$ in BaO layer (15). This difference is expected to be due to the large isotropic hyperfine coupling constant of $\text{O}(2,3)$ in CuO_2 plane. Comparing our previous results with theirs, our T_1 could be associated with $\text{O}(4)$ site in BaO layer. Following us, Wzietek et al. also have observed a distinct enhancement of $1/T_1$ which is associated with $\text{O}(4)$ site (14). On the other hand, Takigawa et al. have reported that T_1 of all oxygen sites including $\text{O}(4)$ site show no enhancement just below T_c (15). Accordingly, the results of T_1 are not consistent with each other. In order to confirm whether or not the enhancement of $1/T_1$ observed for $\text{O}(4)$ site is intrinsic and if the enhancement of $\text{O}(2,3)$ in CuO_2 plane is not observed even at zero magnetic field, further systematic experiments are required. Here we focus on the T_1 results of $\text{O}(2,3)$ for La and Y compounds.

In Fig. 12, $(T_1 T)^{-1}$ of ^{17}O of La compound (16) and $\text{YBa}_2\text{Cu}_3\text{O}_7$ reported by Takigawa, et al (15), are indicated. $(T_1 T)^{-1}$ for Y system is nearly temperature-independent above T_c , while that of La compound, which is at the moment a preliminary result, shows rather weak temperature dependence. Different from those behaviors, $(T_1 T)^{-1}$ of $\text{YBa}_2\text{Cu}_3\text{O}_{6.65}$ above T_c shown in Fig. 13 shows a substantial decrease with decreasing temperature in a similar manner to the susceptibility and the Knight shift (see Fig.

11) (17). As for the increase of $(T_1T)^{-1}$ below around 80 K in $\text{YBa}_2\text{Cu}_3\text{O}_{6.65}$ (see Fig. 13), this anomaly is not due to the magnetic relaxation process, but due to the quadrupole relaxation process, of which the origin is not yet clear (17). The detailed analysis should be referred to the paper (17). When comparing the relaxation behaviors of ^{17}O with those of Cu, we are aware that $(T_1T)^{-1}$ of ^{17}O of O(2,3) in CuO_2 plane has relevance to the uniform susceptibility $\chi_o(T)$ in contrast to the behavior of $(T_1T)^{-1}$ of Cu which is associated with the staggered susceptibility $\chi_Q(T)$.

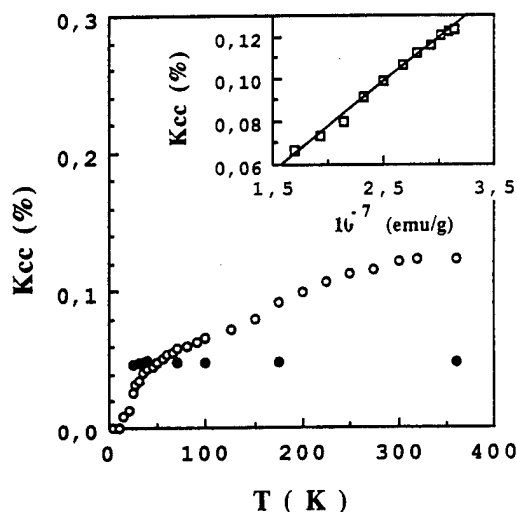


Fig. 11. Temperature dependence of Knight shifts of ^{17}O in $\text{YBa}_2\text{Cu}_3\text{O}_{6.65}$ with $T_c = 61$ K. Open and solid circles indicate the data in CuO_2 and BaO layers, respectively. Inset shows the Knight shift vs. the susceptibility plot with the temperature as an implicit parameter.

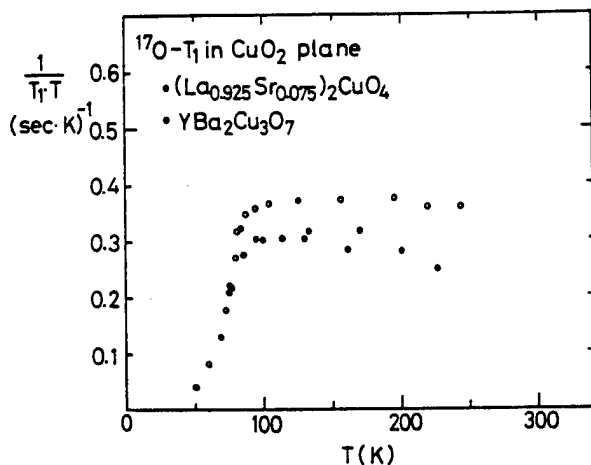


Fig. 12. Temperature dependence of $(T_1T)^{-1}$ of ^{17}O in CuO_2 plane for La (solid circles) and Y (open circles) systems.

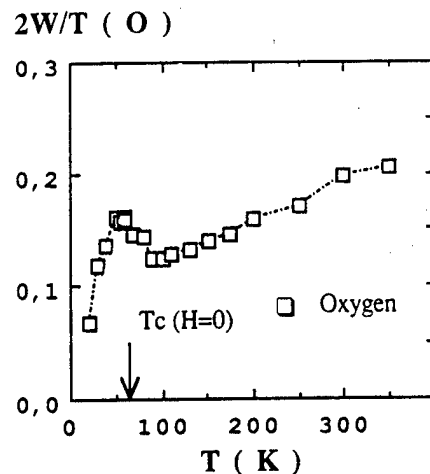


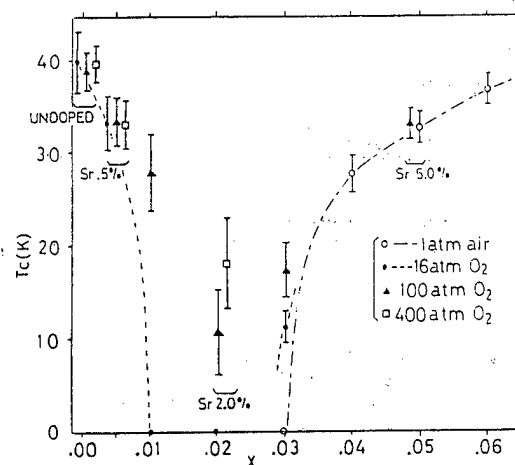
Fig. 13. Temperature dependence of $(T_1T)^{-1}$ of ^{17}O in CuO_2 plane for $\text{YBa}_2\text{Cu}_3\text{O}_{6.65}$ with $T_c = 61$ K.

2. Susceptibility and Resistivity

Electrical and magnetic properties of $(\text{La}_{1-x}\text{Sr}_x)_2\text{CuO}_{4+y}$ annealed in high pressure oxygen gas up to 400 bar has been studied. The superconducting $(\text{La}_{1-x}\text{Sr}_x)_2\text{CuO}_{4+y}$ includes two separate phases: one is superconducting phase with extra oxygen, and the other is the well known antiferromagnetic phase with Neel temperature T_N of 240-300 K depending on the annealing atmosphere. the superconducting phase in the undoped sample becomes unstable by Sr doping. The obtained phase diagram is shown in Fig. 14 (18).

The works on ^{17}O have been performed in collaboration with M. Horvatić, Y. Berthier, P. Butaud, P. Ségransan, C. Berthier (Grenoble), H. Katayama-Yoshida, Y. Okabe and T. Takahashi (Sendai). The d.c. susceptibility measurement has been made by Y. Yamada (Himeji). The samples of Tl compounds were supplied by J.J. Capponi (Grenoble) and Sumitomo company (Tokyo Japan).

Fig. 14. The relation between T_c of $(\text{La}_{1-x}\text{Sr}_x)_2\text{CuO}_{4+y}$ and Sr concentration x . The ends of the bar show the onset and zero resistance temperatures, respectively. The annealing atmosphere are shown in the figure. The data marked with parentheses are for the same Sr concentration.



References

- (1) K. Ishida et al.: J. Phys. Soc. Jpn. 58 (1989) 36.
- (2) K. Ishida et al.: J. Phys. Soc. Jpn. 58 (1989) 2638.
- (3) Y. Kitaoka et al.: IBM Japan Int. Symposium on "Strong Correlation and Superconductivity" eds. by Fukuyama et al. (Springer Series in Solid State Science 89, (1989) p.262)
- (4) Y. Kitaoka et al.: in preparation.
- (5) J.B. Torrance, et al. Phys. Rev. 40 (1989) November.
- (6) G. Shirane et al. p. 236 in ref. (3)
- (7) K. Fujiwara et al.: in preparation.
- (8) G-q. Zheng et al.: J. Phys. Soc. Jpn. 58 (1989) 1910.
- (9) Y. Kohori et al.: to be published in J. Phys. Soc. Jpn.
- (10) H. Yasuoka: private communication.
- (11) K. Ishida, et al.: J. Phys. Soc. Jpn. 57 (1988) 2897.
- (12) M. Takigawa et al: Phys. Rev. B 39 (1989) 300.
- (13) H. Horvatic et al. Physica C159 (1989) 689.
- (14) P. Wzietek et al.: Europhys. Lett. 8 (1989) 363.
- (15) P.C. Hammel et al.: Phys. Rev. Lett. 63 (1989) 1992.
- (16) Ishida et al.: in preparation.
- (17) P. Butaud, et al.: to be published in Physica C.
- (18) Y. Oda et al.: submitted to J. Phys. Soc. Jpn.

Proton NMR Studies of Hydrogen-Doped Superconductor $\text{YBa}_2\text{Cu}_3\text{O}_{6.94}\text{H}_x$

H. NIKI[†], T. HIGA^{*}, S. TOMIYOSHI^{**}, M. OMORI^{**}, T. KAJITANI^{**}, T. SATO^{**},
T. SHINOHARA^{**}, T. SUZUKI^{***}, K. YAGASAKI^{*}, and R. IGEI[†]

Department of Physics, Division of General Education[†] and College of Science^{*},

University of the Ryukyus, Nishihara, Okinawa 903-01, Japan

^{**}Institute for Materials Research, Tohoku University, Sendai 980, Japan

^{***}Institute of Physics, University of Tsukuba, Tsukuba, Ibaraki 305, Japan

Proton NMR in the hydrogen-doped $\text{YBa}_2\text{Cu}_3\text{O}_{6.94}\text{H}_x$ ($x=0.2, 0.5$) was carried out. Relaxation time T_1 of ^1H in $\text{YBa}_2\text{Cu}_3\text{O}_{6.94}\text{H}_{0.2}$ with T_c of 92 K has been measured between 77 K and 300 K. Just below T_c , the spin-lattice relaxation rate T_1^{-1} shows a fairly large enhancement at $0.93 T_c$, followed by sharp decrease with decreasing temperature. This suggests the existence of a superconducting energy gap $2\Delta \approx 13k_B T_c$. The hydrogen atom in $\text{YBa}_2\text{Cu}_3\text{O}_{6.94}\text{H}_{0.5}$ is moving above 200 K but is trapped in the crystal below 150 K, whose behavior is similar to that of $\text{YBa}_2\text{Cu}_3\text{O}_{6.94}\text{H}_{0.2}$.

1. Introduction

Nuclear magnetic resonance (NMR) is one of the most powerful experimental methods for the investigation of superconductivity from a microscopic point of view. Nuclear spin-lattice relaxation time T_1 , line width and Knight shift give detailed information to elucidate the mechanism of superconductivity of high- T_c ceramic.

In this paper we report measurements of proton NMR in hydrogen doped superconductor $\text{YBa}_2\text{Cu}_3\text{O}_{6.94}\text{H}_x$ ($x=0.2, 0.5$) [1,2]. Since the spin of ^1H nucleus is $1/2$ with no quadrupole moment, we can measure T_1 of ^1H without any complexity resulting from quadrupole effect.

2. Experimental

The sample of $\text{YBa}_2\text{Cu}_3\text{O}_{7-\delta}$ was prepared by the method described in previous paper [1]. Before doping hydrogen the samples have T_c of about 92 K and also the oxygen concentration of 6.94 which is estimated by comparing the lattice parameters by neutron diffraction. Hydrogen was doped with an apparatus of Silverts type under the pressure of about 420 Pa at 570 K.

A conventional phase-coherent pulsed NMR spectrometer is employed for measurements of T_1 , T_2 and inverse linewidth parameter T_2^* with a resonance frequency of 33 MHz in the applied magnetic field of about 7.8 kOe. A conventional bridge spectrometer for the measurements of the line width of NMR spectra.

The T_1 is determined by $180^\circ - \tau - 90^\circ$ pulse sequences. The magnetization $M(\tau)$ at time τ after 180° pulse is determined from the height of the free induction decay-tails following the pulse. The T_1 is determined by $\log [(M(\tau) - M_0)/2M_0]$ vs. τ plots, where M_0 is the nuclear magnetization of ^1H in thermal equilibrium.

3. Results and Discussions

3-1. Nuclear spin-lattice relaxation T_1 in $\text{YBa}_2\text{Cu}_3\text{O}_{6.94}\text{H}_{0.2}$

The recovery curves of the nuclear magnetization of the hydrogen nucleus at all temperatures indicate that the long tail part of the recovery curve in the longer time

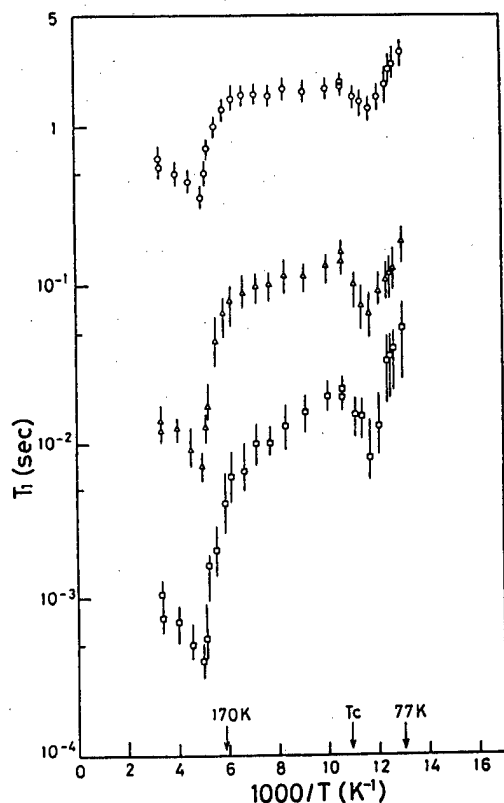


Fig. 1. Temperature dependence of T_1 of ^1H in $\text{YBa}_2\text{Cu}_3\text{O}_{6.94}\text{H}_{0.2}$ as a function of T^{-1} .

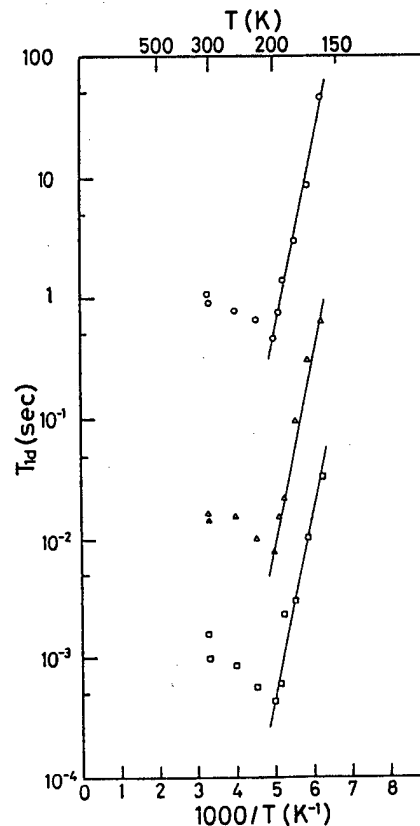


Fig. 2. Temperature dependence of T_{1d} of ^1H in $\text{YBa}_2\text{Cu}_3\text{O}_{6.94}\text{H}_{0.2}$ as a function of T^{-1} .

The value of 30 ± 5 kJ/mol for the activation energy is obtained from the slope of the solid line.

region is straight, but in shorter time region it deviates from the straight line [2]. The non-linear part of the recovery curve has been observed. Since the inverse of the slope of the recovery curve gives T_1 , the deviation from the straight line suggests that several relaxation times should be necessary to reproduce the observed ones [3]. Therefore, we first determined the longest T_1 from the straight part of the curve in longer time region. The next T_1 was determined from the curve remained after subtracting the straight line of the longest T_1 from the original decay curve. The similar processes repeated in sequence gave shorter T_1 's. Three T_1 's thus obtained were found to fit well all of the original decay curves.

Figure 1 shows the temperature dependence of the three T_1 's. As easily seen from this figure the temperature dependence of each T_1 has similar tendency. One of the most interesting tendencies is that the T_1 curves show sharp drops at 170 K. These V-shape curves of T_1 vs. T^{-1} indicate that hydrogen atoms trapped in the crystal begin to move at this temperature [4], which is consistent with the results obtained by continuous wave (cw) method [1]. It should be noticed that all of the onset

temperatures of hydrogen movement determined from the T_1 curves agree very well. If each T_1 results from different hydrogen site, it will give different onset temperature. Thus, we can conclude that the three T_1 curves are caused by the hydrogen atoms trapped in the single atomic site which should be interstitial site between the Cu(1)'s in the two adjacent Cu(1)O chains or vacant O(1) site of $\text{YBa}_2\text{Cu}_3\text{O}_7$ lattice (Hereafter, we call the former H(1) site and the latter H(2) site as determined in Ref. 1.)

The conclusion above has been also confirmed by the analysis of the activation energy as shown below. In this temperature range T_1^{-1} can be written as

$$T_1^{-1} = T_{1d}^{-1} + T_{1t}^{-1},$$

where T_{1d} is the spin-lattice relaxation time which is caused by the contribution from the moving hydrogen atoms, and T_{1t} denotes the contribution from the other mechanisms. The T_{1t} is determined from the lower temperature region where hydrogen atoms are trapped in the crystal. Thus we can obtain the T_{1d} as shown in Fig. 2. All of the three curves are characterized by the same single slope. The activation energy is determined from this slope as 30 ± 5 kJ/mol which also agrees well with the value determined from the analysis of the line width obtained by cw method [1]. This means that the three T_{1d} 's are caused by the hydrogen atoms occupying the single crystallographic site as described above.

In the case of single site, the most plausible origin of the deviation of the decay curve from the straight line will be the paramagnetic impurity center. According to Blumberg [5], if there are paramagnetic impurity centers, the magnetization $M(\tau)$ varies with time τ : for small τ region, $M(\tau) \propto \tau^{1/2}$ and for sufficiently large τ region, $M(\tau) = M_0[1 - \exp(-\tau/T)]$.

We have plotted the $(M_0 - M(\tau))/2M_0$ against $\tau^{1/2}$. The results shows that $M(\tau)$ depends well on $\tau^{1/2}$ both below and above T_c up to 150 K. This suggests that paramagnetic impurities are present in $\text{YBa}_2\text{Cu}_3\text{O}_{6.94}\text{H}_{0.2}$. But above 150 K the $M(\tau)$ does not depend on $\tau^{1/2}$, which is considered due to the movement of hydrogen atoms.

Since we used high purity reagents, paramagnetic impurities other than the constituent elements are not conceivable. The most probable paramagnetic sources are

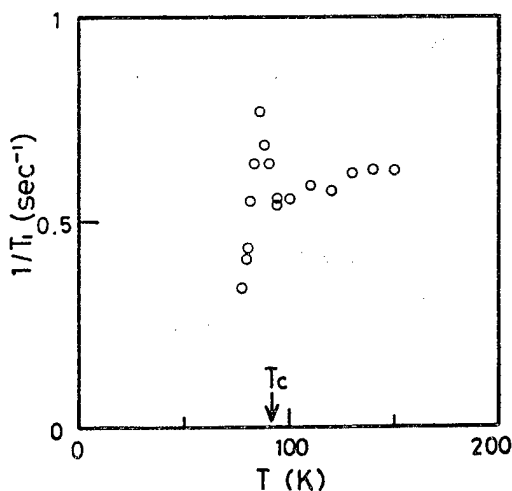


Fig. 3. Temperature dependence of nuclear relaxation rate T_1^{-1} of ^1H in $\text{YBa}_2\text{Cu}_3\text{O}_{6.94}\text{H}_{0.2}$ excluding the effect of paramagnetic impurities.

Cu atoms which occupy Cu(1) site in $\text{YBa}_2\text{Cu}_3\text{O}_{7-\delta}$. The oxygen occupation of O(1) site in the Cu(1)O chain is not perfect and the interstitial site named H(1) site is partly occupied [6]. Randomness of oxygen site-occupation would induce the magnetic moment on Cu(1) atoms. Though the amount of paramagnetic centers is not clear from the present NMR experiments, it would be very small. The T_1^{-1} obtained by excluding the paramagnetic impurity effect below 150 K is shown in Fig. 3.

Above T_c , the temperature dependence of T_1 does not follow the Korringa relation, $T_1 T = \text{const.}$ If the relation could hold, it is limited to the very narrow temperature region just above T_c . This comes from the fact that the contribution from conduction electrons is very weak in the crystal as the T_1 is very long.

Below T_c , the large enhancement of T_1^{-1} has been observed as shown in Fig. 3: the T_1^{-1} has a peak at $0.93T_c$ and decreases sharply with decreasing temperature. After our measurement [7], Morimoto et al. [8] confirmed the existence of the enhancement. The behavior of T_1^{-1} below T_c is very similar to that observed for conventional BCS superconductors, which arises from the formation of energy gap in the conduction bands. The facts shown in Fig. 5 suggest the formation of energy gap in $\text{YBa}_2\text{Cu}_3\text{O}_{6.94}\text{H}_{0.12}$ when it becomes superconducting state. In $\text{YBa}_2\text{Cu}_3\text{O}_7$ system no enhancement of T_1^{-1} has been observed for Cu nuclei, which would be suppressed by spin fluctuation of Cu atoms. Kitaoka and Asayama [9] discussed that enhancement of T_1^{-1} is observed only for O(4) site oxygen in BaO plane because the hybridization of the oxygen atom with 3d hole in $\text{Cu}(2)\text{O}_2$ plane is small compared with that at O(2) and O(3) sites in the $\text{Cu}(2)\text{O}_2$ plane. The peak-temperature of the enhancement of T_1^{-1} for ^1H agrees very well with that of ^{17}O obtained by them. The enhancement of T_1^{-1} of proton suggests that bonding of hydrogen atom with Cu(1) atom may not be so strong as that with O(4) atom. As a result of our NMR measurements [1], hydrogen atom was assigned to H(1) or H(2) site, but this result has not been confirmed by neutron diffraction. In order to understand NMR data further, we need neutron diffraction experiments in more detail.

The energy gap Δ can be extracted from the slope of T_1 vs. T^{-1} curve below the peak if we assume that T_1^{-1} is proportional to $\exp(-\Delta/k_B T)$ derived from BCS theory. The gap determined from the slope is $\Delta = 600$ K, which corresponds to $2\Delta = 13k_B T_c$. This value is rather high compared to BCS value, $2\Delta = 3.5k_B T_c$, but it is comparable to the values $2\Delta = 8k_B T_c$ in the c-plane and $3k_B T_c$ in the direction perpendicular to the c-plane from infrared measurement [10], and $2\Delta = 8k_B T_c$ shown by Photoemission [11]. For more accurate evaluation of the gap, measurement of T_1 in lower temperature region, which is now in progress, is necessary. Besides the consideration of the energy gap, the effect of paramagnetic impurities would contribute to the enhancement of T_1^{-1} and its details would be discussed elsewhere.

3-2. Further Research in $\text{YBa}_2\text{Cu}_3\text{O}_{6.94}\text{H}_x$

The line width of NMR spectra in $\text{YBa}_2\text{Cu}_3\text{O}_{6.94}\text{H}_{0.5}$ was measured in the temperature range from 90 K to 300 K. The line width was determined from peak to peak separation of an absorption derivative ΔH_{pp} . Figure 4 shows the temperature dependence of ΔH_{pp} . The line width is extremely narrow above 190 K due to diffusion or some other dynamical atoms, but it becomes broader below 190 K and keeps almost a constant value of $\Delta H_{pp} = 1.5 \pm 0.5$ Oe in the temperature range from 130 K down to T_c of 92 K. This behavior of the line width suggests that hydrogen atoms are trapped in some sites of the crystal. The temperature dependence of the line width is similar to that of

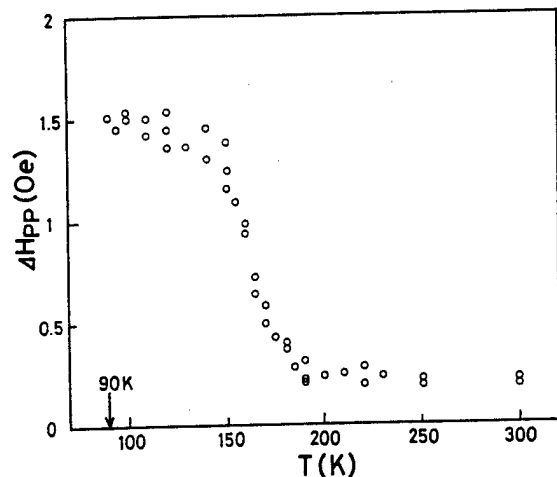


Fig. 4. Temperature dependence of peak to peak separation of the absorption derivative of ^1H NMR in $\text{YBa}_2\text{Cu}_3\text{O}_{6.94}\text{H}_{0.5}$

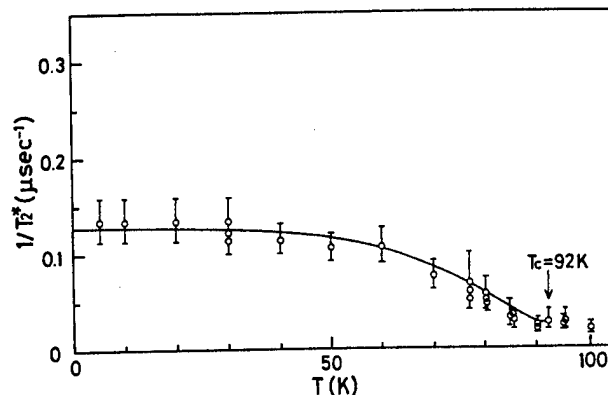


Fig. 5. Temperature dependence of $1/T_2^*$ of ^1H in $\text{YBa}_2\text{Cu}_3\text{O}_{6.94}\text{H}_{0.2}$. The solid line is a curve calculated using $\lambda_0 = 4000 \text{ \AA}$.

$\text{YBa}_2\text{Cu}_3\text{O}_{6.94}\text{H}_{0.2}$ [1]. But T_c is lower by 2 K than that of $\text{YBa}_2\text{Cu}_3\text{O}_{6.94}\text{H}_{0.2}$. Previously [1] we measured the penetration depth of magnetic fields at $T = 0 \text{ K}$ λ_0 from temperature dependence of the line width of NMR spectra below T_c in $\text{YBa}_2\text{Cu}_3\text{O}_{6.94}\text{H}_{0.2}$ and determined the value of λ_0 to be 2500 \AA . Now we measure λ_0 from the temperature dependence of inverse line width T_2^* since we can directly observe inhomogeneous broadening of the line width caused by the change in the penetration depth of magnetic fields. Figure 5 shows temperature dependence of $1/T_2^*$. We obtain the value of λ_0 to be 4000 \AA . This value is slightly larger compared with that of $\text{YBa}_2\text{Cu}_3\text{O}_{6.94}\text{H}_{0.2}$. Its detailed investigation including measurements of temperature dependence of T_2 will be reported elsewhere.

References

- 1) H. Niki, T. Suzuki, S. Tomiyoshi, H. Hentona, M. Omori, T. Kajitani, T. Kamiyama, and R. Igei, Solid State Commun. 69, 547 (1989).
- 2) H. Niki, H. Hentona, S. Tomiyoshi, M. Omori, T. Kajitani, T. Suzuki, T. Kamiyama and R. Igei, Phys. Rev. Lett. to be submitted.
- 3) N. J. Trappeniers, C. J. Gerritsma, and P. H. Oosting, Physica 30, 997 (1964).
- 4) A. Abragam, The Principles of Nuclear Magnetism (Clarendon Press, Oxford, 1961).
- 5) W. E. Blumberg, Phys. Rev. 119, 79 (1960).
- 6) F. Izumi, H. Asano, T. Ishigaki, E. Takayama-Muromachi, Y. Uchida, and N. Watanabe, Jpn. J. Appl. Phys., 26, L1193 (1987).
- 7) H. Niki, T. Suzuki, S. Tomiyoshi, H. Hentona, M. Omori, T. Kajitani, T. Kamiyama, and R. Igei, Read at the 44th Annual Meeting of the Phys. Soc. Jpn., Hiratsuka, March, 1989, 31a-PS-22 (Advance abstracts vol. 3, p.135) [in Japanese].
- 8) K. Morimoto, T. Takabatake, W. Ye, S. Orimo, T. Hihara, and H. Fujii, Physica C, 159, 849 (1989).
- 9) Y. Kitaoka and K. Asayama, Solid State Physics (Agune Gijutsu Center, Tokyo, 1989), Vol. 24, No. 9, p. 43 [in Japanese].

- 10) R. T. Collins, Z. Schlesinger, F. Holtzberg, and C. Feild, Phys. Rev. Lett. 63, 422 (1989).
- 11) J. -M. Imer, F. Patthey, B. Dardel, W. -D. Schneider, Y. Baer, Y. Petroff, and A. Zetttl, Phys. Rev. Lett. 62, 336 (1989).

Hydrogen Absorption in Some High- T_c Copper Oxides

H. Fujii, T. Takabatake, K. Morimoto, W. Ye,
S. Orimo, T. Ekino and T. Hihara

Faculty of Integrated Arts and Sciences,
Hiroshima University, Hiroshima 730

We report on the superconducting properties and nuclear spin-lattice relaxation time of ^1H in $\text{YBa}_2\text{Cu}_3\text{O}_{6.91}\text{H}_x$, $\text{Bi}_2\text{Sr}_2\text{CaCu}_2\text{O}_{8+y}\text{H}_x$ and $\text{Bi}_{1.6}\text{Pb}_{0.4}\text{Sr}_2\text{Ca}_2\text{Cu}_3\text{O}_{10+y}\text{H}_x$. The results indicate that T_c remains almost unchanged with x for $\text{YBa}_2\text{Cu}_3\text{O}_{6.9}\text{H}_x$, T_c in $\text{Bi}_2\text{Sr}_2\text{CaCu}_2\text{O}_{8+y}\text{H}_x$ increases with x for $x \leq 0.4$ and T_c of $\text{Bi}_{1.6}\text{Pb}_{0.4}\text{Sr}_2\text{Ca}_2\text{Cu}_3\text{O}_{10+y}\text{H}_x$ monotonically decreases with x . Based on the variation of the Hall coefficient with x and iodometric analysis, our results are explained by the model that T_c is largely determined by the concentration of mobile holes on the CuO_2 plane. The relaxation rate T_1^{-1} of ^1H in $\text{YBa}_2\text{Cu}_3\text{O}_{6.9}\text{H}_{0.18}$ is found to be enhanced by a factor of two just below T_c and then sharply decreases, while T_1^{-1} in $\text{Bi}_2\text{Sr}_2\text{CaCu}_2\text{O}_{8+y}\text{H}_{0.24}$ drops without showing such an enhancement. The appearance of the enhancement in $\text{YBa}_2\text{Cu}_3\text{O}_{6.9}\text{H}_x$ may originate in the rather weak interaction of ^1H near the $\text{Cu}(1)\text{O}$ plane with electron spin-fluctuations in the $\text{Cu}(2)\text{O}_2$ plane.

1. Introduction

The superconducting transition temperature T_c in high- T_c copper oxides is believed to be a function of the concentration of hole or electron carrier on the CuO_2 plane. Based on the variations of T_c for several series of samples in the $\text{La}_{2-y}\text{Sr}_y\text{CuO}_4$ and $\text{YBa}_2\text{Cu}_3\text{O}_{7-y}$ systems, it has been proposed that there is a maximum in T_c near the mobile hole concentration of 0.15-0.25 per CuO_2 unit /1,2/. In these studies, the hole concentration has been varied by replacing cations and/or changing oxygen concentration. Wide experience has shown that introduction of hydrogen into metallic compounds provides an opportunity of changing carrier density of the system leaving the crystal structure intact /3/. In this paper, we summarize our results of the superconducting properties and the nuclear spin-lattice relaxation time of ^1H in $\text{YBa}_2\text{Cu}_3\text{O}_{6.9}\text{H}_x$, $\text{Bi}_2\text{Sr}_2\text{CaCu}_2\text{O}_{8+y}\text{H}_x$ and $\text{Bi}_{1.6}\text{Pb}_{0.4}\text{Sr}_2\text{Ca}_2\text{Cu}_3\text{O}_{10+y}\text{H}_x$ /4-8/. The results presented here demonstrate that hydrogen absorption is a new method of changing carrier concentration in high- T_c superconducting copper oxides.

2. Superconducting properties in Hydrogenated High- T_c Copper Oxides

We found that $\text{YBa}_2\text{Cu}_3\text{O}_{6.9}$ (YBCO), $\text{Ba}_2\text{Sr}_2\text{CaCu}_2\text{O}_{8+y}$ (BSCCO) and $\text{Bi}_{1.6}\text{Pb}_{0.4}\text{Sr}_2\text{Ca}_2\text{Cu}_3\text{O}_{10+y}$ (BPSCCO) absorb a large amount of hydrogen up to 2, 1 and 3 atoms per formula unit, respectively, leaving the crystal structure and oxygen content intact. The unit cell volume increases by hydrogenation for all the systems. The lattice parameters, however, show different variation depending on the system: For YBCO, the lattice parameter a increases but the parameters b and c decrease with increasing H content x for $x < 0.8$. An orthorhombic to tetragonal transition occurs at $x=0.80$, after that the parameter c becomes almost constant for x while the parameter a continues to increase with x up to $x=1.8$. On the other hand, both the parameters a and c increase with x for BSCCO, whereas the parameter a decreases but c increases with x for BPSCCO.

Figure 1 shows the ac susceptibilities as a function of temperature for all the systems. For the host oxides, an abrupt decrease is observed at T_c , below which the bulk diamagnetic response appears. The onset T_c remains constant up to $x=1.0$ for the YBCO hydride, but the superconducting volume fraction

decreases with x after taking a maximum near $n=0.1$. However, for the BSCCO hydride, T_c shifts to higher temperature up to $x=0.4$. For the BPSCCO hydride, T_c decreases by hydrogen absorption and the volume fraction is more strongly depressed than in BSCCO. The dependence of T_c on x for three systems is compared in Fig. 2. In contrast with the constant T_c for the YBCO hydride, T_c of BSCCO increases with x and exhibits a broad maximum near $x=0.4$, but T_c in BPSCCO monotonically decreases.

For understanding such a significantly different behavior in $T_c(x)$, it is necessary to know the chemical state and the position of hydrogen in the sample. Therefore, we measured the Hall coefficient of the BSCCO hydrides. In Fig. 3, the carrier concentration determined by the Hall coefficient at 290 K is plotted against x . For the host oxide, the hole number of $n_H=3.1 \times 10^{21}/\text{cm}^3$ corresponds to 0.37 holes per CuO_2 unit. It is seen that the hole number decreases linearly with x and all the experimental points are nearly on the solid line expected from the idea that one introduced hydrogen cancels one hole carrier. This asserts that hydrogen behaves as proton H^+ and the transferred electron from hydrogen actually goes into the hole band on the CuO_2 plane. If so, hydrogen might occupy interstitial sites near the CuO_2 plane such as oxygen vacancies in the Ca plane in BSCCO. The linear decrease of n_H observed here is quite similar to that caused by the substitution of Y^{3+} for Ca^{2+} in the system /9,10/. This result confirms that hydrogen preferentially occupies the interstitial sites in the Ca plane. In Fig. 3, we also notice that the magnetic susceptibility at 290 K gradually decreases with increasing x . The decrease in both the hole concentration and magnetic susceptibility with x suggests that the hole band on the CuO_2 plane is gradually filled with electrons transferred from hydrogen. The T_c vs hole concentration relation found in the BSCCO hydride is in analogy with those found for $\text{La}_{2-y}\text{Sr}_y\text{CuO}_4$ and $\text{YBa}_2\text{Cu}_3\text{O}_{7-y}$ /1,2/. The hole concentration per CuO_2 unit which T_c takes a maximum is estimated as ~ 0.18 from the present data. This value is in good agreement with those at the T_c maxima in the above systems. Hence, an universal relation between T_c and mobile hole content is likely to exist among the hole-doped superconductors. In view of this relation, the monotonic decreases of T_c in BPSCCO can be understood as a result of that the hole concentration is at the optimum for superconductivity.

For the YBCO hydride, the average charge per Cu-O unit was determined by an iodometric titration technique. The result indicated that hydrogen also behaves as H^+ in this system. The combined results of lattice parameters /4/ and the core level X-ray absorption spectra /11/ revealed that hydrogen preferentially occupies oxygen

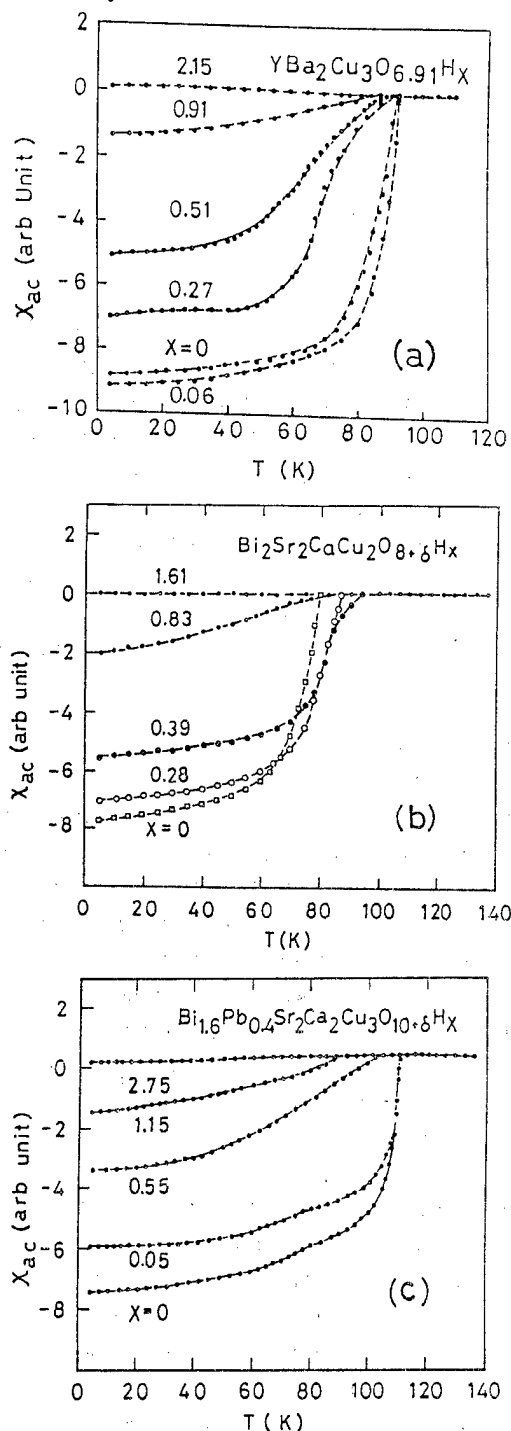


Fig. 1 AC susceptibility as a function of temperature for (a) $\text{YBa}_2\text{Cu}_3\text{O}_{7-y}\text{H}_x$, (b) $\text{Bi}_2\text{Sr}_2\text{CaCu}_2\text{O}_{8+y}\text{H}_x$ and (c) $\text{Bi}_{1.6}\text{Pb}_{0.4}\text{Sr}_2\text{Ca}_2\text{Cu}_3\text{O}_{10+y}\text{H}_x$, respectively.

vacancies or interstitial sites near the Cu(1)O plane. Therefore, the number of holes localized on the plane should decrease by hydrogenation, but the mobile holes on the Cu(2)O₂ plane do not diminish so much. This may lead to the unchanged T_c with x . We have to note that the superconducting volume fraction is diminished by hydrogen absorption for the three systems. This implies that superconductivity in the vicinity of hydrogen is strongly suppressed owing to the extremely short coherence length.

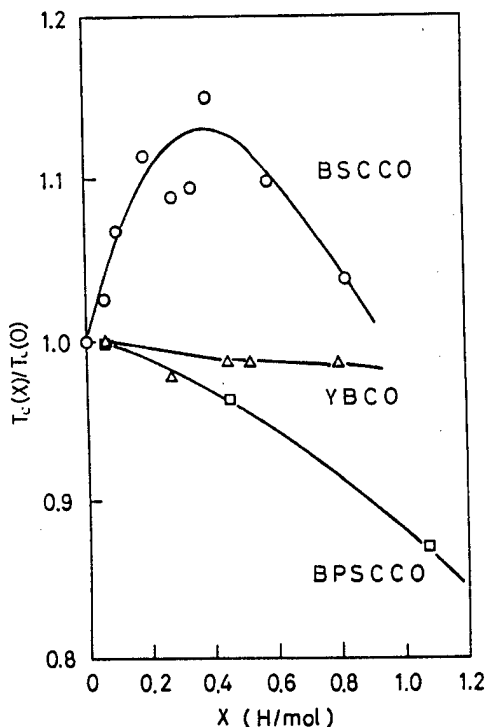


Fig. 2 Relative superconducting transition temperature $T_c(x)/T_c(0)$ plotted against hydrogen concentration x for the YBCO, BSCCO and BPSCCO hydrides.

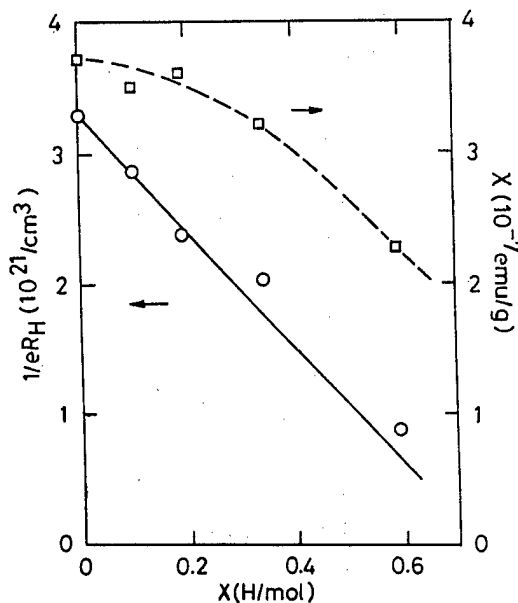


Fig. 3 Carrier concentration and magnetic susceptibility as a function of hydrogen concentration x for the BSCCO hydrides at 290 K.

3. Nuclear Spin-Lattice Relaxation Time of Proton in the Hydrogenated High- T_c Copper Oxides

Figure 4 shows the recovery curves of the nuclear magnetization $M(t)$ of ^1H at 58 MHz in $\text{YBa}_2\text{Cu}_3\text{O}_{6.9}\text{H}_x$. For all the samples, the time dependence of $M(t)$ is not of a single-exponential type in the temperature regions both above and below T_c , but consists of two components with very short and long relaxation times. As is seen in Fig. 4(a), the decay of the short-component strongly depends on the particle size rather than the concentration of hydrogen. Such a short relaxation of ^1H with $T_1 \sim 1$ ms has been reported in degraded and oxygen-deficient surface of powders of YBCO where the Cu-ions have free magnetic moments [12]. Hence, we suppose that the short-component comes from the oxygen deficient surface of the powders. On the other hand, the slope of the $M(t)$ curve of the long-component is independent of the particle size. Thus, the value of T_1 was determined from the slope of the $M(t)$ curve where the relaxation is fully of exponential type.

The relaxation rate $1/T_1$ at 58 MHz for the YBCO hydrides is plotted as a function of temperature in Fig. 5. All the data with $x=0.18$ fall on the same curve for the fine-powder aged 7 months and the coarse-powders aged 4 and 7 months. With decreasing temperature from 294 to 120 K, the rate for $x=0.18$ decreases by one order of magnitude and does not follow the Korringa relation of $T_1 T = \text{const.}$ At a low temperature of ~ 105 K, there appears a small hump, which may not be attributable to a residual diffusion mode of hydrogen. Much more pronounced is the sharp peak just below $T_c=92$ K. At the peak temperature of

86 K ($T/T_c=0.93$), the rate is enhanced by a factor of two. Here, we recall that hydrogen preferentially occupies the oxygen vacancies or interstitial sites near Cu(1)O plane for $x \leq 0.4$. In this plane apart from the Cu(2)O₂ plane, the influence of the spin-fluctuation of the Cu(2) spins may be diminished so that the relaxation rate of ¹H could be as small as in the usual metal hydrides [13]. Therefore, the enhancement in the rate may be understood as the effect of the piling up of the density of states at the gap edge as in the case of ordinary superconductors. In the sample with $x=0.63$, the relaxation rate is higher than that for $x=0.18$ in the overall temperature range, which may be ascribed to mutual spin-flips between neighboring ¹H spins. The broad superconducting transition and the small volume fraction of this sample might have masked the enhancement.

In Fig. 6, we show the variation of $1/T_1$ with temperature for the BSCCO hydrides with $x=0.24$ and 0.42 . Compared the result of $x=0.24$ with that of the YBCO hydride with $x=0.18$, the rate $1/T_1$ is about half of the latter but the temperature dependence is very similar in the normal state. In the range from 100 K to 85 K ($=T_c$), the rate remains constant and commences to decrease at T_c without showing any enhancement. We here recall that hydrogen in BSCCO preferentially occupies interstitial sites in the Ca plane sandwiched by two Cu(2)O₂ planes.

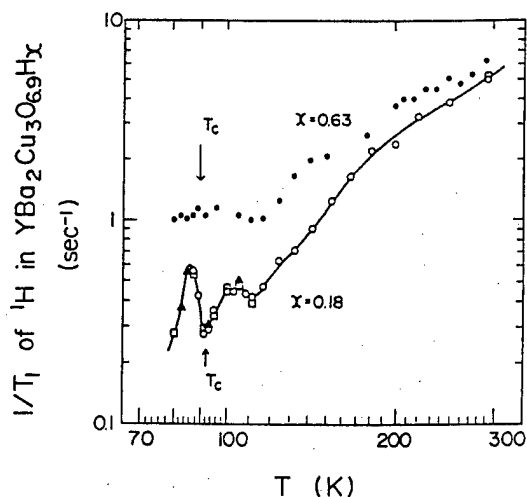


Fig. 5 Temperature dependence of $1/T_1$ of ¹H at 58 MHz in YBa₂Cu₃O_{6.9}H_x with $x=0.18$; ○, coarse-powder aged 4 months; ▲, coarse-powder aged 7 months; □, fine-powder aged 7 months; ●, coarse-powder with $x=0.63$ aged 4 months.

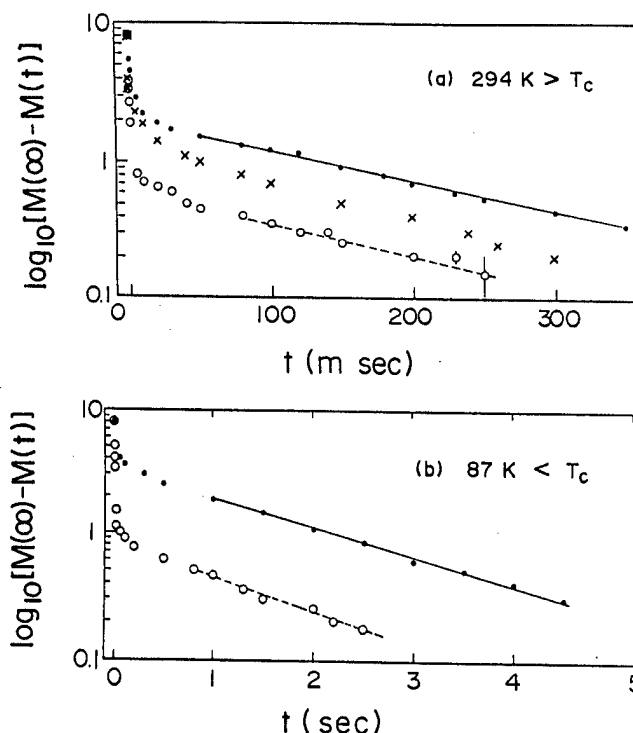


Fig. 4 Time dependence of nuclear magnetization $M(t)$ of ¹H at 58 MHz in Yba₂Cu₃O_{6.9}H_x with $x=0.18$; ●, coarse-powder aged 4 months; ○, fine-powder aged 7 months; ×, coarse-powder with $x=0.63$ aged 4 months at (a) 294 K and (b) 87 K.

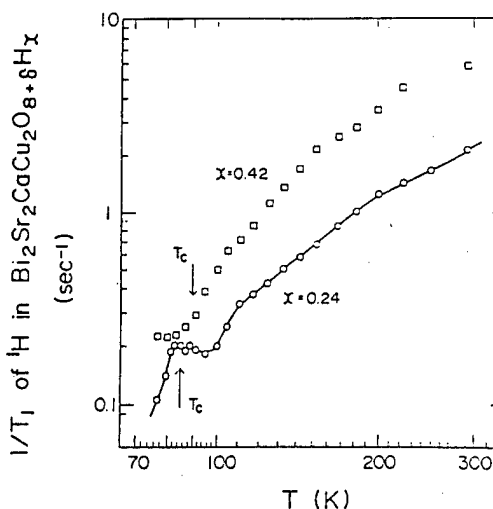


Fig. 6 Temperature dependence of $1/T_1$ of ¹H at 58 MHz in Bi₂Sr₂CaCu₂O_{8+δ}H_x with $x=0.24$ (○) and 0.42 (□).

Hence, the rather small rate suggests that the interaction of hydrogen in the Ca plane with the adjacent Cu(2) spins is also weak. This result seems to be consistent with the very low relaxation rate of ^{69}Y in YBCO /15/, since the crystallographic configuration of the Ca plane in BSCCO is similar to that of the Y plane in YBCO. From the absence of enhancement in the relaxation rate for the BSCCO hydride in Fig. 6, we may deduce that the interaction of ^1H in the Ca plane with the superconducting carriers is weaker than that of ^1H in the Cu(1)O plane in the YBCO hydride.

References

- /1/ J. B. Torrance, Y. Tokura, A.I. Nazzari, A. Bezing, T. C. Huang and S. S. P. Parkin, Phys. Rev. Lett. 61 (1988) 1127.
- /2/ Y. Tokura, J. B. Torrance, T. C. Huang and A. I. Nazzari, Phys. Rev. B38 (1988) 1127.
- /3/ See e. g. G. Alefeld and V. Volkl, eds., Hydrogen in Metals I and II (Springer, Berlin/New York 1978) and L. Sohlapbach, Ed., Hydrogen in Intermetallic Compounds I (Springer, Berlin, 1987).
- /4/ H. Fujii, H. Kawanaka, W. Ye, S. Orimo and H. Fukuba, Jpn. J. Appl. Phys. 27 (1988) L525.
- /5/ T. Takabatake, W. Ye, S. Orimo, H. Kawanaka, H. Fujii, H. Sasakura and S. Minamigawa, Physica C 157 (1989) 263.
- /6/ T. Takabatake, W. Ye, S. Orimo, T. Tamegai and H. Fujii, Intern. M^2S -HTSC Conference, Stanford, California, 1989, to be published in Physica C.
- /7/ K. Morimoto, W. Ye, S. Orimo, T. Takabatake, H. Fujii and T. Hihara, Solid State Commun. 71 (1989) 291.
- /8/ K. Morimoto, T. Takabatake, W. Ye, S. Orimo, T. Hihara and H. Fujii, Physica C 159 (1989) 840.
- /9/ Y. Ando, K. Fukuda, S. Kondoh, M. Sera, M. Onoda and M. Sato, Solid State Commun. 67 (1988) 815.
- /10/ T. Tamegai, K. Koga, K. Suzuki, M. Ichihara, F. Sakai and Y. Iye, Jpn. J. Appl. Phys. 28 (1989) L112.
- /11/ J. P. Burger, J. N. Daue, K. Le Dang, A. M. Flank, P. Lagarde, M. Nicolas, J. P. Renard, P. Vajda and P. Veillet, Solid State Commun. 72 (1989) 705.
- /12/ H. Nishihara, N. Nishida, T. Takabatake, K. Kishio, A. Ohtomo, K. Hayashi, M. Ishikawa, Y. Nakazawa, K. Koga, T. Tamegai and K. Kitazawa, Jpn. J. Appl. Phys. 27 (1988) L1652.
- /13/ K. Morimoto, M. Saga, H. Fujii, T. Okamoto and T. Hihara, J. Phys. Soc. Jpn. 57 (1988) 647.
- /14/ J. M. Markert, T. W. Noh, S. E. Russek and R. M. Cotts, Solid State Commun. 63 (1987) 847.

Study of High T_c Oxide by in-Beam Perturbed Angular Correlation

Fumio Komori, Nobuo Ikeda*, Osamu Hashimoto*, Tomokazu Fukuda*, Shingo Katsumoto, Touru Nomura*, Shun-ichi Kobayashi, Seiichiro Ikehata, and Toshimitsu Yamazaki*

Department of Physics, Faculty of Science, University of Tokyo,
7-3-1 Hongo, Bunkyo-ku, Tokyo 113

*Institute for Nuclear Study, University of Tokyo,
3-2-1 Midorimachi, Tanasi-shi, Tokyo 188

The time differential perturbed angular correlation method, which is an alternative to the ^{17}O substituted NMR, was applied to the study of the high T_c oxides. The spin rotation signal was observed, and the internal field was determined with the accuracy of about 1%.

The hyperfine interaction at oxygen site in oxide superconductors is one of the most informative properties to study high T_c mechanism. So far, the NMR of ^{17}O which substituted ^{16}O in the oxides have been reported. We present in this report the results of the time differential perturbed angular correlation (PAC) method, which is an alternative to the substituted NMR.

The principle of this method is as follows. The 197 keV isomeric state of $^{19}\text{F}(I=5/2, \tau = 128 \text{ nsec})$ is produced by the reaction $^{16}\text{O}(\alpha, p)^{19}\text{F}$. This spin state is highly aligned after the reaction, and its spin rotation in magnetic field can be traced as a time distribution of the γ -rays. When the produced ^{19}F is properly substituted for the oxygen in the oxide, we can obtain internal field at the oxygen site from the rotation pattern. In the case of MnO , [1] the results of the paramagnetic shift implied that ^{19}F is correctly substituted for oxygen.

In the experiment, we first optimized the energy of α -beam from the INS SF-cyclotron to achieve the best signal to noise ratio for the 197 keV γ -ray from ^{19}F isomer. The main sources of the noise γ -ray were ^{68}Ga produced by the reaction $^{65}\text{Cu}(\alpha, p)^{68}\text{Ga}$ and the pair-annihilated positrons emitting 511 keV γ -ray which makes broad peak around 200 keV owing to the Compton scattering. We found the best S/N ratio was obtained at the energy of 21 MeV. For this energy, the period of the beam was fixed to be 133 nsec.

Up to now, we studied $\text{La}_{0.85}\text{Sr}_{0.15}\text{CuO}_4$ ceramics, $\text{YBa}_2\text{Cu}_3\text{O}_7$ ceramics, $\text{Bi}_2\text{Sr}_2\text{CaCu}_2\text{O}_8$ ceramics, $\text{La}_{0.9}\text{Sr}_{0.1}\text{CuO}_4$ single crystal and La_2CuO_4 ceramics at room temperature. We used the samples thick enough to stop the α -beam with the energy of a few tens MeV. An external magnetic field of 1.312 T was applied on the sample perpendicularly to the beam-detectors plane. The γ -ray was detected by a pair of NaI(Tl) scintillators (2" x 1") placed at + 135 degrees to the beam. The time spectrum of γ -ray with energy gates were accumulated on a computer. To see the time spectrum along energy axis in detail, we also accumulated the γ -ray histogram on the energy-time plane on another computer by taking both values of energy and time for

each γ -ray through a parallel interface. We measured time spectrum of each target for about 8 hours.

Figure 1 shows an example of γ -ray count histogram on time-energy plane for the Bi sample. Spin rotation pattern was observed around the peak energy of 197 keV. We observed similar spin rotation patterns for all the samples. We show in Fig.2 the normalized time spectrum of the +135 degree counter (N_+) subtracted from that of the -135 degree counter (N_-) for the $\text{YBa}_2\text{Cu}_3\text{O}_7$ sample. Here we normalized the counts of γ -ray by the total count of γ -ray in the delayed part. The data of the asymmetry $(N_+ - N_-)/(N_+ + N_-)$ is shown in Fig.3 for the same sample.

The observed rotation patterns as shown in Fig.3 were fitted to the formula

$$f(t) = A \sin(2\omega_L t + B) \quad (1)$$

with A , B and ω_L as fitting parameters. The values of the Larmor frequency of ^{19}F , ω_L , were obtained by the χ^2 analysis, and agreed with the reported value[2] within the experimental accuracy of about 1.5 % in all the samples. A part of this error originated from the measured magnetic field strength. The statistical error was less than 1 %.

The fitted value of the asymmetry A was around 6 %, and is about one half of that reported in ref.1 for CoO . In the present experiment, the asymmetry was reduced because the FWHM of the time spectrum of the α -beam was more than 5 nsec and was only one third of the half period of the rotation.

We also analyzed the rotation patterns $(N_+ - N_-)$ by fitting them to the formula

$$g(t) = A \sin(2\omega_L t + B) \exp(-t/\tau) \quad (2)$$

with A , B , ω_L , τ as fitting parameters. Without any source of the relaxation in the spin rotation, the decay constant, τ , should be the life time of the isomer. After the χ^2 analysis, we found that the values of τ agreed with the life time within the experimental accuracy. We observed no sign of spin relaxation within 130 nsec in all the samples. This is quite in contrast to the results in $\mu^-\text{SR}$ at oxygen site. In the latter case, the rotation pattern was missing in $\text{YBa}_2\text{Cu}_3\text{O}_7$ although it was clearly observed in $\text{La}_x\text{Sr}_{1-x}\text{CuO}$.

In these analyses, we found no effect of nuclear quadrupole interaction within our experimental accuracy. The measured quadrupole width of the samples is commonly narrower than a few tens mT. At present, the reason for the absence of the interaction is unknown.

To conclude, we have shown that PAC method can be successfully applied to the high T_c oxides. We are now preparing the measurement of the internal field at low temperatures.

references

- [1] Y. Yoshida, T. Kobayashi, H. Nakayama, H. Yasuoka and T. Yamazaki; *Hyp. Int.* 4 (1987) 448.
- [2] J. Bleck, D.W. Haag and W. Ribbe; *Nucl. Instr. Meth.* 67 (1969) 169.

Fig.1
An example of γ -ray
count histogram on the
time-energy plane.
Data are shown for
the $\text{Bi}_2\text{Sr}_2\text{CaCu}_2\text{O}_8$
ceramics.

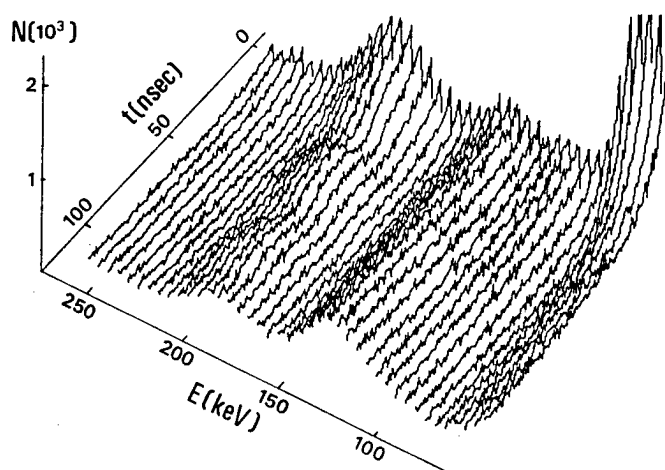


Fig.2
 $N_+ - N_-$ for $\text{YBa}_2\text{Cu}_3\text{O}_7$
ceramics.

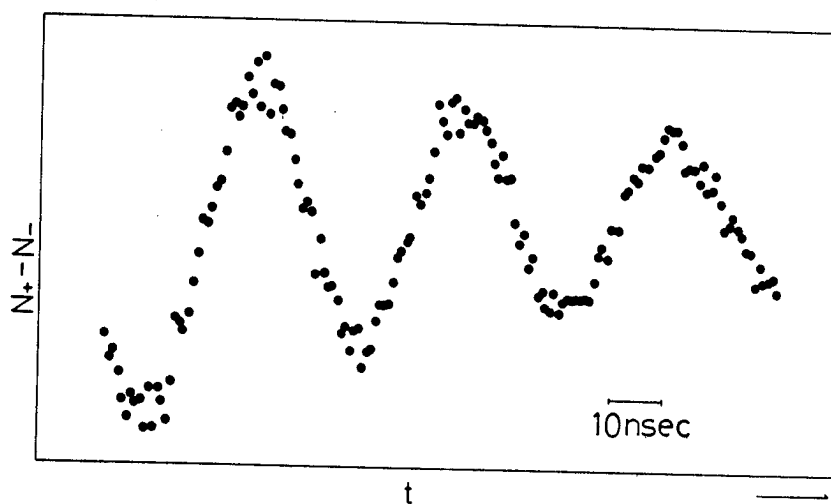
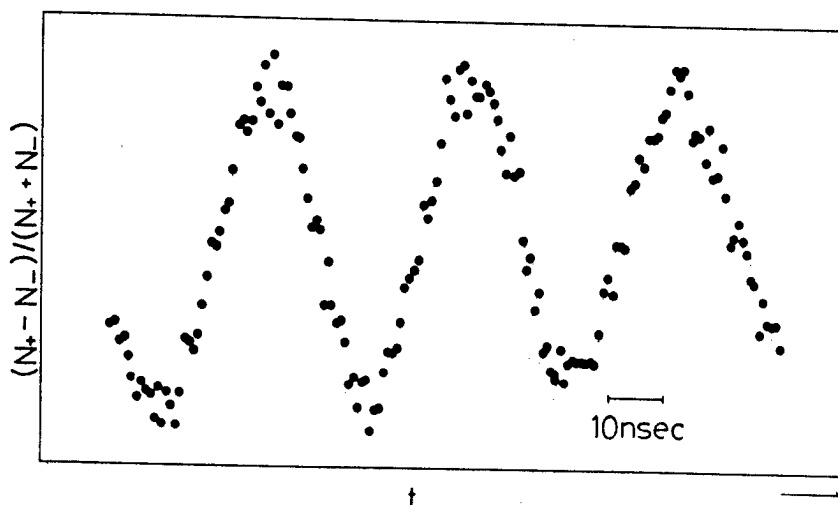


Fig.3
Spin Rotation pattern,
 $(N_+ - N_-)/(N_+ + N_-)$, of
 ^{19}F for $\text{YBa}_2\text{Cu}_3\text{O}_7$
ceramics.



MAGNETISM STUDIES of OXIDE-SUPERCONDUCTORS BY μ^\pm SR

Nobuhiko Nishida

Department of Physics, Tokyo Institute of Technology,
Meguro-ku, Tokyo 152, Japan

Abstract

Magnetic properties of oxide-superconductors have been studied by μ^\pm SR methods.

(A) μ^+ SR studies:

(1) In the $\text{Bi}_{2-x}\text{La}_x\text{Sr}_2\text{CuO}_y$ system, antiferromagnetic orderings have been found in the insulating phase and the magnetic phase diagram was found to be similar to that of $\text{Bi}_2\text{Sr}_2\text{Y}_{1-x}\text{Ca}_x\text{Cu}_2\text{O}_y$ system. The 3-dimensional magnetic ordering temperature T_N seems to have no correlation with the number of $\text{Cu}_2\text{-O}$ layers in these compounds, while the superconducting transition temperatures T_c seem to increase with the number of $\text{Cu}_2\text{-O}$ layers. (2) Antiferromagnetic ordering have been observed in the insulating phase of the newly discovered high- T_c superconductor $\text{Eu}_6\text{Ba}_4\text{Ce}_2\text{Cu}_9\text{O}_y$. (3) In order to consider a possibility of anyon state in high- T_c superconductors, we studied whether there exist a static magnetic field of electronic origin in the superconducting phase of high- T_c superconductor $\text{YBa}_2\text{Cu}_3\text{O}_7$ or not, after the determination of the μ^+ sites in $\text{YBa}_2\text{Cu}_3\text{O}_7$ from the studies of μ^+ local magnetic fields of $\text{YBa}_2\text{Cu}_3\text{O}_6$ and $\text{GdBa}_2\text{Cu}_3\text{O}_7$. (4) $\text{YBa}_2\text{Cu}_{2.76}\text{Fe}_{0.24}\text{O}_7$ samples prepared by different thermal annealing process were studied by μ^+ SR and the clustering of Fe atoms has been observed.

(B) μ^- SR studies:

μ^- paramagnetic shifts at oxygen atom sites were measured in the normal state of various oxide-superconductors ($\text{YBa}_2\text{Cu}_3\text{O}_7$, $\text{La}_{2-x}\text{Sr}_x\text{CuO}_{4-\delta}$, $\text{Nd}_{2-x}\text{Ce}_x\text{CuO}_{4-\delta}$ and LiTi_2O_4) and the related oxide-insulators ($\text{La}_2\text{CuO}_{4-\delta}$ and CuO) and they were compared with one another.

As magnetism may have some relation with a superconducting mechanism of recently-discovered copper-oxide superconductors, we have applied μ^\pm SR methods to magnetism studies of oxide-superconductors. The experiments were performed at KEK-BOOM of Meson Science Laboratory of University of Tokyo, and at TRIUMF, the meson factory at Vancouver in Canada in collaboration with the μ SR group at University of British Columbia and TRIUMF. In the followings, the μ^\pm SR results of this year are summarized.

§1 Studies of Magnetic Properties of Oxide-superconductors by μ^+ SR

1.1 Antiferromagnetism Studies

$\text{Bi}_{2-x}\text{La}_x\text{Sr}_2\text{CuO}_y$ and $\text{Eu}_6\text{Ba}_4\text{Ce}_2\text{Cu}_9\text{O}_y$

The μ^+ SR method was very powerful to detect static or quasi-static magnetic ordering in high- T_c superconductor-related magnetic oxide-insulators, as successfully applied to studies of the magnetic phase diagrams of $\text{YBa}_2\text{Cu}_3\text{O}_x$ [1] or $\text{Bi}_2\text{Sr}_2\text{Y}_{1-x}\text{Ca}_x\text{Cu}_2\text{O}_y$ [2,3].

This means that μ^+ SR method was used as a very sensitive magnetometer. Due to two-dimensional character of the magnetism in these copper-oxide insulators, bulk susceptibility measurements were rather difficult to detect an anomaly at 3-dimensional magnetic ordering temperature T_N .

This year we applied μ^+ SR method to the $\text{Bi}_{2-x}\text{La}_x\text{Sr}_2\text{CuO}_y$ and the newly-discovered $\text{Eu}_6\text{Ba}_4\text{Ce}_2\text{Cu}_9\text{O}_y$ systems. In the insulating phases of both $\text{Bi}_{2-x}\text{La}_x\text{Sr}_2\text{CuO}_y$ [4] and $\text{Eu}_6\text{Ba}_4\text{Ce}_2\text{Cu}_9\text{O}_y$ [5] we have succeeded in finding an antiferromagnetic orderings. In the $\text{Bi}_{2-x}\text{La}_x\text{Sr}_2\text{CuO}_y$ system the magnetic phase diagram similar to those of $\text{La}_{2-x}\text{A}_x\text{CuO}_{4-\delta}$ ($\text{A}=\text{Sr}$ or Ba), $\text{YBa}_2\text{Cu}_3\text{O}_x$, $\text{Bi}_2\text{Sr}_2\text{Y}_{1-x}\text{Ca}_x\text{Cu}_2\text{O}_y$ has been obtained as shown in Fig.1. The studies of $\text{Eu}_6\text{Ba}_4\text{Ce}_2\text{Cu}_9\text{O}_y$ are now in progress.

In all these copper-oxide systems the following picture holds: The superconductivity and the antiferromagnetism have been found to compete against each other; as holes are doped into the parent antiferromagnetic insulators, the superconductivity sets in where the antiferromagnetism disappears.

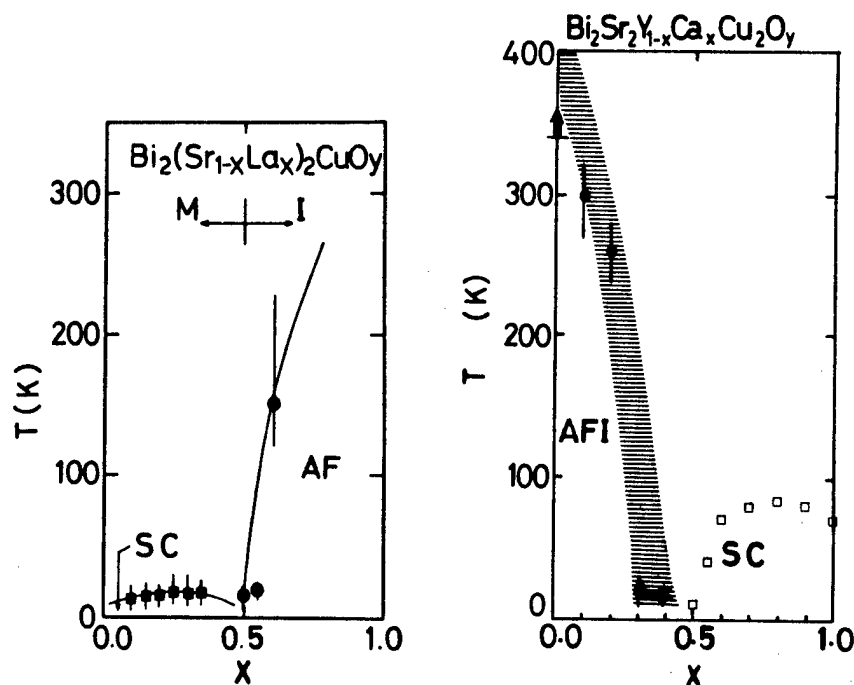


Fig. 1 Magnetic Phase Diagrams of $\text{Bi}_2(\text{Sr}_{1-x}\text{La}_x)_2\text{CuO}_y$ and $\text{Bi}_2\text{Sr}_2\text{Y}_{1-x}\text{Ca}_x\text{Cu}_2\text{O}_y$.

In $\text{Bi}_2\text{Sr}_2\text{Y}_{1-x}\text{Ca}_x\text{Cu}_2\text{O}_y$ (2212 compound with two $\text{Cu}_2\text{-O}$ layers and T_c is about 80K in the superconducting phase) and $\text{Bi}_{2-x}\text{La}_x\text{Sr}_2\text{CuO}_y$ (221 compound with one $\text{Cu}_2\text{-O}$ layer and T_c is 20~30 K), we studied the correlation of 3-d magnetic ordering temperature T_N with the number of $\text{Cu}_2\text{-O}$ layers. There seems no correlation, while the superconducting transition temperature increases with increment of $\text{Cu}_2\text{-O}$ layers. This fact may give information about the interaction between Cu_2O layers and it is now under considerations.

1.2 $\mu^+\text{SR}$ Studies of $\text{YBa}_2\text{Cu}_{2.76}\text{Fe}_{0.24}\text{O}_7$

A lot of Mossbauer experiments were performed on $\text{YBa}_2\text{Cu}_{3-x}\text{Fe}_x\text{O}_7$ to know the electronic state at Fe atoms which are substituted for Cu atoms. However, as the substitution sites have not been well studied, the discussion is not so clear. We performed $\mu^+\text{SR}$ experiments on two samples of $\text{YBa}_2\text{Cu}_{2.76}\text{Fe}_{0.24}\text{O}_7$ which were prepared in two different thermal processes: One was prepared in the same way as $\text{YBa}_2\text{Cu}_3\text{O}_7$ is usually prepared and it is tetragonal. The T_c was about 50K. The other was prepared as follows; at first the oxygen atoms were removed from $\text{YBa}_2\text{Cu}_{2.76}\text{Fe}_{0.24}\text{O}_7$ and insulating $\text{YBa}_2\text{Cu}_{2.76}\text{Fe}_{0.24}\text{O}_6$ was prepared. Then the oxygen atoms were introduced into $\text{YBa}_2\text{Cu}_{2.76}\text{Fe}_{0.24}\text{O}_6$ by annealing the sample. Thus prepared $\text{YBa}_2\text{Cu}_{2.76}\text{Fe}_{0.24}\text{O}_7$ was orthorhombic and the T_c was about 90K. The results of $\mu^+\text{SR}$ on these $\text{YBa}_2\text{Cu}_{2.76}\text{Fe}_{0.24}\text{O}_7$ are as follows: (1) In tetragonal $\text{YBa}_2\text{Cu}_{2.76}\text{Fe}_{0.24}\text{O}_7$, a spin-glass-like ordering was observed at 20 K. (2) In orthorhombic $\text{YBa}_2\text{Cu}_{2.76}\text{Fe}_{0.24}\text{O}_7$, $\mu^+\text{SR}$ revealed that there exist two

magnetically different parts in the sample; they were interpreted as 2/3 magnetic part which seems to make a spin-glass-like ordering at about 40 K and 1/3 superconducting part. In $\text{YBa}_2\text{Cu}_{2.76}\text{Fe}_{0.24}\text{O}_7$ it is considered that a region with rich Fe atoms was formed by annealing and shows a higher magnetic ordering temperature than in tetragonal $\text{YBa}_2\text{Cu}_{2.76}\text{Fe}_{0.24}\text{O}_7$. From the $\mu^+\text{SR}$ studies the superconductivity in both $\text{YBa}_2\text{Cu}_{2.76}\text{Fe}_{0.24}\text{O}_7$ looks percolative. Now detailed analyses of the $\mu^+\text{SR}$ results are in progress as well as Mossbauer experiment results on the same samples.

1.3 Anyon search in high- T_c superconductors by $\mu^+\text{SR}$

As reported in our previous $\mu^+\text{SR}$ work on $\text{YBa}_2\text{Cu}_3\text{O}_x$ [1], in the superconducting phase μ^+ has not detected magnetism of electronic origin. Here, this statement is discussed qualitatively. In Fig.2 are shown the μ^+ spin relaxation function $G_z(t)$'s of $\text{YBa}_2\text{Cu}_3\text{O}_7$ in zero external field: Below 200 K they have the same shape and are well fitted by a static gaussian Kubo-Toyabe function with $\Delta = 0.12 \mu\text{s}^{-1}$. Above 200K they are narrowed due to μ^+ motion. This means that in the superconducting phase at low temperatures static magnetic fields distributed around zero with a standard deviation of 1.4 G have been probed by μ^+ . Recently it was proposed that superconducting states of high- T_c copper-oxide superconductors might be time-reversal-symmetry broken (anyon model) and static magnetic fields might be observed by $\mu^+\text{SR}$ in the superconductor even under zero external field [7]. Let us discuss the above mentioned static magnetic fields observed in superconducting

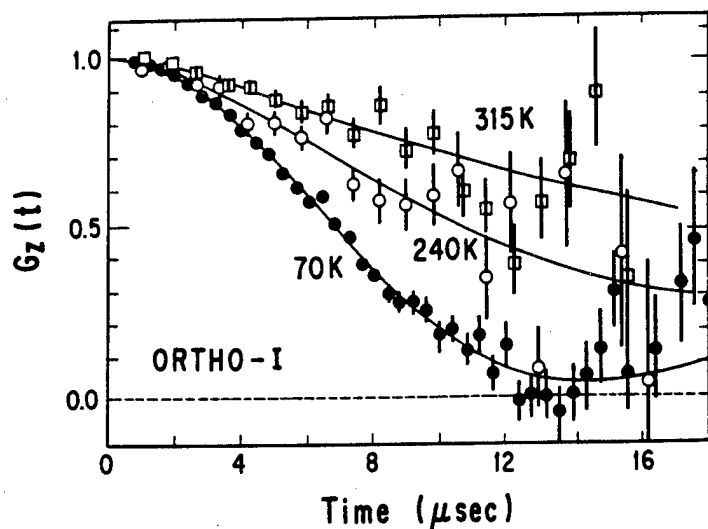


Fig. 2 μ^+ spin relaxation in $\text{YBa}_2\text{Cu}_3\text{O}_7$ under zero external magnetic field at various temperatures.

$\text{YBa}_2\text{Cu}_3\text{O}_7$ qualitatively.

From the analysis of μ^+ hyperfine magnetic fields in antiferromagnetically ordered $\text{YBa}_2\text{Cu}_3\text{O}_6$ and $\text{GdBa}_2\text{Cu}_3\text{O}_7$, we were able to determine the μ^+ sites in $\text{YBa}_2\text{Cu}_3\text{O}_7$ as follows: Implanted μ^+ 's make μ^+ -oxygen bondings (analogous to OH radicals) with any oxygen atoms. The $\text{O}-\mu^+$ takes its orientation as far as possible from cations Cu^{+2} , Ba^{+2} and Y^{+3} and it is slightly modified by being attracted by negative O^{2-} 's. When we calculate the second moments of nuclear magnetic dipolar fields from Cu, Y and Ba nuclear magnetic moments at those proposed μ^+ sites, they almost coincide with the observed experimental value. As the observed static magnetic fields are able to be explained by nuclear magnetic dipolar fields, we should say that anyon states have not been detected by μ^+ SR.

§2 Studies of Oxide-Superconductors by μ^- SR

When μ^- 's are used for studies of oxidesuperconductors, another feature will appear; as μ^- 's implanted into a material are trapped by nuclei and form quasi-nuclei with a large magnetic moment, μ^- SR is able to give information about the electronic state at the oxygen sites of oxide-superconductors ($\text{O}\mu^-$ is equivalent to nitrogen, when it is seen from surrounding electrons). We applied μ^- SR to several oxide-superconductors and the related insulators ($\text{YBa}_2\text{Cu}_3\text{O}_7$, $\text{Nd}_{2-x}\text{Ce}_x\text{CuO}_{4-\delta}$ ($x=0.15$; oxygen-reduced sample (superconductor) and oxygen-annealed sample (non-superconductor)), LiTi_2O_4 , $\text{La}_2\text{CuO}_{4-\delta}$ and CuO) and measured the $\text{O}\mu^-$ paramagnetic shifts in 6 kG at 300K. Good μ^- SR signals have been observed in $\text{Nd}_{2-x}\text{Ce}_x\text{CuO}_{4-\delta}$, LiTi_2O_4 , $\text{La}_2\text{CuO}_{4-\delta}$ and CuO . Nishiyama et al have observed μ^- SR signals in $\text{La}_{2-x}\text{Sr}_x\text{CuO}_{4-\delta}$, too.

However, in $\text{YBa}_2\text{Cu}_3\text{O}_7$ no μ^- precession signal has been observed. Further μ^- SR experiments have been

performed in 6 kG at 100K and 0.3kG at 300K, but still no μ^- SR signal. It was concluded that T_1 of $\text{O}\mu^-$ in $\text{YBa}_2\text{Cu}_3\text{O}_7$ will be very short (shorter than 200 ns). The results on $\text{YBa}_2\text{Cu}_3\text{O}_7$ will be discussed more in detail later. In Fig.3 the paramagnetic shifts of μ^- O thus far measured at 300K are summarized and plotted against the bulk magnetic susceptibilities. In copper-oxides $\text{O}\mu^-$ paramagnetic shifts are all positive and the order of 10^{-3} , whether they are superconductor or insulator. In electron carrier $\text{Nd}_{2-x}\text{Ce}_x\text{CuO}_{4-\delta}$ $\text{O}\mu^-$ paramagnetic shifts were about 3×10^{-3} and do not depend on the oxygen handling procedure. In LiTi_2O_4 , $\text{O}\mu^-$ paramagnetic shift is very small (more than one order), though the bulk magnetic susceptibility is similar to those of copper oxides. This small shift might be explained as follows; in oxide-insulators for transition elements at the latter part in the periodic table, the Cu 3d and O 2p levels are close and strongly hybridized each other. Then, due to a charge transfer between Cu^{++} and O^{--} , a large paramagnetic shift might be expected. On the other hand, in oxide-insulators for those at the early part, O 2p level is situated at a deep position compared with Cu 3d level. Then, a charge transfer will not be expected and a small paramagnetic shift might be observed. The consideration is consistent with photo-emission studies of transition element oxides.

Non-observation of μ SR signal in a stoichiometric $\text{YBa}_2\text{Cu}_3\text{O}_7$ and observation of μ SR signals in doped-oxide superconductors $\text{La}_{2-x}\text{Sr}_x\text{CuO}_{4-\delta}$ or $\text{Nd}_{2-x}\text{Ce}_x\text{CuO}_{4-\delta}$ are very puzzling, but interesting and worthwhile thinking deeply about the reasons. Because (1) $\text{YBa}_2\text{Cu}_3\text{O}_7$ is considered to be more homogenous and uniform than Sr doped $\text{La}_{2-x}\text{Sr}_x\text{CuO}_{4-\delta}$ or Ce-doped $\text{Nd}_{2-x}\text{Ce}_x\text{CuO}_{4-\delta}$ (our sample quality was confirmed by NQR measurement). (2) If we scale $\text{O}\mu^- T_1$ in $\text{YBa}_2\text{Cu}_3\text{O}_7$ from the $\text{O}^{17}\text{-}T_1$ (10 msec at 300K and 35 msec at 100K) only by their magnetic g-factors, $\mu^- T_1$ is

40 times shorter than the $O^{17} T_1$; that is 250 μ sec and 825 μ sec at 300K and 100K. The $O\mu^-$ is considered to be a nitrogen atom for surrounding electrons. From this respect it can be speculated that the carrier-holes are attracted by $O\mu^-$ and localized there; and if they have localized magnetic moments, fast depolarization of μ^- might take place. However, in doped oxide-superconductors such as $La_{2-x}Sr_xCuO_{4-\delta}$ or $Nd_{2-x}Ce_xCuO_{4-\delta}$ or the related insulators $La_2CuO_{4-\delta}$ or CuO we were able to observe μ SR signal easily, as described before. Then, we have to reconsider the μ SR signal in $La_{2-x}Sr_xCuO_{4-\delta}$ or $Nd_{2-x}Ce_xCuO_{4-\delta}$, too. It is interesting if this short T_1 have some relation with the difference of T_c , 80-90K in $YBa_2Cu_3O_7$ and 30-40 K in $La_{2-x}Sr_xCuO_{4-\delta}$ or $Nd_{2-x}Ce_xCuO_{4-\delta}$. The μ SR experiment on another stoichiometric oxide superconductor $Bi_2Sr_2CaCu_2O_y$ will make the problem clearer.

The discussions about the μ^- SR results based on the models proposed to explain high- T_c superconductivity will give us more information to understand them.

acknowledgement

I thank the colleagues at TIT, KEK-BOOM and TRIUMF. I appreciate many collaborators; Y. Hidaka, T. Murakami (NTT) for supplying single crystals $La_2CuO_{4-\delta}$, Y. Ueda (ISSP) for $YBa_2Cu_3O_x$ ($x=6$ and 7) and $LiTi_2O_4$ samples, S. Kambe and H. Yasuoka (ISSP) for making NMR measurements on $Nd_{2-x}Ce_xCuO_{4-\delta}$ to confirm the sample quality, J. Akimitsu (Aoyama-Gakuin) for $Bi_{2-x}La_xSr_2CuO_y$ and $Eu_6Ba_4Ce_2Cu_9O_y$ samples, H. Takagi and S. Uchida (U. of Tokyo) for preparing $Nd_{2-x}Ce_xCuO_{4-\delta}$, and for making stimulating discussions.

REFERENCES

- [1] N. Nishida, H. Miyatake, D. Shimada, S. Okuma, M. Ishikawa, T. Takabatake, Y. Nakazawa, Y. Kuno, R. Keitel, J.H. Brewer, T.M. Riseman, D.Ll. Williams, Y. Watanabe, T. Yamazaki, K. Nishiyama, K. Nagamine, E.J. Ansaldo and E. Torikai, J. Phys. Soc. Jpn. **57** (1988) 599.
- [2] N. Nishida, H. Miyatake, S. Okuma, T. Tamegai, Y. Iye, R. Yoshizaki, K. Nishiyama and K. Nagamine, Physica C156 (1988) 625.
- [3] N. Nishida, H. Miyatake, S. Okuma, R. Yoshizaki, T. Tamegai, Y. Iye, R. Kadono, J.H. Brewer, E.J. Ansaldo, W.N. Hardy et. al., to be published (1990).
- [4] H. Yamazaki, J. Akimitsu, N. Nishida, S. Okuma, J.H. Brewer et al.; in preparation and to be published (1990).
- [5] H. Miyatake, S. Okuma, N. Nishida, J. akimitsu ety al.; in preparation and to be published (1990).
- [6] S. Okuma, N. Nishida, Y. Ueda, K. Kosuge, R. Kadono, J.H. Brwer et al.; in preparation and to be published (1990).
- [7] N. Nishida et al, in preparation and to be published (1990).
- [8] B.I. Halperin, J. March-Russell and F. Wilczek, Phys. Rev. B40 (1989) 8726.

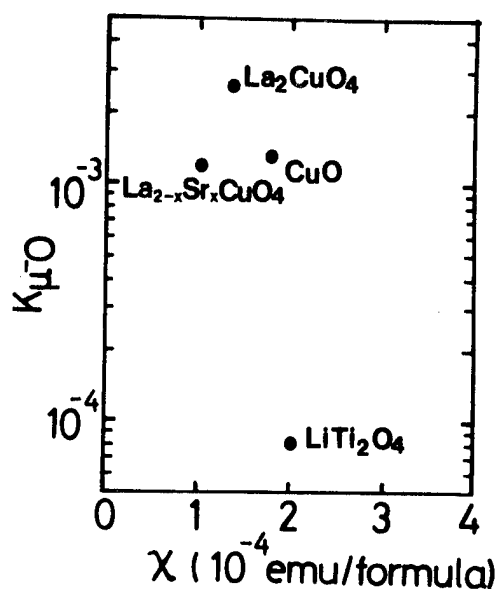


Fig. 3 μ^-O paramagnetic shifts in various oxides at 300K are plotted against the bulk magnetic susceptibility.

^{119}Sn AND ^{57}Fe MOSSBAUER STUDY OF $\text{La}_{2-x}\text{Sr}_x\text{CuO}_4$

T. SHINJO, S. NASU*, T. MIZUTANI, K. SHINTAKU, N. HOSOITO,
K. MATSUKUMA** and T. TAKABATAKE**

Institute for chemical Research, Kyoto University, Uji, Kyoto-fu 611

*Faculty of Engineering Sciences, Osaka University, Toyonaka 560

**Faculty of Integrated Arts and Sciences, Hiroshima University, Hiroshima 730, Japan

Magnetic behaviors of $\text{La}_{2-x}\text{Sr}_x\text{CuO}_4$ ($x=0, 0.15, 0.4$) were studied from ^{119}Sn and ^{57}Fe Mössbauer spectroscopy. For all cases, ^{57}Fe spectra at 4.2K show magnetic hyperfine splittings. On the other hand, a magnetic hyperfine field at Sn nucleus is observed only in the case of $\text{La}_{1.85}\text{Sr}_{0.15}\text{CuO}_4$. The results indicate that the Cu magnetic spins are collectively fluctuating in the superconducting sample.

^{57}Fe RESULTS

Mössbauer results on YBCO were reported last year. This year, by utilizing ^{119}Sn and ^{57}Fe Mössbauer spectroscopy, $\text{La}_{2-x}\text{Sr}_x\text{CuO}_4$ compounds have been studied. Hereafter, La_2CuO_4 , $\text{La}_{1.85}\text{Sr}_{0.15}\text{CuO}_4$ and $\text{La}_{1.6}\text{Sr}_{0.4}\text{CuO}_4$ are abbreviated as Sr(0), Sr(0.15) and Sr(0.4), respectively. Figure 1 shows the Mössbauer spectra at 300K of ^{57}Fe impurities in Sr(0), Sr(0.15) and Sr(0.4) whose Fe concentrations are 1.5% of Cu. All the spectra consist of quadruple doublets. The values of isomer shift and quadruple splitting are listed in Table 1. Except for the case of Sr(0.4), the spectra are well fit by assuming single values for isomer shift and quadruple splitting. The spectrum for Sr(0.4) has somewhat larger line widths and is asymmetric. Therefore a better fitting is obtained by assuming the existence of a minority fraction with slightly different parameters. Since there is only one Cu site in the structure of La_2CuO_4 , the spectra are much simpler than those for $\text{YBa}_2\text{Cu}_3\text{O}_7$ compounds /1/. In order to fit the Mössbauer spectra for Fe-doped $\text{YBa}_2\text{Cu}_3\text{O}_7$ compounds, three (or even more) types of quadruple doublets are necessary to be assumed. The isomer shift values in the present compounds are intermediate between the typical values for Fe^{3+} and Fe^{4+} states. Small dependences on the Sr concentration are observed among the values of isomer shift and quadruple splitting but it seems difficult to discuss the relation with superconductivity.

At 4.2K, all samples show magnetic hyperfine splittings, as shown in Fig. 2. Nishihara et al/2/. Already reported the spectra of Fe impurities in Sr(0) between 290K and 77K, and estimated the Neel temperature to be about 220K. The present result on Sr(0) is in consistent with theirs. It is to be noted that hyperfine fields are also observed in the cases of Sr(0.15) and Sr(0.4). The concentration of Fe impurity is only 1.5% of Cu. If there is no spin correlation among Cu atoms, each Fe atom should behave as paramagnetic and the magnetic hyperfine structure cannot be observed. The present result therefore suggests the existence of collective spin fluctuations in these Cu compounds. Impurity Fe atoms may play a role to pin the spin

fluctuations.

According to the susceptibility measurement on Sr(0.15) sample doped with Fe(Fe/Cu=1%), the onset of superconducting T_c is 10.7K and the diamagnetization at 4.2K is about 40% of non-doped Sr(0.15) sample. Thus, the Fe-doping significantly disturbs the superconductivity in Sr(0.15). From a microscopic viewpoint the doped sample is not a homogeneous superconductor but may be a mixture of super- and non-superconducting domains. However, it is no doubt that the superconducting fraction is not very small and a certain amount of Fe atoms should be included in the superconducting fraction. The obtained spectra indicate that all Fe atoms are in a magnetically ordered state, or participating in collective spin fluctuations with a slow relaxation rate. This result suggests the coexistence of superconductivity and collective spin fluctuations.

The average hyperfine fields at 4.2K are listed also in Table 1. The value for Sr(0) is 486kOe and decreases with the increase of Sr concentration. The spectra of Sr(0.15) and Sr(0.4) are very broad and for the fitting, we have to assume a considerable distribution of hyperfine field. The solid lines in the figure were drawn by assuming static distributions of hyperfine field. However it is very probable that dynamical fluctuations of hyperfine field, like the superparamagnetic case, is a predominant reason for the line broadenings. The temperature dependences are not yet measured and therefore the values at absolute zero are not obtained. For a further discussion, we need spectra with better signal-to-noise ratios as a function of temperature but the measurements require extremely long time.

Comparing the three spectra, we find an interesting feature, in Fig.2, although the spectra are very broad. Because of a quadrupole interaction, the location of magnetically split six lines is not symmetric. The profile suggests that the spin direction in Sr(0.4) is different from the other two. For the interpretation of the spectra for Sr(0) and Sr(0.15), the angle between the magnetic field and the principal axis of electric field gradient (efg) is assumed to be 90° . The sign of efg is taken as positive. In contrast, for the fitting of the Sr(0.4) spectrum, the angle has to be assumed as 0° . If the nature of efg is the same for the three cases, the present result means the change of magnetic spin direction. If the principal axis is along the crystallographic c-axis, the spin direction in the cases of Sr(0) and Sr(0.15) is in the Cu-O plane but that in Sr(0.4) is perpendicular to the plane. At the present stage, the reason of this spin directional change is not clear and whether it is an intrinsic property of the Cu oxide or a phenomenon caused by the Fe-doping cannot be judged.

¹¹⁹Sn RESULTS

The Mössbauer spectra at 300K of ¹¹⁹Sn impurities in Sr(0), Sr(0.15) and Sr(0.4) are shown in Fig. 3. Each spectrum consists of a quadrupole doublet and the values of isomer shift and quadrupole splitting are listed in Table 2, which are typical for Sn⁴⁺ state. The isomer shifts are almost the same but the quadrupole interactions are slightly different. Figure 4 shows the spectra at 4.2K. Although Sr(0) is known to be antiferromagnetic, the spectrum does not show any magnetic hyperfine splitting. If a Sn atom substitutes for a Cu site in the antiferromagnetic La₂CuO₄ crystal, the nucleus has to detect a magnetic hyperfine field. This result indicates that Sn atoms are not dissolved in La₂CuO₄ but are forming an impurity phase. On the other hand, the spectrum for Sr(0.15) shows a very broad splitting which cannot be explained without assuming the existence of magnetic hyperfine field. The magnetic hyperfine field

provides an evidence that Cu atoms are substituting for the Cu site in the sample of Sr(0.15). Therefore the partial substitution of Sr for La seems to be a necessary condition for the solubility of Sn^{4+} impurities in the system.

The measurement on Sr(0.15) was extended down to a very low temperature and the result is shown in Fig. 5. The profile is very broad but the convergence of hyperfine field is better than that at 4.2K. As shown in the figure, the spectrum is roughly fitted by assuming six broad Lorentzians. The average hyperfine field is estimated to be 100kOe. The relative intensity of absorption in the positive velocity side is somewhat larger than that in the negative side. This asymmetry of intensity is caused by a nuclear polarization at the very low temperature, which is a reliable thermometer at very low temperature region. The temperature of the sample is determined to be 20mK.

In the same figure, a spectrum for another Sr(0.15) is shown, whose Sn concentration is less than the former one : $\text{Sn}/\text{Cu}=0.01$. The profile is extremely broad even at the low temperature but the average hyperfine field is almost the same. In both cases, there exist fractions without magnetic splitting. The relative intensity of the magnetic part increases with the decrease of impurity Sn concentration. If the Sn concentration is 0.06, the non-magnetic fraction becomes much more dominant. Therefore, the magnetic fraction is believed to be relating with the intrinsic property of the Cu oxide. For the assignment of the non-magnetic fraction, however, we have not yet a conclusion.

Since a Sn atom itself is non-magnetic, such a large hyperfine field can be induced only if the surrounding Cu atoms have collective spin fluctuations with a rather slow relaxation rate. Usually a magnetic splitting appearing in a Mössbauer pattern corresponds to the temperature dependence of local magnetization and the temperature dependence of hyperfine field is approximated by a Brillouin-like function. However, in the present case, as typically shown in the spectrum for Sr(0.15) at 4.2K, the temperature dependence appears as the broadening. This result means that Cu spins do not have a static magnetic order but are collectively fluctuating.

The ^{119}Sn spectra for Sr(0.4) are entirely non-magnetic at both 300K and 4.2K, although the ^{57}Fe spectrum exhibited a magnetic hyperfine structure. Perhaps the rate of fluctuation is much faster in Sr(0.4) than in Sr(0.15). Since Fe atoms have large local magnetic moments, the relaxation rate of magnetization in Sr(0.4) seems to become much slower by the effect of Fe-doping. It can therefore happen that a Sn-doped sample does not show a magnetic hyperfine splitting although an Fe-doped sample shows.

SUMMARY

^{57}Fe and ^{119}Sn Mössbauer measurements were performed for doped samples of antiferromagnetic La_2CuO_4 , superconducting $\text{La}_{1.85}\text{Sr}_{0.4}\text{CuO}_4$ and non-superconducting $\text{La}_{1.6}\text{Sr}_{0.4}\text{CuO}_4$. Magnetic hyperfine fields at Fe are observed for all the cases, which suggest the existence of strong correlations among Cu spins. On the other hand, a magnetic hyperfine splitting at Sn is observed only in the superconducting case at low temperature. The origin of the magnetic hyperfine field is attributed to collective spin-fluctuations in the Cu oxide with a slow relaxation rate. Thus, the coexistence of superconductivity and collective spin-fluctuations is evidenced. The results on $\text{La}_{1.6}\text{Sr}_{0.4}\text{CuO}_4$ are explained from the different relaxation rates in Fe-doped and Sn-doped samples.

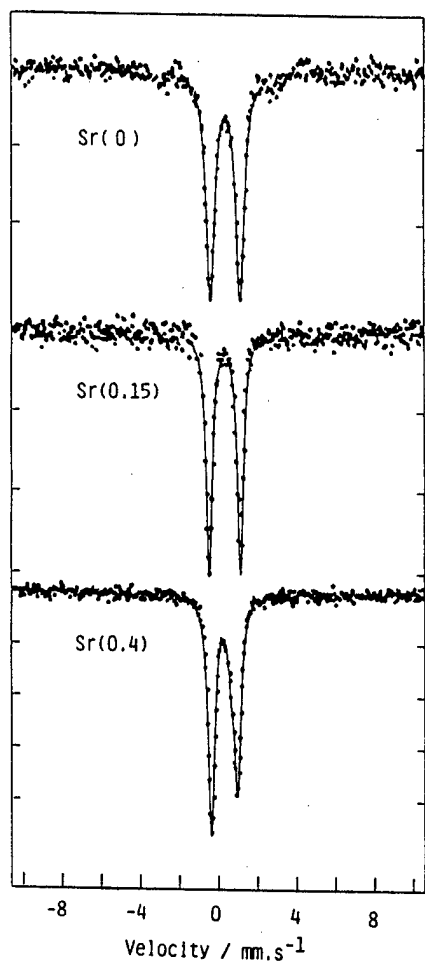


Fig. 1. Mössbauer absorption spectra at 300K for ^{57}Fe impurities in La_2CuO_4 , $\text{La}_{1.85}\text{Sr}_{0.15}\text{CuO}_4$ and $\text{La}_{1.6}\text{Sr}_{0.4}\text{CuO}_4$. $\text{Fe}/\text{Cu}=0.015$.

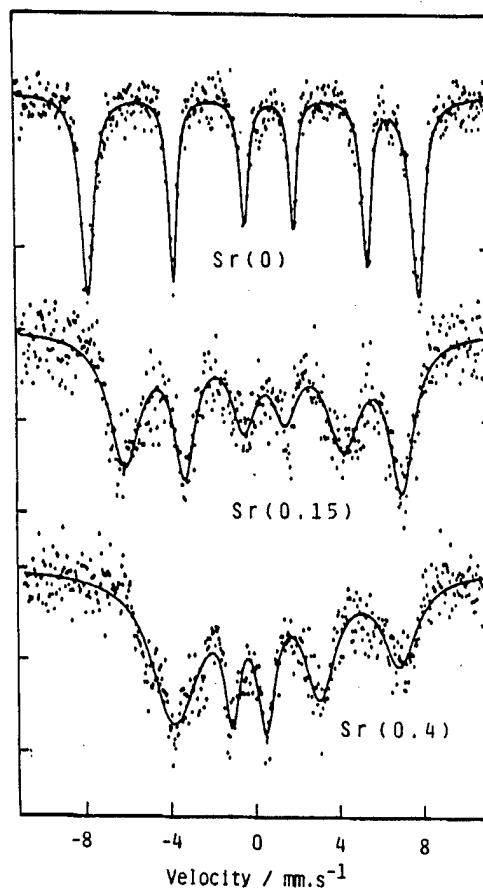
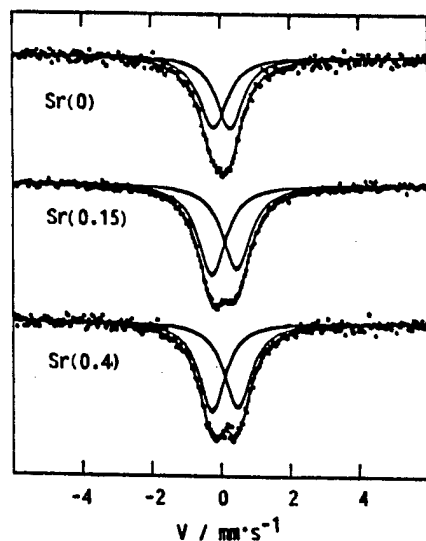


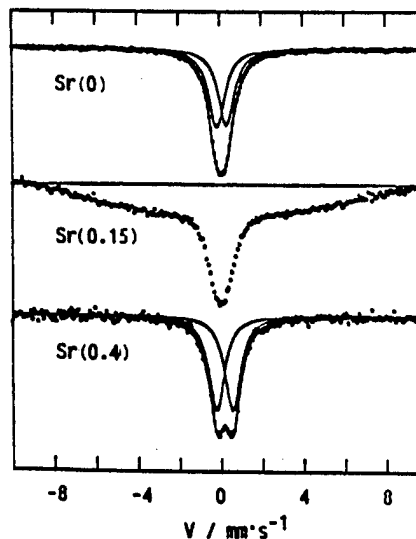
Fig. 2. ^{57}Fe Mössbauer spectra at 4.2K of the same samples as Fig. 1.

Fig. 3. at 300K



Mössbauer spectra for ^{119}Sn impurities in
 La_2CuO_4
 $\text{La}_{1.85}\text{Sr}_{0.15}\text{CuO}_4$
 $\text{La}_{1.6}\text{Sr}_{0.4}\text{CuO}_4$

Fig. 4. at 4.2K



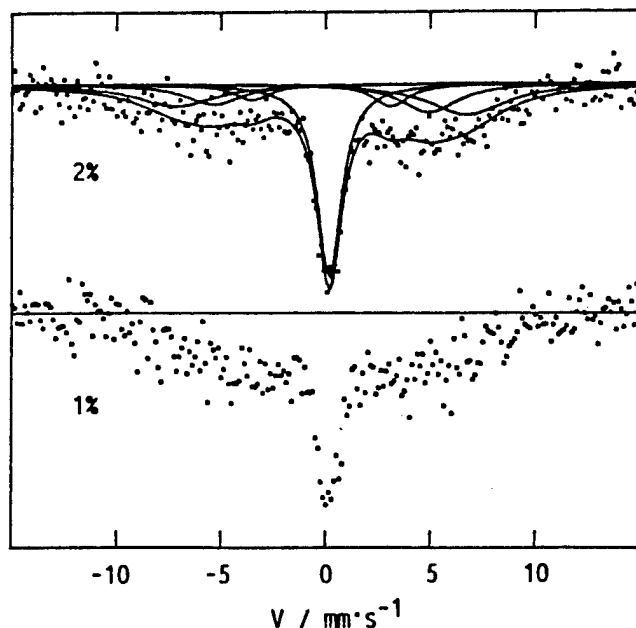


Fig. 5. Mössbauer spectra for ^{119}Sn impurities in superconducting $\text{La}_{1.85}\text{Sr}_{0.15}\text{CuO}_4$ at 20mK. The impurity concentrations, Sn/Cu, are 0.02 and 0.01, respectively.

References

- /1/ e.g., T. Shinjo and S. Nasu, "Mechanisms of High Temperature Superconductivity", ed. by H. Kamimura and A. Oshiyama, Springer-Verlag, 1989, p.166.
 /2/ Y. Nishihara, M. Tokumoto, K. Murata, K. Oka and H. Unoki, J. Phys. Soc. Jpn. 57 (1988) 384.

Table 1. Observed values of isomer shift, quadrupole splitting and magnetic hyperfine field of ^{57}Fe impurities in La-Sr-Cu-O compounds. The concentrations of Fe are 1.5% of Cu.

	La_2CuO_4 [Sr(0)]	$\text{La}_{1.85}\text{Sr}_{0.15}\text{CuO}_4$ [Sr(0.15)]	$\text{La}_{1.6}\text{Sr}_{0.4}\text{CuO}_4$ [Sr(0.4)]	
IS/mm.s $^{-1}$ * at 300K	0.33	0.28	0.23 (0.07)**	* relative to pure Fe at 300K
QS/mm.s $^{-1}$ at 300K	1.53	1.55	1.34 (1.04)**	**values for the minority phase whose intensity is 22% of the total.
H/kOe at 300K	0	0	0	
77K	431	0	0	
4.2K	486	402	337	

Table 2. Observed values of isomer shift relative to BaSnO_3 and quadrupole splitting at 300K of ^{119}Sn impurities in La-Sr-Cu-O compounds.

	La_2CuO_4 Sr(0)**	$\text{La}_{1.85}\text{Sr}_{0.15}\text{CuO}_4$ Sr(0.15)*	$\text{La}_{1.6}\text{Sr}_{0.4}\text{CuO}_4$ Sr(0.4)**	
IS/mm.s $^{-1}$	0.05	0.11	0.12	* Sn/Cu=2%
QS/mm.s $^{-1}$	0.48	0.76	0.74	**Sn/Cu=3%

NEW METHOD FOR ACCURATE ANALYSIS OF MÖSSBAUER SPECTRA OF $\text{YBa}_2(\text{Cu}_{1-x}\text{Fe}_x)_3\text{O}_{7-\delta}$

T. Tamaki, M. Nishizawa, A. Ito and T. Fujita*

Department of Physics, Faculty of Science, Ochanomizu University, Bunkyo-ku,
Tokyo 112, Japan

*Department of Physics, Faculty of Science, Hiroshima University,
Hiroshima 730, Japan

In order to reduce ambiguous factors introduced when the conventional method is applied to decompose the complicated Mössbauer spectra of $\text{YBa}_2(\text{Cu}_{1-x}\text{Fe}_x)_3\text{O}_{7-\delta}$ into several quadrupole doublets, we have used a sophisticated technique by paying attention to a fact that only relative intensities of the Mössbauer spectra are changed by a heat-treatment at 300°C in vacuum. Using this technique, the Mössbauer spectrum of $\text{YBa}_2(\text{Cu}_{0.95}\text{Fe}_{0.05})_3\text{O}_{7-\delta}$ at room temperature is decomposed into four kinds of quadrupole doublets, and their quadrupole splittings ΔE_Q and the center shifts δ are determined precisely. We have shown that the values of ΔE_Q for the doublets D-3 and D-4 (defined in the text) reported previously by many groups of workers should be changed.

Many groups of workers have studied the iron-doped $\text{YBa}_2(\text{Cu}_{1-x}\text{Fe}_x)_3\text{O}_{7-\delta}$ by observing Mössbauer spectra. Although the appearances of most of the Mössbauer spectra are very similar with one another except for relative intensities of the absorption lines, various kinds of assignments for the spectral lines have been reported.¹⁻³ A reason for that comes from their ways of analyses: they decomposed their spectra into several sets of quadrupole doublets by adjusting the quadrupole splittings and the intensities so as to simulate the experimental spectra as well as possible. This method sometimes gives misassignments in the case that some Mössbauer absorption lines are superposed with each other and they are not resolved completely. In order to argue the properties of this system through the doped Fe's, it is clear that assignment of the Mössbauer spectra should be done as precisely as possible. In this report, we describe a sophisticated technique effectual for accurate analyses of Mössbauer spectra of $\text{YBa}_2(\text{Cu}_{1-x}\text{Fe}_x)_3\text{O}_{7-\delta}$, which is also usefully applied for systems in which only relative intensities of Mössbauer spectra are changed by heat-treatments or other methods.

We examined $\text{YBa}_2(\text{Cu}_{0.95}\text{Fe}_{0.05})_3\text{O}_{7-\delta}$ by comparing the Mössbauer spectra taken at room temperature before and after a heat-treatment at 300°C in vacuum of $\sim 10^{-2}$ mmHg for 10 min. It should be noted that the decrease of the superconducting transition temperature T_C is not very large: T_C is about 57 K for the heat-treated sample while 65.4 K for the as-prepared one. In Fig. 1, we show the spectrum of the as-prepared sample [A] and that of the heat-treated one [B], in which the positions of the quadrupole doublets D-1-D-4 are indicated by solid bars on the basis of our results (see Table 1). As seen in the figure, the relative intensities of the absorption lines are largely changed by the heat-treatment. However, we want to emphasize that the positions of the absorption

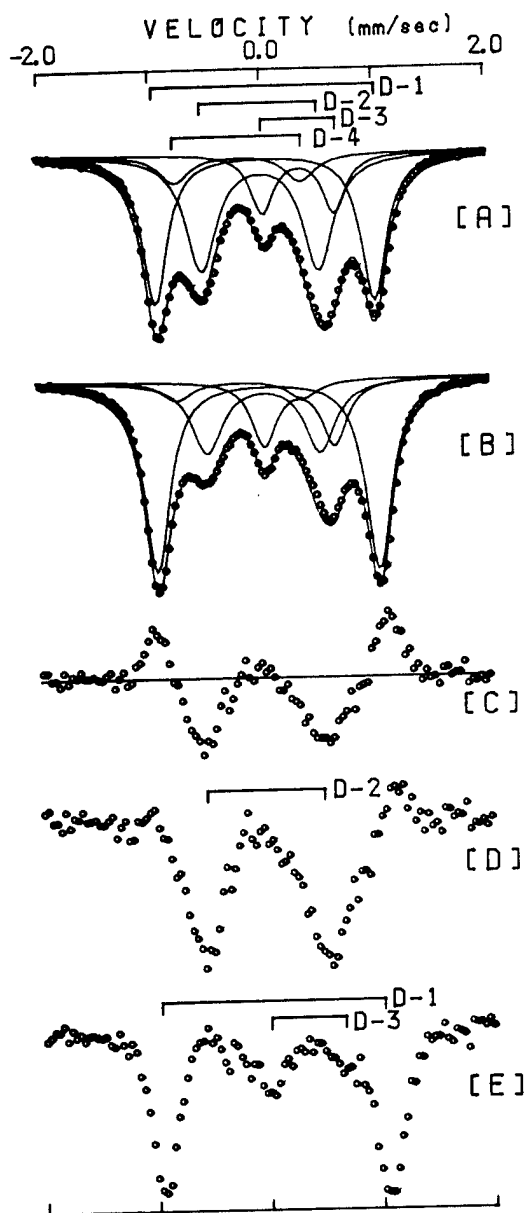


Fig.1

Process how to determine positions of the constituent quadrupole doublets of the Mössbauer spectrum at room temperature for $\text{YBa}_2(\text{Cu}_{0.95}\text{Fe}_{0.05})_3\text{O}_{7-\delta}$. [A] : Mössbauer spectrum of the as-prepared sample. The positions of the quadrupole doublets D-1~D-4 determined by the present work are indicated by solid bars. [B] : Mössbauer spectrum taken after the heat-treatment at 300°C in vacuum for 10 min. [C] : A spectrum of $([A] - [B])$. Before the subtraction, the average back-ground counts of [A] and [B] are normalized to equal. [D] : A spectrum of $([A] + p[C])$, where p is chosen so that the doublet D-1 is canceled. [E] : A spectrum of $([A] - q[D])$, where q is chosen so that the doublet D-2 disappears. The solid line spectrum in [A] or [B] is the calculated one composed by using the values listed in Table 1.

lines are not affected significantly by this heat-treatment. As is shown below, therefore, comparisons of these two spectra [A] and [B] allow us to find locations of less intense lines and unresolved lines. The spectra [C]~[E] are obtained by repeating addition and subtraction between two of various spectra. The spectrum [C] is obtained by subtracting [B] from [A] after normalizing the average back-ground counts of [A] and [B] to equal. From this analysis, both of Fe's giving the doublet D-1 and D-2 are evidenced to sit in the Cu_1 site, details of which are reported in ref.4. The [D] is obtained by adding [C] to [A] as $[A] + p[C]$, where a relative weight p is chosen so that the doublet D-1 is canceled. From the [D], the accurate position of D-2 is determined. The [E] is a subtracted spectrum of $([A] - q[D])$, where q is chosen so that

the doublet D-2 disappears. A noticeable point in the [E] is that the location of the right absorption line of D-3 is clearly seen. The position of this line is observed for the first time by the present treatment. From this, therefore, the position of D-3 is determined unambiguously. The accurate position of D-1 is also determined from the [E]. The values of the quadrupole splitting ΔE_Q and the center shift δ thus determined are listed in Table 1, and the relative intensities are also shown. The position and the intensity of D-4 are determined so that the spectrum [A] or [B] experimentally obtained is reproduced by the calculated spectrum (solid line spectrum).

Table 1.

Quadrupole splitting ΔE_Q , center shift δ and relative intensity I of four constituent doublets of $\text{YBa}_2(\text{Cu}_{0.95}\text{Fe}_{0.05})_3\text{O}_{7-\delta}$ for the as-prepared spectrum [A] and for the heat-treated spectrum [B].

		D-1	D-2	D-3	D-4
ΔE_Q (mm/s)	[A]	1.96	1.05	0.64	1.13
	[B]	1.98	1.02	0.64	1.13
δ (mm/s)	[A]	0.04	0.00	0.35	-0.20
	[B]	0.05	0.01	0.34	-0.20
I	[A]	0.39	0.37	0.15	0.09
	[B]	0.53	0.23	0.17	0.07

Table 2

Comparison of Mössbauer parameters for as-prepared $\text{YBa}_2(\text{Cu}_{1-x}\text{Fe}_x)_3\text{O}_{7-\delta}$ reported by three groups; quadrupole splitting ΔE_Q , center shift δ and relative intensity I.

		x	D-1	D-2	D-3	D-4
ΔE_Q (mm/s)	this work	0.05	1.96	1.05	0.64	1.13
	V. Sedykh et al ²	0.017	1.96	1.17	0.50	1.60
	E.Baggio-Saitovitch et al ¹	0.03	1.91	1.19	0.29	1.48
δ (mm/s)	this work	0.05	0.04	0.00	0.35	-0.20
	V. Sedykh et al ²	0.017	0.03	-0.01	0.27	-0.12
	E.Baggio-Saitovitch et al ¹	0.03	0.047	0.032	0.208	-0.245
I	this work	0.05	0.39	0.37	0.15	0.09
	V. Sedykh et al ²	0.017	0.11	0.53	0.16	0.20
	E.Baggio-Saitovitch et al ¹	0.03	0.31	0.53	0.08	0.08

For comparison, we list in Table 2 the values of ΔE_Q , δ and I reported previously by two other groups for their respective as-prepared samples together with ours. It is noticed in Table 2 that the values of ΔE_Q and δ for D-1 and D-2 determined by three groups agree with one another within a permitted limit if we take into account the variety of samples.¹⁻³ However, our values for D-3 and D-4 are different considerably from others. The doublet D-3 has been assigned as Fe^{3+} replacing $Cu_{2.2.5}$. A value of $\Delta E_Q=0.64$ mm/s for D-3 determined by the present study is fairly large, but it is the most expected value for Fe^{3+} sitting in highly distorted sites such as the Cu_2 site. A value of $\delta=0.35$ mm/s is also quite reasonable for this kind of Fe^{3+} . Our value of $\Delta E_Q=1.13$ mm/s for D-4 is about 30% smaller as compared with any values reported previously. The electronic state of Fe giving D-4 can not readily be determined from a combination of values $\Delta E_Q=1.13$ mm/s and $\delta=-0.20$ mm/s. From each combination of the values of ΔE_Q and δ for D-1, D-2 or D-4, it can be clearly said that the irons giving D-1, D-2 and D-4 are not in well known states such as Fe^{2+} , Fe^{3+} or Fe^{4+} in high-spin or low-spin state. In order to determine the electronic states of them, techniques other than Mössbauer spectroscopy are desired to be used jointly.

References

- 1 E. Baggio-Saitovitch, I. Souza Azevedo, R. B. Scorzelli, H. Saitovitch, S. F. da Cunha, A. P. Guimaraes, P. R. Silva, and A. Y. Takeuchi, *Phys. Rev. B* 37, 7967 (1988).
- 2 V. Sedykh, S. Nasu, and F. E. Fujita, *Solid State Commun.* 67, 1063 (1988).
- 3 R. A. Brand, Ch. Sauer, H. Lütgemeier, B. Rupp and W. Zinn, *Physica C* 156, 539 (1988).
- 4 T. Tamaki, M. Nishizawa, A. Ito and T. Fujita, to be published in *Hyperfine Interactions* (1990), *Proceedings of International Conference on the Applications of the Mössbauer Effect*, Budapest, Hungary, 1989.
- 5 T. Tamaki, T. Komai, A. Ito, Y. Maeno and T. Fujita, *Solid State Commun.* 65, 43 (1988).

Ion-Channeling Studies in Single-Crystal $\text{YBa}_2\text{Cu}_3\text{O}_{7-y}$ and $\text{Bi}_{2.2}\text{Sr}_{1.8}\text{CaCu}_2\text{O}_y$

K. Yamaya, T. Haga and Y. Okajima

Department of Nuclear Engineering, Hokkaido University, Sapporo 060, Japan

The temperature dependence of the Rutherford backscattering in the $\langle 001 \rangle$ axial channeling mode for each constituent atoms of single-crystal $\text{YBa}_2\text{Cu}_3\text{O}_{7-y}$ and $\text{Bi}_{2.2}\text{Sr}_{1.8}\text{CaCu}_2\text{O}_y$ have been carried out to study the change in the structural properties at the superconducting transition. Anomalies of channeling behavior observed across the superconducting transition temperature of $\text{YBa}_2\text{Cu}_3\text{O}_{7-y}$ suggest a structural instability or a change in the lattice. The anomalies of RBS for Y and Ba atoms suggest the phonon softening, while those for Cu and O atoms are not explained in terms of only the phonon softening. On the other hand, in $\text{Bi}_{2.2}\text{Sr}_{1.8}\text{CaCu}_2\text{O}_y$ no anomaly of channeling has been observed across the superconducting transition temperature, because of large yield of the Rutherford backscattering.

The greatest interest in the recently discovered high-temperature superconductors is whether they represent a class of materials in which a new pairing mechanism produces superconductivity. It is therefore important to identify any unconventional behavior in comparison with ordinary superconducting behaviors. It is generally accepted that at the superconducting transition temperatures, T_c 's, the lattices and their properties are essentially unchanged, while some of the properties of the conduction electrons are changed significantly. However, in high- T_c superconductors much anomalous behaviors associated with the lattice properties have been reported by several researchers. For example, the elastic anomalies which cannot be explained within a BCS model have been observed at and below T_c of $\text{La}_{2-x}\text{Sr}_x\text{CuO}_4$ and $\text{YBa}_2\text{Cu}_3\text{O}_{7-y}$ [1-3] and the c-axis of $\text{YBa}_2\text{Cu}_3\text{O}_{7-y}$ exhibits an anomalous change in a narrow temperature range near T_c . [4] More, recently, it has been found from high-pressure studies that the low temperature structural phase transition in $\text{La}_{2-x}\text{Ba}_x\text{CuO}_4$ does suppress the superconductivity. [5] It is likely that the structural anomalies observed in high- T_c oxides have implications for the mechanism of superconductivity.

It is known that the axial ion-channeling mode in Rutherford backscattering spectroscopy (RBS) is highly sensitive to the lattice vibration and small lattice displacements from regular lattice sites. From the minimum yield of RBS in the axial channeling mode, X_{\min} , rms amplitudes of the lattice vibration and displacement of atoms can be derived. Therefore, the channeling technique is very useful to studies of phase transitions (such as Jahn-Teller [6] and charge-density-waves phase transitions. [7,8]), which is accompanied with the structural change.

In the present letter we report the first measurement of X_{\min} of $\langle 001 \rangle$ -aligned channeling for each constituent atom of $\text{YBa}_2\text{Cu}_3\text{O}_{7-y}$ and $\text{Bi}_{2.2}\text{Sr}_{1.8}\text{CaCu}_2\text{O}_y$ for temperatures down to 50K through the superconducting transition.

The standard experimental arrangement for ion backscattering was used with Van de

Graaff-type ion accelerator. The 1.00-MeV He^+ and D^+ ions were used as probe beams. The diameter and the divergence of the ion beam were 1.0 mm and 0.03° , respectively. For RBS and nuclear-reaction experiments, a Si-surface-barrier (annular type) detector was used. The active area, the scattering angle, and the distance between a sample and the detector are 50 mm^2 , 174° , and 35 mm, respectively. For particle-induced x-ray emission (PIXE) experiments, a Si (Li) solid-state detector was used. The active area, the scattering angle, and the distance between a sample and the detector are 30 mm^2 , 150° , and 25 mm, respectively. The sample was set at a position where a beam direction was aligned with a channel axis of the sample by the three-axis goniometer and the sample was cooled down slowly with a cryorefrigeration. It was confirmed at several points that the incident direction of ions paralleled the crystal axis. The temperature of the sample was measured by a Si-Diode thermometer attached on the bottom of the sample and was controlled within $\pm 0.1\text{K}$ with the aid of an additional small heater on the sample holder. In the actual experiment, we paid special attention to the ion fluence in order to minimize the radiation damage of the sample. [7,10] The total ion fluence for one sample was restricted within $\sim 400 \text{ nC}/1.0 \text{ mm } \phi$.

$\text{YBa}_2\text{Cu}_3\text{O}_{7-y}$ (with M. Oda and M. Ido, Department of Physics, Hokkaido University, Sapporo 060, Japan, Y. Tajima and Y. Hidaka, NTT Opto-Electronics, Tohkai 319-11, JAPAN)

$\text{YBa}_2\text{Cu}_3\text{O}_{7-y}$ (YBCO) single crystals were grown by the flux method.[9] Two single crystals with typical dimensions of $2 \times 2 \times 0.1 \text{ mm}^3$ were used for the ion-channeling measurement. Their T_c 's were determined from resistivity measurements by the dc four probe method and magnetic-susceptibility measurements by a SQUID susceptometer.

The T_c 's of two single crystals were determined to be 90 and 91K from resistivity measurements. The temperature dependence of dc magnetic susceptibility for one of the crystals is shown in Fig. 1. This result is consistent with that of resistivity measurements. The results of ion channeling for two single crystals were substantially the same. Figure 2 shows typical RBS energy spectra at room temperature obtained by using 1.00-MeV He^+ ions. In this figure, one spectrum is the channeling one along the $\langle 001 \rangle$ axis, and the other is the random spectrum ($\sim 5^\circ$ off the channeling axis). The magnitude of the RBS yield along the $\langle 001 \rangle$ direction

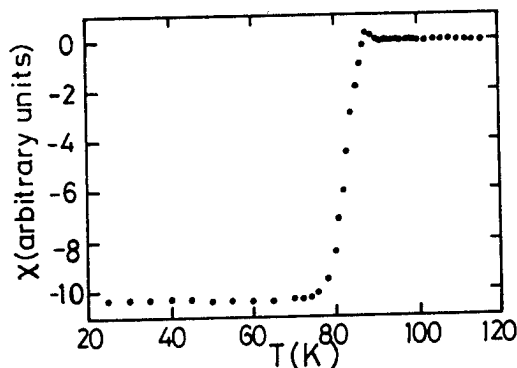


Fig. 1 dc magnetic susceptibility of single-crystal $\text{YBa}_2\text{Cu}_3\text{O}_{7-y}$ as a function of temperature.

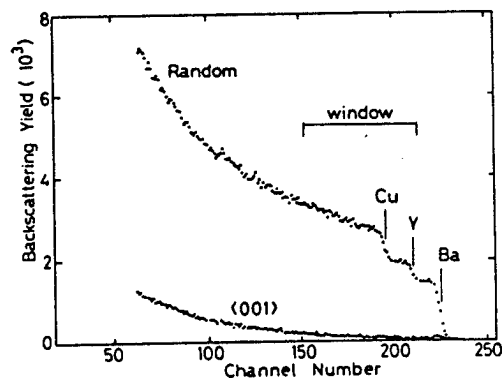


Fig. 2 $\langle 001 \rangle$ -aligned and random RBS energy spectra of single-crystal $\text{YBa}_2\text{Cu}_3\text{O}_{7-y}$.

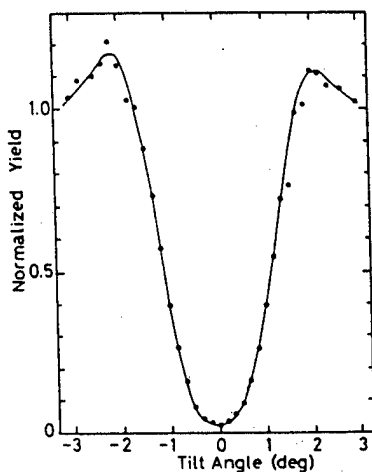


Fig. 3 RBS yields of $\text{YBa}_2\text{Cu}_3\text{O}_{7-y}$ as a function of tilt angle.

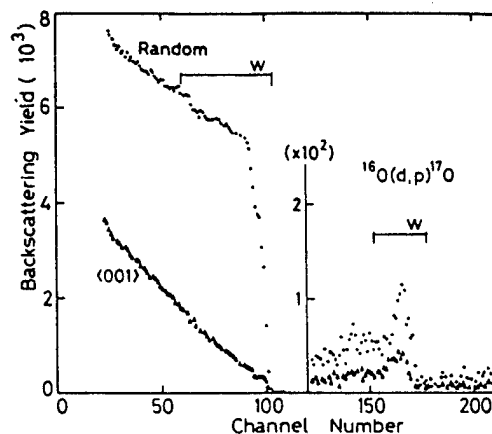


Fig. 4 Typical spectra for RBS and high-energy protons.

is extremely smaller than that of the random direction. Moreover, the normalized RBS yields within the energy window marked in Fig. 2 are shown as a function of the tilt angle in Fig. 3. From these measurements, the normalized minimum yields along the $\langle 001 \rangle$ directions are determined to be of the order of 0.03, which is in good agreement with the results of the ion-channeling in YBCO reported already.[10,11] These facts indicate that the samples used in the present work are very high-quality single crystal.

Furthermore, to obtain the clearly distinguished information on each element of YBCO, we used PIXE and nuclear-reaction methods with 1.00-Mev D^+ ions. Figure 4 shows the $\langle 001 \rangle$ -aligned energy spectrum and the random one for RBS and high-energy protons. Here, the high-energy protons were produced by the nuclear reactions. The information of the O atoms was determined by the nuclear reaction. Figure 5 shows the $\langle 001 \rangle$ -aligned and the random characteristic x-ray spectrum for Y, Ba, and Cu atom obtained by the PIXE method.

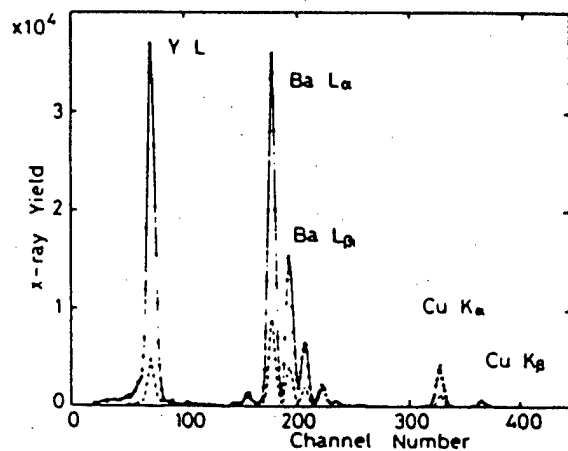


Fig. 5 $\langle 001 \rangle$ -aligned and random PIXE spectra for Y, Ba, and Cu. The dashed line indicates the $\langle 001 \rangle$ -aligned spectrum.

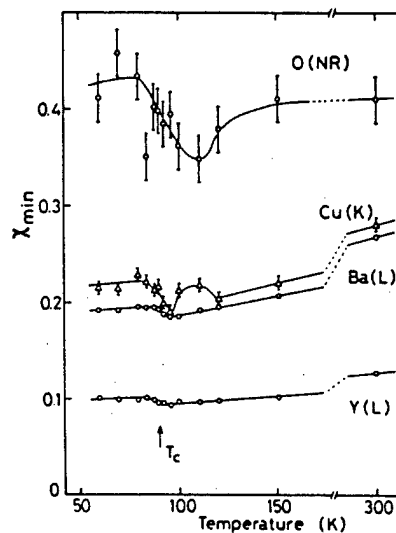


Fig. 6 X_{\min} 's for each element of $\text{YBa}_2\text{Cu}_3\text{O}_{7-y}$ obtained by PIXE and nuclear-reaction method as a function of temperature.

Figure 6 shows the temperature dependence of the X_{\min} for each constituent atoms of YBCO obtained by the PIXE and nuclear reaction methods with 1.00-MeV. In the normal state, the X_{\min} for all constituent atoms monotonically decrease with decreasing temperature, which is similar to the typical temperature dependence of X_{\min} of a conventional solid. However, in the vicinity of T_C , the temperature dependence of X_{\min} for each atom is very curious, especially those for Cu and O atoms. Thus, the abrupt increase in X_{\min} is observed across T_C .

According to Barrett's equation[12], X_{\min} for a monatomic lattice is given by the atomic density of the samples and the rms amplitude of the lattice vibration of the atoms in the plane normal to the channeling axis. In the case of the crystals which consist of many different atoms, the expression for X_{\min} is much more complicated but Barrett's equation can be still used as a guiding principle for searching the fundamental process. It is widely accepted that unless any structural transition occurs, X_{\min} is proportional to the rms amplitude square of the lattice vibration. Therefore, it can be concluded that the decrease in X_{\min} with decreasing temperature in the normal state of YBCO is due to the decrease in the rms amplitude of the thermal vibration; a stiffening of the lattice is observed, while the increase in X_{\min} observed near T_C can not be interpreted in terms of such a thermal vibration of atoms.

The magnitude of X_{\min} depends on not only the rms amplitude of the lattice vibration but also lattice displacements. As possible mechanisms of the increase in X_{\min} with decreasing temperature, the structural change or the softening of the phonon which is related with the structural instability have generally been taken. In fact, it is known that in the Jahn-Teller[6] transition the gradual raise of X_{\min} revealed just above the transition temperature is due to the phonon softening and in the CDW phase transition[7,8] the enormous rise in X_{\min} at the transition temperature is caused by the displacement of atoms from regular sites of the high-temperature phase.

X_{\min} 's for Y and Ba atoms shown in Fig. 6 exhibit the abrupt rise of X_{\min} with decreasing temperature. The behavior is probably interpreted in terms of the phonon softening or the small displacement of atoms, while those for Cu and O atoms begin to reveal the increase or decrease at temperatures above T_C and a large ups and downs change in the X_{\min} are observed with decreasing temperature. These enormous changes in the X_{\min} 's of Cu and O atoms observed in a narrow temperature range are not simply explained in terms of the phonon softening or the small displacement of atoms, which may indicate the complicated lattice dynamics of Cu and O atoms. Here, it should be noted that Sharma et al.[10,13] also observed the abrupt change in the width of the $\langle 001 \rangle$ channeling dips at T_C . However, our interpretation does not agree with theirs. Though the origin of this discrepancy is unclear at this moment, we think that sensitivity of X_{\min} to all types of defects, disorder, etc. is better than that of the width of a channeling dip.

Anomalous behaviors of Cu and/or O atoms in YBCO have been observed near T_C on other measurements also; Debye-Waller factor for the O atoms perpendicular to the c-plane obtained from the EXAFS (Extended X-ray Absorption Fine Structure) method[14] and the breathing-mode vibration of O atoms around Cu atoms determined from the Raman scattering measurement. [15] Furthermore, the measurement of the neutron diffraction exhibits the discontinuous change of Cu-O bond length perpendicular to the c-plane at T_C [16] and that there is the difference on the occupancy ratio of oxygen in the chain

site between in the normal and superconducting states. [17] These results, including the present one strongly suggest that a change in the lattice dynamics of Cu and/or O atom occurs in the vicinity of T_C .

It is known that the Cu and O atoms play an important role for the mechanism of the superconductivity in high- T_C compounds, while Y and Ba atoms are mainly contribute to the crystal bonding, but not directly related to the superconductivity. Therefore, it is very interested whether the structural anomalies observed in YBCO have implications for the mechanism of superconductivity.

Bi_{2.2}Sr_{1.8}CaCu₂O_y (with S. Takekawa, National Institute for Research in Inorganic Materials, Tsukuba 305, JAPAN)

The single crystal Bi₂Sr₂CaCu₂O_y (BSCCO) was grown by the floating-zone method. [18] The chemical composition determined by EPMA measurement is Bi_{2.2}Sr_{1.8}CaCu₂O_y. The samples were carefully cleaved from as-grown crystal into the ab-plane sheets. The samples had smooth and shinny surfaces and were free of major visible defects. The diffraction pattern obtained by the Laue method showed existence of the superstructure along the b-axis. The typical dimensions of our samples for measurement of ion-channeling were 5x5x0.5 mm³. The T_C was determined from measurements of dc resistivity and inductance.

The average value of the T_C of as-grown crystal were determined to be 86(±2)K from both measurements of resistivity and inductance. Figure 7 shows the typical temperature dependence of inductance. The normalized RBS yields obtained with 1.00-MeV He⁺ ions are shown as a function of the tilt angle in Fig. 8. The X_{min} of BSCCO is the order of 0.3, which is an order of magnitude larger than that of YBCO. There are several possible interpretations of this large X_{min} observed in BSCCO; they are (1) existence of the incommensurate superstructure along the b-axis, (2) substitution of Sr and/or Ca atoms in BiO₂-planes, (3) deviation from the chemical composition of Bi:Sr:Ca:Cu=2:2:1:2, and (4) oxygen deficiencies. Especially, (1) and (2) are characteristics in BSCCO. Thus, large X_{min} of BSCCO may be intrinsic.

Figure 9 shows the X_{min} for each constituent atom of BSCCO obtained by the PIXE and nuclear-reaction method as a function of temperature. The X_{min} for all constituent atoms monotonically decreases with decreasing temperature and no anomaly

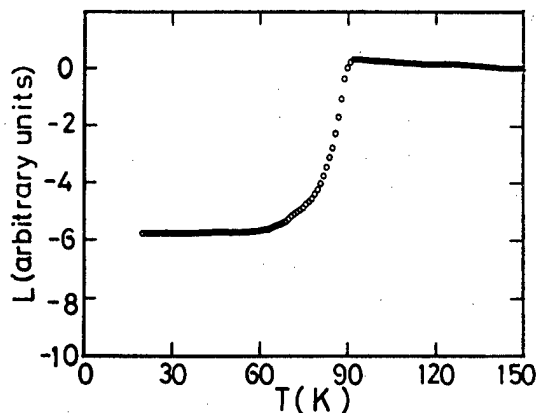


Fig. 7 Inductance of single-crystal Bi_{2.2}Sr_{1.8}CaCu₂O_y as a function of temperature.

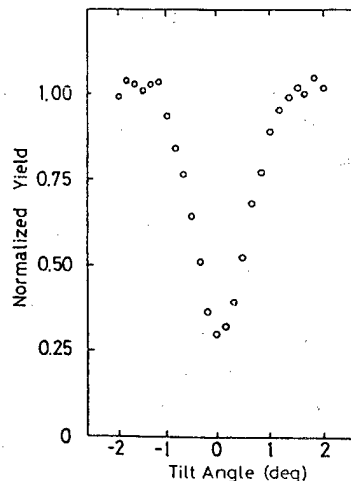


Fig. 8 RBS yield of Bi_{2.2}Sr_{1.8}CaCu₂O_y as a function of tilt angle.

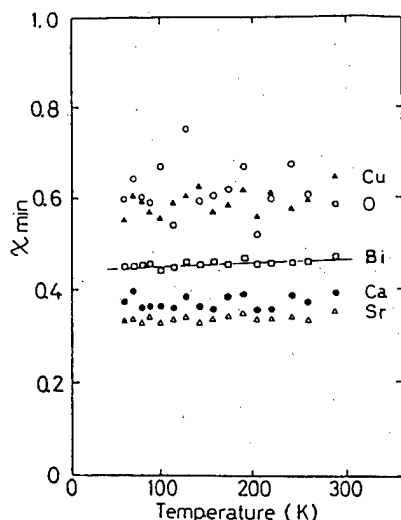


Fig. 9 X_{\min} 's for each element of $\text{Bi}_{2.2}\text{Sr}_{1.8}\text{CaCu}_2\text{O}_y$ obtained by PIXE and nuclear-reaction method as a function of temperature.

is observed in the temperature range measured. Comparing this result with that of YBCO, it is found that the X_{\min} is large and its temperature coefficient is very small, almost constant. This means that the large magnitude of X_{\min} observed in BSCCO is mainly due to the disorder and/or defects of atoms of the samples, and the effect due to the thermal vibration is extremely small. Therefore, even if the lattice vibration anomalies near T_c is intrinsic in BSCCO, it will be hard to detect the anomalies in X_{\min} as observed in YBCO.

In order to make clear the correlation between the superconducting state and the anomalies of X_{\min} , further analysis on the temperature dependence of RBS is in progress on single crystals of high- T_c compounds.

This work was partly supported by a Grant-in-Aid for Scientific Research on Priority Areas "Mechanism of Superconductivity".

References

- [1] H. Mathias, Phys. Rev. B36(1987)2411.
- [2] A. Migliori, T. Chen, B. Alavi, and G. Gruner, Solid State Commun. 63(1987)827.
- [3] S. Bhattacharya, M. J. Higgins, D. C. Jonston, A. J. Jacobson, J. P. Stokes, D. P. Goshorn, and J. T. Lewandowski, Phys. Rev. Letters 60(1988)1181.
- [4] R. Srinivasan, K. S. Girirajan, V. Ganesan, V. Radhakrishnan, and G. V. Subba Rao, Phys. Rev. 38B(1988)889.
- [5] N. Yamada, M. Oda, M. Ido, Y. Okajima, and K. Yamaya, Solid State Commun. 70(1989)1151.
- [6] T. Haga, K. Shimizu, Y. Abe, and Y. Kino, Solid State Commun. 38(1981)187.
- [7] T. Haga, Y. Abe, and Y. Okamoto, Phys. Rev. Letters, 51(1983) 678.
- [8] M. Nunez-Regueiro, B. Daubin, M. Dubus, and C. Ayache, Solid State Commun. 54(1985)457.
- [9] Y. Hidaka, Y. Enomoto, M. Suzuki, M. Oda, and T. Murakami, J. Cryst. Growth 85(1987)581.
- [10] R. P. Sharma, L. E. Rehn, P. M. Baldo, and J. Z. Liu, Phys. Rev. B38(1988)9287.
- [11] N. G. Stoffe, P. A. Morris, W. A. Bonner, and B. J. Wilkens, Phys. Rev. B37(1988)2297.
- [12] J. H. Barret, Phys. Rev. B3(1971)1527.
- [13] R. P. Sharma, L. E. Rehn, P. M. Baldo, and J. Z. Liu, Phys. Rev. Lett. 62(1989)2869.
- [14] H. Maeda, N. Bamba, A. Koizumi, Y. Yoshikawa, T. Ishi, H. Maruyama, M. Hida, Y. Kuroda, H. Yamazaki, and T. Morimoto, J. Phys. Soc. Jpn. 56(1987)3413.
- [15] C. Dongming, M. Chunbo, Q. Yiyai, C. Zhuyao, H. Tianjing, W. Jian, X. Houwen and L. Fan-chen, Solid State Commun. 68(1988)263.
- [16] W. Schafer, E. Jansen, G. Will, J. Faber, Jr. and B. Vcal, Mat. Res. Bulletin 23(1988)1439.
- [17] Q. W. Yan, P. L. Zhang, Z. G. Shen, J. K. Zhao, Y. Ren, Y. N. Wei, T. D. Mao, C. X. Liu, T. S. Ning, K. Sun, and Q. S. Yang, Phys. Rev. B36(1987)8810.
- [18] S. Takekawa, H. Nozaki, A. Umezono, K. Kosuda, and M. Kobayashi, J. Cryst. Growth 92(1988)687.

Electronic Structure of High-Tc Superconductor Studied by Photoemission and X-Ray Absorption

T. Takahashi, H. Matsuyama, H. Katayama-Yoshida, T. Watanabe, T. Ejima,

T. Kashiwakura, S. Suzuki, and S. Sato

Department of Physics, Tohoku University, Sendai 980, Japan

N. Kosugi

Division of Molecular Engineering, Kyoto University, Kyoto 606, Japan

A. Yagishita, K. Tanaka, and H. Maezawa

Photon Factory, KEK, Tsukuba 315, Japan

H. Fujimoto

Department of Chemistry, Kumamoto University, Kumamoto 860, Japan

K. Seki

Department of Material Science, Hiroshima University, Hiroshima 730, Japan

K. Kamiya, S. Shamoto, M. Sato, and H. Inokuchi

Institute for Molecular Science, Okazaki 444, Japan

Electronic structure of the high-Tc superconductor has been studied by various spectroscopies (photoemission, inverse photoemission, x-ray absorption, and scanning tunneling spectroscopy). The experimental results strongly suggest that the electronic structure in the vicinity of the Fermi level forms Fermi-liquid states and has a dominant oxygen $2p_{x,y}$ nature with a "impurity-state"-like origin.

The mechanism responsible for high-Tc superconductivity is controversial even though extensive experimental and theoretical studies have been made. Knowledge of the electronic structure is a key step toward understanding the mechanism of high-Tc superconductivity.

In this paper, we report comprehensive results of our photoemission, inverse photoemission, x-ray absorption, and scanning-tunneling spectroscopy of the high-Tc superconductor. From the results, we propose a model to describe the electronic structure of the high-Tc superconductor.

Angle-resolved photoemission study of $\text{Bi}_2\text{Sr}_2\text{Ca}_{1-x}\text{Y}_x\text{Cu}_2\text{O}_8$

Figure 1 shows angle-resolved photoemission spectra of superconducting $\text{Bi}_2\text{Sr}_2\text{CaCu}_2\text{O}_8$ and the "band structure" determined from the photoemission experiment [1]. The photoemission spectra and resulting band structure clearly shows two dispersive bands which intersect the Fermi level midway between the center and the boundary of the Brillouin zone. This is a direct evidence for the existence of Fermi surface(s) and therefore Fermi-liquid states in the high-Tc superconductor [1]. Next step to approach the high-Tc mechanism is to study the nature and origin of the Fermi-liquid states. Comparison of the electronic "band structure" between the superconducting $\text{Bi}_2\text{Sr}_2\text{CaCu}_2\text{O}_8$ and insulating $\text{Bi}_2\text{Sr}_2\text{Ca}_{0.5}\text{Y}_{0.5}\text{Cu}_2\text{O}_8$ where doped holes are compensated with electrons provided from trivalent Y atoms, would be very helpful for understanding the origin of the Fermi-liquid states.

Figure 2 shows the result of angle-resolved photoemission study of $\text{Bi}_2\text{Sr}_2\text{Ca}_{0.5}\text{Y}_{0.5}\text{Cu}_2\text{O}_8$.

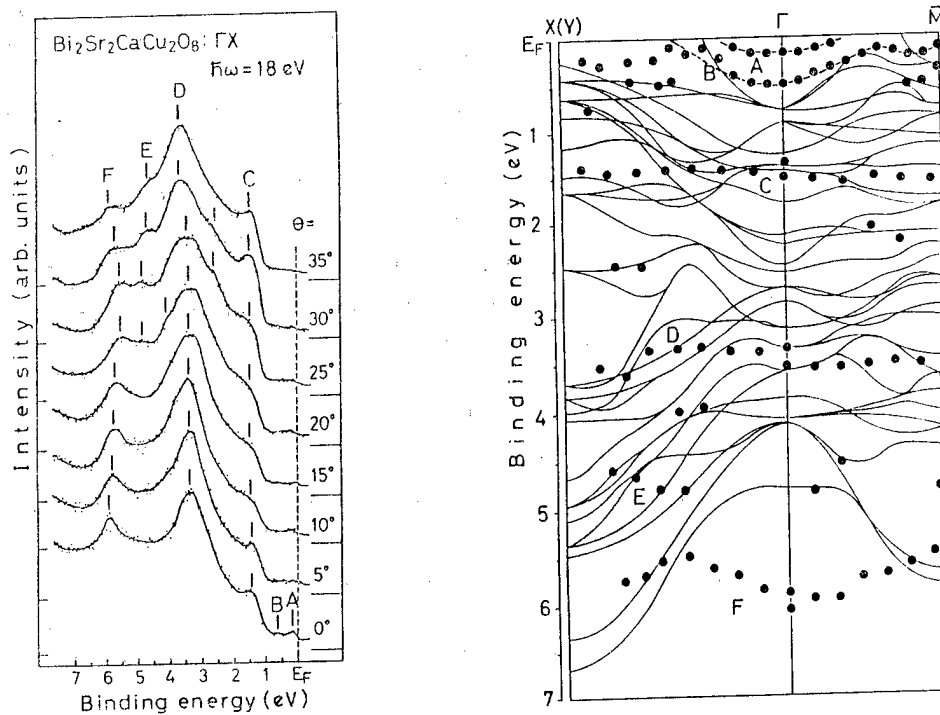


Figure 1 Angle-resolved photoemission spectra of $\text{Bi}_2\text{Sr}_2\text{CaCu}_2\text{O}_8$ (left) and the "band structure" derived from the photoemission experiment (right). A band structure-calculation is shown by thin solid lines for comparison.

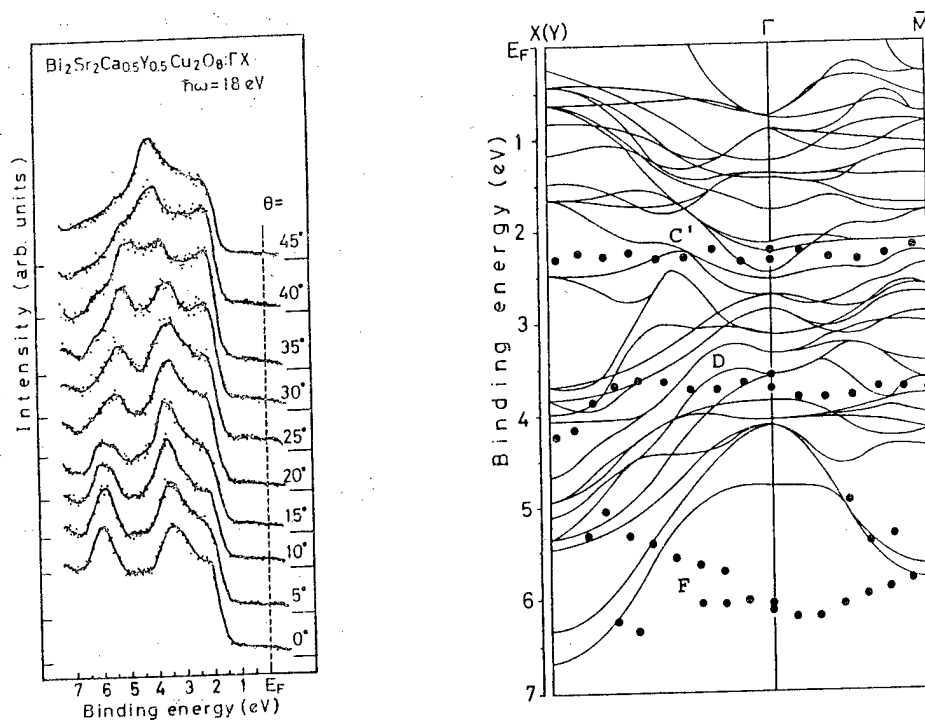


Figure 2 Angle-resolved photoemission spectra of $\text{Bi}_2\text{Sr}_2\text{Ca}_{0.5}\text{Y}_{0.5}\text{Cu}_2\text{O}_8$ (left) and the "band structure" derived from the photoemission experiment (right). A band structure-calculation for $\text{Bi}_2\text{Sr}_2\text{CaCu}_2\text{O}_8$ is shown by thin solid lines for comparison.

As shown in the figure, small structures in the vicinity of the Fermi level (bands A and B) together with a non-dispersive band at 1.5 eV (band C) disappear in the non-superconductor ($x=0.5$) and alternatively a new non-dispersive band appears at 2.3 eV (band C'). A slight energy shift by 0.2-0.3 eV toward the high-binding-energy side is observed for bands D and F in $\text{Bi}_2\text{Sr}_{2-x}\text{Ca}_{0.5}\text{Y}_{0.5}\text{Cu}_2\text{O}_8$. The disappearance of bands which cross the Fermi level obviously indicates the breakdown of one-electron picture proposed from band-structure calculation which expects a rigid shift of the electronic states relative to the Fermi level. The experimental results in Figs. 1 and 2 strongly suggest that the electronic states in the vicinity of the Fermi level (Fermi-liquid states) are a kind of impurity states produced by doping of holes. This conjecture will be reinforced by inverse photoemission and x-ray absorption studies described below.

Inverse photoemission study of $\text{Bi}_2\text{Sr}_2\text{Ca}_{1-x}\text{Y}_x\text{Cu}_2\text{O}_8$

Inverse photoemission spectroscopy has an advantage over photoemission spectroscopy since the former can give a direct information about the unoccupied electronic states which is not accessible by the latter.

Figure 3a shows inverse photoemission spectra of three kinds of high- T_c superconductors; $\text{Bi}_2\text{Sr}_2\text{CaCu}_2\text{O}_8$, $\text{YBa}_2\text{Cu}_3\text{O}_7$, and $\text{La}_{1.8}\text{Sr}_{0.2}\text{CuO}_4$ [2]. As shown in Fig. 3a, the inverse photoemission spectrum of $\text{Bi}_2\text{Sr}_2\text{CaCu}_2\text{O}_8$ has a clear Fermi-edge structure (in other words, a finite density of states at the Fermi level) in support with the photoemission result (Fig. 1). This is an alternative evidence for the existence of the Fermi-liquid states in high- T_c superconductors. Absence or remarkable reduction of the Fermi-edge structure in $\text{YBa}_2\text{Cu}_3\text{O}_7$ and $\text{La}_{1.8}\text{Sr}_{0.2}\text{CuO}_4$ as shown in Fig. 3a may be due to a loss of oxygen at the sample surface under ultra high vacuum.

Figure 3b shows Y-content (hole-concentration) dependence of inverse photoemission spectrum near the Fermi level. When we increase the Y-content (in other words, decrease the hole concentration), the spectral intensity near the Fermi level gradually decreases. This result is quite consistent with the photoemission results shown in Figs. 1 and 2, suggesting the "impurity-state"-like nature of the electronic states near the Fermi level.

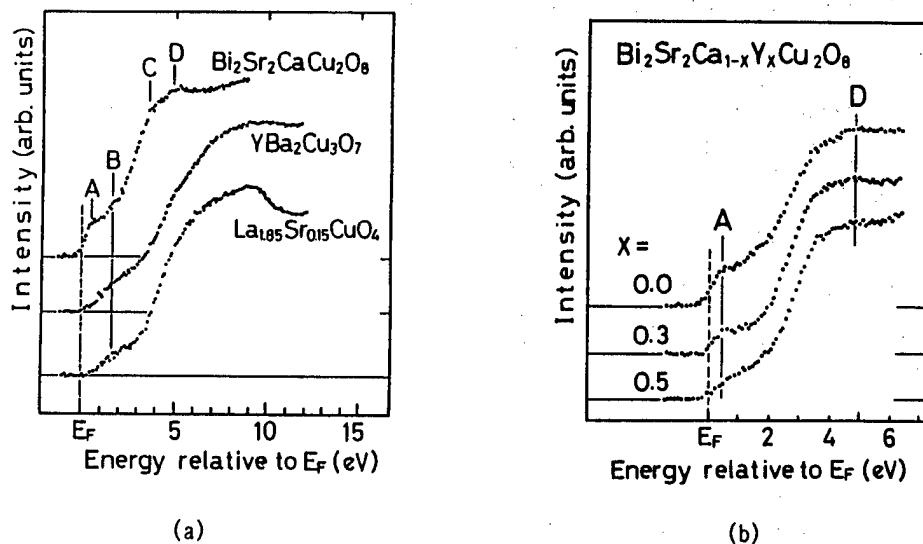


Figure 3 (a) Inverse photoemission spectra of $\text{Bi}_2\text{Sr}_2\text{CaCu}_2\text{O}_8$, $\text{YBa}_2\text{Cu}_3\text{O}_7$, and $\text{La}_{1.8}\text{Sr}_{0.2}\text{CuO}_4$. (b) Inverse photoemission spectra of $\text{Bi}_2\text{Sr}_2\text{Ca}_{1-x}\text{Y}_x\text{Cu}_2\text{O}_8$ ($x=0.0, 0.3$, and 0.5).

X-ray absorption spectroscopy of $\text{Bi}_2\text{Sr}_2\text{Ca}_{1-x}\text{Y}_x\text{Cu}_2\text{O}_8$

X-ray absorption spectroscopy measures an optical transition from a core level of a certain atom to unoccupied electronic state above the Fermi level. Selection rules restrict the final states to which core electrons are optically excited. Therefore x-ray absorption spectroscopy gives information about individual contribution of each atomic orbital to the unoccupied electronic states.

Figure 4a shows oxygen-K absorption spectra of $\text{Bi}_2\text{Sr}_2\text{Ca}_{1-x}\text{Y}_x\text{Cu}_2\text{O}_8$ [3]. The spectrum of $x=0.0$ has a prominent edge-peak at about 528 eV, which we attribute to the optical transition from the oxygen 1s core level to unoccupied oxygen 2p states. The intensity of this edge-peak gradually decreases with increasing the Y content (in other words, decreasing hole concentration). This indicates that doped holes are accommodated mainly in oxygen 2p states at the Fermi level.

Figure 4b shows oxygen-K absorption spectra of single-crystal $\text{Bi}_2\text{Sr}_2\text{CaCu}_2\text{O}_8$ recorded at various incident angles of linearly-polarized light as shown in the figure. The intensity of the edge-peak gradually decreases with the incident angle referred to the surface normal, indicating that the oxygen 2p atomic orbital just above the Fermi level has a x-y (in-plane) symmetry.

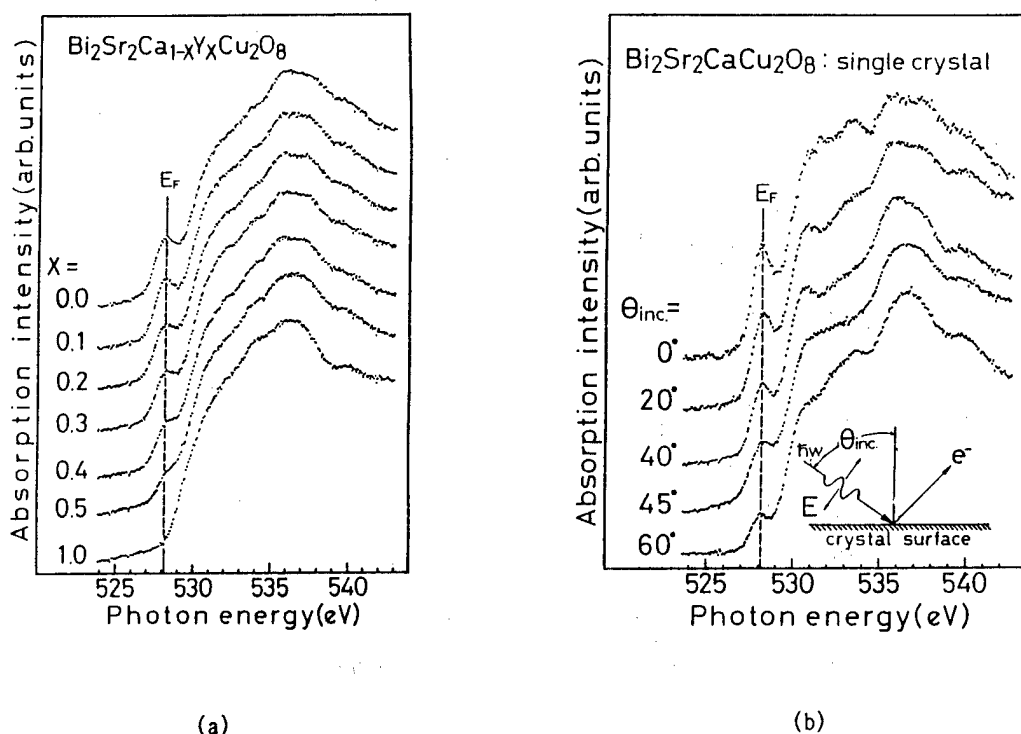


Figure 4 (a) Oxygen-K absorption spectra of $\text{Bi}_2\text{Sr}_2\text{Ca}_{1-x}\text{Y}_x\text{Cu}_2\text{O}_8$ ($x=0.0$ to 1.0). (b) Oxygen-K absorption spectra of single-crystal $\text{Bi}_2\text{Sr}_2\text{CaCu}_2\text{O}_8$ recorded at various incident angle of linearly-polarized light.

Scanning-tunneling spectroscopy of $\text{Bi}_2\text{Sr}_2\text{CaCu}_2\text{O}_8$

The existence of the Fermi-liquid states in $\text{Bi}_2\text{Sr}_2\text{CaCu}_2\text{O}_8$ has been experimentally established by photoemission, inverse photoemission, and x-ray absorption spectroscopy. However it may be claimed that $\text{Bi}_2\text{Sr}_2\text{CaCu}_2\text{O}_8$ is special since it has BiO planes as well as CuO_2 and the Fermi-liquid states observed by photoemission etc. may come from the BiO plane, but not from the CuO_2 plane common to all cuprate superconductors. To elucidate this point, we have performed scanning-tunneling spectroscopy.

Scanning-tunneling spectroscopy is a spectroscopic version of scanning-tunneling microscope which probes atomic structure of top-most layer of a crystal. Therefore scanning-tunneling spectroscopy gives information about the electronic structure of a top-most atomic layer.

Figure 5a shows a scanning-tunneling-microscope image of a cleaved $\text{Bi}_2\text{Sr}_2\text{CaCu}_2\text{O}_8$ crystal [4]. The image shows periodic rows spaced by 2.6 nm, which we attribute to the superstructure of BiO plane already observed for the bulk by electron microscope. This indicates that the cleaved surface is a BiO plane. Figure 5b shows a scanning-tunneling-spectroscopy (STS) spectrum for the cleaved (therefore BiO) plane measured by changing the bias-voltage of a tip. The STS spectrum exhibits a small gap of about 0.3 eV at the Fermi level, suggesting a semiconducting nature of a BiO plane. This indicates that the Fermi-liquid states (electronic states just at the Fermi level) observed by photoemission and inverse photoemission do not reside on BiO planes but spread over CuO_2 planes common to all cuprate high- T_c superconductors.

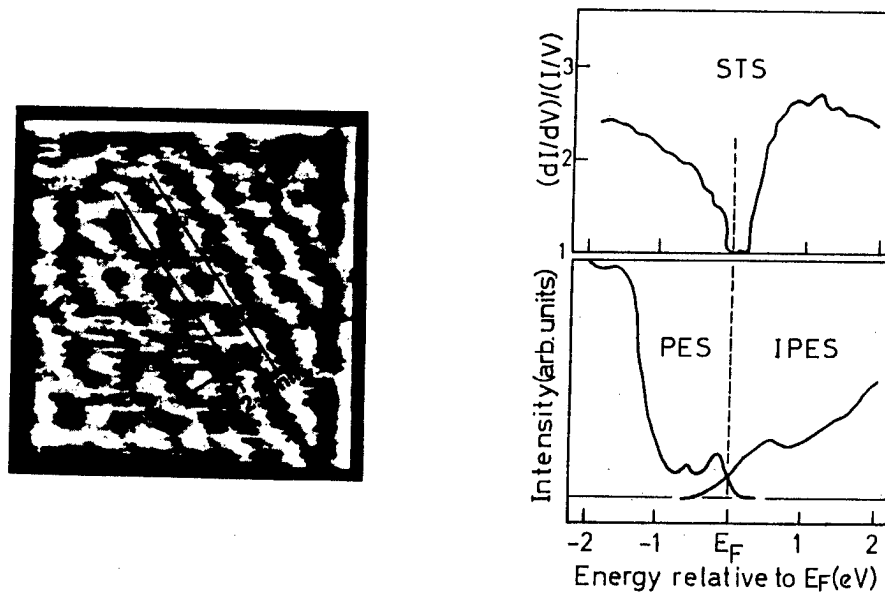


Figure 5 Scanning-tunneling-microscope image of a cleaved $\text{Bi}_2\text{Sr}_2\text{CaCu}_2\text{O}_8$ single crystal (left). Scanning-tunneling-spectroscopy (STS) spectrum compared with combination of photoemission (PES) and inverse photoemission (IPES) spectra (right).

Electronic structure of high-Tc superconductor

From the experimental results described above, we propose a model of the electronic structure of the high-Tc superconductor as shown in Fig. 6. In undoped compound such as La_2CuO_4 , a charge-transfer gap opens because of a large on-site Coulomb repulsion energy of Cu 3d electrons compared with a relatively small charge-transfer energy from O 2p to Cu 3d states. When holes are doped into this system, they are accommodated in O 2p atomic orbitals and resultingly a kind of impurity states are created at the Fermi level. These "impurity states" have a dominant O 2p_{x,y} nature and would be produced through a strong hybridization between the doped O 2p_{x,y} hole orbitals and surrounding Cu 3d_{x²-y²} empty orbitals. When the concentration of holes is increased, the overlapping between the "impurity states" transforms them into bands with energy dispersion of about 0.5 eV as observed by angle-resolved photoemission. Superconductivity would be driven by Cooper-pairing of O 2p holes in the Fermi-liquid states.

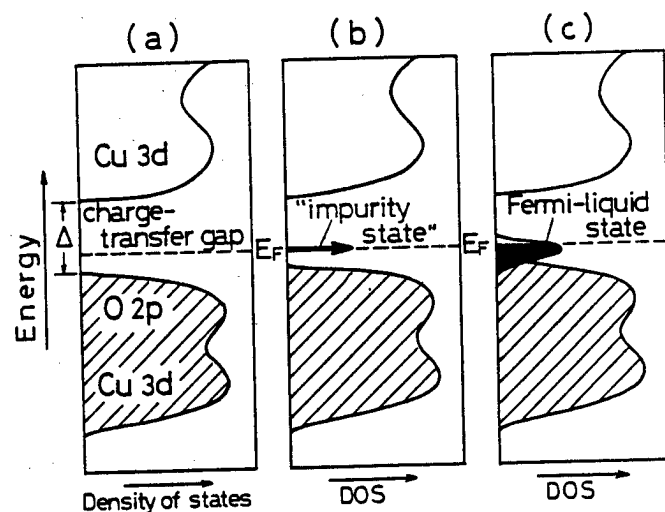


Figure 6 Schematic diagram of the electronic structure of the high-Tc superconductor derived from the present experiment.

Acknowledgement

We thank M. Tanaka, S. Yamazaki, M. Fujinami, W. Mizutani, M. Ono, and K. Kajimura for their collaboration in the scanning-tunneling-spectroscopy measurement.

References

1. T. Takahashi, H. Matsuyama, H. Katayama-Yoshida, Y. Okabe, S. Hosoya, K. Seki, H. Fujimoto, M. Sato, and H. Inokuchi: *Nature* **334**, 691 (1988) and *Phys. Rev. B* **39**, 6636 (1989).
2. H. Ohta, T. Takahashi, K. Murata, H. Matsuyama, S. Suzuki, Y. Okabe, and H. Katayama-Yoshida: *Phys. Rev. B* **39**, 7354 (1989).
3. H. Matsuyama, T. Takahashi, H. Katayama-Yoshida, T. Kashiwakura, Y. Okabe, S. Sato, N. Kosugi, A. Yagishita, K. Tanaka, H. Fujimoto, and H. Inokuchi: *Physica C* **160**, 567 (1989).
4. M. Tanaka, T. Takahashi, H. Katayama-Yoshida, S. Yamazaki, M. Fujinami, Y. Okabe, W. Mizutani, M. Ono, and K. Kajimura: *Nature* **336**, 691 (1989).

Photoemission Study of Electron- and Hole-Doped Cu-Oxide Superconductors

A. Fujimori

Department of Physics, University of Tokyo, Hongo, Bunkyo-ku, Tokyo 113, Japan

We have studied the electronic structure of hole-doped Bi- and La-based Cu-oxide superconductors and electron-doped $\text{Nd}_{2-x}\text{Ce}_x\text{CuO}_4$ by photoemission spectroscopy. As for $\text{Bi}_2\text{Sr}_2\text{CaCu}_2\text{O}_8$, electronic states near the Fermi level are confirmed to arise from d^9 -ligand-hole local singlets within the CuO_2 planes. The results for $\text{Nd}_{2-x}\text{Ce}_x\text{CuO}_4$ show no evidence for occupied d^{10} (Cu^+) states in the bulk compounds. The Fermi level is found to be located well within the charge-transfer gap, suggesting that new states are formed within the gap by Ce doping. A similar behavior is observed for $\text{La}_{2-x}\text{Sr}_x\text{CuO}_4$.

While the electronic structure of undoped Cu oxides is now basically understood [1], the nature of the metallic states of doped materials is far from clear [2]. In order to shed more light on the origin of electronic states near the Fermi level (E_F) in the Cu-oxide superconductors, we have studied the electronic structure of Bi-, La- and Nd-based Cu oxides and related compounds by photoemission spectroscopy.

It is generally accepted that doped carriers conduct through the CuO_2 planes. Our previous results on superconducting $\text{Bi}_2\text{Sr}_2\text{CaCu}_2\text{O}_8$ and insulating $\text{Bi}_2\text{Sr}_2\text{Ca}_{1-x}\text{Y}_x\text{Cu}_2\text{O}_8$ as well as on $\text{Sr}_2\text{CuO}_2\text{Cl}_2$ have supported this idea at least for the Bi-based compounds [3]. On the other hand, Shen et al. [4] suggested that contributions from the BiO planes dominate those from the CuO_2 planes near E_F based mainly on the lack of resonance behavior at the Cu 3p-3d core-absorption threshold. In order to clarify this point, we have made a comparative study of $\text{Bi}_2\text{Sr}_2\text{CaCu}_2\text{O}_8$, $\text{Bi}_2\text{Sr}_2\text{CuO}_6$ and $\text{Bi}_2\text{Sr}_2\text{CoO}_{6+y}$. As shown in Fig. 1, the states closest to E_F disappears on substituting Co for Cu, indicating that these states are not associated with the BiO planes but are indeed derived from the CuO_2 planes. We point out that the lack of resonance is simply due to the small d^8 weight in these final states and is consistent with their CuO_2 -plane origin. We have also observed that the intensity of these states increases with photon energy, suggesting significant Cu d contributions at E_F . However, this does not mean that doped holes have substantial (a few tens %) Cu d character as suggested by Arko et al. [6]. By a simple intensity calculation based on the cluster model, it can be shown that the large (~30 %) Cu d spectral weight is fully consistent with the nearly pure (>90 %) oxygen p character of doped holes [5].

If electrons doped into $\text{Nd}_{2-x}\text{Ce}_x\text{CuO}_4$ occupy Cu 3d orbitals to form d^{10} configurations, which are local singlets, there is an electron-hole symmetry and the t - J model would be considered as a relevant model for the Cu-oxide superconductors. Our results for $\text{Nd}_{2-x}\text{Ce}_x\text{CuO}_4$, however, show no evidence for the presence of Cu d^{10} configuration [7]. Figure 2 shows the Cu 2p x-ray photoemission (XPS) spectra of $\text{Nd}_{2-x}\text{Ce}_x\text{CuO}_4$, showing no sign of Cu d^{10} up to $x = 0.15$. (The filled circle in the insert of Fig. 2 is for a reduced sample, for which the grain boundary may be contaminated by Cu^+ impurity phases.) Our result is

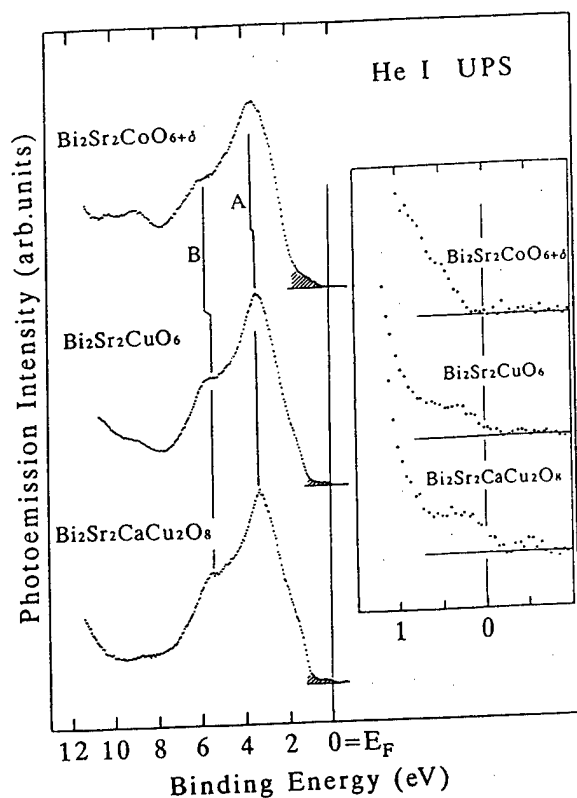


Fig. 1 Ultra-violet photoemission (UPS) spectra of $\text{Bi}_2\text{Sr}_2\text{CoO}_{6+\delta}$, $\text{Bi}_2\text{Sr}_2\text{CuO}_6$, and $\text{Bi}_2\text{Sr}_2\text{CaCu}_2\text{O}_8$ taken with $h\nu = 21.2$ eV. The inset shows spectra near the Fermi level on an expanded energy scale.

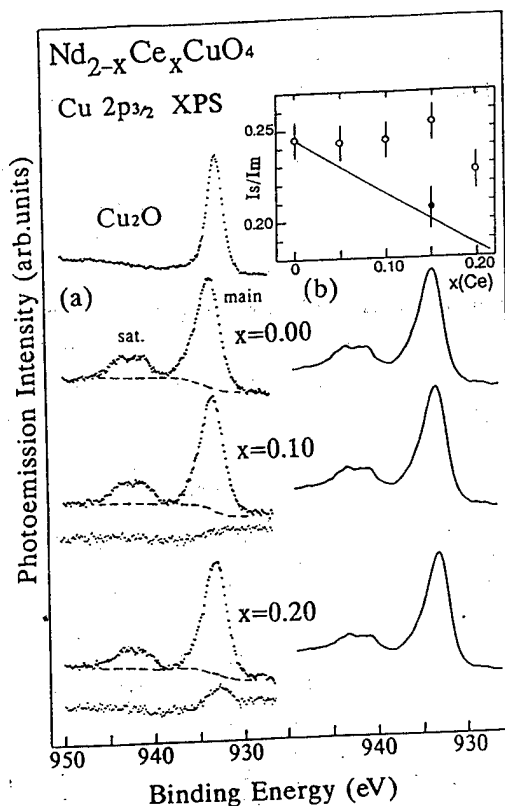


Fig. 2. Cu 2p core-level XPS spectra of $\text{Nd}_{2-x}\text{Ce}_x\text{CuO}_4$ ($h\nu = 1253.6$ eV). (a) Measured spectra. For $x = 0.1$ and 0.2 , difference from $x = 0$ is shown on the bottom of each spectrum. (b) Superposition of the $x = 0$ and Cu_2O spectra to simulate the case where all doped electrons enter the Cu 3d orbitals. In the insert, relative intensity of the satellite to the main peaks is plotted as a function of x . The solid line in the insert shows the expected behavior when all doped electrons occupy the Cu 3d orbitals.

consistent with bulk-sensitive experiments such as Cu K-edge x-ray absorption by Kosugi et al. [8] (An earlier Cu K-edge study [9], which has lead to the conclusion that doped electrons occupy Cu 3d orbitals, is criticized in [8] for its misleading data analyses.) Other photoemission measurements show increasing amount of Cu d^{10} signals with Ce doping [10]. The discrepancy between these and our photoemission experiments may be attributed to the fact that our measurements have been carried out on surfaces scraped at liquid-nitrogen temperature whereas the other experiments have been performed at room temperature. We have observed that the surface of $\text{Nd}_{2-x}\text{Ce}_x\text{CuO}_4$ is degraded within an hour in vacuum at room temperature and that the preparation of well-characterized surfaces is essentially important for surface sensitive experiments such as photoemission spectroscopy.

The XPS spectra of $\text{Nd}_{2-x}\text{Ce}_x\text{CuO}_4$ in the valence-band region reveal weak emission at E_F whose intensity increases with Ce content. In Fig. 3, we compare the valence-band photoemission spectra of $\text{Nd}_{2-x}\text{Ce}_x\text{CuO}_4$ and hole-doped $\text{La}_{2-x}\text{Sr}_x\text{CuO}_4$. We note that the position of E_F in the two types of superconductors are remarkably similar: The position of E_F differs only ~ 0.3 eV between them although the parent compounds, La_2CuO_4 and Nd_2CuO_4 , have band gaps as large as 1.5–2 eV. This indicates that the E_F 's of the doped samples are located well within the band gaps of the parent materials and are pinned by states induced by doping. The E_F 's are not located at the top of the valence band or the bottom of the conduction band as would be expected for a rigid-band picture for the electron and hole doping. The doping-induced states may originate from many-body effects involving Cu 3d-O 2p hybridization [11] or may be induced by the impurity potential of the substitutional Sr and Ce ions [12].

The presence of doping-induced states is clearly seen in the Bremsstrahlung isochromat (BIS) spectra of $\text{La}_{2-x}\text{Sr}_x\text{NiO}_4$ as shown in Fig. 4. In this case, the density of states at E_F is vanishingly small since the samples ($x = 0$ and 0.15) are semiconducting. These states

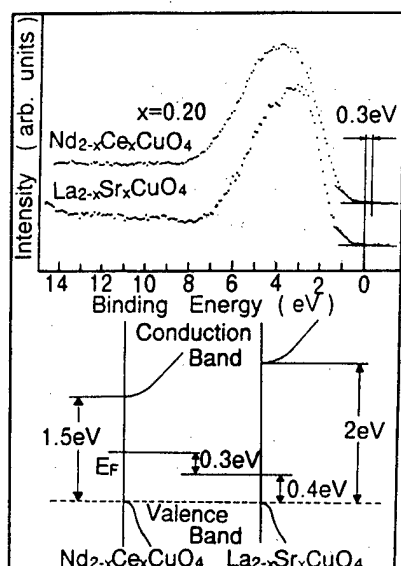


Fig. 3. Top: Comparison of the UPS spectra of $\text{Nd}_{2-x}\text{Ce}_x\text{CuO}_4$ and $\text{La}_{2-x}\text{Sr}_x\text{CuO}_4$ ($h\nu = 40$ eV) which have been shifted so as to align the tops of the valence bands. Bottom: Schematic representation of the electronic structure near the Fermi levels in the two compounds, showing the position of E_F within the band gaps.

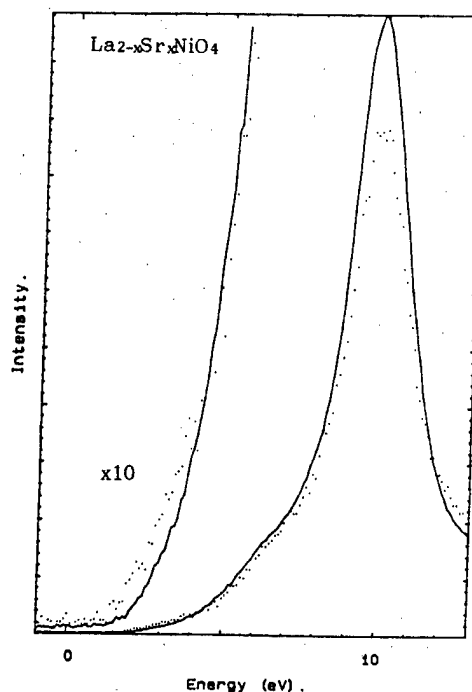


Fig. 4. BIS spectra of $\text{La}_{2-x}\text{Sr}_x\text{NiO}_4$ with $x = 0$ and $x = 0.15$ (solid curve and dots, respectively; $h\nu = 1486.6$ eV). The spectra have been normalized so that the intensity of the La 4f states is proportional the number of La atoms, $2-x$. Doping-induced states appear 1–3 eV above E_F . Unoccupied Ni 3d states are located at ~ 2 –3 eV. The La 5d and Sr 4d bands are observed around 6 eV.

can be naturally explained as due to states which are split off from the O 2p band due to the impurity potential of the substitutional Sr ions and are occupied by the extra holes [12]. Whether the same situation occurs for $\text{La}_{2-x}\text{Sr}_x\text{CuO}_4$ remains to be studied.

I would like to thank my collaborators, H. Eisaki, H. Takagi, S. Uchida, H. Matsubara, S. Suga, S. Hosoya, H. Katayama-Yoshida, P. Kuiper, J. van Elp, G. A. Sawatzky, M. Nakamura, A. Misu, T. Mizokawa, Y. Tokura, and H. Namatame.

References

- [1] A. Fujimori, E. Takayama-Muromachi, Y. Uchida, and B. Okai, *Phys. Rev. B* **35** (1987) 8814.
- [2] See, e.g., *Strong Correlation and Superconductivity*, edited by H. Fukuyama, S. Maekawa, and A. P. Malozemoff (Springer, Berlin, 1989).
- [3] Z.-X. Shen, P. A. P. Lindberg, P. Soukiassian, C. B. Eom, I. Lindau, W. E. Spicer, and T. H. Geballe, *Phys. Rev. B* **39**, 823 (1988).
- [4] A. Fujimori, Y. Tokura, H. Eisaki, H. Takagi, S. Uchida, and M. Sato, *Phys. Rev. B* **40**, 7303 (1989).
- [5] H. Eisaki, H. Takagi, S. Uchida, H. Matsubara, S. Suga, M. Nakamura, K. Yamaguchi, A. Misu, H. Namatame, and A. Fujimori, *Phys. Rev. B*, in press.
- [6] A. J. Arko, R. S. List, R. J. Bartlett, S.-W. Cheong, Z. Fisk, J. D. Thompson, G. G. Olson, A.-B. Yang, R. Liu, C. Gu, B. W. Veal, J. Z. Liu, A. P. Paulikas, K. Vandervoort, H. Claus, J. C. Campuzano, J. E. Schirber, and N. D. Shinn, *Phys. Rev. B* **40**, 2268 (1989).
- [7] A. Fujimori, Y. Tokura, H. Namatame, H. Eisaki, H. Takagi, S. Uchida, and E. Takayama-Muromachi, *Phys. Rev. B*, submitted.
- [8] N. Kosugi, Y. Tokura, H. Takagi, and S. Uchida, *Phys. Rev. B*, submitted.
- [9] J. M. Tranquada, S. M. Heald, A. R. Moodenbaugh, G. Liang, and M. Croft, *Nature* **337**, 720 (1989).
- [10] S. Uji, M. Shimoda, and H. Aoki, *Jpn. J. Appl. Phys.* **28**, L804 (1989); A. Grassmann, J. Strobel, M. Klauda, J. Schlotterer, and G. Saemann-Ischenko, *Europhys. Lett.* **9**, 827 (1989); Y. Fukuda, T. Suzuki, M. Nagoshi, Y. Shono, K. Oh-ishi, and M. Tachiki, *Solid State Commun.*, submitted.
- [11] H. Matsumoto and M. Tachiki, preprint.
- [12] A. Fujimori, p. 300 of Ref. 2.

S.Sugai

Department of Physics, Faculty of Science, Osaka University, Machikaneyama, Toyonaka 560, Japan,

The anomalous spin and doped charge states in copper oxide superconductors and the electron-phonon interacting states in $\text{BaPb}_{1-x}\text{Bi}_x\text{O}_3$ and $\text{Ba}_x\text{K}_{1-x}\text{BiO}_3$ are reviewed through the investigation of Raman spectroscopy. From the anomalies in the magnon scattering in copper oxides the existence of four-spin cyclic exchange interactions are concluded. When carriers are doped, the A_{1g} spectra change into continuous spectra from $\omega=0$ to over 7000 cm^{-1} , which are quite different from the normal Fermi liquid. Those are discussed in connection with the marginal Fermi liquid model. The Raman spectra in $\text{BaPb}_{1-x}\text{Bi}_x\text{O}_3$ and $\text{Ba}_x\text{K}_{1-x}\text{BiO}_3$ show the coexistence of itinerant large polarons and localized bipolarons. The superconductivity model induced by their mutual interactions is the same as Varma's speculative model for the susceptibility of the marginal Fermi liquid.

1. Introduction

The high T_c superconductivity is endowed by the appropriate carrier doping into the specific charge-transfer-type insulators with two-dimensional pseudo-square lattices of CuO_2 . On increasing the doping concentration, the insulators change to superconductors and to normal metals in the sense that they do not undergo superconducting states. In these materials the normal states, insulator phases, and normal metallic phases, as well as the superconducting states are all anomalous. These are reviewed by the Raman scattering spectroscopy.

2. Two-spin and four-spin exchange interactions in undoped antiferromagnetic insulator phases of the copper oxides

Many anomalies in the antiferromagnetic insulator phases and the carrier doped phases have been attributed to the two-dimensional quantum spin effects. They are, for examples, the strong two-dimensional spin correlation even above the antiferromagnetic transition temperature (T_N), the short spin correlation length in spite of the large antiferromagnetic exchange interaction (J), and also the mobility of doped carriers in the antiferromagnetic spin sea. The present Raman scattering experiments revealed the existence of four-spin cyclic exchange interactions in addition to the two-spin exchange interactions.^{1,2} The four-spin exchange interactions have effects to frustrate the antiferromagnetic spin order and modify the system composed of itinerant carriers and localized spins. These four-spin exchange interactions are not included in the Heisenberg model.

Figure 1 shows polarized Raman spectra at 30 K in the insulating phases of $S=1/2$ copper oxides; hole superconductors La_2CuO_4 , $\text{YBa}_2\text{Cu}_3\text{O}_{6.2}$, and $\text{Bi}_2\text{Sr}_2\text{Ca}_{0.5}\text{Y}_{0.5}\text{Cu}_2\text{O}_{8+y}$, electron superconductors Nd_2CuO_4 and Pr_2CuO_4 , and an $S=1$ nickel oxide; La_2NiO_4 .² The incident wavelength (λ_i) is 4579 \AA . The solid curves are the B_{1g} spectra measured at the (x', y') polarization configuration and the dotted curves are the $A_{1g}+B_{2g}$ spectra at (x', x') . The B_{2g} components are about 10% or less. Here (x', y') indicates that the polarization of the incident light is parallel to the $x'=[1, 1, 0]$ direction and the scattered light to the $y'=[1, -1, 0]$, where x, y , and z are the axes of the CuO_2 quasi-square lattice. In the copper oxides the peaks above 7000 cm^{-1} are due to the luminescence. The peaks below 800 cm^{-1} are mainly from one-phonon scattering and the peaks between 800 and 1500 cm^{-1} are from two-phonon scattering. Very strong even-order multi-phonon resonant scattering is observed in the A_{1g} spectra of La_2CuO_4 , when excited with $\lambda_i=5145\text{ \AA}$. The isostructural La_2NiO_4 shows multi-phonon scattering of the 674 and 718 cm^{-1} modes.

The two-magnon scattering peaks are observed in the B_{1g} spectra at 3230 cm^{-1} in La_2CuO_4 , 2730 cm^{-1} in $\text{YBa}_2\text{Cu}_3\text{O}_{6.2}$, 3080 cm^{-1} in $\text{Bi}_2\text{Sr}_2\text{Ca}_{0.5}\text{Y}_{0.5}\text{Cu}_2\text{O}_{8+y}$, 2890 cm^{-1} in Nd_2CuO_4 , 2820 cm^{-1} in Pr_2CuO_4 , and 1640 cm^{-1} in La_2NiO_4 . The estimated J is 1200 cm^{-1} for La_2CuO_4 , 1010 cm^{-1} for $\text{YBa}_2\text{Cu}_3\text{O}_{6.2}$, 1140 cm^{-1}

for $\text{Bi}_2\text{Sr}_2\text{Ca}_{0.5}\text{Y}_{0.5}\text{Cu}_2\text{O}_{8+y}$, 1070 cm^{-1} for Nd_2CuO_4 , 1040 cm^{-1} for Pr_2CuO_4 , and 240 cm^{-1} for La_2NiO_4 , on the assumption that the peak energy is $2.7J$ for the $S=1/2$ copper oxides and $6.7J$ for the $S=1$ nickel oxide.

In La_2NiO_4 the linewidth of the two-magnon peak is narrow and the shape is close to the theoretical curve. On the other hand the copper oxides show theoretically unexpected characteristics. (1) The B_{1g} spectra have secondary scattering intensities near $4J$ (classical cutoff energy for the two-magnon scattering). (2) The A_{1g} spectra have large intensities. The strong A_{1g} spectra are not explained in the known theory of two-magnon scattering. (3) The spectra extend up to $8J$. (4) The widths of the two-magnon peaks are abnormally large.

Singh et al.³ tried to explain the large linewidth of the B_{1g} two-magnon peak in La_2CuO_4 by the $S=1/2$ quantum spin fluctuations and the A_{1g} and B_{2g} spectra by the diagonal-second-neighbor spin-pair excitations permitted by the quantum spin fluctuations. The theoretically estimated second-neighbor exchange energy J_2 is, however, only $5\sim 8\%$,⁴ so that it is very difficult to explain the large scattering intensity up to $8J$. The high energy continuum may exist above the magnon dispersion curve in the quantum spin system. The theoretical work in the two-dimensional $S=1/2$ system has not been done, so that it is difficult to estimate this effects.

If the new $4J$ peaks are assigned to the four-magnon peaks caused by the four-spin cyclic exchange interactions,⁵ the high energy tails up to $8J$ are naturally explained. The energy of the interacting four magnons created on the neighboring four sites on a square is roughly $(4ZS-4)J$, where $Z=4$ is the number of neighboring spins and $S=1/2$. This energy, $4J$, is close to the new peak energy. The recent calculation by Schmidt and Kuramoto⁶ shows that the four-spin exchange interaction (K) is about $\sim 20\%$ of J . Then we conclude that the new peaks are the four-magnon peaks caused by the four-spin cyclic exchange interactions.

In the above discussion it is assumed that the four-spin exchange interactions work directly only in the formation of the four-magnon peaks, but do not alter the magnon states essentially. The four-spin exchange interactions, however, strongly modify the magnon dispersion curves and frustrate the antiferromagnetic orders as observed in the very large linewidths of the two-magnon peaks. The stability of the four-magnon scattering in the doped superconducting cuprates and the definite difference from La_2NiO_4 suggest the importance of the four-spin cyclic exchange interactions for the superconductivity.

3. Electronic states in the spin and charge fluctuations

When holes are doped in the antiferromagnetic states, the interactions between the doped hole spins

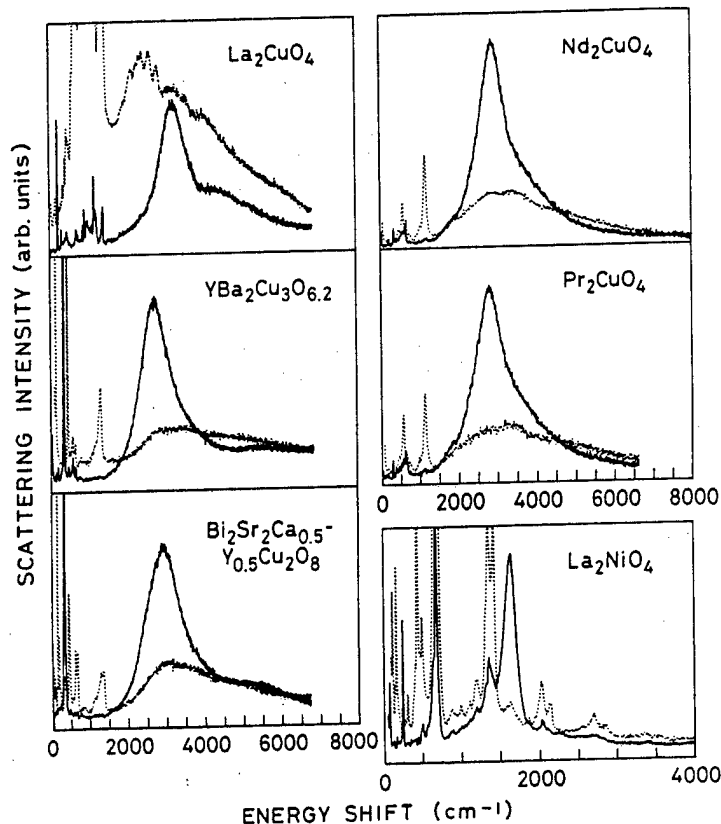
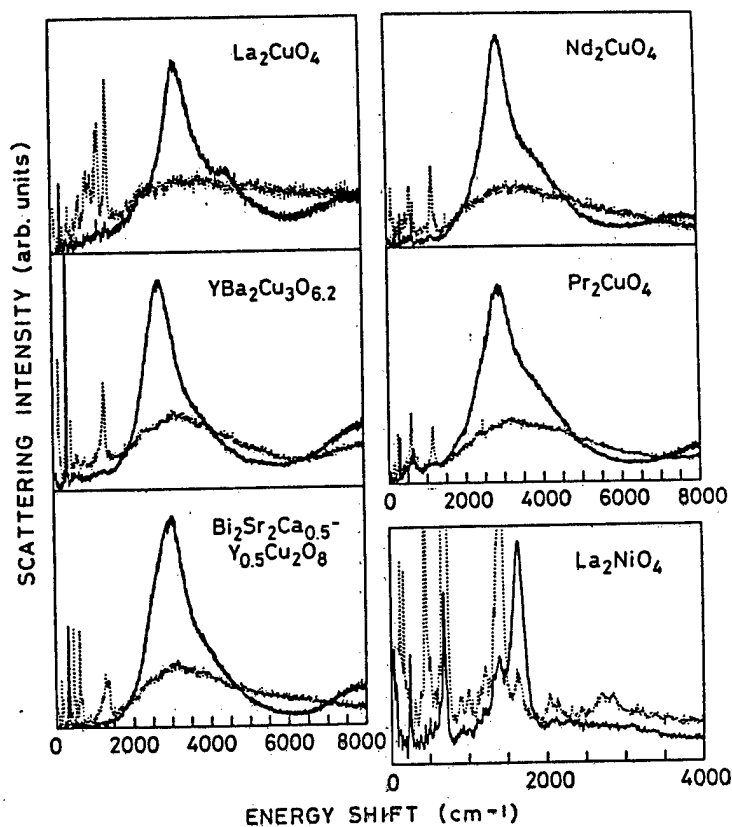


Fig.1 Polarized Raman spectra at 30 K for $\lambda_i=4579\text{ \AA}$. The solid curves are the (x', y') spectra, and the dotted curves are the (x', x') spectra. The (x', x') and (x', y') spectra are plotted with the same scale for each compound.

DEPARTMENT OF PHYSICS
FACULTY OF SCIENCE
OSAKA UNIVERSITY
TOYONAKA, OSAKA 560, JAPAN

March 7, 1990

In the report titled "Raman studies of spins and carriers in oxide superconductors" by S. Sugai which recently appeared in "Research Report on Mechanism of Superconductivity", Science Research on Priority Areas No.031, Ministry of Education, Science and Culture, Japan, p259, a different figure was stuck for Fig.1. The printed figure is the Raman spectra for $\lambda_1=5145 \text{ \AA}$. The spectra for $\lambda_1=4579 \text{ \AA}$ are shown below.



I am very sorry, if this caused confusion.

Sincerely yours,

Shunji Sugai

Shunji Sugai

at O sites and the localized spins at Cu sites produce hole-spin composites (magnetic polarons). It is controversial whether they are Fermi liquid or non-Fermi liquid.

The Raman scattering intensity is given by

$$I(\omega) \sim \frac{(\hat{e}_i \cdot \hat{e}_s)^2 \chi''(q \rightarrow 0, \omega)}{1 - \exp(-\omega/T)}, \quad (1)$$

where \hat{e}_i and \hat{e}_s are the unit vectors of the polarizations of the incident and scattered light, and $\chi''(q \rightarrow 0, \omega)$ is the imaginary part of the susceptibility. $\chi''(q \rightarrow 0, \omega)$ for the charge fluctuation in the normal Fermi liquid is

$$\chi''(q \rightarrow 0, \omega) \sim \begin{cases} \pi N(0) \omega / (2qV_F) & \text{for } |\omega| < qV_F, \\ \sim 0 & \text{for } |\omega| > qV_F, \end{cases} \quad (2)$$

where $N(0)$ is the one-particle density of states and V_F is the Fermi velocity. qV_F is estimated as about 100 cm^{-1} . Therefore no scattering intensity is expected above 100 cm^{-1} , which is quite different from the experimental results.

Recently Varma et al.⁷ proposed a Marginal Fermi liquid model. They claimed, if a phenomenological hypothesis for both charge and spin susceptibility

$$\chi''_{\text{MFL}}(q, \omega) \sim \begin{cases} N(0) \omega / T & \text{for } |\omega| < T, \\ \sim N(0) \text{sgn} \omega & \text{for } |\omega| > T \end{cases} \quad (3)$$

is introduced, many anomalies in the normal states and the superconducting states can be explained. This susceptibility is quite different from the normal Fermi liquid. Very recently Ruvalds and Virosztek⁸ showed that the similar susceptibility χ_{NFL} is obtained in the nested Fermi liquid without any empirical hypothesis.

Figure 2(a) shows the (x', x') spectra with dominantly A_{1g} symmetry and (b) the (x', y') spectra with B_{1g} symmetry from $\text{La}_{2-x}\text{Sr}_x\text{CuO}_4$ measured at 30 K. The samples with $x=0.116$ and $x=0.2$ are superconductors with the $T_c=10$ K and 20 K, respectively. The sample with $x=0.34$ is the normal metal. The (x', x') spectra of $x=0$ and $\lambda_1=5145 \text{ \AA}$ have large even-order multi-phonon scattering components. The magnon component is estimated from the $\lambda_1=4579 \text{ \AA}$ spectra and other cuprates that the intensity increases from 1000 cm^{-1} and reaches the maximum at about 3500 cm^{-1} and then gradually decreases toward 8000 cm^{-1} . The magnon component at 3000 cm^{-1} is estimated as about 1/3 of the observed intensity.

When holes are doped, the A_{1g} and B_{1g} spectra show very different behavior. The A_{1g} spectra immediately change to the continuous spectra from $\omega=0$ to over 7000 cm^{-1} . The susceptibility χ'' obtained by dividing the spectra by the statistical factor $1/(1 - \exp(-\omega/T))$ shows the ω -linear increase from $\omega=0$, and reaches the folding point near T and then gradually decreases. The intensity at high energies decreases with the increase of the hole concentration. In the B_{1g} spectra the intensity slowly increases in proportional to ω . The gradient increases with the increase of the hole concentration, and the folding-point energy shifts to the low energy as shown in Fig. 2(b).

The intraband single particle excitation gives only the A_{1g} component. In order to give the B_{1g} component in YBCO, Monien et al.⁹ introduced the interband excitation between the bands crossing nearby the Fermi energy (E_F). The B_{1g} component are, however, commonly observed in $\text{Bi}_2\text{Sr}_2\text{CaCu}_2\text{O}_{8+y}$ and $\text{La}_{2-x}\text{Sr}_x\text{CuO}_4$. This indicates that the B_{1g} scattering does not depend on the accidental band crossing near E_F . It is natural to suppose that the B_{1g} component of the single particle excitation gains the scattering intensity from the magnon component through the interactions. The difference between the A_{1g} and B_{1g} spectra is directly related to the experimental facts that the superconducting gap in the A_{1g} symmetry is smaller than in B_{1g} .^{10,11}

When Sr concentration changes from $x=0$ to $x=0.34$, the nesting condition of the Fermi surface is

supposed to change largely. Nevertheless the essential change is not observed in the A_{1g} spectra of the doped samples. This suggests that the nested Fermi liquid model is unfavorable. The fact that the A_{1g} spectra of $x=0.34$ extend above 7000 cm^{-1} indicates that the so-called "normal metallic phase" is never normal Fermi liquid.

The characteristic temperature dependence of the low-energy susceptibility in the marginal Fermi liquid, $\chi''_{\text{MFL}} N(0)\omega/T$ for $\omega \ll T$, can be compared

with the experimentally obtained χ'' , if the Raman spectra are divided by the statistical factor. The conclusive results are, however, not obtained at present, because the electron temperature is supposed to rise by the incident laser beam in the present experimental condition.

Varma et al. supposed that the spin and charge susceptibility have the same functional form. Now let us see the case of $\text{Ba}_x\text{K}_{1-x}\text{BiO}_3$ in which spins do not contribute to χ'' . Figure 3 shows the Raman spectra of $\text{Ba}_x\text{K}_{1-x}\text{BiO}_3$ as well as the copper oxides superconductors at 30 K. The solid and dashed curves are the superconductor phases and the dotted curves are the insulator phases. These spectra include both the A_{1g} and

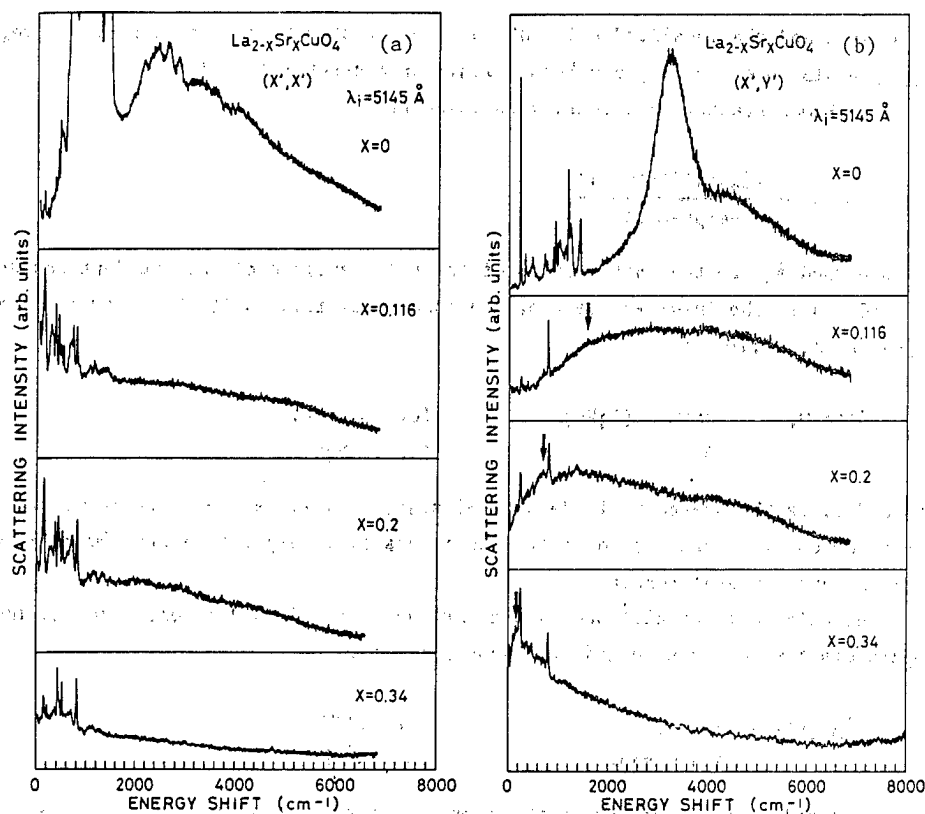


Fig.2 (a) The (x', x') spectra and (b) the (x', y') spectra of $\text{La}_{2-x}\text{Sr}_x\text{CuO}_4$ at 30 K with $\lambda_i=5145\text{ \AA}$.

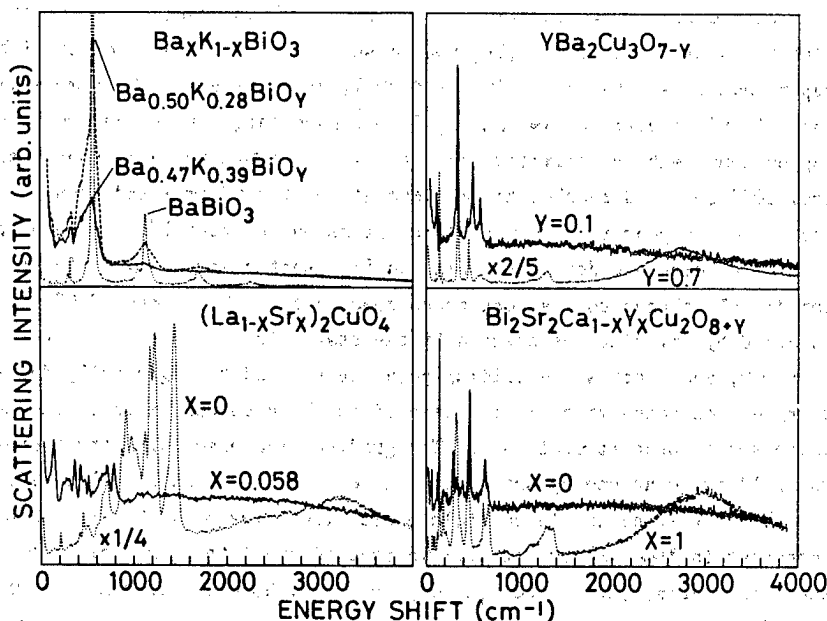


Fig.3 Raman spectra of $\text{Ba}_x\text{K}_{1-x}\text{BiO}_3$ and the copper oxide superconductors at 30 K with $\lambda_i=5145\text{ \AA}$. The solid curves and the dashed curves are the spectra in the superconducting compositions and the dotted curves are in the insulating compositions.

B_{1g} components. $Ba_x-K_{1-x}BiO_3$ as well as copper oxides have the continuous scattering ranging from $\omega=0$ to over 4000 cm^{-1} . This indicates that the non-Fermi liquid behavior in the oxide superconductors is caused not only from the spin fluctuation, but also from the charge fluctuation. The non-Fermi liquid is the universal property in the high T_c superconductors.

Varma speculated that, if the normal state is a mixture of bound pairs of electrons and "free" electrons, then their mutual scattering leads to the

susceptibility of Eq.(3). This is exactly the model that I proposed for the superconductivity mechanism in $BaPb_{1-x}Bi_xO_3$ and $Ba_xK_{1-x}BiO_3$.^{12,13} In these materials the strong electron-phonon interactions of the breathing phonon modes make localized bipolarons in which antiphase vibrations of two neighboring $Bi(Pb)O_6$ octahedra are accompanied by the charge transfer between them. The localized bipolarons and itinerant large single-polarons coexist in the almost whole range of doped electron concentrations. The superconductivity is induced in the appropriate rate of those mixtures.

4. Superconductivity in the mutual interacting system of itinerant large polarons and localized bipolarons in $BaPb_{1-x}Bi_xO_3$ and $Ba_xK_{1-x}BiO_3$

The electric properties of $BaPb_{1-x}Bi_xO_3$ change drastically with the increase of Bi concentration; semimetallic at $x=0$, metallic at $x<0.35$, and insulating at $x>0.35$. On increasing x , the T_c increases with x and reaches maximum at $x=0.25\sim 0.3$, then rapidly decreases in accordance with the metal-insulator transition. The start of opening of an insulating pseudo-gap is observed at $x=0.15$.

Figure 4 shows the Raman spectra of $BaPb_{1-x}Bi_xO_3$ at about 30 K.¹² The drastic change, on increasing x , is observed in the continuum peak ranging from below 100 cm^{-1} to 650 cm^{-1} . This broad continuum is decomposed into five peaks. The energies, relative intensities, and spectral widths are shown in Fig.5.

In order to explain the Raman spectra, an itinerant electronic state and a localized state are introduced. Both states coexist in almost the whole range of Bi concentration. The itinerant state is dominant at small x , and the localized state increases above $x=0.15$. We suppose that the itinerant electronic state has a finite extent of wave function. The metal-insulator transition at $x=0.35$, on increasing x , is interpreted as the disappearance of percolation paths due to the decrease of the extent

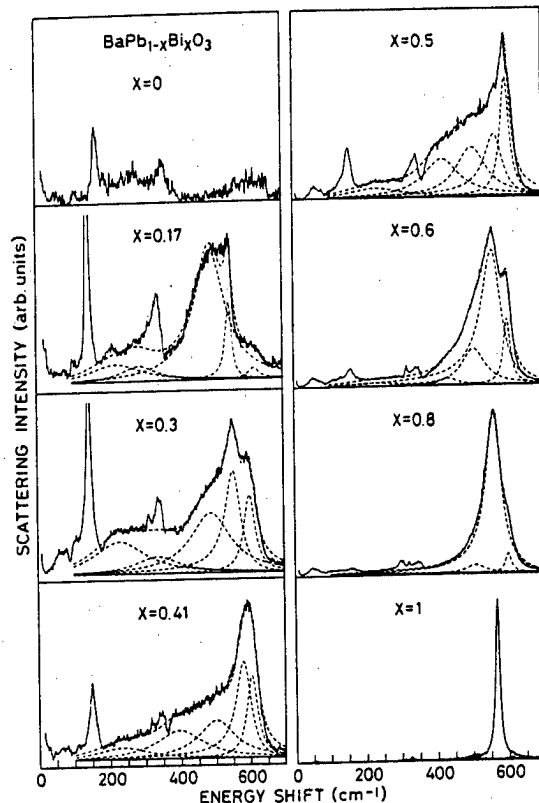


Fig.4 Raman spectra in $BaPb_{1-x}Bi_xO_3$ at about 30 K and the decomposed five peaks and the sum of the decomposed peaks.

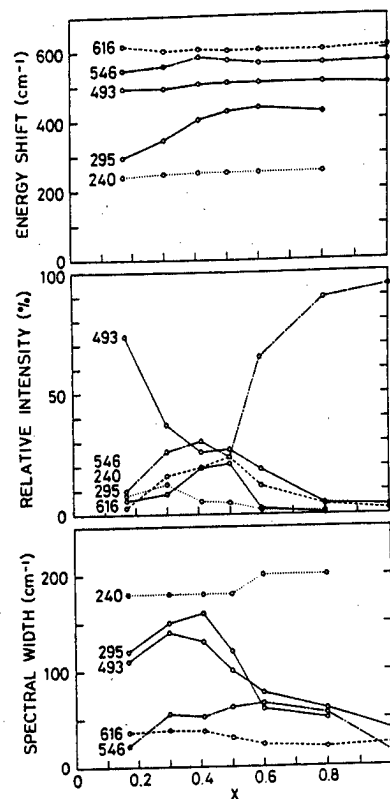


Fig.5 Energies, relative intensities, spectral widths of the decomposed peaks.

of wave function, which is caused by the increase of impurity potentials of Bi on the conductance paths.

All the relevant five modes are assigned to the breathing modes couple with itinerant and localized electrons. The highest energy peak at 616 cm^{-1} with narrow linewidth is assigned to the bare breathing mode of $\text{Pb}(\text{Bi})\text{O}_6$ octahedra with no excess electron. The 546 cm^{-1} mode which has very large scattering intensity in the insulating region is assigned to the out-of-phase vibration of the breathing mode in dimerized $\text{Pb}(\text{Bi})\text{O}_6$ octahedra. This vibration is accompanied by the charge transfer of excess electrons within the dimers, that is bipolarons. The 493 cm^{-1} mode which has large intensity in the metallic region is assigned to the breathing mode coupled with the itinerant electrons. The 295 cm^{-1} mode which shows softening toward $x=0.15$ is assigned to the breathing mode coupled with the electronic transition from the itinerant state to the localized state.

The highest T_c is achieved under the balance of population rate between the localized bipolarons and the itinerant large single-polarons. Robaszkiewicz et al.¹⁴ and Chen Chang-feng et al.¹⁵ showed the enhancement of T_c in the free carrier-bipolaron interacting system.

The utmost difference between $\text{Ba}_x\text{K}_{1-x}\text{BiO}_3$ and $\text{BaPb}_{1-x}\text{Bi}_x\text{O}_3$ is the soft mode energy in the superconductor phases. The energy in $\text{Ba}_x\text{K}_{1-x}\text{BiO}_3$ is as large as in the insulating phase of $\text{BaPb}_{1-x}\text{Bi}_x\text{O}_3$. This indicates that the extent of the itinerant wave function is larger than in $\text{BaPb}_{1-x}\text{Bi}_x\text{O}_3$, and advantages $\text{Ba}_x\text{K}_{1-x}\text{BiO}_3$ to raise T_c by keeping conductive up to the higher electron concentration.

5. Conclusions

The present Raman scattering experiments revealed the existence of the four-spin exchange interactions in copper oxides and the non-Fermi liquid behavior of doped carriers in both copper oxides and $\text{Ba}_x\text{K}_{1-x}\text{BiO}_3$. The experimentally obtained model for the superconductivity in $\text{Ba}_x\text{K}_{1-x}\text{BiO}_3$ and $\text{BaPb}_{1-x}\text{Bi}_x\text{O}_3$, the mutual interacting system of the itinerant large polarons and the localized bipolarons, is the same with the speculative model for the marginal Fermi liquid.⁷ In $\text{Ba}_x\text{K}_{1-x}\text{BiO}_3$ the attractive forces for the bound pairs of electrons are the electron-phonon interactions. In the case of copper oxides the phonon spectra in the superconductor phases are different from those in $\text{Ba}_x\text{K}_{1-x}\text{BiO}_3$. It is speculated that the attractive forces in copper oxides are magnetic interactions. When holes move in the quasi-square lattice with antiferromagnetic spin order, they leave the reversed spin traces which produce self-trapped potentials. The delocalization has been discussed with respect to the quantum spin fluctuations.¹⁶ However, if holes move in pairs, no reversed spin trace is left. This is the possible origin of the bound pairs of holes in copper oxides.

Acknowledgments: The author thanks M.Sato, S.Uchida, H.Takagi, T.Ito, T.Ido, J.Akimitsu, T.Kobayashi, T.Murakami, Y.Enomoto, Y.Hidaka, S.Hosoya, T.Kajitani, and T.Fukuda for providing good single crystals.

1. S.Sugai, preprint.
2. S.Sugai, M.Sato, T.Kobayashi, J.Akimitsu, T.Ito, H.Takagi, S.Uchida, S.Hosoya, T.Kajitani, and T.Fukuda, preprint.
3. R.R.P.Singh, P.A.Fleury, K.B.Lyons, and P.E.Sulewski, Phys. Rev. Lett. **62**, 2736 (1989).
4. J.F.Annett, R.M.Martin, A.K.McMahan, and S.Satpathy, Phys. Rev. **B40**, 2620 (1989).
5. M.Roger and J.M.Delrieu, Synth. Met. **29**, F673 (1989).
6. H.J.Schmidt and Y.Kuramoto, private communication.
7. C.M.Varma, P.B.Littlewood, S.Schmitt-Rink, E.Abrahams, and A.E.Ruckenstein, Phys. Rev. Lett. **63**, 1996 (1989); C.M.Varma, Int. J. Mod. Phys.; Y.Kuroda and C.M.Varma, preprint.
8. J.Ruvalds and A.Virosztek, preprint; A.Virosztek and J.Ruvalds, preprint.
9. H.Monien and A.Zawadowski, Phys. Rev. Lett. **63**, 911 (1989).
10. S.L.Cooper, F.Slakey, M.V.Klein, J.P.Rice, E.D.Bukowski, and D.M.Ginsberg, Phys. Rev. **B38**, 11934 (1988).
11. A.Yamanaka, T.Kimura, F.Minami, K.Inoue, and S.Takekawa, Jpn. J. Appl. Phys. **27**, L1902 (1988).
12. S.Sugai, Solid State Commun. **72**, 1187 (1989).
13. S.Sugai, Y.Enomoto, and T.Murakami, Solid State Commun. **72**, 1193 (1989).
14. S.Robaszkiewicz, R.Micnas, and J.Ranninger, Phys. Rev. **B36**, 180 (1987).
15. Chen Chang-feng and Zhang Li-yuan, Physica **147B**, 175 (1987).
16. J.Inoue and S.Maekawa, J. Phys. Soc. Jpn.

Correlation of the Infrared Anomaly and Superconductivity in
 $\text{YBa}_2(\text{Cu}_{1-x}\text{Co}_x)_3\text{O}_{7-\delta}$

Kohji Ohbayashi, Hideaki Tukamoto, Norio Ogita, Masayuki Udagawa,
Yuji Aoki* and Toshizo Fujita*

Faculty of Integrated Arts and Sciences, Hiroshima University,
Hiroshima 730

*Department of Physics, Faculty of Sciences, Hiroshima
University, Hiroshima 730

For $\text{YBa}_2\text{Cu}_3\text{O}_{7-\delta}$ oxides sintered at various temperatures, the infrared absorption mode of in-plane $\text{Cu}(2)-\text{O}(2,3)$ stretching motions shows the anomalous behavior to disappear for superconducting samples although it is allowed by the selection rule. The correlation between the infrared anomaly and superconductivity has been confirmed systematically for $\text{YBa}_2(\text{Cu}_{1-x}\text{Co}_x)_3\text{O}_{7-\delta}$ system in the Co concentration region of $0 < x < 0.3$ for samples quenched from sintering temperatures of 400, 500, 600, 700 and 800°C. From the continuous variation of the infrared anomaly, itineracy of carriers for semiconductive samples has been estimated to be about 2.2 atomic distances. The fact that hopping carriers have partial itineracy is consistent with the t - J model.

For $\text{RBa}_2\text{Cu}_3\text{O}_{7-\delta}$, sensitive dependence of the infrared spectrum on oxygen content has been reported. Main motivation of this work is to investigate whether the variation of infrared spectra of $\text{RBa}_2\text{Cu}_3\text{O}_{7-\delta}$ may be systematically interpreted by the concept of the infrared anomaly, which we introduced to interpret the infrared spectra of $(\text{La}_{1-x}\text{M}_x)_2\text{CuO}_4$ systems.¹⁾ Superconductivity is controlled both by the carrier concentration and substitution of transition metal ions for Cu ions. In this work, we made $\text{YBa}_2(\text{Cu}_{1-x}\text{Co}_x)_3\text{O}_{7-\delta}$ samples and changed δ by quenching samples from various sintering temperatures.²⁾ The reason that we chose Co ions for substitution is that they are expected to occupy mainly $\text{Cu}(1)$ sites.

The polycrystalline samples were prepared by standard ceramic techniques. As starting materials, Y_2O_3 , BaCO_3 , CuO and CoO were used. The purity of these starting materials was 99.99 %, except for 99.9 % purity of BaCO_3 . Powders of starting materials were combined in appropriate proportions to prepare mixtures with desired compositions. These mixtures were pressed at about 100 kg/cm² to form cylindrical pellets of ≈ 1.5 cm in diameter and ≈ 0.5 cm thick. The pellets were pre-fired at 940°C in air for 10 hours, followed by two-time firing at 970°C for 10 hours with intermittent grinding. For $\text{YBa}_2(\text{Cu}_{1-x}\text{Co}_x)_3\text{O}_{7-\delta}$ system, eleven concentrations of $x = 0, 0.02, 0.04, 0.06, 0.08, 0.1, 0.12, 0.15, 0.2, 0.25$ and 0.3 were chosen. To control the oxygen deficiency δ , samples were fired in air at various temperatures and then quickly quenched into liquid nitrogen. The sintering temperatures were 400, 500, 600, 700 and 800 °C. For $\text{YBa}_2\text{Cu}_3\text{O}_{7-\delta}$, the sintering

temperature was taken also at 850, 900 and 950 °C. To prepare samples with small δ , a set of samples were annealed at 500 °C for 2 days and gradually cooled in a furnace.

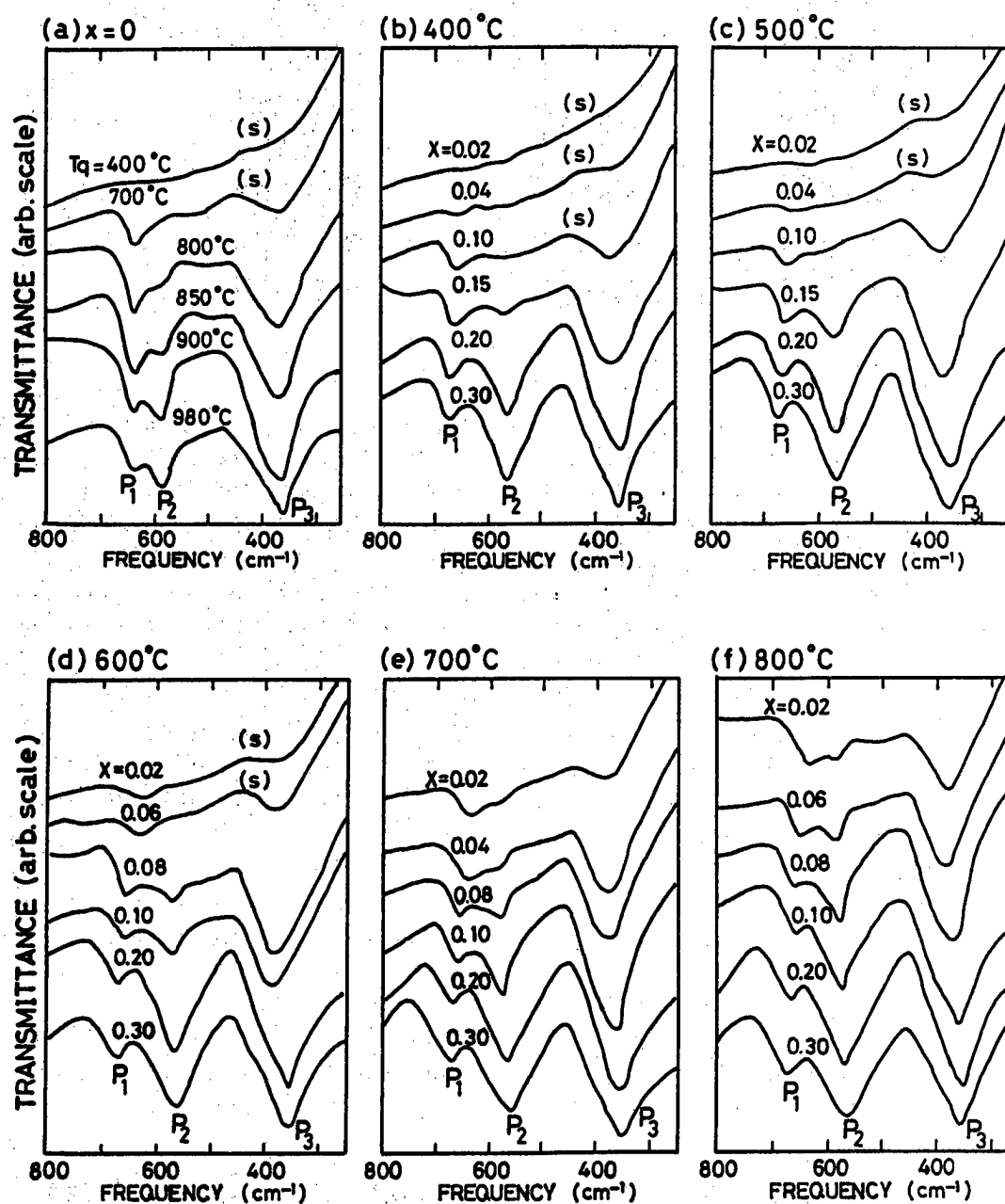


Fig. 1 The infrared absorption spectra of $\text{YBa}_2(\text{Cu}_{1-x}\text{Co}_x)_3\text{O}_{7-\delta}$. The vertical position of each spectrum is suitably shifted to avoid crossing. The three peaks are clearly observed, which are labeled as P_1 , P_2 and P_3 from the higher energy side. (a) The infrared spectra of $\text{YBa}_2\text{Cu}_3\text{O}_{7-\delta}$ sintered at various temperatures, from which samples were quenched. (b)-(f) The infrared spectra of $\text{YBa}_2(\text{Cu}_{1-x}\text{Co}_x)_3\text{O}_{7-\delta}$ sintered at various temperatures indicated at the top of each figure, from which samples were quenched.

Infrared absorption spectra were measured using a HITACHI model 270-50 Infrared Spectrophotometer with a CsI method in the energy region of $250\text{--}4000\text{ cm}^{-1}$. Features due to phonons were observed below 800 cm^{-1} and data are shown in the energy region of $250\text{--}800\text{ cm}^{-1}$. All the infrared measurements were carried out at room temperature. The infrared spectra of $\text{YBa}_2\text{Cu}_3\text{O}_{7-\delta}$ quenched from various sintering temperatures (T_q) are shown in Fig. 1 (a). In the figure, the spectrum depends on T_q sensitively. As T_q increases, three clear peaks appear, which are labeled as P_1 , P_2 and P_3 from the higher energy side. The orthorhombic-tetragonal transition occurs as T_q changes from 700 to 800°C . P_2 is observed only for tetragonal samples and its intensity increases as T_q increases. P_1 and P_3 are observed both for orthorhombic and tetragonal samples. They become less clear as T_q decreases. For the sample of $T_q = 400^\circ\text{C}$, P_1 is not observed and P_3 is traced as a broad feature. The decrease of the number of observable phonons, as a sample transforms from tetragonal to orthorhombic, is a very interesting phenomenon because all the infrared active phonons for the tetragonal $\text{YBa}_2\text{Cu}_3\text{O}_{7-\delta}$ are also allowed for the orthorhombic crystals by the selection rules based on crystal symmetry. Especially, behavior of P_2 is noted because it disappears just at the concentration where the sample becomes superconductive; i.e. the infrared anomaly. The infrared spectra of $\text{YBa}_2(\text{Cu}_{1-x}\text{Co}_x)_3\text{O}_{7-\delta}$ system are shown in Fig. 1 (b)-(f) for various sintering temperatures. In the series of samples sintered at 400°C , superconductivity is observed in the concentration region of $x \leq 0.1$. The intensity of the peak P_2 is essentially zero for all superconducting samples. With an increase of x over 0.1 , the relative intensity of the peak P_2 increases. For the series of the samples sintered at 800°C , all the samples are not superconductive and the peak P_2 is observed for all the samples. Thus correlation of the infrared anomaly with superconductivity is confirmed for the case of substitution of Co atoms for Cu atoms.

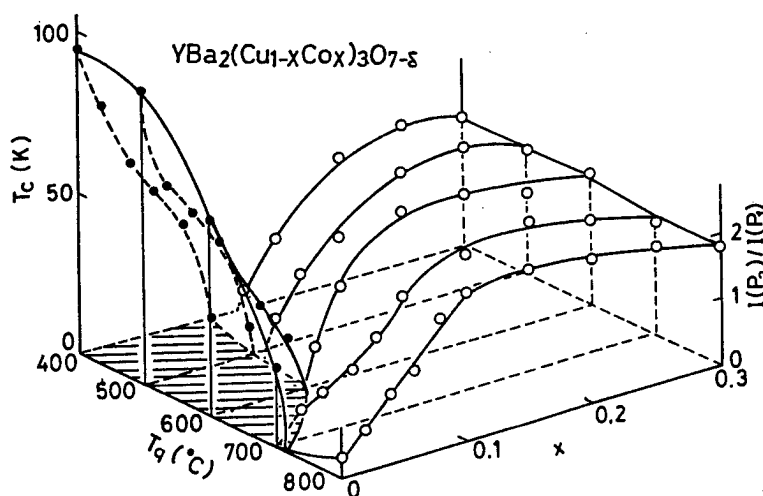


Fig. 2 The superconducting transition temperature T_c and the peak height ratio $I(P_2)/I(P_1)$ are plotted as functions of the sintering temperature and the Co concentration x for $\text{YBa}_2(\text{Cu}_{1-x}\text{Co}_x)_3\text{O}_{7-\delta}$. Clear correlation between appearance of superconductivity and near zero of the peak height ratio is observed.

To characterize the infrared anomaly quantitatively, we use the ratio of the peak height of P_2 to that of P_1 : $I(P_2)/I(P_1)$. Absolute intensity depends on the conductivity of samples and also on the size of pellets used for infrared measurements. However, the relative intensity ratio is less sensitive to these parameters and can be estimated reproducibly. Here we need to admit at most 20 % uncertainty due to difficulty of the base line estimation. The superconducting transition temperature T_c and the intensity ratio are plotted as functions of the sintering temperature T_q and the Co concentration x in a perspective view in Fig. 2. Superconductivity is observed only in the valley region where the intensity ratio is essentially zero. The correlation between increase of the intensity ratio and disappearance of superconductivity is remarkable. We also point out that the decrease of the intensity ratio proceeds gradually towards the concentration region where superconductivity is observed.

In our previous paper on $(La_{1-x}M_x)_2CuO_4$ systems,¹⁾ we considered shielding effects as a possible explanation of the infrared anomaly. One shielding effect is the anisotropic attenuation of incident electromagnetic waves used for optical measurements. Because of anisotropy of electronic conductivity of the sample, electromagnetic waves with their polarization perpendicular to the c -axis are more attenuated than those with their polarization parallel to the c -axis. However, this shielding effect could not explain the infrared anomaly of $(La_{1-x}M_x)_2CuO_4$. Of the three infrared absorption peaks observed in the energy region of $250-800\text{ cm}^{-1}$, two are E_u modes with their polarization perpendicular to the c -axis. One is the Cu-O bond-stretching mode and the other the La-O bond-bending-stretching mode. Only the former shows infrared anomaly. To explain it, we proposed¹⁾ another shielding effect that electric dipole moments of optical phonons corresponding to relative motions of Cu atoms and O atoms in conducting planes are shielded by free carriers directly. For $(La_{1-x}M_x)_2CuO_4$, relative motions of La atoms to O atoms are not shielded directly.

To examine whether the infrared anomaly in $YBa_2Cu_3O_{7-\delta}$ is explained similar way, we need to assign phonon modes. Different assignments have been made by a few authors.³⁻⁶⁾ In our recent paper,²⁾ we compared various experimental data and model calculations. Our assignment of the three peaks P_1 , P_2 and P_3 are shown in Fig. 3. The anomalous peak P_2 is the in-plane Cu(2)-O(2,3) stretching mode, which is a relative motion of atoms in the conductive planes. It is interesting to note that, both for $(La_{1-x}M_x)_2CuO_4$ and $RBa_2Cu_3O_{7-\delta}$ systems, the anomalous mode is the Cu-O bond stretching in the conductive CuO_2 planes. We note that the selective disappearance of the mode occurs continuously as shown in Fig. 2. There are two possibilities for this: the mode is shielded homogeneously or locally. We take the latter possibility because conductivity of a semiconducting sample exhibits a variable-range-hopping-like temperature dependence. The shielding is characteristic for free carriers. In order to explain that the shieldings occur even for semiconducting samples, we need to take into account local itineracy of carriers (holes). They are expected to shield the electric-dipole moments of optical phonons effectively covered by the local itineracy. Then the concentration at which the anomalous mode fully disappears indicates that local conductive regions fully overlap mutually and cover whole the sample. Assuming that the insulative $YBa_2Cu_3O_6$ has no hole, one hole per two O(2,3) atoms is introduced for $YBa_2Cu_3O_7$. As shown in Fig. 2, the peak P_2 fully

disappear for the sample sintered at 700°C with estimated δ value of 0.6. For this value, 0.2 holes per one O(2,3) atom is introduced. From this, the local itinerant region of a single carrier is estimated to be $2.23a \times 2.23a$, a being the lattice parameter. This means an isolated carrier can freely move only to nearest neighbors. If we make a similar calculation for $(La_{1-x}M_x)_2CuO_4$, the itinerant region is estimated to be $5.8a \times 5.8a$, which is larger than that for $YBa_2Cu_3O_{7-\delta}$. It is interesting to note that the more localized the carriers are the higher the superconducting transition temperature.

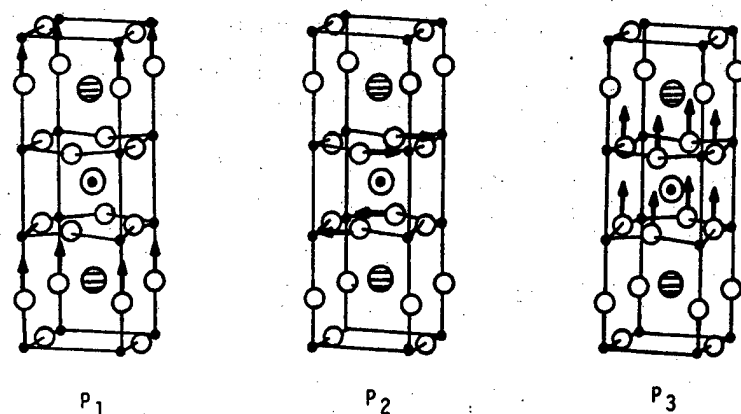


Fig. 3 Eigenvectors of the three lattice vibrational modes P_1 , P_2 and P_3 . Cu; closed circle; O; open circle; Y; dotted circle; Ba; hatched circle.

As mentioned above, carriers in the semiconducting samples are expected to have certain degree of local itineracy while they hop from one localized site to another. This behavior of carriers is consistent with the t - J model.^{7,8} According to the model, motions of carriers accompany modulation of spin arrangement. The modulation effectively produce a potential for carriers. This coherent coupled motions of carriers and spins give carriers certain degree of local itineracy. Thus the infrared anomaly is consistent with the t - J model at least qualitatively.

References

- 1) K. Ohbayashi, H. Tukamoto, H. Yamasita, A. Fukumoto, Y. Utunomiya, N. Ogita, M. Udagawa and S. Funahashi: Submitted to J. Phys. Soc. Japan.
- 2) K. Ohbayashi, H. Tukamoto, N. Ogita, M. Udagawa, Y. Aoki and T. Fujita: Submitted to J. Phys. Soc. Japan.
- 3) S. L. Chaplot: Phys. Rev. B **37** (1988) 7435.
- 4) R. Liu, C. Thomsen, W. Kress, M. Cardona and B. Gegenheimer: Phys. Rev. B **37** (1988) 7974.
- 5) W. Kress, U. Schroder, J. Prade, A. D. Kulkarni and F. W. De Wetts: Phys. Rev. B **38** (1988) 2906.
- 6) F. E. Bates: Phys. Rev. B **39** (1989) 322.
- 7) H. Fukuyama: Buturi **44** (1989) 475.
- 8) C. L. Kane, P. A. Lee and N. Read: Phys. Rev. B **39** (1989) 6880.

HOPPING, FREE CARRIER AND SUPER-CONDUCTION IN FIR OPTICAL CONDUCTIVITY OF Bi-Sr-Ca-Cu-O THIN FILMS

K. Nagasaka, M. Sato and N. Tonosaki

Department of Physics, Science University of Tokyo
Kagurazaka, Shinjuku-ku, Tokyo, 162

Far infrared spectroscopy has been carried out in the range 3 to 500 cm^{-1} , by using a lamellar grating and Michelson Fourier transform spectrometer.

(1) We prepared semiconducting thin films cleaving a crystal which exhibits the superconductivity in the case of the DC measurement. Their thickness is about 5 μm and the size is about $2 \times 2 \text{ mm}^2$. Using the incident electric field in the metallic a-b plane of the crystal, we obtained the absorption coefficient,

$$\alpha = 850 \cdot \omega^s, \quad (s=1/3).$$

From the absorption spectra, the conduction mechanism is attributed to the variable range hopping conduction in the band of Cu-O planes. It is quite different from the free carrier conduction mechanism of the Drude model.

(2) We measured the temperature dependence of the transmission spectrum in the range 50 to 300 cm^{-1} of the superconducting crystal films which were prepared on MgO substrate by the CVD method. From the spectra, we present the ratio of superconducting to normal transmittance minus unity, $(T_s - T_n)/T_n$, where T_s and T_n are its transmittance at temperature below and above the superconducting transition, respectively. This spectrum can be given by using a dielectric constant,

$$\epsilon = \epsilon_{\infty} + f_n \epsilon_D + (1 - f_n) \epsilon_S, \quad (T < T_C),$$

where ϵ_{∞} is the high frequency dielectric constant, ϵ_D that of the Drude model, ϵ_S that of optical conductivity of Mattis-Bardeen theory and f_n the normal electron friction in the total number of conduction electrons in the crystal of which the plasma frequency is about 10^4 cm^{-1} .

(3) We have measured the dependence of the transmittance on magnetic field in the range 0 to 3.7 T. By using the ratio, $T(H)/T(0)$, we can find the qualitative features of the dependence of superconducting energy gap on magnetic field, $\Delta_g(H)$. The curve, Δ_g versus H , gives so fairly close coincidence with Abrikosov and Gor'kov theory. From this experiment, we determined the optical gap, 220 cm^{-1} , and the upper critical magnetic field, 38 T, and consequently obtained the relation $\Delta_g(0) = 2\Delta^P(0) \sim 3.9 k_B T_C$.

INTRODUCTION

There has been considerable attention paid to determining of superconducting energy gap using far infrared spectroscopy. Thomas et al.¹⁾ obtained reflectance $R=1$ at low frequency, and the relationship between the superconducting energy gap at $T=0\text{K}$ and the critical temperature, $2\Delta_0/kT_C=3-4$, using microtwinned crystals $\text{Ba}_2\text{YCu}_3\text{O}_7$ with $T_C=50$ and 68 K. Timusk and Tanner et al.²⁾ measured the reflectance of $\text{Bi}_2\text{Sr}_2\text{CaCu}_2\text{O}_8$ crystals in the superconducting state and a sharp reflectance edge at 300 cm^{-1} associated with a threshold in real part of the optical conductivity. Re-

cently, transmission spectra have been observed in superconducting Bi-Sr-Ca-Cu-O films.³⁾

Using low frequency transmission spectroscopy, we can observe a direct interaction with the elementary excitation which plays an important role in conduction in solids. It is a more direct method of assessing conductivity than the wide range reflectance measurements and the Kramers and Kronig transformation of their spectra. In this paper, we report the far infrared transmission measurement of semiconducting and superconducting Bi-Sr-Ca-Cu-O thin films in the range 3 to 300 cm^{-1} .

1. VARIABLE RANGE HOPPING IN SEMICONDUCTING Bi-Sr-Ca-Cu-O THIN FILM

Measurements were made on thin crystal films (code numbers 1 and 2) prepared by cleaving crystals. They were about $5\mu\text{m}$ thick and about $2\times 2\text{ mm}^2$ in size. These films used for FIR transmission measurements are semiconducting materials. However, DC measurement of slabs of $1\times 2\times 10\text{ mm}^3$ prepared from the same crystals always shows superconductivity.

We measured the far infrared transmission spectra with the incident electric field in a-b plane of our crystal film, using a lamellar grating Fourier spectrometer in the range 3 to 40 cm^{-1} and a Michelson Fourier spectrometer in the range 15 to 500 cm^{-1} . There was no need to compensate for interference in the specimen films because the thickness of $5\mu\text{m}$ is smaller than wavelengths in the range 30 to 3000 μm . We find that a characteristic property in the far infrared transmission spectra of these crystals is quite different of the free carrier behavior of the Drude model.

Figure 1 shows the transmittance spectra for the code number 1 crystal film. In the range from 30 to 150 cm^{-1} transmittance decreases with temperature. We also observed transmission spectra in the range 3 to 100 cm^{-1} at 8K using the code number 2 crystal film (Fig. 1 insert).

To interpret several features of the transmission spectra shown in Fig. 1, we considered the variation of transmittance with ω in the range 5 to 300 cm^{-1} at 8K (Fig. 1 insert). In this region, it is noted that transmittance varies approximately as $1/\omega^s$ ($s=1/3$).

Next, let us discuss the conduction mechanism. For simplicity, we neglected reflectance, and calculated an absorption coefficient of $-1/\text{dln}(I/I_0)$, where I_0 is the intensity of the incident radiation, I is radiation passing through the crystal film and d is thickness. This absorption coefficient versus ω is shown in Fig. 2. From the absorption spectra in the range below 100 cm^{-1} we obtained the absorption coefficient

$$\alpha = 650\omega^s \quad (s=1/3). \quad (1.1)$$

Figure 3 shows $\log \alpha$ versus $\log \omega$. Based on this relationship, we can relate this spectrum to variable range hopping from a localized state to other states. Moreover, because this absorption has temperature dependence and is enhanced by phonon population, this hopping is considered to be a phonon assisted hopping.

Subtracting the absorption coefficient which just above mentioned from the total absorption coefficient, we obtained several absorption peaks with absorption coefficients as large as 500~1000 cm^{-1} . Their frequencies are listed in Table 1; they exhibit fairly close correspondence to those of the Raman scattering spectrum⁴⁾.

2. TEMPERATURE DEPENDENCE OF FAR-INFRARED TRANSMISSION SPECTRA OF SUPERCONDUCTING Bi-Sr-Ca-Cu-O THIN FILM

The $\text{Bi}_2\text{Sr}_2\text{CaCu}_2\text{O}_8$ superconducting film was made by chemical vapor deposition (CVD) method on MgO substrate, which thickness is 400 μm . The film thickness is about

0.1 μm and its grain size was 10-100 μm . The resistivity measured by 4-terminal method gives zero at 81K as shown in Fig.4.

Far-infrared transmission measurements were performed in the range 50 to 300 cm^{-1} using a Michelson Fourier spectrometer. We obtained transmittance spectra for temperatures, 5, 34, 43, 52, 70, 83, 93, 117 and 300K. The MgO substrate introduced limitation to measuring frequencies below 300 cm^{-1} , because the reststrahlen band is at 350 cm^{-1} . The properties of the substrate are slightly temperature, magnetic field and frequency dependent. These effects were eliminated by referencing the sample spectrum to an identical MgO substrate.

Figure 5 shows the transmittance spectra at 5, 52, 83, 117 and 300K. After Tinkham, it is known that the transmittance ratio $(T_s - T_n)/T_n$ has a peak at energy gap where T_s is transmittance of superconducting state and T_n is of normal state. In this case, we chose the transmission spectrum at 83 K for the normal state transmission one. This temperature is just above the transition temperature. Each ratio, $(T - T_n)/T_n$, spectrum has a broad peak for temperatures of the superconducting state of 5, 52 and 70K, and no peak at 93K of the normal state. Furthermore, the peak shifts to lower frequency with increasing temperature. Then we considered that this peak is corresponding to the superconducting energy gap. We determined the gap about 200 cm^{-1} at 0K.

To analyze the transmission spectra, we put a dielectric function of eqs.(2.1) and (2.2), and can calculate a transmission spectra. Comparing experimental spectra to calculated spectra, we can determine four important parameters such as the plasma frequency, the relaxation times of free carriers and quasi particles, the superconducting energy gap and the friction of the normal conduction carriers in superconducting materials.

$$\epsilon_1 = \epsilon_\infty + f_n \epsilon_{d1} + (1 - f_n) \epsilon_{s1} \quad (2.1)$$

$$\epsilon_2 = f_n \epsilon_{d2} + (1 - f_n) \epsilon_{s2} \quad (2.2)$$

where, ϵ_∞ is the dielectric constant at high frequency, f_n is friction of normal, ϵ_{d1} and ϵ_{d2} are real and imaginary part of the Drude free carrier dielectric function given by eqs.(2.3) and (2.4),

$$\epsilon_{d1} = -\frac{\omega_p^2 \tau^2}{\omega^2 \tau^2 + 1} \quad (2.3)$$

and

$$\epsilon_{d2} = \frac{\omega_p^2 \tau}{\omega(\omega^2 \tau^2 + 1)} \quad (2.4)$$

where ω_p is the plasma frequency, τ is the relaxation time and ω is the frequency and ϵ_{s1} and ϵ_{s2} are dielectric functions of superconducting state which is corresponding to Mattis-Bardeen's optical conductivity given by equations,

$$\epsilon_{s1} = -\frac{|\sigma_n|}{\epsilon_0 \omega} S_2 \quad (2.5)$$

and

$$\epsilon_{s2} = \frac{|\sigma_n|}{\epsilon_0 \omega} S_1 \quad (2.6)$$

where

$$|\sigma_n| = \frac{\epsilon_0 \omega_p^2 \tau}{\sqrt{1 + \omega^2 \tau^2}} \quad (2.7)$$

ϵ_0 is the dielectric constant of vacuum, and S_1 and S_2 are Mattis-Bardeen's normal-

ized optical conductivity.

Figure.7 shows a calculated transmittance of (b) curve for completely superconductor ($f_n=0$) with a energy gap at 200cm^{-1} . It has no transmittance below the energy gap. It is due to no real part of optical conductivity below the gap and complete reflectivity. But measured transmittance has finite one below the energy gap. Then we add this superconducting dielectric function with Drude free carrier term which has finite real part of conductivity below the gap. Therefore, we use dielectric function in superconducting state with a finite friction of normal, f_n .

As a result, we got those fitting parameters listed in table 2. Here, we fixed high frequency dielectric constant ϵ_∞ as 5 and a energy gap 2Δ as the value of the peak of the ratio $(T_S-T_N)/T_N$ for each temperature. It is noted that the optical conductivity at normal state is comparable with the DC measured one i.e. $\sigma_{DC}=273\text{ }1/\Omega\text{cm}$ and $\sigma_{op}=480\text{ }1/\Omega\text{cm}$.

We consider the penetration depth λ , mean free length l and coherent length ξ , because these values should determine the optical condition. The coherent length is about 30-40Å obtained by magnetoresistance measurements⁵⁾ and $\xi_0=0.18\hbar v_F/k_B T_C$ from BCS relation where v_F is Fermi velocity, k_B is Boltzmann constant and \hbar is Plank constant. Then, we got $v_F=3.7\times 10^6\text{cm/s}$. Using the relaxation time $\tau\sim 10^{-13}$, we determined the mean free path, $l=v_F\tau\sim 90\text{Å}$. The penetration depth λ , is larger than $0.3\mu\text{m}$ of magnetization experiments⁶⁾. By using our results of the plasma frequency ω_p , the London penetration depth $\lambda_L=c/\omega_p$ (c is velocity of light) was determined to be about $1.4\mu\text{m}$. Additionally, the skin depth at normal state, $\delta=c\sqrt{2}/\omega_p\sqrt{\omega\tau}$ is about $2\mu\text{m}$ at $\omega=200\text{cm}^{-1}$.

Using these values, l , ξ , λ and δ , it is clear that (a) the film thickness d is smaller than λ and δ . It is consistent with the fact that the light can pass through the sample. (b) Since $l\ll\lambda$ and δ , we neglect the anomalous skin effect and can calculate the transmission by using an ordinary equation and also holds following argument. (c) Mattis and Bardeen derived an equation of the optical conductivity at superconducting state assuming anomalous skin effect. But in this case, because the coherent length is smaller than the penetration depth, London local limit is realized. Then, the optical conductivity σ has no k dependence in the Pippard integral. As a result, we use the Mattis-Bardeen's equation for calculating the superconducting optical conductivity. (d) In Mattis-Bardeen's equation, it was assumed that $\Omega_g\tau\ll 1$ where Ω_g is energy gap in frequency, that is, the normal conductivity σ_n is independent of frequency. In this case, because $\Omega_g\tau\sim 1$, we should use eq.(2.7).

Pay attention to the friction of normal metal. For our sample, it is about

0.7~0.8. On the other hand, a pure superconductor which should have $f_n=0$ exhibits a sharp peak in the ratio $(T_s-T_n)/T_n$ spectrum. However, this ratio spectrum is very broad. The feature of the spectrum is consistent with the large value of f_n .

The temperature dependence of the plasma frequency ω_p is explained by enhancement of an effective mass of carrier in the equation $\omega_p^2 = ne^2/\epsilon_0 m^*$. In the superconducting state the effective mass enhancement factor is 1.4 comparing that of normal conduction at 117K.

3. MAGNETIC FIELD DEPENDENCE OF OPTICAL GAP, $\Omega_g(H)$, IN SUPERCONDUCTING Bi-Sr-Ca-Cu-O THIN FILM

Twenty five years ago, theoretical physicists predicted that an applied magnetic field, H , causes a large decrease in the optical gap and in T_c ^{7,8,9,10}) as well as paramagnetic impurities with equivalent inverse collision time, Γ , proportional to H . This effect was studied by tunneling effects through a point contact or superconductor-insulator-metal junction, because the tunneling effect is a direct method of determining the density of states at the gap edge. ^{11,12}) In this section we report a new method for determining optical gap in a magnetic field and magnetic field dependence of the optical gap, $\Omega_g(H)$.

We employed thin films of Bi-Sr-Ca-Cu-O crystal deposited on MgO substrate and oriented with their c-axis perpendicular to the substrate. Crystal preparation is reported elsewhere ¹³). Measurements of far infrared transmission spectra were carried out in the range 110 to 230 cm^{-1} in magnetic field, using a Michelson Fourier spectrometer and a Ge-Ga photoconductor.

We measured transmission spectra, $T(H)$, in the range 110 to 230 cm^{-1} at magnetic field of 0, 0.5, 2.5 and 3.7 T, as shown in Fig.8. The magnetic field was applied in the Faraday configuration and parallel to c-axis of the crystal.

As the applied magnetic field was increased from 0 to 3.7 T, the transmittance spectrum deviated from the spectrum at $H=0$ T. The deviation point decreased with magnetic field. To determine the decrease of the gap, $\Omega_g(H)$, it is convenient to take the ratio of spectra, $T(H)/T(0)$, at 0.5, 2.5 and 3.7 T, as shown in Fig. 9. In this ratio, we can see thresholds at 208, 180, and 172 cm^{-1} , corresponding to magnetic fields, 0.5, 2.5, and 3.7 T, respectively. Provided that the frequency of the threshold is equal to the gap in magnetic field, the ratio of $\Omega_g(H)/\Omega_g(0)$, is given as a function of magnetic field.

For a thin film in a magnetic field which is perpendicular to the film, inverse collision time ¹⁴) for exchange scattering is obtained by

$$\Gamma = \hbar D e H, \quad (3.1)$$

where D is the diffusion constant.

S. Skalski, O. Betbeder-Matibet and P. R. Weiss⁸⁾ derived the ratio of inverse collision time, Γ , to the order parameter at $T=0$ and $H=0$, $\Delta^P(0)$, which is given by

$$\frac{\Gamma}{\Delta^P(0)} = -\frac{4}{\pi} \left\{ \frac{\Delta(0, \Gamma)}{\Delta^P(0)} \right\} \ln \frac{\Delta(0, \Gamma)}{\Delta^P(0)}. \quad (3.2)$$

In addition, Skalski et al gives a condition that, when $2\Gamma/\Delta^P(0)=1$, $\Delta(0, \Gamma)/\Delta^P(0)=0$, where the magnetic field is equal to the upper critical magnetic field, $H=H_{C2}$. From eq(3.1), $2\Gamma/\Delta^P(0)=H/(\Delta(0)/2\hbar De)$, where $(\Delta^P(0)/2\hbar De)$ is constant. Considering the special case mentioned above, we can have

$$2\Gamma/\Delta^P(0)=H/H_{C2}. \quad (3.3)$$

since, $(\Delta^P(0)/2\hbar De)=H_{C2}$. Therefore, we can express the order parameter ratio, $\Delta(0, \Gamma)/\Delta^P(0)$ as a function of H/H_{C2} . Moreover they also derived the ratio of the optical gap at T and H to that at $T=0$ K and $H=0$ T, which is given by

$$\frac{\Omega_g(T, \Gamma)}{\Omega_g(0, 0)} = \frac{\Delta(T, \Gamma)}{\Delta^P(0)} \left\{ 1 - \left(\frac{\Gamma}{\Delta(T, \Gamma)} \right)^{2/3} \right\}^{3/2} \quad (3.4)$$

Assuming $\Delta(T=4.2K, \Gamma) \sim \Delta(0, \Gamma)$ and $\Omega_g(4.2K, \Gamma) \sim \Omega_g(0, \Gamma)$, and using eqs.(3.2) and (3.4), we can obtain

$$\frac{\Omega_g(T, \Gamma)}{\Omega_g(0, 0)} = \frac{\Delta(T, \Gamma)}{\Delta^P(0)} \left\{ 1 - \left(-\frac{4}{\pi} \ln \frac{\Delta(0, \Gamma)}{\Delta^P(0)} \right)^{2/3} \right\}^{3/2} \quad (3.5)$$

Equation(3.5) shows the relation between $\Omega_g(0, \Gamma)/\Omega_g(0, 0)$ and $\Delta(0, \Gamma)/\Delta^P(0)$. Therefore, using eq(3.3), we can express $\Omega_g(0, \Gamma)/\Omega_g(0, 0)$ as a function of H/H_{C2} . From our experiment, we determined three $\Omega_g(H)$ corresponding to each magnetic field, H, which should be able to be shown by the rhombic symbols in Fig. 10. Using the least square method, we fitted the curve of $\Omega_g(H)/\Omega_g(0)$ versus H/H_{C2} to three rhombic points of our experiments. Through this procedure we obtained $\Delta^P(0) \sim 220 \text{ cm}^{-1}$ and the critical magnetic field, $H_{C2} \sim 38 \text{ T}$. Then, in Fig.10, the rhombic symbols indicate our experimental points, Ω (threshold at H)/ $\Omega_g(0)$, and the solid line indicates the theoretical curve of a decrease in the optical gap ratio corresponding to this experiment. In addition, the dashed line indicates a decrease in the order parameter, $2\Delta(H)$, in this system.

CONCLUSION

We observed transmission spectrum in the range from 3 to 300 cm^{-1} in semiconducting Bi-Sr-Ca-Cu-O films. The qualitative features of absorption spectra exhibit the variable range hopping conduction in the semiconducting films which should have small

number of carriers. This is quite different from the free carrier conduction of Duder model. On the other hand, we carried out the transmission measurements in the superconducting thin films, too. Moreover, the transmission spectra were fitted by using the Drude free carrier term and the Mattis-Bardeen's optical conductivity. Even in the superconducting state, we observed the finite optical conductivity below the energy gap. From this experiment, we obtained a clear evidence that there is no hopping conduction carrier but free carriers in the midgap even in the superconducting material below T_C . In addition, the optical gap was determined to be about 220 cm^{-1} and the upper critical magnetic field about 38 T . Therefore, this material exhibits the relation ,

$$2\Delta^P(0) \sim 3.9k_B T_C,$$

where $T_C = 82 \text{ K}$.

References

1. G.A.Thomas, J.Orenstein, Rapikine, M.Capizzi, A.j.Millis, R.N.Bhatt, L.F.Schneemeyer and J.V.Waszcak: Phys.Rev.Lett. 61(1988)1313.
2. M.Reedyk, D.A.Bohn, J.D.Garret, J.E.Greedan, C.V.Stager, T.Timusk, K.Kamaras and D.B.Tanner: Phys.Rev. B38(1988)11981
3. R. A. Hughes, T. Timusk, A. L. Cooper, G. A.Thomas, J. J. Yeh, and M. Hong: Phys. Rev. B40(1989)5162
4. A.Yamanaka, T.Kimura, F.Minami, K.Inoue and S.Takekawa: Jpn.J.Appl.Phys. 27(1988)L1902
5. Y.Matuda et.al.:Phys.Rev.B40, 5176 (1989)
6. S.Mitra et.al.: Phys.Rev.B40, 2674 (1989)
7. A. A. Abrikosov and L. P. Gor'kov, Zh.Eksperim. i Teor. Fiz. 39, 1781 (1960)
8. S.Skalski, O. Betbeder-Matibet, and P. R. Weiss, Phys. Rev.136, 6A (1964)
9. K. Maki, Prog. Theoret. Phys. 31, 5 (1964)
10. A. Larkin, Zh. Eksperim, i Teor. Fiz. 48, 232 (1965)
11. R.Meservey, and D.H.Douglass, Jr.Phys. Rev. 135, A24 (1964)
12. Michael A. Woolf and F.Reif Phys. Rev. 137, A557 (1965)
13. M. Ihara, T. Kimura, H. Yamawaki, and K. Ikeda IEEE Trans. Magn. 25, 2470 (1989)
14. M. Tinkham. Introduction to superconductivity, chap.8, McGraw-Hill, Inc.

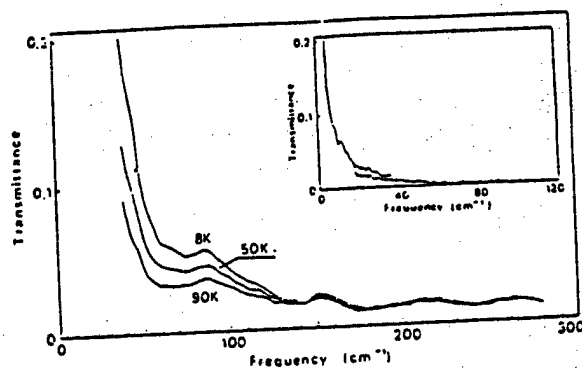


Fig. 1. Measured transmittance of layered crystal film (code number 1) Bi-Sr-Ca-Cu-O crystal at 8, 50 and 90K. Inset: measured transmittance of single crystal film (code number 2) Bi-Sr-Ca-Cu-O at 8K.

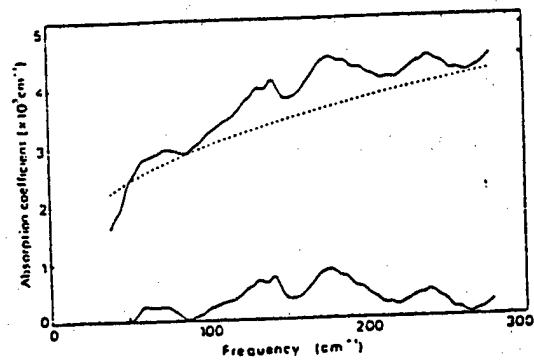


Fig. 2. Measured absorption coefficient, $-(1/d)\log(I/I_0)$ versus frequency, ω , and $\alpha=650\omega^3$ ($s=1/3$). Lower curve exhibits the phonon absorption spectrum.

Table 1 Phonon frequencies observed by far infrared and Raman(4) spectroscopy.

	Frequency (cm ⁻¹)							
FIR	60	130	175	240	(290)			
Raman	-	120	175	225	255	345	470	627

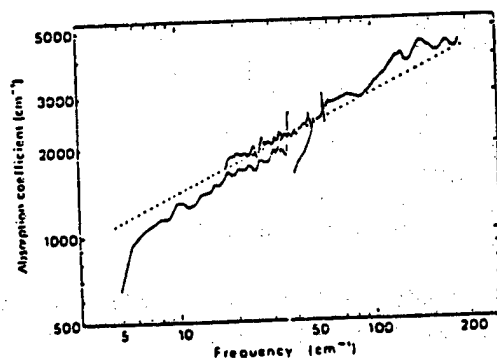


Fig. 3. Absorption coefficient $-(1/d)\log(I/I_0)$ versus frequency ω . The dotted line shows $\alpha=650\omega^3$ ($s=1/3$). The line indicates photon-induced hopping conduction.

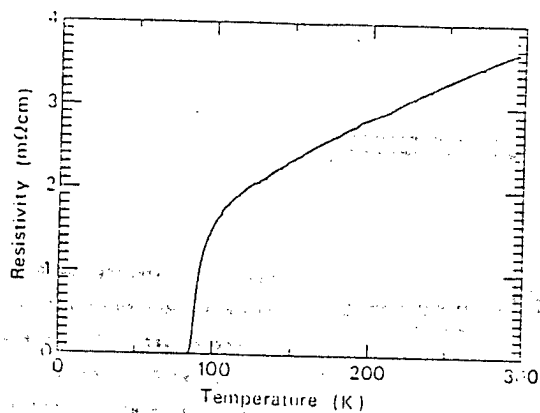


Fig. 4. Temperature dependence of the resistivity of Bi-Sr-Ca-Cu-O thin film deposited on MgO substrate.

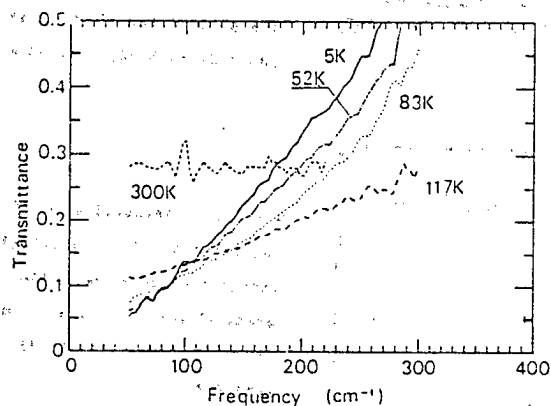


Fig. 5. Far-infrared transmittance of 0.1 μm Bi-Sr-Cu-Cu-O film on MgO substrate for several temperatures above and below T_c .

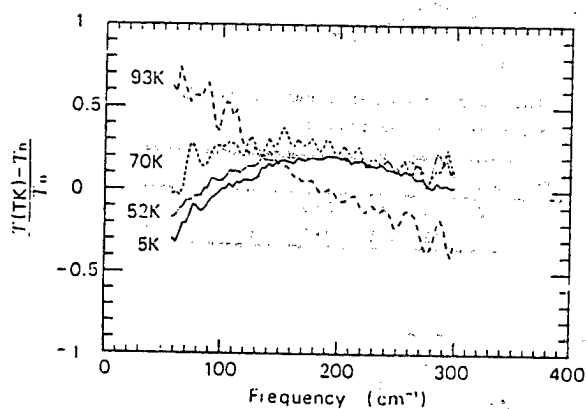


Fig. 6. The ratio of superconducting to normal transmittance S , 51, 70 and 90K, respectively. For normal transmittance, the transmission spectra observed at 83K was employed.

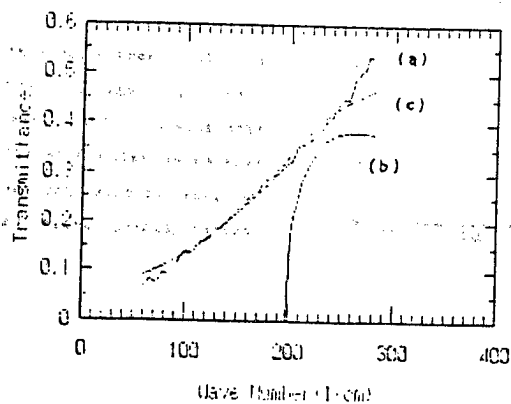


Fig. 7. Measured transmittance spectra are given by curve (a) and calculated spectra by (b) and (c) curves. The parameters for calculation are $\omega_g=200\text{cm}^{-1}$, $\tau=3\times 10^{-13}\text{sec}$, $\omega_p=6900\text{cm}^{-1}$, $f_N=0$ for (b) and $f_N=0.8$ for (c).

Table 2. Fitting parameters

Temperature	T(K)	5	34	43	52	70	83	93	117	300
plasma frequency	ω_p (cm ⁻¹)	6900	7200	7400	7300	7400	7800	8500	9000	11000
relaxation time	τ (x10 ⁻¹³ s)	3.0	2.0	1.9	3.5	2.5	3.6	1.6	1.7	0.5
energy gap	2Δ (cm ⁻¹)	200	190	180	150	150				
friction of normal	f_n	0.8	0.7	0.7	0.8	0.8				

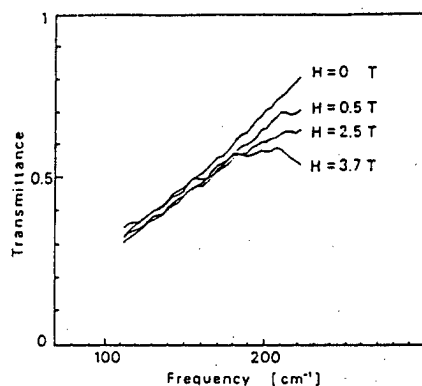


Figure 8 : Magnetic field dependence of transmission spectra of thin superconducting film on MgO substrate.

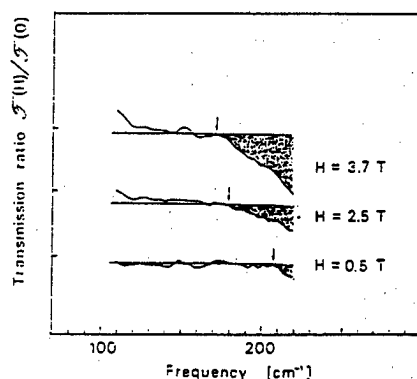


Figure 9: Ratio of transmission spectra at magnetic field, H, to that at 0 T.

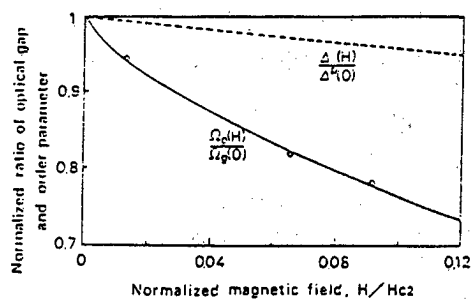


Figure 10: Ratio of optical energy gap at H to that which is to be 220 cm⁻¹ at 0 T versus the normalized magnetic field by the upper critical magnetic field, H_{c2} ~ 38 T, shown by solid line. Rhombic symbols exhibit experimental values. Ratio of order parameter at H to that at 0 T, shown by dotted line.

Oxygen K-edge Fine Structure of Tl-Ba-Ca-Cu-O Studied by
Electron Energy Loss Spectroscopy

D. SHINDO, K. HIRAGA, S. NAKAJIMA⁺, M. KIKUCHI and Y. SYONO

Institute for Materials Research, Tohoku University, Katahira, Sendai 980, Japan

⁺CASIO Computer Co., Ltd, Hachioji-city, Tokyo 192, Japan

The fine structures of oxygen K-edge in the Tl-Ba-Ca-Cu-O superconductors were investigated by electron energy loss spectroscopy (EELS). The peak corresponding to the hole state near the Fermi energy was sensitive to the number of Cu-O layers and the direction of momentum excitation. It was shown that the hole content in $\text{Tl}_2\text{Ba}_2\text{Ca}_{n-1}\text{Cu}_n\text{O}_{2n+4}$ ($n=1-3$) and $\text{Tl}_1\text{Ba}_2\text{Ca}_{n-1}\text{Cu}_n\text{O}_{2n+3}$ ($n=2-4$) decreases with the increase of n and that most holes exist in the O $2p_{x,y}$ orbitals of 2-dimensional Cu-O planes. Holes in $\text{Tl}_2\text{Ba}_2\text{Cu}_1\text{O}_6$ and $\text{Tl}_1\text{Ba}_2\text{Ca}_1\text{Cu}_2\text{O}_7$ are overdoped.

Since the discovery of new high- T_c superconductors [1-4], much effort has been devoted to understand the mechanism of superconductivity. As the carrier of superconductivity in these superconductors was considered to be holes, the determination of the position of the hole and its symmetry was one of the most important clues to understand the mechanism of superconductivity. Recently, absorption spectroscopy techniques such as X-ray absorption spectroscopy [5-6] and EELS [7-9] were employed to examine the unoccupied density of state near the Fermi energy in these superconductors. By investigating samples with different oxygen content, it was reported that the hole was located mainly at oxygen sites in $\text{La}_{2-x}\text{Sr}_x\text{CuO}_4$ [7] and $\text{YBa}_2\text{Cu}_3\text{O}_{7-y}$. [8,9] Some of the present authors also confirmed a direct correlation between the height of the peak at the oxygen K-edge at around 528 eV and oxygen content of $\text{YBa}_2\text{Cu}_3\text{O}_{7-y}$ by in-situ observation [10]. Furthermore by changing the direction of momentum transfer of the incident electrons in EELS, it was also pointed out that near-edge fine structure at the oxygen K-edge in the Y-Ba-Cu-O system was different between on the c-plane and along the c-axis. [8,9] Very recently orientation dependency of momentum transfer of $\text{Bi}_2\text{Sr}_2\text{Ca}_1\text{Cu}_2\text{O}_8$ was reported for single crystals by X-ray absorption spectroscopy [11] and EELS [12].

In this study, we concentrated our attention on the hole state of a Tl-Ba-Ca-Cu-O system. Among the superconductors discovered so far, the Tl-Ba-Ca-Cu-O system has attracted much attention on both its structure and superconducting transition temperature (T_c). The system may be divided into two systems, $\text{Tl}_1\text{Ba}_2\text{Ca}_{n-1}\text{Cu}_n\text{O}_{2n+3}$ with single Tl-O layers [4,13-15] and $\text{Tl}_2\text{Ba}_2\text{Ca}_{n-1}\text{Cu}_n\text{O}_{2n+4}$ with double Tl-O layers [16-19]. In both systems, T_c changes with n . There is a definite difference as to the origin of the supply of holes in the two systems. In $\text{Tl}_1\text{Ba}_2\text{Ca}_{n-1}\text{Cu}_n\text{O}_{2n+3}$, the hole content is given as $1/n$ by assuming the formal valencies (Tl, Ba, Ca, Cu and O have valencies of +3, +2, +2, +2 and -2, respectively), whereas in $\text{Tl}_2\text{Ba}_2\text{Ca}_{n-1}\text{Cu}_n\text{O}_{2n+4}$, the hole content is 0 regardless of the value of n . Recently the mechanism of the supply of holes by the decrease of valency of Tl atoms in $\text{Tl}_2\text{Ba}_2\text{Ca}_{n-1}\text{Cu}_n\text{O}_{2n+4}$ was proposed based on the XPS experiments [20].

A large single crystal of Tl-Ba-Ca-Cu-O is difficult to obtain at this time and we therefore utilized a highly efficient parallel detector installed on a conventional electron microscope to investigate the oxygen K-edge fine structure. In contrast with other superconductors such as the Y-Ba-Cu-O system, the Tl-Ba-Ca-Cu-O system is rather simple and may be well characterized, since the number of Cu-O layers in the unit cell can be controlled and there are no Cu-O chains but only Cu-O planes. Therefore, the fine structure of the oxygen K-edge could be investigated by changing the number of Cu-O layers and the direction of momentum transfer.

Samples were prepared from Tl_2O_3 , BaCuO_2 , CaO and CuO by conventional ceramic procedures. The preparation was carried out in a closed glove box because of the toxicity of thallium compounds. Structure were synthesized from X-ray powder diffraction analysis and T_c obtained from dc susceptibility measurements is listed in Table I.

The EELS and EDX studies were performed with a JEM-2000FX electron microscope at Purdue University and a JEM-100C electron microscope at Japan Atomic Energy Research Institute. The half width of the main peak (0 eV energy loss) in the EELS spectra was 1 eV. The beam diameter for the EELS study was about $0.2\mu\text{m}$. The thickness of the grains for observation was estimated to be a few ten nm. We investigated the chemical composition of constituent metal atoms in each grain by an energy dispersive X-ray spectroscopy (EDX) prior to EELS study. In order to avoid the background of X-rays from the Cu grids commonly used, we used Mo grids instead. In addition to the EDX analysis, we observed an electron diffraction pattern in each grain to confirm the structure. Although the oxygen content was not analyzed accurately, we assumed that the oxygen content follows the formula $\text{Tl}_2\text{Ba}_2\text{Ca}_{n-1}\text{Cu}_n\text{O}_{2n+4}$ and $\text{Tl}_1\text{Ba}_2\text{Ca}_{n-1}\text{Cu}_n\text{O}_{2n+3}$.

Figures 1(a), 1(b) and 1(c) indicate the EELS spectra of $\text{Tl}_2\text{Ba}_2\text{Ca}_{n-1}\text{Cu}_n\text{O}_{2n+4}$ with $n=1-3$, respectively, and Fig. 1(d) indicates that of $\text{Ca}_{0.91}\text{Sr}_{0.09}\text{CuO}_2$ which is isomorphic to the component structure (CaCuO_2) of Tl-Ba-Ca-Cu-O. There is a peak at 528 eV in the spectra of $\text{Tl}_2\text{Ba}_2\text{Ca}_{n-1}\text{Cu}_n\text{O}_{2n+4}$ followed by the large main peak which is shifted by several eV higher energy in each spectrum. It is noted that the relative height of this peak to the main peak decreases with the increase of n ($n=1-3$) and the position of the main peak indicated by a broken line shifts towards higher energy with the increase of n . It is interesting to compare the spectra of $\text{Tl}_2\text{Ba}_2\text{Ca}_{n-1}\text{Cu}_n\text{O}_{2n+4}$ with a spectrum obtained from $\text{Ca}_{0.91}\text{Sr}_{0.09}\text{CuO}_2$. In the spectrum of the latter sample, there are two small peaks above 529 eV, which probably do not correspond to the hole state of the Cu-O bonding, and a large main peak is situated at around 540 eV. The main peak of $\text{Ca}_{0.91}\text{Sr}_{0.09}\text{CuO}_2$ is situated at several eV higher than those of $\text{Tl}_2\text{Ba}_2\text{Ca}_{n-1}\text{Cu}_n\text{O}_{2n+4}$, and so the shift of the main peak of $\text{Tl}_2\text{Ba}_2\text{Ca}_{n-1}\text{Cu}_n\text{O}_{2n+4}$ with the increase of n is reasonably interpreted from the increase of the component CaCuO_2 in the structure. If the hole contents are the same in the Cu-O bonding in the three compounds or the hole contents in the bonding increase with n , the peak at 528 eV may increase with n since the relative number of the Cu-O bonding in the structure increases with n . This behavior of the peak with the increase of n is clearly contradictory to the observation. So we conclude that the average hole content in $\text{Tl}_2\text{Ba}_2\text{Ca}_{n-1}\text{Cu}_n\text{O}_{2n+4}$ decreases with the increase of n .

Figures 2(a) and 2(b) are the EELS spectra of $\text{Tl}_2\text{Ba}_{1.85}\text{La}_{0.15}\text{CuO}_6$. Although the single phase at this composition has not been obtained yet, the most of the grains contain La as seen in the EELS spectrum of Fig. 2(a) where small peaks

corresponding to La $M_{4,5}$ on the large background of Ba $M_{4,5}$ are indicated by arrows. In the oxygen K-edge of Fig. 2(b), the peak at 528 eV is smaller than that of $Tl_2Ba_2Cu_1O_6$ shown in Fig. 1(a), indicating that the hole content decreases. We also observed similar behavior of the peak in the EELS spectra of quenched samples too. By replacing a part of Ba with La, the hole content decreases as observed in EELS and T_c increases as shown in Table I, so we may conclude that the holes in $Tl_2Ba_2Cu_1O_6$ are overdoped.

Figures 3(a), 3(b) and 3(c) indicate the EELS spectra of $Tl_1Ba_2Ca_{n-1}Cu_nO_{2n+3}$ ($n=2-4$) respectively. A peak at 528 eV was considered to correspond to the hole state and the position of the main peak indicated by a broken line shifts at higher energy with the increase of n as in the case of $Tl_2Ba_2Ca_{n-1}Cu_nO_{2n+4}$. It should be noted that the relative height of this peak to the main peak decreases with the increase of n ($n=2-4$) in $Tl_1Ba_2Ca_{n-1}Cu_nO_{2n+3}$. This result indicates that the hole content in $Tl_1Ba_2Ca_{n-1}Cu_nO_{2n+3}$ also decreases with the increase of n and well corresponds to values of the average hole content, $1/n$, estimated by assuming the ideal composition and formal valence state. It was recently shown that decreasing the hole content by replacing a small amount of Ca(+2) with Y(+3) in $Tl_1Ba_2Ca_1Cu_2O_7$, results in the increase of T_c , indicating the overdoping state of $Tl_1Ba_2Ca_1Cu_2O_7$ [21].

Figures 4(a) and 4(b) are schematic illustrations of the experimental conditions for the orientation dependency of momentum excitation in momentum space. By selecting the scattering vector k parallel to a^* with an objective aperture, the momentum transfer q is set to be nearly parallel to a^* under the condition of Fig. 4(a), whereas it is nearly parallel to c^* under that of Fig. 4(b). Figures 5(a) and 5(b) show the oxygen K-edge fine structures of $Tl_1Ba_2Ca_2Cu_3O_9$ under the two conditions corresponding to Figs. 4(a) and 4(b), respectively. The peak of the hole state disappears and only a small shoulder is observable under the condition where the direction of inner electron excitation is nearly parallel to the c -axis as shown in Fig. 4(b). The decrease of the peak directly indicates that the transition of the K-shell electron into the hole state near the Fermi energy is excited strongly in the a or b direction of Cu-O planes, but not in the c direction indicating the hole exists in the O $2p_{x,y}$ orbitals in the Cu-O planes. This conclusion shows close resemblance to the results recently obtained for $Bi_2Sr_2Ca_1Cu_2O_8$ [11,12].

In conclusion, the hole state in Tl-Ba-Ca-Cu-O was investigated by EELS. The average hole contents in both $Tl_2Ba_2Ca_{n-1}Cu_nO_{2n+4}$ ($n=1-3$) and $Tl_1Ba_2Ca_{n-1}Cu_nO_{2n+3}$ ($n=2-4$) decrease with the increase of n , although the origin of the supply of holes is different for each other. Holes in $Tl_2Ba_2Cu_1O_6$ and $Tl_1Ba_2Ca_1Cu_2O_7$ are overdoped. Most holes in Tl-Ba-Ca-Cu-O exist in the O $2p_{x,y}$ orbitals of 2-dimensional Cu-O planes.

Acknowledgments

The authors wish to thank Professors Y. Muto and M. Tachiki, Institute for Materials Research, and also Professor A. Kotani, Physics department of Tohoku University for their interest and discussion. They also thank Professor Sato, Purdue University, and Drs. T. Soga, K. Hojou, S. Furuno and H. Otsu, Japan Atomic Energy Research Institute for Experimental support for EELS study. The work was supported by a grant under the Monbusho International Scientific Research Program and a Grant-in-Aid for Scientific Research on Priority Areas "Mechanism of Superconductivity".

The EELS and EDX studies at Purdue University were supported by the Indiana Center for Innovative Superconductor Technology.

References

- [1] J. G. Bednorz and K. A. Muller: *Z. Phys.* B64 (1986) 189.
- [2] M. K. Wu, J. R. Ashburn, C. J. Torng, P. H. Hor, R. L. Meng, L. Gao, Z. J. Huang, Y. Q. Wang and C. W. Chu: *Phys. Rev. Lett.* 58 (1987) 908.
- [3] H. Maeda, Y. Tanaka, M. Fukutomi and T. Asano: *Jpn. J. Appl. Phys.* 27 (1988) L209.
- [4] Z. Z. Sheng and A. M. Hermann: *Nature* 332 (1988) 138.
- [5] A. Bianconi, M. De Santis, A. M. Flank, A. Fontaine, P. Lagarde, A. Marcelli, H. Katayama-Yoshida and A. Kotani: *Physica C* 153-155 (1988) 1760.
- [6] A. Bianconi, M. De Santis, A. Di Cicco, A. M. Flank, A. Fontaine, P. Lagarde, H. Katayama-Yoshida, A. Kotani and A. Marcelli: *Phys. Rev.* B38 (1988) 7196.
- [7] N. Nücker, J. Fink, B. Renker, D. Ewert, C. Politis, P. J. W. Weijs and J. C. Fuggle: *Z. Phys.* B67 (1987) 9.
- [8] P. E. Batson and M. F. Chisholm: *Phys. Rev.* B37 (1988) 635.
- [9] N. Nücker, J. Fink, J. C. Fuggle, P. J. Durham and W. M. Temmerman: *Physica C* 153-155 (1988) 119.
- [10] D. Shindo, K. Hiraga, M. Hirabayashi, M. Kikuchi, Y. Syono, S. Furuno, K. Houjou, T. Soga and H. Otsu: *J. Electron Microsc.* 38 (1989) 155.
- [11] F. J. Himpsel, G. V. Chandrashekhar, A. B. McLean and M. W. Shafer: *Phys. Rev.* B38 (1988) 11946.
- [12] N. Nücker, H. Romberg, X.X.Xi, J. Fink, B. Gegenheimer and Z. X. Zhao: *Phys. Rev.* B39 (1989) 6619.
- [13] H. Ihara, R. Sugise, M. Hirabayashi, N. Terada, M. Jo, K. Hayashi, A. Negishi, M. Tokumoto, Y. Kimura and T. Shimomura: *Nature* 334 (1988) 510.
- [14] M. A. Subramanian, J. B. Parise, J. C. Calabrese, C. C. Torardi, J. Gopalkrishnan and A. W. Sleight: *J. Solid State Chem.* 77 (1988) 192.
- [15] B. Morosin, D. S. Ginley, J. E. Shirber and E. L. Venturini: *Physica C* 156 (1988) 587.
- [16] S. Nakajima, M. Kikuchi, Y. Syono, T. Oku, D. Shindo, K. Hiraga, N. Kobayashi, H. Iwasaki and Y. Muto: *Physica C* 158 (1989) 471.
- [17] M. Kikuchi, N. Kobayashi, H. Iwasaki, D. Shindo, T. Oku, A. Tokiwa, T. Kajitani, K. Hiraga, Y. Syono and Y. Muto: *Jpn. J. Appl. Phys.* 27 (1988) L1050.
- [18] C. C. Torardi, M. A. Subramanian, J. C. Calafrese, J. Gopalkrishnan, K. J. Morrissey, T. R. Askew, R. B. Flippen, U. Chowdhry and A. W. Sleight: *Science* 240 (1988) 631.
- [19] S. S. Parkin, V. Y. Lee, A. I. Nazzari, R. Savoy, T. C. Hung, G. Gorman and R. Beyers: *Phys. Rev.* B38 (1988) 6531.
- [20] T. Suzuki, M. Nagoshi, Y. Fukuda, Y. Syono, M. Kikuchi, N. Kobayashi and M. Tachiki: *Phys. Rev.* B40 (1989) 5184.
- [21] S. Nakajima, M. Kikuchi, N. Kobayashi, H. Iwasaki, D. Shindo, Y. Syono and Y. Muto: *Proceeding of 2nd International Symposium on Superconductivity at Tsukuba, November 1989 Springer-Verlag, Tokyo, in press.*

Table I T_c of $Tl_2Ba_2Ca_{n-1}Cu_nO_{2n+4}$, $Tl_2Ba_{1.85}La_{0.15}Cu_1O_6$ and $Tl_1Ba_2Ca_{n-1}Cu_nO_{2n+3}$

Sample	T_c (K)
$Tl_2Ba_2Ca_{n-1}Cu_nO_{2n+4}$ $n=1$	0
$n=2$	98
$n=3$	114
$Tl_2Ba_{1.85}La_{0.15}Cu_1O_6$ $n=2$	55
$n=3$	78
$Tl_1Ba_2Ca_{n-1}Cu_nO_{2n+3}$ $n=3$	120
$n=4$	121

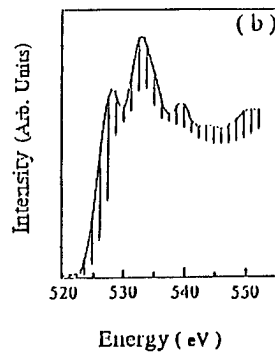
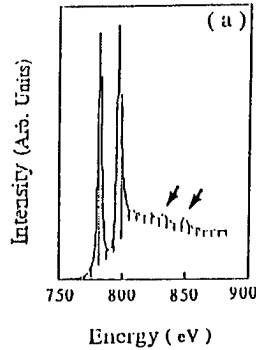


Fig. 2. EELS spectra of $Tl_2Ba_{1.85}La_{0.15}Cu_1O_6$ at energy ranges of 750-900 eV (a) and 520-555 eV (b). Small peaks of La M4,5 are indicated by arrows in (a).

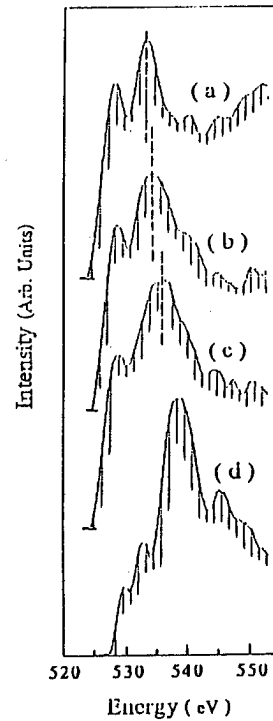


Fig. 1. Fine structures of oxygen K-edge spectra of $Tl_2Ba_2Ca_{n-1}Cu_nO_{2n+4}$ with $n=1$ (a), 2 (b) and 3 (c), and that of $Ca_{0.91}Sr_{0.09}CuO_2$ (d). The positions of the main peaks in the spectra of $Tl_2Ba_2Ca_{n-1}Cu_nO_{2n+4}$ are indicated by broken lines.

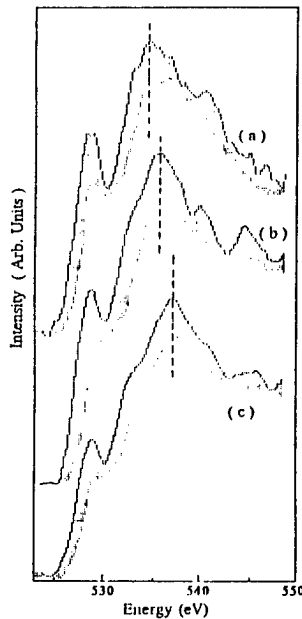


Fig. 3. Fine structures of oxygen K-edge spectra of $Tl_1Ba_2Ca_{n-1}Cu_nO_{2n+3}$ with $n=2$ (a), 3 (b) and 4 (c). The position of the main peak was indicated by a broken line.

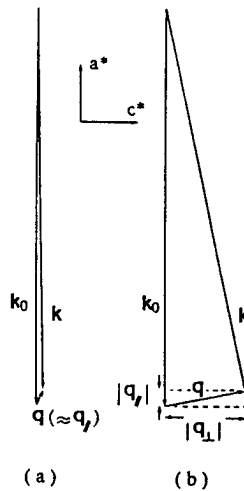


Fig. 4. Schematic illustration of the experimental conditions of the orientation dependency of the momentum transfer. k_0 and k correspond to the wave vectors of incident electron and scattered electron, respectively, and q is the momentum transfer. The parallel and transverse components of q are indicated by $q_{||}$ and q_{\perp} , respectively.

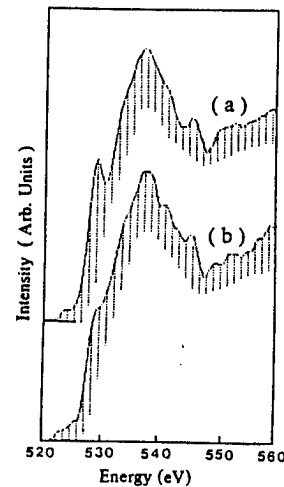


Fig. 5. Fine structures of oxygen K-edge spectra of $Tl_1Ba_2Ca_2Cu_2O_9$ under two conditions corresponding to Figs. 4 (a) and 4 (b), respectively.

Low-energy Electron Energy Loss Spectroscopy on $\text{Bi}_2\text{Sr}_2\text{Ca}_{n-1}\text{Cu}_n\text{O}_{2n+4+x}$ ($n=1,2$)
and Preparation of Thin Film Specimens by Molecular Beam Epitaxy

Atsushi ANDO, LIU Kuang-Yu and Atsushi KOMA

Department of Chemistry, The University of Tokyo
Bunkyo-ku, Tokyo 113, Japan

In-depth profiling of electronic structures of $\text{Bi}_2\text{Sr}_2\text{Ca}_{n-1}\text{Cu}_n\text{O}_{2n+4+x}$ ($n=1,2$) have been done with low-energy electron energy loss spectroscopy. The spectra are almost independent of probing depth, indicating rather extended electronic states of those materials. It has been also found out that the existence of Ca layer does not affect the spectra so much. A thin film specimen of $\text{Bi}_2\text{Sr}_2\text{CaCu}_2\text{O}_{8+x}$ has been grown on a MgO (100) substrate by molecular beam epitaxy, which has become superconducting after annealing in air.

Low-energy electron energy loss spectroscopy (LEELS) is a powerful method to investigate electronic structures in the wide energy range. It also gives informations on in-depth change of electronic structures, when the probing depth is changed by changing the incident electron energies [1]. In the present paper we will report its application to $\text{Bi}_2\text{Sr}_2\text{CaCu}_2\text{O}_{8+x}$ (abbreviated as BSCCO hereafter) and $\text{Bi}_2\text{Sr}_2\text{CuO}_{6+x}$

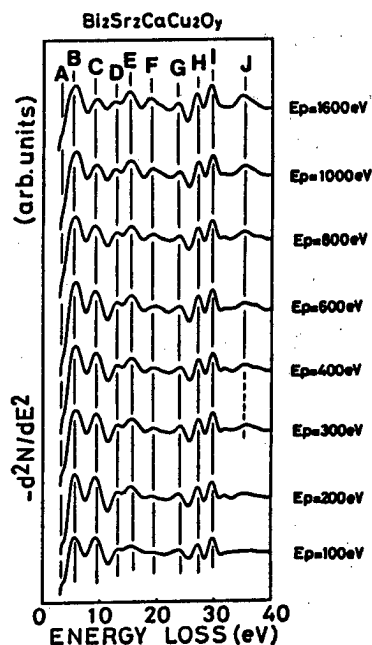


Fig. 1 LEELS spectra of $\text{Bi}_2\text{Sr}_2\text{CaCu}_2\text{O}_{8+x}$

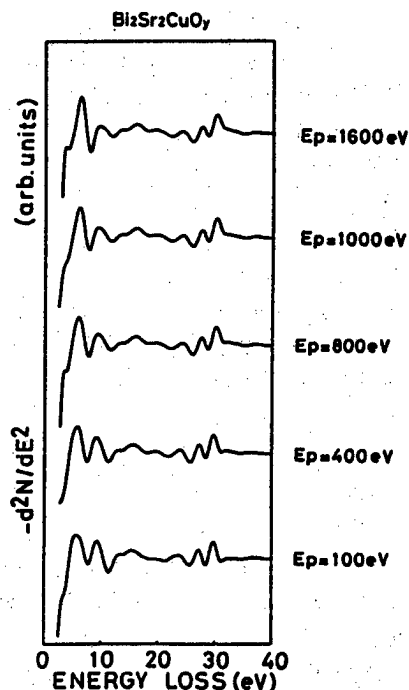


Fig. 2 LEELS spectra of $\text{Bi}_2\text{Sr}_2\text{CuO}_{6+x}$

(abbreviated as BSCO hereafter) to reveal their electronic structures. Clean surfaces were prepared by cleaving single-crystalline samples under the vacuum of 1×10^{-8} Pa. Cleanliness was checked by Auger electron spectroscopy just before LEELS measurements. Previously we have reported that the LEELS spectrum of $\text{YBa}_2\text{Cu}_3\text{O}_{7-y}$ is easily changed by the oxygen desorption from its surface at room temperature [2]. The LEELS spectra of BSCCO and BSCO, however, has not changed so much by the electron irradiation at room temperature. This indicates that the surface oxygen is much more stable in BSCCO and BSCO than in YBCO. Thus all the LEELS spectra shown below have been taken at room temperature. Figs. 1 and 2 show the LEELS spectra of BSCCO and BSCO, respectively. The incident electron energy was changed between 100 eV and 1600 eV to change the probing depth between 0.2 and 1.2 nm [1]. Since the BSCCO and the BSCO are cleaved between two Bi-O planes, the probing regions of LEELS for various incident electron energies will be the ones shown in Fig. 3 in the case of BSCCO. Nevertheless the observed spectra do not change so much when the incident electron energies are changed. This is much different from the case of mica, which has a layered crystal structure similar to BSCCO or BSCO and shows a distinct change in spectra for various incident energies [3]. Small dependence of LEELS spectra on incident electron energies indicates that the electronic structures of BSCCO and BSCO are rather extended and not so much localized as in the case of mica. The peaks observed in those spectra have been assigned as in the followings by taking into account of the results of XPS on BSCCO by Meyer et al. [4] and Zanoni et al. [5]. The prominent twin peaks H and I come from the excitations of Bi $5d_{5/2}$ and Bi $5d_{3/2}$ core electrons, respectively. Peak E comes from Bi 6s core electron excitation, whereas peak G arises from the Sr 4p core electron excitation. Peaks A to D seem to come from oxygen-derived shallow valence band electrons. The origin of the peak F is not clear at the present stage. The final states of those excitations are considered to be the

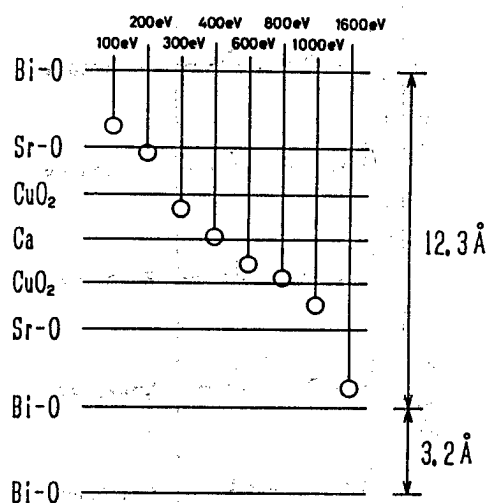


Fig. 3. Probing depth of LEELS

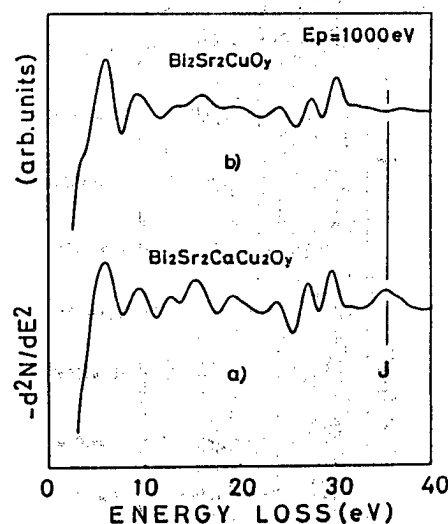


Fig. 4. Comparison of LEELS spectra of BSCCO(a) and BSCO(b).

first conduction band, of which maximum density of states is found to be located at around 3 eV above Fermi level by inverse photoemission [6]. Nearly the same peak assignment is possible for BSCO. The comparison of spectra of BSCCO and BSCO is made in Fig. 4. As is seen in the figure, their spectra are almost the same except the peak J. This shows that the electronic structures of BSCCO and BSCO are very similar to each other, which means that the Ca layer, which exists only in BSCCO, do not affect the overall electronic structure of BSCCO. The only distinct effect of the Ca layer in BSCCO are seen in peak J. It seems to be related with Ca-derived electronic states. It is very interesting to see the peak J can be seen in Fig. 1 only for incident electron energies larger than 300 eV, where probing depth exceeds the depth of Ca layer, as is seen in Fig. 3.

Recently various efforts have been devoted to prepare of thin film specimens of high- T_c superconductors both for the purpose of fundamental research and for the application purpose. So far several growth methods have been tried to get thin film specimens of good quality. Among them molecular beam epitaxy (MBE) seems to be useful to prepare thin film specimens of such high- T_c superconductor with a layered crystal structure as BSCCO, since one can control each layer with atomic-order precision and characterize the growing interface in situ by means of various electron spectroscopic methods. MBE, however, has a disadvantage for the growth of high- T_c superconductor films, because it is usually used under high vacuum atmosphere resulting in the oxygen deficiency in the prepared oxide superconductor films. Thus special care should be taken to promote oxygen atom inclusion into the grown film, if one uses MBE. We have made a few efforts for that purpose as is shown in the followings.

Fig. 5 shows a MBE system (Eiko EL-10), which was specially designed for the present purpose. The growth chamber consists of two differentially pumped rooms.

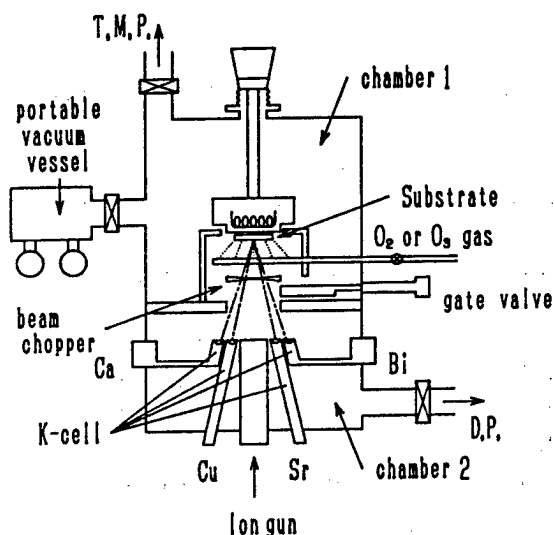


Fig. 5. MBE apparatus

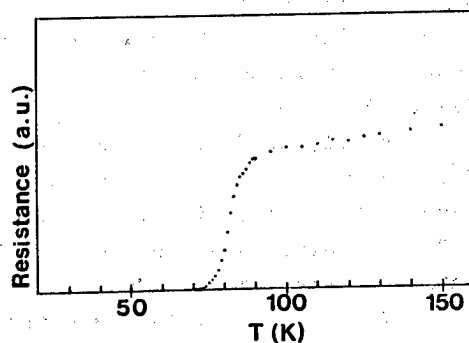


Fig. 6. Superconducting Characteristic of MBE grown film of BSCCO.

The oxygen gas is introduced through small holes on a ring located just below the sample holder. Then the oxygen pressure at the sample surface can be maintained higher than that in the source chamber by about two orders of magnitude. Knudsen cells are used for all sources of Bi, Sr, Ca and Cu. An ozonizer (Nihon Ozone OT-31RL-2) is placed in the oxygen supply line to promote the oxygen incorporation. The ion gun is also equipped to supply oxygen as active ions, but it was not used in the present experiment. BSCCO film was grown on a MgO (100) substrate at 650 °C with a growth rate of 0.05 nm/s. The as-grown film with about 300 nm thickness was not superconducting, and it was annealed at 880 °C for 5 h in air. After annealing the sample has become superconducting as is seen in Fig. 6. The critical temperature at mid-point is about 82 K. Now the growth condition is being adjusted to get as-grown superconducting film specimens. A portable vessel is being prepared to transport a grown sample into the other chamber equipped with AES-LEELS and XPS without exposing to the air [7]. Then in situ characterization of surface and interface of the grown film will become possible.

In conclusion, we have succeeded in growing thin films of BSCCO by MBE. In-depth profiling of electronic structures of BSCCO and BSCO have also been made successfully by LEELS. In the next step we are pursuing to connect both techniques. A specimen having a CuO₂ top layer, which seems to play an essential role in high-T_c superconductivity mechanism, will be prepared by MBE and its characteristic electronic structure will be made clear by in-situ LEELS measurement, which has a capability to show the electronic structure of a film as thin as a few tenths nm.

The authors thank Prof. S. Uchida for giving them single-crystalline samples of BSCCO and BSCO.

References

- [1] K. Yoshimura and A. Koma, Extended Abstracts of 1984 Intern. Conf. Solid State devices and Materials, Kobe, 1984, p.293.
- [2] A. Ando, K. Saiki, K. Ueno and A. Koma, Jpn. J. Appl. Phys. 27 (1988) L304.
- [3] S. Moore, H. Shimizu, A. Masuda, Y. Tadami and A. Koma, Jpn. J. Appl. Phys. 28 (1989) 2309.
- [4] H.M. Meyer III, D.M. Hill, J.H. Weaver, D.L. Nelson and C.F. Gallo, Phys. Rev. B38 (1988) 7144.
- [5] R. Zanon, Y. Chang, Ming Tang, Y. Hwu, M. Onellion, G. Margaritondo, P.A. Morris, W.A. Bonner, J.M. Tarascon and N.G. Stoffel, Phys. Rev. B38 (1988) 11832.
- [6] H. Ohta, T. Takahashi, K. Murata, H. Matsuyama, S. Suzuki, Y. Okabe and H. Katayama-Yoshida, Phys. Rev. B39 (1989) 39.
- [7] K. Ando, K. Saiki, Y. Sato, A. Koma, T. Asano, H. Ishiwara and S. Furukawa, Jpn. J. Appl. Phys. 27 (1988) L170.

Self-Interaction Correction to Local Spin Density Approximation in Solids

Y. Ishii and K. Terakura

Institute for Solid State Physics, University of Tokyo
7-22-1, Roppongi, Minato-ku, Tokyo 106, Japan

The local-spin-density approximation in the spin-density-functional formalism has a serious shortcoming that the self-interaction is not completely canceled out between the Hartree and the exchange-correlation terms. Although a correction for the self-interaction improves the results of the local-spin-density approximation for atoms significantly, such a prescription is not available for solids. Here the work by Svane and Gunnarsson for the Hubbard model is restudied with an aim of applying the method to more realistic cases.

The local-spin-density approximation (LSDA) has made a remarkable contribution in the elucidation of the electronic structures of solids. In particular, the cohesive properties of metals, semiconductors and insulators are well described even quantitatively [1,2]. This is, of course, due to the following fortunate facts: The cohesive properties are determined by the energetics of the ground state; The density functional formalism is concerned with the ground state properties; The total energy is a variationally guaranteed quantity. Besides, there are several examples indicating that LSDA can describe the single-particle excitation spectrum reasonably well. Therefore, the band-structure calculations based on LSDA are now regarded as the first step to the understanding of the new materials.

It turned out, however, that the applicability of LSDA is fairly limited for some classes of materials, where the electron correlation is strong. For example, LSDA cannot reproduce the antiferromagnetism of NiS and some high- T_c related materials like La_2CuO_4 [3,4]. LSDA may overestimate the hybridization of the neighboring orbitals to suppress the antiferromagnetism. One of the origins of this inconvenience may be traced back to the problem of self-interaction. As is well known, the self-interaction is absent in the Hartree-Fock (HF) approximation due to the cancellation between the Hartree and the exchange terms. However, the corresponding cancellation between the Hartree and the exchange-correlation terms in LSDA is not perfect. Nevertheless, the self-interaction does not produce any serious problem for the extended state because it vanishes as the system size goes to infinity. This is one of the reasons of the success of LSDA in the weakly correlated systems. On the other hand, the true eigenstate of the strongly correlated systems may have some localized character, for which the non-vanishing self-interaction in LSDA is a trouble. In fact, it was demonstrated for atoms that the correction for the self-interaction improves the results of LSDA significantly [5]. For solids, a

prescription of the self-interaction correction (SIC) has not been established and there has been no systematic studies on it.

Recently, Svane and Gunnarsson studied the one-dimensional Hubbard model in connection with LSDA and SIC-LSDA [6]. We are interested in this work, because despite the simplicity of the model itself their prescription of incorporating SIC to solids may be generalized to more realistic cases. As the details were not presented in their paper, we first tried to trace their calculations. Concerning the original one-dimensional Hubbard Hamiltonian

$$H = \sum_{\sigma} \left[\epsilon_0 \sum_{i=1}^N \hat{n}_{i\sigma} + t \sum_{i=1}^N (c_{i+1\sigma}^{\dagger} c_{i\sigma} + \text{h.c.}) \right] + U \sum_{i=1}^N \hat{n}_{i\uparrow} \hat{n}_{i\downarrow}, \quad (1)$$

with the periodic boundary condition $C_{N+1\sigma} = C_{1\sigma}$, they assumed a local-spin-density functional for the exchange-correlation energy density as

$$\epsilon_{xc}(n_{i\uparrow}, n_{i\downarrow}) = U(n_{i\uparrow} + n_{i\downarrow})^{1/3} [-a - b f(z_i)], \quad (2)$$

with

$$z_i = n_{i\uparrow} / (n_{i\uparrow} + n_{i\downarrow}), \quad (3)$$

$$f(z) = (1 - 2^{-1/3})^{-1} [z^{4/3} + (1 - z)^{4/3} - 2^{-1/3}]. \quad (4)$$

The total exchange-correlation energy is given by

$$E_{xc}^{\text{LSD}}[n_{i\sigma}] = \sum_i (n_{i\uparrow} + n_{i\downarrow}) \epsilon_{xc}(n_{i\uparrow}, n_{i\downarrow}). \quad (5)$$

Regarding $n_{i\sigma}$ as $n_{\sigma}(r)$ in the ordinary density functional theory in the continuous space, we can easily see the similarity in the functional form of eq.(2) to the corresponding one given by Barth and Hedin [7]. The parameters a and b in eq.(2) were determined by using LSDA results of a free H atom. The total energy in LSDA is given by

$$E_T^{\text{LSD}} = \sum_{\sigma} \left[\epsilon_0 \sum_{i=1}^N n_{i\sigma} + t \sum_{i=1}^N \langle c_{i+1\sigma}^{\dagger} c_{i\sigma} + \text{c.c.} \rangle \right] + \frac{1}{2} U \sum_i (\sum_{\sigma} n_{i\sigma})^2 + E_{xc}^{\text{LSD}}[n_{i\sigma}], \quad (6)$$

where $\langle \dots \rangle$ denotes an expectation value in the ground state. The third term of eq.(6) corresponds to the Hartree energy. Hereafter we consider only the half-filled case.

Now we introduce a unitary transformation such that

$$a_{\alpha\sigma} = \sum_i \xi_{i\alpha}^{\sigma*} c_{i\sigma}, \quad (7)$$

with

$$\sum_i \xi_{i\alpha}^{\sigma*} \xi_{i\alpha'}^{\sigma} = \delta_{\alpha\alpha'}. \quad (8)$$

Then

$$n_{i\sigma} = \langle c_{i\sigma}^{\dagger} c_{i\sigma} \rangle = \sum_{\alpha} f_{\alpha\sigma} \xi_{i\alpha}^{\sigma*} \xi_{i\alpha}^{\sigma}, \quad (9)$$

$$\langle c_{i\sigma}^\dagger c_{j\sigma} \rangle = \sum_{\alpha} f_{\alpha\sigma} \xi_{i\alpha}^{\sigma*} \xi_{j\alpha}^{\sigma}, \quad (10)$$

with the occupation number $f_{\alpha\sigma}$ given by

$$f_{\alpha\sigma} = \langle a_{\alpha\sigma}^\dagger a_{\alpha\sigma} \rangle. \quad (11)$$

We would like to point out the analogy of eq.(9) to the ordinary continuous space expression

$$n_{\sigma}(r) = \sum_{\alpha} f_{\alpha\sigma} |\varphi_{\alpha\sigma}(r)|^2, \quad (12)$$

where $\varphi_{\alpha\sigma}(r)$ is an eigenstate wave function.

The SIC is incorporated by subtracting the self-interaction associated with the orbital $(\alpha \sigma)$ in the Hartree and the exchange-correlation terms in eq.(6). The SIC term to the total energy is given by

$$\Delta E_{xc}^{SIC} = - \sum_{\alpha} \sum_{\sigma} \left\{ \frac{1}{2} U \sum_i [f_{\alpha\sigma} |\xi_{i\alpha}^{\sigma}|^2]^2 + E_{xc}^{LSD} [f_{\alpha\sigma} |\xi_{i\alpha}^{\sigma}|^2, 0] \right\}, \quad (13)$$

and the total energy with SIC is

$$E_T^{SIC} = E_T^{LSD} + \Delta E_{xc}^{SIC}. \quad (14)$$

The equation to determine $\xi_{i\alpha}^{\sigma}$ is obtained by minimizing E_T^{SIC} with a constraint of eq.(8):

$$\frac{\partial}{\partial \xi_{i\alpha}^{\sigma*}} \left[E_T^{SIC} - \sum_{\alpha'} \sum_{\alpha''} \epsilon_{\alpha'\alpha''}^{\sigma} \sum_j \xi_{j\alpha'}^{\sigma*} \xi_{j\alpha''}^{\sigma} \right] = 0. \quad (15)$$

Equation (15) can be expressed as

$$\sum_j (H_{\alpha\sigma})_{ij} \xi_{j\alpha}^{\sigma} = \sum_{\alpha'} \epsilon_{\alpha'\alpha}^{\sigma} \xi_{i\alpha'}^{\sigma}. \quad (16)$$

Not only the diagonal but also the off-diagonal Lagrange multipliers should be included in eqs.(15) and (16), because the effective one-electron Hamiltonian is orbital dependent so that the orthogonality between eigenstates are not guaranteed. It is not easy to solve eq.(16). Some details of the technical aspect may be described in our later publication.

After having reproduced most of the results in ref.6, we tried to understand the physical meaning of the off-diagonal Lagrange multipliers [8]. From eq.(6), $\epsilon_{\alpha\alpha'}^{\sigma}$ is the matrix element of $H_{\alpha\sigma}$ between $(\alpha \sigma)$ and $(\alpha' \sigma)$. As explained in ref.6, the state $(\alpha \sigma)$ becomes localized around the site i for $U \gg t$. In this sense, $\epsilon_{\alpha\alpha'}^{\sigma}$ may be regarded as a hopping integral and the eigen values of the matrix $\epsilon_{\alpha\alpha'}^{\sigma}$ may give us one-electron orbital energies. In Fig.1, we compare the energy dispersion curve obtained along this line with the corresponding ones in LSDA and also in HF approximation to the original Hamiltonian eq.(1). For both of $U/t = 4$ and 8, the dispersion curve of SIC-LSDA coincides with that of HF, while the result of LSDA deviates from both results significantly. Therefore the above process of obtaining the one-electron orbital energy seems to be meaningful. We take this an encouraging result as the first step towards

"beyond LSDA".

We are now studying the effect of hole or electron doping within the present model. We are also interested in applying SIC-LSDA to some realistic cases.

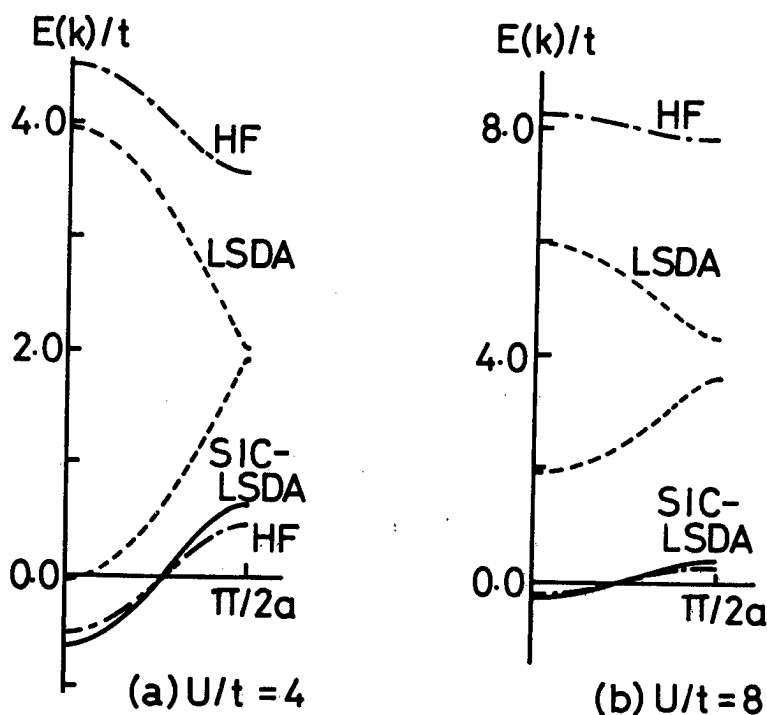


Fig.1 One-electron energy dispersion curves for one-dimensional Hubbard model. (a) for $U/t = 4$ and (b) for $U/t = 8$. The solid lines are for SIC-LSDA, chain lines for HF and the broken lines for LSDA.

References

1. V. L. Moruzzi, J. F. Janak and A. R. Williams, *Calculated Properties of Metals* (Pergamon, New York, 1978).
2. M. T. Yin and M. L. Cohen, *Phys. Rev. B* **26**, 5668 (1982).
3. A. Fujimori, K. Terakura, M. Taniguchi, S. Ogawa, S. Suga, M. Matoba and S. Anzai, *Phys. Rev. B* **37**, 3109 (1988).
4. K. T. Park, K. Terakura, T. Oguchi, A. Yanase and M. Ikeda, *J. Phys. Soc. Jpn.* **57**, 3445 (1988).
5. J. P. Perdew and A. Zunger, *Phys. Rev. B* **23**, 5048 (1981).
6. A. Svane and O. Gunnarsson, *Phys. Rev. B* **37**, 9919 (1988).
7. U. von Barth and L. Hedin, *J. Phys. C* **5**, 1629 (1972).
8. M. R. Pederson and C. C. Lin, *J. Chem. Phys.* **88**, 1807 (1988).

Nature of Doped Electrons in $\text{Nd}_{2-x}\text{Ce}_x\text{CuO}_4$: Electronic Band Structures of Nd_2CuO_4 Type M_2CuO_4 ($\text{M}=\text{La}$, Ce and Th)

Katsuhiko TAKEGAHARA and Tadao KASUYA

Department of Physics, Tohoku University, Sendai 980, Japan

One-electron energy band structures for La_2CuO_4 , Ce_2CuO_4 and Th_2CuO_4 with the Nd_2CuO_4 type crystal structure were calculated by the self-consistent APW method with the local density approximation. The bonding-antibonding splitting between the Cu $3d(x^2-y^2)$ and O $2p$ states on the CuO_2 plane makes a pair of subbands. In La_2CuO_4 , the Fermi energy cuts the middle of antibonding band resulting in the half-filled band. By replacing La with tetravalent Th, the Cu $3d$ states raise due to the increase in the number of Cu $3d$ electron but the bonding band made from Th $6d(3z^2-r^2)$ state falls down. In Ce_2CuO_4 , the Fermi energy cuts the bottom of $4f$ bands. To raise the $4f$ states, a correction is introduced to the Ce potential and then Ce becomes nearly tetravalent resulting in similar band structure to that of Th_2CuO_4 . By considering the strong correlation in the Cu $3d(x^2-y^2)$ state, the doped electrons in $\text{Nd}_{2-x}\text{M}_x\text{CuO}_4$ ($\text{M} = \text{Ce}, \text{Th}$) are thought to be injected into the M $d(3z^2-r^2)$ bonding band.

1. Introduction

Recently, the electron-doped systems $\text{Nd}_{2-x}\text{Ce}_x\text{CuO}_4$ and $\text{Nd}_{2-x}\text{Th}_x\text{CuO}_4$ were found to be a high T_C superconductor [1,2]. This finding may give an important key for the mechanism of high T_C superconductivity because all of the high T_C Cu oxides so far discovered were the hole-doped system. Various spectroscopic studies have been performed in order to clarify the nature of doped electrons. From the x-ray absorption studies, it was shown that the doped electrons are injected into the Cu $3d$ orbitals [3] or a band [4]. On the contrary, from the photoemission spectroscopy, it was suggested that the doped electrons go into the Cu $4s$ orbitals [5]. In this context, the nature of doped electrons is still an open question.

In the previous paper [6], we reported the result of the self-consistent APW band calculation for Nd_2CuO_4 type La_2CuO_4 instead of Nd_2CuO_4 . This is because, for the stable trivalent rare earth compounds, the electronic band structure of corresponding La compound is the same as that of these compounds except for the $4f$ bands position and is better to see the band structure near the Fermi level. Except for the $4f$ band, overall feature of our result on La_2CuO_4 is the same to that of Massidda et al. [7] on Nd_2CuO_4 in which the $4f$ states are treated as the core state. In this paper, we performed the band calculation for the typical tetravalent Th system, Th_2CuO_4 , and the nearly tetravalent Ce system, Ce_2CuO_4 , in order to investigate the effect of the partial replacing of Th or Ce for Nd on the band structure in the vicinity of the Fermi energy. Furthermore, to compare with the typical trivalent system, we performed the re-calculation of La_2CuO_4 with the exactly same condition of numerical computation for Ce and Th systems.

2. Method of calculation

The Nd_2CuO_4 type crystal structure is the body centered tetragonal [8]. The space group is $I4/mmm$ with Nd in $4e$: $(0,0,\pm 0.3513)$, Cu in $2a$: $(0,0,0)$, O1 in $4c$: $(1/2,0,0)$, and O2 in $4d$: $(1/2,0,1/4)$. Note that in the K_2NiF_4 type structure, O2 is in $4e$: $(0,0,\pm 0.182)$. The lattice constants used in the calculations are those observed for Nd_2CuO_4 ; $a = 3.945 \text{ \AA}$ and $c = 12.171 \text{ \AA}$.

The present band calculation is based on the APW method with muffin-tin approximation. The muffin-tin sphere radius of both O1 and O2 is chosen to be 0.8 \AA . Then the muffin-tin radii of Cu and $\text{M}(\text{M}=\text{La}, \text{Ce}, \text{Th})$ are chosen to be the maximum possible values in which the Cu and O1 spheres contact each other and the M and O2 spheres also contact each other. To improve the muffin-tin approximation, we introduce appropriate empty spheres (ES) at $4e$: $(0,0,\pm 0.1611)$. This position and the muffin-tin radius of ES are determined in such a way that the empty sphere contacts with both M and Cu spheres. Then we obtain the following values for muffin-tin radii: $1.526 \text{ \AA}(\text{M})$, $1.173 \text{ \AA}(\text{Cu})$ and $0.788 \text{ \AA}(\text{ES})$. The total muffin-tin spheres occupy 52 % of the unit cell volume. Other details of the method of self-consistent APW calculation are same as those described in the previous paper [6].

3. Energy band structure for La_2CuO_4 (LCO)

Present method of calculation differs from that of the previous paper [6] in the following points; 1) in this paper we use the empty sphere approximation and 2) the muffin-tin sphere radius of O is 0.11 Å smaller than that used in the previous paper and thus the muffin-tin radii of La and Cu become 0.11 Å larger so that to get better information for the d states in La and Cu. However, both methods of calculation give the very similar results and thus the above differences in method do not introduce the large discrepancy in the band structure.

Figure 1 shows the result of present calculation for the energy band structure along the principal symmetry axes in the BZ. In the figure, the tightly bound La 5p and O 2s bands are not shown but the average energy levels are followings, La 5p at -0.61 Ry, O1 2s at -0.85 Ry and O2 2s at -0.84 Ry. The lower 17 bands (from the X_1 state at -0.07 Ry to the X_4 state at 0.53 Ry) consist of the Cu 3d and O 2p states. The narrow bands at about 0.77 Ry are derived primarily from La 4f states. Between the 17 band complex and the 4f bands, there are two bands. In the previous paper, these two bands are separated from the 4f bands causing a gap. In the present calculation, these two bands and the 4f bands overlap slightly.

The charge distribution of the lowest X_1 state is as follows; La d 2 %, Cu s 19 %, Cu d 7 %, O1 p 39 % and O2 p 1 %. Thus this state is the Cu 4s and O1 2p bonding band and the corresponding antibonding state at the X point lies at 1.19 Ry. At the Γ point the Cu 4s state is located at 1.07 Ry. The third band (the X_4 state at 0.04 Ry) and the 17th band of X_4 state are the pair of bonding-antibonding bands between the Cu 3d(x^2-y^2) and O1 2p states on the CuO_2 plane with 0.50 Ry of the splitting width. The charge distribution of the antibonding X_4 state is listed in Table I. The antibonding band is half filled and the Fermi energy E_F cuts the middle of the band at 0.3787 Ry. The 18th band is one of possible states into which the doped electrons are injected. Thus the charge distribution of the Γ_1 and $X_{3'}$ states is listed in Table I. Both states have about 40 % of component in the outer region of muffin-tin spheres but the relatively dominant state in the rest of components is Cu s state for Γ_1 and La d($3z^2-r^2$) state for $X_{3'}$. Table II lists the number of valence electrons of given symmetry within each muffin-tin sphere. Note that in Table II the contributions from the tightly bound La 5p and O 2s bands are included.

4. Energy band structure for Th_2CuO_4 (TCO)

The calculated results for the energy band structure is shown in Fig. 2 in which the Th 6p and O 2s bands are not shown. The average energy levels are as follows; Th 6p at -0.60 Ry, O1 2s at -0.71 Ry and O2 2s at -0.79 Ry. Note that the 2s levels of O1 and O2 are in inverse order as compared with those of LCO because of the change of the Madelung potential. From Table II, the value of effective positive charge at the Th muffin-tin sphere is $10 - 7.424 = 2.576$ while that at La site is $9 - 7.064 = 1.936$. Furthermore, the Th-O2 nearest neighbour distance is 2.326 Å, 0.351 Å shorter than the Th-O1 distance.

The Th 5f bands lie at about 0.9 Ry and have about 1.5 times wider band width than the La 4f band width because the Th 5f state is more extended. As shown in Table II, the number of 5f electron in the Th muffin-tin sphere is 0.6 per atom and is about twice of La 4f electron. However, the most of them is not the atomic f character and thus the Th atom is considered to be tetravalent and the La atom trivalent. Therefore, the Th 6d($3z^2-r^2$) state falls down due to the intra-atomic Coulomb attraction and also due to the inter-atomic Coulomb interaction because the inter-atomic distance between the Th atoms placed at both sides of CuO_2 plane, Th(0,0,z) and Th(0,0,1-z), is short, 3.620 Å, with $z = 0.3513$. Note that the second nearest inter-atomic distance is 3.723 Å between Th(0,0,z) and Th(1/2,1/2,1/2-z) and the third one is 3.945 Å between Th(0,0,z) and Th(1,0,z). On the other hand, the Cu 4s state in the 18th band, the Γ_1 state, shows very little shift because the Cu 4s component decreases but the Cu 3d component increases as shown in Table I.

Two extra valence electrons per formula unit raise the Fermi energy; $E_F = 0.6936$ Ry. Thus, as shown in Table II, the number of d electron in the Cu muffin-tin sphere increases by 0.065 per atom resulting to raise the Cu 3d states, especially the Cu 3d(x^2-y^2) state, the Γ_2 and Z_2 states at 0.51 Ry, due to the intra-atomic Coulomb interaction. The four bands from the Γ_1 state at 0.43 Ry to the Γ_5 state at 0.44 Ry have the Cu 3d character other than the 3d(x^2-y^2) character. They are also shifted up but not so much compared with the 3d(x^2-y^2) state because of the different inter-atomic Coulomb effect. The lower 12 bands are mainly of the O 2p character and there is a gap between the 12th and 13th bands. As the Cu 3d(x^2-y^2) state is raised, the Cu 3d(x^2-y^2) and O1 2p antibonding band shifts up and the Cu 3d component in the X_4 state increases as shown in Table I. As the result, the antibonding band separates from the lower bands. However, the bonding-antibonding splitting width at the X point does not change compared with that of LCO.

Finally we investigated the mixing between the Cu 3d(x^2-y^2) and O1 2p antibonding band and the Th 6d($3z^2-r^2$)

band. At the symmetry axes and the symmetry planes ($k_z = 0$ plane and $k_x = k_y$ plane), these two bands are of the different irreducible representations and thus there is no mixing between two bands. Then we performed the band calculation at the general points; along $k = (1/2, k_y, 1/4)$, $0 \leq k_y \leq 1/2$. Even though these two bands should not intersect by the group theory, we can not find a definitive crossing gap. This means that the mixing between two bands is very small and thus the crossing gap is less than 0.0005 Ry judged from uncertainty in our band calculation.

5. Energy band structure for Ce_2CuO_4

5.1. Case 1: Standard APW method (CCO-1)

At first, we performed the band calculation using the standard APW method, the same as those for LCO and TCO. The calculated results for the energy band structure is shown in Fig. 3. In various trivalent Ce compounds, the electronic band structure is very similar to that of corresponding La compound except for the 4f band position. However, the calculated result as shown in Fig. 3 is different from that of LCO; especially the Cu 3d(x^2-y^2) and O1 2p antibonding band separates from the lower bands. This is because the number of 3d electron in the Cu muffin-tin sphere increases by 0.058 per atom as compared with that of LCO. This situation is essentially the same as that for TCO. The average energy levels of tightly bound Ce 5p and O 2s bands are followings, Ce 5p at -0.76 Ry, O1 2s at -0.83 Ry and O2 2s at -0.87 Ry. The order of 2s levels of O1 and O2 is the same to that of TCO, but the splitting width of levels is about a half of that for TCO because the value of effective positive charge at the Ce site is $10 - 8.008 = 1.992$.

These situations mean that the feature of band structure is very similar to that of TCO. However, the narrow Ce 4f bands shift down and cross the Cu 3d(x^2-y^2) and O1 2p antibonding band. The Fermi level cuts the bottom of the 4f band, $E_F = 0.4927$ Ry, and thus the number of f electron in the Ce muffin-tin sphere increases to be 1.1 per atom. As the result, the Ce 4f component increases in the Γ_1 and $X_{3'}$ states as shown in Table I. It is well known that the calculated f band based on the local density approximation is too close to the Fermi energy due to inadequate treatment of the self-interaction term. Thus, we considered this correction in the next subsection.

5.2. Case 2: Potential correction for Ce atom (CCO-2)

There are various ways to treat the self-interaction problem. In the present paper, to raise the 4f levels, we simply added an extra potential V_{corr} to the Ce potential calculated by the local density approximation. We write V_{corr} as a biquadratic expression of the radial variable r and determine the coefficients by the following conditions. 1) V_{corr} has a maximum value V_0 at $r = 0.458$ Å which is the peak position of the 4f charge density for the trivalent Ce ion. 2) At the muffin-tin sphere radius, $r = r_{MT}$, V_{corr} has a negative value V_1 . 3) $V_{corr} = 0$ at $r = 0.916$ Å. 4) Average potential is zero; $\int_0^{r_{MT}} V_{corr} r^2 dr = 0$. Then we set $V_0 = 0.8$ Ry and $V_1 = -0.2$ Ry and performed the self-consistent calculation.

Figure 4 shows the energy band structure. Due to the extra potential V_{corr} , the Ce 4f bands raise while the Ce 5d states fall down and the Ce 5d($3z^2-r^2$) component increases at the Γ_1 and $X_{3'}$ states as shown in Table I. The energy of $X_{3'}$ state decreases but that of the Γ_1 state decreases only slightly. The number of f electron in the Ce muffin-tin sphere decreases to be 0.79 per atom corresponding to the tetravalent state judged from the results of various other Ce compounds. The Fermi energy is located at 0.5328 Ry.

The Cu 3d states raise and thus the gap appears again between the 12th and 13th bands. However, the splitting width of the bonding-antibonding bands between the Cu 3d(x^2-y^2) and O1 2p states does not change. As the effective positive charge at the Ce site increases to be $10 - 7.918 = 2.082$, the splitting width of the tightly bound O 2s bands increases; O1 2s at -0.82 Ry and O2 2s at -0.88 Ry. The Ce 5p band is located at -0.80 Ry.

6. Discussions

It is well known that the energy dispersion of the usual band calculation has no significant physical meaning but it can reproduce the one particle Green's function, which is observed by the photoemission measurement, for example, fairly well for the weakly correlated systems. It is also well known that, for the strongly correlated system, a proper treatment of correlation, namely the intra-atomic Coulomb interaction, is essentially important and the CuO_2 type high T_C materials belong to this class. Therefore, to get proper informations on the system which we have treated here, some modifications due to the strong correlation, in particular on Cu 3d(x^2-y^2) state, is necessary. Roughly speaking, there are two main modifications. Firstly, the 3d(x^2-y^2) state is shifted up while other 3d states shifted down relatively to O 2p states. Secondly, the bonding and antibonding Cu 3d(x^2-y^2)-O 2p σ bands change character to the lower and upper

Hubbard bands of $d(x^2-y^2)$. By these modifications, the top of the filled bands becomes O $2p\sigma$ bands and the bottom of the upper Hubbard band is expected to be about 2 eV above that, namely a little bit below the position of X_4 state, in La_2CuO_4 . Therefore the X_3 and Γ_1 states are thought to be not the bottom of the unoccupied bands. An isolated Th impurity is thought to be not sufficient to bring the Th $6d(3z^2-r^2)$ state to the bottom. However, the pair of Th to form the bonding $6d(3z^2-r^2)$ state, or their cluster, is thought to bring the bonding band below the Cu $d(x^2-y^2)$ state judging from the present calculation on Th_2CuO_4 . The same thing is expected for the Ce substitution. Therefore the main carrier in $\text{Nd}_{2-x}\text{Ce}_x\text{CuO}_4$ for $x \sim 0.15$ is thought to be of the bonding Ce $5d(3z^2-r^2)$ band.

It is important to note that the mixing of the bonding Ce $5d(3z^2-r^2)$ band with Cu $3d(x^2-y^2)$ and O $2p\sigma$ states is very weak due to the symmetry. In the actual crystal, however, due to random substitution of Ce^{4+} , the symmetry breaking occurs and a moderate amount of mixing is expected. Then the situation is very similar to the Ce, or more precisely Yb, compounds and the dense Kondo behavior is expected. Actually, Date et al. found recently a typical dense Kondo behavior of resistivity in the normal state under high magnetic field [9]. More works are, of course, necessary to confirm the present picture.

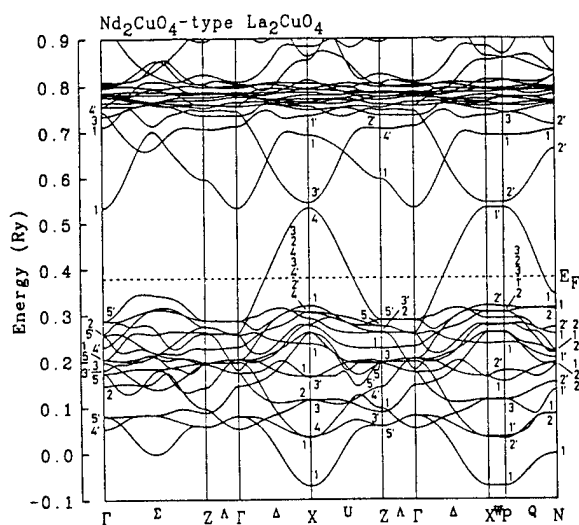


Fig. 1. Self-consistent APW energy band structure for La_2CuO_4 .

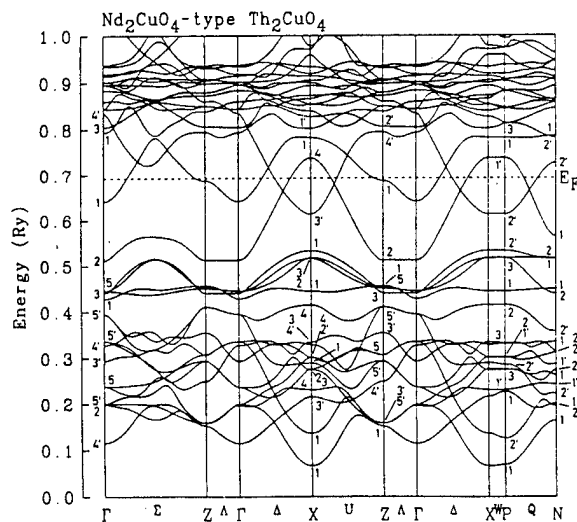


Fig. 2. Self-consistent APW energy band structure for Th_2CuO_4 .

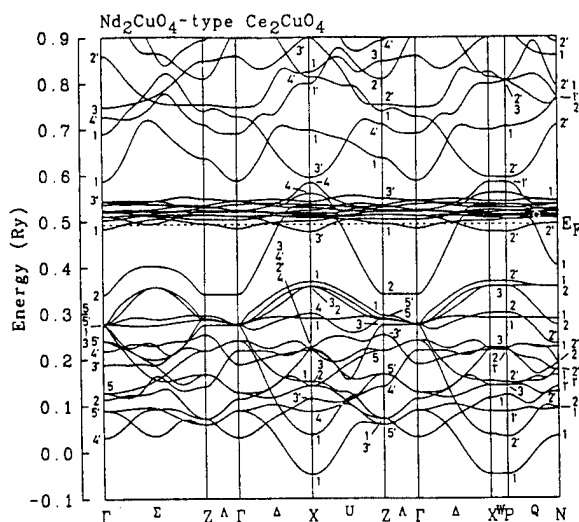


Fig. 3. Self-consistent APW energy band structure for Ce_2CuO_4 (case 1).

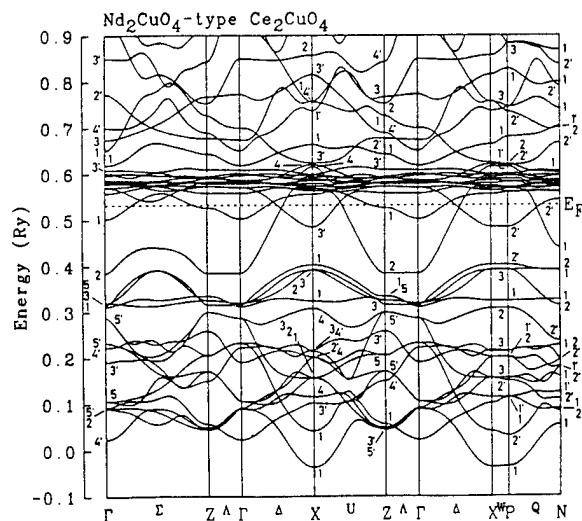


Fig. 4. Self-consistent APW energy band structure for Ce_2CuO_4 (case 2) with potential correction for Ce.

References

- 1) Y. Tokura, H. Takagi and S. Uchida: Nature **337** (1989) 345. H. Takagi, S. Uchida and Y. Tokura: Phys. Rev. Lett. **62** (1989) 1197.
- 2) J. T. Markert and M. B. Maple: Solid State Commun. **70** (1989) 145.
- 3) J. M. Tranquada, S. M. Heald, A. R. Moodenbaugh, G. Liang and M. Croft: Nature **337** (1989) 720.
- 4) E. E. Alp, S. M. Mini, M. Ramanathan, B. Dabrowski, D. R. Richards and D. G. Hinks: Phys. Rev. **B40** (1989) 2617.
- 5) A. Fujimori, Y. Tokura, H. Eisaki, H. Takagi, S. Uchida and E. Takayama-Muromachi: Phys. Rev. **B** (in press).
- 6) K. Takegahara and T. Kasuya: Solid State Commun. **70** (1989) 637.
- 7) S. Massidda, N. Hamada, J. Yu and A. J. Freeman: Physica **C157** (1989) 571.
- 8) HK. Müller-Buschbaum and W. Wollschläger: Z. anorg. allg. Chem. **414** (1975) 76.
- 9) M. Date: private communication.

Table I. Energies and charge distributions of the Γ_1 , X_3 and X_4 states as mentioned in the text for La_2CuO_4 (LCO), Ce_2CuO_4 case 1 (CCO-1) and case 2 (CCO-2), and Th_2CuO_4 (TCO). Components are shown in per cent and the minus sign (-) means that the state is not generated by the symmetry.

	Energy (Ry)	Outer region	M spheres				Cu sphere			O1 spheres		O2 spheres		ESs	
			s	p	d	f	s	p	d	s	p	s	p	s	p
Γ_1 state															
LCO	0.5324	41	3	0	10	6	16	-	9	6	-	2	-	5	0
CCO-1	0.4836	14	1	0	6	65	3	-	8	1	-	0	-	1	0
	0.5873	27	3	0	7	32	12	-	8	5	-	2	-	3	0
CCO-2	0.5027	24	1	0	22	30	3	-	15	2	-	0	-	1	0
	0.6187	11	1	0	12	67	3	-	3	1	-	1	-	1	0
TCO	0.6418	33	3	0	11	11	7	-	25	5	-	1	-	3	0
X_3 state															
LCO	0.5435	41	1	0	17	10	-	9	-	-	-	-	14	7	0
CCO-1	0.4770	21	0	0	10	59	-	4	-	-	-	-	3	3	0
	0.5954	22	1	0	14	40	-	4	-	-	-	-	14	3	0
CCO-2	0.4854	31	1	0	20	27	-	5	-	-	-	-	10	5	0
	0.6243	8	1	0	8	71	-	1	-	-	-	-	9	1	0
TCO	0.6135	43	1	0	17	12	-	8	-	-	-	-	11	7	0
X_4 state															
LCO	0.5321	7	-	-	0	0	-	-	47	-	46	-	0	-	-
CCO-1	0.5842	6	-	-	0	0	-	-	52	-	41	-	0	-	-
CCO-2	0.6158	5	-	-	0	2	-	-	54	-	38	-	0	-	-
TCO	0.7377	5	-	-	0	0	-	-	57	-	38	-	0	-	-

Table II. Number of valence electrons within the muffin-tin spheres.

		La_2CuO_4	Ce_2CuO_4		Th_2CuO_4
			Case 1	Case 2	
Charge content within the muffin-tin spheres (per atom)					
M	s	0.139	0.135	0.143	0.145
	p	5.825	5.898	5.891	5.785
	d	0.727	0.804	1.021	0.817
	f	0.304	1.104	0.793	0.600
	total	7.064	8.008	7.918	7.424
Cu	s	0.348	0.326	0.343	0.365
	p	0.298	0.338	0.331	0.368
	d	9.071	9.129	9.146	9.136
	total	9.775	9.853	9.878	9.927
O1	s	1.538	1.536	1.539	1.536
	p	3.414	3.403	3.383	3.413
	total	4.959	4.949	4.933	4.961
O2	s	1.542	1.547	1.545	1.548
	p	3.541	3.502	3.492	3.578
	total	5.090	5.056	5.044	5.136
ES	s	0.055	0.069	0.074	0.110
	p	0.024	0.023	0.024	0.027
	total	0.085	0.098	0.104	0.144
Outer region (per F.U.)					
		8.830	8.925	9.124	9.744
Total charge (per F.U.)					
		53.0	55.0	55.0	55.0

J. Kanamori, T. Nishino and M. Takahashi

Department of Physics, Faculty of Science, Osaka University
Machikaneyama 1-1, Toyonaka, Osaka 560

The ground state of Cu-O and Ni-O systems is investigated by calculating the wave function for finite size clusters containing more-than-one cations with periodic boundary conditions. In the case of the Cu-O system the electronic structure and correlation of the CuO_2 plane with apex oxygens is investigated by calculating the ground state wave function of a Cu_4O_{12} cluster. The cluster is the smallest among those taking account of the electron transfer between CuO_5 units with the translational invariance of the CuO_2 plane. When extra holes are introduced, they have amplitudes on all the atoms including the apex oxygens unlike the case of a single CuO_5 cluster. No appreciable spin correlation between the apex oxygen p_z orbital and Cu $d(x^2 - y^2)$ is found. Spin correlations between other pairs of orbitals and spin and charge fluctuations of a CuO_5 cluster are also examined. In the case of the Ni-O system the change from the state corresponding to the insulating phase with well developed magnetic moment of Ni to the state corresponding to the nonmagnetic phase with either decreasing the charge transfer energy between Ni and O or decreasing the intraatomic coulomb energy of Ni is investigated by use of a simplified model. It is found that the system makes a transition from the insulating state to an intermediate state where the magnetic correlation between Ni atoms is drastically decreased while retaining a finite atomic magnetic moment.

§1. Cu-O System

The p-type oxide high T_c superconductors so far known possess the CuO_2 planes on which each Cu atom are surrounded pyramidally by four in-plane oxygen atoms and an extra one at the apex site; in the case of the prototype of them, Ba-La-Cu-O system, they are surrounded octahedrally. Those recently found Tl-Ba-Ca-Cu-O and Bi-Sr-Ca-Cu-O systems possess another kind of the CuO_2 planes with Cu atoms surrounded only by four in-plane oxygen atoms without the apex ones. Since T_c as function of the number of the latter kind of the CuO_2 planes decreases after passing a maximum, we may assume that the pyramidal planes are primarily responsible for the superconductivity.

We carried out a calculation of the ground electronic state of a model of the pyramidal plane which corresponds to four pyramids sharing the in-plane oxygens. Details of it have been published already.[1] The ground states of the system with and without extra holes are investigated. The electronic structure of the pyramidal plane has been discussed so far with the models in which a single Cu atom is taken into account. The primary purpose of the present investigation is to elucidate the effect of the hole itinerancy on the electronic structure.

We employ a Cu_4O_{12} cluster, which may contain 4 or 6 holes. (Fig. 1) We confine ourselves to twenty atomic orbitals shown in Fig. 2, that is, eight $\text{Cu } d_y$ orbitals, eight p_σ orbitals of in-plane oxygen atoms and four p_z orbitals of apex oxygen atoms. We take into account the electron (hole) transfer among $\text{Cu } d_y$ and oxygen p orbitals in the LCAO scheme, assuming the same transfer parameters as in Fujimori's single cluster calculation, in-plane $(pp\sigma)=0.5\text{eV}$, $(pd\sigma)=-1.35\text{eV}$, and $(pdm) \propto R^{-3.5}$, $(ppm) \propto R^{-2}$ with 1.23 for the ratio between the off-plane and in-plane Cu-O [2]. Coulomb and exchange interactions between $\text{Cu } d(x^2 - y^2)$ and $d(3z^2 - r^2)$ orbitals are treated exactly; $J=5.3\text{eV}$ and $K=0.8\text{eV}$ are assumed. The coulomb self-energy of the oxygen p orbitals U_p and that of $\text{Cu } d$ orbitals U_d are taken to be 3.0eV and 6.0eV , respectively. There are two remaining parameters $\Delta_{p\sigma}$ and Δ_{pz} which are the charge transfer energies defined by the difference of the one-hole energies between the in-plane or apex oxygen p orbitals and the $\text{Cu } d_y$ orbitals. Since the value of $\Delta_{p\sigma}$ has not been well established yet, we vary it from 0.5eV to 2.5eV with the result that no qualitative change of the ground state is found. The parameter Δ_{pz} is varied within the range $0.0\text{eV} < \Delta_{pz} < \Delta_{p\sigma}$. Since the Hamiltonian conserves the total spin of the system, we investigate the ground state with zero total S_z . The calculation is carried out by use of the Lanczos method.

Deferring details to the publication [1] we summarize the conclusions. We find the hole occupancy of the order of 0.1 per orbital in the p_z of the apical oxygens in the absence of extra holes, i.e. in the case of 4 holes in the system and about 0.2 in the case two extra holes (six holes in the system); the holes in the p_z orbital have no appreciable spin correlation with those in $\text{Cu } d$ orbitals. When extra holes are added, they distribute rather evenly among all the orbitals taken into account in the calculation. Two third of them enter in the oxygen orbitals. It seems to be rather difficult to deduce a simple model such as the t - J model from the present calculation. We discuss in future publication the XAS and XPS on the basis of the present analysis.

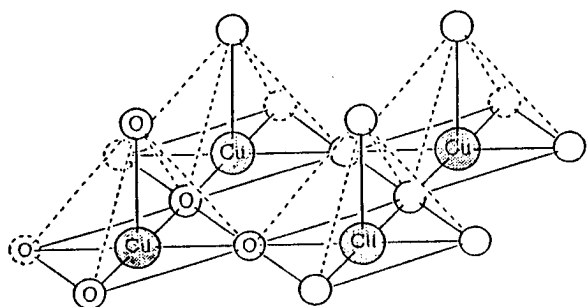


Fig. 1 A Cu_4O_{12} cluster used in the calculation. Large and small spheres denote Cu and oxygen atoms respectively. Periodic boundary conditions are imposed for both directions in the a - b plane.

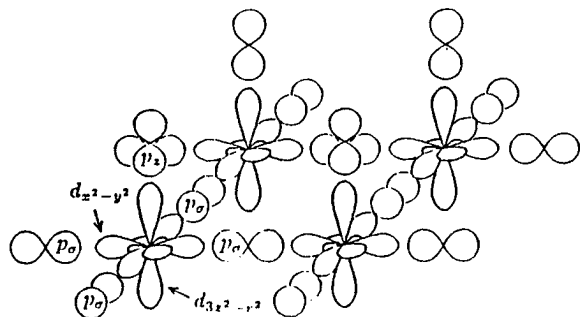


Fig. 2 The atomic orbitals in the Cu_4O_{12} cluster. We treat only the oxygen p orbitals that are σ bonded to the $\text{Cu } d_y$ orbitals.

§2. Ni-O System

NiO was a classical example of the Mott-Hubbard insulator, where the energy cost U required to produce $\text{Ni}(d^7)$ and $\text{Ni}(d^9)$ from two $\text{Ni}(d^8)$ was supposed to suppress the itinerancy of d electrons. However, it has been pointed out first by Fujimori [3] and discussed later more generally by Sawatzky and Allen [4] that the charge transfer energy Δ involved in the process $\text{Ni}(d^8) \rightarrow \text{Ni}(d^9)L$ with L representing a hole in the ligand and replaces U in the discussion of the metal-insulator transition of Ni compounds with the situation that Δ is generally smaller than U . If Δ is sufficiently small, we expect that d electrons are delocalized and Ni atoms will lose their magnetic moment. In fact NiS which is insulating and antiferromagnetic with the atomic moment of about $1.7\mu_B$ at low temperatures becomes metallic at high temperatures or under high pressure; the metallic phase is not antiferromagnetic, though the absence or presence of the atomic moment is not easy to conclude from the susceptibility measurement.

The photoemission experiment on NiS yields the result that the overall spectra do not change appreciably at the metal-insulator transition. [5] It has been discussed by Terakura [6], for example, that we should expect a more conspicuous change of the photoelectron spectra between the nonmagnetic metallic phase and the antiferromagnetic state in the band structure calculation. This apparent discrepancy is one of the motivation of the present study. Another motive is the possibility of the high T_c superconductivity in Ni compounds which would be expected, if any, near or after the transition into the metallic phase. Bearing in the mind that the electron correlation will be important even in the metallic phase, we investigate in the present study the ground state of a cluster consisting of more than one Ni atoms and their ligands by diagonalizing exactly the Hamiltonian including the electron-electron interaction; we find the change of the ground state wave function corresponding to the metal-insulator transition by varying the charge transfer energy and the intraatomic coulomb energy.

Figure 3 illustrates the simplified model adopted in the calculation. So far we have carried out the calculation of the ground state for a chain consisting up to four Ni atoms intervened by atoms corresponding to either oxygen or sulfur with the periodic boundary condition. We assume the hole picture in the calculation; in the limit of large Δ each Ni atom will accommodate two holes. Adopting a tight binding model, we assume for each Ni atom two orbitals which correspond to the d_y orbitals of e_g symmetry and for each intervening ligand atom an orbital corresponding to p_σ of O or S. The electron transfer is assumed to take place between p_σ and either of the d_y orbitals with the same magnitude of the matrix element denoted by t . The intraatomic coulomb interaction among the two d orbitals is taken into account fully under the assumption of the e_g symmetry. The parameter U characterizing its magnitude is defined by $U = J_{uu} - K_{uv}$ which is equal to the energy difference $E(d^9) + E(d^7) - 2E(d^8)$. The calculation is based on the Lanczos method.

Figure 4 shows an example of the result of the calculation. We find that the ground state changes more than one time by decreasing Δ . The change takes place in a narrow range of Δ ; except for this transition range the total spin of the system remains zero. Figure 4 shows the average of the magnitude of the total spin of each Ni atom and the spin correlation between neighboring Ni atoms. The state for large Δ is characterized by a large magnitude of Ni spin and a large antiferromagnetic coupling between neighboring Ni atoms. Decreasing Δ , we reach the next state where the total spin of a Ni atom is still high, corresponding to the magnetic moment larger than

one; it is characterized, however, by a small value of the spin correlation between neighboring Ni atoms. By reducing Δ further we go into the state where holes seem to move more independently and freely between Ni and intervening orbitals.

We have calculated the photoemission spectra with the same model. The calculation shows that the spectra of the intermediate state can remain quite similar to those of the state of high Δ if the transition matrix elements to the free state from the d and p states are of the same order of magnitude.

The present calculation indicates the possibility that electrons in the metallic phase of NiS are still highly correlated corresponding to the intermediate state mentioned above. Details of the calculation and further discussions are deferred to future publication.

Fig. 3 An illustration of the model for Ni compounds.

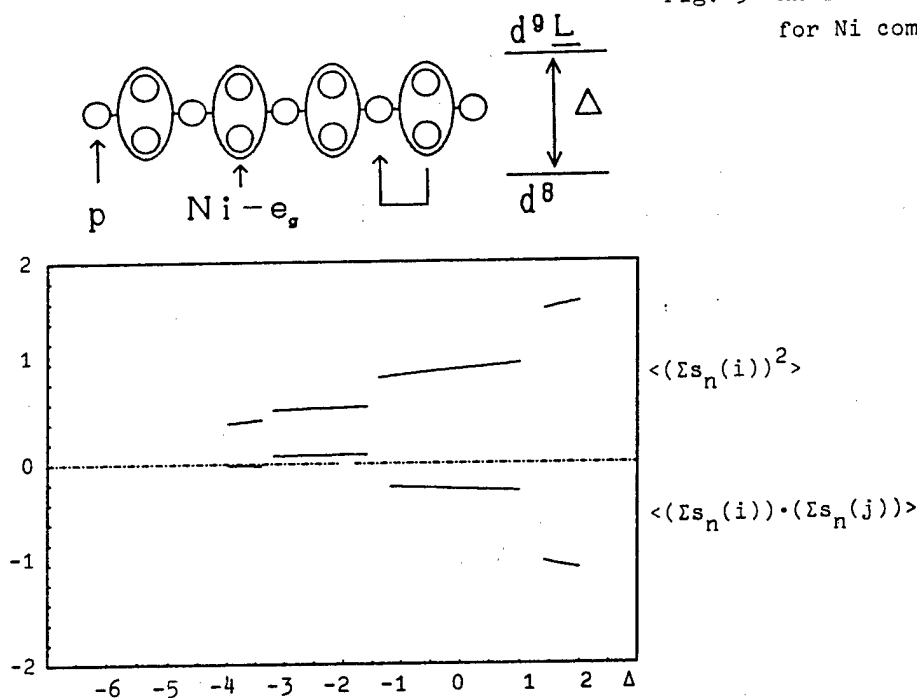


Fig. 4 Calculated dependence of the spin correlations on Δ . $\Sigma s_n(i)$ represents the total spin at i -th site of Ni. The upper part gives the average value of the square of the total spin; the lower part the correlation between neighboring sites of Ni. The calculation assumes $t=1$, $J_{uu}=5$, $J_{uv}=3$, $K_{uv}=1$ and $U_p=3$, where J and K are the coulomb and exchange integrals of the two d_y orbitals and U_p is the coulomb integral for the p orbital.

- [1] T. Nishino and J. Kanamori, J. Phys. Soc. Jpn. 59 (1990) 253.
- [2] A. Fujimori, Phys. Rev. B39 (1988) 793.
- [3] A. Fujimori, F. Minami and S. Sugano, Phys. Rev. B29 (1984) 5225.
- [4] G. A. Sawatzky and J. W. Allen, Phys. Rev. Lett. 53 (1984) 2239.
- [5] A. Fujimori, M. Matoba, S. Anzai, K. Terakura, M. Taniguchi, and S. Suga, J. Mag. and Mag. Mat. 70 (1987) 67.
- [6] K. Terakura, ref.[5] and private communication

Theoretical analysis is presented for the spectra of X-ray photoemission (XPS), X-ray absorption (XAS) and X-ray emission (XES) associated with the Cu 2*p* core level in high- T_c systems and related materials. We use the single-site impurity Anderson model with Cu 3*d* orbitals and O 2*p* valence bands specified by irreducible representations of the D_{4h} symmetry around the Cu atom. By analyzing Cu 2*p*-XPS, we can get information on the hybridization strength between Cu 3*d* and O 2*p* states and the charge transfer energy. In determining the spectral shape of the XPS satellite, it is shown that the interplay between the intraatomic multiplet coupling and the solid-state hybridization plays an essential role. The Cu 2*p*-XAS, especially its polarization dependence, gives most direct information on the site and the symmetry of doped holes. Finally, we show the Cu 2*p*-XES can also be interpreted by using the impurity Anderson model in a manner consistent with XPS and XAS.

1. Introduction

In the study of electronic states of high T_c superconductors, core-level spectroscopic techniques, such as X-ray photoemission (XPS), X-ray absorption (XAS) and X-ray emission (XES), have played an important role.¹⁾ The XPS strongly reflects the effect of the hybridization between Cu 3*d* and O 2*p* states.²⁻⁵⁾ The XAS⁶⁻⁹⁾ and XES^{10,11)} provide us with information on the unoccupied and occupied valence states, respectively. Especially, the polarization dependence of the XAS gives most direct information on the site and the symmetry of the extra-holes doped in high- T_c materials.^{7,8)}

In order to extract useful information from experimental data of core-level spectroscopy, it is necessary to carry out the theoretical analysis by taking account of the many body effect induced by a strong core-hole potential. It is the purpose of the present paper to review our systematic analysis¹²⁻¹⁴⁾ of XPS, XAS and XES of the Cu 2*p* core level in high T_c systems with the use of the single-site impurity Anderson model.

In Section 2, our model is introduced and the method of calculating Cu 2*p*-XPS, XAS and XES is shown. The results of the analysis is presented in Section 3. Section 4 is devoted to the discussion mainly on the effect of the multiplet coupling.

2. Model and Method of Spectral Analysis

We use the impurity Anderson model¹²⁾ consisting of a single Cu ion on the so-called CuO₂ plane, which is commonly included in La-Sr-Cu-O, Y-Ba-Cu-O and Bi-Sr-Ca-Cu-O high T_c systems, and a valence band of O ions. The Hamiltonian is described by

$$\begin{aligned}
 H = & \sum_{\Gamma, \sigma} \epsilon_d d_{\Gamma\sigma}^{\dagger} d_{\Gamma\sigma} + \sum_{\Gamma, \sigma} \sum_{k=1}^N \epsilon_{k\Gamma} a_{k\Gamma\sigma}^{\dagger} a_{k\Gamma\sigma} + \sum_{\Gamma, \sigma} \sum_k \frac{V_{k\Gamma}}{\sqrt{N}} (a_{k\Gamma\sigma}^{\dagger} d_{\Gamma\sigma} + d_{\Gamma\sigma}^{\dagger} a_{k\Gamma\sigma}) \\
 & + \frac{U_{dd}}{2} \sum_{(\Gamma, \sigma) \neq (\Gamma', \sigma')} d_{\Gamma\sigma}^{\dagger} d_{\Gamma\sigma} d_{\Gamma'\sigma'}^{\dagger} d_{\Gamma'\sigma'} - U_{dc} \sum_{\Gamma, \sigma} d_{\Gamma\sigma}^{\dagger} d_{\Gamma\sigma} (1 - a_c^{\dagger} a_c),
 \end{aligned} \tag{1}$$

where the first and second terms on the right-hand side represent, respectively, the Cu 3d state and the O 2p valence band. The index Γ represents the symmetry of the Cu 3d orbital states which are taken as irreducible representation a_{1g} , b_{1g} , b_{2g} and e_g in the D_{4h} point group, and the index k describes the energy levels of the valence band. The third, fourth and fifth terms represent the hybridization between the 3d and valence band states, the Coulomb interaction between 3d electrons and the core hole potential acting on the 3d states, respectively. For the moment, we disregard the effect of the multiplet coupling originating from the multipole Coulomb interaction and the spin-orbit interaction. This effect is discussed in Section 4. Furthermore, when we analyze the polarized Cu 2p-XAS of Y-Ba-Cu-O, we also take account of the contribution from the Cu site on the CuO chain.

The spectra of Cu 2p-XPS and Cu 2p-XAS are expressed, respectively, as

$$F_{XPS}(E_B) = \sum_f |\langle f | a_c | g \rangle|^2 L(E_B - E_f + E_g), \quad (2)$$

and

$$F_{XAS}(\omega) = \sum_f |\langle f | d_{\Gamma\sigma}^+ a_c | g \rangle|^2 L(\omega - E_f + E_g), \quad (3)$$

where $|g\rangle$ and $|f\rangle$ represent the initial and final states with energy E_g and E_f , respectively, E_B is the binding energy, ω is the incident photon energy, and $L(x)$ is the Lorentzian function by which the spectral broadening due to the core hole lifetime τ_c and the experimental resolution is represented. The Cu 2p-XES is expressed, by applying the formula of the second order optical process¹⁴⁾, in the form

$$F_{XES}(\omega) = \sum_f |\langle f | a_c^+ d_{\Gamma\sigma} \frac{1}{H - E_f - \omega - i(\hbar/\tau_c)} a_c | g \rangle|^2. \quad (4)$$

Here we consider the process where a 2p core electron is first excited to a high energy continuum by a monochromatic incident X-ray, and then a 3d electron makes a transition to the 2p level by emitting an X-ray photon with energy ω .

In order to calculate these spectra, we diagonalize numerically the Hamiltonian (1) for a finite system where $\epsilon_{k\Gamma}$ are taken as

$$\epsilon_{k\Gamma} = \epsilon_{v\Gamma}^0 - W/2 + W(k - 1/2)/N. \quad (5)$$

Here, $\epsilon_{v\Gamma}^0$ is the center of the valence band with symmetry Γ , W is the width of each valence band, and $k = 1 \sim N$. The energy dependence of the hybridization is assumed to be semi-elliptical and is given by

$$(V_{k\Gamma})^2 = \frac{8V(\Gamma)^2}{\pi W} [(W/2)^2 - (\epsilon_{k\Gamma} - \epsilon_{v\Gamma}^0)^2]^{1/2}, \quad (6)$$

where $V(\Gamma)$ is the strength of the hybridization. The value of N is taken to be so large that the calculated spectra converge well. The key parameters of our model are $V(\Gamma)$, U_{dd} , U_{dc} and the charge transfer energy $\Delta(\Gamma)$ which represents the energy difference between $d^{10}\underline{L}(\Gamma)$ and $d^9(\Gamma)$ configurations (in the limit of vanishing V), where \underline{L} denotes a hole in the valence band. Namely, $\Delta(\Gamma)$ is defined by

$$\Delta(\Gamma) = \epsilon_d + 9U_{dd} - \epsilon_{v\Gamma}^0. \quad (7)$$

3. Results

First we show the result of our analysis for undoped La_2CuO_4 , a typical mother material of high T_c systems. In La_2CuO_4 the Cu ion is nominally divalent, so that the ground state of the impurity Anderson model includes one hole. There is a general consensus that the symmetry of the hole is b_{1g} , and the ground state is a strongly hybridized state between $3d^9(b_{1g})$ and $3d^{10}\underline{L}(b_{1g})$ configurations.

The calculated results^{12,14)} of Cu 2p-XPS, XAS and XES are shown in Fig. 1 and compared with the corresponding experimental data^{2,9,15)} ($2p_{3/2}$ component) in the inset. In the final state of XPS, the energies of $3d^9(b_{1g})$ and $3d^{10}\underline{L}(b_{1g})$ configurations become very different because of the core hole potential $-U_{fc}$, and the latter configuration gives the main peak of XPS, while the former gives the satellite. In order to reproduce the intensity ratio and energy separation between the main peak and the satellite, as well as to reproduce the other spectra¹²⁾ (e. g. 3d-XPS), we estimate the parameter values as $\Delta(b_{1g}) = 2.0$ eV, $V(b_{1g}) = 2.5$ eV, $U_{dc} = 8.0$ eV and $W = 3.0$ eV. On the difference

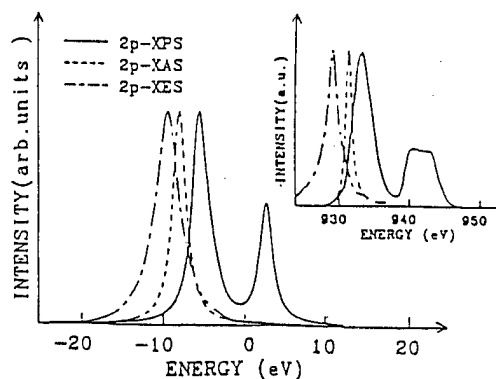


Fig. 1 Calculated results of Cu 2p-XPS, XAS and XES for La_2CuO_4 . Experimental results are shown in the inset.

in the theoretical and experimental spectral shapes of the satellite, we discuss in Section 4.

In the final state of Cu 2p-XAS of La_2CuO_4 , we have only one state with the $3d^{10}$ configuration, so that the spectrum is given by a single peak (which is denoted by white line) as shown in Fig. 1. On the other hand, the XES process is very complicated; the intermediate state consists of $3d^9(b_{1g})$ and $3d^{10}\underline{L}(b_{1g})$ configurations, which is the same as the final state of XPS, and the final state consists of $3d^8$, $3d^9\underline{L}$ and $3d^{10}\underline{L}^2$ configurations with various symmetries and with the hybridization among them. However, when we sum up all the XES processes, we find that XES also has a single peak as shown in Fig. 1, where we used the additional parameter values of $\Delta(a_{1g}) = 1$ eV, $\Delta(b_{2g}) = \Delta(e_g) = 3$ eV, $V(a_{1g}) = 2.0$ eV, $V(b_{2g}) = 1.5$ eV, $V(e_g) = 1.0$ eV and $U_{dd} = 7.0$ eV. The calculated XES spectrum is in fairly good agreement with the experimental result not only in its spectral shape but also in the relative peak position with XPS and XAS. When we change the value of U_{dd} , the XES peak energy changes to some extent. The choice of $U_{dd} = 7.0$ eV is reasonable from the analysis of XES¹⁴⁾, as well as 3d-XPS.¹²⁾

From our parameter values we find $U_{dd} > \Delta$. This means that the system is the so-called charge transfer type insulator¹⁶⁾, and suggests that when holes are doped they enter mainly the O 2p valence band. So, it is interesting to study explicitly the effect of the doped hole with the impurity Anderson model. When an extra-hole with symmetry Γ is added in our model, we have two holes in the system, and the ground state is a linear combination of $3d^8(b_{1g}, \Gamma)$, $3d^9(b_{1g})\underline{L}(\Gamma)$, $3d^9(\Gamma)\underline{L}(b_{1g})$ and $3d^{10}\underline{L}^2(b_{1g}, \Gamma)$. With our parameter values the lowest state of $\Gamma = b_{1g}$ is close to that of $\Gamma = a_{1g}$. When we calculate Cu 2p-XPS, the spectrum is very similar to that of the undoped system¹²⁾, irrespective of $\Gamma = b_{1g}$ or a_{1g} . Experimental data also show that the effect of the doping is very small in Cu 2p-XPS²⁾. This is interpreted that the extra-hole is mainly on the O site while the Cu 2p-XPS is not sensitive to the electronic state on the O site. As a matter of fact, when we calculate the weight of the $3d^8$ configuration in the ground state, we obtain only 6.5% for $\Gamma = b_{1g}$ (only 4.4% for $\Gamma = a_{1g}$), and thus, most of the extra-holes enter the O 2p states.

When we study the effect of the doped hole on Cu 2p-XAS with our model, it is found that the doped hole contributes to a satellite peak on the higher energy side of the white line of the undoped system. The satellite is allowed for $\epsilon \perp c$ in the case of $\Gamma = b_{1g}$, whereas it is allowed for $\epsilon \parallel c$ in the case of $\Gamma = a_{1g}$, where ϵ and c represent the direction of the X-ray electric field and the crystalline c-axis, respectively¹²⁾. According to experimental data for Y-Ba-Cu-O⁷⁾, the extra-holes give rise to a weak satellite about 1.5 eV above the white line, and the relative intensity of the satellite is proportional to the doped hole concentration. A similar satellite is also observed in the Bi-Sr-Ca-Cu-O system⁸⁾. From the polarized XAS measurements, the satellite of Y-Ba-Cu-O is mainly allowed for

$\epsilon \parallel c^7$), while that of Bi-Sr-Ca-Cu-O is mainly allowed for $\epsilon \perp c^8$). A similar result was also obtained by recent EELS measurements.¹⁷⁾

From the theoretical and experimental results mentioned above, we interpret that in the Bi-Sr-Ca-Cu-O system the extra holes are doped in the b_{1g} state, which mainly consists of the O $2p_x$ and $2p_y$ states in the CuO_2 plane. This is also consistent with recent experimental results of O 1s-XAS^{17,18)}, where the XAS near the absorption edge is allowed only for $\epsilon \perp c$. However, in analysing Cu 2p-XAS of Y-Ba-Cu-O, we should be careful, because there are two inequivalent Cu sites: the Cu(1) site on the CuO chain in addition to the Cu(2) site in the CuO_2 plane. In order to treat both Cu(1) and Cu(2) sites, we combine the impurity Anderson model including the Cu(2) site with a cluster model including the Cu(1) site.¹⁹⁾ For the impurity Anderson model, we use the same model as that we have treated so far, because the parameter values for Y-Ba-Cu-O is not very different from those for La_2CuO_4 .¹²⁾ The cluster model consists of the Cu(1) and the neighboring four O atoms for $\text{YBa}_2\text{Cu}_3\text{O}_{7-\delta}$ with $\delta = 0$, while it consists of the Cu(1) and three O atoms for $\delta = 0.5$. The apical O atom is closer to Cu(1) than to Cu(2), so that it is included in the cluster model. The charge transfer energy between O(1) $2p$ and Cu(1) $3d$ states are taken to be 1.0 eV, and that between O(4) $2p$ and Cu(1) $3d$ to be 2.5 eV, where O(1) is the O atom on the CuO chain and O(4) is the apical O atom. The hybridization in the cluster is taken consistently with that in the CuO_2 plane such that the hybridization strength is proportional to $r^{-3.5}$ with the Cu-O distance r .

The calculation of the Cu 2p-XAS is made for $\delta = 0$ and 0.5. For a general value of δ , the results for $\delta = 0$ and 0.5 are superposed with the statistical weight. A result for $\delta = 0.2$ is shown in Fig. 2. This is obtained by assuming that a half of the doped holes enter the CuO_2 plane with the symmetry of $x^2 - y^2$ around Cu(2) and the remaining half enter the CuO chain and the apical O atom around Cu(1).¹⁹⁾ The white line for $\epsilon \perp c$ comes mainly from the undoped Cu(2) site, while the main line and the satellite for $\epsilon \parallel c$ originate from the undoped Cu(1) site and the Cu(1) site with the doped hole on the neighboring O atoms, respectively. The effect of the holes doped in the CuO_2 plane also gives, for $\epsilon \perp c$, a shoulder on the higher energy side of the white line, but it is not clearly separated as a satellite peak. These features agree rather well with those of experimental results.^{7,17)} Therefore, we interpret that

in the Y-Ba-Cu-O system the extra-holes are not doped selectively in a specific oxygen site but a considerable amount of holes enter all of the oxygen sites in the CuO_2 and BaO planes and also on the CuO chain.

4. Discussion

From Fig. 1 it is found that the spectral shape of the satellite of Cu 2p-XPS is different between the calculated and experimental results. As shown by van der Laan *et al.*²⁰⁾, the satellite structure of Cu 2p-XPS for CuCl_2 is explained by the atomic multiplet structure of the $\text{Cu } 2p^5 3d^9$ final state. However, the observed spectral shape of the satellite for La_2CuO_4 is considerably different from that for CuCl_2 . This suggests that the solid-state effect is also important in determining the satellite structure. In order to study how the interplay between the atomic multiplet coupling and the solid-state hybridization affects the spectral shape of Cu 2p-XPS, we incorporate in our Hamiltonian

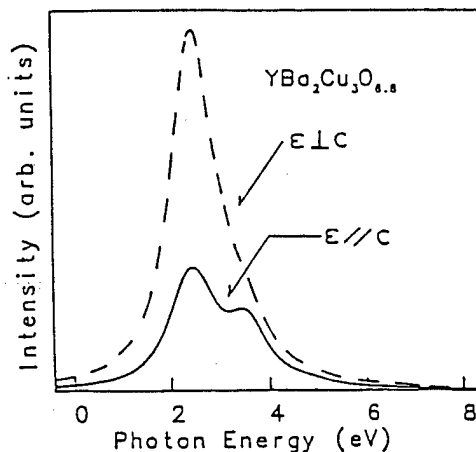


Fig. 2 Polarization dependence of Cu 2p-XAS in $\text{YBa}_2\text{Cu}_3\text{O}_{6.8}$ calculated by taking account of two inequivalent Cu sites.

(1) the interactions described by the Slater integrals F^2 , G^1 and G^3 between $2p$ and $3d$ states, and the spin-orbit interactions in the $2p$ and $3d$ states.¹³⁾ The calculated Cu $2p$ -XPS is shown in Fig. 3, where the line spectra before the convolution is also plotted. The used parameter values are essentially the same as those we estimated before (with some minor modification), and in addition, the Slater integrals of $F^2=7.47$ eV, $G^1=5.62$ eV, $G^3=3.21$ eV and the spin-orbit coupling constants of $\zeta_d=0.13$ eV, $\zeta_p=13.6$ eV are used. Now the experimental spectral shape of the satellite is reproduced fairly well. Furthermore, by changing the contribution from the solid-state hybridization we can explain the systematic variation of the satellite spectral shape¹³⁾, i.e., the rectangle like shape for La_2CuO_4 and CuO , a triangle like shape for CuF_2 , and the atomic multiplet like shape (which has large spectral weight on the low energy side of the satellite) for CuCl_2 . Therefore, the interplay between the atomic multiplet coupling and the solid-state hybridization is essentially important in determining the spectral shape of Cu $2p$ -XPS. According to our preliminary calculation²¹⁾, on the other hand, the effect of the multiplet coupling does not change very much the spectral shape of Cu $2p$ -XES shown in Fig.1. Furthermore, the effect of the multiplet coupling does not affect the Cu $2p$ -XAS of La_2CuO_4 because of the $3d^{10}$ final state, and even for the doped system the effect is very small because the final state is mainly in the $3d^{10}\underline{L}$ configuration.

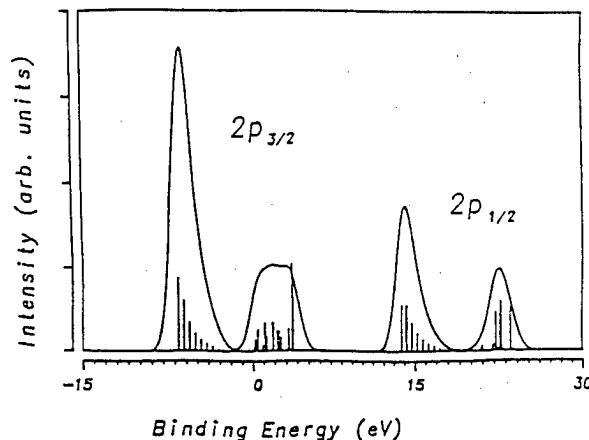


Fig. 3 Cu $2p$ -XPS for La_2CuO_4 calculated by taking account of the multiplet coupling effect.

On the satellite of Cu $2p$ -XAS in the Y-Ba-Cu-O system, Zaanen *et al.*²²⁾ have recently given an interpretation that it comes from the Cu(1) site, consistently with our interpretation, on the basis of the energy band calculation. In our calculation, however, it originates from a well localized state around the Cu(1) site because of the cluster model, but Zaanen *et al.* ascribe it to the van Hove singularity in the Cu(1)-O chain band.

Finally, Bianconi *et al.*²³⁾ have recently made systematic measurements of the polarized Cu $2p$ -XAS for various Bi-Ca-Sr-Cu-O samples with different T_c . They observed a considerable absorption intensity for $\epsilon||c$, in addition to that for $\epsilon \perp c$, in the energy region of the white line. Furthermore, the relative intensity of the $\epsilon||c$ absorption peak increases with increasing T_c , and the energy splitting between $\epsilon||c$ and $\epsilon \perp c$ absorption peaks decreases with increasing T_c . Within the impurity Anderson model with the D_{4h} symmetry, as discussed in the present paper, this absorption for $\epsilon||c$ cannot be explained. In order to analyze this result it will be necessary to extend the model so as to include the effect of a possible rhombic distortion²⁴⁾ and the effect of the translational symmetry.

I would like to thank Dr. K. Okada, Dr. H. Katayama-Yoshida, Mr. S. Tanaka, Mr. Y. Seino and Prof. A. Bianconi for their collaboration and discussion.

References

- 1) *Core-Level Spectroscopy in Condensed Systems*, (eds. J. Kanamori and A. Kotani) : Springer-Verlag, Berlin, 1988.
- 2) P. Steiner, J. Albers, V. Kinsinger, I. Sander, B. Siegwart, S. Hüfner and C. Politis : *Z. Phys. B* **66**, 275(1987).
- 3) N. Nücker, J. Fink, B. Renker, D. Ewert, C. Politis, P. J. W. Weijs and J. C. Fuggle : *Z. Phys. B* **67**, 9(1987).
- 4) A. Fujimori, E. Takayama-Muromachi, Y. Uchida and B. Okai : *Phys. Rev. B* **35**, 8814(1987).

- 5) T. Gourieux, G. Krill, M. Maurer, M. F. Ravat, A. Menny, H. Tolentino and A. Fontaine : Phys. Rev. **37**, 7516(1988).
- 6) P. Kuiper, G. Kruizinga, J. Ghijsen, M. Grioni, P. J. W. Weijs, F. M. F. De Groot, G. A. Sawatzky, H. Verweij, L. F. Feiner and H. Peterson : Phys. Rev. **B 38**, 6483 (1988).
- 7) A. Bianconi, M. De Santis, A. Di Cicco, A. M. Flank, A. Fontaine, P. Lagarde, H. Katayama-Yoshida, A. Kotani and A. Marcelli : Phys. Rev. **B 38**, 7196(1988).
- 8) A. Bianconi, P. Castrucci, M. De Santis, A. Di Cicco, A. Fabrizi, A. M. Flank, P. Lagarde, H. Katayama-Yoshida, A. Kotani, A. Marcelli, Z. X. Zhao and C. Politis : Modern Phys. Letters **B 2**, 1313(1988).
- 9) A. Bianconi, M. De Santis, A. Clozza, A. Congiu Castellano, A. M. Flank, A. Fontaine, P. Lagarde, J. Budnick and A. Gargano : *Core-Level Spectroscopy in Condensed Systems*, (eds. J. Kanamori and A. Kotani) p146 (Springer-Verlag, Berlin, 1988).
- 10) J. M. Mariot, V. Barnole and C. F. Hague : Solid State Commun. **64**, 1203(1987).
- 11) N. Wassdahl : Ph. D. Thesis, Uppsala Univ., Uppsala, Sweden, 1987.
- 12) K. Okada and A. Kotani : J. Phys. Soc. Jpn. **58**, 1095(1989).
- 13) K. Okada and A. Kotani : J. Phys. Soc. Jpn. **58**, 2578(1989).
- 14) S. Tanaka, K. Okada and A. Kotani : J. Phys. Soc. Jpn. **58**, 813(1989).
- 15) T. Takahashi : private communication.
- 16) J. Zaanen, G. A. Sawatzky and J. W. Allen : Phys. Rev. Lett. **35**, 418(1985).
- 17) N. Nücker, H. Romberg, X. X. Xi, J. Fink, B. Gegenheimer and Z. X. Zhao : Phys. Rev. **B 39**, 6619(1989).
- 18) F. J. Himpsel, G. V. Chandrashekar, A. B. McLean and M. W. Shafer : Phys. Rev. **B 38**, 11946(1988); P. Kuiper, M. Grioni, G. A. Sawatzky, D. B. Mitzi, A. Kapitulnik, A. Santaniello, P. de Padova and P. Thiry : to be published in Physica C.
- 19) Y. Seino, K. Okada and A. Kotani : submittd to J. Phys. Soc. Jpn.
- 20) G. van der Laan, C. Westra, C. Haas and G. A. Sawatzky : Phys. Rev. **B 23**, 4369(1981).
- 21) S. Tanaka, K. Okada and A. Kotani : unpublished.
- 22) J. Zaanen, M. Alouani and O. Jepsen : Phys. Rev. **B 40**, 837(1989).
- 23) A. Bianconi, P. Castrucci, A. Fabrizi, M. Pompa, A. M. Flank, P. Lagarde, H. Katayama-Yoshida and G. Calestani : to be published in Proc. Erice school "Earlier and recent aspect of superconductivity" eds. J. G. Bednorz and K. A. Müller (Springer, 1989).
- 24) Y. Seino, A. Kotani and A. Bianconi : unpublished.

Self-Doping in Oxide Superconductors

J. Kondo

Electrotechnical Laboratory
Tsukuba, Ibaraki 305, Japan

It is shown that the actual carrier content of oxide superconductors may be different from the nominal one due to self-doping. The Madelung potential plays an essential role in such a doping mechanism. This mechanism is important for the YBCO system with small oxygen content (<6.5) and for multi-layered Tl-compounds.

1. Introduction

The number of carriers in oxide superconductors is determined by oxygen content and composition of metal elements. Consider, e. g., a compound $A_xB_yCu_zO_\delta$, where nominal valences of the elements are A^{2+} , B^{3+} , Cu^{2+} and O^{2-} . Then the number p defined by

$$2x+3y+2z-2\delta=-p \quad (1)$$

may be called the hole content per unit formula of the compound. When p is negative, the carriers may be electrons. In some cases, however, the actual carrier content (including its sign) may be different from p . This is due to self-doping of carriers, which we will discuss in some detail in this report. Self-doping is defined by charge transfer between nominal valence states, e. g., $A^{2+} Cu^{2+} \rightarrow A^{3+} Cu^+$. In treating such a self-doping, we will take a standpoint of the ionic-crystal model, and consider the sum of the Madelung energy and the energies of the isolated ions as the first approximation for the energy of the compound. We will see that, in some cases, the smallest energy is attained for a valence assignment where self-doping took place. There are two important cases of self-doping in high- T_c oxide superconductors. One is the YBCO system and the other multi-layered Tl-compounds.

2. YBCO system

Tokura et al [1] measured T_c 's of many compounds of formula $(Y,Ca)Ba_2Cu_3O_\delta$ and $Y(Ba,La)_2Cu_3O_\delta$ and obtained a phase diagram in a p - δ plane, where the superconducting and semiconducting regions are divided by a straight line (Fig. 1). An overall feature of the diagram can be explained in terms of the Madelung potential. When δ is close to 7, the oxygen sites in the chain are almost completely filled by O^{2-} ions. Then the Madelung potential for the hole will be very low at the chain sites,

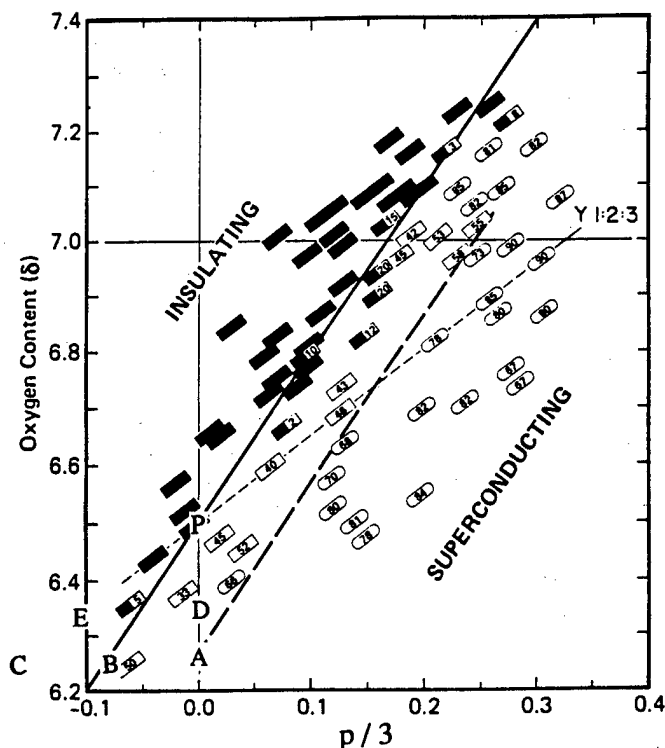


Fig. 1 Superconducting and insulating regions are separated by a straight line in the p - δ plane (from ref. [1]).

and all the holes will occupy them. We then have semiconductors. When the number of holes is increased, the hole potential of the chain will be raised due to the repulsive potential from the holes introduced into the chain. As the number of holes is increased further, some holes will occupy plane sites. We then have superconductors. For smaller δ the attractive potential from the O^{2-} ions will be smaller at the chain sites, and will be overcome by the repulsive potential from the holes in the chain at a smaller hole content. We have shown that this idea explains the diagram semiquantitatively[2].

For $\delta < 6.5$ the diagram shows that the superconducting region extends up to where p is negative. We will study a few cases in this region.

2.1 $Y_{0.5}Ca_{0.5}Ba_2Cu_3O_{6.25}$

This compound is denoted by "A" in Fig. 1. In this compound only one quarter of the oxygen sites in the chain is occupied by O^{2-} ions. Many groups studied oxygen ordering in these compounds[3] and reported that one quarter of the chains is completely filled by O^{2-} ions and the others are empty, so that the superstructure is $4a_0 \times b_0$. Assuming that oxygen ions order in this way and the Y sites are occupied randomly by Y^{3+} and Ca^{2+} ions, we obtain the Madelung potential for the electron at each Cu site as shown in Fig. 2. We see that the potentials at the Cu sites in the empty chain are very low. This is because these sites are coordinated only by two oxygen ions. Such a low potential indicates that the nominal valence assignment is unstable and these Cu ions will attract electrons from other ions, thus giving rise to self-doping. The doped holes may occupy Cu sites or O sites. The ionic-crystal model gives almost the same energy for the hole in the Cu site in the plane and in the O site in the plane. It is difficult to give a definite answer to whether the hole prefer a Cu site or an O site based on the ionic-crystal model, so we here assume that the holes

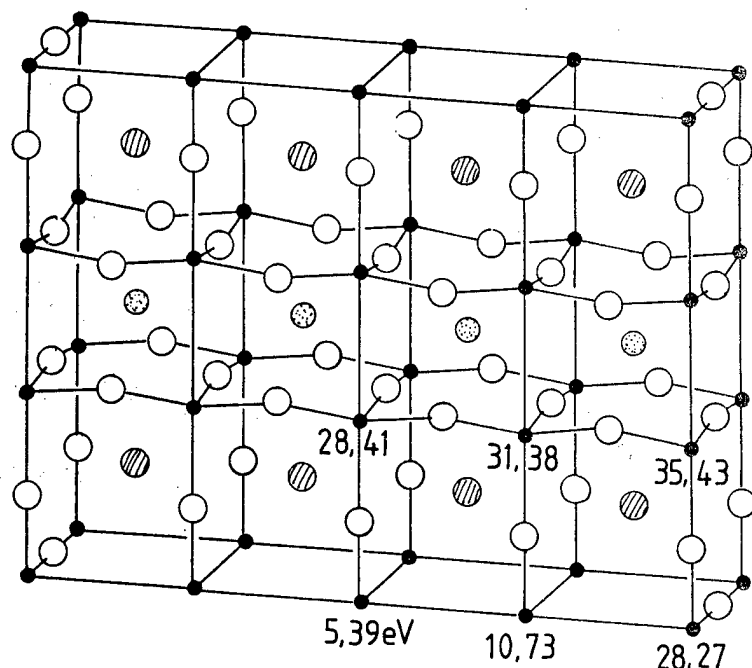


Fig. 2 Crystal structure of $\text{Y}_{0.5}\text{Ca}_{0.5}\text{Ba}_2\text{Cu}_3\text{O}_{6.25}$. An oxygen ordering is assumed in the chain sites. The number indicates the Madelung potential for the electron at each site.

occupy O sites. We have found that the lowest energy is attained when all the Cu ions in the empty chains are Cu^+ , all the O ions in the chains are O^- and there are two holes somewhere in the plane in the unit cell of Fig. 2. Since all the chains have the same total charge in this valence assignment, the potential for the hole in the plane is rather flat. Thus we conclude that the hole number of this compound is 0.25 per Cu in the plane, even though the nominal hole number is zero.

2.2 $\text{YBa}_2\text{Cu}_3\text{O}_{6.25}$

This compound is marked by "C" in Fig. 1. The oxygen ions in the chain sites are assumed to order as in 2.1. The lowest energy is attained when the Cu ions in the empty chains are Cu^+ and the O ions in the chain are O^- . There is no hole in the plane. Thus this compound should be semiconducting. For the compounds on the line between "A" and "C" holes enter plane sites. For example, for the compound "B" there is one hole in a plane site in the unit cell of Fig. 2.

2.3 $\text{Y}^{2/3}\text{Ca}^{1/3}\text{Ba}_2\text{Cu}_3\text{O}_{6\frac{1}{3}}$

This compound is marked by "D" in Fig. 1 and has a nominal hole number $p=0$, but shows self-doping. We assume an oxygen ordering where there is one chain filled by oxygen ions for every three chains. Again at the empty chains the Madelung potential is very low, and the lowest energy is attained when the Cu in these chains are Cu^+ . The compensating holes may enter plane sites as well as chain sites. Since the energy difference is small, it is difficult to determine how many holes enter the plane sites. When all the holes enter the plane sites, the hole number per Cu in the plane is 0.33, but will actually be smaller.

2.4 $\text{YBa}_2\text{Cu}_3\text{O}_{6\frac{1}{3}}$

This is denoted by "E" in Fig. 1 and has $p=-1/3$. If the same oxygen ordering as in 2.3 is assumed, the lowest energy is attained when all the Cu's in the empty chains are Cu^+ , half of the oxygen ions in the chain is O^- and there are $1/12$ holes per Cu in the plane. This number is determined from neutrality condition. Thus this compound should be a hole superconductor, even though the nominal carriers are electrons. These electrons are trapped by Cu^{2+} ions in the empty chains. Furthermore a self-doping takes place, giving rise to the holes in the plane.

2.5 $\text{YBa}_2\text{Cu}_3\text{O}_{6.5}$ "P"

This has a nominal hole content $p=0$. It is reported that in the chain sites chains filled by O^{2-} ions and empty chains alternate[3]. In the lowest energy configuration all the Cu's in the empty chains are Cu^+ and half of the oxygen ions in the chain sites is O^- . There are $1/8$ holes per Cu in the plane from neutrality condition.

Recently Nakazawa and Ishikawa[4] observed that well-annealed samples of $\text{YBa}_2\text{Cu}_3\text{O}_\delta$ show superconductivity for δ as small as ~ 6.2 . This result is explained by the self-doping. When oxygen ions are randomly distributed in the chain, there will be only a small number of "isolated" Cu ions in the chain. By "isolated" Cu ions I mean those with only two nearest neighbouring oxygen ions in the apical positions. The Madelung potential for other Cu ions surrounded by more than two oxygen ions will not be low, so that self-doping will not take place. When oxygen ions are ordered by annealing as in 2.1, 2.3 or 2.5, a substantial fraction of the Cu ions in the chain are isolated, so that self-doping will take place. We have seen that superconductivity should occur for δ down to 6.25. The question why oxygen ions order in the way mentioned above will be discussed in another place.

3. $\text{Tl}_2\text{Ba}_2\text{Ca}_{n-1}\text{Cu}_n\text{O}_{2n+4}$

These compounds have nominal hole content $p=0$, if the nominal valence of Tl is assumed to be +3. Since these are high- T_c superconductors, a question arises where the carriers come from. This question has been answered in terms of the self-doping [5]. As we have shown the Madelung potential in the TlO planes is very low compared with those of the CuO_2 planes for the nominal valence assignment. Then some electrons are transferred from the CuO_2 planes to the TlO planes, thus creating holes in the plane. The same doping mechanism has also been proposed by Shono[6].

References

- [1] Y. Tokura, J. B. Torrance, T. C. Huang and A. I. Nazzari, Phys. Rev. B38 (1988) 7156.
- [2] J. Kondo, Y. Asai and S. Nagai, J. Phys. Soc. Jpn. 57 (1988) 4334.
- [3] See, e. g., C. Chaillout, M. A. Alario-Franco, J. J. Capponi, J. Chenavas, J. L. Hodeau and M. Morezio, Phys. Rev. B36 (1987) 7118 and D. J. Werder, C. H. Chen, R. J. Cava and B. Batlogg, Phys. Rev. B38 (1988) 5130.
- [4] Y. Nakazawa and M. Ishikawa, Physica C158 (1989) 381.
- [5] J. Kondo, J. Phys. Soc. Jpn. 58 (1989) 2884.
- [6] Y. Shono, Workshop on Oxide Superconductors held at Nasu, Sept. 24-26 1989.

Hole Distribution in Cu-Oxide Superconductors

S. Maekawa, Y. Ohta and T. Tohyama

*Department of Applied Physics, Nagoya University,
Nagoya 464-01, Japan*

Starting with the ionic crystal model, the Madelung energy and hole distribution are calculated in various Cu-oxides. The distribution and several electronic properties emerged in the model are examined in the cluster model approach.

1. Introduction

There are several common features in all Cu-oxides superconductors: (i) They have CuO_2 plane as a structural unit. (ii) The parent compounds of the superconductors such as La_2CuO_4 and $\text{YBa}_2\text{Cu}_3\text{O}_6$ are insulators and may be considered as ionic crystals because of the strong electron correlation. (iii) Hole-doping on the plane brings about the superconductivity. It is well-known that the hole concentration on the plane is a crucial parameter to determine the superconducting transition temperature T_c in the oxides. We note, however, that although the optimum concentration of holes is almost unique ($p \simeq 0.15 - 0.2$) [1] in all the hole-doped superconductors, the value of T_c is strongly dependent on materials.

Here, starting with the ionic crystal model, we first calculate the Madelung energy in the compounds and examine hole distribution. We will find that, in addition to the hole concentration on the plane, the difference in the Madelung potential between oxygens in the apical site and those on the plane determines T_c [2]. In the light of the calculation, we propose several possible high- T_c superconductors [2,3].

The cluster model calculation has been used to study the electronic states in the oxides. The advantage of this model is that the strong electron correlation on Cu sites and the charge transfer between Cu and O ions are taken into account on the equal footing [4]. We examine the electronic states in the cluster model and discuss a criterion of high- T_c superconductivity in the oxides [5].

In Sec. 2, we study the Madelung energy in the ionic crystal model [2,3]. In Sec. 3, we calculate the electronic states in the cluster model [5]. Conclusion is given in Sec. 4.

2. Ionic crystal model [2,3]

The total electronic energy of an ionic crystal may be written as a function of the charge distribution $\{Q_i\}$ among the ions under the charge neutrality constraint $\sum_i Q_i = 0$ as

$$E(\{Q_i\}) = E_A(\{Q_i\}) + E_M(\{Q_i\}), \quad (1)$$

$$E_A(\{Q_i\}) = \sum_i \sum_{q=1}^{Q_i} s_i(q), \quad (2)$$

$$E_M(\{Q_i\}) = \sum_{i \geq j} c_{ij} Q_i Q_j, \quad (3)$$

where the i and j summations run over all the ions in the unit cell. Here, $E_A(\{Q_i\})$ represents the atomic energy coming from the ionization energy (electron affinity) associated with removing (adding) electrons from (to) the isolated

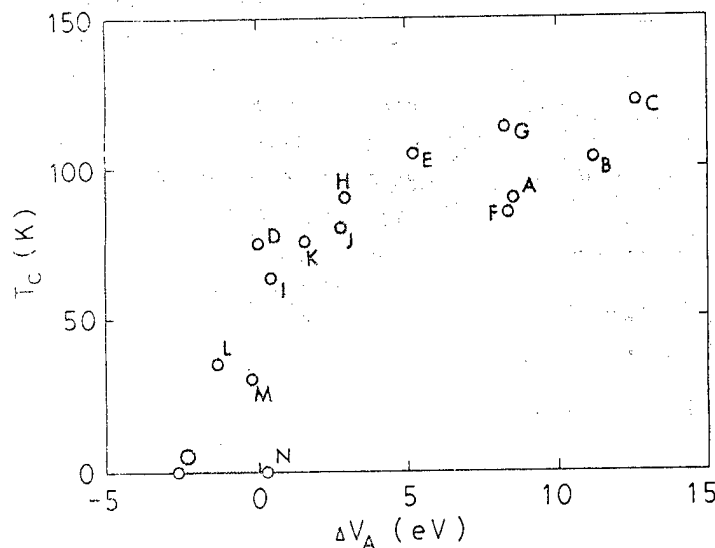


Fig. 1. The T_c vs. ΔV_A correlation in hole-superconductors. All the representative compounds (labelled A-O as below) are collected. Madelung potentials are evaluated for the following parent compounds (valences assigned are shown in parentheses): A: $\text{Ti}_2\text{Ba}_2\text{CuO}_6$, B: $\text{Ti}_2\text{Ba}_2\text{CaCu}_2\text{O}_8$, C: $\text{Ti}_2\text{Ba}_2\text{Ca}_2\text{Cu}_3\text{O}_{10}$, D: $\text{TiBa}_2(\text{Ca-Y})\text{Cu}_2\text{O}_7$ (Ca-Y=3+), E: $\text{TiBa}_2(\text{Ca-Y})_2\text{Cu}_3\text{O}_9$ (Ca-Y=2.5+), F: $\text{Bi}_2\text{Sr}_2\text{CaCu}_2\text{O}_8$, G: $\text{Bi}_2\text{Sr}_2\text{Ca}_2\text{Cu}_3\text{O}_{10}$ (from ref. [12]), H: $\text{YBa}_2\text{Cu}_3\text{O}_{6.5}$ (orthorhombic), I: $\text{YBa}_2\text{Cu}_3\text{O}_{6.5}$ (tetragonal), J: $\text{YBa}_2\text{Cu}_4\text{O}_8$ (O in Cu-O chain = 1.5-), K: $\text{Pb}_2\text{Sr}_2\text{YCu}_3\text{O}_8$ (linearly coordinated Cu = 1+), L: La_2CuO_4 , M: $(\text{Nd}_{1-x-y}\text{Sr}_x\text{Ce}_y)_2\text{CuO}_4$ ($M = 2.8+$ and $M' = 3.2+$), N: $\text{La}_2\text{CaCu}_2\text{O}_6$ (2a-site = 2+ and 4e-site = 3+), and O: $\text{La}_2\text{SrCu}_2\text{O}_6$ (2a-site = 2.5+, and 4e-site = 2.75+). $\text{TiBa}_2\text{CuO}_5$ and $\text{Bi}_2\text{Sr}_2\text{CuO}_6$, which show low T_c 's due to overdoping [12], are excluded.

atoms, where $s_i(q)$ denotes either the q -th ionization energy $I_i(q)$ for cations or the q -th electron affinity $A_i(q)$ for anions. $E_M(\{Q_i\})$ is the Madelung energy gained by condensing the resultant ions to the crystal. The coefficient c_{ij} is a function of the crystal structure and is calculated by the Ewald method. The potential of the i -site for a hole (i.e., the energy required to bring a hole from infinity to the i -site) may be written as

$$P_i = P_i^A + P_i^M, \quad (4)$$

$$P_i^A = s_i(Q_i + 1), \quad (5)$$

$$P_i^M = \sum_j c_{ij} Q_j. \quad (6)$$

The equilibrium charge distribution is determined by minimizing the total energy $E(\{Q_i\})$ with respect to $\{Q_i\}$.

2-1. Correlation between T_c and the Madelung potential [2]

Let us introduce a hole on the CuO_2 plane. Recent experiments indicate that a hole sits on O and not on Cu in the plane. We have calculated the Madelung potential (eq.(6)) of the apical oxygen (O(A)) relative to that of the CuO_2 plane (O(P)), ΔV_A , in various parent compounds.

In Fig. 1, the optimum T_c is plotted as a function of the difference in the Madelung potential, ΔV_A . As seen in the Figure, all the compounds are located in a shaded area exhibiting a characteristic curve. We find the followings in Fig. 1: (i) Compounds with larger ΔV_A have higher T_c . (ii) T_c appears at $\Delta V_A \approx -2$ eV and increases rapidly with increasing ΔV_A . (iii) The curve tends to have a smaller gradient for larger ΔV_A . We may conclude that T_c in hole-doped superconductors is controlled by the energy level of O(A) relative to that of O(P). We note here that T_c 's in Fig. 1 are those in the compounds with optimum hole concentration ($p \approx 0.15 - 0.2$) [1]. Therefore, T_c 's may be considered to have two independent parameters, p and ΔV_A .

It has been observed in $\text{YBa}_2\text{Cu}_4\text{O}_8$ that major effect of pressure is to bring O(A) close to CuO_2 plane [6]. This distortion of O(A) causes the decrease of the hole potential on CuO_2 plane but not O(A). It follows the increase of ΔV_A . In $\text{YBa}_2\text{Cu}_4\text{O}_8$, a measured distortion of the bond length of Cu-O(A), d_A , is given by $d \ln d_A / dP \approx -2.5 \text{ \%/GPa}$. Since we have $d \Delta V_A / d \ln d_A = -14.7$ eV in the ionic crystal model and $d T_c / d \Delta V_A \approx 10 \text{ K/eV}$ in Fig. 1, we obtain $d T_c / dP \approx 4 \text{ K/GPa}$. This value agrees with the experimental one, 5.5 K/GPa [6].

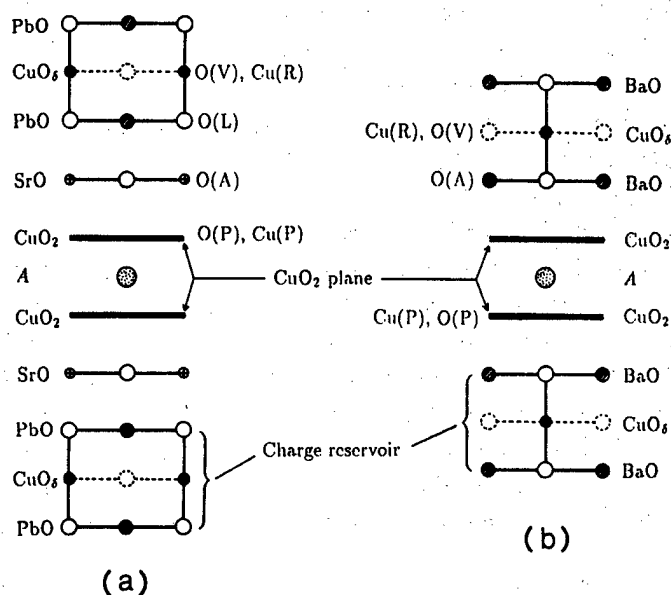


Fig. 2. Schematic representation of the structures of the layered compounds (a) $Pb_2Sr_2ACu_3O_{8+\delta}$ and (b) $ABa_2Cu_3O_{6+\delta}$. Note that the charge reservoirs consist of the $PbO-CuO_\delta-PbO$ block in (a) and the $BaO-CuO_\delta-BaO$ block in (b). In (a) the SrO layer separates the CuO_2 planes from the charge reservoir.

The T_c vs. ΔV_A curve in Fig. 1 indicates the existence of a threshold in ΔV_A (≈ -2 eV), which separates superconducting compounds from metallic but not superconducting ones. Since ΔV_A increases with pressure, the latter class of compounds such as $La_2SrCu_2O_6$ will become superconducting if high pressure of a few GPa is applied. The negative ΔV_A in $La_2SrCu_2O_6$ has also been pointed out by Kondo *et al.* [8].

Compounds with no apical oxygens such as Nd_2CuO_4 [9] may be regarded as the systems with $\Delta V_A \rightarrow \infty$. Thus, we expect that, if these compounds could be doped with holes rather than electrons, they should be superconductors with high T_c of over 100 K-class.

We will discuss the correlation between T_c and ΔV_A through the calculation of the electronic states in Sec. 3.

2-2. Possible new superconducting phases in $Pb_2Sr_2Y_{1-x}Ca_xCu_3O_{8+\delta}$ [3]

Cava *et al.* [10] have discovered a family of high T_c superconductors with formula $Pb_2Sr_2ACu_3O_{8+\delta}$ (A = a mixture of lanthanide and alkaline earth elements). Here, we would like to propose possible new superconducting phases in this family.

The family has the following interesting properties: (i) wide range of oxygen stoichiometry, (ii) capability of substitution by various elements, and (iii) unusual electronic configuration, i.e., the average Cu valence is less than 2+ unlike the other known superconductors which always have the valence greater than 2+.

This family of compounds also exhibits a structural similarity to $ABa_2Cu_3O_{6+\delta}$. As seen in Fig. 2, both families have (i) a pair of CuO_2 layers separated by an O-free A layer and (ii) an O-deficient Cu layer which absorbs/releases O atoms. The structures may be divided into the building blocks: the CuO_2 planes and a $PbO-CuO_\delta-PbO$ or $BaO-CuO_\delta-BaO$ block involving the O-deficient Cu layer which supplies (or absorbs) holes to (or from) the CuO_2 planes. We call the latter block the charge reservoir. In $Pb_2Sr_2ACu_3O_{8+\delta}$, a SrO layer separates the CuO_2 planes from the charge reservoir. Non-equivalent Cu and O atoms in the unit cell are denoted by symbols, $Cu(P)$, $O(R)$, \dots , in Fig. 2.

To examine the charge distributions in $Pb_2Sr_2Y_{1-x}Ca_xCu_3O_{8+\delta}$, we focus on excess $x + 2\delta - 1$ carriers per formula unit, which are either holes or electrons depending on whether the sign is positive or negative. Observed small orthorhombic and superstructural distortions of the crystal are neglected. We assume the followings: (i) Pb is maintained in a 2+ valence state because a possible 4+ state is estimated from the atomic ionization energies to be much higher in energy (by 70.9 eV) than the 2+ state. (ii) The average valence state of Cu is between 1+ and 3+. Finally, we impose the following criterion on the state of the system: if the CuO_2 plane has p holes per unit CuO_2 with $0.05 \leq p \leq 0.32$ [1,11], then the compound is superconducting, and otherwise it is insulating ($0 \leq p < 0.05$) or normal metallic ($p > 0.32$). Values of the ionization energies of Cu and electron affinity of O are: $I_{Cu}(2) = 20.3$ eV, $I_{Cu}(3) = 36.8$ eV and $A_O(2) = -8.1$ eV. Ambiguity of the value of the electron affinity of O makes it difficult to determine whether holes sit on Cu or O in the

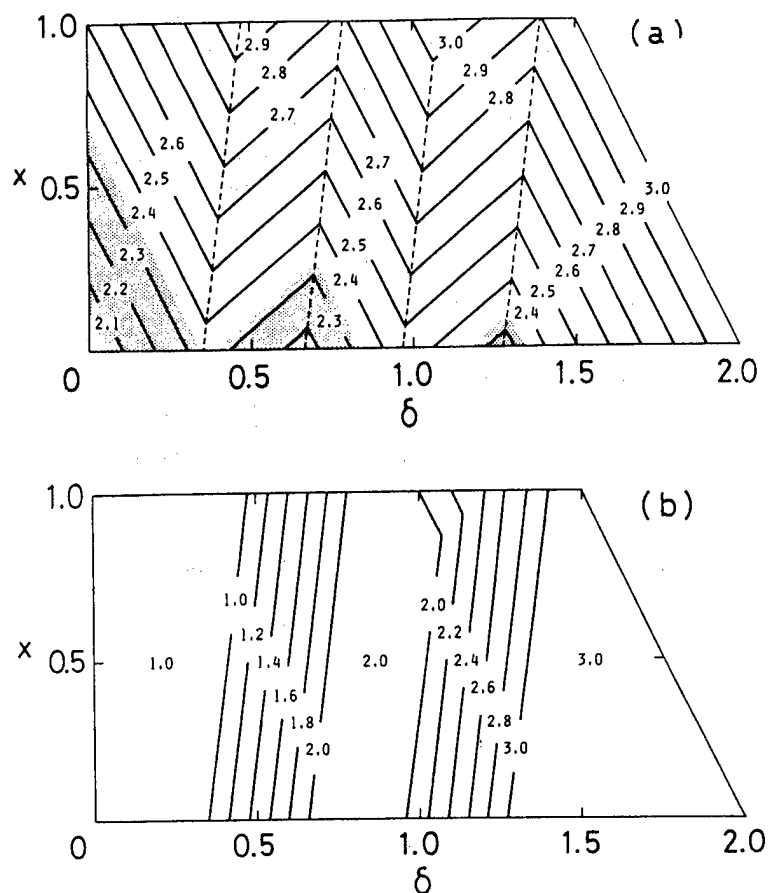


Fig. 3. Average valencies of Cu(P) in (a) and Cu(R) in (b) for $\text{Pb}_2\text{Sr}_2\text{Y}_{1-x}\text{Ca}_x\text{Cu}_3\text{O}_{8+\delta}$. The shaded area represents the superconducting regions.

CuO_2 planes. Here, we assume that holes sit on Cu sites in the plane. However, we can show that the qualitative results do not depend on this assumption.

Figure 3 shows the calculated results for the average valency of the Cu ions, which are obtained by assuming that the O ions are all in the 2- state. We find the following characteristics with increasing δ : (i) The compound is insulating near $x = \delta = 0$ since there are no carriers on the CuO_2 planes. (ii) In the region with $0.1 \leq 2\delta + x \leq 0.64$ the system is superconducting because an appropriate number of holes are in the CuO_2 planes. This is consistent with experiment [10]. (iii) The system becomes normal metallic for $0.32 < \delta \lesssim 0.4$ because there are too many holes in the CuO_2 planes. (iv) Around $0.4 \lesssim \delta \lesssim 0.5$ the valence state of Cu in the reservoir changes by absorbing holes from the CuO_2 planes. (v) As a result, the number of holes in the CuO_2 planes reduces to become appropriate for the superconductivity. We thus have the second superconducting region around $\delta \simeq 0.7$. (vi) For $0.7 \lesssim \delta \lesssim 0.9$ the valence state of Cu in the reservoir is maintained to be 2+, and the number of holes on the CuO_2 planes is again larger than 0.32 and the system is normal metallic. (vii) Following the change from Cu(R)^{2+} to Cu(R)^{3+} for $0.9 \lesssim \delta \lesssim 1.6$, holes are again absorbed by the reservoir. We may therefore have the third superconducting region for $1.2 \lesssim \delta \lesssim 1.3$ although it is rather small.

These results in $\text{Pb}_2\text{Sr}_2\text{Y}_{1-x}\text{Ca}_x\text{Cu}_3\text{O}_{8+\delta}$ are in strong contrast with those in $\text{YBa}_2\text{Cu}_3\text{O}_{6+\delta}$. In the latter compounds, holes introduced by the oxidation are first captured by the charge reservoir. Then, at the stoichiometry of $\delta = 0.5$ in the case where oxygens are at random in the reservoir [8], holes start overflowing into the CuO_2 planes, leading to the emergence of superconductivity.

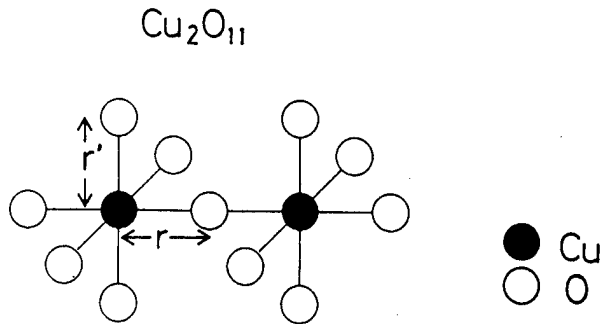


Fig. 4. Cu_2O_{11} cluster used in the cluster model calculation. The ratio r'/r is taken to be 1.275.

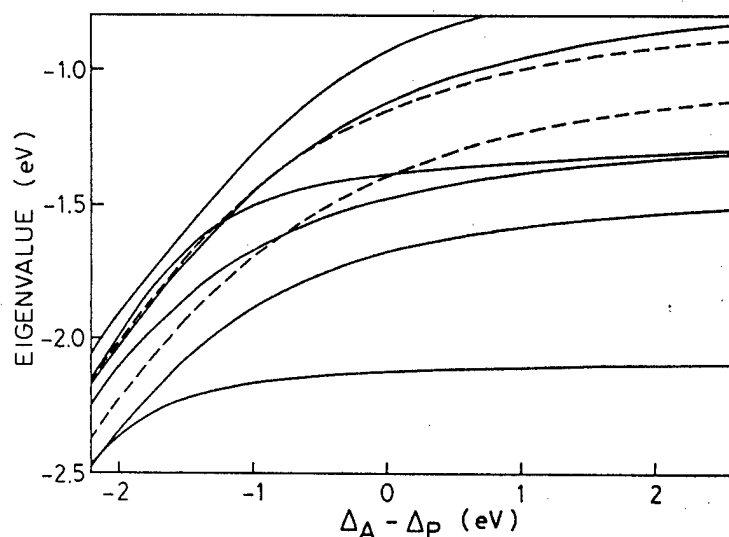


Fig. 5. The low energy eigenvalues of Cu_2O_{11} cluster with three holes as functions of $\Delta_A - \Delta_P$. The solid and dashed lines denote the states with $S_z = 1/2$ (doublet) and $S_z = 3/2$ (quartet), respectively.

3. Electronic states in the cluster model [5]

In the previous section, we have assumed the compound to be essentially ionic crystals. In this section, we examine the role of covalency in the cluster model, where the Madelung energy may be absorbed into the energy level of each atom.

Let us consider the coupled clusters given in Fig. 4 in connection to La_2CuO_4 . In the calculation, we take the Cu-3d orbitals with $(x^2 - y^2)$ and $(3z^2 - r^2)$ symmetries and the O-2p orbitals which cause σ -bonds with Cu-3d orbitals. We define the parameters Δ_P and Δ_A for the energies of O's in the plane and the apical sites, respectively, as $\Delta_P = \epsilon_{2p}(\text{P}) - \epsilon_{3d}(x^2 - y^2)$ and $\Delta_A = \epsilon_{2p}(\text{A}) - \epsilon_{3d}(x^2 - y^2)$, where $\epsilon_{2p}(\text{P})$ and $\epsilon_{2p}(\text{A})$ are the energies of a hole on 2p orbitals in the plane and the apical site, respectively, and $\epsilon_{3d}(x^2 - y^2)$ is the energy of a hole on Cu-3d orbital with $(x^2 - y^2)$ symmetry. The value $\Delta_A - \Delta_P$ and the Madelung energy ΔV_A given in the previous section do not exactly agree with each other. This is because covalency reduces the formal valence of each atom, which has been used to calculate ΔV_A in the ionic model. Nevertheless, we assume that $\Delta_A - \Delta_P$ is proportional to ΔV_A .

In Fig. 5, low energy eigenvalues of the cluster with three holes are shown as functions of $\Delta_A - \Delta_P$. The solid and dashed curves denote the states with $S_z = 1/2$ (doublet) and $S_z = 3/2$ (quartet), respectively. In Table 1, the hole population on each atom for several values of $\Delta_A - \Delta_P$ is also listed. When $\Delta_A - \Delta_P$ is much larger than -2 eV, the ground and first excited states are described as the bonding and anti-bonding states of the local singlet, respectively. With decreasing $\Delta_A - \Delta_P$, the local triplet mixes and the stability of the local singlet decreases. At $\Delta_A - \Delta_P \approx -2.1$ eV, the ground and first excited states cross each other. Therefore, assuming that $\Delta_A - \Delta_P$ is proportional to ΔV_A , we may consider that T_c is related with how the local singlet is stable.

Table III. Hole population on each atom in the Cu_2O_{11} cluster with three holes as a function of $\Delta_A - \Delta_P$. $\Delta_A - \Delta_P = \infty$ corresponds to Cu_2O_7 cluster. g.s. denotes the ground state, and 1st and 2nd denote the first and second excited states, respectively. O(1) is the central oxygen and O(A) is the apical oxygen.

$\Delta_A - \Delta_P$ (eV)	state (symmetry)	Cu ($x^2 - y^2$)	Cu ($3z^2 - r^2$)	O(1)	O(A)
∞	g.s. (2A_g)	0.803	0.011	0.362	—
	1st ($^2B_{1u}$)	0.755	0.085	0.244	—
	2nd ($^2B_{1u}$)	0.530	0.365	0.317	—
2.0	g.s. (2A_g)	0.795	0.019	0.369	0.001
	1st ($^2B_{1u}$)	0.638	0.224	0.315	0.008
	g.s. (2A_g)	0.501	0.396	0.338	0.010
0.0	g.s. (2A_g)	0.786	0.029	0.373	0.005
	1st ($^2B_{1u}$)	0.584	0.272	0.339	0.033
	2nd (2A_g)	0.543	0.335	0.321	0.032
-2.0	g.s. (2A_g)	0.680	0.103	0.306	0.108
	1st ($^2B_{1u}$)	0.634	0.137	0.269	0.151
	2nd (4A_g)	0.624	0.169	0.185	0.163

4. Conclusion

Starting with the ionic crystal model, we examined the Madelung potential and hole distribution in various Cu-oxides compounds. We found that in addition to the hole concentration on the plane, the Madelung potential on the apical oxygen relative to that in the CuO_2 plane, ΔV_A , in the parent compounds is a crucial parameter for T_c . Through the calculation of the potential, we proposed several high- T_c compounds including new phases of $\text{Pb}_2\text{Sr}_2\text{Y}_{1-x}\text{Ca}_x\text{Cu}_3\text{O}_{8+\delta}$. For the superconductivity, there exists a threshold value of ΔV_A (≈ -2 eV). The calculation of the electronic states in the cluster model suggests that T_c is related with how the local singlet is stable. More detailed study of the electronic states is in progress.

Acknowledgement

This work has been supported by Grant-in-Aid for Scientific Research on Priority Areas "Mechanism of Superconductivity".

References

- [1] J. B. Torrance, A. Bezing, A. I. Nazzari and S. S. P. Parkin: *Physica C* **162-164** (1989) 291.
- [2] Y. Ohta, T. Tohyama and S. Maekawa: to be published in *Physica C*.
- [3] Y. Ohta and S. Maekawa: to be published in *Phys. Rev. B*.
- [4] S. Maekawa, J. Inoue and T. Tohyama: *Strong Correlations and Superconductivity*, eds. H. Fukuyama, S. Maekawa and A. P. Malozemoff (Springer Series in Solid State Sciences **89**, 1989) p. 66.
- [5] T. Tohyama and S. Maekawa: to be published.
- [6] E. Kaldos, P. Fischer, A. W. Hewat, E. A. Hewat, J. Karpinski and S. Rusiecki: *Physica C* **159** (1989) 668.
- [7] J. B. Torrance, Y. Tokura, A. Nazzari and S. S. P. Parkin: *Phys. Rev. Lett.* **60** (1988) 542.
- [8] J. Kondo, Y. Asai and S. Nagai: *J. Phys. Soc. Japan* **57** (1988) 4334.
- [9] Y. Tokura, H. Takagi and S. Uchida: *Nature* **337** (1989) 345.
- [10] R. J. Cava *et al.*: *Nature* **336** (1988) 211.
- [11] See also J. B. Torrance *et al.*: *Phys. Rev. Lett.* **61** (1988) 1127 and J. B. Torrance *et al.*: *Phys. Rev. B* **40** (1989) 8872.
- [12] J. Kondo: *J. Phys. Soc. Japan* **58** (1989) 2884.

Theoretical Study of Tunneling Spectra in $\text{Ba}_x\text{K}_{1-x}\text{BiO}_3$

Masafumi SHIRAI, Naoshi SUZUKI and Kazuko MOTIZUKI

Department of Material Physics, Faculty of Engineering Science
Osaka University, Toyonaka 560, Japan

Tunneling spectra of $\text{Ba}_x\text{K}_{1-x}\text{BiO}_3$ (BKB) are studied on the basis of the strong coupling theory of phonon mechanism for superconductivity. By using the electron-lattice coupling, which is calculated microscopically by the use of the realistic electronic band structure and the renormalized phonons, we have calculated the spectral function $\alpha^2F(\omega)$. The gap function $\Delta(\epsilon)$ is obtained by solving the Eliashberg equation at $T=0$ K. The superconducting energy gap Δ_0 is evaluated to be 4.8 meV for $x=0.7$ and 1.0 meV for $x=0.5$. Spectra of differential conductance dI/dV and its derivative d^2I/dV^2 show significant deviations from those predicted by the BCS weak coupling theory. The value of Δ_0 and the line shapes of dI/dV and d^2I/dV^2 are in good agreement with the recent observations.

§1. Introduction

Oxide superconductor $\text{Ba}_x\text{K}_{1-x}\text{BiO}_3$ (BKB) with a cubic perovskite-type structure has been found to have the highest transition temperature ($T_c \approx 28$ K at $x=0.7$) among the Cu-free superconductors.¹⁻³⁾ Since BKB contains no transition-metal element, the magnetic mechanism may not be expected for the superconductivity in BKB. In fact any magnetic order has not been observed in BKB by the μ -on spin rotation experiments⁴⁾ and the magnetic susceptibility in the normal state in BKB shows a Pauli paramagnetic behavior.^{5,6)}

We have intensively made microscopic study on the electron-lattice interaction and the lattice dynamics of BKB and its related compound $\text{BaPb}_{1-x}\text{Bi}_x\text{O}_3$ by using the realistic electronic bands of BaBiO_3 .⁷⁻¹¹⁾ Furthermore, we have evaluated T_c by solving the linearized Eliashberg equation with use of the calculated spectral function $\alpha^2F(\omega)$.^{10,11)} The magnitude and the isotope shift of T_c calculated by us are in good agreement with the experimental data for BKB.^{3,6,12)} Our microscopic study has clarified that the origin of high- T_c of BKB can be ascribed to the strong electron-phonon coupling caused by vibrations of O atoms toward Bi atoms.

In this report tunneling spectra of BKB are studied theoretically to clarify the effects of the strong electron-phonon coupling upon the tunneling spectra. In §2 the results of calculation of the electron-lattice interaction and the lattice dynamics of BKB are reviewed. Then, the tunneling spectra are studied in §3 on the basis of the strong coupling theory for superconductivity.

§2. Electron-Lattice Interaction and Lattice Dynamics

According to the results of the self-consistent LAPW band calculations¹³⁾ the conduction band which acrosses the Fermi level is a hybridized band consisting of O

2p and Bi 6s orbitals. This conduction band is well reproduced by the tight-binding (TB) model with three Slater-Koster transfer integrals between nearest neighbouring Bi and O atoms. By using the TB conduction band we calculate the electron-lattice coupling coefficient which is described as¹⁴⁾

$$g_{\mu}^{\alpha}(nk, n'k') = \sum_{a, \nu} \sum_{b, \nu'} [A^{\dagger}(k)]_{n, \mu, \alpha} [t_{\mu}^{\alpha}(k, k')]_{\mu, a, \nu} [A(k')]_{\nu, b, n'} \quad (1)$$

where $A(k)$ represent the transformation coefficients which diagonalize the transfer matrix of the cubic structure, and $t_{\mu}^{\alpha}(k, k')$ is written in terms of derivatives of the transfer integrals (t'). The values of t' have been estimated to be about $4 \text{ eV} \cdot \text{\AA}^{-1}$ to reproduce the electronic band gap in a charge density wave (CDW) phase of BaBiO_3 . The coupling coefficient $g_{\mu}^{\alpha}(nk, n'k')$ represents the strength of the coupling between two conduction band states nk and $n'k'$ caused by the displacement of the μ th atom along the α direction ($\alpha = x, y, z$). It is found that $g_{\mu}^{\alpha}(nk, n'k')$ has the remarkable wavevector and mode dependences, reflecting the nature of the conduction band. Especially the displacements of O atoms toward the neighboring Bi atoms interact with the conduction band. Since the conduction band of BKB is little affected by doping of K atoms,¹³⁾ we adopt hereafter the rigid-band approximation for the doping effects, i.e. we assume that the TB conduction band is filled gradually without change of its dispersion as x increases.

Next we study the lattice dynamics of BKB by taking account of the effect of the electron-lattice interaction. The dynamical matrix is divided into two parts: the generalized electronic susceptibility χ and the remaining part D_0 . The Fourier transform of χ represents the effective long range forces caused by the electron-lattice interaction, whereas D_0 is usually given by the Fourier transform of inter-atomic short range forces. For D_0 we consider seven kinds of short range forces. They are determined to fit seven phonon frequencies observed in $\text{BaPb}_{0.75}\text{Bi}_{0.25}\text{O}_3$.¹⁵⁾ Since the vibrations of Ba or K atoms are hardly coupled with the conduction band states, we neglect the difference between Ba and K atoms in BKB. It is found that the electron-lattice interaction causes lowering of the frequency and broadening of the line-width of the longitudinal (L) O stretching or breathing mode vibration, which is originally located around 60 meV. The frequency renormalization is remarkable especially in the wavevector region near the Brillouin zone boundaries. The wavevector and mode dependences of the phonon renormalization are originated from the wavevector and mode dependences of $g_{\mu}^{\alpha}(nk, n'k')$. It is noted that the renormalization becomes remarkable as x increases, reflecting the variation of the conduction band states near the Fermi level.

§3. Superconducting Energy Gap at $T = 0 \text{ K}$ and Tunneling Spectra

Tunneling measurement is one of powerful methods to observe directly the superconducting energy gap. It can also provide direct information about the electron-phonon spectral function.¹⁶⁾ The differential conductance dI/dV through the junction between a superconductor and a normal metal is approximately proportional to the electronic density of states $N_s(\epsilon)$ in the superconducting state:¹⁷⁾

$$\left. \frac{dI}{dV} \right|_{eV=\epsilon} \propto \frac{N_s(\epsilon)}{N(E_F)} = \text{Re} \left[\frac{|\epsilon|}{[\epsilon^2 - \Delta(\epsilon)^2]^{1/2}} \right] \quad (2)$$

where $N(E_F)$ denotes the electronic density of states at the Fermi level E_F in the normal state, and $\Delta(\epsilon)$ represents the energy dependent gap function at $T=0$ K, which is determined by solving the Eliashberg equation for $T=0$ K:^{16,17)}

$$\xi(\epsilon) = [1 - Z(\epsilon)]\epsilon$$

$$= \int_{\Delta_0}^{\infty} d\epsilon' \operatorname{Re} \left[\frac{\epsilon'}{[\epsilon'^2 - \Delta(\epsilon')^2]^{1/2}} \right] \int_0^{\infty} d\omega \alpha^2 F(\omega) \left(\frac{1}{\epsilon' + \epsilon + \omega - i\delta} - \frac{1}{\epsilon' - \epsilon + \omega - i\delta} \right), \quad (3)$$

$$\Delta(\epsilon) = \frac{1}{Z(\epsilon)} \int_{\Delta_0}^{\infty} d\epsilon' \operatorname{Re} \left[\frac{\epsilon'}{[\epsilon'^2 - \Delta(\epsilon')^2]^{1/2}} \right] \int_0^{\infty} d\omega \alpha^2 F(\omega) \left(\frac{1}{\epsilon' + \epsilon + \omega - i\delta} + \frac{1}{\epsilon' - \epsilon + \omega - i\delta} \right)$$

$$- \frac{\mu^*}{Z(\epsilon)} \int_{\Delta_0}^{\epsilon_c} d\epsilon' \operatorname{Re} \left[\frac{\epsilon'}{[\epsilon'^2 - \Delta(\epsilon')^2]^{1/2}} \right], \quad (\delta \rightarrow +0) \quad (4)$$

where $\xi(\epsilon)$ is the electronic self-energy of the normal state, $Z(\epsilon)$ is called the mass renormalization function, and Δ_0 denotes the superconducting energy gap defined by $\Delta_0 = \Delta(\Delta_0)$. The Coulomb interaction is treated in terms of an effective parameter μ^* which is about 0.1 in usual metals.

The spectral function $\alpha^2 F(\omega)$ is defined by

$$\alpha^2 F(\omega) = \frac{1}{N(E_F)} \sum_{nn'} \sum_{\mathbf{k}\mathbf{k}'} \sum_{\gamma} \frac{|V^{\gamma}(\mathbf{n}\mathbf{k}, \mathbf{n}'\mathbf{k}')|^2}{2N\omega_{\mathbf{k}'-\mathbf{k}}^{\gamma}} \delta(E_{\mathbf{n}\mathbf{k}}^0 - E_F) \delta(E_{\mathbf{n}'\mathbf{k}'}^0 - E_F) \delta(\omega - \omega_{\mathbf{k}'-\mathbf{k}}^{\gamma}), \quad (5)$$

where $\omega_{\mathbf{k}'-\mathbf{k}}^{\gamma}$ is the phonon frequency of mode γ , $E_{\mathbf{n}\mathbf{k}}^0$ denotes the conduction band energy and $V^{\gamma}(\mathbf{n}\mathbf{k}, \mathbf{n}'\mathbf{k}')$ represents the electron-phonon coupling coefficient given by

$$V^{\gamma}(\mathbf{n}\mathbf{k}, \mathbf{n}'\mathbf{k}') = \sum_{\mu\alpha} \frac{1}{\sqrt{M_{\mu}}} \epsilon_{\gamma, \mu\alpha}(\mathbf{k}'-\mathbf{k}) g_{\mu}^{\alpha}(\mathbf{n}\mathbf{k}, \mathbf{n}'\mathbf{k}') \quad (6)$$

Here, M_{μ} is the mass of the μ th atom, $\epsilon_{\gamma, \mu\alpha}(\mathbf{k}'-\mathbf{k})$ denotes the phonon polarization vector.

Figs.1(a) and 2(a) show the spectral function $\alpha^2 F(\omega)$ and the phonon density of states $F(\omega)$ calculated for $x=0.7$ ($\text{Ba}_{0.7}\text{K}_{0.3}\text{BiO}_3$) and $x=0.5$ ($\text{Ba}_{0.5}\text{K}_{0.5}\text{BiO}_3$), respectively. In the present calculations $t^* = 4.05 \text{ eV} \cdot \text{\AA}^{-1}$ is used. It is clearly seen that the frequency dependence of $\alpha^2 F(\omega)$ is entirely different from that of $F(\omega)$. For smaller value of x (< 0.3) $\alpha^2 F(\omega)$ has some prominent structures only in the frequency range of 0 stretching or breathing mode around 60 meV. Thus the 0 stretching or breathing mode is expected to contribute dominantly to the superconductivity in BKB. As x increases, however, some main peaks in $\alpha^2 F(\omega)$ shift to lower frequency side and the magnitude of $\alpha^2 F(\omega)$ increases in the whole frequency range up to 60 meV as shown in Figs.1(a) and 2(a). This drastic change in $\alpha^2 F(\omega)$ is caused by the frequency renormalization of the 0 stretching or breathing mode.

Once the spectral function $\alpha^2 F(\omega)$ and μ^* are given, $\xi(\epsilon)$ and $\Delta(\epsilon)$ are calculated by utilizing eqs.(3) and (4) in a self-consistent manner. In actual calculations the value of $\mu^*=0.1$ has been used. Further the cut-off energy ϵ_c has been taken to be 200 meV and then $\Delta(\epsilon)$ has sufficiently converged in iteration of several times. In result, the superconducting energy gap Δ_0 is found to be 4.8 meV for $x=0.7$ and 1.0 meV

for $x=0.5$. The energy gap obtained for $x=0.7$ is in good agreement with the recent experimental data $\Delta_0=4.3$ meV determined by optical measurement for $\text{Ba}_{0.6}\text{K}_{0.4}\text{BiO}_3$ ($T_c=29$ K).¹⁸⁾ Since T_c has been evaluated to be 31.3 K for $x=0.7$ and $\mu^*=0.1$, a ratio $2\Delta_0/k_B T_c$ is found to be about 3.6, which is accidentally close to that predicted by the BCS theory. However, the gap function $\Delta(\epsilon)$ exhibits the remarkable energy dependence which is typical in the strong coupling superconductor, and such prominent structures in $\Delta(\epsilon)$ must be reflected in the tunneling spectra.

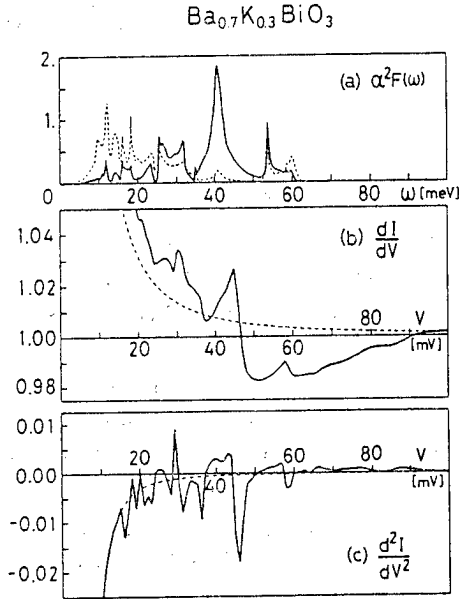


Figure 1. (a) $\alpha^2 F(\omega)$ (full curves) and $F(\omega)$ (broken curves), (b) dI/dV , and (c) d^2I/dV^2 calculated for $x=0.7$. The broken curves in (b) and (c) represent the BCS results.

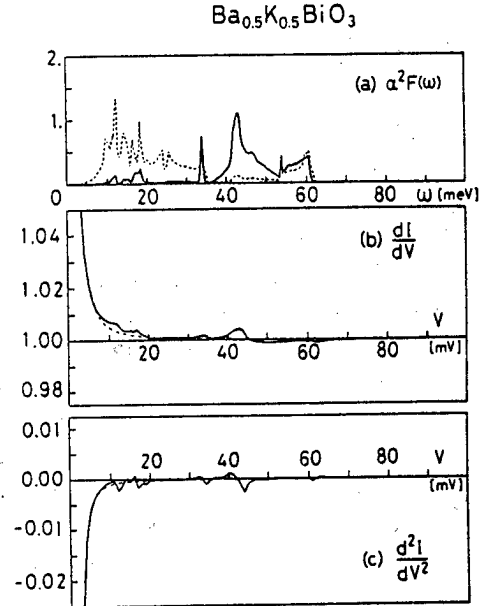


Figure 2. (a) $\alpha^2 F(\omega)$ (full curves) and $F(\omega)$ (broken curves), (b) dI/dV , and (c) d^2I/dV^2 calculated for $x=0.5$. The broken curves in (b) and (c) represent the BCS results.

We have calculated the differential conductance dI/dV given by eq.(2). The results for $x=0.7$ and $x=0.5$ are shown by full curves in Fig.1(b) and 2(b), respectively. The broken curves represent the BCS results which are given by

$$\frac{N_s(\epsilon)}{N(E_F)} \approx \text{Re} \left[\frac{|\epsilon|}{[\epsilon^2 - \Delta_0^2]^{1/2}} \right] \quad (7)$$

Deviations from the BCS results are clearly seen in Figs.1(b) and 2(b). We have calculated also the second derivative spectra d^2I/dV^2 . The results are shown in Figs. 1(c) and 2(c). In general d^2I/dV^2 gives direct information about $\alpha^2 F(\omega)$, i.e. negative peaks (dips) in d^2I/dV^2 correspond to peaks in $\alpha^2 F(\omega)$.¹⁶⁾ By comparing Figs. 1(c) and 1(a) it is clear that our results show certainly such correspondences. It should be noted here that the fine structures in the d^2I/dV^2 spectra are drastically reduced when going from $x=0.7$ to $x=0.5$. This is due to a decrease of the magnitude of the gap function $\Delta(\epsilon)$ as x changes from 0.7 to 0.5.

Recently, tunneling spectroscopy measurements with high resolution have been performed on $\text{Ba}_{0.625}\text{K}_{0.375}\text{BiO}_3$ ($T_c=29$ K).¹⁹⁾ The observed curves of dI/dV and

d^2I/dV^2 have line shapes similar to those shown in Fig.1(b) and (c), respectively. In particular, the dips in d^2I/dV^2 observed below 60 meV show good correspondence to the negative peaks in Fig.1(c). Very recently, tunneling measurements have been performed also on $Ba_{0.5}K_{0.5}BiO_3$ ($T_c = 13$ K)²⁰⁾ and a drastic reduction of prominent structures in d^2I/dV^2 spectra has been observed as predicted by our calculation.

In conclusion, the superconducting properties in BKB, such as the energy gap and the tunneling spectra as well as the magnitude and the isotope shift of T_c , can be understood in the framework of the strong coupling theory of the phonon-mediated pairing mechanism.

References

- 1) L.F.Mattheiss, E.M.Gyorgy and D.W.Johnson, Jr.: Phys. Rev. B37 (1988) 3745.
- 2) R.J.Cava, B.Batlogg, J.J.Krajewski, R.C.Farrow, L.W.Rupp, Jr., A.E.White, K.T.Short, W.F.Peck, Jr. and T.Y.Kometani: Nature (London) 332 (1988) 814.
- 3) D.G.Hinks, B.Dabrowski, J.D.Jorgensen, A.W.Mitchell, D.R.Richards, S.Pei and D.Shi: Nature (London) 333 (1988) 836.
- 4) Y.J.Uemura, B.J.Sternlieb, D.E.Cox, J.H.Brewer, R.Kadono, J.R.Kempton, R.F.Kiefl, S.R.Kreitzman, G.M.Luke, P.Mulheln, T.Riseman, D.L.Williams, W.J.Kossler, X.H.Yu, C.E.Stronach, M.A.Subramanian, J.Gopalakrishnan and A.W.Sleight: Nature (London) 335 (1988) 151.
- 5) B.Batlogg, R.J.Cava, L.W.Rupp, Jr., A.M.Mujsce, J.J.Krajewski, J.P.Remeika, W.F.Peck, Jr., A.S.Cooper and G.P.Espinoza: Phys. Rev. Lett. 61 (1988) 1670.
- 6) S.Kondoh, M.Sera, Y.Ando and M.Sato: Physica C157 (1989) 469.
- 7) M.Shirai, N.Suzuki and K.Motizuki: Solid State Commun. 60 (1986) 489.
- 8) M.Shirai, N.Suzuki and K.Motizuki: JJAP Series 1 (1988) 255.
- 9) M.Shirai, N.Suzuki and K.Motizuki: Ferroelectrics (1989) in press.
- 10) M.Shirai, N.Suzuki and K.Motizuki: J. Phys.: Condens. Matter 1 (1989) 2939.
- 11) M.Shirai, N.Suzuki and K.Motizuki: to be published in Proc. of Int. Conf. on Phonon Phys. (Heidelberg; 1989).
- 12) D.G.Hinks, D.R.Richards, B.Dabrowski, D.T.Marx and A.W.Mitchell: Nature (London) 335 (1988) 419.
- 13) L.F.Mattheiss and D.R.Hamman: Phys. Rev. Lett. 60 (1988) 2681.
- 14) K.Motizuki and N.Suzuki: Structural Phase Transitions in Layered Transition-Metal Compounds, ed. K.Motizuki (Dordrecht, Reidel; 1986) p.1.
- 15) W.Reichardt and W.Weber: JJAP 26, Suppl. 26-3 (1987) 1121.
- 16) W.L.McMillan and J.M.Rowell: Phys. Rev. Lett. 14 (1965) 108.
- 17) J.R.Schrieffer, D.J.Scalapino and J.W.Wilkins: Phys. Rev. Lett. 10 (1963) 336.
- 18) Z.Schlesinger, R.T.Collins, J.A.Calise, D.G.Hinks, A.W.Mitchell, Y.Zheng, B.Dabrowski, N.E.Bickers and D.J.Scalapino: Phys. Rev. B40 (1989) 6862.
- 19) J.F.Zasadzinski, N.Tralshawala, D.G.Hinks, B.Dabrowski, A.W.Mitchell and D.R.Richards: Physica C158 (1989) 519.
- 20) J.F.Zasadzinski: private communication.

Electronic State and Superconductivity in Layered Copper Oxides

M. Tachiki and H. Matsumoto

Institute for Materials Research, Tohoku University
2-1-1 Katahira, Sendai 980, Japan

This report contains two subjects. One is a theoretical study on the electronic state in the metal-insulator transition region of the oxide superconductors using the d-p mixing model. The result shows that a new band arises spontaneously inside the charge transfer gap due to a many body effect, and develops with hole doping. The occurrence of many unusual properties in the oxides is related to the formation of the new band. The other subject is a study on the superconducting properties of the layered copper oxides. The stacking structure of strongly and weakly superconducting layers in the oxides causes a characteristic fine structure inside the tunneling gap in the tunneling spectrum. The layer structure itself works as the strong pinning centers of the flux lines, and plays an important role in realizing a high critical current.

1. Electronic State in Oxide Superconductors

Since the discovery of the high T_c superconductivity in La-Sr-Cu-O [1], many kinds of Cu-oxide superconductors have been found such as Y-Ba-Cu-O [2], Bi-Sr-Ca-Cu-O [3], Tl-Ca-Ba-Cu-O [4] and Nd-Ce-Cu-O [5]. All those materials have the layered structure composed of Cu-O planes. It is now widely accepted that the electronic states on this plane are responsible for the superconductivity. In those materials, the superconductivity appears only in the intermediate region of the insulator-metal transition [6]. When a system becomes too metallic, the superconductivity is destroyed. This suggests that the mechanism of the superconductivity is closely related with properties of electronic states realized near the insulator-metal transition. What kind of the special properties make the superconductive state favourable?

In recent experiments of photoemission [7,9-14], EELS [8] and optical reflection and transmission [15-18], the structures of the electronic state near the Fermi level have been extensively studied. The electronic state near the Fermi level is mainly of the oxygen p-character with a small mixture of the copper d-character [8-12]. There is a strong intra-atomic Coulomb repulsion ($\sim 7\sim 10$ eV) at the Cu-sites [7-10] and the insulator gap ($\sim 1.5\sim 2.0$ eV) [8,15,18] is the charge transfer gap between the p-band and the upper Hubbard-split d-level. The Fermi edge is clearly observed [9-12]. The topological structure of the Fermi surface is very similar to the one obtained from the band calculation [13], but its dispersion is very flat (5-10 factor difference) [9,11,12], forming a very narrow band. The opening of the superconducting gap

in the concerned band is also observed below T_C [12,14]. The experiments of the optical conductivity also reveals the following facts. In the insulator phase of La-Sr-Cu-O, the charge transfer gap is about 2eV, and with increasing hole doping, certain structures at 0.5eV and 1.5eV develop [15,18] in addition to the Drude part. In the metallic phase of Y-Ba-Cu-O [16,17] and La-Sr-Cu-O [15,18], two components structure is observed in the infrared region; the Drude part is sensitive to the doping and temperature, and the mid-infrared structure is less sensitive to temperature and shifts gradually to the low energy region with hole doping. One of the remarkable results in the photoemission and EELS is in the fact that a narrow band seems to develop inside the charge transfer gap, and relative positions of energy levels from the Fermi level are not much changed in the insulator-metal transition. In fact if one assumes the development of a new state at the Fermi level which is situated about 0.5eV above the p-band, the observed double structure in the optical conductivity is naturally understood. However, this means that, quite differently from a simple band theory, holes are not doped to the occupied states of the p-band with lowering the Fermi level, but a new band is formed spontaneously at the Fermi level inside the insulator gap. Since a similar narrow band is observed even in the regular lattice of $\text{Bi}_2\text{Sr}_2\text{Ca}_1\text{Cu}_2\text{O}_8$ [19,20], $\text{TlBa}_2\text{CaCu}_2\text{O}_7$ [21] and its state density decreases in the less metallic samples by substituting Ca with Y, we consider that the spontaneous formation of a narrow band at the Fermi level is intrinsic in those materials.

If the spontaneous creation of a new state at the Fermi level occurs intrinsically in the metal-insulator transition, its mechanism should be closely connected with the formation of the Fermi surface due to a macroscopic amount of hole doping. Note that, in an infinite volume system, N_h (the total hole number) = finite means the hole density $\rho_h (= N_h/V; V$ is the volume) = 0. Even if $\rho_h \ll 1$, the total hole number N_h may be infinite, since V is infinite. If a mechanism applies even when one hole is doped in the insulator phase, such effects should appear in photoemission spectral of the insulator phase, since the photoemission observes the one hole excitation spectral from the ground state. Therefore the mechanism should arise from a many body effect among hole carriers. In those materials, the d-electron levels are Hubbard-splitting due to a strong intra-atomic Coulomb repulsion. Due to the hopping of electrons between O- and Cu-sites, the Cu-spin fluctuates, which produces a strong spin fluctuation. When holes are doped by a macroscopic amount, electrons hop around the lattice sites, receiving the spin scattering at Cu-sites. When the Fermi surface is formed, the Kondo-type effect is induced. We think that this effect is the cause of the forming of a new state at the Fermi level [22]. The above mechanism is also considered as follows. Suppose that we create the Fermi surface at the top of the p-band by hole-doping. Due to the Fermi edge effect, the effective Cu-spin-p-electron-spin interaction is increased. Then the electron states near the Fermi surface have a tendency to split from others by forming a partial singlet state with a Cu-spin, which may cause a spontaneous creation of a new band at the Fermi level.

In order to see the above possibility in the actual calculation [22], we start from the p-d mixing model [23]:

$$H = \sum_{i,\sigma} \epsilon_p p_{i\sigma}^\dagger p_{i\sigma} + \sum_i \left(\sum_{\sigma} \epsilon_d d_{i\sigma}^\dagger + U n_{ii} \right) + \sum_{i,j,\sigma} t_{ij} (p_{i\sigma}^\dagger d_{j\sigma} + d_{j\sigma}^\dagger p_{i\sigma}). \quad (1.1)$$

By assuming the nearest neighbour hopping between $\text{Cu}_{x^2-y^2}$ and O_{p_x, p_y} orbitals, and by

eliminating non-bonding band, we have

$$t_{ij} = \frac{\Omega}{(2\pi)^2} \int_{\Omega_B} d\vec{k} e^{i\vec{k}(\vec{R}_i - \vec{R}_j)} \left[4t \left(\sin^2 \frac{ak_x}{2} + \sin^2 \frac{ak_y}{2} \right) \right]^{1/2}, \quad (1.2)$$

where Ω is a unit volume, a is a lattice length, and R_i and R_j are lattice points. By considering the case of $\epsilon_d \rightarrow -\infty$, $\epsilon_\eta = \epsilon_d + U$ finite, the d-electron freedom is restricted to describe only $n_d = 1 \leftrightarrow 2$ transition, which introduces an operator η_\uparrow , η_\downarrow [24,25],

$$\eta_\uparrow = d_\uparrow n_\downarrow, \quad \eta_\downarrow = d_\downarrow n_\uparrow. \quad (1.3)$$

The p-electron propagator $S_{pp}^\dagger(\omega, \vec{k})$ and d-electron propagator $S_{\eta\eta}^\dagger(\omega, \vec{k})$, which is described by η , are obtained as

$$S_{pp}^\dagger(\omega, \vec{k}) = 1/[\omega - \epsilon_p - t^2(k) \tilde{S}_{\eta\eta}^\dagger(\omega, \vec{k})], \quad (1.4)$$

$$S_{\eta\eta}^\dagger(\omega, \vec{k}) = \tilde{S}_{\eta\eta}^\dagger(\omega, \vec{k}) / [1 - \frac{1}{\omega - \epsilon_p} t^2(k) \tilde{S}_{\eta\eta}^\dagger(\omega, \vec{k})], \quad (1.5)$$

where $\tilde{S}_{\eta\eta}^\dagger(\omega, \vec{k})$ is the one p-electron irreducible part given by

$$\tilde{S}_{\eta\eta}^\dagger(\omega, \vec{k}) = (n/2) / [\omega - \epsilon_\eta - \Sigma(\omega, \vec{k})], \quad (1.6)$$

and n is given by

$$\frac{2-n}{2} = \frac{\Omega}{(2\pi)^2} \int d^2k d\omega \left(-\frac{1}{\pi} \text{Im} S_{\eta\eta}^\dagger(\omega, \vec{k}) \right) (1 - f_F(\omega)). \quad (1.7)$$

By denoting $\eta_{i\sigma}(t) = \eta_\sigma(x)$, $\Sigma_{ij} p_j(t) = p_t(x)$, the irreducible part $\tilde{S}_{\eta\eta}^\dagger$ is evaluated from

$$\left(i \frac{\partial}{\partial t} - \epsilon_\eta \right) \langle R(\eta_\sigma(x) \eta_\sigma^\dagger(y)) \rangle = i \delta(x-y) \frac{n}{2} + \sum_\mu \left(-\frac{1}{2} \sigma^\mu \right) \langle R(\delta n_\mu(x) p_\mu(x) \eta_\sigma^\dagger(y)) \rangle \quad (1.8)$$

with $\sigma^\mu = (-1, \sigma_i)$, $n_\mu = (d^\dagger d, d^\dagger \sigma_i d)$ and $\delta n_\mu = n_\mu - \langle n_\mu \rangle$. By introducing a local decomposition

$$\langle \delta n_\mu(x) \eta_\sigma(z) \eta_\sigma^\dagger(y) \rangle = \sum_{\lambda \lambda'} \langle \delta n_\mu(x) \lambda(z) \rangle \langle \lambda^*(z) \eta_\sigma(z) \lambda'(z) \rangle \langle \lambda'^*(z) \eta_\sigma^\dagger(y) \rangle \quad (1.9)$$

with λ being an complete set of operators satisfying

$$\langle \lambda^*(z) \lambda'(z) \rangle = \delta_{\lambda \lambda'} \quad (1.10)$$

and

$$\langle \eta(z) \delta n_{\mu}(x) \eta^{\dagger}(y) \rangle = \sum_{\lambda \lambda'} \langle \lambda(z) \eta^{\dagger}(y) \rangle \langle \lambda'^*(z) \eta(z) \lambda'(z) \rangle \langle \lambda'^*(z) \delta n_{\mu}(x) \rangle, \quad (1.11)$$

we have

$$\begin{aligned} & \langle R(n(x) p_t(x) \eta^{\dagger}(y)) \rangle \\ &= (-i) \int dz \langle p_t(x) p_t^{\dagger}(z) \rangle \langle \delta n_{\mu}(x) \delta n_{\nu}(z) \rangle J_{\nu}^1 \\ & \quad - \langle p_t^{\dagger}(z) p_t(x) \rangle \langle \delta n_{\nu}(z) \delta n_{\mu}(x) \rangle J_{\nu}^2 \langle R(\eta(z) \eta^{\dagger}(y)) \rangle \end{aligned} \quad (1.12)$$

with

$$J_{\nu}^a = \delta_{\nu i} \begin{bmatrix} -\frac{1}{2-n} & \sigma \\ & i \end{bmatrix} + \delta_{\nu 0} \begin{bmatrix} -\frac{1}{2-n} \\ \frac{1}{n-1} \end{bmatrix} \quad (1.13)$$

By neglecting the effect of the charge fluctuation, we have

$$\begin{aligned} \Sigma(\omega, \vec{k}) &= \frac{3}{2(2-n)} \int dk dk' \frac{\Omega}{(2\pi)^2} \int dk' \frac{\sigma}{p_t p_t^{\dagger}} (k', k') \sigma_s(k, k-k') \\ & \quad (1+f_B(k))(1-f_F(k')) \\ & \quad \times \frac{1}{\omega - k - k' + i\epsilon}, \end{aligned} \quad (1.14)$$

where

$$\sigma_{p_t p_t^{\dagger}}(\omega, \vec{k}) = -\frac{1}{\pi} \text{Im} S_{p_t p_t^{\dagger}}(\omega, \vec{k}) \text{ and } \sigma_s(\omega, \vec{k}) = -\frac{1}{\pi} \text{Im} \chi_s(\omega, \vec{k}). \quad (1.15)$$

By replacing σ_s by its momentum average, assuming

$$\sigma_s(\omega) \frac{1}{2} (1+2f_B(\omega)) \approx \frac{1}{\pi} \frac{\gamma}{\omega^2 + \gamma^2} (2-n) \quad (1.16)$$

and approximating $t(k) \approx 8t(k/q)^2$ and $\frac{\Omega}{(2\pi)^2} \int d^2 k \sim \frac{\Omega}{4\pi} \int_0^2 dk^2$,

we perform the self-consistent numerical calculation to obtain

$$\sigma_{pp_1}^{\dagger}(\omega) = \frac{\Omega}{(2\pi)^2} \int d^2 k \sigma_{pp_1}^{\dagger}(\omega, \vec{k}), \quad \sigma_{\eta\eta}^{\dagger}(\omega) = \frac{\Omega}{(2\pi)^2} \int d^2 k \sigma_{\eta\eta}^{\dagger}(\omega, \vec{k}).$$

The result is shown in Fig. 1. The parameters are chosen as transfer gap $\Delta (= \epsilon_p - \epsilon_{\eta}) = 3.0 \text{ eV}$, $t = 1.3 \text{ eV}$, $\gamma_s = 0.02 \text{ eV}$ and temperature $T = 0.01 \text{ eV}$. By fixing Δ , we decrease

$|\epsilon_p|$, which corresponds to lowering the Fermi level. With doping, a new narrow band develops at the Fermi level inside the charge transfer gap. The distance between the top of the p-band and the Fermi level ($\omega=0$) decreases with increasing doping. This is due to the fact that, when the kinetic term is produced only by the p-d hopping term, there exists a point $t^2(k) = 0$, at which the p-electron state receives no modification. This situation is quite different from the Anderson model, where the mixing t is taken constant. In the latter case, the lower p-band and a newly created narrow band repel each other by the mixing interaction and the change of the gap between p-and the new band is small [22]. In the actual situation, there may exist a direct hopping among p-electrons, and we expect an intermediate situation.

We have seen that, due to the critical spin scattering at the Fermi level, a new narrow band can be spontaneously created at the Fermi level in the metal-insulator transition in the oxide materials. This seems to explain many features of photo-emission, EELS and optical experiments as mentioned previously. Then what is expected for the superconductivity? For the formation of a narrow band, we showed that the spin interaction has played an important role. However once this state is formed, spin interactions are sufficiently renormalized and the effective spin-spin interaction among quasi-particle states may be weakened. On the other hand, due to a narrow band, low frequency charge fluctuation through the charge transfer interaction may be induced, which may work as an attractive force for the superconductivity. When the hole concentration is increased, the band may be broadened and it may shift to a usual metallic band.

Therefore the effect of the charge fluctuation takes its maximum in the intermediate region of the insulator-metal transition. We think that the charge-fluctuation mediated superconductivity [26] is more plausible. We may say that both of spin and charge fluctuation play important roles to create the high T_c -superconductivity, the former works to produce the environment and the latter may cause an additional phase

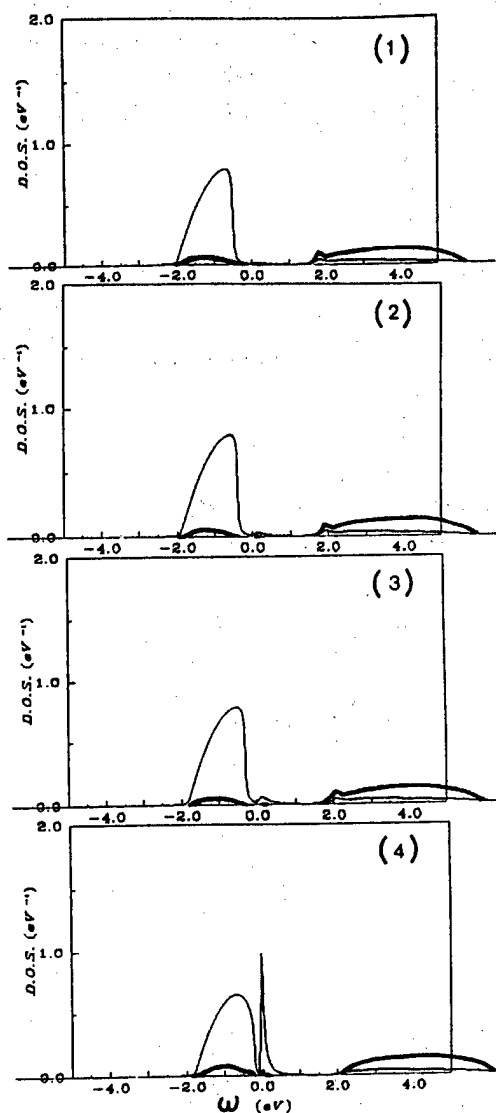


Fig. 1 Electron density of state $\sigma_{pp}^{\dagger}(\omega)$ and $\sigma_{\eta}^{\dagger}(\omega)$. The fine solid lines are for $\sigma_{pp}^{\dagger}(\omega)$ and the bold solid line is for $\sigma_{\eta}^{\dagger}(\omega)$. The parameters are $\Delta(\epsilon_{\eta}-\epsilon_p)=3.0\text{eV}$, $t=1.3\text{eV}$, $T=0.01\text{eV}$, $\gamma_s=0.02\text{eV}$ and ϵ_p is changed as $\epsilon_p = -0.5\text{eV}$ (1), -0.4eV (2), -0.3eV (3) and -0.2eV (4).

$$H_{\text{int}} = \Delta \sum_{\vec{k}, \sigma} [a_{1\uparrow}(\vec{k}) a_{1\downarrow}(-\vec{k}) + \text{c.c.}] + \Delta \sum_{\vec{k}, \sigma} [a_{5\uparrow}(\vec{k}) a_{5\downarrow}(-\vec{k}) + \text{c.c.}] + \frac{2\Delta^2}{I} \quad (2.2)$$

I being the superconducting interaction constant. The superconducting order parameter Δ in Eq.(2.2) is defined by

$$\Delta = I \sum_{\vec{k}} \langle a_{1\uparrow}(\vec{k}) a_{1\downarrow}(-\vec{k}) \rangle, \quad (2.3)$$

where $\langle A \rangle$ denotes the thermal average of A . We calculate the eigenvalues and eigenstates of the Hamiltonian $H + H_{\text{int}}$. Using the eigenstates, we calculate the thermal average value of $\langle a_{1\uparrow}(\vec{k}) a_{1\downarrow}(-\vec{k}) \rangle$ in Eq.(2.3). This quantity is a function of the order parameter Δ . Therefore, Eq.(2.3) gives the self-consistent equation to determine Δ as a function of temperature.

The local density of states at the m -th layer is given by

$$\rho_m(\omega) = -\frac{2}{\pi} \text{Im} \sum_{\vec{k}} (a_{m\uparrow}(\vec{k}), a_{m\uparrow}^\dagger(\vec{k}))_\omega \quad (2.4)$$

where $(a_{m\uparrow}(\vec{k}), a_{m\uparrow}^\dagger(\vec{k}))_\omega$ is the Fourier component of the retarded Green's function with energy ω . The factor 2 in Eq.(2.4) comes from the spin degree of freedom. When the m -th layer of the oxide contacts with the tunnel barrier in the tunnel junction of the oxide and a metal, the tunneling current is mainly brought about by electrons from the m -th layer, since the tunneling probability from the other layers are very small. The tunneling current in this junction is expressed as

$$I_m = A \int_{-\infty}^{\infty} d\omega \rho_m(\omega) [f(\omega) - f(\omega + eV)] \quad (2.5)$$

where $f(\omega)$ is the Fermi-Dirac function $f(\omega) = [\exp(\omega/k_B T) + 1]^{-1}$ and V is the bias voltage. In Eq. (2.5), we assume that the density of states of the normal metal in the junction is independent of energy in the range of eV around the Fermi level. The coefficient A in Eq. (2.5) is a constant related to this density of states of the normal metal and the nature of the junction. Using Eq.(2.5), the tunneling conductance of the junction is calculated as

$$G_m(V) = \frac{\partial I_m}{\partial V} = A \frac{e}{4k_B T} \int_{-\infty}^{\infty} d\omega \rho_m(\omega) \text{sech} \left(\frac{\omega + eV}{2k_B T} \right) \quad (2.6)$$

According to the distribution of the layers at the interface between the oxide and the tunneling barrier, we may measure some average values of the conductances $G_1, G_2 \dots G_5$ in the tunneling experiments. When the layers appear in equal weight at the interface, the average value $\bar{G} = (1/5) \sum_{m=1}^5 G_m$ is measured. Using some values for the parameters of the energy bands and the superconducting interaction constant, we calculated the average value of the conductance \bar{G} . The figure 3 shows the conductance \bar{G} normalized by a constant G_0 as a function of $eV/\Delta(0)$ at 0 K. We see a

fine structure inside the large tunneling gap which mainly comes from the superconducting energy gap on the CuO_2 layer. The fine structure originates from the small superconducting energy gaps on the BaO and CuO layers. The finite conductance at zero bias voltage is caused by gapless excitations in the excitation spectrum. The ruggedness of the tunneling curves in Fig.3 originates from the Van Hove singular-

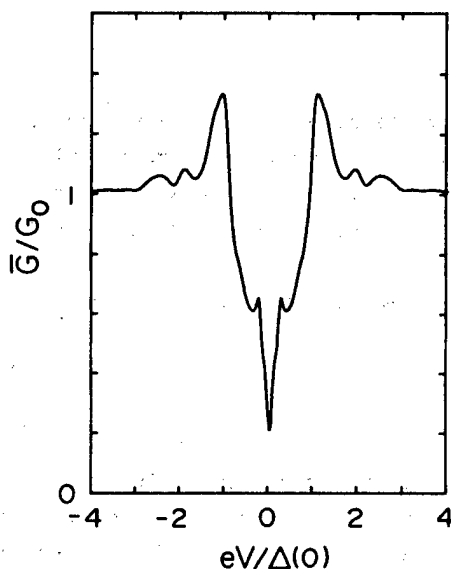


Fig.3 Normalized average tunneling conductance as a function of the normalized bias voltage at $T=0\text{K}$.

ities in the excitation spectrum. The fine structure inside the tunneling gap and the finite conductance at zero bias voltage seen in Fig.3 have been observed actually by the experiments using a junction between a normal metal and $\text{YBa}_2\text{Cu}_3\text{O}_{8-7}$ [27-35], and a junction between a metal and Bi-Sr-Ca-Cu-O [36-38].

critical current

If the oxides have the layered structure of strongly and weakly superconducting layers as mentioned above, we expect that this structure itself works as strong pinning centers in the following [39,40]. The coherence length along the c axis of the oxide crystal is shorter than the lattice constant at low temperatures. When the flux lines are parallel to the layers, the flux lines are stabilized the most when they are placed at the weakly superconducting layers, since the loss of the superconducting cohesive energy due to inclusion of the flux lines is least in this case. Therefore, the weakly superconducting layers work as natural pinning centers. Almost all flux lines are pinned by the weakly superconducting layers and the strength of the pinning force is considerably high. Thus, we expect the high critical current density as large as 10^8A/cm^2 at 4.2 K [39]. We also expect that the critical current density from this mechanism is strongly dependent on the direction of the applied magnetic field [40]. When the direction of the magnetic field is slightly tilted from the layers, the critical current drastically decreases. The high critical current density and the anisotropy of the critical current mentioned above have actually been observed in the experiments using the high-quality single crystal films of $\text{YBa}_2\text{Cu}_3\text{O}_{7-8}$ [41-48].

The present researches were accomplished in cooperation with Dr. T. Koyama, Dr. S. Takahashi, Mr. M. Sasaki, Mr. S. Ishihara, and Mr. N. Takezawa.

References

- [1] J.G.Bednorz and K.A.Müller, Z.Phys. B64, 189 (1986).
- [2] M.K.Wu, J.R.Ashburn, C.J.Torng, P.H.Hor, R.L.Meng, L.Gao, Z.J. Huang, Y.Q.Wang and C.W.Chu, Phys. Rev. Lett. 58, 908 (1987).
- [3] H.Maeda, Y.Tanaka, M.Fukutomi and T.Asano, Jpn. J. Appl. Phys. 27, L209 (1988).
- [4] Z.Z.Sheng and A.M.Hermann, Nature (London) 332, 138 (1988).
- [5] Y.Tokura, H.Takagi and S.Uchida, Nature (London) 337, 345 (1989).
- [6] J.B.Torrance, T.Tokura, A.I. Nazzal, A.Bezinge, T.C.Huang and S.S.P.Parkin, Phys. Rev. Lett. 61, 1127 (1988); J.B.Torrance, A.Bezinge, A.I.Nazzal, T.C.Huang, S.S.P.Parkin, D.T.Keane, S.J.La Placa, P.M.Horn and G.A.Held, Phys. Rev. B40, 8872 (1989).
- [7] A.Fujimori, E.Takayama-Muromachi, Y.Uchida and B.Okai, Phys. Rev. B35, 8814 (1987).
- [8] N.Nucker, J.Fink, J.C.Fuggel, P.J.Durkam and W.M.Temmerman, Phys. Rev. B37, 5158 (1988).
- [9] T.Takahashi, H.Matsuyama, H.Katayama-Yoshida, Y.Okabe, S.Hosoya, K.Seki, H.Fujimoto, M.Sato and H.Inokuchi, Nature 334, 691 (1988).
- [10] A.J.Arko, R.S.List, R.J.Barlett, S-W.Cheong, Z.Fisk, J.D.Thompson, C.G.Olson, A.-B.Yang, R.Liu, C.Gu, B.W.Veal, J.Z.Liu, A.P.Paulikas, K.Vandervoort, H.Claus, J.C.Campuzano, J.E.Schirber and N.D.Shinn, Phys. Rev. B40, 2268 (1989).
- [11] R.Manzke, T.Buslaps, R.Claessen, M.Skibowski and J.Fink, Physica C162-164, 1381 (1989).
- [12] C.G.Olson, R.Liu, A.-B.Yang, D.W.Lynch, A.J.Arko, R.S.List, B.W.Veal, Y.C.Chang, P.Z.Jiang and A.P.Paulikas, Science 245, 731 (1989).
- [13] J.C.Campuzano, G.Jennings, M.Faiz, L.Beaulaigue, B.W.Veal, J.Z.Liu, A.P.Paulikas, K.Vandervoort, H.Claus, R.S.List, A.J.Arko and R.J.Bartlett, (Aogonne N.L. & Los Alamos N.L., Preprint 1990).
- [14] F.U.Hillebrecht, J.Fraxedes, L.Ley, H.J.Trodahl, J.Zaanen, W.Braun, M.Mast, H.Petersen, M.Schaible, J.C.Bourne, P.Pinsukajana, A.Zettl, Phys. Rev. B39, 236 (1989).
- [15] M.Suzuki, Phys. Rev. B39, 2312 (1989).
- [16] G.A.Thomas, J.Orenstein, D.H.Rapkine, M.Capizzi, A.J.Millis, R.N.Bhatt, L.F.Schneemeyer and J.V.Waszcak, Phys. Rev. Lett. 61, 1313 (1988).
- [17] R.T.Collins, Z.Schlesinger, F.Holtzberg, P.Chaudhari and C.Feild, Phys. Rev. B39, 6571 (1989).
- [18] S.Tajima, S.Tanaka, T.Ida and S.Uchida, 2nd Int. Symp. on Superconductivity (Tsukuba, Japan, 1989).
- [19] Y.Fukuda, K.Terashima, Y.Nakanishi, T.Suzuki, M.Nagoshi, Y.Shono and M. Tachiki, Physica C162-164, 1315 (1989).
- [20] H.Matsuyama, T.Takahashi, H.Katayama-Yoshida, T.Kashiwamura, Y.Okaba, S.Saito, N.Kosugi, H.Yagishita, K.Tanaka, H.Fujimoto and H.Inokuchi, Physica C160, 567 (1989).
- [21] D.Shindo, K.Hiraga, S.Nakajima, M.Kikuchi, Y.Shono, N.Kobayashi, K.Hojou, T.Soga, S.Furuno and H.Otsu, Physica C159, 794 (1989).
- [22] H.Matsumoto, M.Sasaki and M.Tachiki, Solid State Commun. 71, 829 (1989).
- [23] V.J.Emery, Phys. Rev. Lett. 58, 2794 (1987).

- [24] J.Hubbard, Proc. Roy. Soc. A276, 283 (1963); *ibid.* 281, 401 (1964).
- [25] H.Matsumoto and H.Umezawa, Phys. Rev. B31, 4433 (1985).
- [26] M.Tachiki and S.Takahashi, Phys. Rev. B38, 218 (1988); *ibid.* B39, 293 (1988).
- [27] J.Geerk, X.X.Xi, and G.Linker, Z.Phys. 73, 329 (1989).
- [28] J.Geerk, G.Linker, O.Mayer, Q.Li, R.-L.Lang, and X.X.Xi, Physica C162-164, 837 (1989).
- [29] M.Gurvitch, J.M.Valles Jr., A.M.Cucolo, R.C.Dynes, J.P.Garno, L.S.Schneemeyer, J.V.Waszcak, Phys.Rev.Lett. 63, 1008 (1989).
- [30] A.Fournel, I.Oujia, and I.Sorbier, Europhys.Lett. 6, 653 (1988).
- [31] I.Takauchi, J.S.Tsai, Y.Simakawa, T.Manako, and Y.Kubo, Physica C158, 83 (1989).
- [32] N.Miyakawa, D.Shimada, T.Kido, and N.Tsuda, J.Phys.Soc.Jpn. 58, L1141 (1989).
- [33] I.Iguchi, S.Narumi, Y.Kasai, and A.Sugishita, Physica, 322 (1987).
- [34] M.Sera, S.Shamoto, and M.Sato, Solid State Commun. 65, 997 (1988).
- [35] J.Tanaka, T.Terashima, Y.Bando, H.Mazaki, K.Iishima, K.Yamamoto, and K.Hirata, Phys.Rev. B40, 4478 (1989).
- [36] M.Lee, D.B.Mitzi, A.Kapitulnik, and M.R.Beasley, Phys.Rev. B39, 801 (1989).
- [37] H.Ikuta, A.Maeda, K.Uchinokura, and S.Tanaka, Jpn.J.Appl.Phys. 27, L1083 (1988).
- [38] T.Enoki and J.Akimitsu, Phys.Rev. B40, 6902 (1989).
- [39] M.Tachiki and S.Takahashi, Solid State Commun. 71, 291 (1989).
- [40] M.Tachiki and S.Takahashi, Solid State Commun. 72, 1083 (1989).
- [41] G.Saemann-Ischenko, B.Hensel, B.Roas, J.Dengler, G.Ritter, S.Klaumunzer, H.E.Hoenig, H.-W.Neumuller, J.Schutzmann, M.Franz, W.Ose, K.F.Renk, And D.L.Nagy, Mod.Phys.Lett. B (in press).
- [42] B.Roas, L.Schultz, and G.Endres, Appl.Phys.Lett. 53, 1557 (1988).
- [43] J.Mannhart, P.Chaudhari, D.Dimos, C.C.Tuei, and T.R.McGuire, Phys.Rev.Lett. 61, 2476 (1988).
- [44] D.K.Christen, C.E.Klabunde, J.R.Thompson, H.R.Kerchner, S.T.Sekula, R.Feenstra, and J.D.Budai, Physica C 162-164, 653 (1989).
- [45] K.Watanabe, H.Yamane, H.Kurosawa, T.Hirai, N.Kobayashi, H.Iwasaki, K.Noto, and Y.Muto, Appl.Phys.Lett. 54, 575 (1988).
- [46] Y.Enomoto, T.Murakami, M.Suzuki and K.Moriwaki, Jpn. J. Appl. Phys. 26, L1248 (1987).
- [47] H.Itozaki, S.Tanaka, K.Higaki and S.Yazu, Physica C153-155 1155 (1988).
- [48] M.Murakami, M.Morita, K.Doi and N.Koyama, Jpn. J. Appl. Phys. 28, L1125 (1989).

Electronic States of the d-p Model

T. Matsuura, H. Jichu[†], Y. Ōno and Y. Kuroda

Department of Physics, Nagoya University, Chikusa-ku, Nagoya 464-01

[†]Aichi College of technology, Gamagori, Aichi 443

The electronic state in the CuO_2 -layer is studied by using the d-p model with the local electronic correlation being fully taken into account. The hole doping brings about a new band around the Fermi level inside the energy gap. Intensity of the band increases as the number of holes increases. The transport properties are discussed due to the new band.

The d-p model is now widely accepted as a model which properly describes the CuO_2 network in the copper-oxide superconductors. The key point in the study of the model is how we take into account the local electronic correlation on the Cu sites. For such purpose the boson technique is useful which was proposed by Coleman[1] and used by Jin and Kuroda[2] for the infinite-U impurity Anderson model. This technique was modified by Ōno et. al.[3] and Kuroda et. al.[4] so to apply to the lattice case. They succeeded in describing the electronic state in the whole temperature range, i.e. the incoherent and coherent regimes and its crossover phenomena in the Anderson lattice.

Jichu et.al.[5] applied the technique to the d-p model and studied the electronic state. We review the technique and the results. Then we study the transport properties.

The d-p model Hamiltonian is given as

$$H = \sum_{k\alpha\sigma} (\varepsilon_p - \mu) C_{k\alpha\sigma}^\dagger C_{k\alpha\sigma} + \sum_{i\sigma} (\varepsilon_d - \mu) d_{i\sigma}^\dagger d_{i\sigma} + \frac{1}{\sqrt{N}} \sum_{k i \alpha \sigma} (V_{kai}^* C_{k\alpha\sigma}^\dagger d_{i\sigma} b_i^\dagger + \text{h.c.}) \quad (1)$$

where $C_{k\alpha\sigma}^\dagger$, $d_{i\sigma}^\dagger$, b_i^\dagger denote creation operators of p_α -hole ($\alpha=x,y$), $d_{x^2-y^2}$ -hole and slave boson at the i -th Cu site. $V_{kai} = 2i \sin(k_\alpha a/2) \exp(ikR_i)$. We impose the local constraint of

$$Q_i = \sum_{\sigma} d_{i\sigma}^\dagger d_{i\sigma} + b_i^\dagger b_i = 1 \quad (2)$$

for each site. In order to enforce the local constraint, we invoke a grand canonical ensemble, $H_1 = H + \sum_i \lambda_i Q_i$. Then, we calculate an expectation value of operator A in such a way as

$$\langle A \rangle = \lim_{\{\lambda_i\} \rightarrow \infty} [\langle A \Pi Q_i \rangle_{\lambda} / \langle \Pi Q_i \rangle_{\lambda}] \quad (3)$$

where $\langle B \rangle_{\lambda} = T_R [\exp(-\beta H_{\lambda}) B] / T_R [\exp(-\beta H_{\lambda})]$. The Dyson equations are given in Figs. 1 and 2.

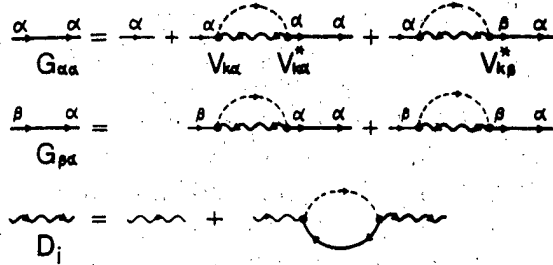


Fig. 1. Dyson equations for single-particle Green's functions. The thin solid, dashed and wavy lines with one arrow denote the bare p -, d -hole and auxiliary boson Green's functions, respectively. The thick lines with two arrows represent the corresponding renormalized Green's functions.



Fig. 2. The correction to the d -hole Green's function.

The guiding principle is essentially due to the $(1/N)$ -expansion method[3,4], i.e. the $(1/N)^0$ terms are included. These equations are coupled and should be solved self-consistently.

We summarize the results in the following.

(i) We define a characteristic energy ω_0 (similar to T_K), a renormalization factor b and a critical temperature $T_0 = \omega_0 / \ln[2/(1-b)]$. Due to the many body correlation at $T < T_0$, the resonance level emerges at $\omega_0 + \mu$ with its residue b . The resonance level mixes with the p -level and forms hybridized bands which are given by

$$E_{\pm}(k) = (\epsilon_p + \omega_0 + \mu + \gamma[(\epsilon_p - \omega_0 - \mu) + 4bW(k)]^{1/2})/2, \quad (4)$$

where $\gamma = \pm$ and $w(k) = (2t)^2 (\cos^2(k_x a/2) + \cos^2(k_y a/2))$ is the hybridization.

(ii) For $T=0$, we calculate ω_0 , b and μ self-consistently with $\bar{\Delta} = (\epsilon_p - \epsilon_d)/2t$ fixed. In Fig. 3, we have plotted b against n for $\bar{\Delta} = 1, 2, 4$. Here n is the total number of holes per unit cell, i.e., $n = n_d + n_c$ with n_d being the hole number in the d -state and n_c the hole number in the band. The system becomes an insulator at $n=1$ for $\bar{\Delta}=4$, since the band width is proportional to b and $b=0$ in that case. This is seen more clearly in Figs. 4 and 5. In Fig. 5, we see that a new midgap band emerges at $n=1$ around $\epsilon_p - 4t^2/\epsilon_d$ and its intensity increases as hole doping. The midgap band is mainly due to the p -holes. In Fig. 6, the density of states of the band at the Fermi level has sharp peak at $n=1$ for $\bar{\Delta}=4$.

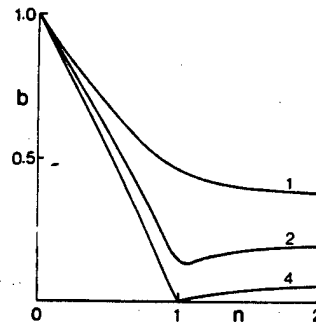


Fig. 3. The residue b vs the total number of holes per unit cell, n . The number attached to each line denotes the value of $\bar{\Delta}$.

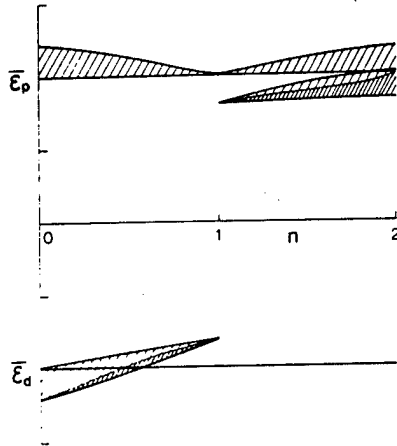


Fig. 4

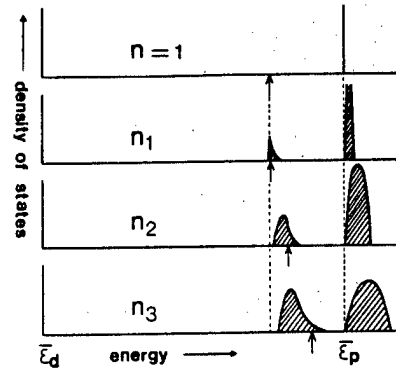


Fig. 5

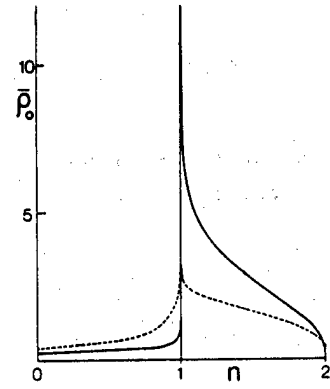


Fig. 6

Fig. 4. The energy scheme for $\bar{J}=4$. $\bar{\epsilon}_p$ and $\bar{\epsilon}_d$ are denoted by two horizontal lines. Each band is shown by the hatched area. The fine-hatched regions indicate the occupied states.

Fig. 5. The schematic density of states corresponding to the band scheme of Fig. 4. The Fermi level is shown by the arrow. $1 < n_1 < n_2 < n_3 < 2$.

Fig. 6. The densities of states at the Fermi level for two values of \bar{J} , i.e., for $\bar{J}=4$ (solid lines) and 2 (dashed lines).

In the case of $T=0$, the Fermi surface is determined by $n_c + n_d = (2/N) \sum_k \theta(-E_-(k) + \mu)$ which satisfies Luttinger's theorem. This means that even at low hole doping $n-1 \sim 0$ the Fermi surface encloses a half of the first Brillouin zone. On the other hand in the case of $T \gg T_0$, the midgap band disappears and a small hole Fermi sphere appears. In this sense, the critical temperature T_0 is a crossover temperature, above or below which the low energy properties such as transportones change drastically.

The expressions of the conductivity and the Hall coefficient in the Fermi liquid were given by Yamada and Yosida[6], Kohno and Yamada[7]. However, here, we study these on the following assumption: (1) The vertex corrections may be neglected in the first approximation, (2) The damping terms are due to the potential scattering by impurities on O-sites, (3) The direct transfer among O-sites exists.

In the case of $T < T_0$, the midgap band carries current. The quasi-particles of the band move mainly through the mixing term when $n \sim 2$, but when n decreases, $n-1$, the mixing term decreases and is dominated by the direct transfer among O-sites. Thus we expect that the Hall coefficient changes its sign from negative to positive on the way from $n=2$ to 1. Here we show the results in the limit $n-1$;

$$\sigma_{xx} = \frac{e^2 \tau n}{m^*}, \quad (5)$$

$$\sigma_{xy} = \frac{e^3}{m^* c} H \tau^2 n \left(\frac{-t_p}{10} a^2 \right), \quad (6)$$

where t_p is the direct transfer $t_p < 0$ and m^* is the effective mass $m^* = 2(\epsilon_p - \omega_0 - \mu)a^2/\pi^2$.

Then the Hall coefficient is given;

$$R_H = \frac{\sigma_{xy}}{\sigma_{xx}} \frac{1}{H} = \frac{1}{ecn} \cdot \frac{\pi^2}{20} \left(- \frac{t_p}{\epsilon_p - \omega_0 - \mu} \right) . \quad (7)$$

On the other hand, at $T \gg T_0$, the Hall coefficient is due to the small Fermi sphere corresponding the hole number $n-1$;

$$R_H \sim \frac{1}{ec(n-1)} . \quad (8)$$

This crossover phenomenon may be observed in the experiment.

References

- [1] P. Coleman, Phys. Rev. B 29 (1984) 3035.
- [2] B. Jin and Y. Kuroda, J. Phys. Soc. Jpn. 57 (1988) 1687.
- [3] Y. Ōno, T. Matsuura and Kuroda, Physica C 159 (1989) 878.
- [4] Y. Kuroda, Y. Ōno, T. Matsuura and H. Jichu, in Strong Correlation and Superconductivity (eds.) H. Fukuyama, S. Maekawa and A.P. Malozemoff (Springer, Berlin, Heidelberg 1989, p.167).
- [5] H. Jichu, T. Matsuura and Y. Kuroda, J. Phys. Soc. Jpn. 58 (1986) 4280.
- [6] K. Yamada and K. Yosida, Prog. Theor. Phys. 76 (1986) 621.
- [7] H. Kohno and K. Yamada, ibid 80 (1988) 623.

To Understand Electronic Properties of High Temperature Superconductors on the Basis of Fermi Liquid Theory. II

HIROSHI KOHNO AND KOSAKU YAMADA

Department of Physics, Kyoto University, Kyoto 606

Electronic properties in the normal state are studied on the basis of the Fermi liquid theory. A general expression for nuclear spin-lattice relaxation rate T_1^{-1} is derived. Implications of this result are discussed.

Characteristic spin dynamics in High- T_c materials has been revealed by microscopic magnetic probes such as neutron scattering^[1] and NMR^[2] experiments. It seems that the properties of undoped systems can be understood on the basis of 2D Heisenberg model.^[3] While it is still controversial as to doped systems,^[4] it is basically the problem of electron correlation which has long been attacked theoretically. We have been studying such correlation effects in normal metals on the basis of the Fermi liquid theory. Here we derive the exact expression for nuclear spin-lattice relaxation rate T_1^{-1} on the basis of diagrammatic perturbation theory. This relaxation rate is the leading-order quantity which reflects the low-frequency dynamics of spin fluctuations.

When the relaxation is due to nuclear-electron hyperfine interaction, T_1^{-1} is expressed in terms of transverse susceptibility $\chi^{+-}(\mathbf{q}, \omega + i0)$ of the electron system:^[5]

$$T_1^{-1} = k_B T (g_n \mu_n)^2 \sum_{\mathbf{q}} |A(\mathbf{q})|^2 \left[\frac{1}{\omega} \text{Im} \chi^{+-}(\mathbf{q}, \omega + i0) \right]_{\omega \rightarrow 0}. \quad (1)$$

Here, $A(\mathbf{q})$ is the hyperfine coupling constant and

$$\chi^{+-}(\mathbf{q}, \omega + i0) = i \int_0^\infty dt e^{i(\omega + i0)t} \langle [S_{\mathbf{q}}^+(t), S_{-\mathbf{q}}^-(0)] \rangle, \quad (2)$$

$$S_{\mathbf{q}}^+ = \sum_{\mathbf{k}} c_{\mathbf{k}\uparrow}^\dagger c_{\mathbf{k}+\mathbf{q}\downarrow}. \quad (3)$$

Before proceeding, we comment on the distinction between T_1^{-1} and static transport coefficients (TC) ; detailed study of the latter was made by Eliashberg^[6] and Yamada *et al.*^{[7][8]} for conductivity and by us for Hall coefficient^[9] and thermal TC^[10]. Both quantities, T_1^{-1} and TC, are similar in that each can be obtained as $[\text{Im} \chi(\omega + i0)/\omega]_{\omega \rightarrow 0}$, where $\chi(\omega + i0)$ is an appropriate susceptibility. The difference is that finite- \mathbf{q} terms contribute to T_1^{-1} as seen from Eq. (1), while transport phenomena are usually meaningful for $\mathbf{q} \rightarrow 0$. Accordingly, T_1^{-1} does not contain the term inversely proportional to quasiparticle damping γ_p (or higher) as opposed to TC, thus requiring rigorous manipulations without any approximations which rely on the smallness of γ_p/ϵ_F employed for TC.

Now we write as

$$\chi^{+-}(\mathbf{q}, i\omega_\lambda) = -T \sum_n \sum_{\mathbf{k}} \mathcal{G}_{\mathbf{k}+\mathbf{q}}(i\varepsilon_n + i\omega_\lambda) \mathcal{G}_{\mathbf{k}}(i\varepsilon_n) K(i\varepsilon_n; i\omega_\lambda), \quad (4)$$

$$K(i\varepsilon_n; i\omega_\lambda) = 1 + T \sum_{n'} \sum_{\mathbf{k}'} \Gamma_{\mathbf{k}, \mathbf{k}'; \mathbf{q}}(i\varepsilon_n, i\varepsilon_{n'}; i\omega_\lambda) \mathcal{G}_{\mathbf{k}'+\mathbf{q}}(i\varepsilon_{n'} + i\omega_\lambda) \mathcal{G}_{\mathbf{k}'}(i\varepsilon_{n'}), \quad (5)$$

where $\mathcal{G}_{\mathbf{k}}(i\varepsilon_n)$ and Γ are renormalized Green function and four point vertex function with imaginary frequency. After analytic continuation they become

$$\begin{aligned} \chi^{+-}(\mathbf{q}, \omega + i0) &= - \int_{-\infty}^{\infty} \frac{d\varepsilon}{4\pi i} \sum_{\ell=1}^3 \lambda_{\ell} g_{\ell} K_{\ell} \\ &\equiv \sum_{\ell=1}^3 \lambda_{\ell} g_{\ell} K_{\ell}, \end{aligned} \quad (6)$$

where

$$\left. \begin{aligned} \lambda_1 &\equiv \lambda_1(\varepsilon; \omega) = \text{th} \frac{\varepsilon}{2T}, \\ \lambda_2 &\equiv \lambda_2(\varepsilon; \omega) = \text{th} \frac{\varepsilon + \omega}{2T} - \text{th} \frac{\varepsilon}{2T}, \\ \lambda_3 &\equiv \lambda_3(\varepsilon; \omega) = -\text{th} \frac{\varepsilon + \omega}{2T}, \end{aligned} \right\} \quad (7)$$

$$\left. \begin{aligned} g_1 &\equiv g_1(\varepsilon; \omega) = G^{\text{R}}(\varepsilon + \omega) G^{\text{R}}(\varepsilon), \\ g_2 &\equiv g_2(\varepsilon; \omega) = G^{\text{R}}(\varepsilon + \omega) G^{\text{A}}(\varepsilon), \\ g_3 &\equiv g_3(\varepsilon; \omega) = G^{\text{A}}(\varepsilon + \omega) G^{\text{A}}(\varepsilon), \end{aligned} \right\} \quad (8)$$

and

$$K_{\ell}(\varepsilon; \omega) = 1 + \int_{-\infty}^{\infty} \frac{d\varepsilon'}{4\pi i} \sum_{m=1}^3 \mathcal{T}_{\ell m}(\varepsilon, \varepsilon'; \omega) g_m(\varepsilon'; \omega). \quad (9)$$

The vertices $\mathcal{T}_{\ell m}$ are related to the analytic continuation of Γ by Eqs. (12) of Ref. [6]. Its subscript ℓm indicates that it is connected to g_{ℓ} (g_m) to the left (right). Here and hereafter, we omit momentum variables unless necessary.

Using irreducible vertex $\mathcal{T}^{(1)}$ with respect to particle-hole channel carrying external momentum \mathbf{q} , which is obtained from $\Gamma^{(1)}$ in the same way as \mathcal{T} from Γ , we obtain the following integral equations:

$$K_{\ell}(\varepsilon; \omega) = 1 + \int_{-\infty}^{\infty} \frac{d\varepsilon'}{4\pi i} \sum_{m=1}^3 \mathcal{T}_{\ell m}^{(1)}(\varepsilon, \varepsilon'; \omega) g_m(\varepsilon'; \omega) K_m(\varepsilon'; \omega). \quad (10)$$

Four- and three-point vertices containing no g_2 -sections, $\mathcal{T}_{\ell m}^{(0)}(\varepsilon, \varepsilon'; \omega)$ and $\Lambda_{\ell}(\varepsilon; \omega)$, respectively, are defined by

$$T_{lm}^{(0)}(\varepsilon, \varepsilon'; \omega) = T_{lm}^{(1)}(\varepsilon, \varepsilon'; \omega) + \int_{-\infty}^{\infty} \frac{d\varepsilon''}{4\pi i} \sum_{j=1,3} T_{lj}^{(1)}(\varepsilon, \varepsilon''; \omega) g_j(\varepsilon''; \omega) T_{jm}^{(0)}(\varepsilon'', \varepsilon'; \omega), \quad (11)$$

$$\Lambda_l(\varepsilon; \omega) = 1 + \int_{-\infty}^{\infty} \frac{d\varepsilon'}{4\pi i} \sum_{j=1,3} T_{lj}^{(0)}(\varepsilon, \varepsilon'; \omega) g_j(\varepsilon'; \omega). \quad (12)$$

From these relations, we get

$$K_i(\varepsilon; \omega) = \Lambda_i(\varepsilon; \omega) + \int_{-\infty}^{\infty} \frac{d\varepsilon'}{4\pi i} T_{i2}^{(0)}(\varepsilon, \varepsilon'; \omega) g_2(\varepsilon'; \omega) K_2(\varepsilon'; \omega), \quad (13)$$

where $i = 1, 3$ and

$$K_2(\varepsilon; \omega) = \Lambda_2(\varepsilon; \omega) + \int_{-\infty}^{\infty} \frac{d\varepsilon'}{4\pi i} T_{22}(\varepsilon, \varepsilon'; \omega) g_2(\varepsilon'; \omega) \Lambda_2(\varepsilon'; \omega). \quad (14)$$

From Eq. (13), Eq. (6) becomes

$$\begin{aligned} \chi^{+-}(\mathbf{q}, \omega + i0) &= \sum_{i=1,3} \lambda_i g_i \Lambda_i + \left[\sum_{i=1,3} \lambda_i g_i T_{i2}^{(0)} + \lambda_2 \right] g_2 K_2 \\ &= \sum_{i=1,3} \lambda_i g_i \Lambda_i + \hat{\lambda}_2 \lambda_2 g_2 K_2. \end{aligned} \quad (15)$$

The last equality of Eq. (15) follows from Eqs. (12) of Ref. [6], and $\hat{\lambda}_l$ is given by λ_l with its left and right reversed. In the second term of Eq. (15), the factor ω is directly obtained from λ_2 .

The next step is to extract terms proportional to ω from the imaginary part of the first term of Eq. (15). The key point is that the first term is real if we put $\omega = 0$ in the thermal factor $\text{th} \frac{\varepsilon + \omega}{2T}$ associated with g_3 . Or, it might be best described as its imaginary part arises due to the difference between $\text{th} \frac{\varepsilon}{2T}$ and $\text{th} \frac{\varepsilon + \omega}{2T}$, which are associated with g_1 and g_3 , respectively. Thus the desired quantity is obtained by picking up the factor ω from the difference between $\text{th} \frac{\varepsilon}{2T}$ and $\text{th} \frac{\varepsilon + \omega}{2T}$ and by setting $\omega = 0$ in the other parts. If we give attention to the section from which the factor ω is picked up in this way, the whole diagram is divided into two parts, the left and the right, and we get the result as

$$\begin{aligned} \left[\frac{1}{\omega} \text{Im} \chi^{+-}(\mathbf{q}, \omega + i0) \right]_{\omega \rightarrow 0} &= -\frac{1}{2} \int_{-\infty}^{\infty} \frac{d\varepsilon}{2\pi} \left(-\frac{\partial f}{\partial \varepsilon} \right) [\hat{\lambda}_1 g_1 \Lambda_1 + \hat{\lambda}_3 g_3 \Lambda_3 - 2\text{Re} \hat{\lambda}_2 g_2 K_2] \\ &= -\frac{1}{2} \int_{-\infty}^{\infty} \frac{d\varepsilon}{2\pi} \left(-\frac{\partial f}{\partial \varepsilon} \right) [\hat{\lambda}_1 g_1 \Lambda_1 + \hat{\lambda}_3 g_3 \Lambda_3 - 2\text{Re} \hat{\lambda}_2 g_2 \Lambda_2] \\ &\quad + \frac{1}{2} \int_{-\infty}^{\infty} \frac{d\varepsilon}{2\pi} \int_{-\infty}^{\infty} \frac{d\varepsilon'}{2\pi} \left(-\frac{\partial f}{\partial \varepsilon} \right) \text{Im} [\hat{\lambda}_2 g_2 T_{22} g_2' \Lambda_2']. \end{aligned} \quad (16)$$

Momentum variables should appear in the formula for periodic systems, although we omit them for simplicity. It may be worthwhile to recognize that no assumption is made so far such as the existence of well-defined quasiparticles and/or even the existence of the Fermi surface.

At zero temperature, $\Lambda_{\mathbf{k}}$'s are all equal and real, and T_{22} vanishes like $\sim T^2$. Thus Eq. (16) reduces to

$$\left[\frac{1}{\omega} \text{Im} \chi^{+-}(\mathbf{q}, \omega + i0) \right]_{\omega \rightarrow 0} = \pi \sum_{\mathbf{k}} a_{\mathbf{k}} \delta(\mu - E_{\mathbf{k}}^*) a_{\mathbf{k}+\mathbf{q}} \delta(\mu - E_{\mathbf{k}+\mathbf{q}}^*) [\Lambda_{\mathbf{k}, \mathbf{k}+\mathbf{q}}(\mu)]^2. \quad (17)$$

Here, $a_{\mathbf{k}}$ and $E_{\mathbf{k}}^*$ are the wavefunction renormalization factor and the excitation energy of a quasiparticle of momentum \mathbf{k} , respectively.

The factor $\Lambda_{\mathbf{k}, \mathbf{k}+\mathbf{q}}$ is expected to be enhanced due to electron-electron interaction U , leading the enhancement of the Korringa constant, i.e., $(T_1 T)^{-1}$ at $T = 0$.

At finite temperature, $(T_1 T)^{-1}$, given by Eq. (16), would decrease from the constant value enhanced by correlation with the T^2 -dependence, as far as normal Fermi liquid phase is assumed. Deriving the coefficient of this T^2 -term remains as a future problem.

Both feature, enhancement of $(T_1 T)^{-1}$ at $T = 0$ and its T^2 -like decrease, are observed in heavy-fermion systems.^[11] As for High- T_c materials, most natural interpretation of experimental results^[2] seems to lie along this line.^[2b]

In discussing the site dependence of T_1^{-1} , \mathbf{q} -dependence of $A(\mathbf{q})$ and $\Lambda_{\mathbf{k}, \mathbf{k}+\mathbf{q}}$ should play the central role. One possible viewpoint is as follows: if the following relation

$$\Lambda_{\mathbf{k}, \mathbf{k}+\mathbf{q}} \simeq A(\mathbf{q}) \simeq \frac{\chi(\mathbf{q})}{\chi^0(\mathbf{q})}, \quad (18)$$

which holds within RPA for the Hubbard model, remains a good approximation even for the exact $\chi(\mathbf{q})$ and $\Lambda_{\mathbf{k}, \mathbf{k}+\mathbf{q}}$, $A(\mathbf{q})$ can be regarded as the enhancement factor of $\chi(\mathbf{q})$ due to correlation. In fact, if one can neglect the \mathbf{k}, ε -dependence of $\Lambda_{\mathbf{k}, \mathbf{k}+\mathbf{q}}(\varepsilon)$, one finds

$$\begin{aligned} \chi(\mathbf{q}) &= - \sum_{\mathbf{k}} \int_{-\infty}^{\infty} \frac{d\varepsilon}{2\pi i} \Lambda_{\mathbf{k}, \mathbf{k}+\mathbf{q}}(i\varepsilon) G_{\mathbf{k}}(i\varepsilon) G_{\mathbf{k}+\mathbf{q}}(i\varepsilon) \\ &\simeq A(\mathbf{q}) \chi^0(\mathbf{q}). \end{aligned} \quad (19)$$

In conclusion, we have demonstrated that the enhancement of $(T_1 T)^{-1}$ and its temperature dependence, observed in heavy-fermion and High- T_c superconducting systems, would be understood most naturally on the basis of the Fermi liquid theory. The reduction of Eq. (1) to Eq. (16) for finite temperature and Eq. (17) for $T = 0$ is the present main results. We hope that more convincing information should be derived from these formulae.

References:

- [0] For a recent progress, see, *e.g.*,
Strong Correlation and Superconductivity, eds. H. Fukuyama, S. Maekawa and A. P. Malozemoff, Springer Ser. Solid-State Sci. (Springer-Verlag, Berlin, Heidelberg, 1989)
- [1] For a review, see
 R. J. Birgeneau and G. Shirane : in *Physical Properties of High Temperature Superconductors*, ed. D. M. Ginsberg (World Scientific Publishing, Feb. 1989)
 G. Shirane : in Ref. [0]
- [2] (a) H. Yasuoka *et al.* : in Ref. [0]
 (b) P. C. Hammel *et al.* : Phys. Rev. Lett. **63** (1989) 1992
- [3] S. Chakravarty *et al.* : Phys. Rev. Lett. **60** (1988) 1057 ; Phys. Rev. **B39** (1989) 2344
- [4] (a) P. W. Anderson : in Ref. [0]
 (b) N. Bulut, D. Hone, D. J. Scalapino and N. E. Bickers : preprint
- [5] T. Moriya : J. Phys. Soc. Jpn. **18** (1963) 516
- [6] G. M. Éliashberg : Sov. Phys.-JETP **14** (1962) 886 [Z. Eksp. Teor. Fiz. **41** (1961) 410]
- [7] K. Yamada and K. Yosida : Prog. Theor. Phys. **76** (1986) 621
- [8] K. Yamada *et al.* : Prog. Theor. Phys. **82** (1989) 689
- [9] H. Kohno and K. Yamada : Prog. Theor. Phys. **80** (1988) 623
- [10] H. Kohno : in preparation
- [11] Y. Kitaoka *et al.* : in *Theoretical and Experimental Aspects of Valence Fluctuations and Heavy Fermions*, eds. L. C. Gupta and S. K. Malik (Plenum Press, New York, 1987)

Fermi Liquid Theory on the Basis of the Periodic Anderson Model with
Spin-Orbit Coupling and Crystalline Field

K. Hanzawa, K. Yosida and K. Yamada*

Department of Physics, Science University of Tokyo, Noda 278, Japan

*Department of Physics, Kyoto University, Kyoto 606, Japan

In order to discuss the normal-state properties of heavy-fermion systems, the Fermi liquid theory is developed on the basis of the periodic Anderson model with arbitrary spin-orbit coupling and crystalline field. For the unperturbed ($U=0$) case, the electronic band structure is determined; then the expressions of T-linear coefficient of specific heat and magnetic susceptibility are derived. For $U \neq 0$, the general expressions for T-linear coefficient of specific heat and magnetization are derived. However, the expression for magnetic susceptibility cannot generally be brought into such a usual form that includes only the quantities on the Fermi surface because of the existence of off-diagonal elements of f-electron self-energy. Therefore, the susceptibility is calculated in the special case that only the lowest Kramers doublet is taken into account.

(published in Prog. Theor. Phys. 81, 960-975(1989))

A Modified Spin-Wave Theory of the Square-Lattice Antiferromagnet

K. Ohara and K. Yosida

Department of Physics, Science University of Tokyo, Noda 278, Japan

A modified spin-wave theory is developed for the square-lattice antiferromagnet under the constraint that the sublattice magnetization vanishes. This constraint gives rise to a highly anisotropic susceptibility. The rotational averaged susceptibility increases linear in temperature from its $T=0$ value which is equal to the average susceptibility at $T=0$ obtained by the usual spin-wave theory. The free energy and specific heat remain essentially unchanged from those obtained by the usual spin-wave theory.

(published in J. Phys. Soc. Jpn. 58, 2521-2530(1989))

T-Square Term of Electrical Resistivity

K. Yamada, M. Nakano, K. Yosida,^{*} K. Hanzawa^{*} and A. Sakurai[†]

Department of Physics, Kyoto University, Kyoto 606, Japan

^{*}Department of Physics, Science University of Tokyo, Noda 278, Japan

[†]Department of Physics, Kyoto Sangyo University, Kyoto 603, Japan

The electrical resistivity, R , in metals at low temperature T is given by $R_0 + AT^2$, where R_0 and A are the residual resistivity due to impurities and the coefficient of T^2 -term due to electron interactions, respectively. In this paper, we discuss the magnitude of A for the systems composed of two kinds of electrons possessing different effective masses, such as transition and rare earth metals. Starting with the Kubo formula, we obtain coupled equations for the current vertex functions of light and heavy electrons. By using these equations, we can show that the resistance of light electrons originates from the collision between the two kinds of electrons (s - d scattering or s - f scattering) as believed. In this mechanism, a mutual interaction between heavy electrons is indispensable for the momentum, transferred from the light electron to heavy electron, to decay. If the system has the mixing term between light and heavy electrons like heavy fermion system, the quasi-particles are composed of the both kinds of electrons. For this case, the contributions of the two kinds of electrons to the conductivity are separated to determine the main contributions for some limiting cases.

(published in Prog. Theor. Phys. 82, 689-701(1989))

Functional Integral Approach to the Low Dimensional Antiferromagnets

K. Hatada and K. Yosida

Department of Physics, Science University of Tokyo, Noda 278, Japan

The ground-state energies of the low-dimensional antiferromagnets are calculated including the triangular lattice by the fermionic mean-field approach. These energies are, as well known, high compared with those of Néel states. For one-dimensional case, the effects of the fluctuations from the mean field are investigated by the functional integral method and these mean-field states are shown to be unstable to the dimer state. Finally, the ground-state energy is calculated by taking into account the fluctuations from the dimer state.

(published in Prog. Theor. Phys. 82, 702-722(1989))

Theory of Normal and Superconducting States of High Temperature Superconductors

Y. Nagaoka, Y. Ōno, T. Matsuura, Y. Kuroda, H. Jichu*, K. Takano,
K. Sano**, I. Doi*** and D.S. Hirashima

Department of Physics, Nagoya University, Chikusa-ku, Nagoya 464-01

*) Aichi College of Technology, Gamagori, Aichi 443

**) Faculty of Education, Mie University, Tsu, Mie 514

***) Department of Physics, College of General Education,
Nagoya University, Nagoya 464-01

Bednorz and Müller's discovery of high temperature superconductivity (HTS) in Cu-O based materials has raised important theoretical questions. What is the nature of the normal state in these materials, what is the mechanism for pairing, and what is the superconducting state (is it the BCS state, or not)? In our group, effort has been paid to answer these questions by various approaches.

- 1) The $1/N$ expansion method was applied to the infinite-U Anderson lattice model and to the d-p model of HTS. (Y. Ōno, T. Matsuura, Y. Kuroda, H. Jichu)[1,2]
- 2) The t-t'-J-J' model was investigated numerically by the direct diagonalization method. (K. Takano, K. Sano, I. Doi)[3,4,5]
- 3) The superconducting state was studied based on the marginal Fermi liquid theory. (Y. Kuroda)[6]
- 4) A model of HTS which leads to consecutive superconducting transitions was studied. (D.S. Hirashima, T. Matsuura)[7]

These works are briefly reviewed in the following.

§1. $1/N$ Expansion of the Anderson Lattice[1] and the d-p Model[2]

To study the infinite-U Anderson lattice at the whole temperature range, we present a modified version of the model with large orbital degeneracy N , which yields finite intersite coherence effects even in the limit $N \rightarrow \infty$ in contrast to the traditional models. By introducing the slave boson operators, b_i and b_i^\dagger , the model Hamiltonian is transformed to

$$H = \sum_{k\sigma} \epsilon_k C_{k\sigma}^\dagger C_{k\sigma} + \sum_i \sum_{m=1}^N f_{im}^\dagger f_{im} + \frac{1}{N} \sum_L \sum_i \sum_{m=1}^N \sum_{(k\sigma) \in S_m} (V_{k\sigma m} C_{k\sigma}^\dagger f_{im} b_i^\dagger e^{-ikR_i} + \text{h.c.}) , \quad (1)$$

with the local constraint

$$\hat{Q}_i = \sum_{m=1}^N f_{im}^\dagger f_{im} + b_i^\dagger b_i = 1 , \quad \text{for all } i . \quad (2)$$

In order to enforce the constraint (2) strictly, a chemical potential λ_i is introduced, and the limit $\lambda_i \rightarrow \infty$ is taken, according to ref.[8]. In the model (1), the

total degrees of freedom for the s-electrons are divided into N subspaces with S_m , i.e., $\sum_m \sum_{(k\sigma) \in S_m} = \sum_{k\sigma}$. This means that the summation over $(k\sigma)$ in a subspace S_m yields a factor of $O(1/N)$, in contrast to the conventional models where $V^2 \propto (1/N)^1$ [3].

The most dominant terms in power of $1/N$ for the single particle Green's functions are described by the Dyson equations illustrated in Fig.1. Then the s-electron self-energy is obtained by

$$\Sigma_{k\sigma}(i\omega_n) \approx a\varphi(T) |V_{k\sigma m}|^2 [i\omega_n - E_0]^{-1} \quad ((k\sigma) \in S_m). \quad (3)$$

Where a and E_0 are the parameters of $(1/N)^0$ to be determined self-consistently, and

$$\varphi(T) \equiv [N^{1-T_0/T} + 1]^{-1} \approx \begin{cases} 1 & (\text{at } T \lesssim T_0) \\ (1/N)^1 & (\text{at } T \gg T_0) \end{cases} \quad (4)$$

with $T_0 = E_0 / \log N$.

At $T \lesssim T_0$, the coherence factor $\varphi(T)$ is of $(1/N)^0$, so that the electrons form the renormalized bands. The band width is of $O(E_0)$, and the phase volume enclosed by the Fermi surface satisfies the Luttinger sum rule. While at $T \gg T_0$, $\varphi(T)$ diminishes to be of $(1/N)^1$, then the system is reduced to one with the bare s-band plus the Kondo impurities. On the other hand, in the conventional models where one assume $V^2 \propto (1/N)^1$, the intersite coherence effect, i.e. $\Sigma_{k\sigma}$ in eq.(3) comes in only as a higher order correction over the whole temperature range.

The life time τ to the order $(1/N)^1$ is given by

$$\frac{1}{2\tau} \propto \begin{cases} N^{-1} E_0^{-2} ((\pi T)^2 + \omega^2) & (\text{at } T \ll T_0) \\ N^{-1} \log(T_K/T) & (\text{at } T \gtrsim T_K) \end{cases} \quad (5)$$

Here the Kondo temperature T_K is determined by the same way for the single Kondo problem [8]. If one neglects the k -dependence of V_k and the s-electron's density of states, E_0 is identical to T_K . However, in general, they are not identical with each other. When T_0 is considerably larger than T_K , the Kondo anomalies at $T \gtrsim T_K$ may not be observed. The CuO_2 network is supposed to be such a system, if the d-p model describes it correctly.

In the hole representation, the d-p model with infinite intra atomic repulsion on d-sites is given by

$$H = \sum_{k\alpha\sigma} \varepsilon_p C_{k\alpha\sigma}^\dagger C_{k\alpha\sigma} + \sum_{i\sigma} \varepsilon_d d_{i\sigma}^\dagger d_{i\sigma} + \frac{1}{\sqrt{N_L}} \sum_{k\alpha\sigma} \sum_i (V_{k\alpha m} e^{-ikR_i} + C_{k\alpha\sigma}^\dagger d_{i\sigma} b_i^\dagger + \text{h.c.}) \quad (6)$$

The above method is applied to this model, and numerical calculations are done at $T=0$. The energy scheme and the density of states are illustrated in Figs.2 and 3.

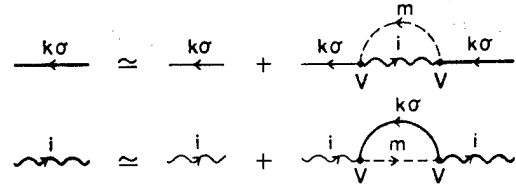


Fig.1 Dyson equations for the periodic Anderson model (1). The solid, broken and wavy lines denote the s-, f-, and slave boson Green's functions, respectively.

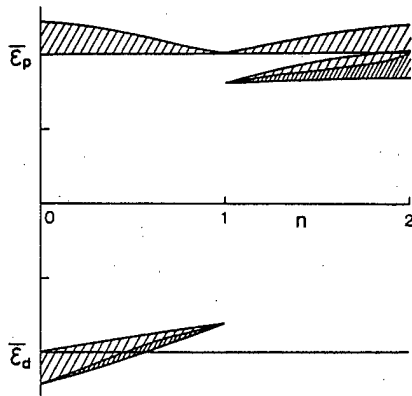


Fig.2 The energy scheme of the d-p model (6). Each band is shown by the hatched area with varying the total hole number n ($n=1$ in the half-filled and $n>1$ in the hole doping case).

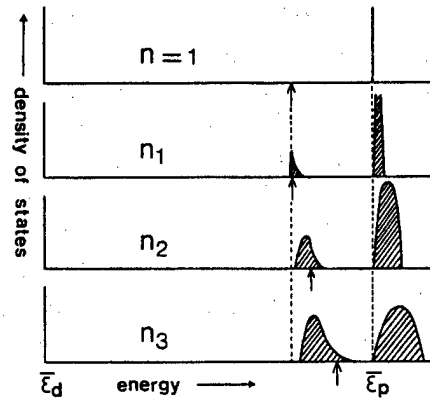


Fig.3 The schematic density of states corresponding to the band scheme of Fig.2. The Fermi level is shown by the arrow. $1 < n_1 < n_2 < n_3 < 2$.

We note that, in the half-filled case ($n=1$) the system is an insulator with a energy gap of $O(|\varepsilon_p - \varepsilon_d|)$, and that as holes are doped ($n>1$), a new band grows up inside the gap with the Fermi level midst of the band. This scheme may explain the experimental features.

§2. Numerical Study of the t-t'-J-J' Model[3,4,5]

We employed the t-t'-J-J' model and examined the ground state and excited states by direct numerical diagonalization. The model describes a simple strongly correlated electron system, which has possible relevance to high- T_c superconductivity, and is given by the Hamiltonian

$$H = -t \sum_{i\sigma} c_{i\sigma}^\dagger c_{j\sigma} - t' \sum_{i\sigma} c_{i\sigma}^\dagger c_{j'\sigma} + J \sum_i S_i \cdot S_j + J' \sum_i S_i \cdot S_{j'} \quad (7)$$

where t (J) is the nearest-neighbor transfer (exchange interaction) and t' (J') the next-nearest-neighbor one.

In the two-dimensional and half-filled case, this model reduces to the AFHM on a square lattice with frustrated interactions J and J' . By numerical analysis we obtained the following results[3]. When frustration parameter J'/J increases starting from 0 (the case of a simple square lattice), the ground state varies without any discontinuity. Excitation energies for finite systems (up to 24 lattice sites) follow the finite size scaling based on a spin-wave-analysis and are extrapolated to a gapless excitation in the thermodynamic limit (Fig.4). This result strongly suggests that the ground state has a magnetic long-range order and the low excited states are described by spin waves. In particular, frustration does not make a chiral-spin or FQHE-like state the ground state. We also checked AFHM's in triangular lattices and obtained the same conclusion.

Next, we examined the 1-hole case, in which one electron is removed from the just half-filled system. The hopping terms with transfers t and t' come to work accordingly. We found that these terms have a peculiar magnetic effect which

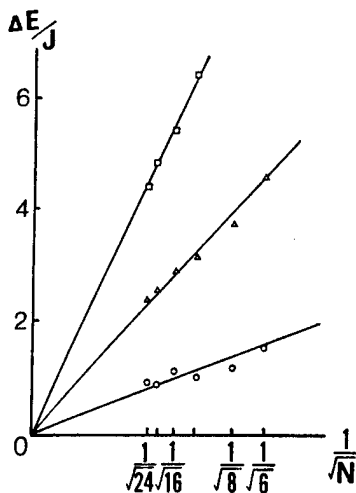


Fig.4 Excitation energies for various values of system size N in a frustrated antiferromagnetic Heisenberg model in the case of $J'/J=0.5$. Extrapolation based on a finite size scaling for the free boundary condition gives gapless excitation in the limit of large N .

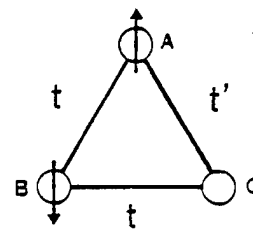


Fig.5 Triangle of 3 sites with 2 electrons. Special kinds of hole motions generate a singlet state for $t' > 0$ and a triplet state for $t' < 0$. This triangle effect survives locally even in large systems.

vanishes when $t'/t=0$. To clarify this effect we examine the simplest system consisting only of 3 lattice sites and 2 electrons in the case of $J=J'=0$ (Fig.5). A simple calculation shows that the ground state for positive t' is a spin-singlet state and that for negative t' is a spin-triplet one. Special kinds of hole motions in the triangle of the 3 sites generate these magnetic states. We call this magnetic effect the triangle effect to distinguish it from the other magnetic effects by J and or J' .

We asserted and confirmed that the triangle effect survives even in the case of large systems. We examined mainly the one-dimensional case numerically[4]. In Fig.6 we show the phase diagram for a 9-site system in the plane of $J/|t|$ and $t'/|t|$, where we take J' as $J'=(t'/t)^2J$. We found a region of $S=1$ (S ; the total spin) in the plane of $t' < 0$ and $J > 0$ and a region of $S=S_{\max}-1$ in the plane of $t' > 0$ and $J < 0$. We examined the same calculation for systems with 5 to 11 lattice sites, and found that the shape and the size of these regions change little. It suggests that there exists a local singlet (triplet) in the sea of a ferromagnetic (singlet) spins for $t' > 0$ and $J < 0$ ($t' < 0$ and $J > 0$). Analyzing numerical wave functions in detail in the region of $S=S_{\max}-1$, we confirmed that a hole and a short singlet pair form a bound state or a

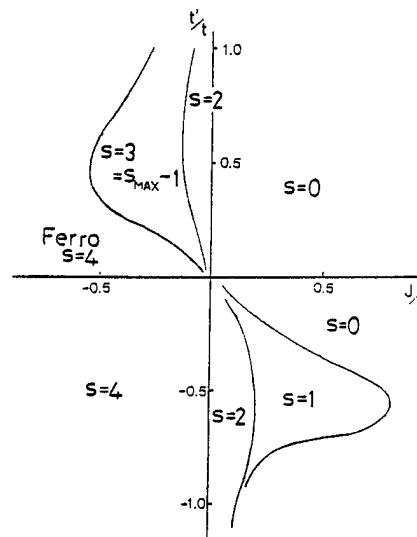


Fig.6 Phase diagram of the one-dimensional t - t' - J - J' model in the plane of $J/|t|$, where $J'=(t'/t)^2J$. There are two soliton regions of $S=1$ and $S=S_{\max}-1$. They appear by the triangle effect.

soliton and move as a whole. This soliton appeared due to the triangular effect mentioned above. The hole can move to one of the next-nearest-neighbor site by two successive hoppings of t and move back to the original site by a hopping of t' . This hole motion is essentially the same as that in the triangle lattice mentioned above, and survives in large systems to create such a soliton.

We also obtained the phase diagram in the two-dimensional case. We found the regions of $S=1$ and $S=S_{\max}-1$ again. In the plane of $t'>0$ and $J>0$, however, there appear three regions with $S=0$, which are not similar to the one-dimensional case. This complex structure was discussed in Ref.5.

§3. Marginal Fermi Liquid and Superconductivity[6]

It is well known that many of the normal state properties are unlike those observed in any other metal or expected for a Fermi-liquid. The electrical resistivity $\rho(T)$, the thermal conductivity $\kappa(T)$, the optical conductivity $\sigma(\omega)$, the Raman scattering intensity $S(\omega)$, tunnelling conductance as a function of voltage $g(V)$, the nuclear relaxation rate $T_1^{-1}(T)$ and the hall coefficient $R_H(T)$, are all anomalous. Except for the temperature dependence of $R_H(T)$, they are also qualitatively the same in all Cu-O based high T_C compounds. Very recently Varma et. al.[10] have shown that these normal state anomalies except for R_H follow from a single hypothesis about the excitation spectrum. Such state described by the hypothesis is not a Fermi liquid in its exact sense but a marginal Fermi liquid, because the quasiparticles therein have life time proportional to $(\epsilon-\epsilon_F)^{-1}$, and moreover their intensity vanishes at $\epsilon=\epsilon_F$, where ϵ and ϵ_F are their energies and the Fermi energy, respectively.

In contrast to the normal state, the superconductive state of the Cu-O's presents few qualitatively new phenomena. London penetration depth measurements [9] yield a superfluid density which approaches zero as $T \rightarrow 0$ with zero slope; this is consistent with s-wave pairing. A direct measurement of the low temperature one-particle spectrum by photoemission [10] is consistent with an unusually large gap: $2\Delta(0)/T_C=8$. The only anomaly discovered [11] is the absence of the BCS coherence peak in nuclear relaxation rate, T_1^{-1} just below T_C ; in fact T_1^{-1} sharply decreases in $\text{YBa}_2\text{Cu}_3\text{O}_{6.9}$ with $(d\ln T_1^{-1}/d\ln T)_{T_C} \approx 5$.

In [6], we have shown that the excitation spectrum which leads to the normal state anomalies or the marginal Fermi liquid also leads the observed behavior of T_1^{-1} . We have also shown that the ratio $2\Delta(0)/T_C$ is enhanced while at the same time the mean-field jump $\Delta C_S/C_N$ in the specific heat is reduced when compared to traditional superconductivity.

Our calculation is just the familiar strong coupling modification of the BCS theory; only the spectrum of excitations exchanged by the electrons is unusual. The hypothesis [8] about the excitation in the normal state is that there exists a contribution to the polarizability, over most of the range of momentum, both for charge and spin excitation of the form

$$\begin{aligned} \text{Im } P(\omega) &= N(0)\text{th}(\omega/2T), & |\omega| < \omega_C, \\ &= 0, & |\omega| > \omega_C. \end{aligned} \quad (8)$$

We follow essentially the same physics to construct the Eliashberg equation as

$$u(\varepsilon_n) = \frac{\varepsilon_n}{\Delta_n} + \frac{\lambda_p}{\Delta_n} \frac{T \Sigma}{\omega_m} F(i\omega_m) \frac{u(\varepsilon_n + \omega_m) - u(\varepsilon_n)}{(1 + u^2(\varepsilon_n + \omega_m))^{1/2}} + \frac{\lambda_s}{\Delta_n} \frac{T \Sigma}{\omega_m} F(i\omega_m) \frac{u(\varepsilon_n + \omega_m) + u(\varepsilon_n)}{(1 + u^2(\varepsilon_n + \omega_m))^{1/2}}, \quad (9)$$

where $F(i\omega_m)$ is given by

$$F(i\omega_m) = (1/\pi) \int dx \text{Im}P(x) (i\omega_m - x)^{-1}, \quad (10)$$

and $u(\varepsilon_n)$ is defined in terms of the normal and the pairing self-energies Σ_1 and Σ_2 as

$$u(\varepsilon_n) = (\varepsilon_n + i\Sigma_1(i\varepsilon_n)) / (\Delta_n - \Sigma_2(i\varepsilon_n)). \quad (11)$$

Here n denotes the Matsubara frequencies, and Δ_n is the contribution of the pairing self-energies due to excitations not included in (8). Now we simply assume that $\text{Im}P(x)$ in the superconducting state is also given by (2) at $T=T_C$ while its low frequency contributions with $|x| < \Delta(0)$ diminish at $T=0$. Then these equations can be solved analytically in the limit, $\lambda_+ \gg \lambda_-$, where $\lambda_{+(-)} \equiv \lambda_p + (-)\lambda_s$. Using these results, we can calculate T_C , $\Delta C_s/C_n$ and $(d\ln T_1^{-1}/d\ln T)$ at $T=T_C$, and $\Delta(0)$. Those explicit forms are rather tedious and should be referred to the original paper [6]. Here we only give some of the numerical results. The normal properties suggest that $\omega_C \approx 2 \sim 3 \times 10^3 \text{ K}$, $\lambda_+ \approx 3$ and $\lambda_s \approx 0.8$ for $\text{YBa}_2\text{Cu}_3\text{O}_{6.9}$. These figures lead to $T_C \approx 90 \sim 110 \text{ K}$, $\Delta C_s/C_n \approx 0.64 \sim 0.70$, $(d\ln T_1^{-1}/d\ln T)_{T_C} \approx 2.8 \sim 3.4$, and $2\Delta_0/T_C \approx 7.7 \sim 7.9$. The experimental values to be compared are 90K, not available (the BCS value is 1.43), 5 and 8.

§4. A Description of the Superconducting Phase of High-Temperature Superconductors

It is said that superconducting properties of HTS can be more or less explained in the framework of the conventional BCS theory. Making a closer inspection, however, we note that there are also controversial problems. For example, although no enhancement in $1/T_1$ just below $T=T_C$ [13] implies that the order parameter is anisotropic, e.g., of d -wave character, the exponential temperature dependence of the penetration depth at low temperatures [14] shows that the order parameter is isotropic, i.e., nodeless. Furthermore, anomalous temperature dependence of the lower critical field H_{c1} has recently been observed. [15]

Understanding the anomalous superconducting properties mentioned above is useful to understand HTS completely. We thus try to give a description of the superconducting phase of HTS consistent with the observations. [7]

It has been found that H_{c1} suddenly increases below a temperature T_C^* ($< T_C$); this implies that the condensation energy abruptly increases below T_C^* . It is known [16] that in the presence of two attractive forces, such as s - and d -wave ones, consecutive superconducting transitions can take place: For example, the normal phase is first condensed into the d -wave superconducting phase at $T=T_C$ and at $T=T_C^*$ ($< T_C$) s -wave component is added to the d -wave phase. Since with the second transition the condensation energy abruptly increases, H_{c1} is also expected to increase abruptly.

Now, if the pairing interaction dominantly originates from an attractive interaction between the nearest neighbor sites, it is given by,

$$V(\mathbf{p}, \mathbf{p}') = \sum_{\mathbf{p}, \mathbf{p}'} (v_I \gamma_{\mathbf{p}} \gamma_{\mathbf{p}'} + v_{\eta} \eta_{\mathbf{p}} \eta_{\mathbf{p}'}), \quad (12)$$

with $\gamma_{\mathbf{p}} = \cos p_x + \cos p_y$, $\eta_{\mathbf{p}} = \cos p_x - \cos p_y$ and $v_I \approx v_{\eta}$. Similarly, if it originates from an attractive interaction between the next nearest neighbor sites, it is given by,

$$V(\mathbf{p}, \mathbf{p}') = \sum_{\mathbf{p}, \mathbf{p}'} (v_{\zeta} \zeta_{\mathbf{p}} \zeta_{\mathbf{p}'} + v_{\phi} \phi_{\mathbf{p}} \phi_{\mathbf{p}'}), \quad (13)$$

with $\zeta_{\mathbf{p}} = 2 \cos p_x \cos p_y$, $\phi_{\mathbf{p}} = 2 \sin p_x \sin p_y$ and $v_{\zeta} \approx v_{\phi}$. In both cases there exist s- (v_I , v_{ζ}) and d- (v_{η} , v_{ϕ}) wave attractive forces. We thus see that if the pairing interaction originates dominantly from near neighbor attractive force, the consecutive superconducting transitions are likely to occur.

Furthermore, we have found that if the normal phase is assumed to be first condensed into the d-wave phase ($\Delta(\mathbf{p}) = \Delta_{\eta} \eta_{\mathbf{p}}$ or $\Delta_{\phi} \phi_{\mathbf{p}}$), the phase below T_c^* would be characterized by a complex order parameter ($\Delta(\mathbf{p}) = \Delta_{\eta} \eta_{\mathbf{p}} \pm i \Delta_I \gamma_{\mathbf{p}}$ or $\Delta_{\phi} \phi_{\mathbf{p}} \pm i \Delta_{\zeta} \zeta_{\mathbf{p}}$), i.e., d+is-phase; this phase generally has no nodes in the excitation energy in contrast to the d-wave phase. We therefore expect that just below $T=T_c$ there is little enhancement in $1/T_1$, because the order parameter is of the d-wave character, and that at low temperatures ($T < T_c^*$) thermodynamic quantities follow the exponential temperature dependence as in the case of the conventional BCS superconductors; these are consistent with the experimental observations in HTS.

In the present model, at $T=T_c^*$, some anomalies will also appear in thermodynamic quantities other than H_{c1} , e.g., specific heat and penetration depth. It is therefore helpful to make a closer investigation of those quantities around the temperature where H_{c1} suddenly increases.

References

- [1] Y. Ōno, T. Matsuura and Y. Kuroda, Physica C **159** (1989) 878; Y. Kuroda, Y. Ōno, T. Matsuura and H. Jichu, in Strong Correlation and Superconductivity (eds.) H. Fukuyama, S. Maekawa and A.P. Malozemoff (Springer, Berlin, Heidelberg 1989), p.167.)
- [2] H. Jichu, T. Matsuura and Y. Kuroda, J. Phys. Soc. Jpn. **58** (1989) 4280.
- [3] K. Sano, I. Doi and K. Takano, in preparation.
- [4] I. Doi, K. Sano and K. Takano, in preparation.
- [5] K. Takano and K. Sano, Phys. Rev. B **39** (1989) 7367.
- [6] Y. Kuroda and C.M. Varma, preprint (1989).
- [7] D.S. Hirashima and T. Matsuura, J. Phys. Soc. Jpn. **59** (1990) No.1.
- [8] B. Jin and Y. Kuroda, J. Phys. Soc. Jpn. **57** (1988) 1687.
- [9] C.M. Varma, P.B. Littlewood, S. Schmitt-Rink, E. Abrahams and A. Ruckenstein, Phys. Rev. Letters **63** (1989) 1996.
- [10] D. Harshmann et al., Phys. Rev. **B39** (1989) 851, L. Krusin-Elbaum et al., Phys. Rev. Letters **62** (1989) 217.

- [11] J.M. Imer et al., Phys. Rev. Letters 62 (1989) 336, C.G. Olson et al., Phys. Rev. Letters (to be published).
- [12] See, for example, articles by R.E. Walstedt and W. Warren, Y. Kitaoka et al, and H. Yasuoka in " Mechanisms of High Temperature Superconductivity", edited by H. Kamimura and A. Oshiyama, Springer Verlag, Heidelberg (1989).
- [13] For example, P.C. Hammel, M. Takigawa, R.H. Heffner, Z. Fisk and K.C. Ott, Phys. Rev. Lett. 63 (1989) 1992.
- [14] For example, A.T. Fiory, A.F. Hebard, P.M. Mankiewich and R.E. Howard, Phys. Rev. Lett. 61 (1988) 1419.
- [15] N. Kobayashi, H. Iwasaki, S. Terada, K. Noto, A. Tokiwa, M. Kikuchi, Y. Shono and Y. Muto, Physica C 153-155 (1988) 1525; M. Sato, S. Shamoto, M. Sera and H. Fujishita, Solid State Commun. 72 (1989) 689.
- [16] D.S. Hirashima, Prog. Theor. Phys. 80 (1988) 840.

Fluctuations in High Temperature Superconductors in Strong Magnetic Field

TOSHIHIKO TSUNETO, RYUSUKE IKEDA AND TETSUO OHMI

Department of Physics, Faculty of Science, Kyoto University, Kyoto 606, Japan

A series of our works on the renormalized fluctuation theory relevant to high temperature superconductors in a strong magnetic field is briefly reviewed. Simplified expressions for the fluctuation conductivities are given to facilitate comparisons with experimental data.

In high temperature superconductors (HTSC) with the extremely short coherence length fluctuations in the superconducting order parameter ψ are not negligible near the transition and become crucially important when enhanced by a strong magnetic field. While in ordinary superconductors the so-called Gaussian theory of fluctuations suffice at least for bulk samples, it badly fails to account for the broadening of the transition induced by the field in HTSC.¹⁾ The broadening is most clearly seen in resistivity²⁾ but also present in specific heat and magnetization data.^{3),4)} To describe large fluctuations with 1-dimensional character imposed by the field, we have to keep the non-linear term $\propto |\psi|^4$ in the GL free energy functional and hence to develop the non-Gaussian theory of superconducting fluctuation.

We first calculated the fluctuation conductivity by means of a theory in which we treated the vertex part perturbationally and renormalized the self-energy part of the correlation function $\langle \psi(x)\psi^\dagger(0) \rangle$.⁵⁾ The agreement of our theoretical results with the observed data is satisfactory as can be seen from Fig.1.⁶⁾ The theory correctly predicted that the same broadening of the transition should be observed in both geometries, $B \perp I$ and $B // I$, where I is measuring current.⁷⁾ This is difficult to explain on the basis of the flux creep theory.

According to the theory, the bare mass $\mu_0 = \ln(T/T_0) + h \sim T - T_{cH}$ is renormalized to μ_R through a relation

$$\left. \begin{aligned} \Delta t &= \mu_0/g^{2/3} = f(x) \\ g &\propto B \\ x &= g/\mu_R^{3/2} \end{aligned} \right\} \quad (1)$$

where we have used the notations given in ref.5. This relation is valid and universal as long as the lowest Landau levels are dominant, and expresses the scaling relation $T - T_{cH} \sim B^{2/3}$ which has been noticed by many experimental groups.^{2),3)} In ref.5, the function $f(x)$ was obtained perturbationally, i.e., as a power series in x . Subsequently we have tried to extend the theory to lower temperatures by the method of Padé approximants and by a partial resummation approximation (called SPH) similar to RPA.⁸⁾ The results of the resistivity⁸⁾ are illustrated in Fig.2, where the contributions of higher Landau levels are neglected as a reasonable approximation at lower temperatures. In addition to the resistivity we have studied the specific heat and the correlation function $\langle |\psi(x)|^2 |\psi(0)|^2 \rangle$ which should reflect the short range order corresponding to Abrikosov flux lattice.

Concerning the conductivities we would like to mention following interesting points. According to our calculation the resistivity $\rho_{||}(=\sigma_{||}^{-1})$ decreases with T more rapidly than $\rho_{\perp}(=\sigma_{\perp}^{-1})$ for the same value of B , in agreement with the data.^{2),9)} Moreover, the curves of $\rho_{\perp}(T)$ have an inflection⁹⁾ as T is lowered and seem to go over smoothly to one obtained from the model of a uniformly sliding flux lattice⁸⁾ as seen in Fig.2. In good samples the effect of pinning apparently sets in below the temperature of this cross-over, making $\rho_{\perp}(T)$ to vanish exponentially. This seems to explain the shoulder (or knee) in $\rho_{\perp}(T)$ curves observed in good quality samples and also its absence in $\rho_{||}(T)$.⁹⁾ Possible effects of pinning on the fluctuation conductivities are an interesting problem for future works.

Since our expressions for the fluctuation conductivities are fairly complicated, we would like to present following simplified formula in order to facilitate comparisons with experimental data. When we neglect the vertex correction in the Kubo formula and assume that the renormalized mass for the n -th Landau level is simply approximated by $\mu_R + 2nh$, we get

$$\sigma_{\perp} \cong \frac{e^2}{8\hbar\xi_{c0}} \sum_{n=0} (n+1) \left[f_n + f_{n+1} - 2f_{n+\frac{1}{2}} \right] \quad (2)$$

$$\sigma_{||} \cong \frac{e^2}{32\hbar\xi_{c0}} \left(\frac{\xi_{c0}}{\xi_0} \right)^2 h \sum_{n=0} f_n^3 \quad (3)$$

where

$$f_n = 1 / \sqrt{(\mu_R + 2nh) \left(1 + \left(\frac{s}{2\xi_{c0}} \right)^2 (\mu_R + 2nh) \right)} \quad (4)$$

To relate the renormalized mass μ_R in these expressions to μ_0 , i.e., to $T - T_{cH}$, we give in Fig.3 a solution of eqn(1) which we calculated with the SPH approximation.⁸⁾ Since, as noted before, this relation between x and $\mu_0/h^{2/3}$ is universal to a good approximation, one has only to scale the variables appropriately for individual cases.

To conclude this report we would like to mention another work¹⁰⁾ related to the subject. It seems to be more convenient at low temperatures to start with the mean field solution of the flux lattice and, for instance, to consider its melting. As is well known, the Abrikosov's solution possesses soft modes which are obviously important for stability of the lattice. The solution is, however, constructed by a superposition of the lowest Landau level and hence approximate. Therefore, one suspects that the soft modes are also a consequence of using only the degenerate lowest Landau level to start with. We have proved that, even when we include higher Landau levels and also consider coupling with the gauge field, there still exist the soft modes. Assuming the flux lattice state does take place, one would expect the soft modes to be important for its melting. More generally, effects of fluctuations in the flux lattice state are yet to be studied.

References

- 1) T. Tsuneto, J. Phys. Soc. Jpn. **57** (1988) 3499.
- 2) Y. Iye et al., J. Appl. Phys. Series 1 (1988) 46 ; K. Kitazawa et al., in *Strong Correlation and Superconductivity* (Springer-verlag, 1989).
- 3) M.B. Salamon et al., Phys. Rev. **B38** (1988) 885.
- 4) U. Welp et al., Phys. Rev. Lett. **62** (1989) 1908.
- 5) R. Ikeda, T. Ohmi and T. Tsuneto, J. Phys. Soc. Jpn. **58** (1989) 1377.

- 6) R. Ikeda, T. Ohmi and T. Tsuneto, *Physica C*, 162-164 (1989) 1693.
- 7) R. Ikeda, *J. Phys. Soc. Jpn.* 58 (1989) 1906.
- 8) R. Ikeda, T. Ohmi and T. Tsuneto, submitted to *J. Phys. Soc. Jpn.*
- 9) J.N. Li et al., *Physica C* 161 (1989) 313 and references therein.
- 10) R. Ikeda, T. Ohmi and T. Tsuneto, submitted to *J. Phys. Soc. Jpn.*

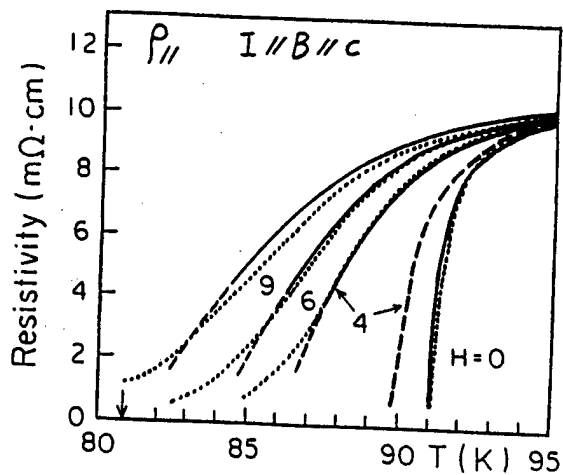
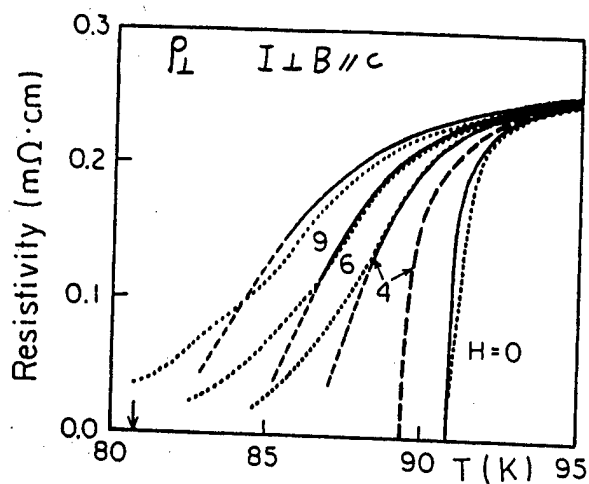


Fig.1

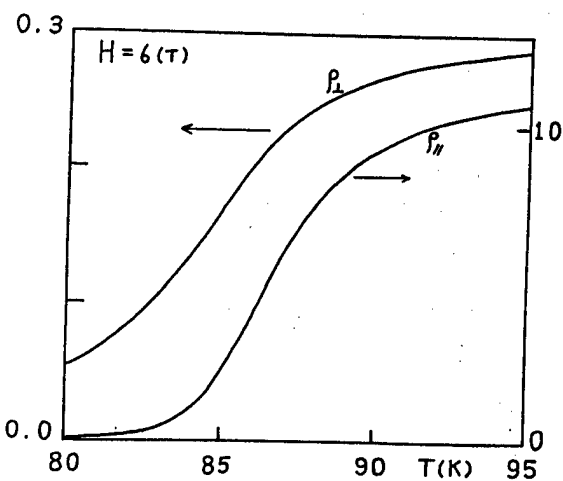


Fig.2

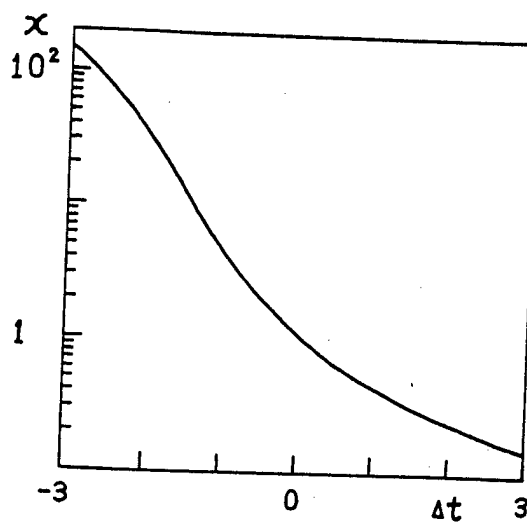


Fig.3

Magnetic Properties of Time-Reversal Breaking Superconductors

M. Sigrist*, T.M. Rice** and K. Ueda*

* University of Tsukuba, Institute of Materials Science, Tsukuba, Ibaraki 305, Japan

** Theoretische Physik, Eidgenössische Technische Hochschule-Honggerberg, 8093 Zurich, Switzerland

A time reversal breaking superconductor has been investigated in the region of a domain wall and at the surface. The finite local magnetization found at these inhomogeneities yields a small paramagnetic response via a movement of domain walls in an external field. We examined line defects in the domain walls which are vortices enclosing a fraction of the standard magnetic flux quantum.

Experiments in the low magnetic field region - the externally applied field is well below the lower critical field H_{c1} experimentally reported - show an unusual behavior in several High- T_c , organic and heavy Fermion superconductors. Mota and co-workers discovered a small paramagnetic response, i.e.: a slow and continuous penetration of magnetic flux in these systems under a small external field [1]. These experiments have been the motivation to study the magnetic properties of time-reversal symmetry breaking superconductors in detail (noticed already by Volovik and Gor'kov [2])[3].

We concentrate on the simplest non-trivial example of an anisotropic superconductor which belongs to the 2-dim. representation of the tetragonal point group D_{4h} . The Ginzburg-Landau free energy has the general form

$$F_s - F_n = \frac{H_c^2 \xi^3}{4\pi} \int d^3r \left[-\frac{1}{2}(|u|^2 + |v|^2) + \left(\frac{1}{8} + \frac{1}{2}\beta_2\right)(|u|^2 + |v|^2)^2 + \frac{1}{2}\beta_2(u^*v - uv^*)^2 + \frac{1}{8}\beta_3(|u|^2 - |v|^2)^2 \right. \\ \left. + k_1(|d_x u|^2 + |d_y v|^2) + k_2(|d_x v|^2 + |d_y u|^2) + k_3\{(d_x u)^*(d_y v) + (d_y u)^*(d_x v) + \text{c.c.}\} \right. \\ \left. + k_4(|d_x u|^2 + |d_x v|^2) + \kappa^2 b^2 \right] \quad (1)$$

where dimensionless units are used with the coherence length ξ of the basal plane as length scale and the vector potential $\mathbf{a} = \mathbf{A}/\sqrt{2}H_c\delta$ (δ : London penetration depth, $\kappa = \delta/\xi$) defining the magnetic field as $\mathbf{b} = \nabla \times \mathbf{a}$. The gradient is $\mathbf{d} = \nabla - i\mathbf{a}$. The coefficients β_i and k_i are real ($k_1 + k_2 = 1$). If we assume $4\beta_2 > \beta_3$ and $\beta_2 > 0$ the homogeneous solution of the Ginzburg-Landau equations is the time-reversal breaking phase $(u, v) = (1, \pm i)e^{i\phi}$ with the even parity gap-function $\hat{\Delta}(\mathbf{k}) \propto i\hat{\sigma}_y k_z(k_x \pm ik_y)$ which is two fold degenerate.

Magnetic properties of that type of superconducting phase can be illustrated by considering a domain wall between the two degenerate states [2]. For that reason we analyse the simple situation determined by the boundary conditions $(u, v) \rightarrow (1, \pm i)$ for $x \rightarrow \pm\infty$ which lead to a one dimensional problem where the domain wall position can be fixed at

$x = 0$. Under the assumption $|u| \approx |v|$ - this is justified in the case $\beta_2 \ll \beta_3$ - we obtain the approximate solution for the order parameter

$$|u(x)| \approx 1 - \frac{4\beta_2}{\cosh^2(\sqrt{2}x/\tilde{\xi})} \quad (2)$$

$$\gamma(x) \approx \arcsin(\tanh(\frac{\sqrt{2}x}{\tilde{\xi}}))$$

where γ is defined by $(u, v) = |u|(1, e^{i\gamma})$ and $\tilde{\xi}$ is the thickness of the domain wall ($= \sqrt{k_1 k_2 / \beta_2}$). The order parameter is slightly suppressed at $x = 0$. The loss of superconducting condensation energy leads to a positive domain wall energy. Thus the existence of a domain wall in a superconductor is only justified by the supposition that they are generated during the superconducting phase transition and then pinned at defects of the crystal lattice.

From the London equation derived from Eq.(1) by variation with respect to \mathbf{a} we find a persistent current flowing in the domain wall homogeneously in y -direction. It induces a magnetic field $\mathbf{b} = (0, 0, b)$ with opposite sign on the two sides which is screened within the London penetration depth towards the bulk region due to diamagnetic supercurrents oppositely directed (Fig. 1). Because the local magnetizations on both sides cancels each other exactly there is no net magnetization due to this effect.

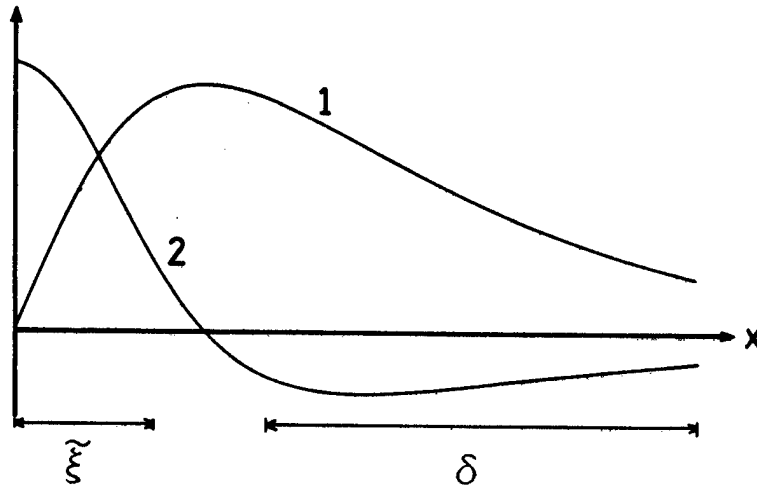


Fig. 1: Magnetic field and current at the domain wall: 1. magnetic field b : odd function of x ; 2. current distribution $-j_y$: even function of x .

The structure of the domain wall considered is degenerate. Beside the solution in Eq.(2) where γ passes from $-\pi/2$ to $+\pi/2$ through $\gamma = 0$, there exists an equivalent way through $\gamma = \pi$. This two structures, if present in a domain wall, are

separated by a line defect similar to a Bloch line in a ferromagnetic domain wall. The topological structure of this line defect - γ is winding once around the line - bears a magnetic flux quantization which is shifted compared to the standard quantization (Φ_0 : standard flux quantum).

$$\Phi \approx \Phi_0(n + k_2) \quad (3)$$

where $0 < k_2 < 1$ and n is an integer number. Consequently, the minimal flux quantum is smaller than Φ_0 : $\Phi \approx \pm k_2 \Phi_0, \pm(1 - k_2) \Phi_0$. In the case $\kappa \gg \tilde{\xi} \gg 1$ the line energy can be calculated easily considering only the contribution of the field and the kinetic energy ($\Phi = k_2 \Phi_0$).

$$\tilde{\varepsilon} = \frac{\Phi_0^2}{2\pi} k_2 [k_2 \ln \kappa + (1 - k_2) \ln \tilde{\xi}] \quad (4)$$

which leads to a critical field $\tilde{h} = \tilde{\varepsilon}/2\kappa^2 \Phi$ which is lower than the usual lower critical field $h_{c1} = \ln \kappa / 2\kappa^2$ for conventional vortices. The structure of this type of vortex do not include a normal core. Only one component of the order parameter has to vanish in the center to ensure topological stability.

The fluxes of two consecutive line defects on a domain wall add to an integer flux quantum of Φ_0 , since there is no net winding around the two lines. Therefore a splitting of a conventional vortex on a domain wall into two fractional vortices is possible and lead to an energy gain $\Delta\varepsilon = -4\pi k_2(1 - k_2) \ln(\kappa/\tilde{\xi})$. A similar effect could happen also with vortices in the bulk region giving rise to a splitted vortex structure with no normal core as presented by several authors [4].

The surface of an anisotropic superconductor is also a region where the order parameter has some spatial variation due to the non-trivial reflection properties of the anisotropic Cooper pairs. We formulate the boundary conditions of the Ginzburg-Landau equations taking into account that the symmetry lowering at the surface allows to add some further second order terms to the Ginzburg-Landau free energy. For the example of a plane surface perpendicular to the y -axis the surface symmetry is $C_{2v}(y) \subset D_{4h}$ yielding the terms

$$F_{sf} = \frac{H_c^2 \xi^3}{4\pi} \int d^3r [g_1(|u|^2 + |v|^2) + g_2(|v|^2 - |u|^2)] \delta(y) \quad (5)$$

where the g_i are real coefficients. For simplicity we consider the case of a specularly reflecting surface choosing $g_1 = g_2$. Thus the component $|u|$ remains constant, whereas $|v|$ obeys the following equations in one dimension (neglecting the vector potential).

$$\frac{\partial^2}{\partial y^2} |v| + 2\alpha(|v| - |v|^3) = 0 \quad (6)$$

$$(k_1 \frac{\partial}{\partial y} |v| + 2g_1 |v|)|_{y=0} = 0$$

with $\alpha = (1 + 4\beta_2 - \beta_3)/8k_1$. The first equation is the Ginzburg-Landau equation of $|v|$. The second is the boundary condition derived from Eq.(1) and (5). The solution is rather simple

$$|v| = \tanh(\alpha(y - y_0)) \text{ with } 2\alpha y_0 = \text{arsinh}(k_1 \alpha / g_1) \quad (7)$$

Similarly to the domain wall a persistent current parallel to the surface is driven by this spatial dependence of the order parameter as easily is found by analysing the London equation.

$$j_z = \frac{k_3}{2\kappa^2} \frac{\alpha \sin \gamma}{\cosh^2(\alpha(y - y_0))} \quad (8)$$

The induced magnetic field $\mathbf{b} = (0, 0, b)$ is again screened towards the bulk region. However, contrary to the domain wall the total magnetization is finite: $M_z \approx \sqrt{2}k_3 \sin \gamma H_c \delta / \kappa$ per unit surface area. Even a single domain superconducting sample would therefore possess a finite total magnetization $M_z \sim H_c \delta / \alpha \kappa$, where a is the sample size.

In a multi domain sample surface magnetizations of neighboring domains have opposite sign. An external magnetic field leads to a difference of the energy density $g = f - 2\kappa^2 \mathbf{b} \cdot \mathbf{h}_{ext}$ in the two domains. The total energy can be lowered by a movement of the domain wall between them enlarging the domain with the surface magnetization parallel to the z -component of the external field (Fig. 2). Since the domain wall is pinned at defects this movement is rather slow and mainly determined by thermal activation processes.

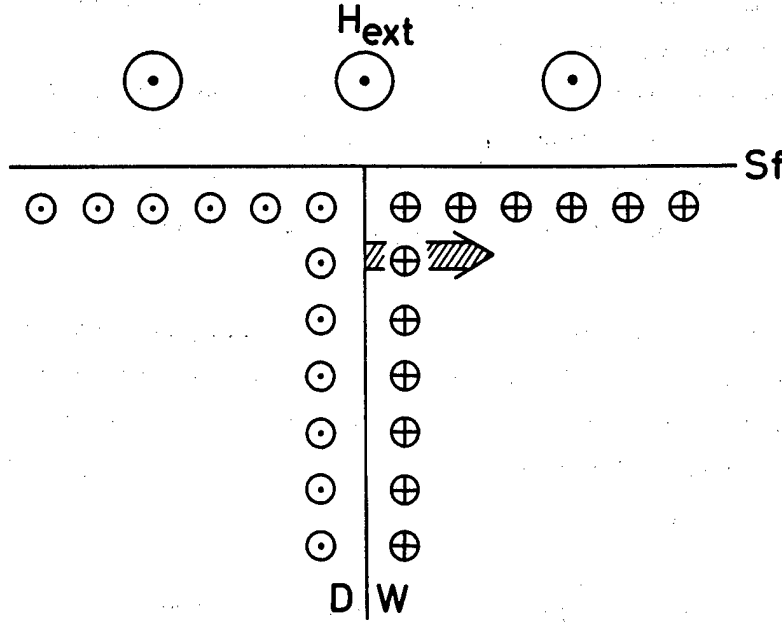


Fig. 2: Paramagnetic response of the superconductor via a domain wall movement due to different surface magnetization in neighboring domains (DW: domain wall; Sf: surface).

The occurrence of local magnetization at the domain wall and at the surface can be traced to the existence of a finite magnetic moment of the Cooper pairs. In the example considered here this moment is aligned with the z -axis. In the bulk region this magnetic moment is screened due to the Meissner effect of the superconductor. However, at inhomogeneities of the superconducting phase it has to appear because of imperfect screening or mismatch of the screening length scale δ and the coherence length of the order parameter.

Summarizing, the magnetic properties of a time-reversal breaking superconducting phase become obvious at inhomogeneities of the order parameter. We have found that in multi component superconductors also various structures of vortices are possible. Especially, on the domain wall vortices with a flux quantum lower than the conventional one can occur. Finally, a finite surface magnetization can yield a small paramagnetic response and gives a possible mechanism which could explain the observation mentioned initially.

References

- [1] A.C. Mota, G.Juri, P. Visani and A. Pollini, *Physica (Amsterdam) C* (to be published) and references therein.
- [2] G.E. Volovik and L.P. Gor'kov, *Pis'ma Zh. Eksp. Teor. Fiz.* **39**, 550 (1984) [*JETP Lett.* **39**, 674 (1984)]; *Zh. Eksp. Teor. Fiz.* **88**, 1412 (1985) [*Sov. Phys. JETP* **61**, 843 (1985)].
- [3] M. Sigrist, T.M. Rice and K. Ueda, *Phys. Rev. Letts.* **63**, 1727 (1989)
- [4] A. Schenstrom, M.-F. Xu, Y. Hong, Y. Tokuyasu, D.W. Hess, J.B. Ketterson, J.A. Sauls and D.G. Hinks, *Phys. Rev. Letts.* **62**, 332 (1989); Yu.A. Izyumov and V.M. Laptev (to be published); T.A. Tokuyasu, D.W. Hess and J.A. Sauls (to be published); H. Ebisawa (private communication).

THEORETICAL STUDY OF TWO-DIMENSIONAL CuO_2 SYSTEMS

Masatoshi IMADA

Department of Physics, College of Liberal Arts,
University of Saitama, Shimo-Okubo, Urawa 338

Numerical results from Monte Carlo simulation in the ground state and at finite temperatures as well as the exact diagonalization and the transfer matrix method obtained at our group are reviewed. Perturbational treatments of the coupled spin-fermion model are also summarized.

§1. Quantum Monte Carlo Simulation²⁾

Recently developed Monte Carlo algorithm for low temperature properties of lattice fermion models^{1,2)} has been examined extensively. Efficiency and applicable range of parameters are investigated in detail.

The Hubbard model defined by the Hamiltonian

$$H = -t \sum_{\langle ij \rangle, \sigma} (c_{i\sigma}^\dagger c_{j\sigma} + c_{j\sigma}^\dagger c_{i\sigma}) + U \sum_i n_{i\uparrow} n_{i\downarrow}, \quad (1)$$

has been investigated by using this newly developed algorithm. We have obtained following properties of the Hubbard model on a square lattice.

i) Magnetic property

The ground state Monte Carlo results show that the presumable long range antiferromagnetic order in the half-filled system is drastically suppressed away from the half-filling and show the short-ranged incommensurate correlation in the Fourier transform of the equal time spin-spin correlation. The incommensurate correlation increases with the increase of U . It, however, seems to remain quite short ranged.

ii) Superconducting correlation

In the ground state of the Hubbard model, we do not have numerical data to support the tendency to a superconducting state. It raises a serious doubt on the relevance of the Hubbard model as a model for the high- T_c superconductivity.

§2. One-Dimensional $t - J$ Model^{2,3)}

The superconducting and magnetic correlation of the one-dimensional $t - J$ model defined by

$$H = -t \sum_{\langle ij \rangle} ((1 - n_{i,-\sigma}) c_{i\sigma}^\dagger c_{j\sigma} (1 - n_{j,-\sigma}) + h.c.) - 2J \sum_{\langle ij \rangle} \vec{S}_i \cdot \vec{S}_j, \quad (2)$$

has been investigated by the checker board Monte Carlo method and the real space transfer matrix method. In the doped systems, magnetic correlation shows incommensurate peak for small J/t similarly to the Hubbard model. The superconducting correlation is small in this parameter space. However, the superconducting correlation shows striking enhancement at low temperatures when one increases the ratio J/t . This seems to be consistent with the attractive interaction of two holes observed for large J/t in the exact diagonalization study.

§3. Perturbational Treatment of Coupled Spin-Fermion Model⁴⁾

The coupled spin-fermion model is defined from

$$\begin{aligned}
 H = & -t \sum_{\langle i,j \rangle \sigma} (c_{i\sigma}^\dagger c_{j\sigma} + c_{j\sigma}^\dagger c_{i\sigma}) \\
 & + J_K \sum_{\langle i,l \rangle} \vec{S}_l \cdot \vec{\sigma}_i + J'_K \sum_{\langle i,l \rangle, \langle j,l \rangle, i \neq j} \sum_{s,s'} \vec{S}_l \cdot (c_{i,s}^\dagger(\vec{\sigma})_{s,s'} c_{j,s'}) \\
 & + J_S \sum_{\langle l,m \rangle} \vec{S}_l \cdot \vec{S}_m,
 \end{aligned} \quad (3)$$

where

$$\vec{\sigma}_i = \frac{1}{2} c_{i\sigma}^\dagger (\vec{\sigma})_{\sigma\sigma'} c_{i\sigma'}.$$

We have applied the perturbational method using the diagrammatic expansion with respect to J_K and J'_K . For the Heisenberg spin systems, spin-wave approximation has been employed. The logarithmic singularity appears in the fermion self-energy in the order of J_K^4 . The logarithmic divergence comes from the coupling of fermions to long-wave-length mode of the spin wave excitation in two-dimension. This divergence indicates that a doped fermion forms a localized state self-trapped by the distortion of spins. When the fermion concentration is increased, the doped fermions remains localized until a critical concentration δ_c . Above the critical concentration, there seems to be a region where the fermi liquid with small fermi surface coexists with the anti-ferromagnetic order of Heisenberg spins, if the Kondo coupling is small enough. The self-trapped state of fermions and spins in the low doping region might have some relevance in the optical and photoemission experiments. In particular, we expect a peak of the frequency dependent optical conductivity within the charge transfer gap. This seems to be consistent with the mid-infrared peak observed in the experiments of high-Tc oxides.^{5,6)}

§4. On the Possibility of TP Symmetry Breaking with Chiral Spin and/or Flux Order⁷⁾

The possibility of chiral symmetry breaking and the flux state is examined in frustrated and non-frustrated quantum spin systems. The spin-1/2 Heisenberg model is defined by the Hamiltonian

$$H = -2J \sum_{\langle i,j \rangle} \vec{S}_i \cdot \vec{S}_j. \quad (4)$$

The chirality defined by

$$c_{123} = \vec{S}_1 \cdot (\vec{S}_2 \times \vec{S}_3) \quad (5)$$

on the unit triangle has been examined to investigate the possibility of time reversal and parity symmetry breaking and hence fractional statistics. The fluctuation of the chirality has been calculated in the exact diagonalization of finite systems with the railroad trestle extrapolation to the thermodynamic limit. The numerical data show that the chiral symmetry breaking is unlikely both on square and triangular lattice.

The chirality correlation shows similar behavior even when the next nearest neighbor exchange coupling J' has the same strength with the nearest neighbor coupling J on the triangular lattice. The square lattice with the next nearest neighbor interaction $J' = J/2$ also shows similar behavior. It indicates that regularly frustrated spin systems with the ordinary form of Heisenberg exchange coupling is not likely to show the chiral order. Similarly the correlation of the flux does not seem to show growth with the increase of system size in the two-dimensional Hubbard model at $U = 4$ away from the half-filling. At this moment, we have no data supporting the appearance of the time reversal and the parity symmetry broken state in realistic models of high- T_c oxides.

Acknowledgements

This research has been proceeded by the collaboration with Y. Hatsugai and N. Furukawa.

References

- 1) S. Sorella, E. Tosatti, S. Baroni, R. Car and M. Parrinello: *Int. J. Mod. Phys. B* 1 (1988) 993.
S. Sorella, S. Baroni, R. Car and M. Parrinello: *Europhys. Lett.* 8 (1989) 663.
- 2) M. Imada and Y. Hatsugai: *J. Phys. Soc. Jpn.* 58 (1989) 3752.
- 3) M. Imada: *Proceedings of the Workshop "Quantum Simulation of Condensed Matter Phenomena"* ed. by J. Gubernatis (World Scientific, Singapore) to be published
- 4) N. Furukawa and M. Imada: submitted to *J. Phys. Soc. Jpn.*
- 5) G. A. Thomas et al.: *Phys. Rev. Lett.* 61 (1988) 1313.
- 6) S. Uchida, H. Takagi and Y. Tokura: to be published in the proceedings of $M^2S - HTSC$ Conference, Stanford (1989).
I. Terasaki, T. Nakanishi, S. Takebayashi, A. Maeda and K. Uchinokura: *Physica C* (in press).
- 7) M. Imada: *J. Phys. Soc. Jpn.* 58 (1989) 2650 and in preparation.

Y. Takahashi and H. Tsunetsugu

Institute for Solid State Physics, The University of Tokyo
Roppongi, Minato-ku, Tokyo 106, Japan

Single hole propagation doped into a quantum antiferromagnet is studied taking into account the effect of finite exchange interaction up to the first order among antiferromagnetic spin background. Both even and odd moments of the hole density of states are evaluated up to 8th order based on the spin wave approximation including the effect of local spin relaxation around the hole. The results of the lower order moments suggest the existence of the string effect, which leads to the hole localization in the small concentration region.

Behavior of the small concentration of holes doped in a half-filled antiferromagnetic Mott insulator is important since a lot of physical properties of high- T_c superconductors are subject to the behavior of these holes. Current high- T_c copper oxide compounds are characterized by their relatively large exchange interaction J among the background spin system. Therefore the finite J correction is very important in this case. As a generalization of the moment expansion treatment by Nagaoka [1] and Brinkman and Rice [2], Takahashi [3] treated the finite J effect of a single hole assuming the simple antiferromagnetic Ising spin configuration. Hirsch [4] also discussed the same problem in a somewhat different model. These studies suggest the existence of the string effect, *i.e.*, exchange energy cost increases with the hopping distance of a hole from the origin. Subsequent works dealing with the finite J effect [5-11], however, questioned the existence of the string effect. It was argued that the hole actually propagates through the crystal, but the effective band width is greatly reduced to be of the order of J . It was also argued that the exchange energy cost by the hole in the resonating valence bond (RVB) [12] state is much smaller than that in the antiferromagnetic (AF) state, which will favor the stabilization of the RVB state against AF state by hole doping. The purpose of the present work is to clarify these points by extending our work [13-16] by taking into account the effect of finite J correction on the hole propagation based on the moment expansion method. We can show that the moments of the hole density of states are evaluated from the multi-spin correlation functions [15-17]. From the recent numerical Monte Carlo simulation [18], the spin wave approximation was found to give a good estimate of the ground state energy and the spontaneous magnetization of the $S = 1/2$ 2D Heisenberg antiferromagnet. According to our previous work [16], we estimate these higher spin correlation functions based on the spin wave approximation.

We study here the following t - J model:

$$H = H_0 + H_1$$

$$H_0 = J \sum_{ij} (\mathbf{S}_i \cdot \mathbf{S}_j - \rho_i \rho_j / 4), \quad H_1 = -t \sum_{ij\sigma} c_{i\sigma}^\dagger c_{j\sigma}. \quad (1)$$

where $c_{i\sigma}$ ($c_{i\sigma}^\dagger$) is an electron annihilation (creation) operator on i -th lattice site with σ -spin direction and the summation on i, j is over all the lattice sites which are nearest neighbor with each other. We solve the Hamiltonian (1) in terms of the continued fraction method. Starting from an initial wave function ψ_0 , we successively introduce an orthonormal wave function ψ_n ($n > 0$) by

$$b_1 \psi_1 = H \psi_0 - a_0 \psi_0$$

$$b_{n+1}\psi_{n+1} = H\psi_n - a_n\psi_n - b_n\psi_{n-1} \quad (2)$$

The coefficients a_n and b_n are related to the moments:

$$\langle \psi_0 | (H_0 + H_1)^n | \psi_0 \rangle = \langle H_0^n \rangle + \langle H_1 H_0^{n-1} \rangle + \dots$$

where $\langle \dots \rangle$ is the expectation value with respect to ψ_0 . If the initial wave function ψ_0 is not the real eigenstate of H_0 , we can define higher order wave functions ψ_n even in the absence of the term H_1 , which serve us to find the exact ground state energy of H_0 . Then we have to treat the terms such as $\langle H_0^n \rangle$ which are in general not equal to a_0^n . Because a_0 is a macroscopic quantity, *i.e.* the exchange energy of the total system, we cannot discard the difference, $\langle H_0^n \rangle - a_0^n$. We are however not interested in the eigenvalue problem of H_0 . We are rather interested in the coupled effect arising from both H_0 and H_1 . In order to bypass complexities related to the eigenvalue problem of H_0 , we assume that ψ_0 is the eigenstate of H_0 with the eigenvalue a_0 , *i.e.*, $H_0\psi_0 = a_0\psi_0$, and all the energies are measured relative to the exact eigenvalue a_0 of H_0 which is assumed to be given. The moments we evaluate here are defined by

$$A_n = \langle (H - a_0)^n \rangle, \quad (3)$$

and the diagonal element a_n in eq.(3) is given by

$$a_n = \langle \psi_n | (H - a_0) | \psi_n \rangle \quad (4)$$

The coefficient a_0 no longer appears in the formalism and all the coefficients a_n and b_n are of the order $O(1)$. For example with the use of the following relations:

$$\begin{aligned} \langle H \rangle &= a_0 \\ \langle H^2 \rangle &= a_0^2 + \langle H_1^2 \rangle \\ \langle H^3 \rangle &= a_0^3 + 2a_0\langle H_1^2 \rangle + \langle H_1 H_0 H_1 \rangle = a_0^3 + 3a_0\langle H_1^2 \rangle + \langle H_1 [H_0, H_1] \rangle \end{aligned}$$

the first non-trivial odd moment A_3 is evaluated as follows:

$$\langle (H - a_0)^3 \rangle = \langle H^3 \rangle - 3a_0\langle H^2 \rangle + 3a_0^2\langle H \rangle - a_0^3 = \langle H_1 [H_0, H_1] \rangle$$

In the present nearest neighbor hopping model, the diagonal coefficients a_n is an odd function of J and proportional to J for small J value, whereas b_n^2 is an even function of J . Up to the first order of J , moments are given by

$$\begin{aligned} A_1 &= 0 \\ A_2 &= \langle H_1^2 \rangle = b_1^2 \\ A_3 &= \langle H_1 H_1^{(1)} \rangle = a_1 b_1^2 \\ A_4 &= \langle H_1^4 \rangle = b_1^2(b_1^2 + b_2^2) \\ A_5 &= \text{Re}\{3\langle H_1^3 H_1^{(1)} \rangle + \langle H_1^2 H_1^{(1)} H_1 \rangle\} = b_1^2\{b_2^2 a_2 + 2(b_1^2 + b_2^2)a_1\} \\ A_6 &= \langle H_1^6 \rangle = b_1^2\{b_2^2 b_3^2 + (b_2^2 + b_1^2)^2\} \\ A_7 &= \text{Re}\{5\langle H_1^5 H_1^{(1)} \rangle + 3\langle H_1^4 H_1^{(1)} H_1 \rangle + \langle H_1^3 H_1^{(1)} H_1^2 \rangle\} \\ &= b_1^2[b_2^2 b_3^2 a_3 + 2b_2^2(b_3^2 + b_2^2 + b_1^2)a_2 + \{2b_2^2 b_3^2 + 3(b_1^2 + b_2^2)^2\}a_1] \\ A_8 &= \langle H_1^8 \rangle = b_1^2\{b_2^2 b_3^2(b_4^2 + b_3^2 + 2b_2^2 + 2b_1^2) + (b_2^2 + b_1^2)^3\} \end{aligned} \quad (5)$$

where Re means the real part and $H_1^{(1)}$ is defined as the commutation relation:

$$\begin{aligned} H_1^{(1)} &= [H_0, H_1] \\ &= -tJ \sum_{\delta, k, l} (c_{k\mu}^\dagger \sigma_{\mu\nu} c_{l\nu}) \cdot (\mathbf{S}_{k+\delta} - \mathbf{S}_{l+\delta}) \end{aligned} \quad (6)$$

In eq. (6) the summation of δ is over the nearest neighbor sites of k and l . However both $k + \delta = l$ and $l + \delta = k$ are excluded because of the electron double occupancy prohibition. In the present treatment since we only deal with the first order correction with respect to J , the odd moment A_{2n+1} is proportional to $J(-t)^{2n}$. In the following we assume energy units, $t = 1$, and introduce the parameter $\alpha = J/| -t |$ to characterize the magnitude of the exchange term. Since the operator $H_1^{(1)}$ represent an electron hopping process, odd moments are expressed as the sum of various hopping processes which starts from the origin and after several steps returns to the origin again. From the simple operator algebra and the singly occupied electron constraint, we can show that contributions from these paths reduce to the evaluation of various multi-spin correlation functions in the ground state [19].

We have evaluated pair spin correlation functions in the spin wave approximation. Multi-spin correlation functions are estimated by using the decoupling approximation (see [16] for details). The effect of the quantum spin fluctuations is taken into account by the spin wave approximation down to the order S^0 and the effect of local defect (the absence of the spin on the origin) is also treated in the same approximation. Both of even and odd moments A_n , parameters a_n and b_n^2 are shown in Table I. We also evaluated individual contributions from retraceable and non-retraceable paths for A_{2n+1} and a_n separately. The values of a_n are sensitive to the distant spin pair correlations. For comparison we have estimated the values of a_1 and a_2 for nearest neighbor RVB wave function of the finite 32-site cluster with two holon with the periodic boundary condition [14]. Here four spin correlations $\langle (S_1 \cdot S_2)(S_3 \cdot S_4) \rangle$ are evaluated in terms of pair correlations by the decoupling approximation:

$$\langle (S_1 \cdot S_2)(S_3 \cdot S_4) \rangle = \langle S_1 \cdot S_2 \rangle \langle S_3 \cdot S_4 \rangle + \frac{1}{3} \{ \langle S_1 \cdot S_3 \rangle \langle S_2 \cdot S_4 \rangle + \langle S_1 \cdot S_4 \rangle \langle S_2 \cdot S_3 \rangle \}$$

The result is: $a_1 = 2.53$ and $a_2 = 5.01$. The smaller value of these values are derived from the short spin correlation of the RVB state. The effect of the spin relaxation due to the defect is found to be relatively small, but we see the tendency approaching towards the RVB limit.

Table I Moments and coefficients of continued fraction expansion coefficient a_l and b_l in the case without defect. Retraceable path contribution, a_l^{ret} , is given in the parenthesis.

l	A_{2l-1}/α	A_{2l}	a_l (a_l^{ret})	b_l^2
1	0	4	3.1669 (3.1669)	4
2	3.167	26.248	5.8459 (7.2629)	2.5621
3	56.541	200.67	9.1533 (14.3553)	2.7738
4	798.83	1652.52		2.4734

The most dominant contributions to A_{2n+1} come from retraceable paths. When we evaluate a_n by eq.(5), these terms however cancel with each other and non-retraceable path contributions have the sizable weight in a_n . The magnitude of the retraceable contribution to a_n increases faster than the linear n -dependence with increasing n . However the sum of both contributions seems to increase linearly with n at least for small n . Due to the quantum spin fluctuations retraceable path contributions are enhanced as compared with the case of Ising spin alignment. This effect is compensated by the negative non-retraceable path contributions. The resultant a_1 , for example, for AF has nearly the same value as the Ising case.

The continued fraction representation amounts to transforming the original Hamiltonian matrix into a tridiagonal one. If we represent the eigenfunction of H by the superposition of ψ_n :

$$\psi^{(\nu)} = \sum_n c_{n\nu} \psi_n \quad (\nu = 0, 1, 2, \dots) \quad (7)$$

the original eigenvalue problem is transformed into the following matrix form.

$$\begin{pmatrix} a_0 & b_1 & & \\ b_1 & a_1 & b_2 & \\ & b_2 & a_2 & b_3 \\ & & & \ddots \end{pmatrix} \begin{pmatrix} c_{0\nu} \\ c_{1\nu} \\ \vdots \end{pmatrix} = \epsilon_\nu \begin{pmatrix} c_{0\nu} \\ c_{1\nu} \\ \vdots \end{pmatrix} \quad (8)$$

In the preceding section, we have shown that the coefficients a_n behave as

$$a_n = q_0 n + q_1 \quad (9)$$

If we assume eq.(9) for larger n , the problem is reduced to solving the electronic states on the Bethe lattice. In order to see the effect of diagonal terms we have numerically diagonalized the tridiagonal matrix of dimension N by assuming the diagonal elements given by eq. (8) with $q_0 = 3\alpha$, $q_1 = 0$. For subdiagonal elements b_n for $n \leq 4$ we employed the values listed in Table I and assumed $b_n = b_4$ for $n > 4$. We checked that the band width for the case of $\alpha = 0$ well reproduces our previous estimate $|\varepsilon_0/4t| = 0.79$ [16]. The lowest energy level $\varepsilon_0(\alpha)$ increases with α according to

$$\varepsilon_0(\alpha) - \varepsilon_0(0) \propto \alpha^\beta$$

with $\beta = 0.65 \sim 0.7$, which agrees with [7] for the Ising spin configuration. The presence of the diagonal terms has a significant effect on the energy spectrum of the system. When $\alpha = 0$ ($J = 0$), minimum energy separation δ_{min} between a pair of neighboring levels,

$$\delta_\nu = \varepsilon_{\nu+1} - \varepsilon_\nu$$

decreases with increasing N , and energy levels form continuous spectrum for infinite N . In this model minimum value of δ_ν occurs at the band edges. The behavior of $\delta_{min} \propto N^{-p}$ with $p > 1$ reflects the divergent behavior of the density of states. On the other hand, δ_{min} in the case of finite α converges to a finite value of about q_0 . Although eigenvalues of eq.(8) extend to higher energies, the overlap of ψ_0 with these eigenstates becomes extremely small above some energy ε_c . We can therefore define an effective band width W by $\varepsilon_c - \varepsilon_0$. Then we found W remains nearly unchanged. This means that continuous energy spectrum of the system becomes a finite number ($\sim W/q_0$) of discrete levels. It follows then that the local density of states consists of a number of delta-functions, *i.e.*,

$$\rho(\omega) = \sum_\nu |c_{0\nu}|^2 \delta(\omega - \varepsilon_\nu) \quad (10)$$

The value of $|c_{0\nu}|^2$ is negligible for $\varepsilon_\nu - \varepsilon_0 \geq W$, the band width ($W \sim 6.1t$). When diagonal term increases with n and becomes greater than the band energy, the state ψ_0 cannot mix with the state ψ_n . The problem (8) then effectively reduces to the one in a finite dimension. Note that the wave function, ψ_n , is defined successively from ψ_0 by applying the hole transfer Hamiltonian. From this construction, n is the measure of the spatial extension of the hole wave function, the area covered by the hole motion within n steps from the origin. The weight $|c_{n0}|^2$ becomes very small for n larger than W/q_0 . This clearly shows the spatial localization of the hole wave function. Note that the actual localization length is still smaller because the wave function ψ_n in general contains the state with a hole on the origin but with different spin configuration from ψ_0 .

In the present paper we discussed the effect of the finite exchange interaction on the propagation of a hole doped into an antiferromagnetic Mott insulator. Our lower order estimate of the diagonal elements of the continued fraction representation indicates the existence of the string effect for the diagonal elements a_n . This means that the potential energy of a hole increases proportional to the hopping length from the original hole position. This gives rise to the confinement of the hole, *i.e.* the spatial localization of the hole wave function. This implies the degeneracy of the low lying energy levels because two spatially separated holes are almost orthogonal with each other. We suppose, although this conclusion reflects an aspect of the effect of exchange interaction J , the result comes from the present linear approximation of J . In the present nearest neighbor hopping model, the effect of J on the delocalization start from J^2 term, but this is neglected here. If the subdiagonal element b_n grows and overcomes the effect of the diagonal ones, the above degeneracy will be finally lifted and discrete levels will form a narrow continuous energy band again. The band width is then scaled by J . If the linear n -dependence will saturate at some value of n , it also favors the delocalization. Nevertheless we suppose main feature of the local density of states are well reproduced by taking the effect of J discussed here.

In the case of $\text{La}_{1-x}\text{Sr}_x\text{CuO}_4$, hole wave functions are spatially localized in the small concentration region just before the appearance of superconductivity. The temperature dependence of the transport properties seem to be fitted

well with the variable range hopping [20]. In view of the fact that the potential fluctuation introduced by the Sr-doping is well confined to the LaO layers, and the effect on CuO₂ layers is relatively small, the observed localization behavior will possibly be ascribed to the string effect which originates from many-body effect discussed here.

On the relative stability of the RVB and AF states, our estimates of a_n do not show much difference for both cases; AF is slightly disfavored. On the other hand in the present nearest neighbor RVB model the lowest eigenstate a_0 of H_0 is higher than the one in AF [21]. Therefore it is not easy to conclude that the slight difference of a_n for RVB and AF is the main stability energy of the RVB state upon doping, which agrees with our previous conclusion in the case of $J/t = 0$ limit [16].

This work was supported by Grant-in-Aid for Scientific Research on Priority Areas "Mechanism of Superconductivity".

References

- [1] Y. Nagaoka: Phys. Rev. **147** 392 (1966).
- [2] W.F. Brinkman and T.M. Rice: Phys. Rev. **B2** 1324 (1970).
- [3] Y. Takahashi: Z. Physik **B 67** 503 (1987).
- [4] J.E. Hirsch: Phys. Rev. Lett. **59** 228 (1987).
- [5] S.A. Trugman: Phys. Rev. **B 37** 1597 (1988).
- [6] S.A. Trugman: preprint.
- [7] B.I. Shraiman and E.D. Siggia: Phys. Rev. Lett. **60** 740 (1988).
- [8] S. Sachdev: Phys. Rev. **B 39** 12232 (1989).
- [9] J. Inoue, M. Miyazaki, and S. Maekawa: Physica **C157** 209 (1989).
- [10] S. Maekawa, J. Inoue, and M. Miyazaki: *Mechanism of High Temperature Superconductivity*, Springer Series in Materials Science, edited by H. Kamimura and A. Oshiyama (Springer, Berlin, 1989) p.68.
- [11] M. Miyazaki, J. Inoue, and S. Maekawa: Phys. Rev. **B 40** 6611 (1989).
- [12] P.W. Anderson: Science **235** 1196 (1987).
- [13] P. Lederer and Y. Takahashi: Z. Phys. **B71** (1988) 415.
- [14] P. Lederer and Y. Takahashi: *High Temperature Superconductivity and Other Related Topics*, Proc. of the 1st Asia-Pacific Conf. on Condensed Matter Physics, eds. B.E. Baaquie, C.K. Chew, C.H. Lai, C.H. Oh, and K.K. Phua (World Scientific, Singapore, 1989) p.154.
- [15] Y. Takahashi: Z. Phys. **B71** (1988) 425.
- [16] H. Tsunetsugu and Y. Takahashi: J. Phys. Soc. Jpn. **58** 4184 (1989).
- [17] R. Joynt: Phys. Rev. **B 37** 7979 (1988).
- [18] J.D. Reger and A.P. Young: Phys. Rev. **B 37** 5978 (1988).
- [19] Y. Takahashi and H. Tsunetsugu: preprint.
- [20] M.A. Kastner, R.J. Birgeneau, C.Y. Chen, Y.M. Chiang, D.R. Gabbe, H.P. Jenssen, T. Junk, C.J. Peters, P.J. Picone, T. Thio, T.R. Thurston, and H.L. Tuller: Phys. Rev. **B 37** 111 (1988).
- [21] M. Kohmoto: Phys. Rev. **B 37** 3812 (1988), M. Inoue, T. Chikyu, X. Hu, and M. Suzuki: J. Phys. Soc. Jpn. **57** 3733 (1988), C. Dasgupta: Phys. Rev. **B 39** 386 (1989).

THE HOLON-DOUBLON OPERATOR FORMALISM

Sadao NAKAJIMA

Department of Physics, Tokai University
Hiratsuka, Kanagawa 259-12

A few theoretical remarks are given concerning the operator formalism to describe vacant and doubly occupied sites in the single-orbital Hubbard model.

The aim of this note is to make a few remarks concerning the operator formalism of the single-orbital Hubbard model, particularly in the form of the tJ model, which P. Anderson¹⁾ proposed as a theoretical model to describe newly discovered high-T_c cuprates²⁾. The physical situation is more complicated in p-type high-T_c cuprates than in the single-orbital Hubbard model^{3),4),5)} since the doped hole is experimentally known to spend most of time in oxygen p-states rather than in copper d-states. The model may apply to n-type high-T_c cuprates, provided that the doped electron goes into copper d-states.

We assume the on-site Coulomb energy U large compared with the hopping energy t in the Hubbard model, so that the energy spectrum splits into two bands separated by a gap of the order of U. Corresponding to this splitting, the operator c_{is}, which annihilates the electron with spin s at site i, is decomposed uniquely as

$$c_{is} = a_{is} + b_{is} \quad (1)$$

$$a_{is} = (1 - n_{i-s})c_{is}, \quad b_{is} = n_{i-s}c_{is} \quad (2)$$

where $n_{is} = c_{is}^\dagger c_{is}$. The a-operator creates a vacant site, i.e., the holon in the terminology of Anderson, whereas b[†] creates a doubly occupied site, which we may call the doublon. Half-filling, which corresponds to the undoped, insulating cuprate, means the full a-band and empty b-band:

$$a_{is}^\dagger \Psi = 0, \quad b_{is} \Psi = 0 \quad (3)$$

An advantage of using the a-operators is that the so-called Gutzwiller projection, which is often satisfied only on average in the usual formalism, is automatically taken care of. On the other hand, they satisfy non-linear, spin-dependent anticommutation relations:

$$\begin{aligned} \{ a_{is}, a_{js}^\dagger \} &= \delta_{ij} (1 - n_{i-s}) \\ \{ a_{is}, a_{j-s}^\dagger \} &= \delta_{ij} S_i^{(\pm)} \end{aligned} \quad (4)$$

Where $S_i^{(+)} = c_{i\uparrow}^\dagger c_{i\downarrow}$ is the spin operator. Similarly,

$$\begin{aligned} \{ b_{is}, b_{js}^\dagger \} &= \delta_{ij} n_{i-s} \\ \{ b_{is}, b_{j-s}^\dagger \} &= -\delta_{ij} S_i^{(\pm)} \end{aligned} \quad (5)$$

Now, in terms of these operators, the tJ model Hamiltonian may be written as⁴⁾

$$H = H_t + H_U + H_J \quad (6)$$

with

$$H_t = \sum t (a_{is}^\dagger a_{js} + b_{is}^\dagger b_{js}) \quad (7)$$

$$H_U = \frac{1}{2} \sum U b_{is}^\dagger b_{is} \quad (8)$$

$$H_J = \sum J \{ a_{is}^\dagger a_{i-s} a_{j-s}^\dagger a_{js} - a_{is}^\dagger a_{is} a_{j-s}^\dagger a_{j-s} \} \quad (9)$$

The exchange interaction H_J might appear to commute with the doublon operators b_{is} , but actually it does not since

$$\{ a_{is}, b_{j-s} \} = \delta_{ij} c_{is} c_{i-s} \quad (10)$$

Even the hopping term H_t , which appears to be spin-independent, gives rise to a strongly spin-dependent hopping through (4) and (5). To illustrate this complexity, let us apply the so-called many-body tight binding approximation⁶⁾.

Suppose thus we have one doublon doped into a half-filled state Ψ which satisfies (3). For simplicity, we assume that Ψ is a non-magnetic state such as the RVB state. The many-body tight binding Bloch function of the doublon may be taken as

$$\Psi_k = \{2/N\}^{1/2} \sum \exp\{ik \cdot R_i\} b_{is}^\dagger \Psi \quad (11)$$

The expectation value of (6) can be written as

$$\langle \Psi_k | H | \Psi_k \rangle = E_0 + \epsilon(k) \quad (12)$$

where

$$E_0 = \langle H \rangle \quad (13)$$

$$\epsilon(k) = [2/N] \sum \exp[ik \cdot (R_i - R_j)] T_{ij} \quad (14)$$

$$T_{ij} = - \langle [b_{is}, [b_{js}, H]] \rangle \quad (15)$$

Here $\langle \dots \rangle$ means the expectation value with respect to the half-filled state Ψ .

We denote the many-body transfer matrix elements by T_{ij}^t which we obtain by substituting H_t in (15).

Then

$$T_{ij}^t = t \langle \frac{1}{2} + 2S_i \cdot S_j \rangle \quad (16)$$

Note that the expression in the bracket on the right is the spin exchange operator whose eigenvalues are ± 1 for triplet and singlet states, respectively.

References

1. P.W.Anderson: Science 235 (1987) 1196
2. G Bednorz and K.A. Muller: Z. Phys. B Condensed Matter 64 (1986) 189
3. J. Hubbard: Proc. Roy. Soc. A276 (1963) 238
4. K.A. Chao, J. Spalek and A.M. Oles: J. Phys. C10 (1977) L271
5. H. Fukuyama, H. Matsukawa and Y. Hasegawa: J. Phys.Soc. J. Phys. Jpn 58 (1989) 364
6. See S. Maekawa, J. Inoue and T. Tohyama: "Strong Correlation and Superconductivity" (Proc. IBM Jpn International Symposium 1989), ed. H. Fukuyama, S. Maekawa and A.P. Malozemoff (Springer Verlag) p.66

Slave-Fermion Theory of the t - t' - J Model

Daijiro Yoshioka

Department of Physics, Kyushu University
4-2-1 Ropponmatsu, Fukuoka 810, Japan

As a model for the CuO_2 plane of the oxide superconductor, the t - t' - J model is investigated by a slave-fermion formalism. Three limiting cases are considered: (1) The half-filled case where the model reduces to the Heisenberg model. (2) Near half-filled where only the nearest neighbor transfer is allowed (t - J Model) (3) Near half-filled with finite t' , but $t \ll J$. For the Heisenberg model the present scheme gives reasonable results. For the case (3) it is shown that spin-fluctuation leads to high temperature superconductivity.

§1. Introduction

It is widely believed that the two-dimensional CuO_2 layer is responsible for the high transition temperature superconductivity of the copper oxides. The t - J model is one of the models to represent this CuO_2 layer,[1] and various investigations have been conducted on this model. In the original t - J model, only the nearest-neighbor transfer was considered. However, recently the importance of the next-nearest or farther neighbor transfer (t' -term) has been pointed out.[2] This is the t - t' - J model. It has been argued that t' -term is necessary to represent the CuO_2 layers by this kind of model.[3,4] Thus, our ultimate goal is to understand the t - t' - J model. However, this model is not so easy to be investigated, so we analyze the model step by step.

We employ the Schwinger boson-slave fermion method. Then the Hamiltonian of the t - t' - J model is given as $\mathcal{H} = \mathcal{H}_J + \mathcal{H}_t$, where

$$\mathcal{H}_J = -\frac{J}{2} \sum_{\langle i,j \rangle} \sum_{\sigma} \sum_{\sigma'} \text{sgn}(\sigma\sigma') s_{i\sigma}^{\dagger} s_{j-\sigma}^{\dagger} s_{j-\sigma'} s_{i\sigma'}, \quad (1)$$

and

$$\mathcal{H}_t = - \sum_{\langle i,j \rangle} \sum_{\sigma} t_{ij} [e_i e_j^{\dagger} s_{i\sigma}^{\dagger} s_{j\sigma} + \text{h.c.}]. \quad (2)$$

Here, the electron operator $c_{i\sigma}$ at lattice site \mathbf{r}_i has been expressed by a Schwinger boson operator $s_{i\sigma}$ and a slave-fermion (holon) operator e_i as $c_{i\sigma} = s_{i\sigma} e_i^{\dagger}$. Thus, the order parameter for the superconductivity may be expressed as $\langle c_{i\sigma} c_{j-\sigma} \rangle = \langle e_i^{\dagger} e_j^{\dagger} \rangle \langle s_{i\sigma} s_{j-\sigma} \rangle$. The summation $\sum_{\langle i,j \rangle}$ in \mathcal{H}_J is taken only for nearest-neighbor bonds. That in \mathcal{H}_t is taken up to the third-neighbors. Hereafter, the transfer integral t_{ij} is written as t for $|\mathbf{r}_i - \mathbf{r}_j| = 1$, t' for $|\mathbf{r}_i - \mathbf{r}_j| = \sqrt{2}$, and t'' for $|\mathbf{r}_i - \mathbf{r}_j| = 2$, where the lattice constant is taken to be unity.

We first apply this method to the half-filled case. In this case the \mathcal{H}_t term disappears from the Hamiltonian, and the model reduces to the antiferromagnetic Heisenberg model. We

assume the existence of the RVB-type order parameter, and solve the Hamiltonian by a mean field approximation.[5-7] We find there is long-range antiferromagnetic spin correlation at $T = 0$. At finite temperature the spin correlation decays exponentially. The spin-correlation length, spin susceptibility, and specific heat show reasonable agreement with Monte Carlo simulation [8-10] and neutron scattering experiment.[11]

This success of the Schwinger boson-slave fermion method at the half-filled encourages us to apply this model to the less-than-half filled case. We first consider the case where $t' = t'' = 0$. This is the t - J model. By a mean field approximation we find that there also exists long-range spin correlation at $T = 0$ but with period incommensurate to that of the lattice.[12,13] This incommensurability comes from the fact that in the commensurate state the holons are localized with no gain in the kinetic energy, but they are delocalized in the incommensurate phase which lowers their kinetic energy.

The situation is quite different for the t - t' - J model. The holons are transferred by the t' -term even in the commensurate phase. Therefore, the holons can gain the kinetic energy without destroying the (short-range) commensurate Néel order. Thus we assume that the spin system remains essentially the same as the half-filled case, and include the effect of t and t' terms by the perturbation. We find that in a wide region in the parameter space of t , t' and t'' , interaction between holons mediated by spinons become attractive.[14]

This paper is organized as follows. In the next section the results for the Heisenberg model are shown. In §3 the results for the t - J model are shown. In the final section those for t - t' - J model are presented.

§2. Heisenberg model

At half-filled case the constraint of the t - t' - J model that there should be no doubly occupied site becomes a constraint that there is only one spinon at each lattice site. Therefore there is no holon in the system, and the Hamiltonian consists only of \mathcal{H}_J . This Hamiltonian is equivalent to that of the Heisenberg model. We consider this model in the presence of an external magnetic field. Then the Hamiltonian is given as follows.

$$\begin{aligned} \mathcal{H} = & \frac{J}{2} \sum_{\langle i,j \rangle} \sum_{\sigma} (s_{i,\sigma}^{\dagger} s_{j,-\sigma}^{\dagger} s_{j,\sigma} s_{i,-\sigma} - s_{i,\sigma}^{\dagger} s_{j,-\sigma}^{\dagger} s_{j,-\sigma} s_{i,\sigma}) \\ & - \frac{1}{2} \mu_s B \sum_i (s_{i,\uparrow}^{\dagger} s_{i,\uparrow} - s_{i,\downarrow}^{\dagger} s_{i,\downarrow}) + \mu \sum_i \sum_{\sigma} s_{i,\sigma}^{\dagger} s_{i,\sigma} . \end{aligned} \quad (3)$$

Here μ_s is gyromagnetic ratio and the chemical potential μ has been introduced to make the system to satisfy the constraint

$$s_{i,\uparrow}^{\dagger} s_{i,\uparrow} + s_{i,\downarrow}^{\dagger} s_{i,\downarrow} = 1, \quad (4)$$

on the average. To solve this Hamiltonian by a mean field approximation we introduce the following order parameter, which gives the amplitude of the nearest neighbor singlet pairs.

$$\Delta_z = \frac{1}{2} \langle s_{i,\downarrow} s_{i+\hat{z},\uparrow} - s_{i,\uparrow} s_{i+\hat{z},\downarrow} \rangle, \quad (5)$$

where $z = x$ or y , and $i + \hat{z}$ is a site next to the site i in the z -direction. After decoupling the Hamiltonian, we rewrite the operator by its Fourier transform:

$$s_{i,\sigma} = \frac{1}{\sqrt{N}} \sum_{\mathbf{k}} e^{i\mathbf{k} \cdot \mathbf{r}_i} s_{\mathbf{k},\sigma}, \quad (6)$$

where N is the total number of the lattice sites, and \mathbf{k} is two-dimensional wave vector. The Hamiltonian is diagonalized by the Bogoliubov transformation. We obtain the following self-consistent equations.

$$n_{\uparrow} + n_{\downarrow} = 1, \quad (7)$$

$$n_{\uparrow} - n_{\downarrow} = 2m, \quad (8)$$

$$\Delta_z = \frac{J}{N} \sum_{\mathbf{k}} \sin k_z \frac{\Delta_x \sin k_x + \Delta_y \sin k_y}{E_{\mathbf{k}}} [\langle \alpha_{\mathbf{k}} \alpha_{\mathbf{k}}^{\dagger} \rangle + \langle \beta_{\mathbf{k}}^{\dagger} \beta_{\mathbf{k}} \rangle], \quad (9)$$

where

$$n_{\uparrow} = \langle s_{i,\uparrow}^{\dagger} s_{i,\uparrow} \rangle = \frac{1}{N} \sum_{\mathbf{k}} [|u_{\mathbf{k}}|^2 \langle \alpha_{\mathbf{k}}^{\dagger} \alpha_{\mathbf{k}} \rangle + |v_{\mathbf{k}}|^2 \langle \beta_{\mathbf{k}}^{\dagger} \beta_{\mathbf{k}} \rangle], \quad (10)$$

$$n_{\downarrow} = \langle s_{i,\downarrow}^{\dagger} s_{i,\downarrow} \rangle = \frac{1}{N} \sum_{\mathbf{k}} [|v_{\mathbf{k}}|^2 \langle \alpha_{\mathbf{k}} \alpha_{\mathbf{k}}^{\dagger} \rangle + |u_{\mathbf{k}}|^2 \langle \beta_{\mathbf{k}}^{\dagger} \beta_{\mathbf{k}} \rangle], \quad (11)$$

$$\langle \alpha_{\mathbf{k}}^{\dagger} \alpha_{\mathbf{k}} \rangle = \frac{1}{\exp[E_{\alpha}(\mathbf{k})/T] - 1}, \quad \langle \beta_{\mathbf{k}}^{\dagger} \beta_{\mathbf{k}} \rangle = \frac{1}{\exp[E_{\beta}(\mathbf{k})/T] - 1}, \quad (12)$$

$$E_{\alpha}(\mathbf{k}) = E_{\mathbf{k}} - (1/2)\mu_s B + 2mJ, \quad E_{\beta}(\mathbf{k}) = E_{\mathbf{k}} + (1/2)\mu_s B - 2mJ, \quad (13)$$

$$E_{\mathbf{k}} = \sqrt{\lambda^2 - |\gamma_{\mathbf{k}}|^2}, \quad (14)$$

$$\lambda = \mu - J, \quad (15)$$

$$\gamma_{\mathbf{k}} = 2iJ(\Delta_x \sin k_x + \Delta_y \sin k_y) \equiv |\gamma_{\mathbf{k}}| e^{i\theta_{\mathbf{k}}}, \quad (16)$$

and

$$u_{\mathbf{k}} = \frac{1}{\sqrt{2}} \sqrt{\frac{\lambda}{E_{\mathbf{k}}} + 1} \exp\left(\frac{i}{2}\theta_{\mathbf{k}}\right), \quad v_{\mathbf{k}} = \frac{1}{\sqrt{2}} \sqrt{\frac{\lambda}{E_{\mathbf{k}}} - 1} \exp\left(\frac{i}{2}\theta_{\mathbf{k}}\right). \quad (17)$$

For $T > 0$ the spectrum $E_{\alpha}(\mathbf{k})$ and $E_{\beta}(\mathbf{k})$ must be greater than zero, but at $T = 0$ it is possible that at some \mathbf{k} , E_{α} or E_{β} becomes zero. In the following we consider s -wave state, where $\Delta_x = \Delta_y$. This state is degenerate with the d -wave state, where $\Delta_x = -\Delta_y$. These states have the lowest free energy. In this s -wave state, the minimum of $E_{\alpha}(\mathbf{k})$ and $E_{\beta}(\mathbf{k})$ occurs at $\mathbf{k} = \mathbf{K}_{\pm} = \pm(\pi/2, \pi/2)$. At $T = 0$ the energy should become zero at these wave vectors, and we have the Bose condensation there. We define occupation numbers n_{α} and n_{β} at these condensation wavevectors:

$$\langle \alpha_{\mathbf{k}}^{\dagger} \alpha_{\mathbf{k}} \rangle = n_{\alpha}, \quad \text{at } \mathbf{k} = \mathbf{K}_{\pm}, \quad (18)$$

$$\langle \beta_{\mathbf{k}}^{\dagger} \beta_{\mathbf{k}} \rangle = n_{\beta}, \quad \text{at } \mathbf{k} = \mathbf{K}_{\pm}. \quad (19)$$

This n_{α} or n_{β} becomes macroscopic, only when $E_{\alpha}(\mathbf{K}_{\pm}) = 0$ or $E_{\beta}(\mathbf{K}_{\pm}) = 0$, respectively.

In a finite magnetic field we can assume $B > 0$ without loss of generality. Then m becomes positive. We can show that $E_{\alpha}(\mathbf{k})$ is smaller than $E_{\beta}(\mathbf{k})$, thus only n_{α} can be macroscopic. We define n_B by,

$$n_B = \frac{n_0}{N} = \frac{\lambda n_{\alpha}}{E_{\mathbf{K}_{+}} N}, \quad (20)$$

where n_0 is one half of the number of bosons which are Bose condensed. In the limit of $B \rightarrow 0$ Δ and n_B are given as $n_B(0) = 0.3034$, and $\Delta(0) = 0.5790$.

Finite value of n_B means that there is long-range antiferromagnetic spin correlation. At low magnetic field the spin-spin correlation in the limit of infinite separation between two spins is given as

$$\langle \mathbf{S}_i \cdot \mathbf{S}_{i+\mathbf{R}} \rangle = (-1)^{X+Y} \left[\frac{3}{2} n_B^2 - m^2 \right] + \frac{3}{2} m^2, \quad (21)$$

where X and Y are the x - and y -components of \mathbf{R} in units of the lattice constant. This value of the spin correlation is about 1.5 times greater than that of the Monte Carlo simulation. However, qualitative feature of the model, the existence of the long-range order at $T = 0$, is correctly described.

At finite temperature the spin-correlation decays exponentially. The correlation length is given by

$$\xi = \sqrt{2\Delta} \frac{J}{T} \exp\left(\frac{2\pi J\Delta}{T} n_B\right). \quad (22)$$

This temperature dependence coincides with the result of one-loop approximation of the non-linear- σ model by Chakravarty et al.[15] Neutron scattering experiment [11] also shows this kind of behavior.

At finite temperature we can also calculate the specific heat and the susceptibility. At low temperature these can be expanded as a power series in T . To the lowest order we obtain

$$\frac{C}{N} = \frac{3}{2\pi} \zeta(3) \left(\frac{T}{J\Delta(0)} \right)^2 \simeq 1.712 \left(\frac{T}{J} \right)^2, \quad (23)$$

and

$$\chi(T) \simeq \frac{\mu_s^2}{2J} \frac{n_B}{4\Delta + 2n_B} \left[1 + \frac{2}{\pi} \frac{n_B}{4\Delta + 2n_B} T \right] = \frac{\mu_s^2}{J} (0.05190 + 0.03726 \frac{T}{J}). \quad (24)$$

These results agree with a Monte Carlo simulation.[9,10]

§3. t - J model

Having seen that present Schwinger boson-slave fermion method gives reasonable results at half-filled case, we apply this model to the t - J model.[12] Here we consider only the nearest neighbor hopping. The Hamiltonian is now given as follows

$$\begin{aligned} \mathcal{H} = & -t \sum_{\langle i,j \rangle} \sum_{\sigma} [e_i^\dagger e_j^\dagger s_{i,\sigma}^\dagger s_{j,\sigma} + \text{h.c.}] - \frac{J}{2} \sum_{\langle i,j \rangle} \sum_{\sigma} [s_{i,\sigma}^\dagger s_{j,-\sigma}^\dagger s_{j,-\sigma} s_{i,\sigma} - s_{i,\sigma}^\dagger s_{j,-\sigma}^\dagger s_{j,\sigma} s_{i,-\sigma}] \\ & - \mu_e \sum_i e_i^\dagger e_i - \mu_s \sum_i \sum_{\sigma} s_{i,\sigma}^\dagger s_{i,\sigma}. \end{aligned} \quad (25)$$

The last two terms with the chemical potential μ_e and μ_s are added to enforce the constraint that $\langle e_i^\dagger e_i \rangle = \delta$ and $\langle s_{i,\sigma}^\dagger s_{i,\sigma} \rangle = (1/2)(1 - \delta)$, where δ is the hole concentration.

We treat this hamiltonian by a mean field approximation, introducing the following order parameters.

$$\Delta_z = \frac{1}{2} \langle s_{i+\hat{z},\uparrow} s_{i,\downarrow} - s_{i+\hat{z},\downarrow} s_{i,\uparrow} \rangle, \quad (26)$$

$$\kappa_{z,\sigma} = \langle s_{i,\sigma}^\dagger s_{i+\hat{z},\sigma} \rangle, \quad (27)$$

and

$$\epsilon_z = \langle e_{i+\hat{z}}^\dagger e_i \rangle. \quad (28)$$

We consider the case where all the order parameters are real and $\Delta_x = \Delta_y = \Delta$, $\kappa_{x,\uparrow} = \kappa_{x,\downarrow} = \kappa_{y,\uparrow} = \kappa_{y,\downarrow} = \kappa$, and $\epsilon_x = \epsilon_y = \epsilon$, since this choice makes the free energy minimum. The fermion (holon) part of the mean field Hamiltonian only consists of hopping terms. Therefore it is diagonalized in the momentum space. The band width is finite, when κ becomes finite, and there is a finite Fermi surface. The boson (spinon) part of the mean field Hamiltonian is diagonalized by the Bogoliubov transformation in the momentum space as before.

In the present model the energy of the spinon becomes zero at $\mathbf{k} = \mathbf{K}_{\pm} = \pm(K_0, K_0)$, where $\cos K_0 = -\tilde{t}\epsilon/\sqrt{(\tilde{t}\epsilon)^2 + (J\Delta)^2}$. Here $\tilde{t} = t + J\kappa/2\epsilon$. At small δ K_0 is given as

$$K_0 \simeq \frac{\pi}{2} + 1.24 \frac{t}{J} \delta, \quad (29)$$

The deviation of K_0 from $\pi/2$ means that the long-range spin correlation at $T = 0$ becomes incommensurate to the lattice. This incommensurability is necessary to gain the kinetic energy of holons. Incommensurate spin correlation has been observed experimentally.[16]

§4. t - t' - J model

Here we consider t - t' - J model.[14] Namely we consider the second neighbor transfer (t') and the third neighbor transfer (t'') together with the nearest neighbor transfer. Although t' and t'' are smaller than t , the effects of these terms are not small. As we have seen in the previous section, holons cannot move in the commensurate state. However, the t' and t'' terms allow holons to hop in the commensurate state. Therefore the holons can gain the kinetic energy even in the commensurate phase. Thus, we first solve the Hamiltonian, taking into account only the exchange term by a mean field theory. This is what we have done in §2. The effects of the transfer terms are considered as perturbations. This treatment is justified when the hole concentration δ is small enough.

In this section we divide the lattice into A and B sublattices, because in the present treatment holons transfer only in the same sublattices. We use operators a and b for holon destruction operators on A and B sublattices, respectively, and operators s^A and s^B for spinon operators on A and B sublattices, respectively. Then the transfer part of the Hamiltonian in the Fourier space is given as follows

$$\begin{aligned} \mathcal{H}_t = & \frac{1}{N} \sum_{\mathbf{k}_1} \sum_{\mathbf{k}_2} \sum_{\mathbf{q}} \sum_{\sigma} \{ [t(\mathbf{k}_1 - \mathbf{k}_2) e^{i(h_{1x} - h_{2x})} b_{\mathbf{k}_1}^{\dagger} a_{\mathbf{k}_1 + \mathbf{q}} s_{\mathbf{k}_2 + \mathbf{q}\sigma}^{A\dagger} s_{\mathbf{k}_2\sigma}^B + \text{h.c.}] \\ & + t'(\mathbf{k}_1 - \mathbf{k}_2) [a_{\mathbf{k}_1}^{\dagger} a_{\mathbf{k}_1 + \mathbf{q}} s_{\mathbf{k}_2 + \mathbf{q}\sigma}^{A\dagger} s_{\mathbf{k}_2\sigma}^A + b_{\mathbf{k}_1}^{\dagger} b_{\mathbf{k}_1 + \mathbf{q}} s_{\mathbf{k}_2 + \mathbf{q}\sigma}^{B\dagger} s_{\mathbf{k}_2\sigma}^B] \}, \end{aligned} \quad (30)$$

where $t(\mathbf{k}) = 2t(\cos k_x + \cos k_y)$, $t'(\mathbf{k}) = 4t' \cos k_x \cos k_y + 2t''(\cos 2k_x + \cos 2k_y)$. In the first-order perturbation, thermal average of $s^{\dagger}s$ is taken. Then we obtain the energy spectrum for the holes:

$$\langle \mathcal{H}_t \rangle_s = \sum_{\mathbf{k}} E_h(\mathbf{k}) (a_{\mathbf{k}}^{\dagger} a_{\mathbf{k}} + b_{\mathbf{k}}^{\dagger} b_{\mathbf{k}}), \quad (31)$$

where $E_h(\mathbf{k}) = (1/N) \sum_{\mathbf{k}_1} \sum_{\sigma} t'(\mathbf{k} - \mathbf{k}_1) \langle s_{\mathbf{k}_1\sigma}^{A\dagger} s_{\mathbf{k}_1\sigma}^A \rangle$. This $E_h(\mathbf{k})$ has the same form as $t'(\mathbf{k})$, except that t' and t'' are renormalized to be $0.8977t'$ and $0.8364t''$, respectively. The minimum of $E_h(\mathbf{k})$ occurs at $\mathbf{k} = \mathbf{K}_h$, where

$$\mathbf{K}_h = \begin{cases} (\pi/2, -\pi/2) & \text{for } t' > \max(1.86t'', 0) \\ (\pi/2, \pi/2) & \text{for } t' < \min(-1.86t'', 0) \\ (0, 0), (\pi, 0) & \text{otherwise.} \end{cases} \quad (32)$$

We refer to these three cases as case I, case II and case III, respectively. A small Fermi surface of holons is created around \mathbf{K}_h . The Fermi momentum is given by $k_F = \sqrt{2\pi\delta}$, when the energy band can be regarded as parabolic and when only a single valley is occupied. It should be remarked that the actual hole is a composite particle of a holon and a spinon. Therefore the energy band of holes become minimum at $\mathbf{K}_h + (\pi/2, \pi/2)$.

Effective interaction between A and B holons emerges from the second-order perturbation where holons exchange a pair of spinons. Since we are interested in the possibility of superconductivity, we consider interaction between holons on different sublattices with the total momentum $2\mathbf{K}_h$. At $T = 0$, the result is given as follows:

$$\mathcal{H}_{\text{eff}} = \frac{1}{N} \sum_{\mathbf{k}_1} \sum_{\mathbf{k}_2} V(\mathbf{k}_1, \mathbf{k}_2) a_{\mathbf{K}_h + \mathbf{k}_2}^\dagger b_{\mathbf{K}_h - \mathbf{k}_2}^\dagger b_{\mathbf{K}_h - \mathbf{k}_1} a_{\mathbf{K}_h + \mathbf{k}_1} e^{i(\mathbf{k}_1 - \mathbf{k}_2) \cdot \mathbf{r}}. \quad (33)$$

The effective interaction $V(\mathbf{k}_1, \mathbf{k}_2)$ is given after angular averaging as

$$\langle V \rangle = \frac{16J\Delta[n_B - (1/2)\delta]v}{[E_h(\mathbf{K}_h - \mathbf{k}_1) - E_h(\mathbf{K}_h - \mathbf{k}_2)]^2 - E_s(K + k_F)^2}, \quad (34)$$

where

$$v = \begin{cases} 4\pi^2\delta^2 t^2 + 32(t' - t'')^2 & \text{for case I} \\ -16\pi\delta t^2 + 32(t' + t'')^2 & \text{for case II} \\ -16\pi\delta t^2 + 16\pi^2\delta^2 t'^2 + 32t''^2 & \text{for case III.} \end{cases} \quad (35)$$

Equations (33) and (34) have the same form as the ordinary phonon-mediated interaction between electrons. Thus, if the interaction is attractive, condensation of holon pairs occurs. The symmetry of the pair is s -wave, which is the same as the RVB order-parameter. Thus, we can expect condensation of the Cooper pair of the real holes in the presence of the holon pair condensation and the RVB order. The interaction is attractive for $|E_h(\mathbf{K}_h - \mathbf{k}_1) - E_h(\mathbf{K}_h - \mathbf{k}_2)| < E_s(\mathbf{K}_s + k_F) \simeq 4\sqrt{\pi\delta}J\Delta$, if v is positive. As seen from eq.(35) v is positive for case I and also positive for cases II and III when δt^2 is small enough. The density of states of holon becomes large around the boundary between the regions I and III and between regions II and III. Thus high transition temperature is expected around these boundaries.

References

- [1] F.C.Zhang and T.M.Rice: Phys. Rev. B **37** (1988) 3759.
- [2] P.A.Lee: Phys. Rev. Lett. **63** (1989) 680.
- [3] L.H.Tjeng, H.Eskes and G.A.Sawatzky: *Strong Correlation and Superconductivity*, ed. H.Fukuyama, S.Maekawa and A.P.Malozemoff, Springer Ser. Solid-State Sci. (Springer, Berlin, Heidelberg 1989) p33.
- [4] H.Matsukawa and H.Fukuyama: J. Phys. Soc. Jpn. **58** (1989) 3687.
- [5] D.Yoshioka: J. Phys. Soc. Jpn. **58** (1989) 32.
- [6] D.Yoshioka: J. Phys. Soc. Jpn. **58** (1989) 3733.
- [7] A.Auerbach and D.P.Arovas did the same calculation. However, their results are not exact: Phys. Rev. Lett. **61** (1988) 617, and Phys. Rev. B **38** (1988) 316.
- [8] J.D.Reger and A.P.Young: Phys. Rev. B **37** (1988) 5978.
- [9] Y.Okabe and M.Kikuchi: J. Phys. Soc. Jpn. **57** (1988) 4351.
- [10] Y.Okabe, M.Kikuchi and A.D.S. Nagi: Phys. Rev. Lett. **61** (1988) 2971.
- [11] G.Shirane, Y.Endoh, R.J.Birgeneau, M.A.Kastner, Y.Hidaka, M.Oda, M.Suzuki, and T.Murakami: Phys. Rev. Lett. **59** (1987) 1613.

- [12] D.Yoshioka: J. Phys. Soc. Jpn. **58** (1989) 1516.
- [13] C.L.Kane, P.A.Lee, T.K.Ng, B.Chakraborty and N.Read: preprint.
- [14] D.Yoshioka: J. Phys. Soc. Jpn. **58** (1989) 4276.
- [15] S.Chakravarty, B.I.Halperin and D.R.Nelson: Phys. Rev. Lett. **60** (1988) 1057.
- [16] R.J.Birgeneau, Y.Endoh, K.Kakurai, Y.Hidaka, T.Murakami, M.A.Kastner, T.R.Thurston, G.Shirane, and K.Yamada: Phys. Rev. B **39** (1989) 1868.

On the Stability of Flux State and Chiral Spin State

Hiroyuki Shiba and Masao Ogata*

Department of Physics, Tokyo Institute of Technology

Oh-okayama, Meguro-ku, Tokyo 152

*Theoretische Physik, ETH - Hönggerberg

CH - 8093 Zürich, Switzerland

The stability of the chiral spin state, which was proposed for the two-dimensional frustrated antiferromagnet on the square lattice, is examined by taking the local constraint into account. It is shown that the chiral spin state is relatively high in energy, suggesting it to be unstable. The instability of the flux state against the antiferromagnetic order is also demonstrated in this connection.

§1 Introduction

One of the most fascinating ideas, which have been proposed so far in connection with high- T_c superconductivity, is Laughlin's scenario based on fractional statistics.¹⁾ Although the relevance of this mechanism to Cu-oxide superconductors is controversial, it is extremely interesting to see in what system this idea is materialized. Wen, Wilczek and Zee²⁾ (WWZ) have recently claimed that the two-dimensional $S=1/2$ Heisenberg antiferromagnet frustrated with the next-nearest-neighbor antiferromagnetic exchange interaction

$$H = J \sum_{ij}^{\text{nn}} \vec{S}_i \cdot \vec{S}_j + J' \sum_{jl}^{\text{nnn}} \vec{S}_j \cdot \vec{S}_l \quad (1)$$

may have a chiral spin state for J'/J greater than a threshold value. According to WWZ this model may then substantiate Laughlin's fractional statistics superconductivity, when the system is doped with holes. The purpose of this paper is to examine the stability of the chiral spin state in the model (1) and some related problems.³⁾

§2 Importance of Local Constraint

By introducing fermion operators with $\vec{S}_j = \sum_{\sigma\sigma'} \vec{S}_{\sigma\sigma'} c_{j\sigma}^+ c_{j\sigma'}$, the model (1) can be written in the form:

$$H = P_G H_{\text{fermion}} P_G, \quad (2)$$

$$H_{\text{fermion}} = -\frac{J}{2} \sum_{ij}^{\text{nn}} \left(\sum_{\sigma\sigma'} c_{i\sigma}^{\dagger} c_{j\sigma'}^{\dagger} c_{i\sigma} c_{j\sigma'} + \frac{1}{2} \right) \\ - \frac{J'}{2} \sum_{jl}^{\text{nnn}} \left(\sum_{\sigma\sigma'} c_{j\sigma}^{\dagger} c_{l\sigma'}^{\dagger} c_{j\sigma}^{\dagger} c_{l\sigma'} + \frac{1}{2} \right) \quad (3)$$

where the Gutzwiller projection operator $P_G = \prod_j [(1-n_{j\uparrow})n_{j\downarrow} + n_{j\uparrow}(1-n_{j\downarrow})]$ represents a local constraint onto the physical subspace in which each site is occupied by a single electron.

In the variational theory applied to (2) the energy is given by

$$E_V = \langle \Psi_V | P_G H_{\text{fermion}} P_G | \Psi_V \rangle / \langle \Psi_V | P_G | \Psi_V \rangle, \quad (4)$$

where Ψ_V is a variational wave function. E_V is then minimized to determine variational parameters in Ψ_V . However the local constraint P_G is completely ignored in the "mean field" theory as

$$\tilde{E}_V = \langle \Psi_V | H_{\text{fermion}} | \Psi_V \rangle / \langle \Psi_V | \Psi_V \rangle \quad (5)$$

and \tilde{E}_V is minimized instead of E_V , by taking a Slater determinant. Wen, Wilczek and Zee also follow the latter line of approach, which lacks any justification.

Table 1: One Dimensional Heisenberg Model

Table 2: Two Dimensional Heisenberg Model

	$\langle S_i \cdot S_j \rangle$ per bond	ref.
Neel state	-1/4=-0.25	
Bethe's exact solution	$(-\ln 2 + 1/4) \cdot 2$ =-0.4431	
"mean field" theory	$-2/\pi^2$ =-0.203	4
Gutzwiller-projected "mean field" theory	$-(3/2\pi) \cdot \text{Si}(\pi)$ =-0.4421	12
"mean field" dimer state	-1/4=-0.25	
Gutzwiller-projected dimer state	-3/8=-0.375	

	$\langle S_i \cdot S_j \rangle$ per bond	ref.
Neel state	-1/4=-0.25	
current best estimate	-0.334~-0.335	10
"mean field" s wave (Baskaran et al.)	$-8/\pi^4$ =-0.082	4
"mean field" dimer	-1/8=-0.125	
"mean field" flux state	-0.115	
Gutzwiller-projected a wave	-0.265	13
Gutzwiller-projected flux state	-0.32	14
Gutzwiller-projected dimer state	-3/16=-0.1875	

The role of P_G can be easily recognized if one takes the $J' = 0$ case and compares E_V and \tilde{E}_V with each other. Tables 1 and 2 show such a comparison for the one-dimensional chain and the two-dimensional square lattice, respectively. The energy for the "Gutzwiller-projected" states represents E_V . The lesson we can learn from the Tables is as follows. First, the "mean field" energy \tilde{E}_V is too high.⁵⁾ Secondly the dimer state has the lowest energy within the "mean field" theory as pointed out by Dombre and Kotliar,⁶⁾ while that is not the case in the Gutzwiller-projected states, which properly take into account P_G as in (4). Notice that the dimer state is not competitive at all in energy in the latter. This clearly demonstrates the necessity of the Gutzwiller projection in discussing the stability of WWZ's chiral spin state. The results will be described in the next section.

§3 Energy of Chiral Spin State

Let us switch on J' . Following WWZ, we take as Ψ_V a generalized Hartree-Fock-type state⁷⁾ having the bonds shown in Fig. 1. For simplicity $\chi_1 \sim \chi_4$ are fixed at $\chi_1 = \chi_2 = \chi_3 = \chi_4 = e^{i\pi/4}$. As for χ_6 and χ_8 we take up 4 cases including WWZ's chiral spin liquid: i) $\chi_6 = -\chi_8 = \text{real}$, ii) $\chi_6 = \chi_8 = \text{real}$, iii) $\chi_6 = -\chi_8 = \text{pure imaginary}$ and iv) $\chi_6 = \chi_8 = \text{pure imaginary}$. The case i) corresponds to WWZ's chiral spin state, in which the chirality in each elementary triangle is uniform and nonvanishing. On the other hand ii) has a staggered chirality and the chirality is vanishing in iii) and iv).

To determine the energy (4) for a given value of χ_6 we employ the variational Monte Carlo (VMC) method,⁸⁾ which has already been tested on several systems and is presumably the most reliable way to evaluate such a quantity as (4). In practice the VMC calculation is carried out on finite lattices; the limit for the infinite lattice is guessed from the size dependence. In the present calculation 4×4 , 6×6 and 8×8 lattices have been studied by imposing the boundary condition periodic in x and antiperiodic in y direction.⁹⁾

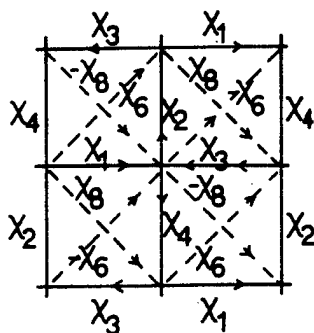


Fig. 1

The definition of the bonds $\chi_1 \sim \chi_8$.

The energy for the states i) and iii) is shown in Figs. 2 and 3, respectively as a function of χ_6 . Here the system size is 8×8 . For $J'/J \leq 0.5$ the minimum point is located at $\chi_6 = 0$, (i.e. the flux states) in both i) and iv). However for $J'/J \geq 0.5$ the state iv) is evidently lower than i). The state ii) having a staggered chirality has turned out to be much higher than i) and iv). There is a small difference between iii) and iv), which is due to the boundary condition chosen and decreases as the system size increases from 4×4 through 8×8 . In the 8×8 lattice the energy for iii) is not much different from iv). From the symmetry both iii) and iv) should give the same energy for the infinite lattice.

Figure 4 shows the energy as a function of J'/J , which is compared with the exact energy for 4×4 lattice under the periodic boundary condition. We can conclude from this result that the states i) and iv) are lower in energy than WZ's chiral

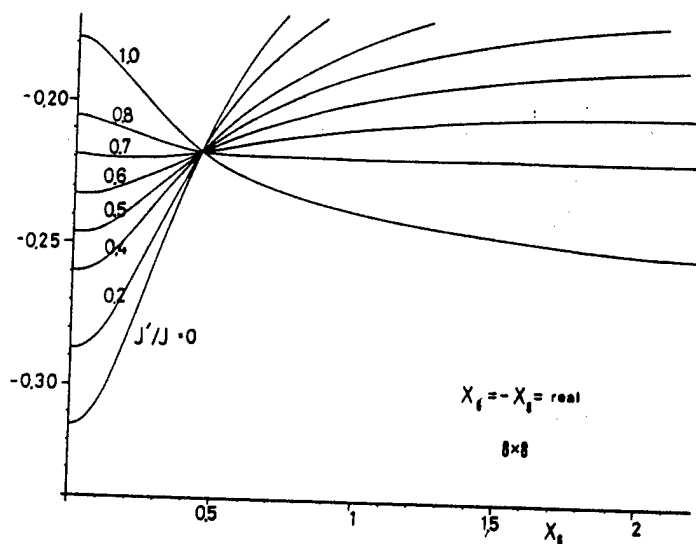


Fig. 2

Energy as a function of χ_6 for the state i) which has a chirality.

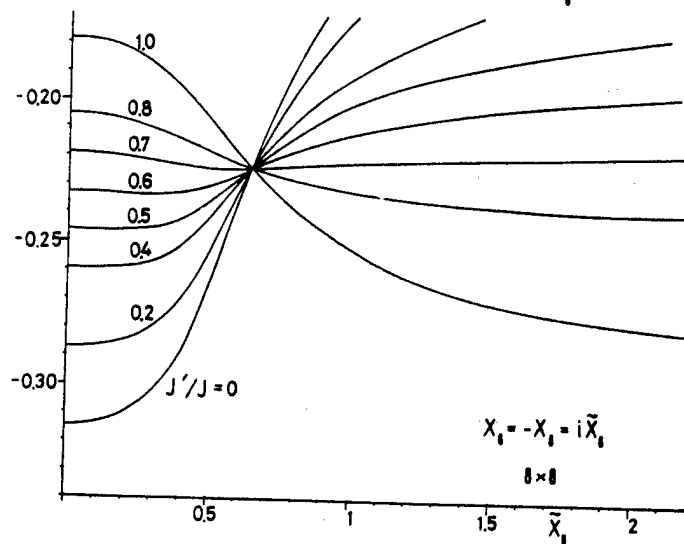


Fig. 3

Energy as a function of $\tilde{\chi}_6$ for the state iii) having no chirality.

spin state i). Therefore the latter state is not stable in contrast to the conclusion of the "mean field" theory.

§4 Is Flux State Stable?

We have also examined if the flux state is stable or not with respect to the antiferromagnetic (AF) long-range order corresponding to the 2-sublattice antiferromagnetism. The AF order is incorporated in Ψ_v by introducing a staggered magnetic field. The results for $J' = 0$ are presented in Fig. 5, which convinces us that the flux state is unstable against the AF order. Domber and Kotliar⁶⁾ pointed out within the "mean field" theory, that the flux state is unstable against the dimer state. The present calculation, which properly takes into account the local constraint, shows the flux state is unstable rather against the AF state. The dimer state is fairly high under the local constraint, as evident in Table 2. This result seems reasonable, since it is a general consensus that the AF long-range order exists for $J' = 0$ at $T = 0$ K.¹⁰⁾

The energy of the flux state modified by the AF order is included in Fig. 4, which demonstrates that the AF state progressively loses its stability with the increase of J'/J . We observe that for $J'/J \geq 0.6$ the energy of iii) and iv) is still

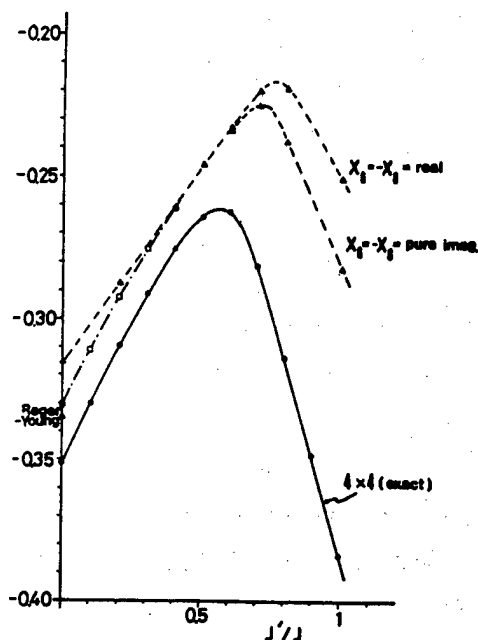


Fig. 4 Ground state energy as a function of J'/J : the open squares denote the flux state modified with antiferromagnetic LRO.

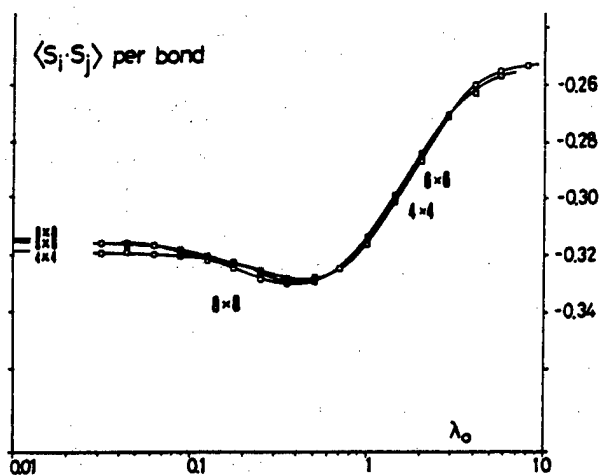


Fig. 5 Energy of the flux state as a function of λ_0 describing the anti-ferromagnetic LRO.

high compared with 4×4 . It is natural to conclude from this that the AF order between the second nearest-neighbor spins should be present in $J'/J \gtrsim 0.6$.¹¹⁾

Summing up, it is very likely that WWZ's chiral spin state is not stable in the model (1).

References

1. R. B. Laughlin : Science 242, 525(1988); Proceedings of 2nd NEC Symposium on Mechanisms of High Temperature Superconductivity (Springer, 1989), p.76.
2. X. G. Wen, F. Wilczek and A. Zee : Phys. Rev. B39, 11413(1989).
3. H. Shiba and M. Ogata : in preparation.
4. For instance G. Baskaran, Z. Zou and P. W. Anderson : Solid State Comm. 69, 973(1987); R. B. Laughlin : unpublished lecture note.
5. F. C. Zhang, C. Gros, T. M. Rice and H. Shiba : Superconductor Science and Technology 1, 36(1988).
6. T. Dombre and G. Kotliar : Phys. Rev. B39, 855(1989).
7. P. W. Anderson, B. S. Shastry and D. Hristopoulos : preprint.
8. For a review on variational Monte Carlo studies see H. Shiba : Two-Dimensional Strongly Correlated Electronic Systems (ed. by Z. Z. Gan and Z. B. Su, Gordon and Breach, 1989), p.161.
9. This boundary condition has been chosen to have a nondegenerate state for Ψ_V .
10. J. D. Reger and A. P. Young : Phys. Rev. B37, 5978(1988).
11. P. Chandra and B. Doucot : Phys. Rev. B38, 9335(1988).
12. F. Gebhard and D. Vollhardt : Phys. Rev. Lett. 59, 147(1987).
13. H. Yokohama and H. Shiba : J. Phys. Soc. Jpn. 56, 2570(1987).
11. C. Gros : Phys. Rev. B38, 931(1988).

Effective Hamiltonian for CuO_2 Layers and Fractional Statistics

Hidetoshi Fukuyama

*Institute for Solid State Physics
University of Tokyo
7-22-1, Roppongi, Minato-ku, Tokyo 106, Japan*

The effective Hamiltonian for CuO_2 layers has been derived based on the $d-p$ model with various parameters deduced from the analysis of photoemission spectroscopy. It is demonstrated that the low lying excitation associated with a single extra hole on oxygens is properly described by the Zhang-Rice singlet with appreciable spatial extent, and then that the $t-J$ model with possible modifications with more extended transfer integral(s) (and exchange interaction) will be the relevant model (the extended $t-J$ model). Effects of apical oxygens are investigated within this framework in the context of the pressure effect on T_c in T^* and T' structures. At the same time it is pointed out that if two holes are located around the same Cu spin those holes interact attractively, one of whose features is been explored.

A mean field theory based on the slave-boson formalism has been worked out for the extended $t-J$ model with special emphasis on the possible chiral spin state. It has been shown that the chiral spin state is stabilized for some range of the parameters in the case of finite doping, which is in contrast to the undoped case. The fluctuations around such mean field solutions have been treated systematically in terms of the gauge theory in (2+1) dimension. It is shown that there exists the Chern-Simons term whose prefactor depends on the degree of doping. By this finding we could for the first time derive anyons for the case of a finite doping. Discussions on anyons based on commensurate flux state are also given.

§1. Introduction

It is by now widely accepted that CuO_2 layers support the high T_c in Cu-oxides. In spite of such a consensus it is not yet fully agreed on which is the relevant model to describe the essence of low-lying excitation of the system; a typical question is which kind of fluctuations is dominant, magnetic or charge. The subtlety arises from the fact that Cu-oxides are not Mott insulators but the charge-transfer type insulators in the undoped case with relatively small gap energy as has been explored by photoemission and optical spectroscopy.

In this report we have first derived the effective Hamiltonian for the low-lying excitation in the doped case by use of various parameters characterizing the large energy scale properties deduced from the photoemission spectroscopy as shown in Fig.1 and Table 1. Detailed discussions on this effective Hamiltonian will be given. Based on these it is indicated that the extended $t-J$ model will be the relevant one, the knowledge of whose implications will be indispensable to the full understanding of high T_c oxides.

Next we will explain the result of a mean field theory of the extended $t-J$ model with particular emphasis on the chiral spin state, which is shown to be stabilized for some range of parameters. Based on this the Chern-Simons term has been obtained for the gauge field representing fluctuations around the mean field solutions and anyons are derived for the first time (not argued!) in the presence of finite doping. Various problems associated with the gauge field resulting from the local constraint are indicated.

§2. Effective Hamiltonian for CuO_2 Layers

By the fact that the Cu^{++} state appears to be stable even in the presence of doping (i.e. the absence of Cu^{+++} state) and that extra holes due to doping are located mainly on oxygen sites (though, of course, those holes have some component of Cu: d wave function because of mixing), it is natural to treat the mixing integral, t_0 , between Cu: $d_{x^2-y^2}$

and $O : p_\sigma$ orbitals as a perturbation. Such a perturbation theory has resulted in the following Hamiltonian in the second order of $t_0^{1,2}$

$$\begin{aligned}
 H_{eff} = & J_d \sum_i ' [\sum_{\alpha} ' \{ S_i \cdot p_{\alpha s}^+ \sigma_{ss'} p_{\alpha s'} (A_1 + A_2 \sum_{\beta \neq \alpha} n_{\beta}) \\
 & + A_3 n_{\alpha} + A_4 n_{\alpha \uparrow} n_{\alpha \uparrow} + A_5 n_{\alpha} \sum_{\beta \neq \alpha} n_{\beta} \} \\
 & + \sum_{\alpha \neq \beta} ' \{ S_i \cdot p_{\alpha s}^+ \sigma_{ss'} p_{\beta s'} (A_6 + A_7 \sum_{\gamma \neq \alpha, \beta} n_{\gamma} + A_8 (n_{\alpha} + n_{\beta})) \\
 & + (p_{\alpha \uparrow}^+ p_{\beta \uparrow} + p_{\alpha \downarrow}^+ p_{\beta \downarrow}) (A_9 + A_{10} \sum_{\gamma \neq \alpha, \beta} n_{\gamma} + A_{11} (n_{\alpha} + n_{\beta})) \}] \\
 & + J_s \sum_{(i \neq k)} ' S_i \cdot S_k + H_0.
 \end{aligned} \quad (1)$$

Here $J_d = t_0^2/U_d$ and S_i is the Cu-spin at the i -th site, whereas $p_{\alpha s}$ and $n_{\alpha s}$ are the hole annihilation operator at the α -th site around the i -th Cu site and the hole number operator at the α -th site for spin s . All the terms except the last two with J_s and H_0 are due to the presence of doping and the numerical factors, A_i ($i=1 \sim 11$), are determined by parameters given in Table 1 and found to be very sensitive functions of these parameters. The term J_s represents the superexchange interaction between Cu spins, which is present even in the undoped insulating state, whereas the last term H_0 represents the direct transfer integrals between oxygens and the on-site Coulomb interaction, U_p , on each oxygen. Equation (1) reveals the essential features of the problem; interaction process between Cu spins and oxygen holes, the indirect transfer integral between oxygens via Cu-sites and the interaction between holes on oxygens around the same Cu-site, which is induced by the charge transfer excitations. The existence of these various kinds of interaction processes will be the case for wide range of parameters as far as the basic condition of the stability of Cu^{++} state is justified. Quantitatively, however, the numerical values of A_i should not be taken literally but be understood with some allowance factors because of the relatively small value of charge transfer excitation gap, Δ , and then contributions from the next order perturbation will not be completely negligible.

Equation (1) is already complicated enough, and is not fully understood. However in the case of a single extra hole in the whole crystal this H_{eff} is apparently simplified as follows³;

$$\begin{aligned}
 H = & J_K \sum_i ' \sum_{\alpha, \beta} S_i \cdot p_{\alpha s}^+ \sigma_{ss'} p_{\beta s'} \\
 & + J'_K \sum_i ' \sum_{\alpha} S_i \cdot p_{\alpha s}^+ \sigma_{ss'} p_{\alpha s'} \\
 & - \sum_i ' \sum_{\alpha \beta} T_{\alpha \beta} p_{\alpha s}^+ p_{\beta s} + J_s \sum_{i \neq k} ' S_i \cdot S_k,
 \end{aligned} \quad (2)$$

where $J_K \sim 1\text{eV}$, $J'_K \sim -0.3\text{eV}$, $J_s \sim 0.1\text{eV}$ and $T_{\alpha \beta}$ has both direct (t_1 and t_2) and indirect transfer (T_0) integrals. The difficulty to solve eq.(2) results from the periodic array of Cu-spins. Since J_K is the largest energy is the problem, it will be natural to take account of this coupling first. We then first solved the problem of a single Cu spin and a single extra hole in the Bloch band in a way similar to but different from that by Eskes and Szatzky⁵ (the difference lies in that the indirect transfer via Cu-sites are fully taken throughout the crystal in the present scheme hence affecting the structure of hole Bloch band in an important way). The result^{3,4} is the strong stabilization of the Zhang-Rice singlet⁶ between the Cu spin and oxygen spin, and hence the low-lying excitations in the case of low doping will be described by the hopping of this singlet state through the crystal; i.e. the $t - J$ model will have the essence as first proposed by Anderson⁷. It turned out, however, by the detailed numerical calculations that the state is not localized completely on the neighboring four oxygen sites but that it is spatially more extended. By this we proposed that the model with more extended transfer integrals will be more relevant. This model is called extended $t - J$ model. Based on a different consideration Lee⁸ also indicated the possible importance of such an extended transfer integral.

In the course of this study we have realized that the spatial extent of the Zhang-Rice singlet is very sensitive to the choice of parameters reflecting the fact that the actual Cu-oxides will be located in a very delicate region of material parameters. This has led us to investigate⁹ the implication of the experiment by Murayama *et al.*¹⁰ of the pressure effect on critical temperature, T_c : large $d \ln T_c / d \ln p$ in NdCeSrCuO_4 (T'' -structure) but none in NdCeCuO_4 (T' -structure).

We found⁸⁾ that the apical oxygens present in T° -structure have profound effects on the spatial extent of the Zhang-Rice singlet, which might have some consequence on the remarkable experimental finding.

So far we have confined ourselves to the exploring the implication of eq.(2) but not the original one, eq.(1). The main difference between eq.(1) and (2) is that there exists in eq.(1) the attractive interaction between two oxygen holes if they are located around the same Cu-site. One of this feature is being investigated¹¹⁾ from the viewpoint of the classification of BCS pairing. The true problem, however, which takes account of Cu-spins at the same time, is to be studied.

§5. Mean Field Theory for the Extended $t - J$ model

As has been discussed in the preceding section we decided that the study of the extended $t - J$ model will be needed to pin down the hardest question of the mechanism of high T_c in oxides. The model is defined by

$$\begin{aligned} H_{t-J} = & J \sum_{n,n.} S_i \cdot S_j + J' \sum_{n,n.n.} S_i \cdot S_j \\ & - t \sum_{n,n.} c_{i\sigma}^{\dagger} (1 - n_{i,-\sigma}) (1 - n_{j,-\sigma}) c_{j\sigma} \\ & - t' \sum_{n,n.n.} c_{i\sigma}^{\dagger} (1 - n_{i,-\sigma}) (1 - n_{j,-\sigma}) c_{j\sigma} - \mu \sum_{i,\sigma} c_{i\sigma}^{\dagger} c_{i\sigma}. \end{aligned} \quad (3)$$

where various parameters are shown in Fig.2. In this model we take that t_{ij} and J_{ij} are independent parameters but that the exclusion of double occupancy is imposed on every site, which is the essence of the present problem of strong correlations. This model is again very hard to attack. Even in the case without J_{ij} the ground state is not known. (Very recently Wiegmann¹²⁾ proposed an interesting framework to this problem based on the transverse gauge field representing the local constraint.) Quite often the numerical calculations are resorted to for this kind of problem, which are admittedly useful to see overall features of electronic states. The nature of true low-lying excitations, however, will be very hard to be traced in such calculations at least with the present limit of attainability. Both analytical and computational methods should be complemented by each other.

Eq.(3) is often treated based on the slave-boson framework. In this the electron operator $c_{i\sigma}$ is represented by the product of the fermion operator, $f_{i\sigma}$, and the boson operator, b_i , as $c_{i\sigma} = f_{i\sigma} b_i^{\dagger}$. Here the boson operator represents the unoccupied state. By these operators the local constraint that each site is at most occupied by one particle is expressed by introducing the Lagrange multiplier, λ_i , as

$$H = H_{tJ} + \sum_i \lambda_i \left(\sum_{\sigma} f_{i\sigma}^{\dagger} f_{i\sigma} + b_i^{\dagger} b_i - 1 \right). \quad (4)$$

In our first treatment^{13,14)}, which is essentially the same as (but a little bit of extension of) the theory by Baskaran, Zou and Anderson¹⁵⁾ on the original $t - J$ model without t' and J' we employed the mean field approximation to this problem of the coupled bosons and fermions replacing λ_i by its average uniform in space, λ , and ignored completely the effect of fluctuations around these mean field solutions. Within this approximation the statistics of slave fermions and bosons remain the same as the original ones, and then fermions have RVB pairing whereas bosons are condensed independently in essence; obviously a very crude approximation.

Recent paper by Wen, Wilczek and Zee¹⁶⁾ has opened our eyes on this problem. They investigated the undoped case with both J and J' and searched for the chiral spin state, which breaks the parity and time-reversal symmetry, based on the mean field theory by taking the hopping, $\langle \chi_{ij} \rangle \equiv \sum_{\sigma} \langle f_{i\sigma}^{\dagger} f_{j\sigma} \rangle$ and $\langle b_i^{\dagger} b_j \rangle$, as order parameters (bond order parameters). Though the chiral spin state is found not to be stabilized within $J - J'$ model and some other terms were claimed for the stability, they have shown that the fluctuations around the mean field solution can be treated in a systematic way;

$$\lambda_i = \lambda + a_0(i), \quad (5.a)$$

$$\langle \chi_{ij} \rangle = \langle \chi_{ij} \rangle_0 \exp[i \int_i^j \vec{a} \cdot d\vec{l}], \quad (5.b)$$

where $\langle \chi_{ij} \rangle_0$ is the mean field solutions. The functions $a_{\alpha}(i)$ ($\alpha = 0, 1 (= x), 2 (= y)$) can be considered as the gauge field in (2+1) dimension. In the chiral spin state these gauge fields have the Chern-Simons term rendering

a test particle injected into the system a semion, a particle with $1/2$ -statistics. This paper has made it clear that the local constraint has profound consequences on the low energy properties of electrons; even the statistics of particles can change! This has stimulated our following research in various directions.

The first problem was under what condition the chiral spin state is actually stabilized at least within the mean field approximation. The effects of more extended exchange interaction (e.g. that between the third neighbors, J'') and the spin-orbit interactions have been investigated for the undoped case.¹⁷⁾

Next for the case of finite doping we have found that there is some region of parameters where the chiral spin state is actually stabilized.^{18,19)} By use of the similar procedures to that of Wen *et al.*¹⁶⁾ for this case, we obtained the Chern-Simons term also in this case and then could derive fractional statistical particles (anyons) microscopically for the first time for the doped case.¹⁸⁾ Interestingly the prefactor of the Chern-Simons term and hence the statistics turn out to depend on the degree of doping.

The possibility of such a new concept of anyons has also been explored²⁰⁾ without recouring to the chiral spin state but based on the commensurate flux state.²¹⁾

It is of interest to study the physical properties of such anyon systems on one hand and at the same it is important to critically assess the relevance of this new view.

References

- 1) H. Fukuyama, H. Matsukawa and Y. Hasegawa, J. Phys. Soc. Jpn. **58**, 364 (1989).
- 2) H. Matsukawa and H. Fukuyama, J. Phys. Soc. Jpn. **58**, 2845 (1989).
- 3) H. Matsukawa and H. Fukuyama, J. Phys. Soc. Jpn. **58**, 3687 (1989).
- 4) H. Fukuyama and H. Matsukawa, Proc. of IBM Japan Intern. Symp. on *Strong Correlation and Superconductivity* ed. H. Fukuyama, S. Maekawa and A. Malozemoff (Springer Verlag, 1989) p.45.
- 5) H. Eskes and G. Sawatzky, Phys. Rev. Lett. **61**, 1415 (1988).
- 6) F.C. Zhang and T.M. Rice Phys. Rev. B **37**, 3759 (1988).
- 7) P.W. Anderson, Science **235**, 1196 (1987).
- 8) P.A. Lee, Phys. Rev. Lett. **63**, 680 (1989).
- 9) H. Matsukawa and H. Fukuyama, ISSP Tech. Rept. No.2222 (Nov. 1989).
- 10) C. Murayama, N. Mori, S. Yomo, H. Takagi, S. Uchida and Y. Tokura, Nature **339**, 293 (1989).
- 11) A. Miyanaga, Y. Hasegawa and H. Fukuyama; in preparation.
- 12) P.B. Wiegmann, talk at Los Alamos Symposium on High Temperature Superconductivity, (Dec. 6-8, 1989).
- 13) Y. Suzumura, Y. Hasegawa and H. Fukuyama, J. Phys. Soc. Jpn. **56**, 401 (1988); *ibid* **57**, 2768 (1988).
- 14) H. Fukuyama, Y. Hasegawa and Y. Suzumura, Physica C **153-155**, 1630 (1988).
- 15) G. Baskaran, Z. Zou and P.W. Anderson, Solid State Commun. **63**, 973 (1987).
- 16) X.G. Wen, F. Wilczek and A. Zee, Phys. Rev. B **39**, 11413 (1989).
- 17) T. Tanamoto, Master Thesis, Univ. of Tokyo (Feb. 1990).
- 18) H. Fukuyama, O. Narikiyo and K. Kuboki, submitted to J. Phys. Soc. Jpn.
- 19) O. Narikiyo, K. Kuboki and H. Fukuyama, to be submitted to J. Phys. Soc. Jpn.
- 20) Y. Hasegawa, O. Narikiyo, K. Kuboki and H. Fukuyama, to be submitted to J. Phys. Soc. Jpn.
- 21) Y. Hasegawa, P. Lederer, T.M. Rice and P.B. Wiegmann, Phys. Rev. Lett. **63**, 907 (1989).

for holes in unit of eV	[1]	[2]	[3]
U_d	8		7.5 ~ 8
U_p	4		5 ~ 6
V_0	1		≤ 1
t_0	1		1.2 ~ 1.4
t_1	0.6		0.5
t_2	0.2		
$\Delta = \epsilon_p - \epsilon_d$	2		2.5 ~ 3

Table 1. Values of Parameter

- 1) K.T. Park, T. Terakura, T. Oguchi, A. Yanase and M. Ikeda: J. Phys. Soc. Jpn. **57**, 3445 (1989).
- 2) A.K. McMahan, R.M. Martin and S. Satpathy: Phys. Rev. B **38**, 6650 (1988).
- 3) A.G. Sawatzky: *IBM Japan International Symposium on Strong Correlation and Superconductivity*, (Mt.Fuji, May, 1989) (Springer Verlag 1989) p.33.

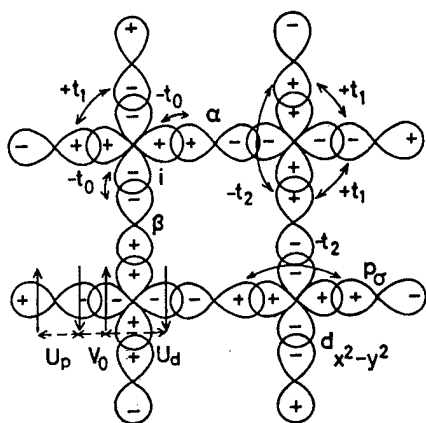


Fig.1 Parameters characterizing the CuO_2 layers.

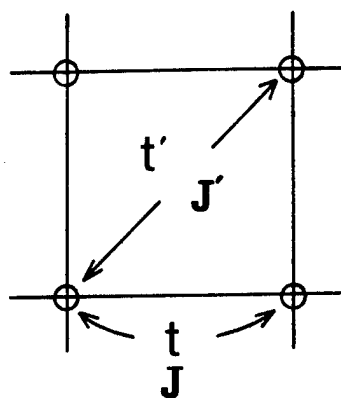


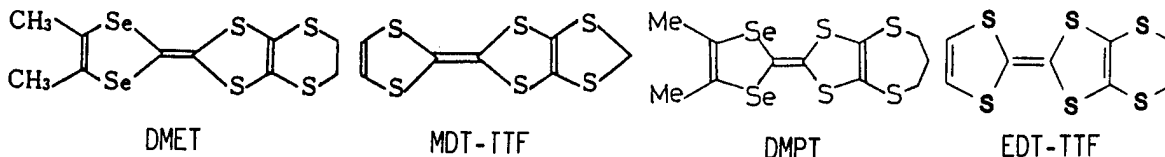
Fig.2 Parameters in the extended t - J model.

I. Ikemoto, K. Kikuchi and K. Saito

Department of Chemistry, Faculty of Science, Tokyo Metropolitan University,
Fukazawa, Setagaya-ku, Tokyo 158, Japan

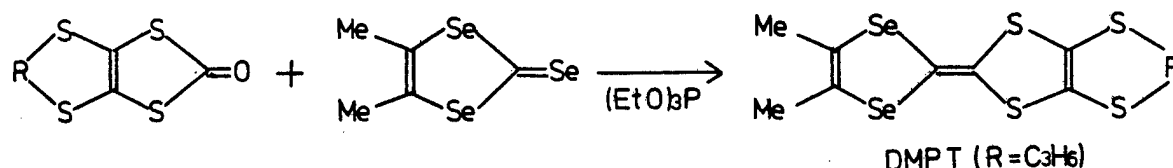
DMPT and EDT-TTF, which are the derivatives of DMET and MDT-TTF respectively, were synthesized and their radical salts were prepared by the electrochemical oxidation. Their physical properties were investigated and the crystal structures were determined. Several salts were found to show the metallic behavior.

DMET and MDT-TTF are the unsymmetrical donors which produce organic superconductors. DMET has half structures of TMTSF and BEDT-TTF, and MDT-TTF those of TTF and BMDT-TTF. The change of the length of side alkyl substituent of half structure of BEDT-TTF or BMDT-TTF is expected to bring about little change of the electrical properties of salts of DMET or MDT-TTF since molecular skeletons which are responsible for the electrical conductivities are the same. Since DMPT is made of half structures of TMTSF and BPDT-TTF, and EDT-TTF is made of half structures of TTF and BEDT-TTF, the salts based on DMPT and EDT-TTF are expected to show the similar physical properties to those of DMET and MDT-TTF respectively. In this report we present the physical properties and crystal structures of some radical salts of DMPT and EDT-TTF.



Physical properties and crystal structures of DMPT salts

DMPT was obtained by cross-coupling of the appropriate 1,3-dithiole-2-ketone and 1,3-diselenole-selenone in toluene with triethyl phosphite. Separation of DMPT from symmetrical co-products was accomplished by chromatography on a SiO_2 column followed by a recycle preparative gel permeation chromatography. DMPT radical salts were prepared by the electrochemical oxidation in the presence of $(n\text{-Bu})_4\text{NX}$ (X = counter anion) in chlorobenzene using a constant current (2 μA).



The electrical conductivities at room temperature, the activation energies and the temperatures of metal-insulator transition are summarized in Table 1. Except

Table 1. Electrical properties of DMPT salts.

anion	$\sigma_{RT} / \text{Scm}^{-1}$	E_a / eV
PF_6	140	0.11
AsF_6	76	0.12
SbF_6	37	0.15
BF_4	7	0.10
ClO_4	46	0.24
ReO_4	24	0.12
AuCl_2	1	0.06
$\text{Au}(\text{CN})_2$	87	metal ($T_{M-I} = 130 \text{ K}$)
$\text{Ag}(\text{CN})_2$	10	metal ($T_{M-I} = 170 \text{ K}$)

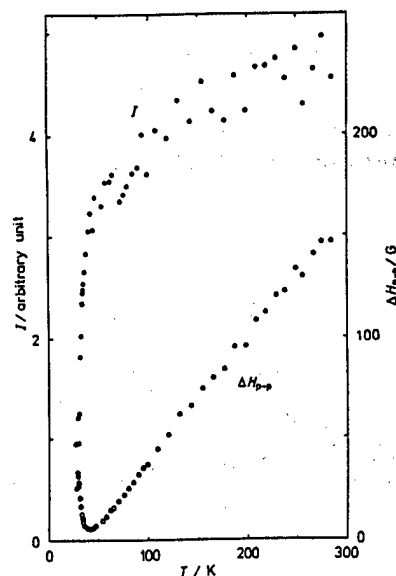


Fig. 1. Linewidth and intensity of ESR of $(\text{DMPT})_2\text{PF}_6$.

$\text{Ag}(\text{CN})_2$ and $\text{Au}(\text{CN})_2$ salts, all other salts showed semiconductive behavior at room temperature. Figure 1 shows the temperature dependence of EPR linewidth and spin susceptibility of PF_6 salt. Around 40 K the susceptibility decreases suddenly and the width of the EPR line increases sharply. This fact suggests that the low temperature phase of PF_6 salt is antiferromagnetic. The antiferromagnetic transition was observed at 35 K in AsF_6 salt. In some DMET salts, the antiferromagnetic transitions were observed, but the temperature of the transition were much lower than those in DMPT salts. It is interesting that little molecular change of a donor molecule affects the transition temperature largely.

The crystal data of $(\text{DMPT})_2\text{PF}_6$ are; triclinic, $\bar{P}1$, $a = 7.871(1)$, $b = 6.967(1)$, $c = 15.845(3) \text{ \AA}$, $\alpha = 95.14(2)$, $\beta = 100.56(1)$, $\gamma = 71.26(1)^\circ$, $V = 808.5(3) \text{ \AA}^3$, $Z = 1$, $R = 0.038$. The crystal structure of PF_6 salt is shown in Fig. 2. $(\text{DMPT})_2\text{PF}_6$ has a similar columnar structure to DMET salts. The distances between the planes of donor molecules are 3.76 and 3.55 \AA , and this suggests that there exists large dimerization. Between the neighboring columns, there is only one short contact as shown in Fig. 2, and therefore $(\text{DMPT})_2\text{PF}_6$ is considered to have little two-dimensional character.

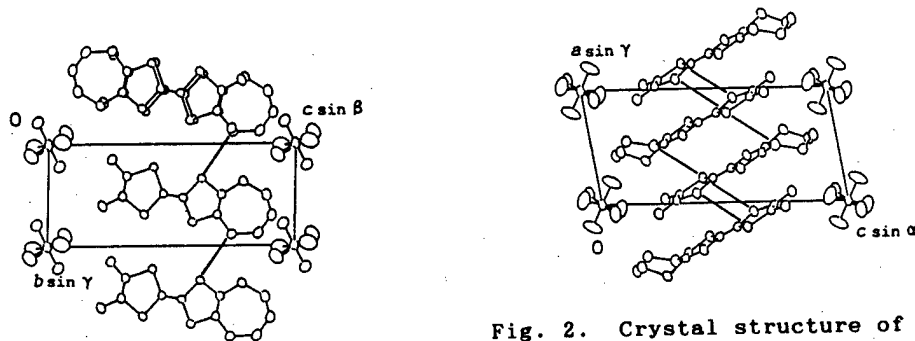


Fig. 2. Crystal structure of $(\text{DMPT})_2\text{PF}_6$.

The crystal data of $(\text{DMPT})_2\text{ReO}_4$ are; monoclinic, $C2/c$, $a = 30.453(4)$, $b = 7.882(1)$, $c = 13.433(1) \text{ \AA}$, $\beta = 90.56(1)^\circ$, $V = 3224.2(7) \text{ \AA}^3$, $Z = 4$, $R = 0.043$. The crystal structure of ReO_4 salt is shown in Fig. 3. In this salt there are four donor

columns in the unit cell and the donor molecule in the neighboring columns are tilted alternately. This structure has not been observed in any DMET salts. The distances between the donor molecular planes are 3.76 and 3.55 Å which implies large dimerization in (DMPT)₂ReO₄. Therefore this salt has little two-dimensional character.

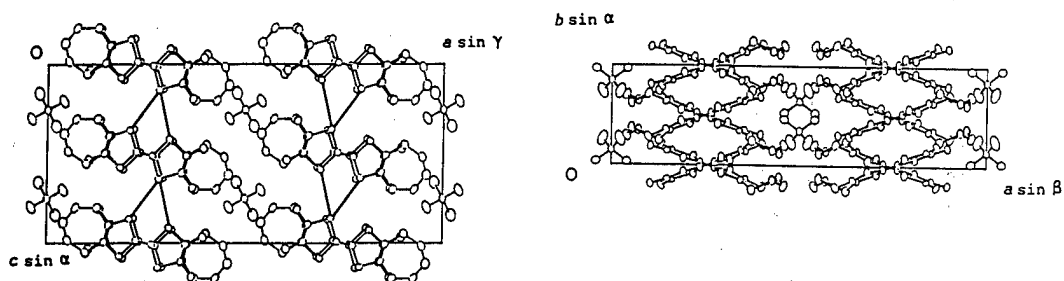


Fig. 3. Crystal structure of (DMPT)₂ReO₄.

Electrical properties and crystal structures of EDT-TTF salts

EDT-TTF was synthesized by the following route. 5,6-dihydro-1,4-dithiino[2,3-d]-1,3-dithiole-2-ketone and 4-acetyl-1,3-dithiole-2-thiol were cross-coupled. The unsymmetrical product was isolated by SiO₂ column chromatography. Then, acetyl group was removed using hexamethylphosphoric triamide and LiBr. EDT-TTF radical salts was obtained by electrochemical oxidation in the presence of (n-Bu)₄NX (X = counter anion) in 1,1,2-trichloroethane, chlorobenzene, or tetrahydrofuran using a constant current (2 μA).

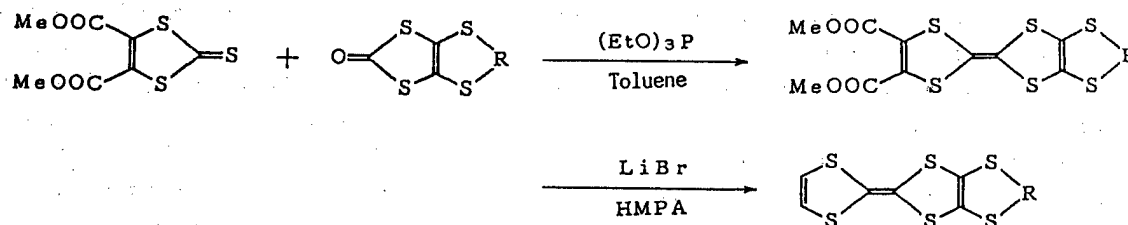


Table 2. Electrical properties of EDT-TTF salts.

anion	$\sigma_{RT} / \text{Scm}^{-1}$	E_a / eV
PF ₆	1300	metal
AsF ₆	8	metal
ClO ₄	7	metal
AuI ₂	21	metal ($T_{M-I} = 170 \text{ K}$)
I ₃	0.002	0.15
Au(CN) ₂	100	metal
IBr ₂	180	metal ($T_{M-I} = 80 \text{ K}$)
I ₂ Br	90	metal

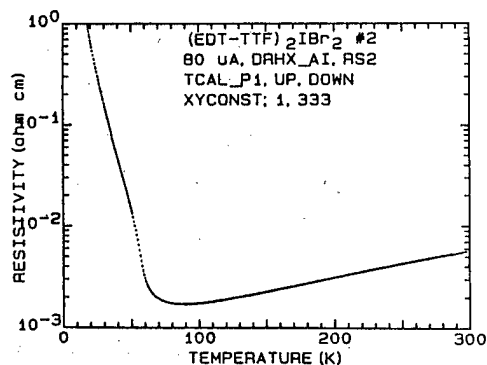


Fig. 4. Resistivity of (EDT-TTF)₂IBr₂.

In Table 2, the electrical conductivities at room temperature, the activation energies and the temperatures of metal-insulator transition of EDT-TTF salts are behaviors from those reported earlier[1]. $(\text{EDT-TTF})_2\text{Au}(\text{CN})_2$ was reported to show a summarized. We found the crystals of $\text{Au}(\text{CN})_2$ and IBr_2 salts that exhibit different semiconducting behavior at room temperature, but our crystal of $\text{Au}(\text{CN})_2$ salt is metallic at room temperature. $(\text{EDT-TTF})_2\text{IBr}_2$ was reported to show a metallic behavior down to low temperature, but our crystal of IBr_2 salt have a sharp metal-insulator transition around 80 K as shown in Fig. 4.

The crystal data of our crystal of $(\text{EDT-TTF})_2\text{IBr}_2$ are; triclinic, $P\bar{1}$, $a = 8.618(7)$, $b = 6.406(5)$, $c = 13.350(9)$ Å, $\alpha = 95.05(6)$, $\beta = 92.68(7)$, $\gamma = 68.53(6)^\circ$, $V = 683.2(9)$ Å³. The crystal structure is shown in Fig. 5. The structure is different from that already reported[2]. Therefore our crystal is a different phase from that already reported. In our $(\text{EDT-TTF})_2\text{IBr}_2$, columns seem to exist, but within a column there are only short contacts (shown with a line) between molecules in a dimer, and there are many short interstack contacts. Thus there is larger interaction between columns rather than within a column.

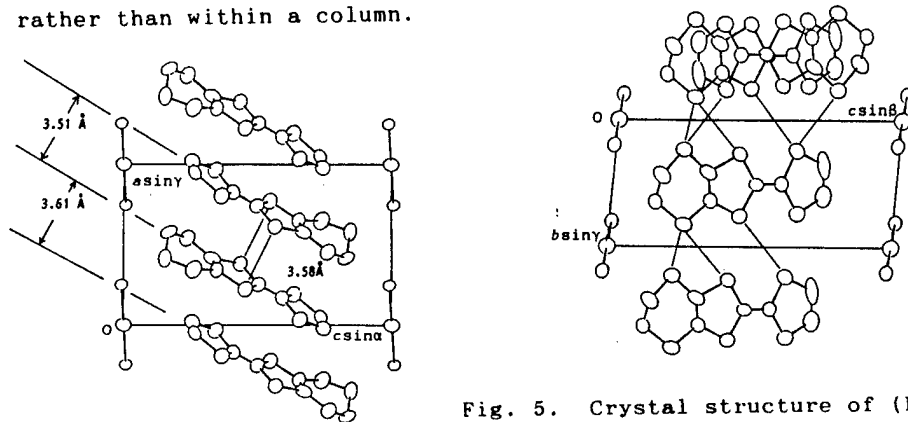


Fig. 5. Crystal structure of $(\text{EDT-TTF})_2\text{IBr}_2$.

Figure 6 shows the temperature dependence of resistivity of I_2Br salt. This salt showed a metallic behavior down to 0.7 K, but not a superconductivity. The absence of superconductivity of this salt may be due to the disorder of the orientation of I_2Br anions.

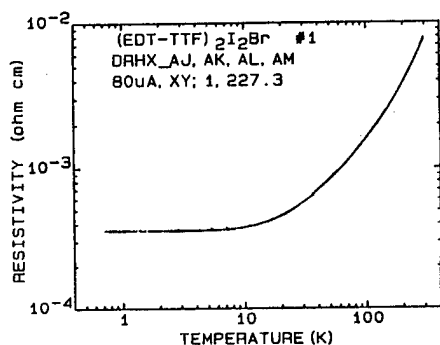


Fig. 6. Resistivity of $(\text{EDT-TTF})_2\text{I}_2\text{Br}$.

References

- [1] G. C. Papavassiliou, G. A. Mousdis, J. S. Zambounis, A. Terzis, A. Hountas, B. Hilti, C. W. Mayer, and J. Pfeiffer, *Synthetic Metals*, **27**, B379 (1988).
- [2] A. Terzis, A. Hountas and G. C. Papavassiliou, *Solid State Commun.*, **66**, 1161 (1988).

Design of Molecular Metals with Various Types of Band Structures
— One-Dimensional and Two-Dimensional π Bands and $p\pi$ -d Mixing Bands

Hayao Kobayashi, Reizo Kato and Akiko Kobayashi*

Department of Chemistry, Faculty of Science, Toho University, Funabashi,
Chiba 274, Japan

*Department of Chemistry, Faculty of Science, the University of Tokyo,
Hongo, Tokyo 113, Japan

Recent our studies on the development of new molecular metals with various types of electronic structures are reported, which are : (1) organic metals based on asymmetric π -acceptor molecule EDT-TTF, (2) stable molecular metal with "solid-crossing segregated stacks" of donor and acceptor molecules, (3) two-dimensional metal based on π -acceptor molecule, $Ni(dmit)_2$ and (4) molecular metal with $p\pi$ -d mixing band, DCNQI-Cu system.

During the last decade, a lot of works have been devoted to search new molecular superconductors. In the first half of 1980s, the systematic "molecular designing analyses" based on simple tight-binding band structure calculations have been started. It has been considered that the design of the molecular metals with 2D intermolecular S(Se)...S(Se) contacts is a short cut to get molecular superconductors. As a result, the recent studies for searching new molecular superconductors have been concentrated on the conducting systems based on the multi-sulfur (selenium) π -donor and/or π -acceptor molecules. In fact, all the molecular superconductors reported so far are this type of molecular conducting systems. Besides the superconductivity, unique physical phenomena such as oscillatory magnetoresistance have been reported in these systems. However, it must be said that the motif of the design of molecular metals (or superconductors) is rather limited. Considering the variety and flexibility of the (organic) molecular systems, there still remains large possibility to find the similar multi-chalcogen π -molecules which will give superconductors with fairly high T_c . But in order to explore a new field of the molecular conducting systems, another types of the molecular conducting systems are also desirable.

In this report, we will present the synthesis and characterizations of new conducting systems obtained in the course of the studies on the development of new molecular superconductors.

(I) $(EDT-TTF)_2X^{1,2)}$

Up to now, we have synthesized and examined many conductors based on various multi-sulfur(selenium) π -donor molecules such as BEDT-TTF(ET), BMDT-TTF(MT), BPDT-TTF(PT), BEDT-TSF(ES), BPDS-TSF and so on. Among them, ET complexes have been most intensively studied because of easiness of the synthesis and the formation of complexes. Very recently, we have succeeded in synthesizing another hopeful π -donor

molecule BEDT-TSF with a reliable yield. Preliminary examination of the complexes made by electrochemical crystallization gave promising results, which will be reported soon.

Besides the above mentioned symmetrical π -donors, asymmetric π -donor molecules have attracted much attention recently, because two of them (DMET and MDT-TTF) gave organic superconductors. EDT-TTF is a hybrid between TTF and BEDT-TTF molecules, which was obtained by cross-coupling reaction of 1,3-dithiolene-2-thione and 1,3-dithiolene-2-one in triethylphosphite. Cation radical salts of EDT-TTF were prepared by electrochemical oxidation in presence of $(n\text{-Bu})_4\text{NX}$ ($\text{X}=\text{PF}_6, \text{AsF}_6, \dots$). Crystal data and electrical properties are listed in Table 1.

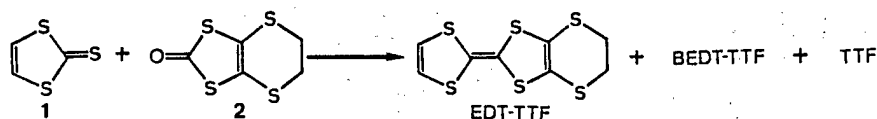


Table 1. Crystal data and electrical properties of $(\text{EDT-TTF})_2\text{X}$

X	$\text{Au}(\text{CN})_2$	TaF_6	$\text{AsF}_6(\alpha)$	$\text{AsF}_6(\beta)$	PF_6	ReO_4	ClO_4	BF_4
space group	$\text{P}\bar{1}$	$\text{P}\bar{1}$	$\text{P}\bar{1}$	Pccn	Pccn	C2/c	C2/c	C2/c
a/Å	14.752	15.213	14.855	28.303	28.014	29.720	29.283	29.133
b/Å	7.225	7.049	7.043	7.120	7.122	7.185	7.145	7.134
c/Å	6.388	6.463	6.457	12.706	12.650	12.416	12.417	12.379
$\alpha/^\circ$	106.15	102.22	102.38					
$\beta/^\circ$	101.56	102.57	96.15			110.56	111.54	111.85
$\gamma/^\circ$	90.50	98.77	101.68					
Z	1	1	1	4	4	4	4	4
$V/\text{\AA}^3$	639.2	646.7	638.1	2560.5	2523.9	2482.4	2416.5	2388.0
R	0.074	0.088	0.037	0.090	0.063	0.115	0.129	0.064
$\sigma_{\text{R.T.}} / \text{S cm}^{-1}$	5	10^2	50	30	10^2	10	10^2	10
$T_{\text{M-I}}/\text{K}$	semicon.	57	50	ca.50	42	150	ca.100	170

In all these compounds, the asymmetric EDT-TTF molecules stack alternately to form almost uniform columns. The EDT-TTF molecules is almost planar except the ethylenedithio fragment. The cation radical salts of EDT-TTF are classified into three almost isostructural groups.

(1) The triclinic group contains the $\text{Au}(\text{CN})_2$, TaF_6 and AsF_6 (α form). Molecular packing is similar to that of the well-known Bechgaard salt, $(\text{TMTSF})_2\text{X}$ (Fig. 1). Band energy calculations show a psuedo 1D Fermi surface. Although the room-temperature conductivity is fairly high and the metal-insulator (MI) transition temperature is fairly low, the MI transition cannot be suppressed at least up to 12 kbar (Fig. 2).

(2) The orthorhombic group includes AsF_6 (β form) and PF_6 salts. Four almost equivalent donor columns run along the b axis. Since four EDT-TTF molecules are in the 2D unit cell of each donor sheet, the system has two pairs of quasi-1D Fermi surfaces (Fig. 3).

(3) The monoclinic group contains the salts with tetrahedral anions (BF_4 , ClO_4 and ReO_4). The band structure is almost the same to that of orthorhombic group compound. Narrow ESR signal ($\Delta H < 13$ G) suggested the strong electron correlation.

As mentioned above, every EDT-TTF compounds loses its conductivity at low temperature. Contrary, its homolog MDT-TTF gave a superconducting system ((MDT-TTF)₂AuI₂). The origin of the difference between two groups is not clear.

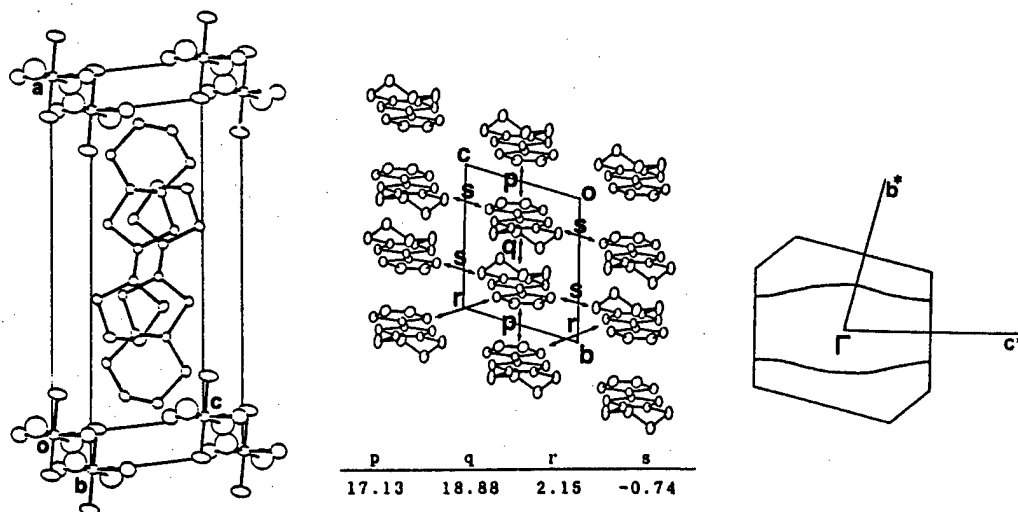


Fig. 1. Crystal structure and 1D Fermi surface of α -(EDT-TTF)₂AsF₆.

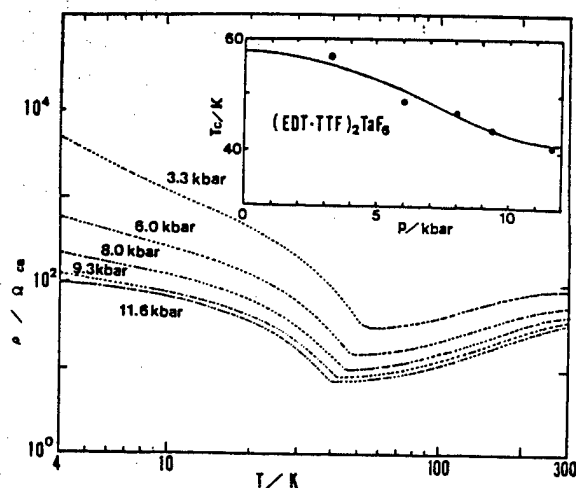


Fig. 2. Electrical resistivity of (EDT-TTF)₂TaF₆.

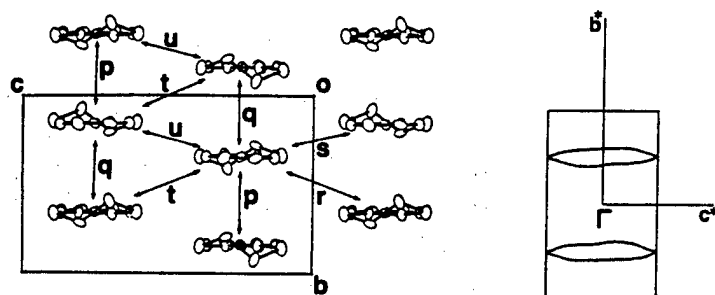


Fig. 3. Fermi surface of β -(EDT-TTF)₂AsF₆.

(II) (EDT-TTF)[Ni(dmit)₂]^{2,3)}

Intensive studies on the π -electron donor-acceptor(DA) complexes analogous to the first metallic molecular crystal, (TTF)(TCNQ) have revealed that the CDW instability is inherent in the 1D molecular metal system with segregated D and A columns. However, we have recently found the DA complex, (EDT-TTF)[Ni(dmit)₂], which retain metallic state down to 1.5 K.

(EDT-TTF)[Ni(dmit)₂] is polymorphic (α , β). The α form is triclinic and the β form is monoclinic. The β form has the mixed stacks of donors(EDT-TTF) and acceptors(Ni(dmit)₂). While the α form has segregated columns of D and A molecules. In the crystal of α -(EDT-TTF)[Ni(dmit)₂], the planar Ni(dmit)₂ molecules form a uniform column along the b axis with the interplanar distance of 3.52 Å (Fig. 4) ($a=6.658$, $b=7.627$, $c=27.385$ Å, $\alpha=93.23$, $\beta=91.43$, $\gamma=119.29^\circ$). The asymmetric EDT-TTF molecules stack alternately along [110] direction. That is, the columns of D and A molecules are not parallel to each other but have the "solid crossing arrangement". The room-temperature conductivity is 100 S cm⁻¹. Upon cooling, the resistivity decreases monotonously down to 20 K, where the resistivity begins to increase. Around 14 K, the resistivity takes its maximum and decreases again (Fig. 5). This resistivity anomaly is somewhat sample-dependent and is suppressed at high pressure. Superconductivity was not observed. X-Ray diffraction

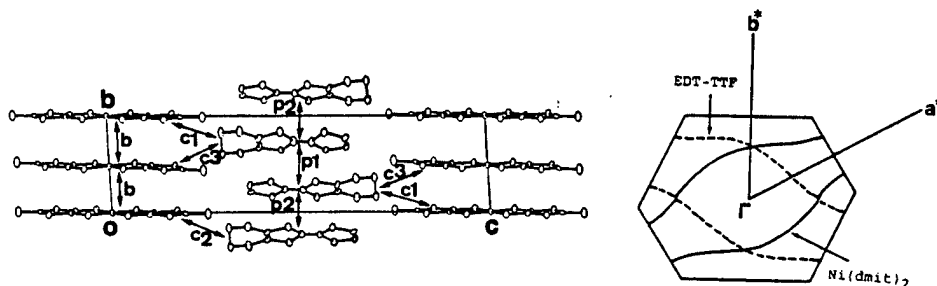


Fig. 4. Crystal structure and Fermi surface of α -(EDT-TTF)[Ni(dmit)₂].

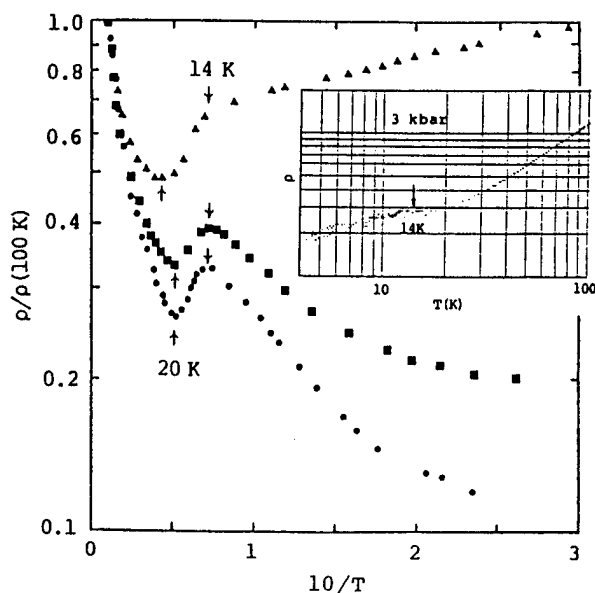


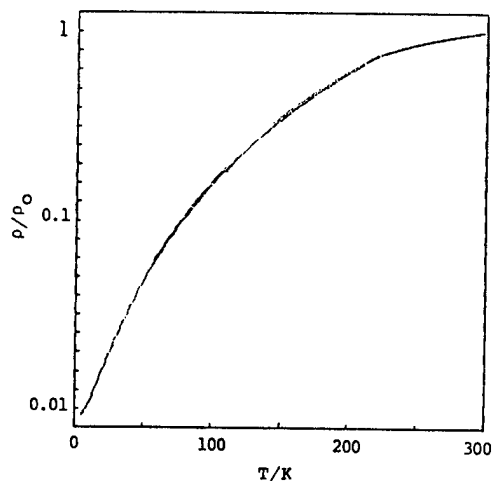
Fig. 5. Electrical resistivity of α -(EDT-TTF)[Ni(dmit)₂].

photograph taken at 15 K gave no indication of the structure change. As shown in Fig. 4, the crystal is composed of the metal sheets of D molecules and those of A molecules, which arranged alternately along the c axis. The calculated energy bands consists of two quasi-1D metal bands, corresponding to those of the D and A sheets. The Fermi surfaces have two pairs of "warped" planes. Similar band structure has been obtained in π -acceptor superconductor, $(\text{CH}_3)_4\text{N}[\text{Ni}(\text{dmit})_2]_2$. Reflectance spectra suggested a small anisotropy of the electronic structure.

(III) 2D π -acceptor metal⁴⁾

Recently, we have reported the first 2D metal derived from the π -acceptor molecules, $\alpha\text{-(DMeDEtN)[Ni(dmit)}_2]_2$. The 2D metal nature has been confirmed by the analyses of the characteristic molecular arrangement of Ni(dmit)_2 , the extended Huckel band structure calculation and reflectance spectra. Unlike the case of the multi-sulfur π -donor molecules such as ET, the intermolecular interaction between Ni(dmit)_2 molecules in side-by-side arrangement cannot be large, owing to the b_{2g} symmetry of the lowest unoccupied molecular orbital. In this system, the 2D nature arises from the unique molecular arrangement named as "spanning overlapping mode" (one molecule overlaps on two molecules). Although the calculated Fermi surface is a cylindrical one similar to those of θ - and $\kappa\text{-ET}_2\text{I}_3$, superconducting behavior was not observed down to 1.5 K and up to 5 kbar. Since the positional disorder of the cation is considered to be unfavorable to observe the superconductivity, we tried to remove the disorder of the cation molecule. By introducing N-dimethylpiperidinium, $(\text{CH}_3)_2\text{C}_5\text{H}_{10}\text{N}^+$, we have succeeded in obtaining the new stable 2D metallic system $[(\text{CH}_3)_2\text{C}_5\text{H}_{10}\text{N}][\text{Ni(dmit)}_2]_2$, which is isomorphous to $\alpha\text{-(DMeDEtN)[Ni(dmit)}_2]_2$. The electrical resistivity decreases with decreasing temperature down to 4.2 K (Fig. 6). further experiments are now in progress.

Fig. 6. Electrical resistivity of $[(\text{CH}_3)_2\text{C}_5\text{H}_{10}\text{N}][\text{Ni(dmit)}_2]_2$.



(IV) DCNQI-Cu systems^{5,6)}

As mentioned before, all the molecular superconductors hitherto reported are compounds based on multi-chalcogen π -molecules, which can be regarded as π -metal systems. In order to contribute to the better understanding of the molecular superconductors, design of the other types of molecular metals (or superconductors) will be highly desirable. In this sense, $(\text{DMe-DCNQI})_2\text{Cu}$ is important (DMe-DCNQI = 2,5-dimethyl-dicyanoquinonediimine). Soon after the discovery of $(\text{DMe-DCNQI})_2\text{Cu}$ by Aumuller et al. (1986), we have pointed out that this system has "p π -d mixing band". Owing to the coexistence of the mixed-valent Cu atoms and p π conduction electrons of DCNQIs, many unique electric and magnetic properties have been observed.

(DMeO-DCNQI)₂Cu is metallic down to 0.5 K at 1 bar but it exhibits an anomalous temperature dependence of the resistivity (ρ (metal-semiconductor-metal) between 8 kbar and 10 kbar (Fig. 7). The ρ -T curve of the low-temperature metallic state does not seem to be a simple extrapolation of that of the high-temperature metallic state. Magnetic susceptibilities (χ) indicate that the magnetic ions (Cu²⁺) emerge when p_r conduction electron disappear. Large enhancement of χ of (DMe-DCNQI)₂Cu was observed below 100 K (at 1 bar). The alloy system [(DMe)_{1-x}(MeBr)_x-DCNQI]₂Cu, showed the resistivity anomaly similar to that observed at high pressure ($x < 0.1$). Low-temperature specific heat suggested that the effective mass of the metal electron becomes "heavy" in this "small-x region". In (MeBr-DCNQI)₂(Cu_{1-y}Li_y), the metal-insulator transition accompanied by the lattice distortion was observed at the intermediate temperature between the transition temperature of (MeBr-DCNQI)₂Cu and that of (MeBr-DCNQI)₂Li.

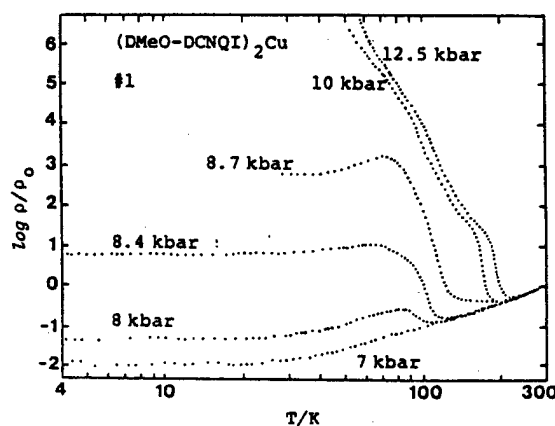


Fig. 7. Resistivity of (DMeO-DCNQI)₂Cu at high pressure.

Acknowledgements

We wish to express our sincere thanks to Profs. W. Sasaki and K. Kajita, Dr. Y. Nishio and Mr. A. Miyamoto of Toho University, Profs. S. Kagoshima of The University of Tokyo and Prof. T. Watanabe of Tokyo University of Fisheries for the collaborations. Our thanks are also due to Prof. H. Fukuyama of The University of Tokyo for his encouragement.

References

- 1) R. Kato, H. Kobayashi and A. Kobayashi, Chem. Lett., 1989, 781-784.
- 2) A. Kobayashi, R. Kato and H. Kobayashi, to be published.
- 3) R. Kato, H. Kobayashi, A. Kobayashi, T. Naito, M. Tamura, H. Tajima and H. Kuroda, Chem. Lett., 1989, 1839-1842.
- 4) A. Kobayashi et al., to be published.
- 5) R. Kato, H. Kobayashi and A. Kobayashi, J. Am. Chem. Soc., 111, 5224-5232 (1989).
- 6) H. Kobayashi, A. Miyamoto, R. Kato, A. Kobayashi, Y. Nishio, K. Kajita and W. Sasaki, Solid State Commun., 72, 1-5 (1989).

A Novel Type of Halogen-Bridged One-Dimensional Metal Complexes : Syntheses,
Structures and Solid State Properties of $-Ni(III)-X-Ni(III)-$ Compounds ($X=Cl$ and Br)

M.Yamashita, K.Hirao, K.Toriumi[†], H.Okamoto[†], T.Mitani[†] and Y.Wada^{††}

College of General Education, Nagoya University, Chikusa-ku, Nagoya 464-01, Japan

[†]Institute for Molecular Science, Okazaki National Research Institutes, Myodaiji, Okazaki 444,
Japan

^{††}National Institute for Research in Inorganic Materials, Tsukuba 305, Japan

Halogen-bridged linear chain compounds, $Ni(chxn)_2X_3$ ($X=Cl$ and Br ; $chxn=1R,2R$ -cyclohexanediamine) were synthesized and the novel one-dimensional $-Ni(III)-X-Ni(III)-$ structures with no Pelerls distortion, which were to our knowledge the first examples, have been confirmed on the basis of careful consideration of single-crystal X-ray diffraction results. On the basis of their reflectance spectra, electrical conductivities, magnetic susceptibility and ESR, these Ni complexes are considered one-dimensional Hubbard systems, that is, Mott-insulators, which is composed of $-Ni(III)-X-Ni(III)-$. The magnetic behavior of $Ni(chxn)_2Br_3$ shows very strong antiferromagnetic coupling between electronic spins ($S=1/2$) on the $Ni(III)$ atoms with $J \sim 3600K$. The two-dimensionality of the fairly tight hydrogen-bond network among chains may play an important role of stabilizing such rare and interesting states.

Introduction

Halogen-bridged one-dimensional $M(II)-M(IV)$ mixed-valence compounds of Pt, Pd and Ni show interesting physical properties due to strong electron-lattice interaction such as the strong intervalence charge transfer absorption, the luminescence with a large Stokes-shift, the long overtone progression in the resonance Raman spectra, and the midgap absorptions attributed to polaron or soliton.¹⁻³ Their physical properties have been extensively investigated to clarify the nature of the ground state, excited state and relaxation process in the half-filled Pelerls Hubbard system, where the four physical parameters (S, T, U, V) are in competition with each other.³ Generally the undistorted $-M(III)-X-M(III)-$ structures are unstable due to the strong electron-lattice interaction, which is characteristic of the quasi-one-dimensional electronic system. Then, the bridging halogen ions in these compounds are slightly deviated from the middle point between the adjacent metal ions, resulting in the charge density wave (CDW) or $M(II)-M(IV)$ mixed-valence state. As a result, the half-filled d_{z^2} electron band is split into the valence and conduction bands with a finite energy gap or Pelerls gap. So far about two hundred compounds have been synthesized with the general formula of $[M(II)(AA)_2][M(IV)X_2(AA)_2]Y_4$ ($M=Pt, Pd, Ni$; AA =diamines etc.; $X=Cl, Br, I$; $Y=ClO_4, X$ etc.). The relation between the Pelerls energy gaps and the lattice distortion has been established by a number of the structural and optical studies.^{4,5} From such experimental and theoretical results, it has been expected that a Ni system should be most suitable to synthesize the undistorted $-M(III)-X-M(III)-$ compound, which is one extreme limit of $M(II) \cdots X-M(IV)-X$ compound and is particularly interesting in its electronic structure and physical

properties.^{7,8}

Experimental

Lustrous golden needle crystals of $\text{Ni}(\text{chxn})_2\text{Cl}_3$ (1) were grown by slow diffusion of Cl_2 into 2-methoxyethanol solution of $[\text{NiCl}_2(\text{chxn})_2]$ under N_2 atmosphere. Black prismatic crystals of $\text{Ni}(\text{chxn})_2\text{Br}_3$ (2) were prepared by the similar method using Br_2 and $[\text{NiBr}_2(\text{chxn})_2]$.

Single crystal X-ray analyses were carried out at room and low temperature. Intensity data were collected on Enraf-Nonius CAD4 and Rigaku AFC-5 four-circle diffractometers with graphite monochromated $\text{MoK}\alpha$ radiation. Crystal data at low temperature are : (1) $\text{C}_{12}\text{H}_{28}\text{N}_4\text{NiCl}_3$, orthorhombic, $I222$, $Z=2$, $a=23.975(5)$, $b=4.894(1)$, $c=6.913(1)\text{\AA}$, $V=811.1(3)\text{\AA}^3$, $D_x=1.611\text{gcm}^{-3}$, $\mu(\text{Mo K}\alpha)=16.78\text{cm}^{-1}$; (2) $\text{C}_{12}\text{H}_{28}\text{N}_4\text{NiBr}_3$, orthorhombic, $I222$, $Z=2$, $a=23.501(4)$, $b=5.157(1)$, $c=7.090(1)\text{\AA}$, $V=859.3(3)\text{\AA}^3$, $D_x=2.036\text{gcm}^{-3}$, $\mu(\text{Mo K}\alpha)=85.24\text{cm}^{-1}$.

The physical property measurements were carried out by the methods described elsewhere.^{4,5,7}

Results and Discussion

Both the crystal structures of 1 and 2 are isomorphous with each other. The $\text{Ni}(\text{chxn})_2$ moieties, lying on the special position of 222, are bridged by halogen atoms and stacked along the b -axis, constructing a linear chain structure. The neighboring $\text{Ni}(\text{chxn})_2$ moieties along the same chain are linked by four $\text{NH}\cdots\text{X}\cdots\text{HN}$ hydrogen-bonds. Moreover, as shown in Fig.1, the hydrogen-bond network extended among the chains constructs a two-dimensional structure parallel to the bc plane. In order to discuss their electronic structures, it is essential to decide whether the bridging halogen atoms are located at the midpoints between two Ni atoms ($\text{Ni(III)}-\text{X}-\text{Ni(III)}$) or deviated from the midpoints ($\text{Ni(II)}\cdots\text{X}\cdots\text{Ni(IV)}$). On the basis of careful consideration of the X-ray diffraction results as shown below, it was confirmed that they have the linear chain $\text{Ni(III)}-\text{X}-\text{Ni(III)}$ structures. Firstly, both the $\text{Ni(III)}-\text{X}$ distances of the chain compounds 1 and 2 are significantly shorter than those of the discrete Ni(III) compounds, respectively. Secondly, the structure analyses do not indicate positional disorders of the bridging halogen atoms. Thirdly, neither diffuse scattering nor satellite peak relating to a superstructure have been observed on the X-ray oscillation and Weissenberg photographs. Finally, the full-matrix least-squares refinements including occupancy factors of the bridging and counter halogen atoms revealed the stoichiometric structures.

In the reflectance spectra polarized parallel to the chain, strong structures are observed. But there are no significant structures in the spectra perpendicular to the chain. The ϵ_2 spectra are relatively sharp and remarkably asymmetric with a long tail extending to the higher energy region, being considerably different from those of the Pt and Pd compounds in the CDW states. The peak energies of the absorption are 1.9eV for 1 and 1.28eV for 2. They can be assigned to the CT exciton in such a way as $\text{Ni(III)}+\text{Ni(III)} \rightarrow \text{Ni(IV)}+\text{Ni(II)}$, because the discrete Ni(III) compounds show no strong absorptions in these regions. These compounds show neither luminescence nor progressive resonance Raman spectra which are characteristic of the CDW states. Single crystal electrical conductivity measurements show very small activation energies and relatively high conductivities,

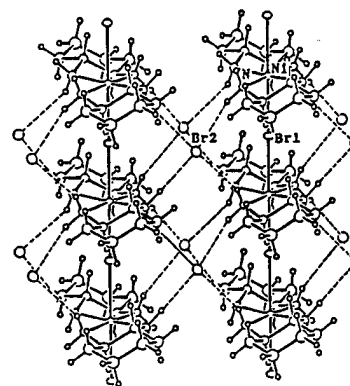


Fig.1 Structure of $\text{Ni}(\text{chxn})_2\text{Br}_3$

compared with the compounds in the CDW states. The room temperature conductivities and activation energies along the chain axes were $1 \times 10^{-3} \Omega^{-1} \text{cm}^{-1}$ and 0.19 eV for 1, and $2 \times 10^{-2} \Omega^{-1} \text{cm}^{-1}$ and 0.11 eV for 2, respectively. Therefore, these compounds are regarded as one-dimensional Hubbard systems, that is, Mott-insulators.

With decreasing temperature from room temperature, the magnetic susceptibility of 2 (χ_M) is almost constant ($\sim 10^{-5} \text{ emu mol}^{-1}$) down to about 50 K and shows a sharp increase at the lower temperature. The latter component which follows the Curie law is attributable to non-interacting spins. χ_M shows no significant anisotropy. ESR spectra of 2 were also measured from at room temperature and below. An ESR signal with a Lorentzian line shape was observed around $g=2$. The integrated intensity is plotted as spin susceptibility χ_s in Fig. 2. The result is essentially consistent with that of χ_M . The observed isotropic and temperature-independent behavior seems to be characteristic of the one-dimensional Heisenberg ($S=1/2$) chain with a strong antiferromagnetic exchange interaction. If it is assumed that the concentration of non-interacting spins is 0.22% and the exchange energy $J=3600 \text{ K}$, the characteristic feature of χ_s is well reproduced as shown in Fig. 2, in which the calculated curve plotted by broken lines is the sum of the Bonner-Fisher curve and the Curie curve.

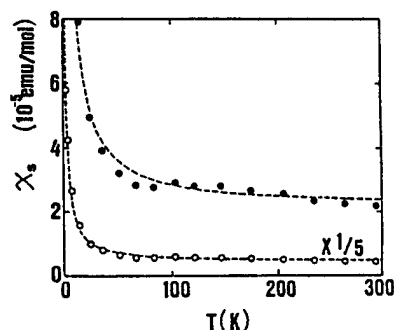


Fig. 2 Temperature-dependence of the spin susceptibility of $\text{Ni}(\text{chxn})_2\text{Br}_2$. The broken lines represent the linear combination of the Bonner-Fisher curve and the Curie curve.

Generally, in the half-filled quasi-one-dimensional Hubbard system, dimeric lattice distortions with the period of twice the lattice constant occur by the effect of site-diagonal or site-offdiagonal (spin-Peierls type) electron lattice interaction at low temperature. Therefore, in the Ni compounds, the two-dimensionality of the hydrogen-bond network may suppress the effect of electron-lattice interaction.

References

- 1) R.J.H.Clark, *Advances in Infrared and Raman Spectroscopy*, 11, 95(1984).
- 2) H.Tanino and K.Kobayashi, *J.Phys.Soc.Jpn.*, 52, 1446(1983).
- 3) N.Kuroda, M.Sakai, Y.Nishina, M.Tanaka and S.Kurita, *Phys.Rev.Lett.*, 58, 2122(1987).
- 4) Y.Wada, T.Mitani, M.Yamashita and T.Koda, *J.Phys.Soc.Jpn.*, 54, 3143(1985).
- 5) Y.Wada, T.Mitani, K.Toriumi and M.Yamashita, *J.Phys.Soc.Jpn.*, 58, 3013(1989).
- 6) K.Nasu, *J.Phys.Soc.Jpn.*, 19, 209(1983) ; 53, 302(1984) ; 53, 427(1984).
- 7) K.Toriumi, Y. Wada, T.Mitani, S.Bandou, M.Yamashita and Y.Fujii, *J.Am.Chem.Soc.*, 111, 2341(1989).

T. Mori and H. Inokuchi

Institute for Molecular Science, Okazaki 444, Japan

A new organic conductor, (EDT-TTF)₂AuBr₂, where EDT-TTF is an unsymmetrical donor, ethylenedithiotetrathiafulvalene, exhibits a metal-to-semiconductor transition at 20 K. Above this transition, a considerable Curie-like enhancement of the spin susceptibility is observed. There are investigated the crystal structure, the energy band structure, the resistivity under pressure, the thermoelectric power, and the ESR.

The discovery of superconductivity in the organic conductors of unsymmetrical electron donors has elucidated that unsymmetry of a donor is no more the origin of disorder, which is disadvantageous to superconductivity, but is a useful means to hybridize two different components to construct a novel organic donor molecule. The hybrid is naively expected to show the intermediate properties of the original symmetrical donors. Then it is interesting to explore the properties of EDT-TTF complexes, where EDT-TTF is a hybrid of the well-known organic donors, BEDT-TTF (bis(ethylenedithio)tetrathiafulvalene) and TTF (tetrathiafulvalene). We have systematically investigated the halogenometal complexes of EDT-TTF, and obtained a comparatively high-conducting complex, (EDT-TTF)₂AuBr₂, which is metallic down to 20 K [1].

Crystals in the form of very thin elongated plates were grown by electrochemical crystallization. Crystal data: monoclinic, space group C2/m, $a = 7.200(3)$, $b = 28.974(7)$, $c = 6.647(2)$ Å, $\beta = 111.68(3)^\circ$, $V = 1288.7(8)$ Å³, and $Z = 2$. There appear considerably intense three-fold reflections along the c axis, which originate in the anion lattice. The analysis of this three-fold structure has not succeeded, and only the average structure is analyzed, where the bromine atoms are treated as disordered.

As shown in Fig. 1, the donors are stacked along the a axis, along which the shape of the crystal is elongated. Along this stack, the ethylenedithio parts (outer rings) of EDT-TTF are arranged alternately, and there is no disorder on the donors. This is common to other complexes of unsymmetrical donors. The terminal carbon atom of the ethylenedithio moiety is about $0.45(5)$ Å out of the TTF plane, as observed in the BEDT-TTF complexes. The interplanar spacing of the donors is $3.60(2)$ Å. The donors have considerable interstack interaction to form conducting sheets parallel to the ac plane.

The tight-binding energy band structure is calculated as shown in Fig. 2. The Fermi surface is open perpendicularly to the a axis, while it is considerably corrugated due to the interstack interaction. The ratio of the intrastack to the interstack interactions is $S_a/S_c = 3$. This value is somewhat larger than the BEDT-TTF complexes ($S_{//}/S_{\perp} < 2$), but smaller than the (TMTSF)₂X family ($S_{//}/S_{\perp} = 10$) (TMTSF: tetramethyltetraselenafulvalene). Hence the dimensionality decreases in the order: BEDT-TTF > EDT-TTF > TMTSF > TTF. The single ethylenedithio moiety of EDT-TTF makes the interstack interaction considerably stronger than TTF, but not strong enough to

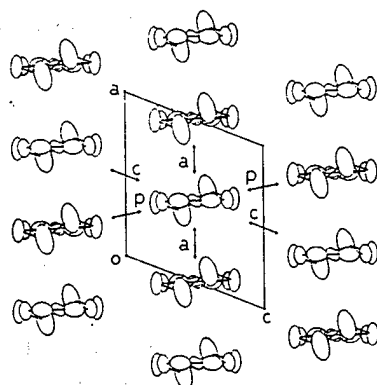


Fig. 1. Crystal structure, projection along the b axis.

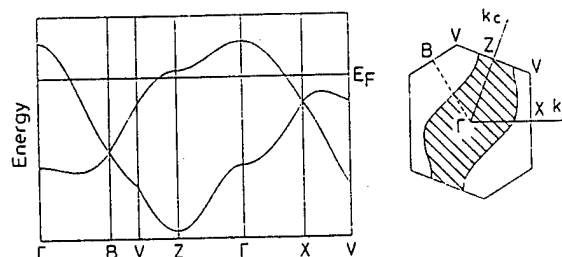


Fig. 2. Tight-binding band structure and the Fermi surface. Overlap integrals are $a=-22.3$, $b=-7.4$, and $c=2.9 \times 10^{-3}$.

make the Fermi surface closed as has been observed in some BEDT-TTF complexes [6].

The temperature dependence of the dc resistivity is shown in Fig. 3. The conductivity is about 200 Scm^{-1} at room temperature, and is metal-like down to about 30 K. Below this temperature, the resistivity increases gradually, and more steeply below 18 K. When cooling, we observed frequent resistance jumps in the metallic region, while no resistance jump is observed in the heating run.

Application of pressure gradually reduces the low-temperature resistance rise; $R(1.5 \text{ K})/R_{\min} = 33$ at ambient pressure decreases to 3 at 12 kbar. The pressure, however, lowers the transition temperature very slowly; the resistivity minimum is 14 K even at 12 kbar. The resistance jumps of the high-temperature metallic region observed in the cooling run do not occur under pressure. No indication of superconductivity has been observed at the temperature down to 1.5 K and under the

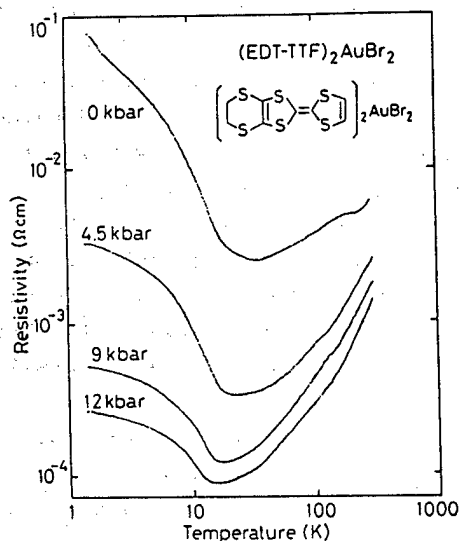


Fig. 3. Temperature dependence of the dc resistivity under pressure, measured along the a axis.

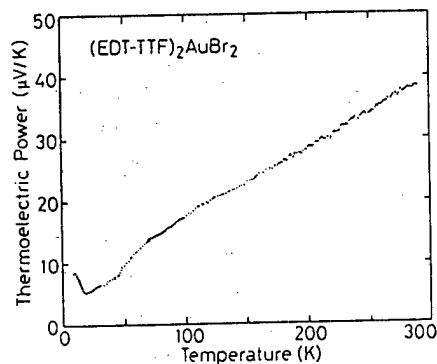
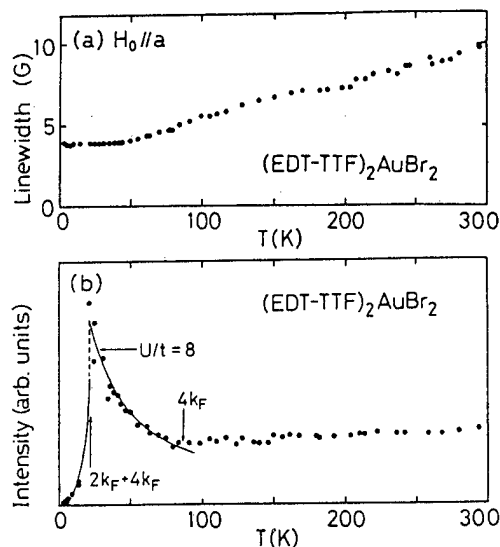


Fig. 4. Temperature dependence of the thermoelectric power measured along the a axis.

Fig. 5. ESR results. (a) Temperature dependence of the peak-to-peak linewidth. (b) Temperature dependence of the ESR intensity. The solid curve and the $4k_F$ and the $2k_F+4k_F$ transitions are taken from the theoretical expectation [2].



pressure up to 12 kbar.

Figure 4 shows the temperature dependence of the thermoelectric power. The positive value indicates that the carriers are holes on the donors. It is linearly dependent on the temperature in the metallic region. Some BEDT-TTF conductors, which have comparatively complicated two-dimensional band structures, exhibit complicated temperature dependences. The simple linear temperature dependence of the present complex suggests a simple band structure. The above-mentioned band calculation shows the one-dimensional band is a good approximation. Assuming the one-dimensional tight-binding band, the temperature gradient of the thermoelectric power affords the bandwidth $4t_a = 0.63$ eV.

Figure 5 shows the results of the ESR measurement. The observed line shape is a single Lorentzian over the whole temperature range. The g -value is essentially temperature-independent, and the linewidth shows linear temperature dependence (Fig. 5(a)). Below 20 K, the linewidth is almost constant. From room temperature to 80 K, the ESR intensity shows almost constant Pauli-like behavior (Fig. 5(b)). Below 80 K, it shows a Curie-like rise, succeeded by a discontinuous decrease at 20 K, below which it decreases by an activated fashion. The Curie-like behavior suggests a highly correlated system, in which the Hubbard U is fairly large. A discontinuity is seen when the spin degrees of freedom are lost in such a case as a spin Peierls transition. The results of a reported model calculation [2] depicted in Fig. 5 seem to reproduce the experiment fairly well. However, the origin of the 20 K transition, whether spin-Peierls or spin-density waves, is yet unclear only from the present observations.

References

- [1] T. Mori and H. Inokuchi, *Solid State Commun.*, **70** (1989) 823.
- [2] S. Huizinga, J. Kommandeur, H. T. Jonkman, and C. Haas, *Phys. Rev. B* **25**, (1982) 1717.

"2K-Superconducting State" in the Organic Superconductor β -(BEDT-TTF)₂I₃

S.Kagoshima, M.Hasumi, Y.Nogami*, N.Kinoshita**, M.Tokumoto**, T.Sasaki***,
N.Toyota***, H.Anzai** and G.Saito****

Department of Pure and Applied Sciences, University of Tokyo, Komaba 3-8-1, Meguro, Tokyo 153, Japan. *Department of Physics Kyoto University, Sakyo-ku, Kyoto 606, Japan. **Electrotechnical Laboratory, Umezono, Tsukuba, Ibaraki 305, Japan. ***Institute for Materials Research, Tohoku University, Katahira 2-1-1, Sendai 980, Japan. ****Institute for Solid State Physics, University of Tokyo, Roppongi 7-22-1, Minato, Tokyo 106, Japan.

Annealing of the title compound at about 110K for 20-40 hr causes a change in the superstructure, and gives rise to two superconducting states with the critical temperature of 2K and -7.5K. The former state is found to occupy most of the sample volume. This state having T_c of 2K has a lower resistance and a narrower EPR line width in its normal state than this compound without annealing has. Furthermore the critical field anisotropy decreases in this 2K-superconducting state. These results suggest that the randomness of this system decreases or the interlayer coupling of electrons increases during annealing. Discussion is made on possible phase diagram of this compound.

1. INTRODUCTION

The significance of organic superconductivity is two-fold: First, organic conductors may possibly present superconductivity of novel type even though we refrain from talking about the high-temperature superconductivity. Second, they provide more clues than other materials do to find out and investigate actual mechanisms of superconductivity. These are brought about by a peculiarity of organic materials; low-dimensionality of their electron systems, softness of the lattice, designability of molecules constituting the lattice etc.

From the latter point of view we have been studying possible origins for the difference between the critical temperatures of the so-called "low- T_c " and the "high- T_c " states of β -(BEDT-TTF)₂I₃. It is well-known that the "low- T_c " state, whose critical temperature T_c is 1-1.5K, appears when an applied pressure is lower than a critical value -0.4kbar [1,2] and the "high- T_c " one with T_c -8K in the higher pressure range. An incommensurate superstructure, which is expected to be present in the pressure range same as that of the "low- T_c " state, has been expected to play an important role in dominating the critical temperature. [3,4]

In a preceding paper [5] we verified directly the presence of the superstructure in the lower pressure range mentioned above. Furthermore we found that the superstructure, which appears below 175K at ambient pressure, became unstable below about 110K. The stable state, which is realized when an annealing is made for 20-40 hr at about 110K, was found to have the superstructure with a wave vector different from that of the sample without annealing. We found also an associated increase of the

superconducting critical temperature: Annealed samples undergo a superconducting transition at 2K, which is higher than that of the "low- T_c " state. In addition, another superconducting state with $T_c \sim 7.5K$ is found to appear in a small volume of samples. [6]

In the present study we examine properties of the two superconducting states found in annealed samples, and investigate possible origins for the difference in critical temperatures between annealed and quenched samples.

2. EXPERIMENTS

Sample crystals were prepared by a conventional electrochemical method. By EPR measurements we verified no inclusion of α -(BEDT-TTF) $_2$ I $_3$, which may turn into the β -phase and make experimental results ambiguous. Dc resistance of samples was measured by a conventional four probe method with gold wires of 10 μ m dia. glued with gold paint onto the two-dimensional ab-plane of samples. Magnetization measurements were made under the magnetic field of 10 Oe in a SQUID magnetometer. EPR measurements of carriers were made in the X-band on a single crystal, whose c^* -axis was parallel to the magnetic field.

3. RESULTS AND DISCUSSION

1) Presence of two superconducting states in annealed samples

As we showed in the preceding report, [5] the electrical resistance of annealed samples suggests the presence of two superconducting transitions at $\sim 7.5K$ and $2K$. (Fig.1) The former appears to be a partial superconductivity in the sample, while the latter is expected to be a superconductivity of the whole volume. In contrast, the same sample without annealing, i.e. cooled down through the temperature range 120-100K with a conventional cooling speed, just starts to become superconducting at about 1.5K as shown in Fig.1. Thus two superconducting states with T_c of about 7.5K and 2K appear as a result of annealing.

Magnetization measurements of annealed samples tell, as shown in Fig.2, that the 2K-superconducting state amounts to almost bulk superconductivity while the diamagnetic signal due to 7.5K-superconducting state is approximately an order of magnitude smaller than the latter.

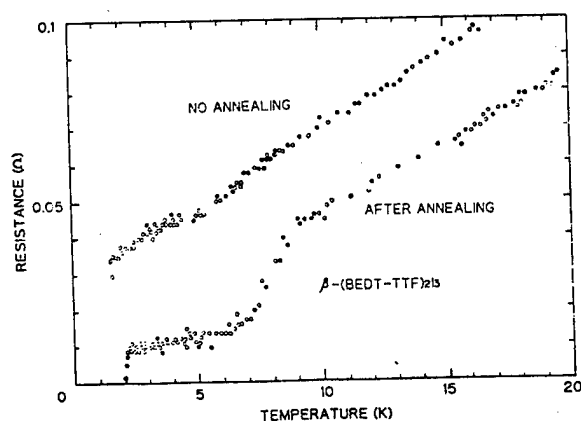


Fig.1 Temperature dependence of the dc resistance of a sample of β -(BEDT-TTF) $_2$ I $_3$ with and without annealing. The annealing was made at about 106K for 100hr.

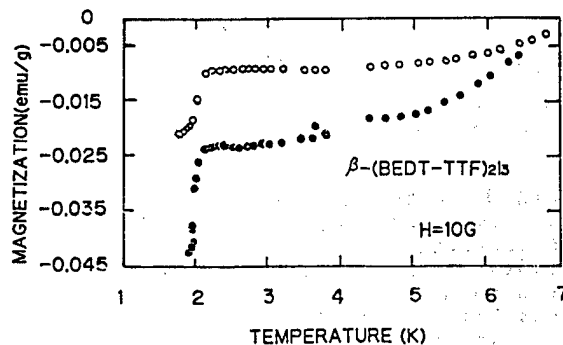


Fig.2 Temperature dependence of the magnetization of β -(BEDT-TTF) $_2$ I $_3$ annealed at about 110K for 135hr. Open circles denote the results of a field-cooled sample and the closed ones the shielding current effect measured with the field of 10 Oe.

Thus we conclude that the annealing at about 110K brings predominantly about an increase of the critical temperature from -1.5K to 2K. The superconductivity with T_c -7.5K is possibly a by-product of the annealing.

2) Properties of the 2K- and the 7.5K-superconducting states

What is happening during the annealing at about 110K? In the preceding report [5] we showed that the wave vector specifying the superstructure changes below about 110K when we annealed samples there. We measured, as shown in Fig.3, the wave vector, the sample resistance and the EPR linewidth of independent samples as functions of time during the annealing. The results strongly suggest that these changes in structure, resistance and spin-relaxation have a common origin. The wave vector changes continuously as keeping the long-range order. [7] It is not given by a superposition of the initial and the final states of the annealing. In addition, also the resistance and the EPR linewidth decrease monotonically with time.

The structural study by x-ray and the EPR measurements probe bulk properties and most of the sample volume undergoes a superconducting transition at 2K. Therefore we consider that the change of properties during the annealing shown in Fig.3 should be related with the appearance of the 2K-superconducting state.

What is the nature of the state with T_c -2K? Evidently the annealed samples has a lower resistance and a narrower EPR linewidth than the sample without annealing has.

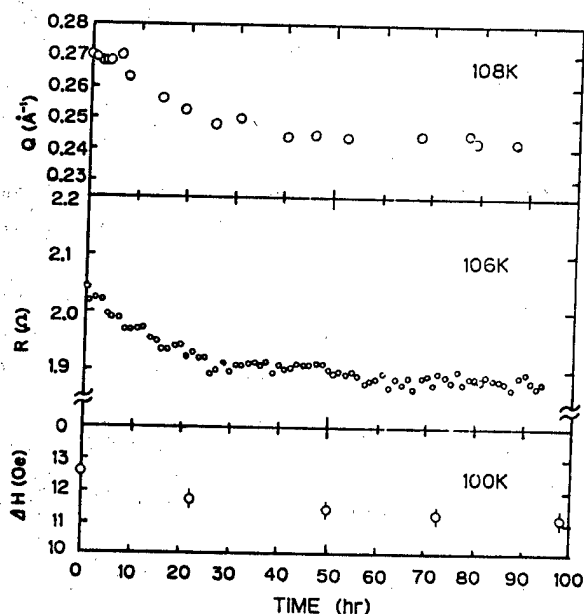


Fig.3 Time dependence of the absolute value of the wave vector Q specifying the superstructure, the sample resistance R and the EPR linewidth ΔH of the independent samples of β -(BEDT-TTF) $_2$ I $_3$ during the annealing at about 110K.

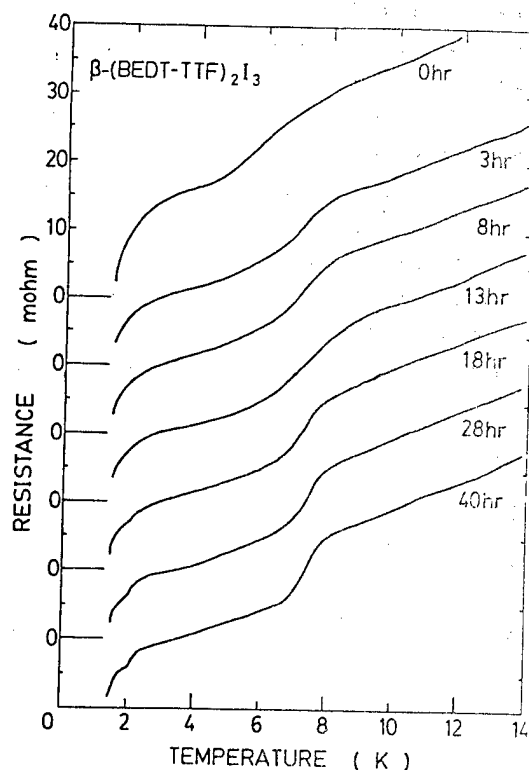


Fig.4 Temperature dependence of the resistance of a sample of β -(BEDT-TTF) $_2$ I $_3$ during annealing. Each set of results was obtained by suspending the annealing followed by cooling down to low temperatures. The figures 3hr, 8hr, shown in the figure denote the total time of annealing at about 106K.

These results imply a decrease of scattering probability of carriers in the annealed state having the critical temperature of 2K. Hence one may conjecture that the increase of T_c from 1.5K to 2K is brought about by the reduction of disorder in samples. It is important to note, however, that the increase of T_c is not continuous as shown in Fig.4. Critical temperatures intermediate between -1.5K and 2K cannot be found. This leads to the conclusion that the 2K- superconducting state is another phase of superconductivity which is qualitatively different from the "low- T_c " state.

In the light of this consideration we would point out a possibility that a disorder concerning the conformational degree of freedom of BEDT-TTF molecules plays a key role as it is discussed in the preceding report [5]. It is believed that the A- and B-type conformations coexist in the "low- T_c " state although only the A-type is present in the "high- T_c " state. Therefore a certain degree of disorder is expected to be inevitably present in the conformation because it must be involved in the superstructure which is incommensurate. [3] We conjecture that all molecules turn into the A-type when the wave vector of the superstructure is changed by annealing. EPR results of the present study support this idea because the EPR linewidths at the beginning and at the end of the annealing processes are similar to those of the "low- T_c " and the "high- T_c " states, respectively, observed by Hurdequint et al. [8]

Measurements of the upper critical field H_{C2} provides another clue to examine properties of the superconducting states. [9] Figure 5 shows temperature dependence of H_{C2} of the "low- T_c " and the 2K-superconducting states. They look quite similar to each other except the difference in T_c . Careful analyses suggest, however, a bit of reduction in the anisotropy of H_{C2} in the 2K-superconducting state. This is consistent with the above idea of the conformational change during the annealing, because the conformational change involves an intramolecular structural change near the edge of a BEDT-TTF molecule. This type of change is expected to affect the interlayer coupling.

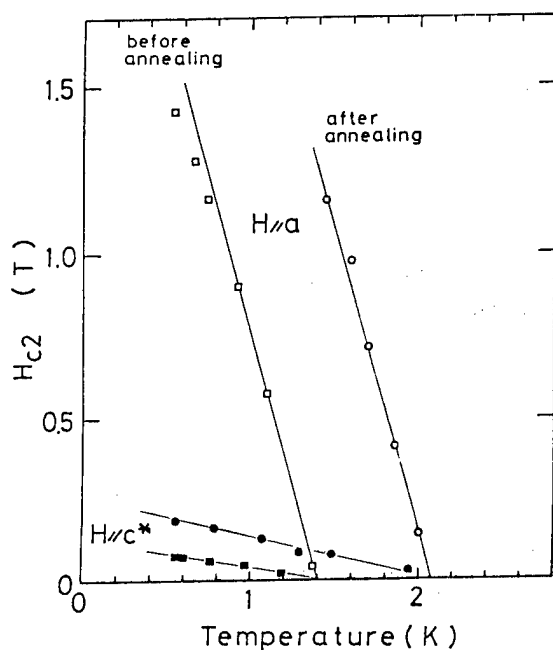


Fig.5 Temperature dependence of the upper critical field H_{C2} in both states before and after annealing.

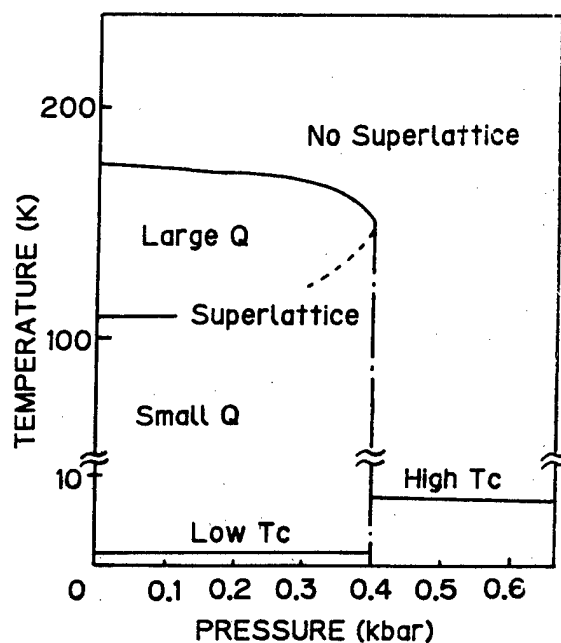


Fig.6 The obtained phase diagram of β -(BEDT-TTF) $_2$ I $_3$

With respect to the 7.5K-superconducting state, H_{C2} as a function of temperature is found to be essentially the same as that of the "high- T_c " state. The similarity of both T_c and $H_{C2}(T)$ suggests that the 7.5K-superconducting state is nothing but the "high- T_c " state, which has only the A-type of conformation of BEDT-TTF molecules and has no superstructure. We conjecture that the 7.5K-superconducting state is presumably brought about in a small volume of samples by the structural change during the annealing, because the structural change will generate a local pressure in samples leading to killing off of the superstructure.

3) Possible phase diagrams of β -(BEDT-TTF) $_2$ I $_3$

We have presented above the following picture, depicted in Fig.6, for the structural and superconducting states of the present material: When a sample is cooled down with an ordinary speed, it becomes structurally metastable below about 110K and undergoes a superconducting transition at 1-1.5K. This is the well-known "low- T_c " state having both A- and B-types of BEDT-TTF molecules. When we anneal the sample at about 110K allowing the structural change to occur, the sample enters a stable state with, presumably, the A-type only and, therefore, has less disorder. Its critical temperature is raised up to 2K discontinuously because the conformational change is expected to cause the discontinuous reduction of disorder in the conformation of BEDT-TTF molecules. During the annealing process a small volume of the sample loses the superstructure because of a local pressure generated by the structural change. Those parts of the sample belong to the so-called "high- T_c " state with T_c -7.5K. The difference of T_c between the "high- T_c " state and the "low- T_c " or the 2K-superconducting state is presumably ascribed to the superstructure.

We should keep another possibility for the ground state at ambient pressure. Above picture assumes the ground state to have still the superstructure although the conformation of BEDT-TTF molecules has only the A-type. However, magnetization measurements suggest [10] that the 7.5K-superconducting state appears to surpass the 2K-one in volume fraction when the annealing is continued for a very long time. This result cannot lead to a unique conclusion but leave a few possibilities because the samples experience many times of thermal cycling between the annealing temperature 110K and lower temperatures for the observation of the change in superconducting properties during the annealing. This process may increase the volume fraction of the "high- T_c " state by giving local pressures to the samples. It is left for further studies whether the 2K-superconducting state is the ground state at ambient pressure or the real ground state is the "high- T_c " state having no superstructure.

Acknowledgements

We are grateful to T.Osada of University of Tokyo, T.Takahashi and K.Kanoda of Gakushuin University and K.Murata of Electrotechnical Laboratory for illuminating discussion.

REFERENCES

1. W.Kang, G.Creuzet, D.J  rome & C.Lenoir: J. Physique 48 (1987) 1035.
2. I.F.Schegolev: Japan. J. Appl. Phys. 26, Suppl. 26-3 (1987) 1972.
3. V.B.Ginodman, A.V.Gudenko, P.A.Kononovich, V.N.Laukhin & I.F.Schegolev: to be published in J. Mol. Elec.

3. P.C.W.Leung, T.J.Emge, M.A.Beno, H.H.Wang & J.M.Williams: J. Am. Chem. Soc. 106 (1984) 7644.
4. See for example, A.J.Schultz, M.A.Beno, H.H.Wang & J.M.Williams: Phys. Rev. B33 (1986) 7823.
5. S.Kagoshima, Y.Nogami, M.Hasumi, H.Anzai, M.Tokumoto, G.Saito and N.Mori: Research Report on Mechanism of Superconductivity, ed. Y.Muto (1989) p.279.
S.Kagoshima, Y.Nogami, M.Hasumi, H.Anzai, M.Tokumoto, G.Saito and N.Mori: Solid State Commun. 69 (1989) 1177.
6. S.Kagoshima, M.Hasumi, Y.Nogami, N.Kinoshita, H.Anzai, M.Tokumoto and G.Saito: Solid State Commun. 71 (1989) 843.
7. Y.Nogami, S.Kagoshima, H.Anzai, M.Tokumoto, N.Mori, N.Kinoshita and G.Saito: to be published in J. Phys. Soc. Jpn. 59 (1990).
8. H.Hurdequint, F.Creuzet and D.Jerome: Synthetic Metals 27 (1988) A183.
9. T.Sasaki, N.Toyota, M.Hasumi, T.Osada, S.Kagoshima, H.Anzai, M.Tokumoto and N.Kinosita: J. Phys. Soc. Jpn. 58 (1989) 3477.
10. K.Kanoda, K.Akiba, K.Suzuki, T.Takahashi and G.Saito: to be published in "The Physics and Chemistry of Organic Superconductors", ed. G.Saito and S.Kagoshima (Springer-Verlag, 1990).

Unconventional Superconductivity in the Organic Superconductor,
 κ -(BEDT-TTF)₂Cu(NCS)₂

Toshihiro Takahashi and Kazushi Kanoda

Department of Physics, Gakushuin University
1-5-1 Mejiro, Toshima-ku, Tokyo 171, Japan.

Unconventional natures of the superconductivity in the organic superconductor, κ -(BEDT-TTF)₂Cu(NCS)₂, were revealed by ¹H-NMR relaxation and complex susceptibility measurements. The existence of new relaxation mechanism, very probably related to vortex dynamics in the superconducting state, was found. The temperature dependence of magnetic-field penetration depth, λ , was found to follow a power law at low temperatures, instead of an exponential behavior expected in the BCS theory. This result strongly suggests anisotropic superconductivity of gapless nature.

Extensive research on material science has provided several exotic metals such as heavy electron, organic and oxide superconductors. It has become a practical problem whether the superconductivity in these materials is of conventional BCS-type or not. Among them, the heavy electron systems have increasing evidences that these are not conventional superconductors. This finding came in part from the measurements of temperature dependences of specific heat [1], nuclear spin-lattice relaxation rate [2], ultrasonic attenuation [3] and magnetic field penetration depth [4].

The title compound, κ -(BEDT-TTF)₂Cu(NCS)₂, has the highest transition temperature, $T_c \sim 10.4$ K, among the organic superconductors to date [5]. This compound consists of alternating sheets of BEDT-TTF molecules and Cu(NCS)₂ ions, and is characterized by a quasi-two-dimensional electronic state. Several experiments aiming at the clarification of the type of superconductivity have been made. Specific heat was measured by Katsumoto et al. [6], who found that it follows the T^3 law at low temperatures. However, possible large contribution of phonons did not allow them to deduce the temperature dependence of electronic part. The ¹H nuclear spin-lattice relaxation rate, T_1^{-1} was measured by our group [7]. The observed temperature dependence of T_1^{-1} , however, was far from any behaviors already predicted. This strongly suggests the existence of some other relaxation mechanism, never considered. In the first part of this report, we summarize the previous results at finite fields and also present new data obtained at zero field by using field cycling technique.

Magnetic-field penetration depth, λ , probes the type of superconductivity. We made precise measurements of complex susceptibility, χ , for single crystals of κ -(BEDT-TTF)₂Cu(NCS)₂ and derived penetration depth in two directions of external field. An evidence of anisotropic superconductivity of gapless nature is reported. This is the second topic of this report.

¹H Nuclear Spin-Lattice Relaxation

The nuclear spin-lattice relaxation rate is a powerful probe to investigate the

type of superconductivity. There have been observed two different temperature dependences of the nuclear spin-lattice relaxation rate, T_1^{-1} , in the superconducting states, depending on the type of electron pairing: For s-wave pairing with isotropic nature as in the BCS model, T_1^{-1} increases just below T_C , and then decreases exponentially due to the presence of finite gap [8]. In anisotropic superconductivity with a gapless nature, the enhancement below T_C does not appear and the low temperature variation follows a power law [9]. The latter behavior of the unconventional superconductivity has been reported in a typical organic superconductor, $(TMTSF)_2ClO_4$ [10]. The organic conductors are now intriguing materials from the viewpoint of physics of the superconductivity.

In κ -(BEDT-TTF) $_2$ Cu(NCS) $_2$, we have reported an unusual enhancement of relaxation rate never observed in the usual superconductors [7]. The temperature dependences of T_1^{-1} at finite fields are summarized as follows: At 3.28 kOe, T_1^{-1} was greatly enhanced below T_C , forming a peak around 4 K, and then decreases rapidly at lower temperatures toward zero. The peak value was about 30 times as large as that at 10 K. At a higher field, 11.7 kOe, the enhancement of T_1^{-1} was reduced and the peak position shifted to a lower temperature, 3 K. The anomaly took place well below the superconducting transition. The large field dependence was indicative of a close relation to the superconductivity. The recovery of the nuclear magnetization fitted well to a single exponential curve for the whole measurements.

The enhancement was exceptionally large compared with the usual superconductors and cannot be explained by any theory either for the isotropic or anisotropic superconductivity, mentioned above. At present we consider that the enhancement is caused by the field fluctuations generated by the vortex dynamics. This type of motion, in general, causes the so-called BPP-type relaxation, which is given by [11]; $T_1^{-1} \sim \gamma_n^2 h_0^2 \tau_c / (1 + \omega_n^2 \tau_c^2)$, where γ_n , h_0 , τ_c and ω_n are the gyromagnetic ratio of the nucleus, the amplitude and the correlation time of the field fluctuation, and the Larmor frequency. The maximum of $T_1^{-1} \sim \gamma_n^2 h_0^2 / 2\omega_n$ appears when the temperature dependent τ_c satisfies $\tau_c \omega_n = 1$. In order to explain the observed peak value, 0.25 s^{-1} , at 3.28 kOe, h_0 should be 0.4 Oe, which is not unrealistic. Considering the sharpness of the peak, vortex lattice melting is favorable as the origin of the required dynamics. Note that this compound has strong two dimensional electronic states. Indeed, the estimated melting temperature using the transport data yields 2.7 K which is close to the temperature where the anomaly occurs [7].

To get further information we have applied the field cycling technique to investigate zero field relaxation. Above T_C , the recovery of the nuclear magnetization in time is single exponential as was in the field. Figure 1 shows the temperature dependence of T_1^{-1} at zero magnetic field together with that at 11.7 kOe. In the temperature range between 10 and 30 K, T_1^{-1} follows the Korringa relation, $(T_1 T)^{-1} = (650 \text{ sec K})^{-1}$. The value of $(T_1 T)^{-1}$ at zero field is enhanced by the factor of 1.7 compared with that at 11.7 kOe. This agrees well the theoretical value of 2 for uncorrelated local fields [12]. Above 30 K, T_1^{-1} gets to deviate from the linearity while the deviation at 11.7 kOe occurs above 100 K. This is reasonably attributed to an additional relaxation due to thermal motions of the ethylene group.

Below T_C , the decay of the nuclear magnetization gets non-single exponential. The profile of the decay curve is shown in Fig. 2. As the temperature decreases, the non-single exponential nature becomes more pronounced. In particular, the initial slope of the decay is surprisingly steep and is even larger by two order of magnitude than the relaxation rate at 11.7 kOe. Furthermore, the decay time of the long component is much

longer than the measured time range. The field dependence of the relaxation profile was precisely investigated at 4.2 K; with increasing the field, the non-single exponential decay at zero field was found to turn gradually into a single exponential curve; the relaxation rate becomes smaller for further increase of the field, and tends continuously to the results at 3.28 and 11.7 kOe.

The results below T_C are not inconsistent with the vortex dynamics discussed above. The non-single exponential decay means inhomogeneous relaxation of nuclei. Since the relaxation in the normal state is homogenous, the vortex structure is the most probable candidate for the origin of the inhomogeneity. Even at 'zero' field in the process of the field cycling, we must suppose the existence of considerable amount of vortices. There should be vortex motions, such as flux creep or, although speculative, the motions of bound vortex-antivortex pairs. In order to confirm this picture, the relaxation measurements for ^{13}C -enriched sample are under way. We also hope the ^{13}C relaxation will reveal the hyperfine contribution which have been masked in the present ^1H relaxation.

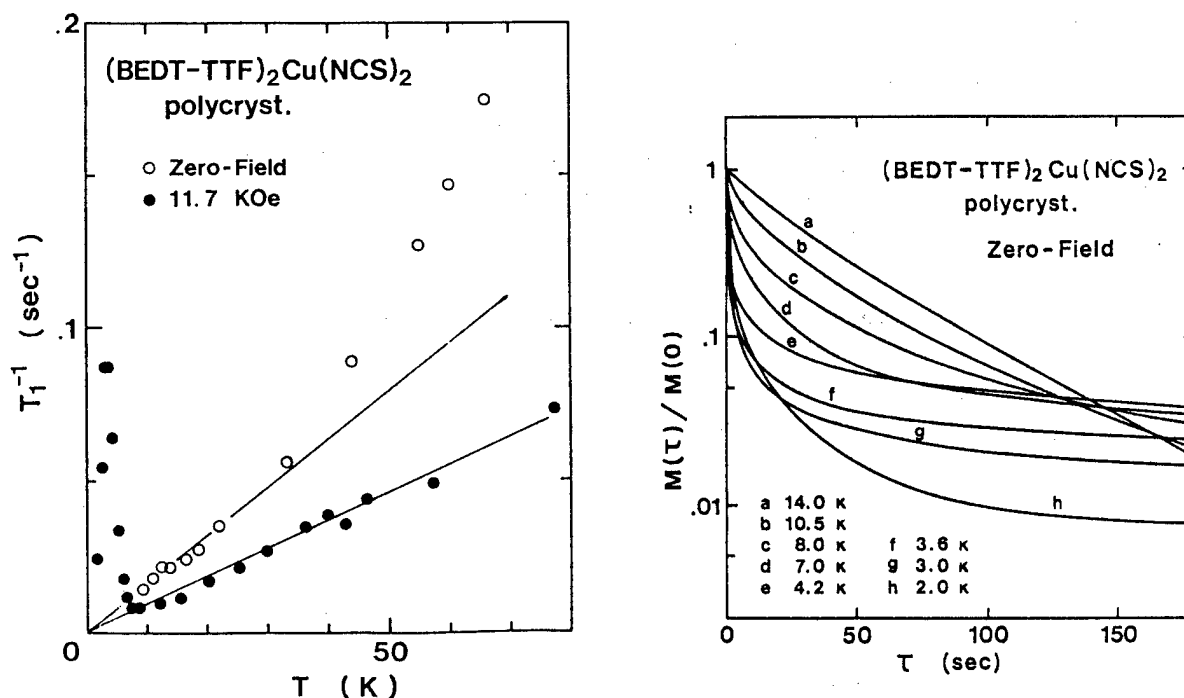


Fig. 1 (Left) ^1H -NMR relaxation rate at zero-field and at 11.7 kOe. The two straight lines show the Korringa behaviors, $T_1T = 650 \text{ secK}$ and $T_1T = 1100 \text{ secK}$, at zero and at 11.7 kOe, respectively.

Fig. 2 (Right) Relaxation profile of the nuclear magnetization at nominal zero field. Non-single exponential decays are observed below T_C .

Magnetic-Field Penetration Depth Determined by Complex Susceptibility

The complex susceptibility χ ($\chi = \chi' - i\chi''$) was measured down to 1.5 K, with a Hartshorn-type mutual inductance bridge, resolution of which is $\sim 5 \text{ nH}$. The ac field was applied either perpendicular or parallel to the crystal layer. In the parallel case, where the demagnetizing effect can be neglected, the absolute value of the susceptibility was determined. For calibration, we used the complete diamagnetism of Sn

films (7-500 μm thick).

At perpendicular fields χ' exhibits a sharp transition at 9.2 K. With increasing the field, χ' around T_C becomes depressed gradually but the low-temperature values lie on a "universal curve" in the zero field limit when the applied ac field is less than 2 Oe. The imaginary part, χ'' , forms a sharp peak only around the transition region. Vanishing χ'' except the vicinity of T_C implies that no vortices enter into the samples. In the perpendicular direction of the field, χ' shows almost a perfect diamagnetism, the deviation from which is quite small. Moreover, the demagnetization effect is large and the correction is not easy for crystals of irregular shape. Thus one cannot determine absolute value of λ from the susceptibility data. It is, however, possible to obtain the deviation from the minimum value of λ in the case of thin crystal with a diameter of $2R$ and a thickness of $2d$ ($R \gg d$), by taking into account the χ' -dependence of the demagnetization factor. The calculation is straightforward [13] and the final formula for $R \gg \lambda_{\min}$ is given as $\lambda(T) - \lambda_{\min} = R[1 - (\chi'(T)/\chi'(T_{\min}))^{1/3}]$. The results thus obtained from χ' at 116 mOe are plotted as a function of $(T/T_C)^2$ in Fig. 3(a). (χ'' at 116 mOe is considered as those in the zero-field limit in the temperature range, $T/T_C < 0.95$.) The temperature dependence of λ is well approximated by the T^2 -law at low temperatures of $(T/T_C)^2 < 0.35$, i.e. $T/T_C < 0.6$. Experimentally, the exponent, α , of the power-law, T^α , is in the range of 1.7-2.2. Such a power law is in remarkable contrast to the BCS behavior, where λ varies exponentially in temperature, as considered later.

Next, the results in the ac field parallel to the crystal layers are given. In this geometry of the field, we can determine the absolute value of the penetration depth since the absolute values of χ' are measured. The results were independent of the amplitude of the ac field at least up to 1.2 Oe. The imaginary part, χ'' , is zero throughout the entire temperature range at the field below 1.2 Oe. The deviation from the perfect diamagnetism ($-4\pi\chi' < 1$) in the low field region is caused by the field penetration, as in the perpendicular geometry. It should be noted that when the field is applied parallel to the crystal surface the penetration can take place both from the surface in a direction perpendicular to the layers and from the edges in the parallel direction. In layered materials, the latter is often dominant. Detailed measurements and analysis were made for several crystals with different dimensions and revealed that the parallel penetration shown in the inset of Fig. 3(b) determines χ' in the present system. (Details were described in Ref. 13.) λ is calculated by the equation $-4\pi\chi' = 1 - (2\lambda/D)\tanh(D/2\lambda)$, where D is the dimension of the sample in the direction of field penetration. The obtained penetration depth, which is normalized to the minimum value, is shown as a function of $(T/T_C)^2$ in Fig. 3(b), as well as the empirical Gorter-Casimir law, $\lambda \sim [1 - (T/T_C)^4]^{-1/2}$, and the model calculation of the Josephson-coupled layers based on the BCS framework [14]. The latter gives the same temperature dependence as in the dirty local limit, namely, $\lambda \sim \Delta(T)\tanh(\Delta(T)/2kT)$, which yields exponential dependence in T at low temperatures. As seen in the figure, our results exhibit T^2 -dependence, $\lambda(T)/\lambda(0) = 1 + 0.45(T/T_C)^2$, at low temperatures. Now the temperature dependence of λ is again of a power-law, instead of an exponential BCS behavior. The results were fairly reproducible for four measurements on different crystals.

The temperature dependence of the penetration depth at low temperatures generally probes the gap structure in the density of states of the quasi-particle excitation. The BCS theory predicts the exponential temperature dependence due to the finite gap in the excitation. For example, in the local limit which is relevant to our compound, $\lambda(T) - \lambda(0) = \lambda(0)(2\pi\Delta/kT)^{1/2}e^{-\Delta/kT}$ at $T \ll \Delta/k$. On the other hand, a power-law dependence means the existence of non-vanishing density of states above the ground state and is

expected for anisotropic superconductors with nodes of the gap parameter on the Fermi surface. The present results give an evidence that the superconductivity in the organic conductor, κ -(BEDT-TTF)₂Cu(NCS)₂, has a gapless nature of this kind similar to the heavy electron systems. The possibility of anisotropic superconductivity and its characteristics, if any, in the quasi-two-dimensional organic systems were discussed in the context of nonlocal attractive and on-site Coulomb interactions by Hasegawa and Fukuyama [15].

In conclusion, the organic superconductor (BEDT-TTF)₂Cu(NCS)₂ exhibits power-law temperature dependence of the penetration depth. Anisotropic pairing with nodes of the gap parameter on the Fermi surface was suggested for this material.

Acknowledgments

The present experiments have been performed in collaboration with K. Akiba, K. Sakao, M. Watabe (Gakushuin University), H. Mori (ISTEC), and G. Saito (Kyoto University). The authors would like to thank K. Suzuki for sample preparation and M. Mori for technical assistance. This work was supported by a Grant-in-aid for Scientific Research from the Ministry of Education, Science, and Culture of Japan.

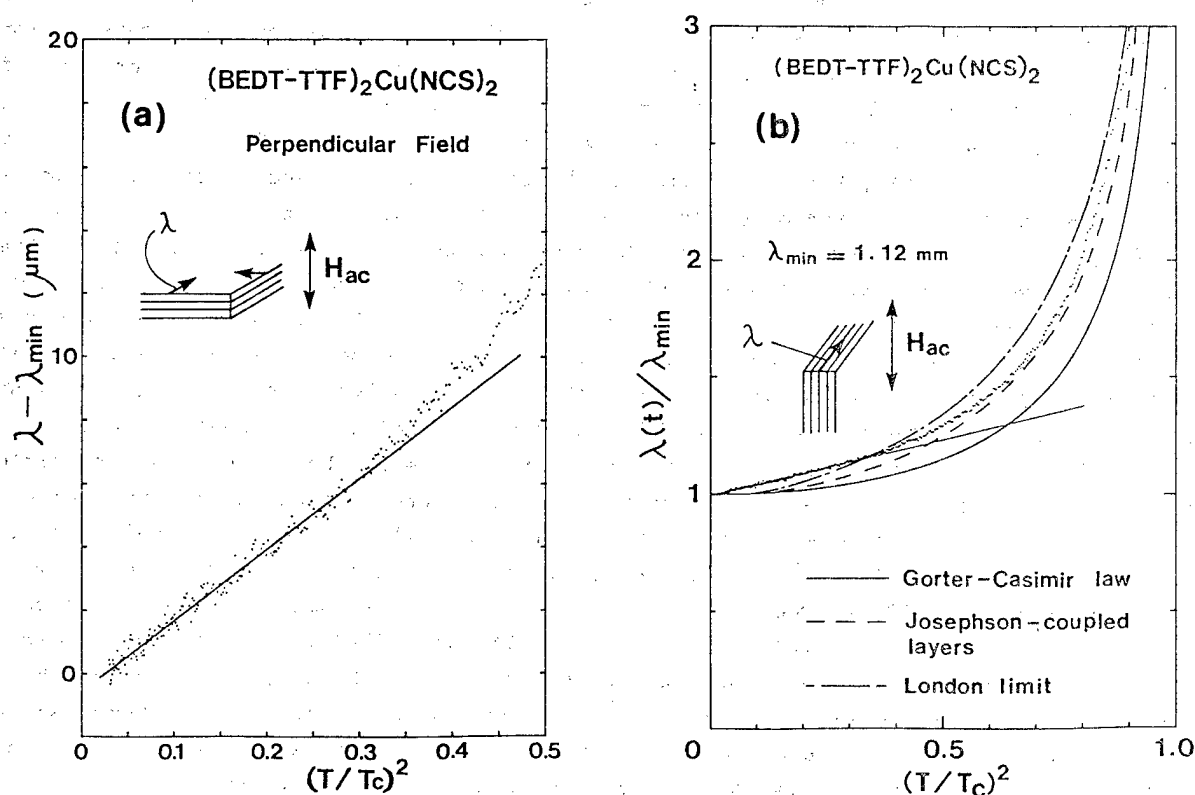


Fig. 3(a) Deviation of the penetration depth from the minimum value, $\lambda - \lambda_{\min}$, plotted as a function of $(T/T_C)^2$. Inset shows the directions of the applied ac field and the penetration with respect to the crystal layer.

(b) Normalized penetration depth, λ/λ_{\min} , plotted as a function of $(T/T_C)^2$. Note that the directions of the applied ac field and the penetration are different from those in (a).

References

- [1] H. R. Ott, H. Rudigier, T. M. Rice, K. Ueda, Z. Fisk, and J. L. Smith, *Phys. Rev. Lett.* **52**, 1915 (1984).
- [2] D. E. McLaughlin, Cheng Tien, W. G. Clark, M. D. Lan, Z. Fisk, J. L. Smith, and H. R. Ott, *Phys. Rev. Lett.* **53**, 1833 (1984).
- [3] D. J. Bishop, C. M. Varma, B. Batlogg, and E. Bucher, *Phys. Rev. Lett.* **53**, 1009 (1984).
- [4] D. Einzel, P. J. Hirschfeld, F. Gross, B. S. Chandrasekhar, K. Andres, H. R. Ott, J. Beuers, Z. Fisk, and J. L. Smith, *Phys. Rev. Lett.* **56**, 2513 (1986).
- [5] H. Urayama, H. Yamochi, G. Saito, K. Nozawa, T. Sugano, M. Kinoshita, S. Sato, K. Oshima, A. Kawamoto, and J. Tanaka, *Chem Lett.* **1988**, 55 (1988).
- [6] S. Katsumoto, S. Kobayashi, H. Urayama, H. Yamochi, and G. Saito, *J. Phys. Soc. Jpn.* **57**, 3672 (1988).
- [7] T. Takahashi, T. Tokiwa, K. Kanoda, H. Urayama, H. Yamochi, and G. Saito, *Physica C* **153-155**, 487 (1988); *Synth. Met.* **27**, A319 (1988).
- [8] L.C. Hebel and C.P. Slichter, *Phys. Rev.* **113**, 1504 (1959).
- [9] Y. Hasegawa and H. Fukuyama, *J. Phys. Soc. Jpn.* **56**, 877 (1987).
- [10] M. Takigawa, H. Yasuoka, and G. Saito, *J. Phys. Soc. Jpn.* **56**, 873 (1987).
- [11] C.P. Slichter, Principles of Magnetic Resonance (Springer-Verlag, 1980) p.167.
- [12] A. Abragam, Principles of Nuclear Magnetism (Oxford University Press, 1961) p.363.
- [13] K. Kanoda, T. Takahashi, G. Saito, in *Proceedings of the International Conference on M²S-HTSC*, Stanford, 1989 (to be published in *Physica C*); K. Kanoda, K. Akiba, S. Suzuki, T. Takahashi, G. Saito, (to be published).
- [14] G. Deutscher and O Entin-Wohlman, *J. Phys. C* **10**, L433 (1977).
- [15] Y. Hasegawa and H. Fukuyama, *J. Phys. Soc. Jpn.* **56**, 2619 (1987).

ANOMALOUS MAGNETOTRANSPORT PHENOMENA IN ORGANIC CONDUCTORS

K.Kajita, Y.Nishio, T.Takahashi, W.Sasaki, R.Kato, H.Kobayashi,

*A.Kobayashi and **Y.Iye

Faculty of Science, Toho University, Miyama 2-2-1, Funabashi 274, Japan

*Faculty of Science, Tokyo University, Bunkyo 113, Japan

**ISSP, Tokyo University, Minatoku 106, Japan

Anomalous magnetotransport phenomena observed in θ -(BEDT-TTF)₂I₃, α -(BEDT-TTF)₂I₃ are discussed based on the dimensionality of electron energy spectrum. Two types of the anomalies, one in low magnetic fields and one in high magnetic fields are reviewed.

1. INTRODUCTION

A θ type crystal of (BEDT-TTF)₂I₃ is an organic crystal having metallic character down to low temperatures and undergoing the superconducting transition with T_c of about 3.6K[1]. This crystal exhibits fairly strong two dimensional properties. The conductivity is high in the ab-crystal plane and low along the c*-crystal axis.

In the course of the investigation of the superconductivity of the crystal, we have noticed that the magnetoresistance in the normal state is anomalous. The magnetoresistance seems not to be determined by the Lorentz force. First, it is too large to be expected from the Lorentz force. Moreover, it is anomalous in that the effect is not sensitive to the angle between the magnetic field and the electric current, but it is determined by the direction of the magnetic field[2]. Such an anomaly seems somewhat universal to two dimensional organic conductors, such as κ -(BEDT-TTF)₂Cu(NCS)₂ and α -(BEDT-TTF)₂I₃.

When we extend the magnetoresistance measurement of θ -(BEDT-TTF)₂I₃ into higher fields, we encounter another anomaly of the magnetoresistance in θ -(BEDT-TTF)₂I₃, which is an oscillation of the magnetoresistance against the change of the magnetic field direction[3,4,5].

2. EXPERIMENTAL RESULTS

A. Low Field Anomaly

Figure 1 gives the magnetic field effect on the resistivity of θ -(BEDT-TTF)₂I₃ in the field one normal to the two dimensional plane and one in the plane. For both magnetic fields, we notice the linearly increasing resistivity instead of the quadratic rise. A much important feature of the phenomena is that the increment of the resistivity is the larger when the magnetic field is parallel to the conductive plane than when it is normal to the 2D plane. Another experiment has shown us that the direction of the magnetic field is the crucial parameter which determines the strength of the magnetoresistance. The angle between the magnetic field and the current is not important in the phenomena. These exclude the possibility that the effect results directly from the Lorentz force on carriers.

Figure 2 gives the magnetoresistance for the magnetic field in the bc*-plane at several temperatures. Analyzing these data, we have found that the function is given as

$$M = \rho_0^{-3/2} (C_a H_a^2 + C_b H_b^2 + C_c H_c^2) / H,$$

where ρ_0 is the zero field resistivity, C_a , C_b and C_c are parameters which are independent of temperature or the magnetic field strength. Relative amplitude of parameters C_a , C_b and C_c is determined in one sample, as $C_a:C_b:C_c=0.7:2:0.5$. This means that the effect is weak for the field in the direction normal to the two dimensional plane. For the fields in the 2D plane, the anisotropy of the effect is such that it is stronger when the field is in the b-axis and weak when it is in the a-axis.

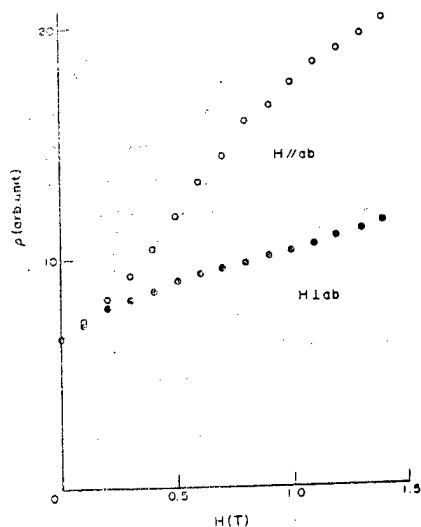


Fig. 1 Resistivity at 1.5 K as a function of the magnetic field which is applied one in the ab -plane and one normal to the ab -plane (along the c^* -axis). The electric current is in the ab -plane.

Similar phenomena are seen in α -type crystals of $(\text{BEDT-TTF})_2\text{I}_3$ under high hydrostatic pressure. An α -(BEDT-TTF) $_2\text{I}_3$ crystal is known to undergo the metal-nonmetal transition at about 135 K. Under high hydrostatic pressure, the critical temperature moves towards lower temperatures. Figure 3 gives the temperature dependence of the resistivity for $P=10\text{ kbar}$. A metal-nonmetal transition takes place at about 90 K. For this pressure, the increase of the resistivity in the low temperature phase is not so large and the resistivity saturates in the lowest temperature region. This implies that some portion of the Fermi surface survives after the metal-nonmetal transition. The magnetotransport experiments are done for this remaining Fermi surface.

The magnetic field direction is rotated in a plane containing the direction normal to the conducting plane which corresponds to $\Theta=0$ in the horizontal axis (Fig. 4). The magnetoresistance increases as the field is tilted from the direction normal to the conducting plane except for a region near $\Theta=-90$ where curves have large dips. If we neglect these dips, the experimental results show that the magnetoresistance is the larger when the field is parallel to the conducting plane. When the magnetic field is rotated in the conducting plane, the magnetoresistance shows anisotropy as seen in Fig. 5. These features are parallel to those we have observed in θ -(BEDT-TTF) $_2\text{I}_3$.

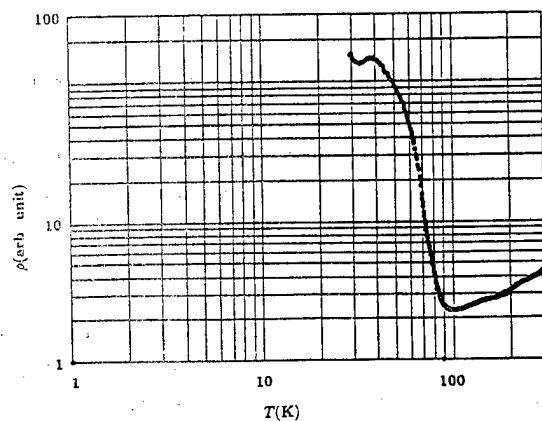


Fig. 3 Temperature dependence of the resistivity of α -(BEDT-TTF) $_2\text{I}_3$. The crystal is in a hydrostatic pressure of about 10 kbar.

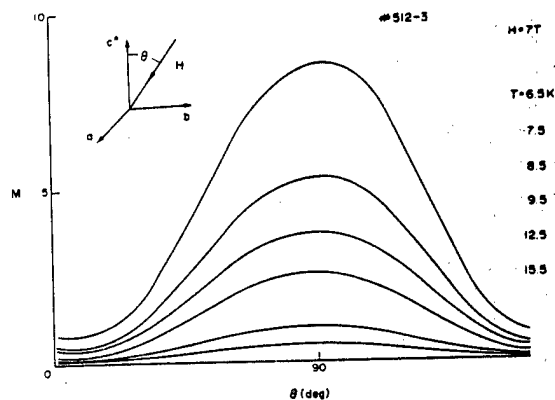


Fig. 2 Magnetoresistance at $H=7\text{ T}$ for several temperatures.

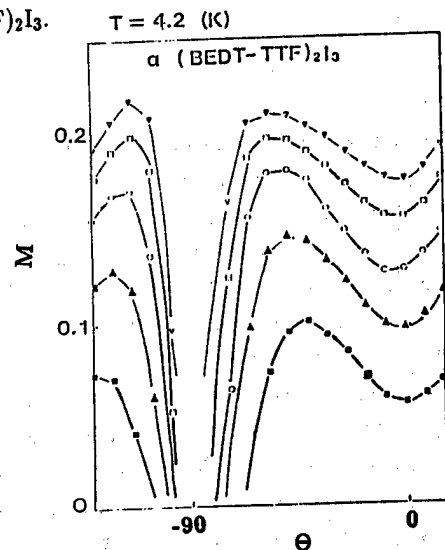


Fig. 4 Magnetoresistance for several magnetic fields ($H=0.4, 0.6, 0.8, 1.0, 1.2, 1.4\text{ T}$). $\Theta=0$ corresponds to the magnetic field direction in the conducting plane and $\Theta=90$ to that normal to the conducting plane.

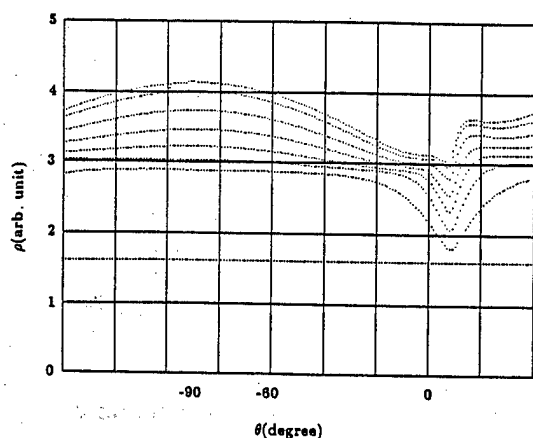


Fig.5 Resistance plotted against the magnetic field direction. Magnetic fields ($H=0,1,2,3,4,5,6,6.5\text{T}$) is rotated in the conducting plane.

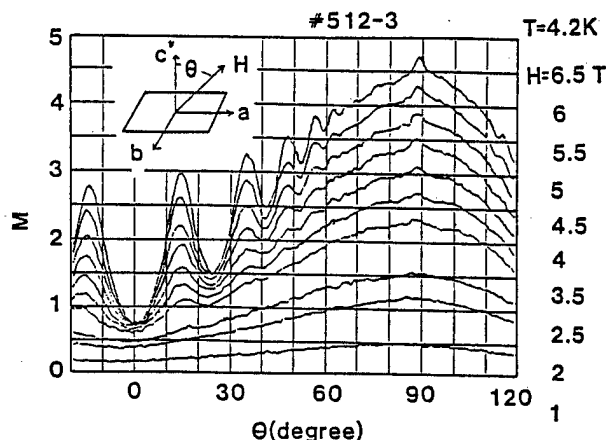


Fig.6 Magnetoresistance of θ -(BEDT-TTF) $_2$ I $_3$ plotted against the direction of magnetic field.

b. High field Anomaly

When we go into higher magnetic field region, a qualitative change of the behavior of the resistivity takes place. Figure 6 gives the magnetoresistance for a θ -(BEDT-TTF) $_2$ I $_3$ crystal plotted against the angle of the magnetic field direction measured from the direction normal to the 2D plane. An oscillatory behavior of the magnetoresistance is apparent for $H \geq 3\text{T}$.

This figure tells that positions of the peaks and bottoms are independent of the strength of the magnetic field. Another experiment evidences that the direction of the electric current is not important in the effect. The important parameter to determine the peak positions is the direction of the magnetic field. Thus, the phenomena is not the Shubnikov-de Haas oscillation.

The bottoms and the peaks of the oscillation appears at the field $H=(H_a, H_b, H_c)$ directions which satisfies

$$a|H_a/H| + b|H_b/H| = N \quad (N=1,2,3,\dots) \quad (\text{for bottoms, } = N+1/2 \text{ for peaks}). \quad (1)$$

On the other hand, the amplitude of the oscillation is determined by the magnetic field normal to the two dimensional plane. The amplitude is very sensitive to the carrier scattering as shown in Fig.7.

3.DISCUSSIONS

Among two types anomalies, the origin of magnetoresistance oscillation has been ascribed to the effective dimensionality of the electron energy spectrum in the magnetic field as follows.

In a magnetic field, the cyclotron mass of an electron is given as $m_H = (\hbar^2/2\pi) d\Lambda/d\epsilon$, where Λ is the area of a region surrounded by an electron trajectory which is on the Fermi surface and normal to the magnetic field. The Landau energy gap is given as $\Delta\epsilon = \hbar(eH/m_Hc)$. For a 2D electron system, magnetic field gives a drastic change to the electronic properties because of the qualitative change of the energy spectrum, from a continuous type to a deltafunction type Landau energy spectrum.

In real materials such as θ -(BEDT-TTF) $_2$ I $_3$, the electron energy spectrum always contains finite three dimensionality and thus, the Fermi surface waves sinusoidally along the direction normal to the 2D plane. In that case, the Landau levels broadens because of the distribution of m_H and the effect of the magnetic field will become weak.

Yamaji has shown that there are special magnetic field directions where the distribution of the value of m_H is very narrow[6]. The width of Landau energy level is sharp for these field directions. The application of the magnetic field in these directions enhances the two dimensionality of the system and that gives rise to the increase of the magnetoresistance. An important point is that the analysis of the oscillation allows us to reconstruct the Fermi surface of the electron. For a square like Fermi surface, we have obtained the peak positions as in Fig.8. This figure represents the experimental results given in eq.(1) at least qualitatively.

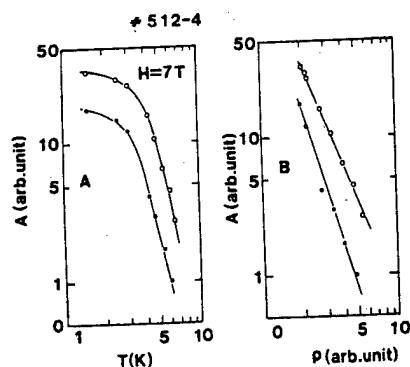


Fig. 7. (A) Temperature dependence of the amplitude A of the oscillation. The indexes of the oscillation for the curves are 3 and 4. (B) A replot of the data in (A). Here, the data are plotted against the zero field resistivity ρ_0 .

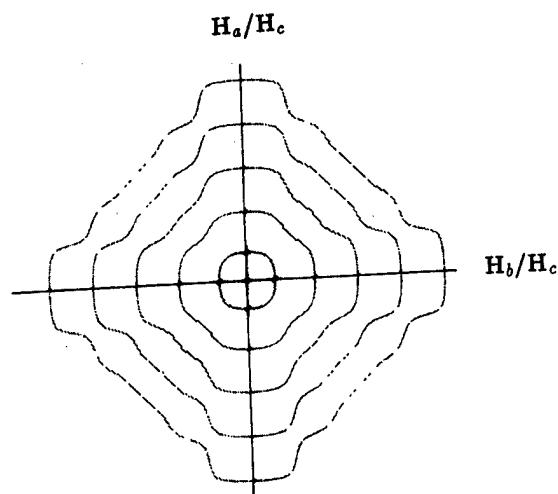


Fig.8 The positions of peak of the magnetoresistance calculated for a square Fermi surface.

Another problem is the low field anomaly of the magnetoresistance. Is the origin of the phenomena is the same with that of the high field oscillation? There are some similarities among these two. Both of them is independent of the direction of the electric current. They are determined by the direction of the magnetic field. Both of them are very sensitive to the temperature and they depend on temperature through the change of the resistivity. These points make us to expect that they come out of the same origin. We already knows that the magnetoresistance oscillation is characteristic to electron systems with two dimensional nature together with weak three dimensionality. We postulate that the low field anomaly of the magnetoresistance effect also comes out of the weak three dimensionality in two dimensional electrons system. Recently, a theory appeared which tells that in such electron systems, the magnetoresistance in the magnetic field parallel to the two dimensional plane is larger than that in the direction normal to it.

REFERENCES

- [1] K.Kajita et al, *solid state commun.* **64** 1279(1987).
- [2] K.Kajita et al, *solid state commun.* **70** 1181(1989).
- [3] K.Kajita et al, *solid state commun.* **70** 1189(1989).
- [4] M.V.Kartsovnik et al, *JETP Lett.* **48** 541(1988).
- [5] T.Osada et al, in *Proceedings of ISSP ISOS* (1990).
- [6] K.Yamaji, *J. Phys. Soc. Jpn.* **58** 1520(1989).

N. Toyota

Institute for Materials Research, Tohoku University, Katahira 2-1-1, Sendai 980, Japan

We report on the recent studies on (BEDT-TTF)-based organic superconductors, which have been made at IMR in the 1989 fiscal year. Three topics will be outlined in focus on the problems still unsettled. (For the details and full literatures, see the original paper.)

1. Magnetoresistance and Shubnikov-de Haas effect in β -(BEDT-TTF)₂IBr₂

T. Sasaki, N. Toyota, T. Fukase, K. Murata, M. Tokumoto and H. Anzai

to be published in Proceedings of The First ISSP Symposium on the Physics and Chemistry of Organic Superconductors (Springer-Verlag, 1990)

The angular dependence of the magnetoresistance and the Shubnikov-de Haas effect have been measured on β -(BEDT-TTF)₂IBr₂ ($T_c=2.3K$, $RRR=1500$) at ambient pressure. This study is based on an extension experiment to the previous observations^{1, 2)} of SdH quantum oscillations in this material and other related organic superconductors. Figure 1 shows the angular dependence of the magnetoresistance at 1.7K in a b^*-c^* plane. The magnetoresistance takes a minimum when the field is applied near the c^* -direction, being normal to the layered plane. The data reveal a weakly oscillatory behavior as a function of the angle, which are, as shown in the figure, superposed on the background magnetoresistance. The peak positions are periodic in $\tan\theta$, where θ is the angle between the resistance minimum direction and the applied field. This phenomenon has been originally discovered by Kajita and his collaborators³⁾ in θ -(BEDT-TTF)₂I₃ and explained by the Yamaji's model⁴⁾ that all the cross-sectional area enclosed by the cyclotron orbits on the slightly warped cylindrical Fermi surface will be completely equal to each other when the field is applied along some directions tilted from the cylinder axis. (For details, refer to Kajita's report.) For the present system, this model reproducing $\tan\theta$ -periodicity results in $S_{FS} \approx 0.3S_{BZ}$, where $S_{FS}(S_{BZ})$ is a cross-sectional area in the basal plane of the Fermi surface (the first Brillouin zone). This prediction is in well agreement with $S_{FS} \approx 0.28S_{BZ}$ determined from SdH observations. This new phenomenon has been already observed by Kartsovnik et al.⁵⁾ who obtained $S_{FS} \approx 0.5S_{BZ}$ (half filled), being almost twice larger than the present result. It is noted here that their single crystals with $RRR=2000-3000$ and $T_c=2.8K$ seems to be of higher quality than ours. For the large difference in not only S_{FS} , but also in-plane cyclotron mass $m_c(\approx 0.5m_0$ for us, and $\approx 5m_0$ for them), we have reached a question as to whether our single crystals might undergo a structural modulation like an incommensurate superstructure observed in an iso-structural β -(BEDT-TTF)₂I₃. The detailed x-ray diffraction measurements by Kagoshima, however, has revealed no positive sign for such a structural change down to helium temperature. The problem still stands over to be clarified in future.

1. K. Murata et al, J. Phys. Soc. Jpn. **57** (1988) 1540
2. N. Toyota et al, J. Phys. Soc. Jpn. **57** (1988) 2616
3. K. Kajita et al, Solid State Commun. **70** (1989) 1189
4. K. Yamaji, J. Phys. Soc. Jpn. **58** (1989) 1520
5. M. V. Kartsovnik et al, JETP Lett. **48** (1988) 541

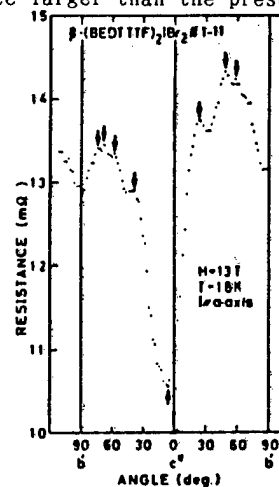


Fig. 1

I. Critical Field Anisotropy in "2K-Superconducting State" of Organic Superconductor β -(BEDT-TTF) $_2$ I $_3$

T. Sasaki, N. Toyota, M. Hasumi, T. Osada, S. Kagoshima, H. Anzai, M. Tokumoto and N. Kinoshita,
J. Phys. Soc. Jpn. **58** (1989) 3477 and *ibid.* in I.

The title compound undergoes a superconducting transition at 1.1-1.5 K at ambient pressure. However, if the sample is cooled from room temperature under small pressure of about 1 kbar, the T_c jumps to 7-8 K which is so called the high- T_c state.¹⁾ It has been revealed that an incommensurate superstructure develops below 175 K at ambient pressure.²⁾ The development of the superstructure makes the terminal ethylene groups of the BEDT-TTF molecules disordered. The pressure easily suppresses the superstructure and also the associated disordering, which could be responsible for the high- T_c state. Recently Kagoshima and his collaborators³⁾ have found that, even at ambient pressure, the superstructure becomes unstable below about 110 K and the wave-vector Q characterizing the superstructure changes from 0.27 to 0.24 Å by keeping the sample at 110 K for 20-40 hours. Thus an annealed sample exhibits successive superconducting transitions at 7-8 and 2 K, these of which show, respectively, the incomplete and complete Meissner effect. Since the annealing-induced increase of bulk T_c from 1.1-1.5 to 2.0 K is reproducibly observed, this phenomenon can be intrinsic and might be deeply related with the change in superstructure. The present paper concerns the effects of annealing on the resistivity and superconducting upper critical field H_{c2} in the 2K-state.

Figure 1 shows the logarithmic plot of the temperature dependence of the resistance. During annealing at 109 K for 120 hours, the resistance decreases by about 8 % and exhibits a saturation. On cooling after this annealing, the temperature dependence becomes equal to that without annealing, except that two superconducting transitions appear at 7-8 and 2 K. Table I lists up the GL coherence length for the in-plane (ℓ) and inter-plane (ℓ) order-parameters, and the anisotropy of H_{c2} , for both states. Parameters in the pressurized states⁴⁾ are also included. The most significant change by annealing is found in the increase of $H_{c2\perp}$, associating the 30 % decrease in an H_{c2} -anisotropy which results in the in-plane coherence length with the inter-plane one unchanged. It is noted that the T_c , anisotropic coherence-length and H_{c2} are comparable in magnitude to those of pressurized states at 3.5-5.0 kbar. This suggests that the 2K-state might be understood by the "lattice pressure" model.⁵⁾ Taking into account that the in-plane coherence length is inversely proportional to the square root of the in-plane transport mass, our results indicate a significant enhancement of the density of states at the Fermi-level. This is favorable to an increase of T_c . Table I leads us to the empirical rule in the present system that the increase of T_c associates a decrease of an H_{c2} -anisotropy.

Finally, although the transport mass is not necessarily equal to the cyclotron mass, they are interrelated each other. The big difference in the in-plane cyclotron mass of $0.5m_0$ in low- T_c state⁶⁾ and $4.5m_0$ in high- T_c state⁷⁾ is already revealed. The important question remains: *whether a continuous change in the cyclotron mass will occur or not in the intermediate states between these states.* For the pressurized states, Murata and his collaborators are extensively studying the SdH oscillations, while, for the 2K-state, we will try again to observe SdH oscillations.

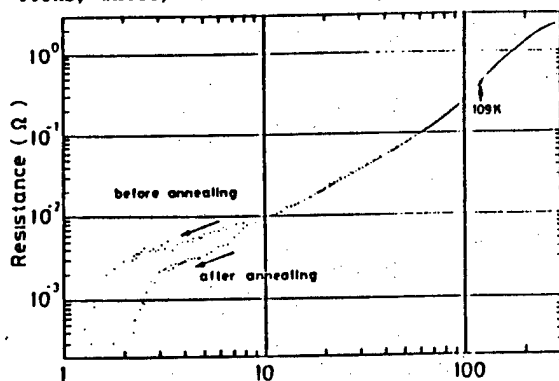


Figure 1 Temperature (K)

Table I

	T_c (K)	P (kbar)	$\xi_{GL\parallel}(0)$ (Å)	$\xi_{GL\perp}(0)$ (Å)	$H_{c2\parallel}/H_{c2\perp}$
Before annealing state	1.40	0	508.5	24.3	20.9
After annealing state	2.08	0	354.6	24.5	14.5
Pressurized state	6.55	1.6	131	10	13.1
	3.06	3.5	355	22.7	15.7
	2.18	5	488	31	15.6

1. K. Murata et al, J. Phys. Soc. Jpn. **54** (1985) 1236 and V.N. Laukhin et al, JETP Lett. **41** (1985) 81
2. T.J. Emge et al, Phys. Rev. **B30** (1984) 6780 and for recent review, S. Kagoshima and Y. Nogami, Research Report on New Superconducting Materials and High Temperature Oxide Superconductors (1984-1987) p.171
3. S. Kagoshima et al, Solid State Commun. **69** (1989) 1171 and **71** (1989) 843, and Y. Nogami et al, J. Phys. Soc. Jpn. **59** No.1 (1990)
4. K. Murata et al, Synth. Metals **19** (1987) 151
5. M. Tokumoto et al, Synth. Metals **13** (1986) 9
6. N. Toyota et al, ref.2 in 1
7. W. Kang et al, Phys. Rev. Lett. **62** (1989) 2559

II. Evidence of Many-Body Renormalizations in Some Organic Conductors

N. Toyota, E.W. Fenton, T. Sasaki and M. Tachiki

Solid State Commun. **72** (1989) 859 and ibid in 1

One of the recent progress in research fields of organic superconductors is a success in detecting SdH quantum oscillations in (BEDT-TTF)-based salts. Hence reliable informations on the electronic states near the Fermi level such as a Fermi surface (FS), cyclotron mass m_c and Dingle temperature $T_D = \hbar / (2\pi)^2 k_B \tau$, where τ is an electron life-time, have become available from these measurements. The FS in β -(BEDT-TTF)₂I₃ without superstructure (high- T_c state; see I.)¹⁾ is a little warped cylinder occupying almost 50% area (a half-filling) of S_{BZ} , while that with a superstructure (low- T_c state)²⁾ occupies 25-30% (almost a quarter-filling) of S_{BZ} . (For β -(BEDT-TTF)IBr₂, the consensus is not yet reached, as described in I.) The band-structure calculations³⁾ based on a two-dimensional tight binding approximation for the overlapping $p(\pi)$ molecular orbitals had predicted a single hole-band with half-filled for a β -phased salt without any lattice modulation. In the meantime, κ -(BEDT-TTF)₂Cu(NCS)₂, which has so far the highest T_c among organic salts, has a little warped cylindrical FS with $S_{FS} = 16\text{-}20\%$ of S_{BZ} .⁴⁻⁶⁾ This is reasonably assigned to be a lens-like closed orbit for holes centered at Z-point, expected from the band-structure calculations.⁴⁾ Figure 1 shows the band-structures calculated for this κ -phased salt.⁷⁾ As shown in this figure, another orbit for electrons is also expected to be open along the $Y-M$ (c^*) direction. Recently Muller et al⁷⁾ have observed a magnetic breakdown to occur across the small energy gap on a $M-Z$ line between these close and open orbits. This experiment gives a strong support to the band-structure calculations. It can be concluded that rather simple band-structure calculations could well reproduce the topology of FS in these salts.

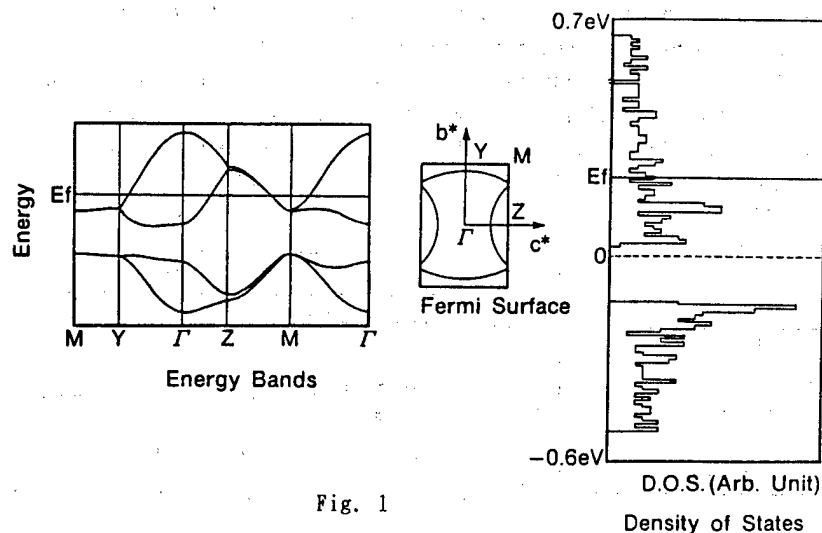


Fig. 1

Figure 2 shows a logarithmic plot of the ratio, m_c/m_0 , versus T_D . The straight lines give the necessary condition for the quantum oscillations to be observable at specified magnetic inductions B , i.e., $\omega_c \tau \geq 1$, where $\omega_c = eB/m_c c$ is a cyclotron frequency. From this figure, it is recognized that the data could be categorized into two groups: the light-mass (less than $0.5m_0$) and high- T_D (several to 10 K); the heavy-mass ($(2-5)m_0$) and low- T_D (less than 1 K). Roughly speaking, the product $m_c T_D$ is nearly constant in a variety of materials and states. To investigate further this systematic, we have analyzed the mean free path $l = v_F \tau$ by use of only SDH parameters for the light-mass group, β -(BEDT-TTF)₂I₃ (low- T_D state) and β -(BEDT-TTF)₂IBr₂, and for the heavy-mass group, κ -(BEDT-TTF)₂Cu(NCS)₂. We find that all three salts have nearly the same magnitude of l which about 1000 Å. As will be proven later, l defined by $v_F \tau$ is a good measure for the quality of a crystal. Therefore the degree of purity of the crystals belonging to different groups must be almost the same. This is also supported by the fact that the residual resistivity ρ_0 and RRR exhibit only minor difference among these salts. The reason why T_D is obtained so low in the heavy-mass group might be simply understood in terms of a classical picture that a slowly moving electron with a heavy mass is scattered by fixed impurities with less probability than a light-mass electron.

The question concerns an origin of the heavy mass: Whether is it ascribed to either a purely band effect or many-body renormalizations? The former possibility might be excluded, since the band-structure calculations, which can reliably reproduce the observed FSs of κ -(BEDT-TTF)₂Cu(NCS)₂ and β -(BEDT-TTF)₂I₃, result in too wide a band-width (0.5-0.7 eV), correspondingly too small a band-mass (about $1m_0$ at most) to explain the measurements. We have pointed out that just this discrepancy in m_c and the agreement of the FS-topology between experiments and calculations could be a direct evidence of the many-body renormalizations in these materials. Therefore we might conclude that these materials are of highly correlated Fermi liquid which satisfies the Luttinger's theorem that the volume enclosed by FS in momentum space is unaffected by the many-body interactions, but the effective mass is enhanced. The essential point of the renormalization theory is that any many-body interaction necessarily leads to the quasi-particle states with the renormalized mass $m = Zm_b$ and life-time⁹⁾ $\tau = Z\tau_b$, where Z is a renormalization constant defined as $1 - \delta\Sigma/\delta(i\omega) \geq 1$ (Σ is a self-energy), m_b is a bandmass and τ_b a bare, unrenormalized life-time.

As have been established in an electron-phonon interaction, many-body interaction enhances the cyclotron mass which enters into the temperature damping factor in the Lifshitz-Kosevich formulation, but it does not affect the mass which enters into the Dingle factor. If this complication is ignored, as is usually done (data in Fig.2) because of difficulty in determining Z , then the bare life-time, which is a good measure for the degree of purity of a crystal, is related to the deduced τ : $\tau_b = \tau/Z$. Thus will be disclosed the above-mentioned "trick" on too small T_D in the renormalized group.

The remaining question is: what is a many-body interaction exerted in the organic conductors? If we take the band mass $m_b \approx 1m_0$, we find $Z \approx 3-4$. For this large Z , we have proposed that Coulomb correlations of the extended Hubbard model might be important, especially in a dimerized system as κ -(BEDT-TTF)₂Cu(NCS)₂.

Similar suggestions have been made independently by Oxford group.⁶⁾ They have estimated the on-site Coulomb interaction $U \approx 1.3$ eV and the inter-site one $V = 0.2-0.5$ eV, the latter of which might be expected to be largest for the neighboring molecule with the largest transfer integral: in this material, the other half of the dimer will be a dominant neighboring site.

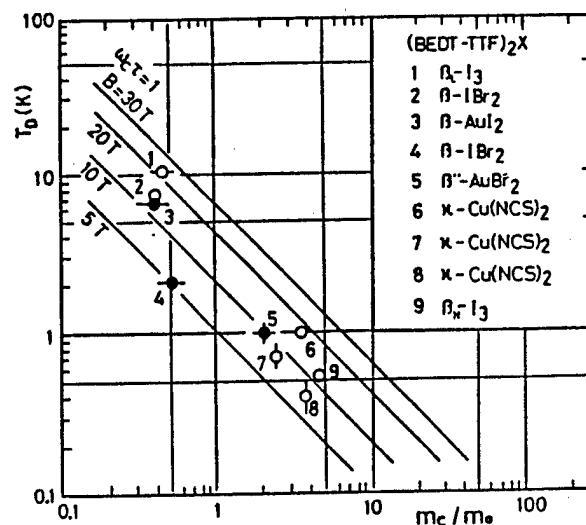


Fig. 2

Finally, the temperature- and field-dependence of the quantum oscillations observed in these organic conductors are consistent with the predictions from Lifshitz-Kosevich theory based on the independent particle model. And band structure calculations well reproduce the FS-topology, but fails to explain the observed heavy-mass. Therefore we are lead to the conclusion that the Luttinger's theorem -- a Fermi-liquid picture -- could hold in the present organics. It is quite surprizing that these theories could still hold, no matter how highly the electrons correlate each other. Similar surprise has already been accumulated in Heavy-Fermion business and will probably be put in High- T_c oxides.

1. W.Kang et al, ref.7 in I.
2. K.Murata et al, and N.Toyota et al, refs. 1 and 2 in I.
3. T.Mori et al, Chem. Lett. 1984 (1984) 957
4. K.Oshima et al, Phys. Rev. B38 (1988) 939
5. N.Toyota et al, ref.2 in I
6. F.L.Pratt et al, to be published in J. Phys. Condes. Matter
7. H.Kusuhara et al, submitted to Solid State Commun.
8. M.Muller et al, ibid. in I
9. M.Tachiki and S.Maekawa, Phys. Rev. B29 (1984) 2497

The present studies have been made in collaboration with a doctor student, T. Sasaki (IMR), Prof. Kagoshima, Dr. T. Osada and a doctor student M. Hasumi (University of Tokyo), Dr. H. Anzai, M. Tokumoto, and Dr. N. Kinoshita (ETL), Prof. T. Fukase, Prof. M. Tachiki (IMR) and Dr. E. W. Fenton (NRC-Canada). I would like to sincerely thank these scientists for making their efforts and letting us enjoying the physics concerned, and Prof. Y. Muto for his distinguished leadership of the Project. These works were supported in part by Grant-in-Aid for Special Project Research from the Ministry of Education, Science and Culture of Japan.

Superconducting and Normal State Properties of Organic Metals (BEDT-TTF)₂X

Madoka Tokumoto, Nobumori Kinoshita, Keizo Murata, Hiroshi Bando,

Kunihiko Yamaji and Hiroyuki Anzai

Electrotechnical Laboratory, 1-1-4 Umezono, Tsukuba, Ibaraki 305

Recent progress in the superconducting and normal state properties of BEDT-TTF based organic metals, including β -(BEDT-TTF)₂X and κ -(BEDT-TTF)₂Cu(NCS)₂, are presented. In addition to the low- and high- T_c states, with $T_c=1$ K and 8 K, respectively, a new superconducting state with $T_c=2$ K was found in β -(BEDT-TTF)₂I₃. DC Hall effect of the low- T_c state of β -(BEDT-TTF)₂I₃ has been studied. Tunneling spectroscopy on κ -(BEDT-TTF)₂Cu(NCS)₂ single crystals by a low-temperature scanning tunneling microscope (STM) is reported. In addition to the Shubnikov-de Haas and de Haas-van Alphen effects, a new oscillatory phenomenon, discovered in the angular dependence of magnetoresistance in β -(BEDT-TTF)₂IBr₂ and θ -(BEDT-TTF)₂I₃, is shown to be a new powerful tool to study Fermi surfaces of quasi two-dimensional electronic systems.

1. Introduction

Superconductivity of BEDT-TTF based organic metals has been found to be quite sensitive to defects, disorders and impurities. In quasi-one dimensional metals, such as (TMTSF)₂X, the conduction path of electrons along the stacking donors can be seriously disturbed by the presence of defects or disorder. However, in two-dimensional system like BEDT-TTF salts, electronic conduction path forms a two-dimensional network so that the presence of point defects cannot cause a serious effect on the electrical conduction. Therefore it is not obvious why the superconductivity of BEDT-TTF based organic metals are so sensitive to the presence of non-magnetic impurities and defects. Two outstanding characteristics of the BEDT-TTF based organic superconductors, i.e. superconductivity at ambient-pressure and relatively high- T_c , are advantageous features for an extensive and quantitative study of superconducting properties in these organic metals.

In this paper we report on recent progress made at Electrotechnical Laboratory in the study of the superconducting and normal state properties of organic superconductors (BEDT-TTF)₂X.

2. Correlation between T_c and Resistivity in β -(BEDT-TTF)₂X[24,25]

First, we show some typical examples where superconducting transition temperature (T_c) and resistivity seems to be closely related with each other in β -(BEDT-TTF)₂X, which forms an isostructural family of organic metals. An important structural feature of β -(BEDT-TTF)₂I₃ is an incommensurate lattice modulation[1], which appears

below 175K at ambient pressure. The presence of this incommensurate superstructure is considered to suppress its T_c from 8.1 K to 1.1-1.5 K. Another important feature in β -(BEDT-TTF) $_2$ I $_3$ is the presence of disordered ethylene group as designated as A-type vs. B-type[2] (or staggered vs. eclipsed[3]) at one end of the molecule and the ordered group at the opposite end. The latter additional structural disorder can possibly be eliminated, as was confirmed in β -(BEDT-TTF) $_2$ IBr $_2$ and β -(BEDT-TTF) $_2$ I $_2$ Br[4], where the former superstructure is also absent.

The best example which demonstrates a high correlation between T_c and resistivity is seen in β -(BEDT-TTF) $_2$ trihalide mixed crystal system. The substitution of anions in β -(BEDT-TTF) $_2$ I $_3$ was found to produce a series of isostructural crystals of β -(BEDT-TTF) $_2$ X. Complete substitution of I $_3$ with IBr $_2$ [5] and AuI $_2$ [6] was found to suppress the incommensurate superstructure and realized the high- T_c state in β -(BEDT-TTF) $_2$ X. However, substitution of I $_3$ with asymmetric anion I $_2$ Br[7] did not give a superconductivity[8] although the "lattice pressure" model[8] predicted higher T_c and both the incommensurate superstructure and the disorder of the ethylene group were missing[4]. Partial substitution of anions corresponds to alloying in metals. It was found that we can prepare β -(BEDT-TTF) $_2$ trihalide mixed crystals, namely β -(BEDT-TTF) $_2$ (I $_3$) $_{1-x}$ (IBr $_2$) $_x$, β -(BEDT-TTF) $_2$ (IBr $_2$) $_{1-x}$ (I $_2$ Br) $_x$ and β -(BEDT-TTF) $_2$ (I $_2$ Br) $_{1-x}$ (I $_3$) $_x$, for a wide composition range[9]. Temperature dependence of electrical resistance in these β -(BEDT-TTF) $_2$ trihalide mixed-anion crystals indicates that the mixed crystals of β -(BEDT-TTF) $_2$ -trihalides constitute a clean alloy system, where the scattering of conduction electrons are predominantly due to phonons at temperatures above around 100 K even in high concentration (1:1) mixed crystals. The effect of alloying on the resistivity appears as a difference in the residual resistance ratio or residual resistivity at very low temperatures. From the residual conductivity(σ_R), which is inverse of residual resistivity, and T_c in β -(BEDT-TTF) $_2$ trihalide mixed crystals, we can see a clear correlation between T_c and residual conductivity(σ_R) for a wide range of composition[10], that is, as we increase the amount of substituent(x or $1-x$), the residual conductivity decreases and the T_c decreases accordingly. Another interesting feature is the presence of a clear boundary, at σ_R =6000 S/cm, between the superconducting and non-superconducting samples, indicating the presence of *minimum conductivity* (6000 S/cm) required for realization of superconductivity in this system[11]. This value obtained from the above experimental results was found to be in fair agreement with a theoretical estimation based on the weak localization effect[12]. Also, this empirical rule explains why β -(BEDT-TTF) $_2$ I $_2$ Br does not show superconductivity.

The second example which shows a correlation between T_c and resistivity is β -(BEDT-TTF) $_2$ I $_3$ itself in which two superconducting states are known to exist at ambient pressure, i.e. the low- T_c state (T_c =1.1-1.5K) and the high- T_c state (T_c =7-8K). The difference between the two states is considered to be the *incommensurate lattice modulation*[1] which appears below 175K, where temperature dependence of resistance changes its slope or derivative[11,13]. Figure 1(a) shows a temperature dependence of resistance(R), and Figure 1(b) shows a temperature derivative of resistance(dR/dT) of β -(BEDT-TTF) $_2$ I $_3$. At 175 K a crossover between the crystal structures with and without the incommensurate lattice modulation takes place. The former(β_L) is stable at lower temperature while the latter(β_H) is stable at higher temperature. And from Fig. 1(a), β_L state with the incommensurate superstructure seems to have higher resistance than β_H state without the superstructure at temperatures below 175 K.

The high- T_c state without the incommensurate superstructure(β_H) can be realized by releasing the pressure at low temperature after cooling under pressure[14,15]. A

more direct difference in resistivity between β_H and β_L states were reported by Hamzic et al.[13] in which they observed an abrupt resistance increase due to a first order structural phase transition from the metastable β_H state to β_L state when the β_H sample was warmed up to about 130 K, although they do not mention the difference in residual resistivity at low temperature. A difference in residual resistivity at low temperature between the two states was reported by Ginodman et al.[16]. The result shows that the resistivity of metastable β_H state is much lower than that in β_L state at low temperatures, indicating that correlation between T_c and residual resistivity also holds in this case.

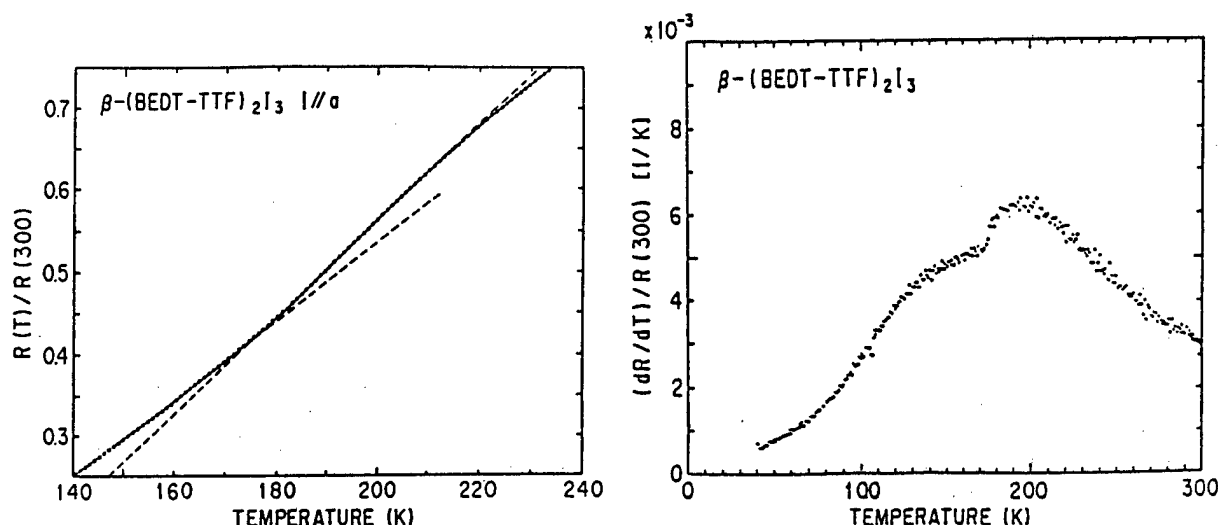


Fig. 1. (a) (left) Temperature dependence of resistance(R) of β -(BEDT-TTF) $_2$ I $_3$.
(b) (right) Temperature dependence of dR/dT of β -(BEDT-TTF) $_2$ I $_3$.

3. DC Hall Effect of the Low- T_c state of β -(BEDT-TTF) $_2$ I $_3$ [26]

The Hall effect was studied in β -(BEDT-TTF) $_2$ I $_3$ in order to survey the problem of the low- T_c and the high- T_c states and the general interest to the Fermi surface of this material. i) Our measurement revealed that this material is a metal with almost constant hole numbers down to 20 K. By the estimate of $R_H = 1/nec$, the hole number seems to be less than one per unit cell. ii) In the temperature dependence of R_H in detail, we found a pronounced stepwise decrease by 8 % in Hall voltage when temperature is lowered through 175 K but not through 110 K. iii) Further, below 20 K, Hall voltage was found to decrease.

As shown in the inset of Fig. 2, the current terminals were placed at both ends in full width to achieve a uniform current along the a -axis. The Hall voltage was taken by the difference in voltage in fields between + and - 5 T during cooling. Part of the results are shown in Fig. 2. Figure 3 shows the temperature dependence of the Hall voltage, which is the difference between 5 T and -5 T. Two distinct transitions are noticeable. One is a stepwise decrease in R_H below 175 K. The other one is depicted by the sudden start of decrease in the Hall voltage below 20 K.

The absolute value of the Hall coefficient of β -(BEDT-TTF) $_2$ I $_3$ is consistent with the crude model of metals, which consists of one electron charge transfer from two BEDT-TTF molecules to one I $_3$. However, upon more precise examination, the absolute value of the apparent carrier number itself seems to be smaller than 1 per unit cell. By

lowering temperature through 175 K, where the structural transition takes place, the Hall coefficient decreases by 8 % in a stepwise way. This result proved that the 175 K transition is accompanied by a transition in the electronic state. The decrease in Hall coefficient is contradictory to the suppression of T_c from 8 K to 1 K, if we recognize the difference of the high- T_c and low- T_c states as a difference of the density of states and if the association of carrier number with density of states is allowed. At temperatures below 20 K, the Hall coefficient starts to decrease significantly. The possibility of a fluctuating phase below 20 K is proposed.

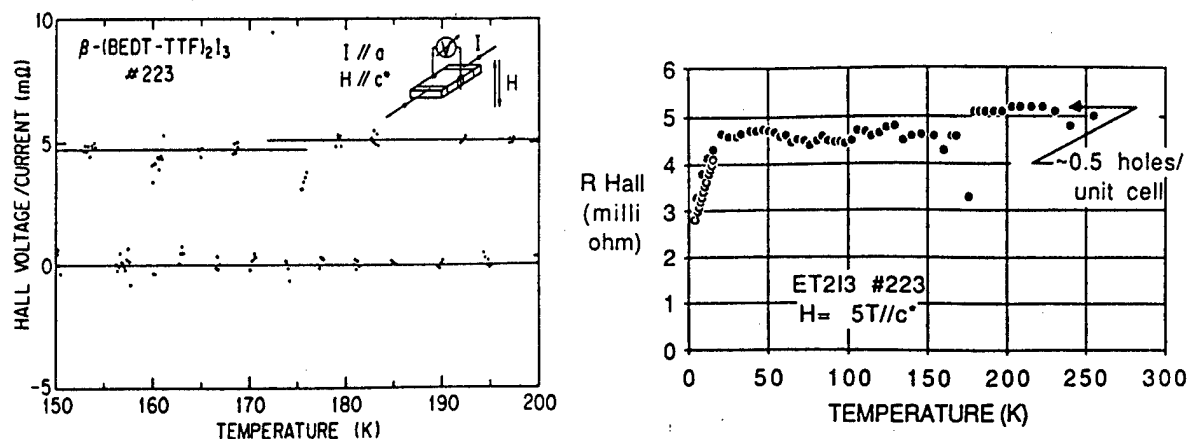


Fig. 2(left) Hall voltage/current of β -(BEDT-TTF) $_2$ I $_3$ as a function of temperature. The difference in the vertical scale between the higher dots (in field of 5 T) and the lower dots (in fields of -5 T) is the Hall voltage signal. Inset shows the configuration of current and fields. The value above 175 K corresponds to 0.50 ± 0.05 holes per unit cell for this sample, when $n = 1/R_{Hec}$ is used.

Fig. 3(right) Hall coefficient, R_H , of β -(BEDT-TTF) $_2$ I $_3$ as a function of temperature. Stepwise reduction of R_H through 175 K, and steep decrease below 20 K are significant. Closed circles were taken by reversing fields during cooling. Open circles are the difference in R_{xy} voltage between those at 5 T and -5 T of the temperature sweep.

4. 2 K Superconducting State in β -(BEDT-TTF) $_2$ I $_3$ [19,25]

Recently, annealing at about 110 K was found to result in a change of the incommensurate superstructure[17]. It was also found that a new superconducting state with $T_c = 2$ K appears as a result of annealing[18,19], although its origin or structural difference responsible to the change of T_c has not been identified yet. Annealing at 110 K is also accompanied by a decrease in resistance in addition to the change of incommensurate superstructure and appearance of the 2 K state. Fig. 4. shows time dependence of resistance (i/c^*) of β -(BEDT-TTF) $_2$ I $_3$ due to annealing. The resistance decrease by as much as 10%, indicating that the new 2 K state has lower resistivity than the original low- T_c state. Fig. 5. shows temperature dependence of resistance of β -(BEDT-TTF) $_2$ I $_3$ before(.....) and after annealing(---). A vertical line at 106 K in the figure indicates the decrease in resistance by annealing. This annealed 2 K state with lower resistance is also metastable, and gradually goes back to the

original low- T_c (1.1-1.5 K) state with higher resistance when the sample is warmed up to about 120 K as seen in Fig. 5.

Now, what about the residual resistance at low temperature? Surprisingly, the temperature dependence of resistance in Fig. 5 shows that the difference in the resistance between the two states, which is as much as 10% at around 100 K, completely disappears as temperature goes down to below 40 K. More or less the same temperature dependence was observed for resistance with current flowing parallel to the conducting plane (i//a) [20]. It is, however, consistent with the ESR linewidth result as shown in Fig. 6. It is well known that structural disorder in β -(BEDT-TTF) $_2$ X provides an additional scattering mechanism for the carriers which increases the residual (low-temperature) ESR linewidth [21]. It is also reported that in β -(BEDT-TTF) $_2$ I $_3$, the linewidth in β_H state is much narrower than that of β_L state [22]. Figure 6 indicates that annealing at 100 K causes an appreciable decrease of the ESR linewidth at high temperature, but the reduction of linewidth due to annealing is much smaller at low temperatures, in contrast to the case of high- T_c (8 K) state [22]. These observations seem to indicate that the change of T_c is not accompanied by the change of the low-temperature residual resistance, or scattering, in the case of 2 K superconducting state. These results suggest that we must look for other reasons which can be related to the change of T_c in this case. The reduction of the critical field anisotropy in 2 K state [20] could give us a clue to obtain a better understanding of the effect of annealing. The anisotropy of H_{c2} , $H_{c2\parallel}/H_{c2\perp}$, is reported to show a significant decrease from 20.9 to 14.5, caused by annealing [23].

It has been found by recent magnetization measurement that an extended annealing at about 110 K results in appearance of appreciable amount of the "high- T_c " state with $T_c=7.5$ K, while the bulk 2 K state gradually loses its volume fraction [19]. Figure 7 shows annealing conditions, i.e. annealing temperature (T_a) and annealing time, for each step of annealing. The effect of annealing performed in 17 steps in total can be classified into three stages. In the first stage, i.e. steps 1 through 7 where $107\text{ K} \leq T_a \leq 111\text{ K}$, we observed coexistence of two superconducting states with

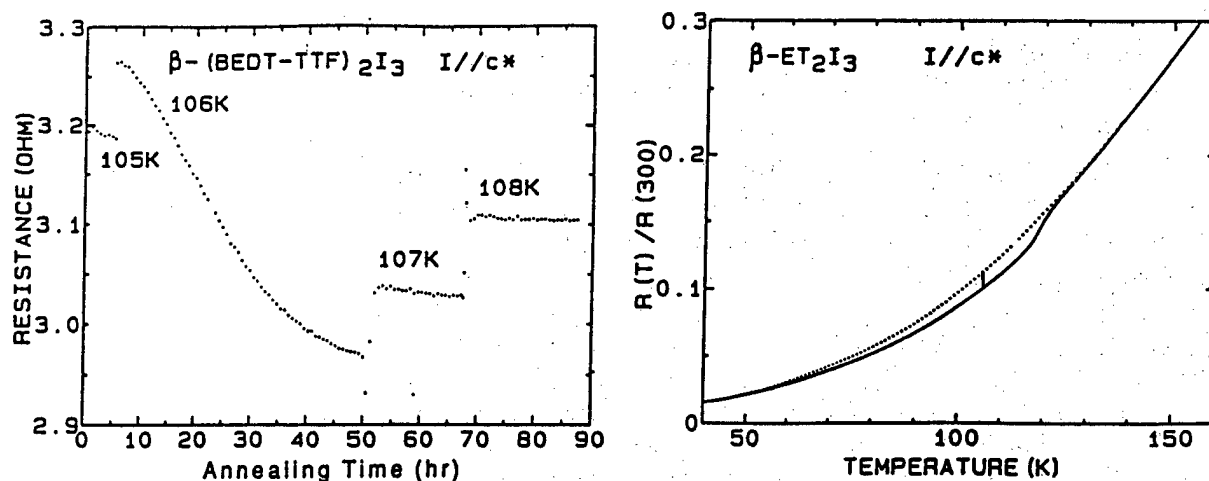


Fig. 4(left) Time dependence of resistance (i//c*) of β -(BEDT-TTF) $_2$ I $_3$ due to annealing.
 Fig. 5(right) Temperature dependence of resistance of β -(BEDT-TTF) $_2$ I $_3$ before (.....) and after annealing (---). A vertical line at 106 K in the figure indicates the decrease in resistance by annealing.

$T_c=2\text{ K}$ and 7.5 K , as shown in Fig. 8. The diamagnetic shielding of the 2 K state is quite large ($\sim 1.3 \times 10^{-1}\text{ emu/g}\cdot\text{Oe}$) corresponding to the whole sample volume. In the second stage, i.e. steps 8 through 12 where $112\text{ K} \leq T_a \leq 118\text{ K}$, we observed only the 7.5 K state as shown in Fig. 9. In the third stage, i.e. steps 13 through 17, where $120\text{ K} \leq T_a \leq 126\text{ K}$, further annealing started to ruin the 7.5 K state and decrease the superconducting volume fraction without appreciable decrease in T_c . The structural difference between these superconducting states with different T_c has not been clarified yet, and needs further study on the superstructure and ethylene ordering.

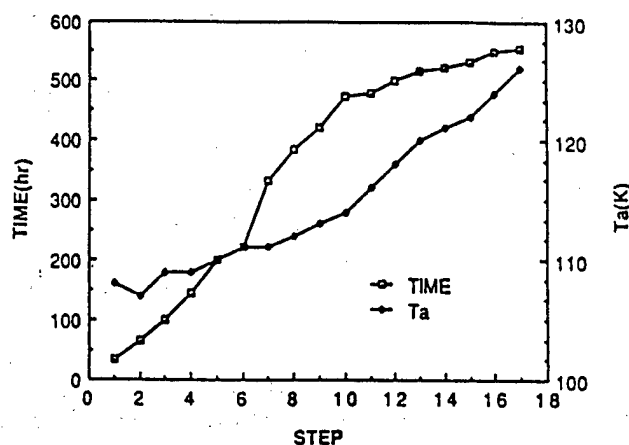
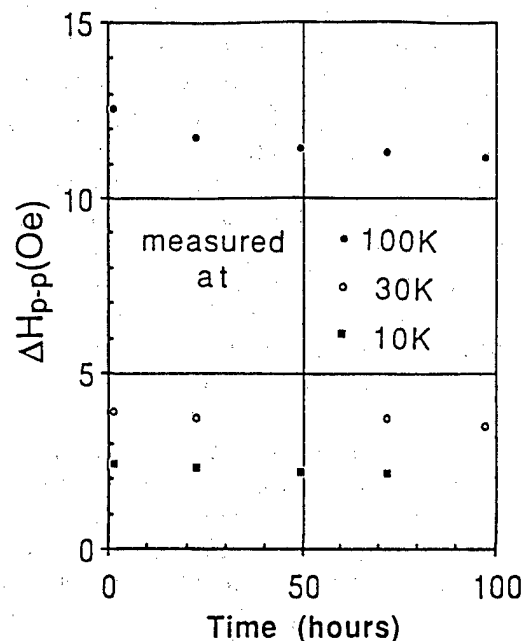


Fig. 6(left) Peak-to-peak ESR linewidth versus annealing time at 100 K and at low temperatures after each annealing process at 100 K .

Fig. 7(right) Annealing Temperature (T_a) and annealing time for each step.

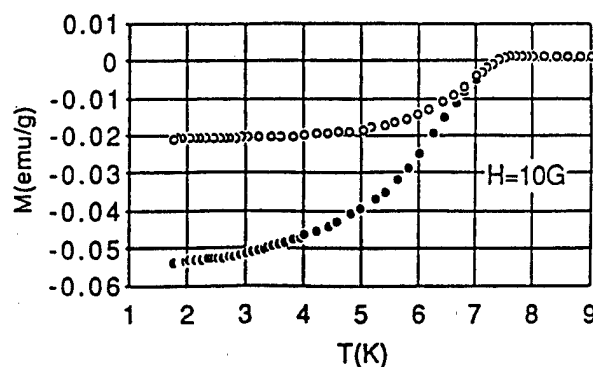
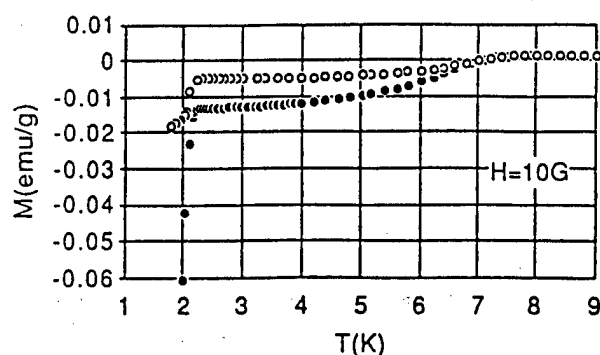


Fig. 8(left) Diamagnetic shielding (●) and Meissner effect (○) after the annealing of step 5 ($T_a=110\text{ K}$) in stage 1.

Fig. 9(right) Diamagnetic shielding (●) and Meissner effect (○) after the annealing of step 8 ($T_a=112\text{ K}$) in stage 2.

5. STM Measurements of Superconducting Properties in κ -(BEDT-TTF)₂Cu(NCS)₂[27,28]

Tunneling spectroscopy on κ -(BEDT-TTF)₂Cu(NCS)₂ single crystals by a low-temperature scanning tunneling microscope (STM) was studied. The superconducting gap at 1.9 K, estimated from Fig. 10, was $2\Delta = 4.8 \pm 1.1$ meV. Both its magnitude and temperature dependence, as shown in Fig. 11, were consistent with the BCS theory. However, the line shape of dI/dV - V characteristics deviated from the BCS theory, indicating some distribution in the energy gap magnitude. We suppose it is possible to interpret the previously reported results of tunneling spectroscopy[29,30] if they sensed subsets of the distribution according to the configurations.

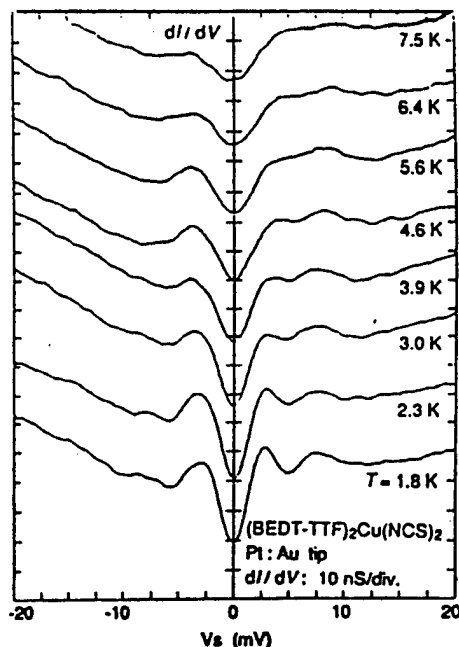
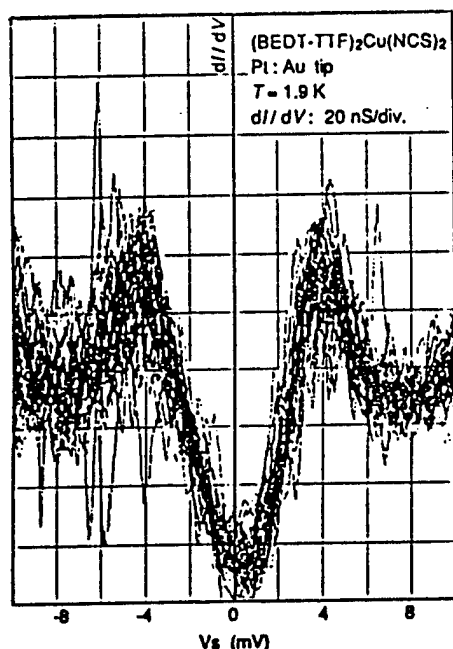


Fig. 10(left) Differential conductance measured at 1.9 K. Traces of dI/dV - V characteristics of 60 continuous sweeps were plotted.
Fig. 11(right) Temperature dependence of differential conductance.

6. Angle-Dependence of Magnetoresistance in Organic Superconductors[33,35]

The newly discovered angle-dependent oscillation of magnetoresistance in the β -(BEDT-TTF)₂IBr₂ [31] and θ -(BEDT-TTF)₂I₃ [32] has been found to arise from a nearly complete discretization of Landau levels or two-dimensionalization of Landau level distribution in the vicinity of the Fermi energy. This feature occurs since the Landau levels lose the dependence on the wave number, determined only by the Landau quantum number. This is shown by a semiclassical argument to occur at special angles for a weakly corrugated cylinder form of Fermi surface, as shown in Fig. 12. These angles are approximately given by

$$ck_F \tan \phi = \pi(n - 1/4), \quad n = 1, 2, 3, \dots \quad (1)$$

where ϕ defines the angle by which the applied magnetic field is tilted from the normal of the conducting plane[33]. At these special angles the magnetoresistance makes peaks, since almost all one-electron states become localized in the vicinity of the Fermi energy in the two-dimensionalized situation due to the same reason why the two-dimensional system loses conductivity in the quantum Hall state. Theoretical values of the angles are in good agreement with the observed peak angles, as shown in Fig. 13, including the value of the slope of the fitting line.. This success gives a support to the validity of the tight-binding bands based on a single HOMO of the BEDT-TTF molecule for BEDT-TTF based superconductors [34]. We have also treated the case of the general form of in-plane Fermi surface and compared the results with experiments, finding a reasonable agreement between theory [35] and experiment [36,37]. These findings open a new method to determine the form of the Fermi surface of quasi two-dimensional metals, the first target of which is the organic superconductors.

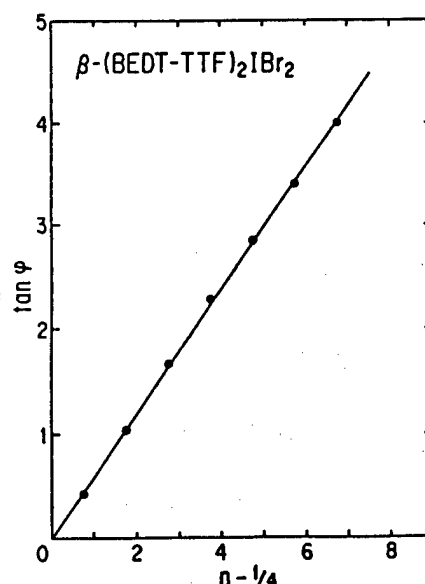
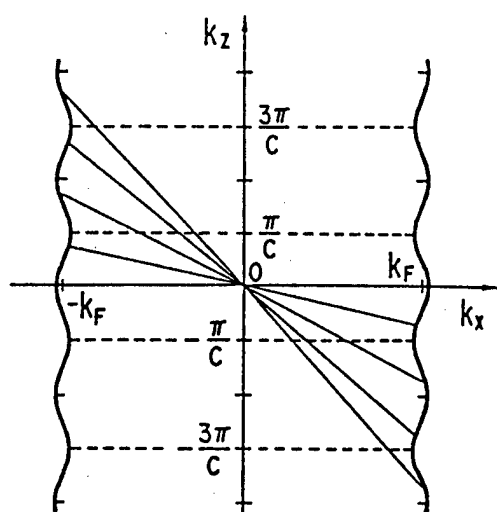


Fig. 12(left) Semiclassical-orbital planes satisfying (1) are shown by oblique lines. Here the special angle ϕ corresponds to the angle between the oblique and horizontal lines.

Fig. 13(right) Values of $\tan \phi$ at peaks of the magnetoresistance (curve 1 in Fig. 1 [31]) versus $n-1/4$ where n numbers the peaks from the $\phi=0$ side.

7. Summary

Recent progress in the superconducting and normal state properties characteristic to the BEDT-TTF based organic metals, including β -(BEDT-TTF)₂X and κ -(BEDT-TTF)₂Cu(NCS)₂, are presented. In addition to the low- and high- T_c states, with $T_c=1$ K and 8 K, respectively, a new superconducting state with $T_c=2$ K was found in β -(BEDT-TTF)₂I₃. DC Hall effect of the low- T_c state of β -(BEDT-TTF)₂I₃ was studied. Tunneling spectroscopy on κ -(BEDT-TTF)₂Cu(NCS)₂ single crystals by a low-temperature scanning tunneling microscope (STM) is reported. In addition to the Shubnikov-de Haas and de Haas-van Alphen effects, a new oscillatory phenomenon characteristic to a quasi two-dimensional electronic system has been shown to be a new powerful tool in the study of Fermi surface in quasi two-dimensional metals.

Acknowledgments

This paper is a summary of recent publications[24-28, 33, 35] by the present authors. The authors would like to thank coauthors of each publication. They would also like to thank Professor S. Kagoshima of the University of Tokyo, and Professor N. Toyota and Mr. T. Sasaki of Tohoku University for useful discussions through a collaborative study on the 2 K superconducting state in β -(BEDT-TTF)₂I₃.

References

1. T. J. Emge, P. C. W. Leung, M. A. Beno, A. J. Schultz, H. H. Wang, L. M. Soma and J. M. Williams, *Phys. Rev.* **B30**, 6780 (1984).
2. P. C. W. Leung, T. J. Emge, M. A. Beno, H. H. Wang, J. M. Williams, V. Petricek and P. Coppens, *J. Am. Chem. Soc.*, **107**, 6184 (1985).
3. J. M. Williams, H. H. Wang, T. J. Emge, U. Geiser, M. A. Beno, P. C. W. Leung, K. D. Carlson, R. J. Thorn, A. J. Schultz and M. -H. Wangbo, *Prog. Inorg. Chem.*, **35**, 51 (1987).
4. P. C. W. Leung, T. J. Emge, A. J. Schultz, M. A. Beno, K. D. Carlson, H. H. Wang, M. A. Firestone and J. M. Williams, *Solid State Commun.*, **57**, 93 (1986).
5. J. M. Williams, T. J. Emge, H. H. Wang, M. A. Beno, P. T. Copps, L. N. Hall, K. D. Carlson and G. W. Crabtree, *Inorg. Chem.*, **23**, 3839 (1984).
6. H. H. Wang, M. A. Beno, U. Geiser, M. A. Firestone, K. S. Webb, L. Nunez, G. W. Crabtree, K. D. Carlson, J. M. Williams, L. J. Azevedo, J. F. Kwak and J. E. Schirber, *Inorg. Chem.*, **24**, 2465 (1985).
7. H. Kobayashi, R. Kato, A. Kobayashi, G. Saito, M. Tokumoto, H. Anzai and T. Ishiguro, *Chem. Lett.*, **1985**, 1293.
8. M. Tokumoto, H. Bando, K. Murata, H. Anzai, N. Kinoshita, K. Kajimura, T. Ishiguro and G. Saito, *Synthetic Metals*, **13**, 9 (1986).
9. H. Anzai, M. Tokumoto, K. Takahashi and T. Ishiguro, *J. Cryst. Growth*, **91**, 225 (1988).
10. M. Tokumoto, H. Anzai, K. Murata, K. Kajimura and T. Ishiguro, *Synth. Metals*, **27**, A251 (1988).
11. M. Tokumoto, H. Anzai, K. Murata, K. Kajimura and T. Ishiguro, *Jpn. J. Appl. Phys.*, **26-S3**, 1977 (1987).
12. Y. Hasegawa and H. Fukuyama, *J. Phys. Soc. Jpn.*, **55**, 4265 (1986).
13. B. Hamzic, G. Creuzet and C. Lenoir, *Europhys. Lett.*, **3**, 373 (1987).
14. F. Creuzet, G. Creuzet, D. Jerome, D. Schweitzer and H. J. Keller, *J. Phys.(Paris) Lett.*, **46**, L-1097 (1985).
15. V. G. Ginodman, A. V. Gudenko, I. I. Zasavitskii and E. B. Yagubskii, *JETP Lett.*, **42**, 472 (1985).
16. V. B. Ginodman, A. V. Gudenko, L. N. Zherikhina, V. N. Laukhin, E. B. Yagubskii, P. A. Kononovich and I. F. Shegolev, *Acta Polymerica* **39**, 533 (1988).
17. S. Kagoshima, Y. Nogami, M. Hasumi, H. Anzai, M. Tokumoto, G. Saito and N. Mori, *Solid State Commun.*, **69**, 1177 (1989).
18. S. Kagoshima, M. Hasumi, Y. Nogami, N. Kinoshita, H. Anzai, M. Tokumoto and G. Saito, *Solid State Commun.*, **71**, 843 (1989).
19. M. Tokumoto, Y. Yamaguchi, N. Kinoshita and H. Anzai, in Proc. 1st ISSP Symposium on the Physics and Chemistry of Organic Superconductors (Springer-Verlag, to be published).
20. T. Sasaki, N. Toyota, M. Hasumi, T. Osada, S. Kagoshima, H. Anzai, M. Tokumoto and

- N. Kinoshita, J. Phys. Soc. Jpn., 58, 3477 (1989).
21. E. L. Venturini, J. E. Schirber, H. H. Wang and J. M. Williams, Synth. Metals, 27, A243 (1988).
 22. H. Hurdequint, F. Creuzet and D. Jerome, Synth. Metals, 27, A183 (1988).
 23. T. Sasaki, N. Toyota, M. Hasumi, T. Osada, S. Kagoshima, M. Tokumoto, N. Kinoshita and H. Anzai, in Proc. 1st ISSP Symposium on the Physics and Chemistry of Organic Superconductors (Springer-Verlag, to be published)
 24. M. Tokumoto, Researches of the Electrotechnical Laboratory, No. 892 (1988).
 25. M. Tokumoto, N. Kinoshita, K. Murata, H. Bando, and H. Anzai, to be published in "Advanced Organic Solid State Materials"(MRS)
 26. K. Murata, M. Ishibashi, Y. Honda, M. Tokumoto, N. Kinoshita and H. Anzai, J. Phys. Soc. Jpn. 58, 3469(1989)
 27. H. Bando, S. Kashiwaya, H. Tokumoto, H. Anzai, N. Kinoshita, and K. Kajimura: to be published in J. Vac. Sci. Technol. A8, no.1 (1990).
 28. H. Bando, S. Kashiwaya, H. Tokumoto, H. Anzai, N. Kinoshita, M. Tokumoto, K. Murata and K. Kajimura: to be published in Proc. of the First ISSP Intl' Symposium on the Physics and Chemistry of Organic Superconductors (Springer-Verlag)
 29. M. E. Hawley, K. E. Grey, B. D. Terris, H. H. Wang, K. D. Carlson and J. M. Williams: Phys. Rev. Lett. 57, 629 (1986).
 30. Y. Maruyama, T. Inabe, H. Urayama and G. Saito: Solid State Commun. 67, 35 (1988).
 31. M.V. Kartsovnik, P.A. Kononovich, V.N. Laukhin, I.F. Shchegolev: JETP Lett. 48, 541 (1988)
 32. K. Kajita, Y. Nishio, T. Takahashi, W. Sasaki, R. Kato, H. Kobayashi, A. Kobayashi, Y. Iye: Solid State Commun. 70, 1189 (1989)
 33. K. Yamaji: J. Phys. Soc. Jpn. 58, 1520 (1989)
 34. T. Mori, A. Kobayashi, Y. Sasaki, H. Kobayashi, G. Saito, H. Inokuchi: Chem. Lett. 957 (1984)
 35. K. Yamaji: to be published in Proc. of the First ISSP Intl' Symposium on the Physics and Chemistry of Organic Superconductors (Springer-Verlag)
 36. I.F. Schegolev, P.A. Kononovich, V.N. Laukhin, M.V. Kartsovnik: to be published in Chemica Scripta (Proc. Gen. Meeting of CMD of EPS in Nice, 1989)
 37. T. Sasaki, N. Toyota, T. Fukase, K. Murata, M. Tokumoto and H. Anzai: to be published in Proc. of the First ISSP Intl' Symposium on the Physics and Chemistry of Organic Superconductors (Springer-Verlag)

T. Ishiguro and Y. Nogami

Physics Department, Kyoto University
Sakyo-ku, Kyoto 606, Japan

Uniaxial stress effects on the low-dimensional molecular Superconductors are investigated. Preliminary results show that the uniaxial tensile strain applied in the conducting plane of κ -(BEDT-TTF)₂Cu(NCS)₂ increases T_C and enhances the resistance peak near 90 K. The increase in T_C is rather weak compared to the calculation. This suggests that the neglected interlayer interaction for calculation may take principal part in determining T_C . The controlled tensile strain experiments are now in progress. The ultrasonic attenuation in high frequency region is to be measured by means of the parametric phonon echo method.

In the organic charge transfer salts exhibiting the superconductivity, the electronic properties are dominated by the electron transfer between radical molecules. Since the molecules are stacked segregatedly, forming columns or layers, the intermolecular bondings are anisotropic depending on the directions parallel or perpendicular to the columnar axes or layer planes, respectively. Consequently the electronic structures are of the reduced dimensionality and the interesting ordered phases such as the charge density waves, the spin density waves and the superconductivity emerge in relation to the low-dimensionality of the electronic structure.

For the hydrostatic pressure, the degree of the low-dimensionality is varied due to the difference in the rigidity of the bonding nature against the pressure: the softer bondings which are usually determining the low-dimensionality are strengthened and hence the degree of the dimensionality is raised. For example, for (TMTSF)₂X salts the hydrostatic pressure increases the transverse transfer energy remarkably and suppresses the nesting of the Fermi surface resulting in the emergence of the superconductivity.

Secondly the suppression of the superconducting transition temperature T_C by pressure is observed widely in organic superconductors [1,2]. The pressure may be either physical or chemical: the effect of pressure to the molecular crystal is represented by the reduction in the intermolecular spacing, which may be realized either by externally applied pressure or by the substitution of counter ions with smaller size due to the so-called the chemical pressure effect. For the charge transfer salts exhibiting the superconductivity, it is found as a general trend that the reduction in the intermolecular spacing results in the decrease in T_C [2].

Based on these two facts we remark here the usefulness of a tensile stress to the organic superconductors. Concerning the pressure dependence of the T_C , it is preferable to apply negative pressure or to elongate the spacing between molecules, in order to increase T_C . This is eventually possible if one can apply tensile stress in

the conduction axis or layer. Although the low-dimensional materials are easily broken by mechanical stress along the least conducting axis due to weak bonding, moderate tensile stresses can be applied along the stacking axes or planes.

With these tensile stress we can expect two effects ; the first is the enlarging the spacing along the stacking axis which may result in increase of T_c , while the second is the decrease in the spacing between conducting columns and layers which results in suppressing the nesting due to the transverse transfer integrals. Further, the combination of the informations deduced from the uniaxial stress with the hydrostatic stress is interesting, which make possible to test the validity of the models formed through the studies by the hydrostatic pressure experiments.

In order to apply the tensile stress we have adopted two approaches : one is the suppression of the thermal contraction [3,4] and the second is the artificial elongation of a sample by using a stress transformer. Since the thermal contraction of the molecular crystals is much larger than ordinary metals or inorganic materials, by cooling one can apply tensile stress to a sample when the ends of the samples are stucked to a holder with small thermal contraction. The estimated changes in lattice parameters for κ -(BEDT-TTF)₂Cu(NCS)₂ by cooling down to 0 K from room temperature are $\Delta b/b=9.5 \times 10^{-3}$, $\Delta c/c=2.7 \times 10^{-2}$ and $\Delta a/a=-9.0 \times 10^{-3}$, where the b and the c axes lie in the conducting plane and the minus sign added to the lattice spacing along the a direction denotes the thermal expansion by cooling [5]. The corresponding thermal contraction ratio for Cu is 3.2×10^{-3} .

The disadvantages of this elongation method are that one cannot artificially control the strain externally and further that the amount of the thermally induced strain itself changes with temperature. To compensate these shortages, we are adopting the stress transformer as shown in Fig. 1, in which the externally applied stresses which are strong enough to break the sample if they are applied directly.

We are carrying out experiments by using the transformer but in this report we describe the preliminary results reduced by the tensile strain caused by the difference in thermal contractions. The effects of the tensile strain are found as the increase in T_c for the superconductivity and also as the enhancement of the resistance peak appearing near 90 K. The effect of the tensile stress is not so prominent as expected from the band structure calculation based on the crystal structure as shown in Fig. 2. We calculated the T_c by using the Yamaji formula based on the electron molecular vibrational coupling in TTF type molecules [6]. The electronic band parameters are calculated through the overlap integrals between adjacent molecules and the tight binding band calculation [7]. The difference between the calculated and the observed is partly due to the fact that the roles of interlayer interaction is neglected for calculation and this indicates that the significance of the interlayer interactions for the superconductivity.

The enhancement of the resistivity peak is represented in Fig. 3, where the height of the peak is increased extraordinarily by the elongation along the b-axis. The origin of the resistivity peak is not clear, but it is suggested that the formation of the polaron due to the strong electron phonon interaction, e.g. via the electron molecular vibration coupling, may be responsible to it.

The remarkable influence of the uniaxial strain to the electronic structure re-

minds us the significance of the ultrasonic study : the longitudinal wave corresponds the oscillating uniaxial strain mode in itself. It is considered that the low-dimensional conductors are not attenuated if it does not accompany the relaxation of the electron distribution associated by the change in the Fermi surface. When the uniaxial strain wave modify the transverse transfer integrals, e.g. suppressing the nesting conditions, the attenuation should occur reflecting the relaxation of the normal carriers. For, the transverse modes, the modification of the nesting condition is not expected in the first approximation, but the attenuation associated by the screening is expected. However, to observe the attenuation from the electrons, it is essential to use ultrasonic waves higher than 100 MHz. It is expected that the ultrasonic attenuation in the superconducting transition region will give essential information in determining the pairing types of superconductivity.

The organic superconductors have limitations to introduce of the high frequency ultrasonic waves. To overcome this difficulty, we are developing a new method for the generation and receipt of the acoustic waves by phonon echo (GRAPE) method. In this method the strain waves of frequency ω is coupled parametrically with the electromagnetic waves of 2ω , resulting in the formation of the backward strain echoes of frequency ω [8]. The echo signals are formed in bonded piezoelectric crystals as shown in Fig. 4 and therefore they are not affected by the irregularity of the end surfaces of crystals whose parallelism is essential for the ordinary ultrasonic pulse echo method. So far we are developing the method of the parametric phonon echoes which is appropriate for the ultrasonic study for the organic crystals with the plate or needles.

We are much obliged to Dr. Y. Ueba and Mr. H. Kusunaga of Sumitomo Electric Co. Ltd., for their collaboration in the tensile strain experiment. We also thank to Mr. H. Ito and Mr. T. Sato for their experimental assistance.

References

1. G. Saito et al., *Synth. Metals* **27** A331 (1988).
2. M. Tokumoto et al., *Physica* **143B** 338 (1986).
3. H. Kusunaga, Y. Sakata, Y. Ueba, K. Toda, M. Kaji and T. Ishiguro, "Tensile Stress Effects on Superconducting Transition Temperature in $(\text{BEDT-TTF})_2\text{Cu}(\text{NCS})_2$ to be published in Proceedings of ISSP Conference on Physics and Chemistry of Organic Superconductors.
4. H. Kusunaga, Y. Sakata, Y. Ueba, K. Toda, M. Kaji and T. Ishiguro, "Tensile Stress Effect on Transport Properties of $(\text{BEDT-TTF})_2\text{Cu}(\text{NCS})_2$ " submitted to *Solid State Commun.*
5. G. Saito and H. Urayama, *Kotaibutsuri* **23**, 198 (1988) (in Japanese)
6. K. Yamaji, *Solid State Commun.* **61** 413 (1987).
7. T. Mori et al., *Bull. Chem. Soc. Jpn* **57** 627 (1984).
8. K. Fossheim and R.M. Holt, *Physical Acoustics Vol. XVI ed., Mason and Thuston* (Academic Press, 1982) p. 217.

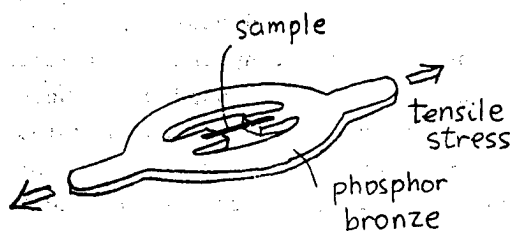


Fig. 1 Strain transformer device.

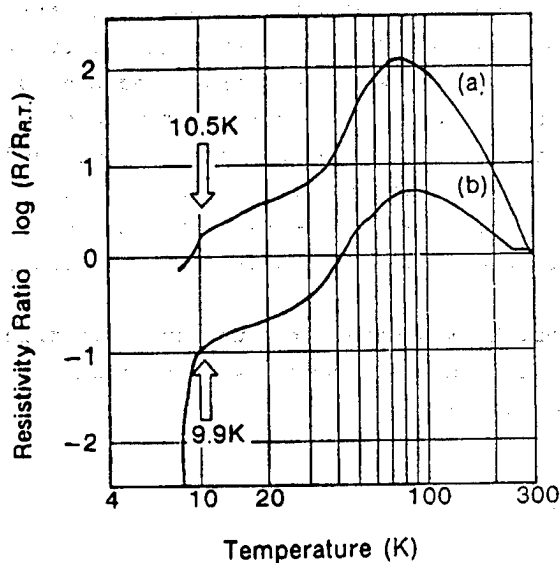


Fig. 3

Temperature dependence of the resistivity normalized with the room temperature value for the sample elongated the b direction (a) and for stress free sample (b).

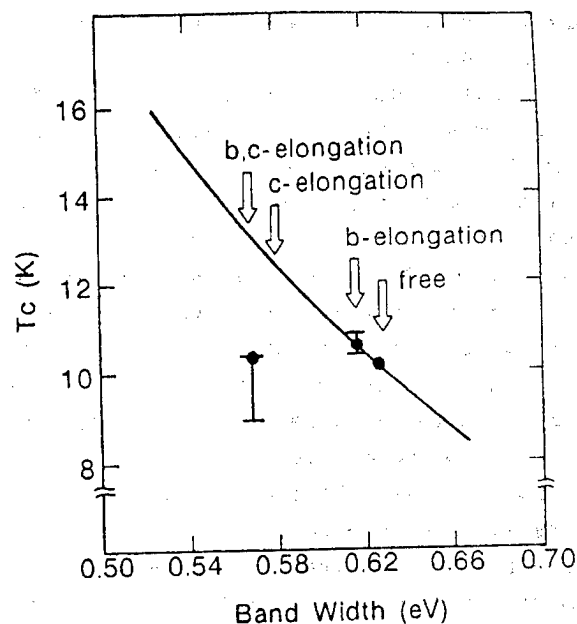


Fig. 2 Band width dependence of T_c for κ -(BEDT-TTF)₂Cu(NCS)₂ after Yamaji formula [6]. Closed circles represent experimental data for samples strain free, elongated along the b axis and elongated along the b and c axes.

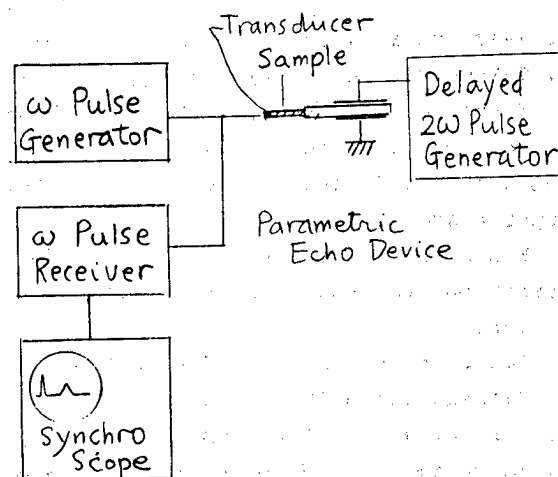


Fig. 4 Block diagram of the parametric phonon echo method.

- END -

This is a U.S. Government publication. Its contents in no way represent the policies, views, or attitudes of the U.S. Government. Users of this publication may cite FBIS or JPRS provided they do so in a manner clearly identifying them as the secondary source.

Foreign Broadcast Information Service (FBIS) and Joint Publications Research Service (JPRS) publications contain political, economic, military, and sociological news, commentary, and other information, as well as scientific and technical data and reports. All information has been obtained from foreign radio and television broadcasts, news agency transmissions, newspapers, books, and periodicals. Items generally are processed from the first or best available source; it should not be inferred that they have been disseminated only in the medium, in the language, or to the area indicated. Items from foreign language sources are translated; those from English-language sources are transcribed, with personal and place names rendered in accordance with FBIS transliteration style.

Headlines, editorial reports, and material enclosed in brackets [] are supplied by FBIS/JPRS. Processing indicators such as [Text] or [Excerpts] in the first line of each item indicate how the information was processed from the original. Unfamiliar names rendered phonetically are enclosed in parentheses. Words or names preceded by a question mark and enclosed in parentheses were not clear from the original source but have been supplied as appropriate to the context. Other unattributed parenthetical notes within the body of an item originate with the source. Times within items are as given by the source. Passages in boldface or italics are as published.

SUBSCRIPTION/PROCUREMENT INFORMATION

The FBIS DAILY REPORT contains current news and information and is published Monday through Friday in eight volumes: China, East Europe, Soviet Union, East Asia, Near East & South Asia, Sub-Saharan Africa, Latin America, and West Europe. Supplements to the DAILY REPORTs may also be available periodically and will be distributed to regular DAILY REPORT subscribers. JPRS publications, which include approximately 50 regional, worldwide, and topical reports, generally contain less time-sensitive information and are published periodically.

Current DAILY REPORTs and JPRS publications are listed in *Government Reports Announcements* issued semimonthly by the National Technical Information Service (NTIS), 5285 Port Royal Road, Springfield, Virginia 22161 and the *Monthly Catalog of U.S. Government Publications* issued by the Superintendent of Documents, U.S. Government Printing Office, Washington, D.C. 20402.

The public may subscribe to either hardcover or microfiche versions of the DAILY REPORTs and JPRS publications through NTIS at the above address or by calling (703) 487-4630. Subscription rates will be

provided by NTIS upon request. Subscriptions are available outside the United States from NTIS or appointed foreign dealers. New subscribers should expect a 30-day delay in receipt of the first issue.

U.S. Government offices may obtain subscriptions to the DAILY REPORTs or JPRS publications (hardcover or microfiche) at no charge through their sponsoring organizations. For additional information or assistance, call FBIS, (202) 338-6735, or write to P.O. Box 2604, Washington, D.C. 20013. Department of Defense consumers are required to submit requests through appropriate command validation channels to DIA, RTS-2C, Washington, D.C. 20301. (Telephone: (202) 373-3771, Autovon: 243-3771.)

Back issues or single copies of the DAILY REPORTs and JPRS publications are not available. Both the DAILY REPORTs and the JPRS publications are on file for public reference at the Library of Congress and at many Federal Depository Libraries. Reference copies may also be seen at many public and university libraries throughout the United States.